O-001

The discovery and characterization of [18F]MK-8553, a novel PET tracer for imaging O-GlcNAcase (OGA)

Wenping Li[1], Cristian Salinas[1], Kerry Riffel[1], Patricia Miller[1], Zhizhen Zeng[1], Talakad Lohith[1], Harold G. Selnick[1], Mona Purcell[1], Marie Holahan[1], Xiangjun Meng[1], Hyking Haley[1], Liza Gantert[1], Guy Bormans[2], Koen Van Laere[2], Michel Koole[2], Kim Serdons[2], Jan de Hoon[2], Ernest McEachern[3], David Vocadlo[3], Corinne Vandermeulen[2], Inge De Lepeleire[4], Ruben Declercq[4], Tom Reynders[4], Arie Struyk[1], Sean Smith[1], Jeff Evelhoch[1], and Eric Hostetler[1]

[1]Merck Research Laboratories, West Point, PA, [2]UZ Leuven and KU Leuven, Leuven, Belgium
[3]Alectos Therapeutics Inc., Burnaby, BC Canada, [4]Merck Sharp & Dohme (Europe) Inc., Brussels, Belgium

Objectives: O-GlcNAcase (OGA) enzyme regulates protein O-GlcNAcylation which is a common post-translational modification that plays a role in regulating protein stability.   Preclinical data demonstrates that OGA inhibition significantly reduces tau aggregation in human neurons and neurodegeneration in the Tg4510 transgenic mouse model of tauopathy. Sustained OGA inhibition is expected to provide therapeutic benefit in reducing tau aggregation and thereby slowing neurodegeneration in progressive supranuclear palsy (PSP) patients. An OGA inhibitor PET tracer would permit the study of this target and measuring central enzyme occupancy by potential therapeutic compounds in preclinical and clinical studies.

Methods: [18F]MK-8553 was prepared by nucleophilic displacement with [18F]KF/Kryptofix 222 in good yield with high radiochemical purity and specific activity. In vitro tissue homogenate binding assays to determine K_d values and autoradiographic studies to determine regional distribution of tracer binding were performed in rhesus monkey and human brain samples.   PET scans under baseline and blocking conditions were carried out in Tg4510 mice, wild type rat, and rhesus monkey to determine binding specificity. Clinical PET scans were also performed to determine human dosimetry and test/retest variability.

Results: Tissue homogenate binding assays revealed MK-8553 has high affinity for the OGA enzyme and autoradiographic studies in rhesus monkey and human brain slices showed highest binding in striatum, frontal cortex, globus pallidus, and hypothalamus. [18F]MK-8553 showed promising imaging characteristics *in vivo*: a large, reversible, specific tracer distribution in the brain, and a regional distribution consistent with the OGA distribution pattern *in vitro*. The specificity of tracer distribution was demonstrated by complete blockade of [18F]MK-8553 binding with a potent, structurally diverse OGA-specific inhibitor in animals. In the clinic [18F]MK-8553 reported an effective dose of 17.0 ± 1.4 microSv/MBq and a test-restest variability of the main quantitative PET outcome of 4% which makes it an ideal tracer to evaluate OGA enzyme target engagement.

Conclusions: [18F]MK-8553 is a high affinity, selective OGA inhibitor with properties suitable for imaging OGA and determining central enzyme occupancy in both preclinical and clinical studies. Currently [18F]MK-8553 is being utilized in humans as a PET tracer to assess CNS target engagement to select a dose for clinical proof of concept trials with a small molecule OGA inhibitor. The target engagement data generated with [18F]MK-8553 will ensure proper testing of the OGA mechanism and increase the probability of a successful clinical trial with OGA inhibitors.

In vivo characterization of an agonist dopamine D1 receptors tracer [18F]MNI-800 (PF-8477) in non-human primates

Cristian C. Constantinescu[1], Lei Zhang[2], Thomas Morley[1], Caroline Papin[1], David L. Gray[3], Che-wah Lee[2], Anabella Villalobos[2], Rikki N. Waterhouse[3], Timothy J. McCarthy[3], Olivier Barret[1], David Alagille[1], Gilles, D. Tamagnan[1]

[1]Molecular NeuroImaging, LLC, New Haven, CT, [2]Worldwide Medicinal Chemistry, Pfizer Inc., Cambridge, MA, [3]Neuroscience and Pain Research Unit, Pfizer Inc., Cambridge, MA

Objective: D1 receptors, which couple to inhibitory G-proteins, have been shown to regulate neuronal growth and development, mediate some behavioral responses, and modulate dopamine receptor D2-mediated events [1]. Its function has been shown to be altered in schizophrenia [2]. To date, there is a lack of agonist PET tracers for the D1 receptors labeled with ^{18}F with relevance in clinical studies. We report the evaluation in non-human primates of [18F]MNI-800 (PF-8477), a novel PET radiotracer of the D1 receptors.

Methods: Eight brain PET studies, 4 baselines (2 test/retest) and 4 blockade studies using SCH23390 were conducted for 120 min in two rhesus monkeys with [18F]MNI-800 (dose 177 ± 7 MBq). Different doses (0.03-0.485 mg/kg) of SCH23390 were used, which were administered i.v. as 15 min infusion starting 25 min before tracer injection. PET data were modeled with 2-tissue compartmental model (2T), Logan graphical analysis (LGA), and non-invasive Logan graphical analysis (NI-LGA) with cerebellar cortex as reference region to estimate total distribution volume V_T, and binding potential BP_{ND}. Occupancy was estimated from BP_{ND} at baseline and post blockade. Two whole-body PET studies were performed in one male and one female rhesus monkey, and radiation absorbed dose estimates and effective dose (ED) were estimated with OLINDA/EXM 1.0.

Results: [18F]MNI-800 penetrated the brain with a peak whole-brain uptake up to ~3% ID at ~ 6 min post injection and showed a fast washout. The highest signal was found in the caudate, putamen, with moderate extrastriatal uptake. The lowest signal was in the cerebellum. BP_{ND} values were up to ~0.85 in the caudate and putamen. Test-retest reproducibility was ≤ 5% for both V_T and BP_{ND} in the striatal regions. Occupancy of D1 receptors by SCH23390 estimated with [18F]MNI-800 was dose dependent, with ED_{50} ~ 0.1 mg/kg. Occupancy estimates were very similar between 2T, LGA, and NI-LGA. From whole-body imaging ED was estimated to be 0.025 mSv/MBq for female and 0.021 mSv/MBq for male rhesus, with tracer being eliminated primarily via hepatobiliary pathway.

Conclusions: Our work showed that [18F]MNI-800 is a promising agonist PET radiotracer for imaging D1 receptors that can be quantified non-invasively and has favorable dosimetry. [18F]MNI-800 is a promising tracer for imaging of should be a very useful tool for studies that target D1 density.

References:
[1] ML Paul, AM Graybiel, JC David, and HA Robertson, "D1-like and D2-like dopamine receptors synergistically activate rotation and c-fos expression in the dopamine-depleted striatum in a rat model of Parkinson's disease," Journal of Neuroscience vol. 12, no. 10, pp. 3729–3742, 1992. [2] A. Abi-Dargham, O.Mawlawi, I. Lombardo et al., "Prefrontal dopamine D1 receptors and working memory in schizophrenia," Journal of Neuroscience, vol. 22, no. 9, pp. 3708–3719, 2002.
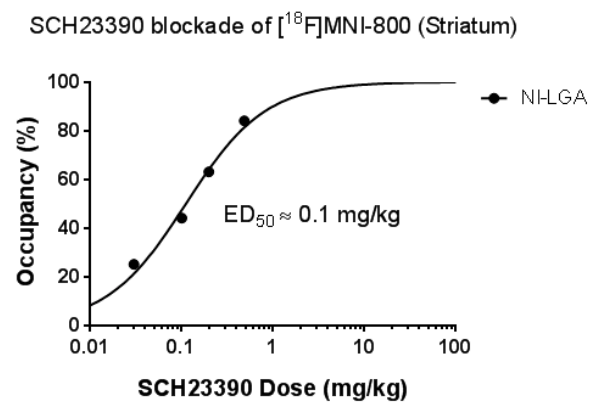
SCH23390 blockade of [^{18}F]MNI-800 (Striatum)

Figure 1. Non-linear regression between average D1 receptor occupancy in the striatum and administered dose of SCH23390.

O-003

Two novel sigma-1 receptor PET radiotracers with favorable imaging properties: evaluation in nonhuman primates

Zhengxin Cai[1], Evan Baum[1], Fred Bois[1], Daniel Holden[1], Shu-fei Lin[1], Teresa Lara- Jaime[1], Michael Kapinos[1], Yuanyuan Chen[2], Winnie Deuther-Conrad[3], Steffen Fischer[3], Bernhard Wünsch[4], Peter Brust[3], Hongmei Jia[2], Yiyun Huang[1]

[1]PET Center, Department of Radiology and Biomedical Imaging, Yale University School of Medicine, New Haven, CT, USA, [2]Ministry of Education Key Laboratory of Radiopharmaceuticals, College of Chemistry, Beijing Normal University, Beijing, China, [3]Helmholtz-Zentrum Dresden-Rossendorf, Research Site Leipzig, Leipzig, Germany, [4]Westfälische Wilhelms-Universität Münster, Department of Pharmaceutical and Medicinal Chemistry, Münster, Germany

Objectives: Sigma-1 receptors (Sig-1Rs) are intramolecular chaperone proteins, the abnormal expression of which has been indicated in a variety of CNS disorders [1]. As a result, Sig-1R is proposed as a therapeutic target for schizophrenia, depression, and Alzheimer's disease. PET imaging of Sig-1Rs would provide an in vivo tool to investigate their involvement in these diseases, and to assist in drug development. Hence, great efforts have been devoted to the development of effective PET radiotracers for Sig-1Rs, though most have failed to reach the human evaluation stage due to unfavorable pharmacokinetic and imaging properties. Through our Sig-1R PET ligand discovery programs, we have identified a number of spirocyclic piperidine analogs with attractive characteristics for development as *in vivo* imaging agents [2-4]. The objective of this study was to evaluate the two most promising ligands in rhesus monkeys in preparation for clinical translation.

Methods: The two ^{18}F-labeled radiotracers (**1** and **2**) were prepared by nucleophilic displacement of the tosylate on the precursors and evaluated in the same rhesus monkeys (n = 2). Baseline scans of 4-h duration were obtained on a FOCUS 220 scanner after injection of ~5 mCi radioactivity. Blocking scans were performed with pre-administration of the selective Sig-1R agonist SA4503. Arterial blood was collected at pre-selected time points for measurement of plasma activity and HPLC analysis of radiometabolites to generate the plasma input functions for the parent tracer. Analysis of brain regional time-activity curves (TACs) was performed with one-tissue (1T), two-tissue (2T), and the multilinear analysis-1 (MA1) models to estimate kinetic parameters and regional volumes of distribution (V_T). Tracer free fraction (f_P) in plasma was measured via ultrafiltration method. Log D of each radiotracer was determined by the shake-flask method.

Results: Radiotracer **1** and **2** were prepared in high radiochemical purity and specific activity. In rhesus monkeys both tracers displayed moderate rates of metabolism, with 35% and 19% of parent fraction for **1** and **2** at 60 min post-injection. Plasma f_P values were 2% and 17% for **1** and **2**, in line with their respective measured Log D values of 2.8 and 2.5. Both radiotracers exhibited excellent brain uptake (peak SUV > 4) and fast tissue kinetics (activity peaked in all regions at <30 min post-injection) (**Fig. 1**). Both the 1T and MA1 models provided good fits of regional TACs and reliable V_T estimates. Overall, ligand **2** displayed higher uptake levels, greater differential uptake among brain regions and higher regional V_T values than **1**. SA4503 (0.5 mg/kg. iv) blocked ~85% (**1**) and ~95% (**2**) of radiotracer uptake, indicating the binding specificity of both radiotracers in the monkey brain.

Conclusions: The novel Sig-1R radiotracers **1** and **2** display excellent brain uptake, fast tissue kinetics, and high levels of specific binding *in vivo*. Both have proved to be suitable for the imaging and quantification of Sig-1R in the monkey brain, therefore, further evaluation in humans is warranted. In comparison, tracer **2** has a ten-fold higher f_P, higher brain uptake, and greater V_T values in rhesus monkey.

References:
1. Maurice T and Su T-P, Pharmacol Ther, 2009. **124**:195.
2. Brust P et al., J Nucl Med, 2014. **55**:1730.
3. Li Y et al., J Med Chem, 2013. **56**:3478. 4. Chen Y-Y et al., Bioorg Med Chem, 2014. **22**:5270.
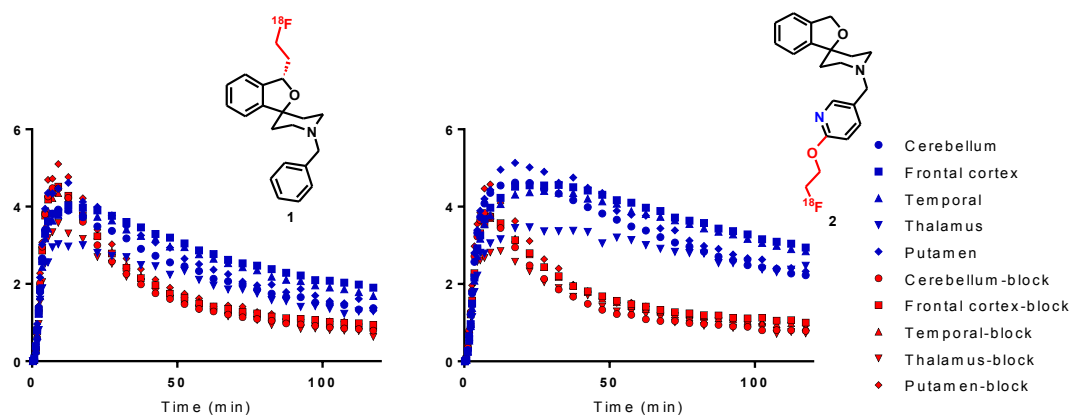
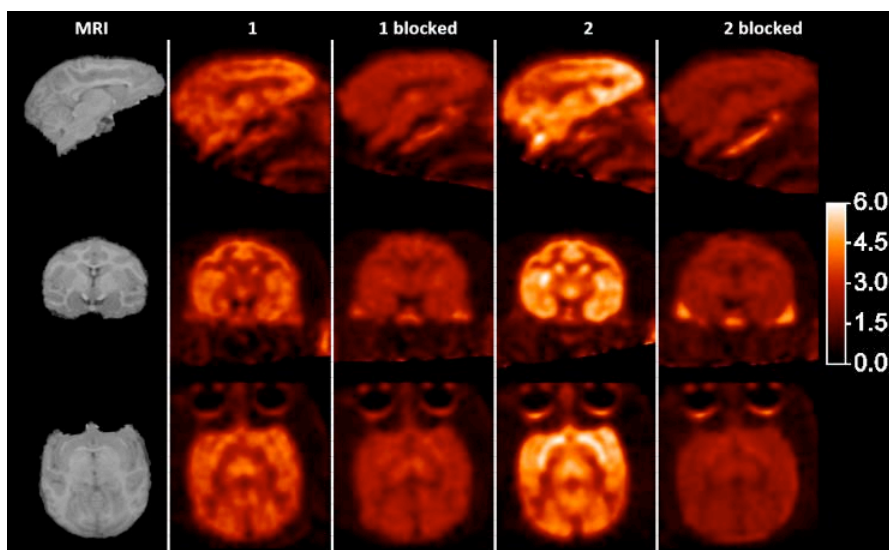**Fig. 1**. Baseline and blocking scan TACs of ligands **1** and **2** in selected brain regions.

Figure 2. Baseline and blocking PET Images summed from 20 to 40 min for ligands **1** and **2** in the same rhesus monkey.

O-004

NMDA-receptor occupancy with [^{11}C]NB1 in rats and the evaluation of a perfusion-independent quantification method in the absence of a reference region or an input function

S. D. Krämer[1], T. Betzel[1], L. Mu[2], M. Szermerski[3], R. Schibli[1], B. Wünsch[3], S. M. Ametamey[1]

[1]ETH, Zurich, Switzerland, [2]University Hospital Zurich, Zurich, Switzerland, [3]Westfälische Wilhelms-Universität, Münster, Germany.

Introduction: We have developed the PET tracer [^{11}C]NB1 (7-[^{11}C]methoxy-3-(4-phenylbutyl)-2,3,4,5-tetrahydro-1H-benzo[d]azepin-1-ol) to image the density and occupancy of NMDA receptors, more specifically the GluN2B modulatory or ifenprodil binding site. [^{11}C]NB1 binds with a K_i of 5.4 nM to human NMDA receptors and has an unmet selectivity over sigma receptors (K_i >180 nM) [1].
Clinical therapy trials with GluN2B-targeting modulators were disappointing so far. Owing to the lack of a suitable tracer, no receptor occupancy studies were performed to better understand their intriguing pharmacology. In this work, we evaluated [^{11}C]NB1 in an NMDA-receptor occupancy study with eliprodil (K_i 13 nM) in rats.
We evaluated two input-function independent parameters for quantification: the averaged standardized uptake value (SUV) and the mean residence time (MRT) by comparison with parameters revealed from kinetic modelling with an input function. Unlike SUV, MRT is in theory independent of K_1 (the tracer clearance from blood to brain) and, therefore, of perfusion.

Methods: We first characterized the kinetics of [^{11}C]NB1 under baseline conditions in isoflurane-anaesthetized rats by modelling with an input function. Data were analysed with a two-tissue compartment model and input-function independent parameters were compared with the modelling results. For the receptor occupancy study, eliprodil (0.25-2000 µg/kg) was co-administered with the tracer. No input function was recorded. Receptor occupancy was calculated with the averaged SUV and the MRT.

Results: Modelling with an input function revealed for whole brain (5 rats) high K_1 (1.24±0.08) mL/min/cm^3, indicating perfusion-limited brain uptake. V_T was 4.15±0.46 ($K_1/k_2(1+k_3/k_4)$) and was stable (±5%) from 14 min onwards. V_T from the Logan graphical analysis was 4.29±0.37. SUV averaged over the complete scan (SUV$_{0-60min}$) correlated with V_T (5 rats, 14 brain regions each) with an r 0.95 (Figure 1A). However, SUV weakly correlated with K_1 (r 0.42; Figure 1B), indicating that it is sensitive to alterations in perfusion. As expected, MRT was independent of K_1 (r 0.27) and better correlated with V_T/K_1 than with V_T (r 0.60 vs 0.49).
[^{11}C]NB1 accumulation in brain was reduced by eliprodil in a dose-dependent manner. When calculated with SUV$_{0-60min}$, 50 % receptor occupancy was reached at 3.8 nmol/kg (1.3 µg/kg; Figure 1C). Calculated with the MRT, the dose for half saturation was 10-fold higher (38 nmol/kg; Figure 1D). The TACs of the scans with the highest shifts comparing the two dose-occupancy diagrams (red broken arrows in Figure 1C/D) had a low SUV$_{0-60min}$ but a shape similar to TACs in the absence of eliprodil. Note that K_1 affects the height of the TAC (and, therefore the SUV) while k_2 and the receptor-related k_3 and k_4 together with the input function define its shape (and thus both SUV and MRT).

Conclusion: The non-invasive quantification of the density and occupancy of ifenprodil-binding NMDA receptors is now possible with [^{11}C]NB1. The perfusion-independent MRT allows quantification in the absence of an input function or a reference region.

References:
[1] Tewes et al. 2010. *ChemMedChem*. 5:687;
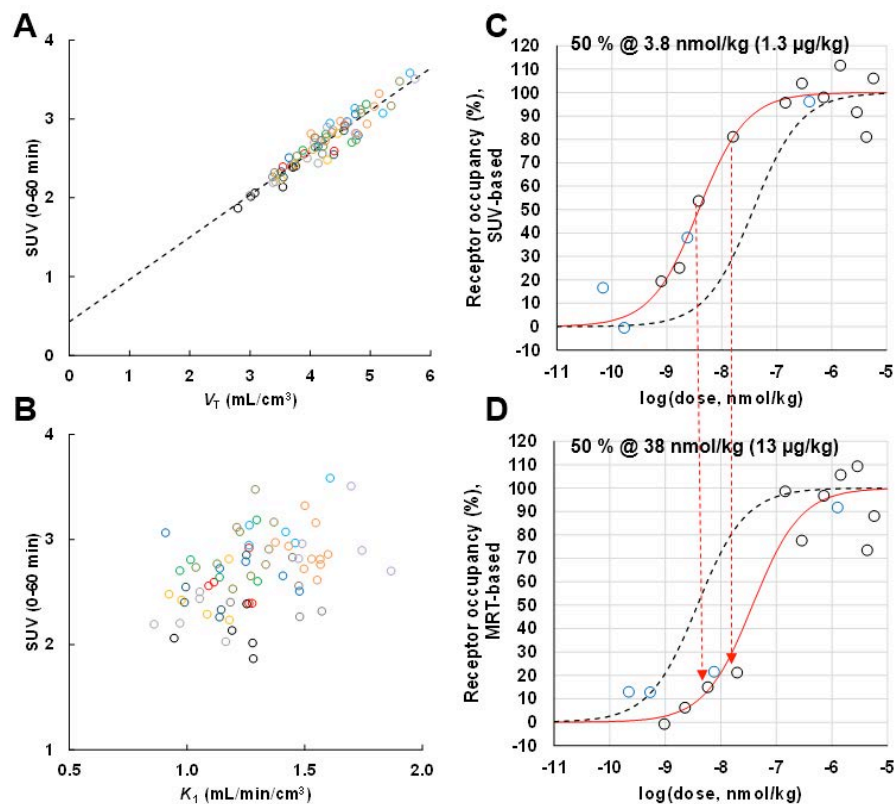[2] Müller et al. 2015. *J. Neurochem*. 133:330.

Figure A) Correlation between $SUV_{0-60min}$ and V_T. Colours indicate individual brain regions. **B)** Influence of K_1 on $SUV_{0-60min}$. **C, D)** Receptor occupancy calculated with the $SUV_{0-60min}$ (**C**) or the mean residence time (MRT; **D**). Dose at 50% occupancy was 10-fold higher with the MRT-based calculations (as indicated). Blue symbols, [^{11}C]NB1/NB1 only (dose equivalents fit from data); red lines, fit functions; black broken lines, fit functions of alternative method for direct comparison; red arrows, shift from >50% to <50% occupancy.

Diphenhydramine is a specific and selective probe to study the H+/antiporter function at the blood-brain barrier: application to ^{11}C-diphenhydramine PET imaging

S Auvity[1,2], H Chapy[2], S Goutal[1], F Caillé[1], B Hosten[2], M Smirnova[2], N Tournier[1], S Cisternino[2]

[1]*Imagerie Moléculaire In Vivo, IMIV, CEA, Inserm, CNRS, Univ. Paris-Sud, Université Paris Saclay, CEA-SHFJ, Orsay, France,* [2]*Variabilité de réponse aux psychotropes, INSERM, Paris, France; Université Paris Descartes, Paris, France; Université Paris Diderot, Paris, France*

Context: Evidence for a cationic drug H$^+$/antiporter from the solute carrier transporter (SLC) family, also known as "clonidine antiporter", has been functionally demonstrated at the blood-brain barrier (BBB). Several in vivo/in situ and in vitro studies have confirmed the unique functional properties of this transport, which does not correspond to any other known SLC transporters at the BBB [1]. This transporter controls the brain distribution of many psychoactive drugs, including clonidine, oxycodone, nicotine, cocaine and diphenhydramine, a sedative H$_1$-histamine receptor antagonist. Drug H$^+$/antiporter function at the BBB challenges the assumption that only passive diffusion controls the distribution of psychoactive drugs to the brain.

Methods: ^{14}C-diphenhydramine *in situ* brain perfusion was performed in mice for 60s. After the systemic blood flow being stopped, the in situ perfusion method replaces the brain vasculature content by an artificial perfusate. This perfusate set up in order to study the impact of drug concentrations that cannot be reached *in vivo*. In situ experiments were performed to measure ^{14}C-diphenhydramine brain uptake clearance (K$_{in}$), in different conditions (n=4-6): *i)* ^{14}C-diphenhydramine baseline transport (vehicle) *ii)* concentration-dependency of diphenhydramine BBB transport (from 0 to 30 mM) *iii)* competitive inhibition using known H$^+$/antiporter inhibitor (clonidine 10 mM) *iv)* P-gp and Bcrp efflux using *Abcb1a/1b/Abcg2* triple knockout mice. Diphenhydramine was then radiolabeled with carbon-11 to validate ^{11}C-diphenhydramine as a PET probe and quantify drug H$^+$/antiporter function *in vivo*. Four rats were injected ^{11}C-diphenhydramine (~37 MBq) followed by 60 min microPET scanning. Brain and plasma radiometabolites were measured using radio-HPLC analysis. ^{11}C-diphenhydramine brain uptake clearance (Cl$_{uptake}$) was calculated using the integration plot analysis from 0 to 2 min using the metabolite-corrected arterial input function measured in 3 additional animals.

Results: Baseline brain uptake clearance of ^{14}C-diphenhydramine measured by in situ mouse brain perfusion was K$_{in}$ = 1.91± 0.18 mL.min^{-1}.g^1. Concentration-dependency experiments showed a carrier-mediated influx of diphenhydramine (K$_m$ = 4.4 ± 1.6 mM; V$_m$ = 162 ± 44 nmol.s^{-1}.g^{-1}), with a passive diffusion component accounting for only 28% of the total diphenhydramine BBB transport for concentrations lower than the K$_m$ (pharmacological situation). Co-infusion of clonidine significantly inhibited ^{14}C-diphenhydramine brain transport (69.3 ± 0.3% of baseline K$_{in}$; p<0.001). P-gp/Bcrp deficiencies did not impact diphenhydramine BBB transport (92.8 ± 3.7% of baseline K$_{in}$). In rats, ^{11}C-diphenhydramine brain uptake was substantial and homogeneously distributed within the brain parenchyma. 15 min after injection, ^{11}C-diphenhydramine radiometabolites accounted for 72 % in plasma and <2 % in the brain. PET-based estimation of brain ^{11}C-diphenhydramine Cl$_{uptake}$ was 0.99± 0.18 mL.min^{-1}.cm^{-3}.

Conclusion: Diphenhydramine brain distribution is mainly controlled by H$^+$/antiporter function at the BBB which contribution to the BBB transport is 3.6-fold higher than the passive diffusion component. Moreover, diphenhydramine BBB transport is not influenced by P-gp/Bcrp efflux at the BBB. In the absence of brain radiometabolites in the brain distribution phase, ^{11}C-diphenhydramine can be reliably used for the non-invasive quantification of the drug H$^+$/antiporter function at the BBB using PET.

References:
[1] P. André, M. Debray, J.-M. Scherrmann, S. Cisternino, Clonidine transport at the mouse blood-brain barrier by a new H+ antiporter that interacts with addictive drugs, J. Cereb. Blood Flow Metab. Off. J. Int. Soc. Cereb. Blood Flow Metab. 29 (2009) 1293–1304. doi:10.1038/jcbfm.2009.54.

O-006

The search for a subtype selective PET imaging agent for the GABA$_A$ receptor complex: evaluation of the novel radiotracer [11C]ADO in non-human primates

Yiyun Huang[1], Fred Bois[1], Daniel Holden[1], Nabeel Nabulsi[1], Richard Pracitto[1], Hong Gao[1], Shu-fei Lin[1], Jo-Ku Teng[1], Anupama Shirali[1], Jim Ropchan[1], Richard E. Carson[1], Charles S. Elmore[2], Neil Vasdev[3]

[1]PET Center, Department of Radiology and Biomedical Imaging, Yale University School of Medicine, New Haven, CT, USA, [2]AstraZeneca Pharmaceuticals, Mölndal, Sweden, [3]Division of Nuclear Medicine and Molecular Imaging, Department of Radiology, Massachusetts General Hospital & Harvard Medical School, Boston, MA, USA

Objectives: Gamma-aminobutyric acid (GABA) is the predominant inhibitory neurotransmitter in the brain, and its myriad functions are regulated by three receptor families: GABA$_A$, GABA$_B$ and GABA$_C$. The GABA$_A$ complex is further divided into many subtypes, with the benzodiazepine binding a$_1$, a$_2$, a$_3$, and a$_5$ subunits being the most abundant and each mediating different pharmacological effects. For example, the sedative activity of benzodiazepines is attributed to the a$_1$ subunit, the a$_2$ and a$_3$ subunits mediate anxiolytic effect, and action at the a$_5$ subunit is believed to be procognitive. Availability of subtype-selective radiotracers would provide valuable tools to elucidate the functions of these GABA$_A$ subunits in vivo, and help in the development of therapeutics with optimal benefit-side effect profiles. The most widely used GABA$_A$ radiotracer [11C]flumazenil and its analogs are subtype-nonselective, while [11C]Ro15-4513 has a$_5$-preferential binding (1). The objective of this study was to characterize the in vivo binding profile of a new radiotracer, [11C]ADO (Figure 1), which has been indicated to have functional selectivity for the a$_2$/a$_3$ subunits (2, 3).

Methods: [11C]ADO was prepared by ^{11}C-methylation of the 2-pyridinol precursor (Figure 1). PET scans were performed on the Focus-220 scanner in rhesus monkeys. Arterial blood samples were taken for measurement of radioactivity and metabolite analysis to construct the plasma input function. Binding specificity and subtype selectivity of the radiotracer was assessed in blocking scans with the non-selective GABA$_A$ ligand flumazenil, the a$_1$-selective zolpidem, or the a$_5$-selective Ro15-4513. Regions of interest were defined on the MR template and time-activity curves (TACs) generated for 15 regions. Kinetic analysis was carried out with compartmental models to derive regional distribution volume (V_T).

Results: [11C]ADO was prepared in >95% radiochemical purity and high specific activity (24.6 ± 8.0 Ci/μmol, n = 9). [11C]ADO metabolized at a moderate rate, with ~30% parent tracer in plasma at 30 min post-injection. In the brain [11C]ADO displayed good uptake, with highest levels in cortical areas, intermediate in cerebellum and thalamus, and lower uptake in striatal regions (Figure 2). Tissue kinetics were fast, with peak uptake within 20 min of tracer injection in all brain regions. The 1-tissue compartment model provided good fits for regional TACs and reliable estimates of kinetic parameters. Mean V_T values were 11.3, 9.0, 8.5, 8.2, 7.0, 5.3, 4.3, and 3.6 for occipital, cingulate, frontal, and temporal cortices, cerebellum, thalamus, putamen, and caudate (n = 6). Pretreatment with flumazenil (0.2 mg/kg) led to complete blockade of specific binding (98.7%), indicating the binding specificity of the radiotracer. Using a dose of Ro15-4513 (0.03 mg/kg) or zolpidem (1.7 mg/kg) estimated to block 50% of a$_5$ or a$_1$ subunit (1), 53% receptor occupancy was observed for Ro15-4513 (n = 2), and 77% for zolpidem (n = 1) across the brain, with no obvious regional differences.

Conclusions: [11C]ADO is a specific radiotracer for the GABA$_A$ receptor with several favorable properties: high brain uptake, fast tissue kinetics, and high specific binding signals. Despite the subtype selectivity observed in functional assays, there is no obvious subtype binding selectivity for [11C]ADO in the monkey brain.

References:
1. Maeda J et al. *Synapse* 2003; **47**:200; 2. Alhambra C et al. *Bioorg Med Chem* 2011; **19**:2927; 3. Moran MD et al. *Bioorg Med Chem* 2012; **20**:4482.
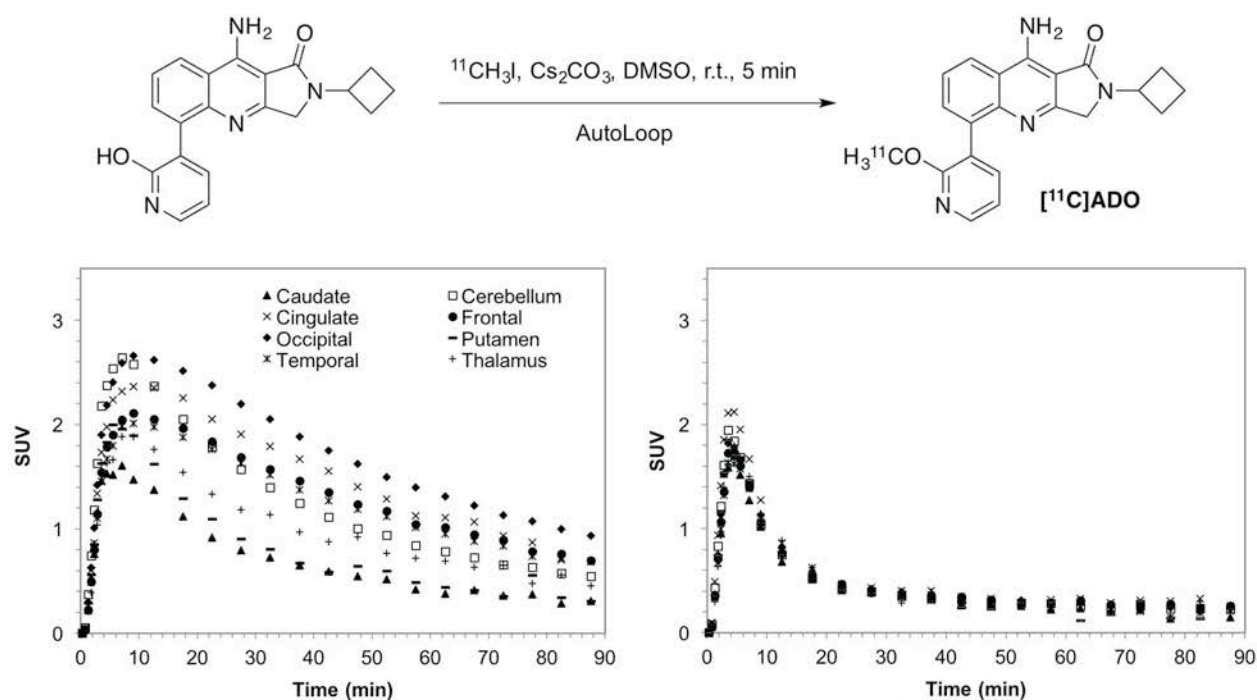
Figure 1. Top: Radiosynthesis of [^{11}C]ADO; Bottom: Regional time-activity curves of [^{11}C]ADO from a baseline scan (left) and a blocking scan (right) with pretreatment of the animal with 0.2 mg/kg of flumazenil.

A regularized full reference tissue model for PET neuroreceptor mapping

Joseph. B. Mandeville[1], Christin Y.M. Sander[1], Hsiao-Ying Wey[1], Jacob M. Hooker[1], Hanne D. Hansen[2], Claus Svarer[2], Gitte M. Knudsen[2], Bruce R. Rosen[1]

[1]*A.A. Martinos Center for Biomedical Imaging, Massachusetts General Hospital, Charlestown, MA, USA,*
[2]*University of Copenhagen*

Objectives: A full reference tissue model (FRTM, [1]) generally is considered to be a better physiological model than the "single-tissue" approximation of the simplified reference tissue model (SRTM), and on this basis, numerous investigations have described biases associated with SRTM (e.g. [2]). We introduce a regularized FRTM (rFRTM) that employs a global estimate of the dissociation rate constant within a basis-function approach, with the goal of providing an alternative to SRTM that reduces parameter bias while simultaneously achieving comparable parameter variance.

Methods: Equation 1 is an exact description of FRTM in a form selected to mimic the basis-function approach to SRTM. Convolution ($\otimes$) of the tissue derivative with an exponential function differentiates SRTM from Eq. 1.

$$C_T = R_1 C_R + k_2 \int \left(C_R - \dot{C}_T \otimes E \right) - k_{2a} \int \left(C_T - \dot{C}_T \otimes E \right) \quad , \quad E(t) = \exp\left(-k_4 \left(1 + BP_{ND} \right) t \right) \qquad (1)$$

Eq. 1 becomes SRTM in the limit that k_4 approaches infinity, but this introduces bias into estimates of binding potential (BP_{ND}) and the reference-region outflow rate constant ($k_2' = k_2/R_1$). Importantly, k_2' is evaluated repeatedly for every region or voxel, which enables a simple optimization strategy: <u>choose k_4 to produce invariance in k_2' across different levels of BP_{ND} from different regions/voxels</u>. The model can be solved using linear methods starting with SRTM to initially estimate BP_{ND} and then iterating by repeated application of Eq. 1 to reach convergence in parameter estimates. Simulated data were generated from first-order differential equations governing FRTM with the addition of noise, and these data were analyzed by SRTM, rFRTM, and two-parameter reductions of these models (SRTM2 and rFRTM2) obtained by fixing k_2' [3]. Simulations in the figure used input parameters appropriate for [11C]raclopride. Maps of BP_{ND} and R_1 obtained in a non-human primate (NHP) were used as the basis for generating simulated data, which were analyzed by each method. Data were obtained in anesthetized NHP for four different radioligands (raclopride, NNC-112, AZ-10419369, and fallypride) and analyzed by rFRTM in order to estimate k_4 values and to observe regional differences in BP_{ND} relative to SRTM.

Results: Using SRTM and SRTM2, simulations suggested bias in BP_{ND} (up to 15%), k_2', and occupancy. rFTRM and rFRTM2 significantly reduced bias without increasing variance. Analyses of simulated occupancy using SRTM and SRTM2 were dominated by false positive results outside the right nucleus accumbens (a). rFRTM2 more accurately identified the localized increase in occupancy. In vivo analysis of NHP data (b) identified the best global k_4 value by removing bias in k_2' versus BP_{ND}. Raclopride and AZ-10419369 exhibited the smallest dissociation time constants (about 10 min) and fallypride the longest (nearly one hour). Relative to SRTM2 and consistent with simulations, maps of BP_{ND} by rFRTM2 for the dopaminergic tracers exhibited smaller values of BP_{ND} in high-binding basal ganglia but higher values in low-binding regions.

Conclusions: Theoretical considerations and simulations suggest that rFRTM reduces parameter bias relative to SRTM without compromising parameter variance. Applications of the model to *in vivo* data demonstrated results consistent with simulations. The main applications of the new model are likely to be functional studies that investigate small changes in occupancy, and *in vivo* estimates of the dissociation rate constant.

References:
[1] Lammertsma et al. 1996. J Cereb Blood Flow Metab 16: 42-52; [2] Salinas et al. 2015. J Cereb Blood Flow Metab 35:304-311; [3] Wu and Carson 2002. J Cereb Blood Flow Metab 22:1440-1452
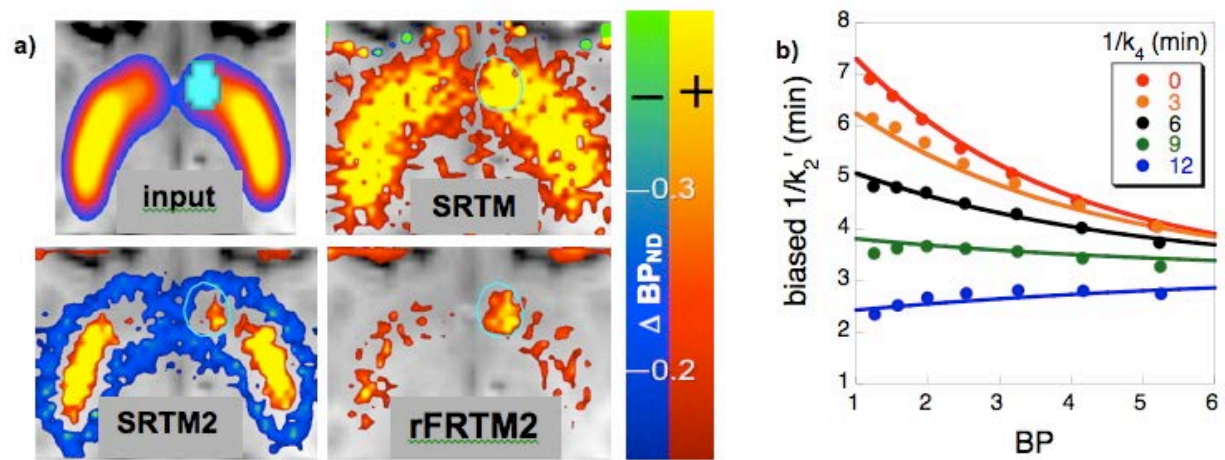
a) Simulations employing an in vivo map of BP_{ND} with a hypothetical 10% change in occupancy in nucleus accumbens (cyan pixels) at 40 minutes were analyzed by SRTM, SRTM2, and rFRTM2. b) Data obtained using [^{11}C]raclopride in anesthetized NHP were analyzed by rFRTM using different values of $1/k_4$ from 0 (red=SRTM) to 12 min (blue) in steps of 3 min; fitting of curves estimated an invariant value of k2' using a global k_4 value of 10.4 min.

Estimation of the binding potential (BP_{ND}) without a reference region or blood samples

Martin Schain[1,2], Francesca Zanderigo[2,3], J John Mann[2,3,4], R. Todd Ogden[2,3,5]

[1]Raymond and Beverly Sackler Postdoctoral Research Fellow in the Laboratory of Image Analysis at the Department of Psychiatry, Columbia University, New York, NY, USA, [2]Division of Molecular Imaging and Neuropathology, Columbia University and New York State Psychiatric Institute, New York, NY, USA, [3]Department of Psychiatry, Columbia University, New York, NY, USA, [4]Department of Radiology, Columbia University, New York, NY, USA, [5]Department of Biostatistics, Columbia University, Mailman School of Public Health, New York, NY, USA

Background: The binding potential (BP_{ND}) is a commonly used outcome measure because it can be estimated without blood sampling. Accurate estimate of BP_{ND}, however, requires identification of at least one brain region that is devoid of the target of interest. For most targets, no such region exists, and quantification instead depends on distribution volume (V_T) for which arterial blood sampling is required. Here, we present and evaluate a new method that allows for accurate calculation of BP_{ND} without requiring either blood samples or a reference region.

Methods: We have previously proposed a method that, by coupling K_1 and k_2 in the 2-tissue compartment model (2TCM) and fitting several brain regions simultaneously, enables estimation of the non-displaceable distribution volume (V_{ND}) without requiring a reference region[1]. This approach however requires an arterial input function (AIF). Theoretically, if the AIF shape but not the amplitude is known (which is typically assumed for population-based input functions, PBIFs), V_T and V_{ND} will display a similar relative bias (here denoted α), which tends to cancel out in the calculation of BP_{ND} (=$\alpha V_T/\alpha V_{ND}$-1).
This method was evaluated using simulations and data from 49 control subjects (five of whom were scanned twice each for test-retest purposes) imaged with the serotonin 1A receptor radioligand [11C]WAY-100635, for which cerebellar white matter is a valid reference region[2]. Simulated data consisted of 5 noiseless time-activity curves (TACs) obtained using an AIF and 2TCM with K_1/k_2 equal to the V_T in cerebellum, to which 1000 instances of realistic simulated noise were added. A PBIF was obtained by normalizing each of 44 subjects' AIF so that its area under curve was equal to one, and averaging normalized curves across subjects. For each noise instance, the simulated TACs were fitted simultaneously using the un-scaled PBIF, (biased) estimates of V_T and V_{ND} (i.e., αV_T and αV_{ND}) were obtained, and regional BP_{ND} was calculated as $\alpha V_T/\alpha V_{ND}$ -1. For the real data (i.e., the [11C]WAY-100635 measurements), regional BP_{ND} was calculated the same way, and compared to BP_{ND} obtained from V_T/V_{ND}-1, where V_T were calculated using an input function and the 2TCM with K_1/k_2 constrained to V_{ND}, which itself was estimated as V_T in the reference region.

Results: For the simulations, regional estimates of BP_{ND} were in very good agreement with the true values, with an average difference of 1.4±8.5% for anterior cingulate cortex, hippocampus, temporal cortex, and occipital cortex, and 13.4±85.6% for thalamus. In the [11C]WAY-100635 data, simultaneously estimated BP_{ND} (without blood samples and reference region) were strongly correlated with values obtained using AIFs and the validated reference region (r^2=0.80) , although they were 17.1±18.1% lower. In the test-retest data, simultaneously estimated BP_{ND} resulted in similar test-retest scores as those obtained using AIFs and the validated reference region (10.7±19.1% and 6.6±18.1% difference, respectively).

Conclusion: For some radioligands, it is possible to estimate BP_{ND} reliably without a reference region or blood samples. We will further evaluate this method using blocking studies with multiple radioligands.

References:
1. Ogden RT, Zanderigo F and Parsey RV. Estimation of in vivo nonspecific binding in positron emission tomography studies without requiring a reference region. *Neuroimage*. 2015; 108: 234-42. 2. Parsey RV, Arango V, Olvet DM, Oquendo MA, Van Heertum RL and John Mann J. Regional heterogeneity of 5-HT1A receptors in human cerebellum as assessed by positron emission tomography. *Journal of cerebral blood flow and metabolism: official journal of the International Society of Cerebral Blood Flow and Metabolism*. 2005; 25: 785-93.
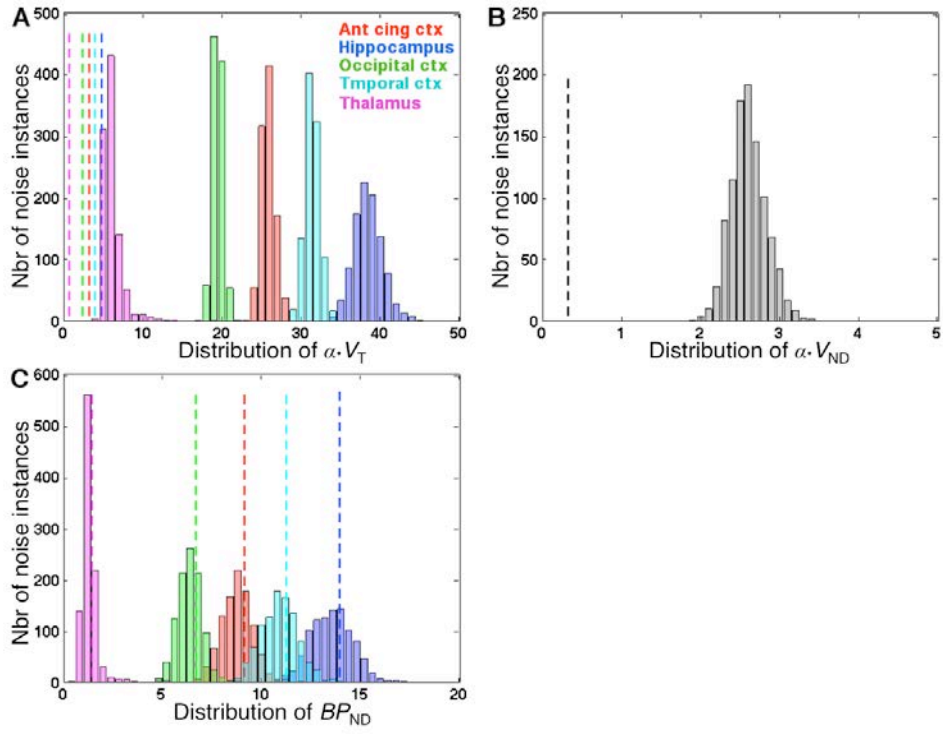
Figure 1. Distributions of $\alpha \cdot V_T$ (**A**), $\alpha \cdot V_{ND}$ (**B**) and BP_{ND} (**C**) obtained from simulated TACs, where α corresponds to the bias introduced by the un-scaled input function. The dashed vertical lines indicate the true value in respective histogram. Since a similar bias is introduced in V_T and V_{ND}, the estimates of BP_{ND} becomes unbiased.

O-009

PET compartmental model selection using sequential Monte Carlo

Yan Zhou[1], John Aston[2], Adam Johnasen[3]

[1]*National University of Singapore*, [2]*University of Cambridge*, [3]*University of Warwick*

Introduction: In almost all tracer kinetic studies, one of the first tasks is to determine the best underlying model for analysis. However, it is common that no one model is entirely suitable. In many cases, one-, two- and even three-tissue compartmental models provide adequate fits according to a chosen measure of goodness-of-fit, such as cross-validation, AIC or BIC.   Turkheimer et al (2003) suggested that in the case where there are common parameters within or derived from the models, such as V_T, then one approach might be to use information from all models, weighted by the model evidence, which gave rise to the notion of Akaike weighted estimates. We follow this line of reasoning but choose to use a computational approach to determine the weights based on a complete description of the underlying parameter distribution from a technique known as Sequential Monte Carlo (SMC).

Methods: SMC (see Doucet and Johansen (2009) for a comprehensive review) is a methodology for determining posterior distributions of quantities of interest, such as V_T. The essential idea is that of a genetic algorithm where parameter values contained in particles are proposed and then mutated and selected such that the particles give a good approximation to the distribution of the parameters. Until recently, these methods would not have been viable for typical PET data due to their computational costs, but recent advances in both parallel technology (using hardware advances such as GPUs) and automated methods have made their use promising even for voxelwise PET analysis (Zhou et al, 2016).
We apply SMC Samplers (Del Moral et al, 2006) to [^{11}C]-Diprenorphine data with associated arterial input function to determine both V_T and model order in a normal control subject. From the SMC output, it is possible to both quantify the empirical distribution of the parameters as well as perform model selection. Using adaptive techniques, a fully automated process can be used, taking advantage of biologically informed prior distributions for the model parameters, yielding full posterior distributions of the model parameters which can then be combined using model averaging or chosen using model selection. The output shown in Figure 1 was determined using 500 particles and 100 intermediate distributions with a fully adaptive and automated choice of tuning parameters (see Zhou et al, 2016).

Results: As can be seen in Figure 1, SMC is able to produce output that looks in many ways similar to that from conventional PET modelling, in that it is able to obtain voxelwise estimates of V_T and other parameters. However, it is also able to produce complete posterior descriptions and use these to determine model selections or obtain model averaging solutions.

Discussion: Full Monte Carlo approaches to PET analysis have not been routinely performed, as a major bottleneck to their usage has been computational limitations. The eminently parallelizable nature of SMC allows parallel computations both within and across voxel computations. This can yield fully Bayesian approaches to model selection and averaging, negating the need to make a-priori model choices for analysis.

References:
Del Moral, P., Doucet, A. and Jasra, A., 2006. Sequential monte carlo samplers. Journal of the Royal Statistical Society: Series B (Statistical Methodology), 68(3), pp.411-436; Doucet, A. and Johansen, A.M., 2009. A tutorial on particle filtering and smoothing: Fifteen years later. Handbook of Nonlinear Filtering, 12(656-704), p.3.; Turkheimer, F.E., Hinz, R. and Cunningham, V.J., 2003. On the Undecidability Among Kinetic Models: From Model Selection to Model Averaging. Journal of Cerebral Blood Flow & Metabolism, 23(4), pp.490-498; Zhou, Y., Johansen, A.M. and Aston, J.A., 2016. Towards automatic model comparison: an adaptive sequential Monte Carlo approach. Journal of Computational and Graphical Statistics, (in press).
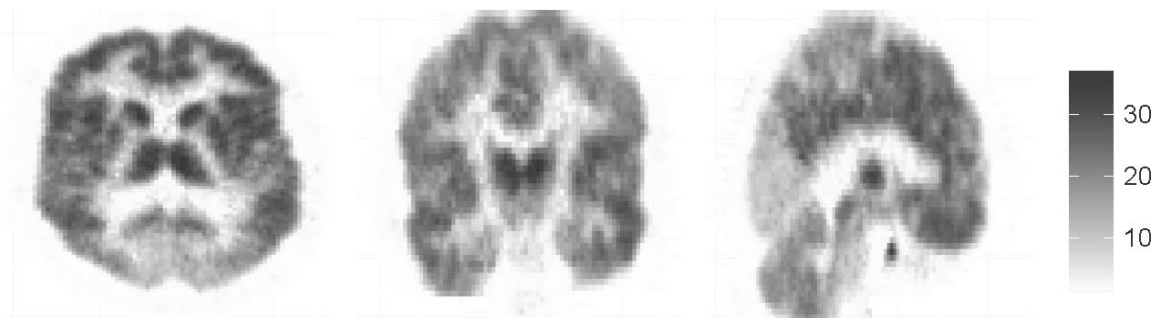
Figure: V_T image from ^{11}C-Diprenorphine produced using Sequential Monte Carlo Samplers with 100 intermediate distribution and 500 particles. The V_T was obtained as the mean of the particle distributions and selected from one-, two- or three-tissue compartmental models as most appropriate at each voxel, using a Bayes Factor model selection choice.

Parametric imaging of brain PET data using a variational Bayesian inference approach

Gaia Rizzo[1], Marco Castellaro[1], Matteo Tonietto[1], Mattia Veronese[2], Federico E. Turkheimer[2], Michael A. Chappell[3], Alessandra Bertoldo[1]

[1]Department of Information Engineering, University of Padova, Italy, [2]Department of Neuroimaging, Institute of Psychiatry, Psychology and Neuroscience, King's College London, UK, [3]Institute of Biomedical Engineering, University of Oxford, Oxford, UK

Introduction: Full quantification at the voxel level of dynamic PET images based on compartmental modeling is a challenging task due to the low signal-to-noise ratio of the voxel activities. Bayesian approaches, which incorporate prior information on the tissue kinetic, have been shown to provide robust estimates also at the voxel level [1-3]. However, these methods are either computationally expensive or they do not have the required flexibility to be generalized to all the most used compartmental models in PET.
In this study, we implemented a Variational Bayesian (VB) estimator for PET parametric mapping. VB is a technique for the statistical inference of the model parameters previously used in magnetic resonance studies [4], which was adapted in this work to the specific noise distribution of PET data [5]. Furthermore, we propose a hierarchical approach to define the parameter priors directly from the images in an Empirical Bayesian scheme.

Methods: VB was tested on 2 different radioligands: L[1-^{11}C]leucine (3 healthy subjects) and [^{11}C]WAY100635 (3 healthy subjects). The priors (mean and variance) were derived from the regional model estimates following a hierarchical approach. Estimates of volume of distribution V_T [mL/cm^3] for [^{11}C]WAY100635 and net trapping rate K_i [mL/cm^3/min] for 1[1-^{11}C]leucine were corrected for failures and outliers (i.e. values with a coefficient of variation > 100% or with less than 5% difference from the priors). VB values were compared with those obtained voxel-wise by using a weighted non-linear least square estimator (WNLLS), considered as reference values. The comparison was carried out in the intersection of voxels where both methods gave reliable estimates. Results were compared in terms of correlation (Pearson's coefficient R^2), slope and intercept of the regression analysis and mean relative difference (MRD).

Results: In both cases VB outperformed the conventional WNLLS, by providing accurate and robust estimates, with a low percentage of outliers. WNLLS had the highest percentage of outliers (34%±20% for 1[1-^{11}C]leucine and 60%±12% for [^{11}C]WAY100635). On the contrary, VB showed a remarkable improvement both in terms of outliers (1%±1% and 8%±9% for the two tracers respectively) and in terms of parametric maps quality (Figure, panels A and B). Since VB solves the compartmental model voxel-wise, it allows the estimation of the model microparameters thus obtaining other parameters of interest, such as the influx rate constant for 1[1-^{11}C]leucine (K_1, mL/cm^3/min) and the nondisplaceable binding potential (BP_{ND}) from the ratio of k_3 over k_4 for [^{11}C]WAY100635 (Figure, panels C and D). Computationally, it was at least 25% faster than WNLLS, completing a single brain analysis in less than 50 min.
In both datasets, VB showed an excellent agreement with the reference WNLLS values (L[1-^{11}C]leucine: R^2=0.98, MRD=3%±6%, m=1.05, q=-0.0001; [^{11}C]WAY100635: R^2=0.93, MRD=5%±12%, m=1.07 and q=-0.03).

Conclusion: VB is applied for the first time to PET data. When applied to real data on a paradigmatic set of PET tracers, VB was able to generate reliable parametric maps in reduced computational time even in presence of high noise in the data. VB is compatible with clinical practice, even when complex compartmental model are employed.

References:
[1] Rizzo et al. (2012) *Neuroimage;* [2] Zanderigo et al. (2010) *Nucl Med Biol;* [3] Zhou et al., (2013) *J Appl Stat;* [4] Chappell et al. (2009) *IEEE Trans Sign Proc;* [5] Mazoyer et al. (1986) *J Comp Ass Tomography*
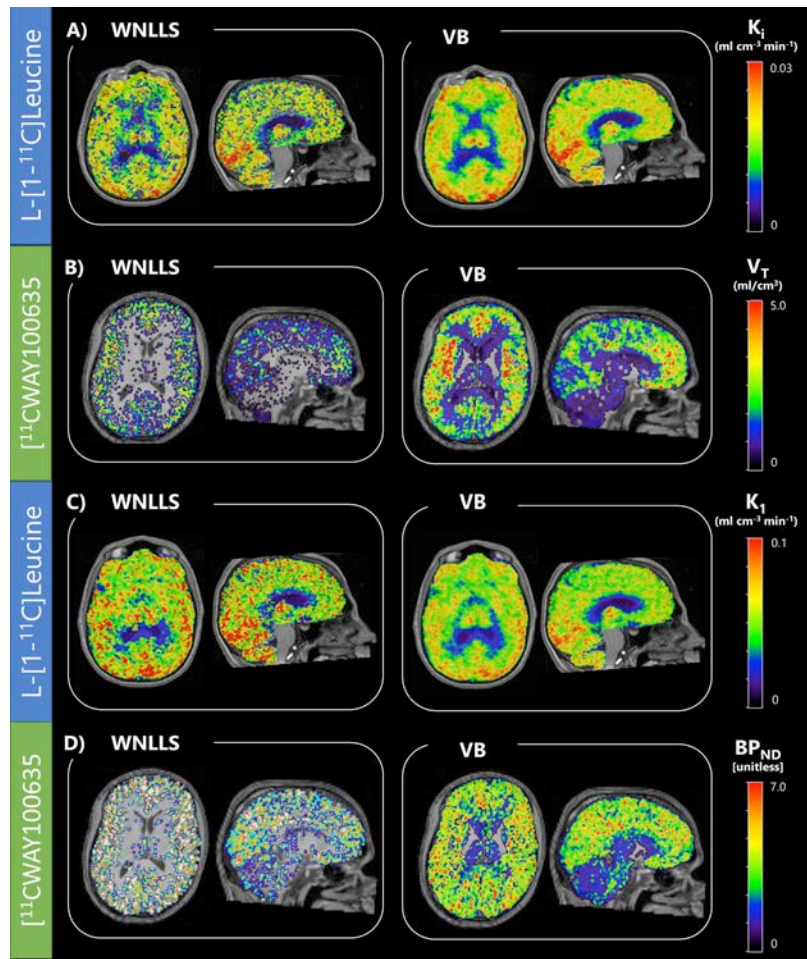
Figure: Parametric maps of K_i and K_1 (A and C, L-[1-^{11}C]Leucine), V_T and BP_{ND} (B and D, [^{11}C]WAY100635) obtained with WNLLS and VB. For each dataset results refer to a transaxial and a sagittal slice for a representative subject. Parametric maps are presented in their raw form without any smoothing.

Reproducibility of volumetric and surface-based smoothing techniques for PET data analysis: A test-retest study with [11C]SCH-23390

Granville J. Matheson[1], Per Stenkrona[1], Pontus Plavén-Sigray[1], Lars Farde[1], Simon Cervenka[1]

[1]Centre for Psychiatry Research, Department of Clinical Neuroscience, Karolinska Institutet, Stockholm, Sweden

Objectives: The use of parametric images in PET research allows for exploratory statistical analysis by comparing each voxel of the brain independently, which is commonly applied in the absence of a strong a-priori regional hypothesis. Due to the inherent imprecision of single voxel measurements, these values are usually spatially smoothed with neighbouring voxels before statistical analysis can be performed. Smoothing has traditionally been applied in three dimensions, irrespective of surrounding tissue types. This procedure may be suitable for subcortical structures, but is potentially problematic for cortical regions for which grey matter often constitutes only a small proportion of the smoothed signal. New methods have been developed for surface-based smoothing in which smoothing is restricted to neighbouring regions along the cortical grey matter, which should theoretically produce more biologically valid results (*1*). In this study, we aimed to measure the reproducibility of parametric receptor binding values obtained after surface-based smoothing in comparison to volumetric smoothing. We contrasted this with a standard ROI-based approach.

Methods: 15 healthy young males were examined using the ECAT Exact HR 47 PET system and the D1-dopamine receptor radioligand [11C]SCH-23390. Each subject was measured twice during one day. Parametric BP_{ND} images were generated using wavelet-aided parametric imaging, applying the non-invasive Logan plot with cerebellar grey matter as reference (*2*). Volumetric normalisation and smoothing of BP_{ND} images was performed using FSL (version 5.0) (*3*), and cortical surface-based normalisation and smoothing was performed using FreeSurfer (www.surfer.nmr.mgh.harvard.edu, version 5.3). Mean absolute percentage variability of BP_{ND} values was calculated as a measure of reproducibility for individual grey-matter voxels and surface vertices using both smoothing methods, as well as for averages of unsmoothed voxels within ROIs. We will also compare these with surface-based smoothing performed on the dynamic PET data prior to kinetic modelling in an ongoing analysis. For the cortical analysis we focused on the frontal cortex in particular, as this region is of relevance for the use of this radioligand in schizophrenia research (*4, 5*).

Results: Volume-based smoothing methods yielded a median voxel-wise variability in the frontal cortex of 31.8%, and BP_{ND} values were decreased from median 0.28 to 0.22 after smoothing. Surface-based methods exhibited less frontal cortex vertex-wise variability (median: 22.3%) and were less negatively biased, from median 0.34 to 0.33 after smoothing. BP_{ND} values obtained by ROI-analysis however showed less variability for subregions of the frontal cortex *(*regional median: 16.8*%)*. Volume-based smoothing in the striatum produced a median voxel variability of 10.5%, which was higher than for the ROI-based analysis (regional median: 7.0%).

Conclusions: These results suggest that traditional volumetric smoothing methods are less suitable for the analysis of PET data in cortical regions than they are for subcortical structures. Surface-based smoothing methods improve cortical BP_{ND} reproducibility and are less biased. In comparison to both parametric approaches, ROI-based methods exhibited better reproducibility. Taken together, these findings imply that surface-based smoothing should be utilised for exploratory parametric analysis of PET data in the cortex, however this approach should be applied only in the absence of an a-priori regional hypothesis.

References:
1. D. N. Greve *et al.*, *Neuroimage* **92**, 225 (2014). 2. Z. Cselényi, H. Olsson, L. Farde, B. Gulyás, *Neuroimage* **17**, 47 (2002). 3. M. Jenkinson, C. F. Beckmann, T. E. J. Behrens, M. W. Woolrich, S. M. Smith, *Neuroimage* **62**, 782 (2012). 4. E. M. Poels, R. R. Girgis, J. L. Thompson, M. Slifstein, A. Abi-Dargham, *Psychopharmacology (Berl).* **228**, 167 (2013). 5. J. Kosaka *et al.*, *Life Sci.* **86**, 814 (2010).

BP_{ND}

Mean Abs
% Dif

O-012
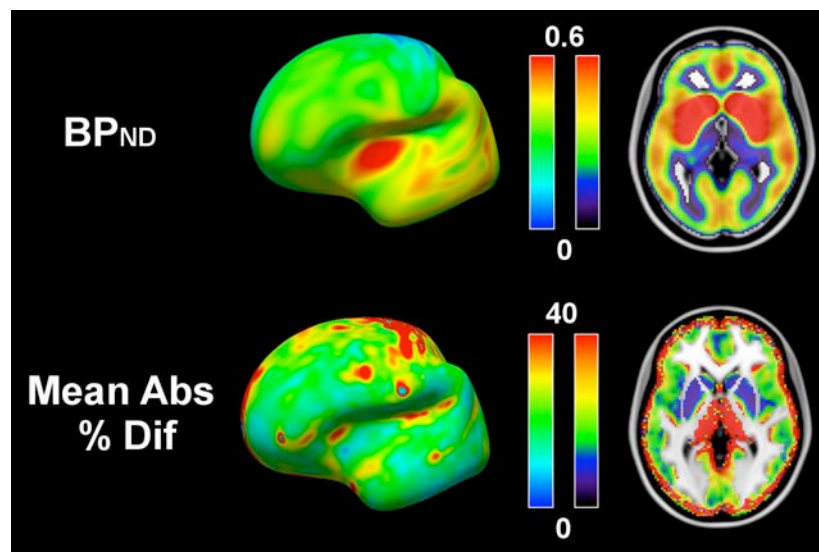
A new method for measuring specific receptor binding of a PET radioligand in human brain without pharmacological blockade

Mattia Veronese[1], Paolo Zanotti-Fregonara[2,3], Gaia Rizzo[4], Alessandra Bertoldo[4], Robert B. Innis[2] and Federico E. Turkheimer[1]

[1]Centre for Neuroimaging Sciences, IoPPN, King's College London, London, UK, [2]Molecular Imaging Branch, National Institute of Mental Health, Bethesda, Maryland, USA, [3]INCIA UMR-CNRS 5287, Université de Bordeaux, Bordeaux, France, [4]Department of Information Engineering, Padova University, Padova, Italy

Introduction: PET radioligands allow in vivo imaging of the distribution and availability of brain receptors. Amongst the criteria for a successful radioligand a high level of specific binding is of prominent importance. The PET signal, however, is the sum of the fraction of radioligand that is specifically bound to the target receptor and the non-displaceable fraction (i.e. the non-specifically bound radioligand plus the free ligand in tissue). Therefore, measuring the non-displaceable fraction, which is generally assumed to be constant across the brain, is a necessary step to obtain regional estimates of the specific fractions.
The nondisplaceable binding can be directly measured if a reference region, i.e. a region devoid of any specific binding, is available. Many receptors are however widely expressed across the brain, and a true reference region rarely available. In these cases, the nonspecific binding can be obtained after competitive pharmacological blockade, which is often contraindicated in humans.

Objectives: In this work we introduce the genomic plot for estimating the nondisplaceable fraction using baseline scans only. The genomic plot is a transformation of the Lassen graphical method in which the brain maps of mRNA transcripts of the target receptor obtained from the Allen Brain Atlas are used as a surrogate measure of the specific binding [3]. Thus, the genomic plot allows the calculation of the specific and nondisplaceable components of radioligand uptake without the need of pharmacological blockade.

Methods: We first assessed the statistical properties of the method with computer simulations. Then we sought ground-truth validation using human PET datasets of seven different neuroreceptor radioligands, where nonspecific fractions were either obtained separately using drug displacement or available from a true reference region. Our datasets included: 1) [11C]WAY100635, targeting the serotonin 5-HT1A receptor [2]; 2) [11C]Ro15-4513 targeting the GABA alpha5 receptor [3]; 3) [11C]LY2795050 targeting the kappa opioid receptor [4]; 4) [18F]FIMX, targeting the metabotropic glutamate receptor 1 [5]; 5) [11C]NOP-1A targeting the nociceptin/orphanin FQ peptide receptor [6]; 6) [11C](R)rolipram, targeting the phosphodiesterase 4 enzyme [7]; 7) [11C]Raclopride, targeting the dopamine D2 receptors [8].

Results: The population nondisplaceable volumes of distribution (V_{ND}) estimated by the genomic plot were very close to those measured by actual human blocking studies (mean relative difference between 2% and 7%). However, these estimates were valid only when mRNA expressions were predictive of protein levels (i.e. there were no significant post-transcriptional changes) (Figure). This condition can be readily established a priori by assessing the correlation between PET and mRNA expression.

Conclusions: The genomic variant of the Lassen plot, or genomic plot, allows the estimation of a PET radioligand nondisplaceable fraction in the absence of reference region and without requiring target-competition studies. The method has general applicability to any neuroreceptor PET tracer, because it relies on mRNA brain maps of the whole human genome. Nevertheless, its precision is dependent on the ability of mRNA expression to predict protein density. Therefore, the consistency between mRNA and PET should be verified a priori.

References:
[1] Lassen, N. *et al.*, Benzodiazepine receptor quantification in vivo in humans using [11C] flumazenil and PET: application of the steady-state principle. JCBFM (1995). [2] Bose, S.K. *et al.*, Presynaptic 5-HT1A is related to 5-HTT receptor density in the human brain. Neuropsychopharmacology (2011). [3] Stokes, P.R. *et al.*, Acute increases in synaptic GABA detectable in the living human brain: A [11 C] Ro15-4513 PET study. Neuroimage (2014). [4] Naganawa, M. *et al.*, Kinetic modeling of 11C-LY2795050, a novel antagonist

radiotracer for PET imaging of the kappa opioid receptor in humans. JCBFM (2014). [5] Zanotti-Fregonara, P. *et al.*, The positron emission tomographic radioligand 18F-FIMX images and quantifies metabotropic glutamate receptor 1 in proportion to the regional density of its gene transcript in human brain. Journal of Nuclear Medicine (2015). [6] Lohith, T.G. *et al.*, Retest imaging of [11 C] NOP-1A binding to nociceptin/orphanin FQ peptide (NOP) receptors in the brain of healthy humans. Neuroimage (2014). [7] Rizzo, G. *et al.*, Voxelwise quantification of [(11)C](R)-rolipram PET data: a comparison between model-based and data-driven methods. JCBFM (2013). [8] Pavese, N. *et al.*, Microglial activation correlates with severity in Huntington disease A clinical and PET study. Neurology (2006).

O-013
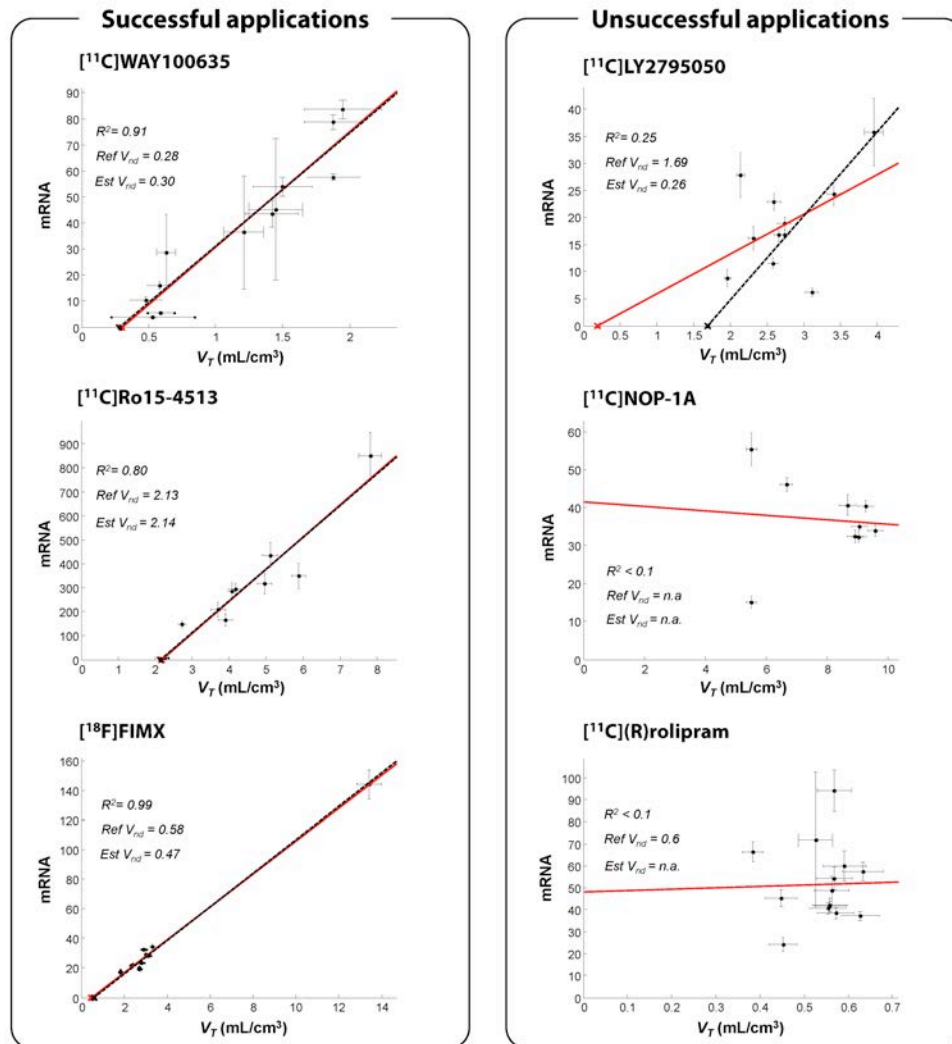
A test-retest study of the same-day variation in estimates of metabotropic glutamate receptor subtype 5 binding measured with [11C]ABP688 and [18F]FPEB

Jean-Dominique Gallezot[1], Christine DeLorenzo[4,5,8], John Gardus[4], Jie Yang[7], Beata Planeta[1], Keun-poong Lim[1], Nabeel Nabulsi[1], R. Todd Ogden[8], David C. Labaree[1], Yiyun Huang[1], J. John Mann[8], Ramin V. Parsey[4,6], Richard E. Carson[1,2], Irina Esterlis[1,3]

[1]Yale University Departments of Radiology and Biomedical Imaging, [2]Biomedical Engineering, and [3]Psychiatry, [4]Stony Brook University Departments of Psychiatry, [5]Biomedical Engineering, [6]Radiology, and Family, [7]Population and Preventive Medicine, [8]Columbia University Department of Psychiatry.

INTRODUCTION: Glutamate is the principal excitatory neurotransmitter in the brain, and the glutamatergic system has been implicated in various neurological or psychiatric disorders. Both [11C]ABP688 and [18F]FPEB have been developed to target the metabotropic glutamate receptor subtype 5 (mGluR5) with PET, to provide quantification of the brain mGluR5 *in vivo* in humans. Both tracers bind to the negative allosteric site on mGluR5. In a previous [11C]ABP688 human test retest study, significant binding increases were observed in the retest scans when both studies were performed on the same day[1]. Conversely, little deviation was reported when scans were >7 days apart for both [11C]ABP688[2] and [18F]FPEB studies[3]. Both previous [11C]ABP688 test-retest studies included only male subjects. The first goal of the present study was to replicate the previous same-day test-retest study in a cohort including females. The second goal was to investigate if the same binding increases could be observed with [18F]FPEB in a same-day test-retest study design.

METHODS: Ten subjects were scanned twice on the same day with [11C]ABP688 (4M, 6F) and 4 (2M, 2F) with [18F]FPEB, using the High-Resolution Research Tomograph (HRRT, Siemens, Knoxville, TN). 631±84 MBq of [11C]ABP688 and 109±52 MBq of [18F]FPEB were injected as a bolus. The two same-day scans were separated by 3.4±0.7 hours and 3.0±0.1 hours for [11C]ABP688 and [18F]FPEB, respectively. A metabolite-corrected arterial input function was measured for all scans. Time-activity curves were computed in 9 regions: anterior cingulate cortex, medial prefrontal cortex, orbitofrontal cortex, ventral striatum, parietal lobe, putamen, caudate, amygdala and hippocampus. The influx rate constant K_1 and the volume of distribution V_T were estimated using the two-tissue compartment (2TC) model for both tracers. For [18F]FPEB, an additional scan of 15-min was performed just before the injection of [18F]FPEB for the retest scan and the 2TC model was extended to account for residual activity from the first injection. The test-retest variability was quantified by computing the percent difference (PD) between test and retest parameter p estimates as

$$100 \times (p_{retest}/p_{test} - 1).$$

RESULTS: For [11C]ABP688, the present study confirmed large within-subject variability in binding. V_T increased in most subjects from scan 1 to scan 2, with little variation across region for a given subject. V_T PD ranged from -7%±2% to 108%±5%. For [18F]FPEB, binding estimates also increased between scans (V_T PD ranged from 5%±5% and 39%±9%). For both tracers, the V_T increase tended to be larger in females than in males, though the gender difference did not reach significance. Additionally, [11C]ABP688 K_1 values were significantly higher during retest scans (test: 0.26±0.17, retest: 0.33±0.15 across all regions and subjects, $p<0.01$) while [18F]FPEB K_1 values were not significantly higher (test: 0.37±0.07, retest: 0.39±0.11 across all regions and subjects, $p=0.26$). For both tracers, plasma clearance significantly increased between scans ($p=0.02$ for [11C]ABP688 and $p=0.01$ for [18F]FPEB).

CONCLUSION: This replication study, and extension to [18F]FPEB, suggests that observed within-day variations in [11C]ABP688 binding are due to characteristics of the mGluR5 receptor or glutamatergic system, and that biological diurnal variations may affect measurement of the mGluR5 receptor.

REFERENCES:
1. DeLorenzo C, Kumar JD, Mann J, Parsey R. *In vivo* variation in metabotropic glutamate receptor subtype 5 binding using positron emission tomography and [11C]ABP688. *Journal of Cerebral Blood Flow & Metabolism.* 2011;31:2169–2180. 2. Burger C, Deschwanden A, Ametamey S, Johayem A, Mancosu B, Wyss M, Hasler G, Buck A. Evaluation of a bolus/infusion protocol for 11C-ABP688, a PET tracer for mGluR5. *Nucl Med Biol.* 2010;37:845-851. 3. Park E, Sullivan J, Planeta B, Gallezot J, Lim K, Lin S, Ropchan J, McCarthy T, Ding Y, EDMorris, Williams W, Huang Y, Carson R. Test-retest reproducibility of the metabotropic glutamate receptor 5 ligand [18F]FPEB with bolus plus constant infusion in human. *European Journal Nuclear Med.* 2015;Epub ahead of print.
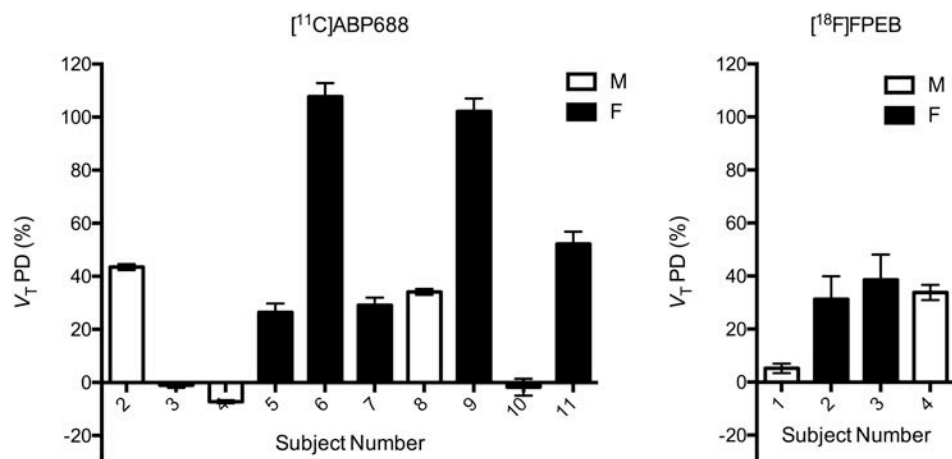
Percent Difference (PD) between test and retest V_T values was computed as $100*(V_T^{retest}/V_T^{test} - 1)$.
For each subject, data is presented as Mean±SD across brain regions.

Validation of reference tissue quantification of [11C]-IMA107 for PDE10A enzyme availability in the human brain

Ayla Mansur[1], Robert Comley[2], Christophe Boetsch[3], Patricia Sanwald-Ducray[3], Roger N Gunn[1,4], Eugenii A. Rabiner[1,5], Graham Searle[1]

[1]Imanova, Centre for Imaging Sciences, London, UK, [2]Roche Pharmaceutical Research and Early Development, Roche Innovation Center Basel, Switzerland, [3]Clinical Pharmacology, Roche Innovation Centre Basel, Switzerland, [4]Division of Brain Sciences, Imperial College, London, UK ,[5]Centre for Neuroimaging Sciences, King's College, London, UK

Introduction: The Phosphodiesterase 10A (PDE10A) enzyme has been proposed to be a useful target for the pharmacological treatment of conditions such as Parkinson's disease and schizophrenia. [11C]-IMA107 was developed as a PET radiotracer to quantify PDE10A availability in the human brain. Previous work demonstrated good test-retest variability of the binding potential derived using a metabolite corrected arterial input function and a two tissue compartmental model (2TCM), with the cerebellum as a reference tissue (BP_{ND}^{2TCM})(Searle et al, NRM 2014). Although post-mortem data indicate that the cerebellum has low PDE10A expression, a formal pharmacological evaluation of its suitability as a reference tissue for the analysis of [11C]-IMA107 data has not been presented. Here, we evaluate the validity of the cerebellum as a reference tissue using competition data with a selective PDE10A inhibitor (RG7203) and compare the binding potential derived from the simplified reference tissue model (SRTM: BP_{ND}^{SRTM}) with that of the 2TCM (BP_{ND}^{2TCM}) for [11C]-IMA107.

Methods: Nine healthy volunteers had a baseline and up to 2 post-dose [11C]-IMA107 PET scans. Fifteen post-dose PET scans were obtained between 3 and 76 hours following single oral administration of various doses of RG7203. Arterial blood was collected during each PET scan, and metabolite corrected arterial plasma input functions were generated. Dynamic PET images were registered to each subject's MRI scan and corrected for motion using frame-to-frame registration with a normalised mutual information cost function. The cerebellum (Cer), dorsal caudate (DCa), dorsal putamen (DPu) and ventral striatum (VStr) were defined as regions of interest (ROI) on volumetric MRI scans collected for each individual. The cerebellum was defined as ventral cerebellum grey matter and used as a reference region for analysis. Total volume of distribution (V_T) was estimated for each ROI using the 2TCM and BP_{ND}^{2TCM} (= (V_T^{Target}- V_T^{Cer})/ V_T^{Cer}). Regional BP_{ND}^{SRTM} was estimated via the SRTM with cerebellum as reference region. Analyses of the PET data were performed using MIAKAT[TM] software (version 4.2.6).

Results: Administration of RG7203 resulted in a dose dependent decrease of striatal V_T to levels similar to the estimated V_{ND}, with no change in cerebellar V_T (Figure 1A - 1B). BP_{ND}^{SRTM} correlated highly with the BP_{ND}^{2TCM}, and SRTM based occupancy estimates were consistent with those derived from the 2TCM (Figure 1C-1D).

Conclusions: These data demonstrate that the cerebellum is a suitable reference tissue for the quantification of PDE10A availability using [11C]-IMA107. The SRTM produces outcome parameters consistent with the "gold standard" 2TCM quantification, and can be used for future [11C]-IMA107 studies evaluating PDE10A availability in the human brain, without the need to collect arterial blood data.
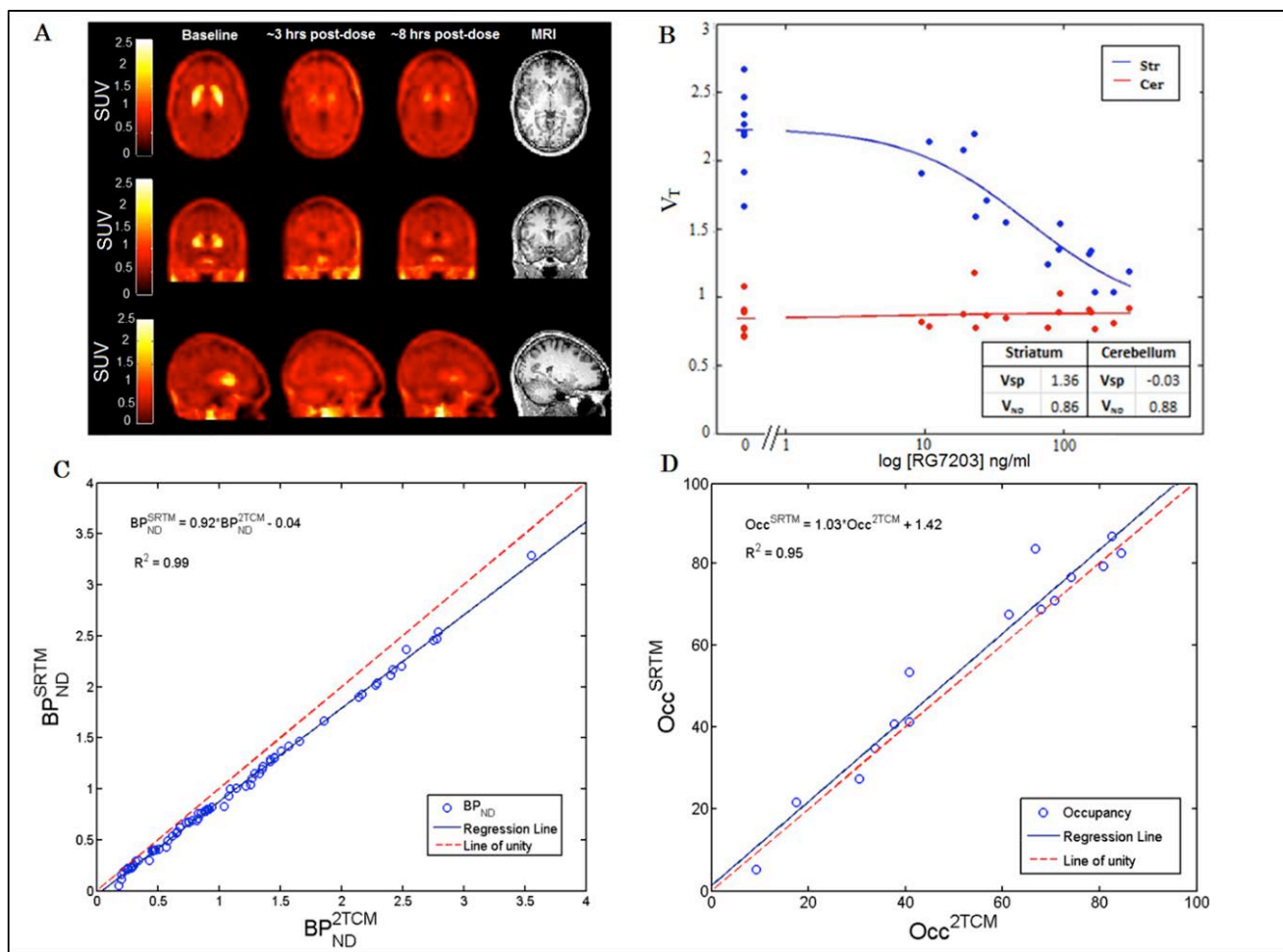
FIGURE 1 A. Corresponding orthogonal cross sections of co-registered PET (SUV:10-90min) and MR (T1) images from a representative subject. From left to right columns, images are PET baseline, PET 2 ~3 hr post-dose, PET 3 ~8 hr post-dose and T1 MRI. **B.** Change in striatal and cerebellar V_T with increasing dose of RG7203 **C.** Binding potential relative to the nondisplaceable component derived from the 2TC and SRTM methods. **D.** Occupancy data derived from the 2TC and SRTM methods.

O-015

Optimal tracer kinetic model for the tau tracer [18F]AV-1451

Sandeep SV Golla[1], Tessa Timmers[1,2], Rik Ossenkoppele[1,2], Colin Groot[1], Sander Verfaillie[2], Philip Scheltens[2], Wiesje van der Flier[2], Patrick Schober[3], Lothar Schwarte[3], Mark Mintun[4], Robert Schuit[1], Albert D Windhorst[1], Adriaan A Lammertsma[1], Ronald Boellaard[1], Bart NM van Berckel[1,2], Maqsood Yaqub[1]

[1]*Department of Radiology & Nuclear Medicine, VU University Medical Center, Amsterdam, Netherlands,*
[2]*Alzheimer Center, Department of Neurology, VU University Medical Center, Amsterdam, Netherlands,*
[3]*Department of Anaesthesiology, VU University Medical Center, Amsterdam, Netherlands,* [4]*Avid Radiopharmaceuticals, Inc., United States*

Introduction: [18F]AV-1451 (formerly known as T807) is a promising ligand for imaging tau deposition. Increased uptake of [18F]AV-1451 in Alzheimer's disease (AD) patients compared with healthy controls (HC) has been shown, with a strong correlation between tracer uptake and cognitive decline. Most studies, however, have used the standardized uptake value ratio (SUVr) derived from a static scan (80-100 min). It is known that this parameter may be flow dependent and, especially for longitudinal studies, it needs to be validated against full kinetic modelling. The objective of this study was to identify the optimal pharmacokinetic model for measuring tau load using [18F]AV-1451.

Methods: Following intravenous injection of 228±8 MBq [18F]AV-1451, 130 min dynamic PET scans were performed in 3 biomarker confirmed AD patients and 3 HC. Combined continuous and manual arterial blood sampling was used to obtain a metabolite corrected plasma input function. PVELAB[1] with the Hammers template[2] was used to delineate regions of interest (ROIs) on a co-registered T1 weighted MRI scan. Next, regional time-activity curves were generated by projecting these ROIs onto the dynamic PET frames. These curves were analyzed using reversible and non-reversible single and two tissue compartment models, both with and without fractional blood volume parameter.

Results: The reversible single tissue compartment model with blood volume parameter (1T2k_V_B) was the preferred model for all HC. For AD patients, however, model preference shifted towards a reversible two tissue compartmental model with blood volume parameter (2T4k_V_B), as shown in Figure 1a. The preference for 2T4k_V_B was more pronounced for regions with high distribution volume ($V_T > 9$ mL·cm^{-3}). In HC, a good correlation ($r^2 = 1.00$, slope = 1.01) was observed between V_T derived from 1T2k_V_B and 2T4k_V_B (Figure 1b). In contrast, for AD subjects an increasing discrepancy ($r^2 = 0.93$, slope = 0.76) between models was observed for increasing V_T (Figure 1c). Figure 1d shows 2T4k_V_B derived V_T for several ROIs. Figure 1d also suggests that cerebellum may be used as a reference region in AD.

Conclusion: This preliminary study suggests that model preference of [18F]AV-1451 may depend on subject status and, in particular, V_T. The relationship between model preference and V_T suggests that (higher) tau load may be reflected by a second tissue compartment. Nevertheless, it seems that consistent results can be obtained using a reversible two tissue compartment model. Further studies are needed to substantiate these findings.

References:
(1) Svarer C, Madsen K, Hasselbalch SG et al. MR-based automatic delineation of volumes of interest in human brain PET images using probability maps. *Neuroimage* 2005;24:969-979. (2) Hammers A, Allom R, Koepp MJ et al. Three-dimensional maximum probability atlas of the human brain, with particular reference to the temporal lobe. *Hum Brain Mapp* 2003;19:224-247.
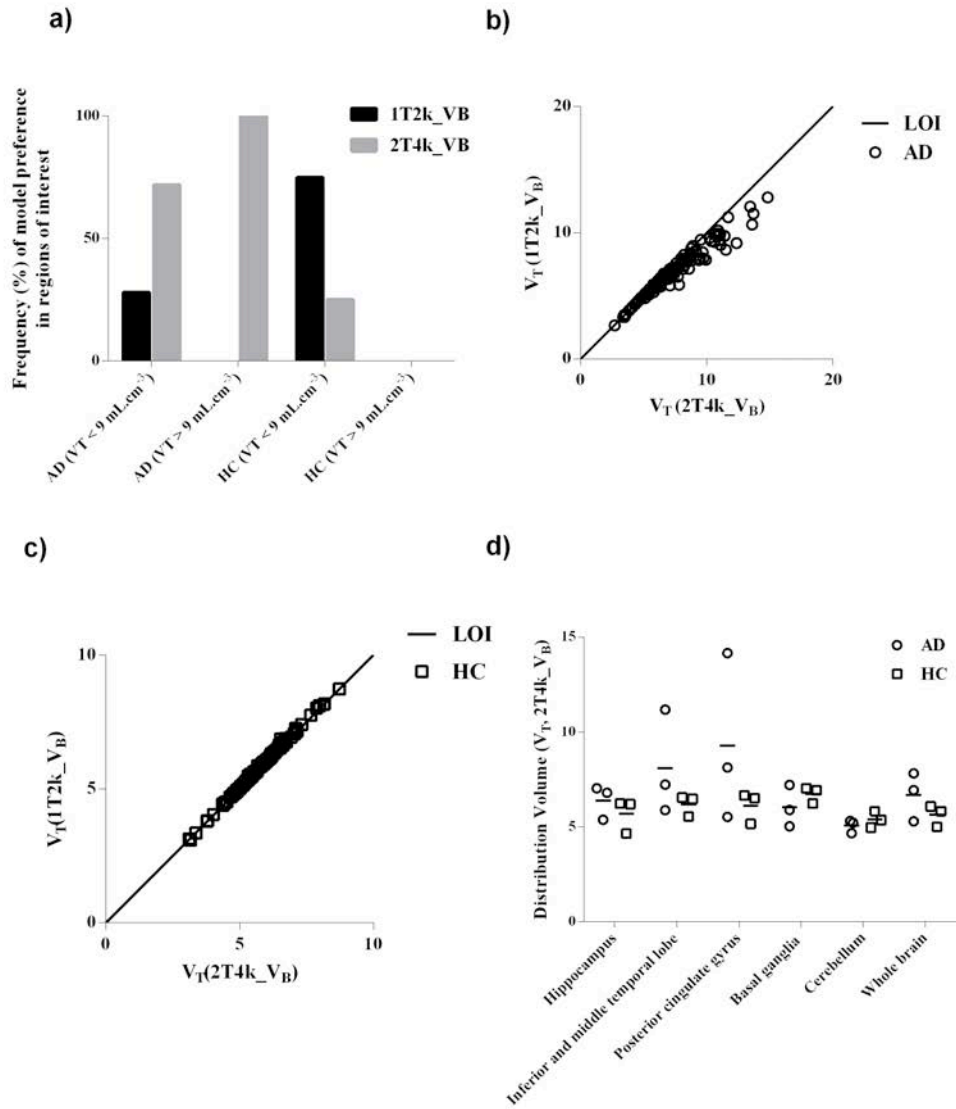
a) Frequency (%) of model preference in regions of interest

b) V_T (1T2k_V$_B$) vs V_T (2T4k_V$_B$), LOI, AD

c) V_T (1T2k_V$_B$) vs V_T (2T4k_V$_B$), LOI, HC

d) Distribution Volume (V_T, 2T4k_V$_B$), AD, HC

Figure 1a) Model preference for ROIs with V_T higher and lower than 9 mL.cm^{-3} in both AD and HC; b) Correlation between 1T2k_V$_B$ and 2T4k_V$_B$ derived V_T in HC; c) Correlation between 1T2k_V$_B$ and 2T4k_V$_B$ derived V_T in AD; d) 2T4k_V$_B$ derived V_T for several (tau specific) ROIs in AD and HC; LOI = line of identity.

O-016

In vivo mapping of the dopamine transporter (DAT) within the nigro-striatal pathway of Parkinson´s disease patients and control subjects using [18F]FE-PE2I and high-resolution positron emission tomography

Patrik Fazio[1], Per Svenningsson[3], Zsolt Cselenyi[1,2], Christer Halldin[1], Lars Farde[1,2] and Andrea Varrone[1].

[1]Karolinska Institutet, Department of Clinical Neuroscience, Centre for Psychiatry Research, Stockholm, Sweden,
[2]AstraZeneca Translational Science Centre at Karolinska Institutet, Stockholm, Sweden,
[3]Karolinska Institutet, Department of Neurology and Clinical Neuroscience, Centre for Molecular Medicine, Stockholm, Sweden.

Background and aims: The DAT is a plasma membrane protein expressed exclusively in nigrostriatal dopaminergic neurons. To date, DAT imaging in humans has been focused mainly on the visualization of the protein in the striatum. DAT is highly enriched in the striatal terminals, but it is also present on the cell body of the dopaminergic neurons in the substantia nigra (1). In addition, immunocytochemistry studies have been able to localize DAT also in dendritic and axonal plasma membranes (2, 3), suggesting that the protein is expressed along the whole nigro-striatal pathway. The objective of the present work was to evaluate *in vivo* with high resolution positron emission tomography (PET), the relative loss of the dopamine transporter (DAT) in the axonal terminals as compared with the cell bodies and the axons, in early stages of Parkinson´s disease (PD).

Method: Sixteen PD patients (13M/3F, 61.5 ± 8.8y, Disease duration 2.88 ± 2.9y; UPDRS-m: 19.06 ± 6.9) and 14 control subjects (CS) (12 M/2F, 60.6 ± 6.8y) underwent PET measurements with the DAT radioligand ^{18}F-FE-PE2I using the HRRT system. High-resolution wavelet-aided parametric images of the binding potential (BP_{ND}) were generated from all the subjects. A DAT template was generated from 10 CS parametric images using a two-steps linear normalization procedure using various tools of the FMRIB Software Library (FSL). The template enabled visualization of DAT binding along distinct pathways. Template-based regions of interest (ROIs) were delineated for the substantia nigra (SN), striatum (STR) and for the nigro-striatal (NST), nigro-pallidal (NPT) and nigro-thalamic (NTT) tracts and then applied to each parametric image to obtain individual BP_{ND} values. Differences between groups were assessed with unpaired t-test ($p<0.05$). Pearson correlation analysis was used to evaluate the relationships between BP_{ND} values in the SN and the striatum with the BP_{ND} values in the different tracts.

Results: BP_{ND} values in PD patients were lower ($p<0.001$) than BP_{ND} values in CS in both STR (1.73 ± 0.7 vs 4.07 ± 0.5) and SN (0.59 ± 0.1 vs 0.83 ± 0.1). No statistically significant difference of BP_{ND} in NST (0.50 ± 0.09 vs. 0.50 ± 0.13) and NTT (0.37 ± 0.12 vs. 0.39 ± 0.11) was observed between PD patients and CS. In the NPT, the difference of BP_{ND} between PD patients and CS (0.32 ± 0.11 vs 0.41 ± 0.13) reached a trend level ($p=0.051$). A strong and significant correlation between BP_{ND} in NPT and in STR was observed in CS ($r=0.888$, $p<0.01$) but not in PD patients ($r=0.279$, n.s.). The correlation between BP_{ND} in NPT and in SN was significant in CS ($r=0.725$, $p<0.01$) and in PD patients ($r=0.544$, $p<0.05$).

Conclusions: High-resolution PET imaging with [18F]FE-PE2I enabled the visualization and quantification of the DAT in the whole nigro-striatal pathway, and for the first time also along the tracts and axons originating from the SN. The findings of this study indicates that at an early stage of PD there is a greater DAT loss in the striatal terminals and a relative preservation of the DAT at level of the cell bodies (SN) and axons, which might be relevant for neuroprotective treatment strategies.

References:
1. Torres GE, Gainetdinov RR, Caron MG. 2003. Plasma membrane monoamine transporters: structure, regulation and functions. Nat Rev Neurosci. Jan;4(1):13-25. 2. Hersch SM, Hong YI, Heilman CJ, Edwards RH, Levey AI. 1997. Subcellular localizationand molecular

topology of the dopamine transporter in the striatum and substantia nigra. J Comp Neurol.;388:211–227. 3. Nirenberg MJ, Vaughan RA, Uhl GR, Kuhar MJ, Pickel VM. 1996. The dopamine transporter is localized to dendritic and axonal plasma membranes of nigrostriatal dopaminergic neurons. J Neurosci. 16:436–447.
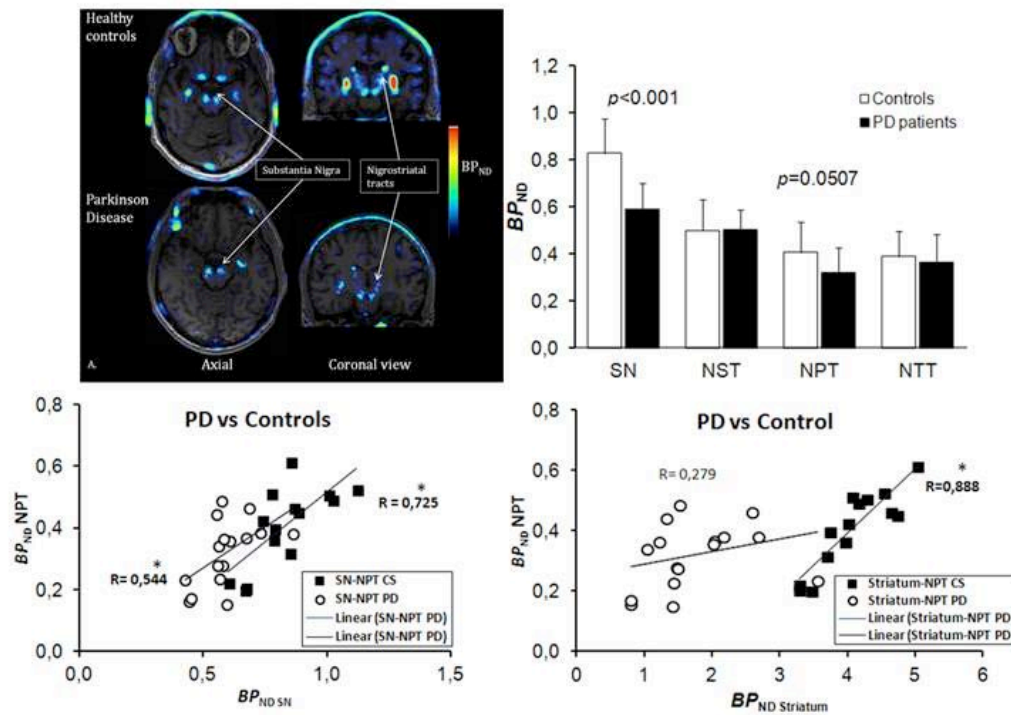
Fig.1 A-B (1-2-3) A. Representative High Resolution DAT PET images in a control subject (upper panel) and in one patient with Parkinson Disease (1.5 Hoehn&Yahr). B1 Summary of the quantification of the regions of interest (SN= Substantia Nigra, NST=Nigrostriatal tract, NPT= NigroPallidal tract, NTT= Nigro thalamic tract). B2-3. Results of the correlation analysis beteween one of the tract (NPT) and the corresponding projecting regions (STR/SN).

High serotonin 1B receptor binding is related to high trait anger and heightened amygdala and striatal reactivity to provocations

Sofi da Cunha-Bang[1,2], Patrick MacDonald Fisher[1], Liv.V.Hjordt[1,2], Erik Perfalk[1,2], Gitte Moos Knudsen[1,2]

[1]*Neurobiology Research Unit, Rigshospitalet, Denmark,* [2]*University of Copenhagen, Denmark.*

Amygdala reactivity to threat-related facial expressions is influenced by serotonin signalling in healthy adults, but in vivo serotonin signalling has never been investigated in the context of provocative stimuli in aggressive individuals. In this study, we evaluated whether brain serotonin 1B receptor ($5\text{-}HT_{1B}$) availability, brain reactivity to provocations and the personality feature trait anger are linked. We used a unique multimodal neuroimaging strategy integrating positron emission tomography (PET) and functional magnetic resonance imaging (fMRI) in 18 male violent offenders and 22 healthy male control subjects. We quantified regional $5\text{-}HT_{1B}$ binding using [^{11}C]AZ10419369 PET (raphe nuclei, amygdala, striatum, anterior cingulate (ACC) and orbitofrontal cortex (OFC)). We measured brain activation following provocations using the point-subtraction aggression paradigm (PSAP) adapted for fMRI. In this task, the participants had the opportunity to pursue monetary rewards or act aggressively, while a fictive opponent regularly stole money with the purpose of provoking participants. Trait anger was measured with the State-Trait Anger Expression Inventory. We used a single latent variable model framework to test for a common association between these three measures. Across all participants, one latent variable (u) was significantly positively associated with $5\text{-}HT_{1B}$ binding (all regions $p < 0.001$, confidence intervals are shown in figure 1), trait anger ($p=0.003$), amygdala ($p=0.039$) and striatal ($p=0.056$) reactivity to provocations (figure 1). Thus, our findings directly support a common underlying construct linking serotonin signalling, aggression-related brain function and trait anger. In other words, high trait anger and heightened amygdala and striatal responsiveness were related to high $5\text{-}HT_{1B}$ binding within the ACC, OFC, raphe nuclei, amygdala and striatum. These novel findings reinforce that serotonin signalling modulates amygdala reactivity, highlighting $5\text{-}HT_{1B}$ as influencing brain responses to provocations in the context of social aggression. Our findings suggest that reducing aggressive and violent behaviours might be achieved through $5\text{-}HT_{1B}$ interventions by reducing heightened neural responsiveness to provocative stimuli.

O-018
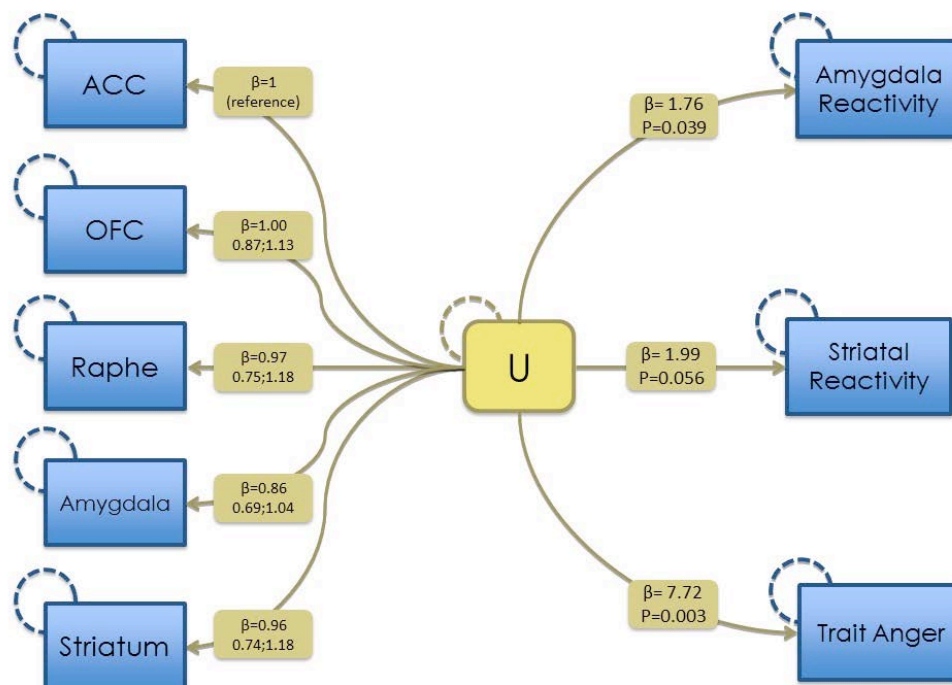
cAMP signaling in brain is decreased in unmedicated depressed patients and increased by treatment with a selective serotonin reuptake inhibitor

Masahiro Fujita[1], Erica M. Richards[1], Sami S. Zoghbi[1], Jinsoo Hong[1], Sanjay Telu[1], Victor W. Pike[1], Carlos A. Zarate Jr[1], and Robert B. Innis[1]

[1]*National Institute of Mental Health*

Background: Basic studies have demonstrated the importance of the cyclic adenosine monophosphate (cAMP) cascade in major depressive disorder (MDD); the cAMP cascade is downregulated in MDD and upregulated by antidepressant treatment. Our previous rodent studies found that PET measurement of ^{11}C-(*R*)-rolipram binding to phosphodiesterase-4 (PDE4)—the primary enzyme in brain that metabolizes cAMP to the inactive monophosphate—reflects in vivo activity of the cAMP cascade. We investigated cAMP cascade activity in MDD by imaging PDE4 using ^{11}C-(*R*)-rolipram in unmedicated MDD patients experiencing a major depressive episode (MDE) and again after approximately eight weeks of treatment with a selective serotonin reuptake inhibitor (SSRI).

Methods: ^{11}C-(*R*)-rolipram PET scans were performed in 44 unmedicated MDE patients (38±11 years, 12F/32M) and 35 healthy controls (36±11 years, 11F/24M). Among the 44 patients, 23 had a follow up ^{11}C-(*R*)-rolipram PET scan after approximately eight weeks of treatment with an SSRI. Patients were moderately depressed (Montgomery-Asberg Depression Rating Scale (MADRS)=30±6) and about half were treatment-naïve. ^{11}C-(*R*)-rolipram binding was measured using arterial sampling to correct for individual differences in metabolism and distribution of the radioligand as well as binding to plasma proteins.

Results: Unmedicated MDE patients showed a widespread, ~20% reduction in ^{11}C-(*R*)-rolipram binding compared to controls (p=0.001). The magnitude of the decrease was similar across brain regions. The decrease was not caused by possibly smaller volumes of gray matter because partial volume correction did not change the results. Unmedicated patients who were cigarette smokers (n=10) showed significantly lower rolipram binding (-23%) than patients who were not smokers (n=34) (P=0.027); however, smoker and non-smoker healthy controls showed almost the same levels of rolipram binding.   SSRI treatment significantly increased rolipram binding (11%, P<0.001) with a significantly greater increase in older patients (P<0.001). A significant age-related decrease in rolipram binding was seen only before treatment and disappeared after treatment (Fig.). Healthy subjects showed almost no age-related decreases. The magnitude of the increase was similar across regions. However, rolipram binding did not correlate with the severity of depressive or anxiety symptoms at baseline, and the increase in rolipram binding during treatment did not correlate with symptom improvement. Age and gender appeared to be confounding factors that may cloud the interpretation of any possible relationship between rolipram binding and symptoms.

Conclusions: Consistent with the cAMP theory of depression, PDE4 was decreased in unmedicated MDE patients and increased after two months of treatment with an SSRI. The lack of correlation between increased PDE4 binding and symptom improvement could reflect the heterogeneity of the disease and/or the target, as PDE4 has four subtypes, only one of which may be involved in antidepressant response. These results suggest that PDE4 inhibitors—which increase activity of the cAMP cascade—may be useful as antidepressants. Improvements over the prototype inhibitor, rolipram, would be necessary; this agent was tried as an antidepressant in the 1980s and failed. However, rolipram is not selective among the four PDE4 subtypes; selectivity to one subtype and allosteric modulating properties that do not cause full blockade would be possible improvements.
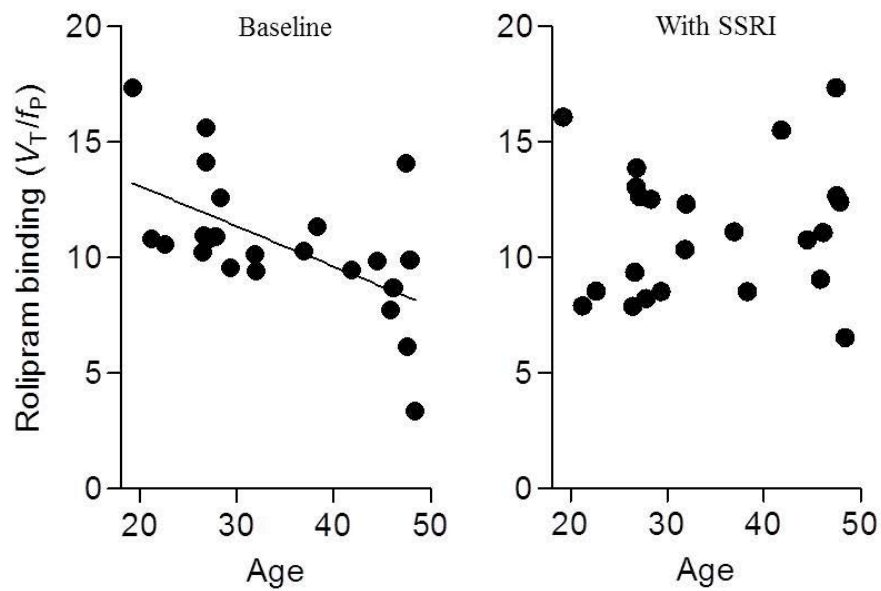
Relationship between age and ^{11}C-(R)-rolipram binding levels before (left) and after (right) starting treatment with a selective serotonin reuptake inhibitor (SSRI). Before starting SSRI treatment, there was significant negative correlation between age and rolipram binding (P=0.001–0.013 across brain areas; left graph). The significant correlation disappeared after patients started SSRI treatment (P>0.39; right). This is because older patients showed significantly greater increases in rolipram binding after treatment. The graphs show data averaged across the 10 large brain regions.

O-019

Comparison in healthy subjects of four PET radioligands to image translocator protein 18 kDa (TSPO)

Robert B. Innis[1], Masahiro Fujita[1], Masato Kobayashi[1], Masamichi Ikawa[1], T.H. Jiang[1], Mohammad B. Haskali[1], Sanjay Telu[1], S. Castellano[2], S. Taliani[3], S.S. Zoghbi[1], Victor W Pike[1]

[1]*Intramural Research Program, National Institute of Mental Health, Bethesda, Maryland, USA,* [2]*Department of Medicine and Surgery, University of Salerno, Italy,* [3]*Department of Pharmacy, University of Pisa, Italy*

Objectives: In 1984, the first PET radioligand to image translocator protein 18 kDa (TSPO)—[^{11}C]PK11195—was reported. Several second-generation radioligands that have been developed more recently are widely thought to have a greater "signal to noise" ratio than [^{11}C](*R*)-PK11195, based largely on blockade studies in monkeys. For example, we found that the BP_{ND} (i.e., the ratio of specific to nondisplaceable uptake) in monkey brain was about 60-fold higher for [^{11}C]PBR28 than for [^{11}C](*R*)-PK11195 (Kreisl et al., *NeuroImage.* 49: 2924, 2010). In the present study, we sought to compare the performance in healthy subjects of [^{11}C](*R*)-PK11195 to three second-generation radioligands: [^{11}C]DPA713, [^{11}C]ER176, and [^{11}C]PBR28 using the TSPO blocking drug XBD173.

Methods: [^{11}C](*R*)-PK11195, [^{11}C]DPA713, and [^{11}C]ER176 were studied in 50 healthy subjects who received either whole body imaging (n=9) or kinetic brain imaging (n=63 scans) combined with arterial blood sampling for compartmental analysis. Results from these radioligands were compared with those published for [^{11}C]PBR28. Specific binding was measured in two ways: within-subject baseline and blocking studies using the TSPO agonist XBD173 (45 or 90 mg PO) or between-subject comparison using the polymorphism plot.

Results:
1) [^{11}C](*R*)-PK11195 showed no sensitivity of brain uptake to the single nucleotide polymorphism (SNP) rs6971; in contrast, all three second-generation radioligands showed marked sensitivity (Table 1). [^{11}C]ER176, an analog of (*R*)-PK11195, was tested in humans because it showed no sensitivity to this polymorphism based on in vitro receptor binding; however, for unknown reasons, [^{11}C]ER176 showed marked sensitivity in vivo, based on whole body imaging of the three genotypes.
2) XBD173 was administered to genetically homogeneous high affinity binders (HABs) and provided reliable estimates of V_{ND} based on the Lassen occupancy plot.
3) The polymorphism plot, which compares uptake in HABs and MABs, gave measurements of variable reliability for the four radioligands, which may have been caused by the variable ratio of binding in HABs to MABs. That is, if HABs and MABs have similar V_T values, the difference between the two is poorly identified.
4) V_T was well identified and stably estimated over time for [^{11}C]DPA713 and [^{11}C]ER176, but not for [^{11}C]PBR28 and [^{11}C](*R*)-PK11195, suggesting that the latter two generate brain-penetrant radiometabolites.
5) The value of BP_{ND} was highest for [^{11}C]DPA713, followed by [^{11}C]ER176, [^{11}C]PBR28, and [^{11}C](*R*)-PK11195 (Table 1).

Table: Performance characteristics of four PET radioligands for TSPO

Radioligand	In vivo genotype sensitivity	Ratio of V_T HAB : MAB	Reliability polymorphism plot	HAB V_T (mL·cm^{-3})	HAB V_{ND} (mL·cm^{-3})	HAB BP_{ND}
[^{11}C]DPA-713	Yes	2.1	excellent	4.2	0.49	7.8
[^{11}C]ER176	Yes	1.2	poor	3.3	0.65	4.2
[^{11}C]PBR28*	Yes	1.5	good	4.3	1.9	1.2
[^{11}C]-*R*-PK11195	No	1.0	impossible	0.76	0.43	0.8

HAB: high-affinity binder; MAB: mixed-affinity binder
*Owen et al. *JCBFM* 34:989, 2014.

Conclusion: This comparative study in healthy subjects suggests that, among these four radioligands, TSPO in brain is most robustly quantified by [^{11}C]DPA713. The study also provided two cautionary notes. First, in vitro and in vivo

sensitivity to the polymorphism rs6971 may differ, as was the case for [^{11}C]ER176. Second, TSPO is now known to exist as a dimer (Li et al., *Science* 347:555, 2015), which means that MABs have three types of TSPO: 25% homo-dimer HAB/HAB, 25% homo-dimer LAB/LAB, and 50% heterodimer HAB/LAB. The variable ratio of binding of MABs to HABs suggests that the heterodimer in MABs (i.e., the HAB/LAB dimer) variably modulates the affinity of these four radioligands.

Correlations between [11C]PBR28 binding to TSPO in brain and blood cells in healthy human subjects

Naoki Kanegawa[1], Karin Collste[1], Anton Forsberg[1], Martin Schain[1], Ryosuke Arakawa[1], Aurelija Jucaite[1], Mats Lekander[2,3], Caroline Olgart Höglund[4,6], Eva Kosek[2], Jon Lampa[5], Christer Halldin[1], Lars Farde[1], Andrea Varrone[1], Simon Cervenka[1,*]

[1]*Department of Clinical Neuroscience, Centre for psychiatry research, Karolinska Institutet,* [2]*Department of Clinical Neuroscience, Osher Center for Integrative Medicine, Karolinska Institutet,* [3]*Stress Research Institute, Stockholm University, Sweden* [4]*Department of Physiology and Pharmacology, Karolinska Institutet,* [5]*Department of Medicine, Rheumatology Unit, Center of Molecular Medicine (CMM), Karolinska Institutet,* [6]*Department of Medicine Solna and CMM, Karolinska Institutet and Karolinska University Hospital Solna, Stockholm, Sweden.*

Objective: The 18-kDa translocator protein (TSPO) is expressed in immune cells in brain as well as in the periphery. *In vitro* binding of the TSPO radioligand [11C]PBR28 in blood cells has previously been shown to correspond to TSPO genotype, and hence also to [11C]PBR28 binding in brain *in vivo* (1). However, thus far there are no published quantitative studies on TSPO binding in peripheral blood cells *in vivo*, and its relationship to TSPO binding in brain has not been explored.

Methods: We examined 32 healthy individuals using positron emission tomography (PET) and [11C]PBR28. In 26 individuals, two measurements were performed. In a subgroup of 19 individuals, of which 12 had repeat examinations, leukocyte numbers in blood was measured on each day of PET measurements. All individuals were genotyped for TSPO polymorphism and categorized as high (HAB), mixed (MAB), and low (LAB) affinity binders. TSPO binding in whole brain expressed as Volume of distribution (V_T) ($V_{T\,Brain}$) was calculated using Logan graphical analysis, with metabolite-corrected arterial plasma as input function. For calculation of V_T in blood cells ($V_{T\,Blood\,cells}$), the radioactivity in each time point was calculated from blood and plasma radioactivity and hematocrit value (HCT) according to the equation:

$$C_{Blood\,cells} = \frac{\left[C_{Blood} - C_{Plasma} \cdot \left(1 - HCT\right) \right]}{HCT}$$

Results: At PET1, the average value of $V_{T\,Brain}$ in MAB was 67 % of that in HAB subjects (p=0.007). Similarly, HAB, MAB and LAB had high, middle and low binding in blood cells, and the average value of $V_{T\,Blood\,cells}$ in MAB was 76 % compared to that in HAB, a difference which was at trend-level significance (p=0.066). For HABs and MABs, $V_{T\,Blood\,cells}$ was strongly and positively correlated to $V_{T\,Brain}$ at baseline (n=31, r=0.85, p=2.1 x 10^{-9} , corrected for genotype) (Fig 1). A correlation was also observed when analyzing change in V_T values in brain and blood between two PET examinations (n = 25, *r* = 0.60, p=0.002). Finally, there was a significant correlation between change of leukocyte numbers and change in $V_{T\,Brain}$, and a trend-level correlation to change in $V_{T\,Blood\,cells}$. When dividing $V_{T\,Brain}$ with $V_{T\,Blood\,cells}$, the intra-individual variability was reduced compared to non-normalized V_T in brain (COV% 40.4 to 23.4 for HABs and MABs combined).

Conclusions: These *in vivo* findings indicate an association between immunological cells in blood and brain *via* intact BBB, suggesting a functional interaction between these two compartments, such as interchange of peripherally derived cells or a common regulatory mechanism. Measurement of radioligand binding in blood cells may be a way to control for peripheral immune function and decrease variability in PET studies using TSPO as a marker of brain immune activation.

References:
Kreisl, W.C., Jenko, K.J., Hines, C.S., Lyoo, C.H., Corona, W., Morse, C.L., Zoghbi, S.S., Hyde, T., Kleinman, J.E., Pike, V.W., McMahon, F.J., Innis, R.B.; Biomarkers Consortium PET Radioligand Project Team. 2013. A genetic polymorphism for translocator protein 18 kDa affects both in vitro and in vivo radioligand binding in human brain to this putative biomarker of neuroinflammation. J. Cereb. Blood Flow Metab. 33 (1), 53-58.
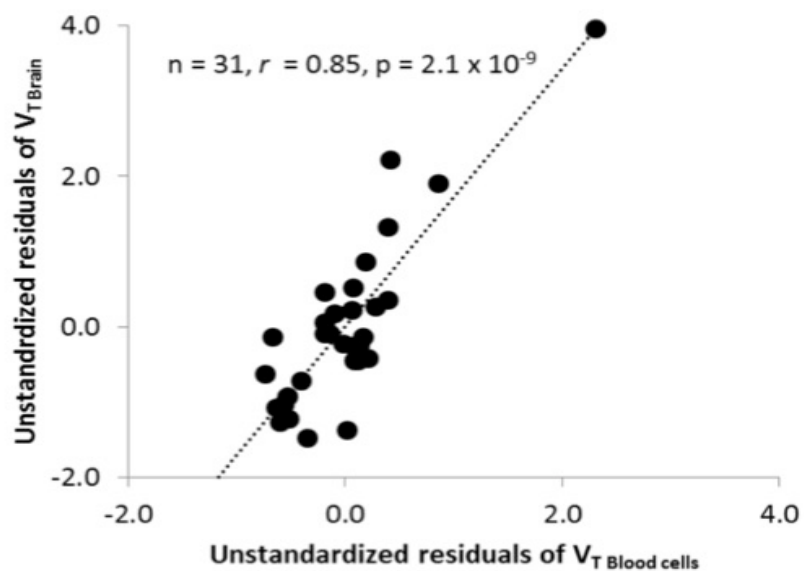
Partial correlation plot of [11C]PBR28 binding in brain ($V_{T\ Brain}$) and blood cells ($V_{T\ Blood\ cells}$) at PET1, showing unstandardised residuals after accounting for genotype

Impact of vascular trapping of ^{18}F-DPA714 on binding parameter estimates in the healthy human

Catriona Wimberley[1], Sonia Lavisse[2,3], Marie-Anne Peyronneau[1], Simon Stute[1], Anthonin Reilhac[4], Vincent Brulon[1], Claude Comtat[1], Claire Leroy[1], Philippe Remy[2,3,5,6], Bruno Stankoff[7,8], Irene Buvat[1], Michel Bottlaender[1,9]

[1]IMIV, Inserm, CEA, Paris-Sud Univ, Orsay, France, [2]MIRCen, CEA, Fontenay-aux-Roses, France, [3]CNRS-UMR9199, Univ Paris-Sud, Fontenay-aux-Roses, France, [4]CERMEP, Lyon, France, [5]Centre Expert Parkins, Neurology Department, CHU Henri Mondor, AP-HP, Créteil, France, [6]Paris-Est University, Créteil, France, [7]Institut du Cerveau et de la Moelle épinière, ICM, Paris, France; Inserm, U 1127, Paris, France and Sorbonne University, UPMC Univ Paris 06, UMR S 1127, Paris, France, [8]CNRS, UMR 7225, F-75013, Paris, France, [9]Neurospin, CEA, Gif-sur-Yvette, France

Introduction: TSPO has been identified as a marker for neuroinflammation that may occur in neurodegenerative diseases. [18F]DPA-714 is one of several second generation TSPO tracers used in PET imaging. Quantification of [18F]DPA-714 faces several challenges including the TSPO expressed on vessel walls and differences in binding affinity between subjects. To perform classical compartmental modelling arterial blood sampling is required. The sampling is not easy to obtain so it would be useful to find a simplified method of quantification. To this end, we should first understand the behaviour of [18F]DPA-714. Based on the Lavisse et al. study[1] we investigated the binding of the ligand to vascular binding sites across the brain using a compartmental model including an irreversible compartment for trapping,[2] the impact on binding parameters if vascular trapping is ignored and further, if it is assumed to be the same anywhere within the brain.

Methods: Eight healthy subjects (5 high affinity binders, HAB; 3 mixed, MAB) underwent [18F]DPA-714 PET on the HRRT scanner with arterial sampling. The scans were reconstructed with AB-EMML[3], PSF modelling and post-smoothing[4]. A 4D iterative deconvolution and spatiotemporal regularisation were used for spatial resolution recovery and noise removal[5]. Two models (2TCM and with vascular compartment, 2TCM-1K[2]) were applied using a metabolite corrected arterial input function for 11 brain regions. To explore the impact of assuming a region-independent vascular trapping, the rate constant for tracer binding to vasculature (kB) was coupled across all regions in the brain and the Vt and BPnd were analysed.
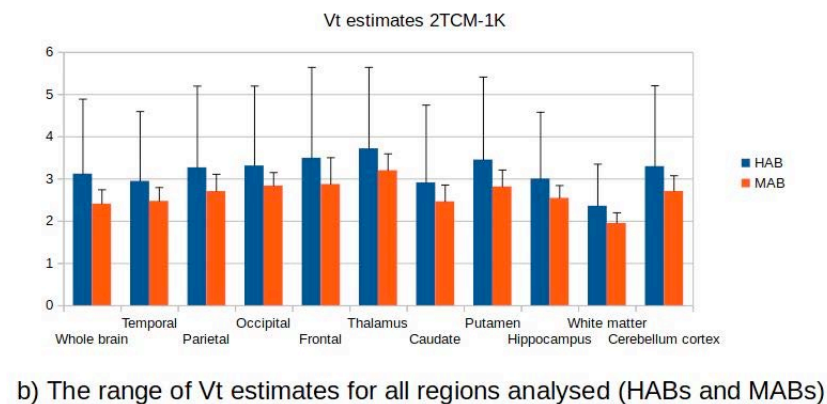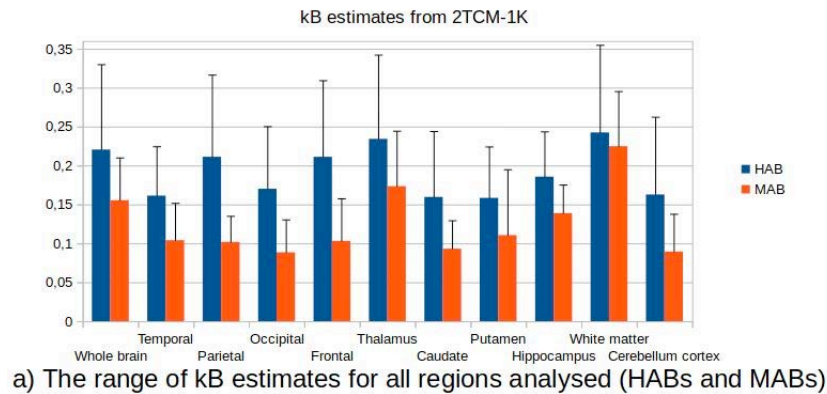
Results: The 2TCM-1K model was a more appropriate model than the 2TCM based on visual assessment and Akaike criterion (AIC lower in 2TCM-1K for all curves). The mean 2TCM-1K regional estimates varied from 2.36 to 3.72 mL/cm3 for Vt, and 1.71 to 2.11 for BPnd in HABs; from 1.94 to 3.20 mL/cm3 for Vt, and 1.02 to 1.25 for BPnd in MABs. The regional Vt and BP values were significantly lower (p<0.01) in the MABs than in the HABs. The Vt values estimated by the 2TCM were on average 57% (HABs) and 27% (MABs) higher than those estimated by the 2TCM-1K.
For 2TCM-1K, the Vt and BPnd estimates with and without coupling kB across all regions were highly correlated (Vt: $r^2>0.98$ and BPnd: $r^2>0.94$) and the average difference was 5.5% (HABs) and 6.4% (MABs) for Vt and 6.85% (HABs) and 4.6% (MABs) for BPnd. The average coupled kB estimated for HABs was 0.19±0.09 and for MABs 0.1±0.05.

Conclusion: This study shows that it is necessary to account for the vascular binding in [18F]DPA-714 by using the 2TCM-1K. However, forcing the vascular trapping parameter to be stationary across the brain does not substantially impact the resulting parameter estimates. This could be because the kB is linked to the blood volume (vB) parameter and therefore the amplitude of the vascular binding curve is moderated by this parameter. These findings should help determine which simplified model to use (eg. SRTMvb as proposed by Tomasi et al.[6]) and how to modify the model if necessary.

References:
(1) Lavisse, S; Garcia-Lorenzo, D; Peyronneau, MA et al.; Optimized Quantification of Translocator Protein Radioligand [18F]DPA-714 Uptake in the Brain of Genotyped Healthy Volunteers; J Nucl Med. (2015), 56(7):1048-54.
(2) Rizzo, G; Veronese, M; Tonietto, M et al.; Kinetic modeling without accounting for the vascular component impairs the quantification of [11C]PBR-28 brain PET data.; JCBFM (2014), 34(6):1060-9
(3) Van Slambrouck, K; Stute, S; Comtat, C et al.; Bias Reduction for Low-Statistics PET: Maximum Likelihood Reconstruction With a Modified Poisson Distribution, IEEE Transactions on Medical Imaging 34 (2015), 126-136.

(4) Stute, S and Comtat, C.; Practical considerations for image-based PSF and blobs reconstruction in PET; Physics in Medicine and Biology 58 (2013), 3849-3870.
(5) Reilhac, A; Charil A; Wimberley, C et al.; 4D PET iterative deconvolution with spatiotemporal regularization for quantitative dynamic PET imaging; Neuroimage (2015), 118:484-93
(6) Tomasi, G; Edison, P; Bertoldo, A et al. Novel Reference Region Model Reveals Increased Microglial and Reduced Vascular Binding of 11C-(R)-PK11195 in Patients with Alzheimer's Disease; J Nucl Med (2008), vol 49 no. 8, 1249-1256

a) The range of kB estimates for all regions analysed (HABs and MABs)

b) The range of Vt estimates for all regions analysed (HABs and MABs)

Evaluating the role of Neuroinflammation in Huntington's Disease using [11C]-PBR28 PET/MRI

C. Lois[1], I. Gonzalez[1], P. Wilkens[2], N.R. Zürcher[1], J. Hooker[1], H.D. Rosas[2]

[1]*A.A. Martinos Center for Biomedical Imaging, Massachusetts General Hospital, Charlestown, MA, USA,*
[2]*Department of Neurology, Massachusetts General Hospital, Boston, MA, USA*

Introduction: Huntington's disease (HD) is a devastating neurodegenerative genetic disease causing progressive motor dysfunction, emotional disturbances, and cognitive impairment. Unfortunately, no treatment can cure or slow down the progression of the disease. Neuroinflammation has been shown to be present since early stages of the disease and is known to be damaging and to promote neurodegeneration. Therefore, it is considered a promising target for therapeutic intervention.

There are many potential treatments targeting inflammatory pathways, however there are no clinical or biological markers that can be used in premanifest or early manifest HD subjects to assess whether the treatments engage their targets and impact neuroinflammation. Because HD is so variable and slowly progressive, such markers would be invaluable for determining which anti-inflammatory treatments merit later phase efficacy studies.

The main goal of this study is to use a novel PET ligand, [11C]PBR28, which binds preferentially to reactive astrocytes and activated microglia, in conjunction with high resolution MRI to assess the regional neuroinflammation in prodromal and early HD.

Methods: Seven patients with early symptomatic HD (F:M 2:5, age 56. ± 8.4) and three healthy controls (F:M 2:1, age 58.7 ± 13.8) participated in our study. Each subject underwent a PET/MR scan in a Siemens Biograph mMR using [11C]-PBR28 as PET tracer (mean injected dose 13.5 ± 1.6 mCi; data acquisition 60-90 min post-tracer injection). Simultaneously, an anatomical MPRAGE was acquired for anatomical localization and generation of attenuation correction maps.

PET data were reconstructed with OP-OSEM 3D and SUV images were calculated and normalized by the whole brain uptake (SUVR) in order to account for differences in global signal across subjects. Regions of interest (ROIs) were defined on the individual MPRAGE images using FreeSurfer automated segmentation. Individualized ROIs were subsequently used to sample PET images and obtain SUVR values in caudate, putamen, pallidum, and thalamus. For each patient, left and right ROIs were merged and analyzed together. Principal component analysis (PCA) was used to obtain a blinded classification of disease of based on imaging, using a few statistical quantities per ROI (average, median, first and third quartile, maximum and minimum values) as features to describe each patient.

Results: We found distinct patterns of [11C]-PBR28 uptake in HD patients compared to controls, observed at the individual level in all HD subjects. We noted increased regional microglial activation in the putamen and the pallidum of HD. Our main finding is that, when quantifying HD progression, the pallidum plays a key role while the caudate only plays a minor one. We conclude that [11C]-PBR28 provides a better signal compared to previous PET tracers targetting neuroinflammation and has the potential to assess HD progression. Our results suggest [11C]-PBR28 might provide the necessary sensitivity and specificity for clinical trials evaluating therapies targeting neuroinflammation.
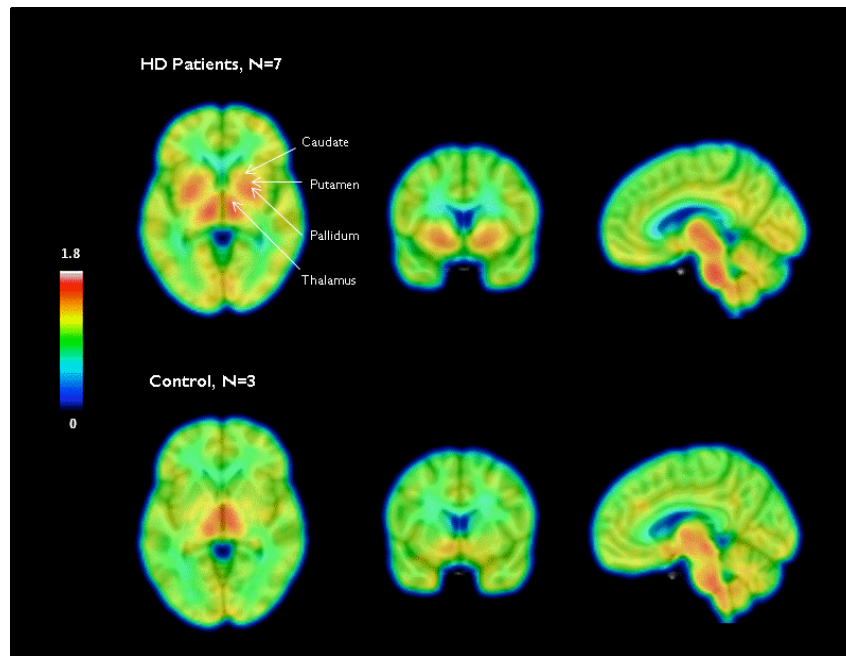
Figure 1: Average [11C]PBR28 uptake for early stage HD patients (top) and controls (bottom). Increased uptake can be observed in the putamen and pallidum of HD patients compared to controls. In addition, all subjects show uptake in other brain regions like the thalamus or brainstem.

Initial evaluation of [18F]GE-180 as an imaging biomarker in natalizumab therapy of multiple sclerosis

Sujata Sridharan[1], Rainer Hinz[1], Hervé Boutin[1], Alexander Gerhard[1], Will Trigg[2], Christopher Buckley[2], David Brooks[3,4], Richard Nicholas[5], Joel Raffel[5]

[1]*Wolfson Molecular Imaging Centre, University of Manchester, United Kingdom,* [2]*GE Healthcare, The Grove Centre, Amersham, United Kingdom,* [3]*Division of Brain Sciences, Imperial College London, Hammersmith Hospital Campus, United Kingdom,* [4]*Institute of Clinical Medicine, Aarhus University, Denmark,* [5]*Faculty of Medicine, Department of Medicine, Imperial College London, United Kingdom*

Introduction: Multiple sclerosis (MS) is an autoimmune disease primarily characterised by demyelination, with grey and white matter neuroinflammation. MRI is the preferred imaging modality for clinical diagnosis, but it has limitations in measuring disease activity, and does not always correlate with clinical disability as measured by the expanded disability status scale (EDSS) [1, 2]. Relapsing-remitting (RRMS) patients can be treated with the monoclonal antibody natalizumab, which blocks passage of inflammatory immune cells through the blood brain barrier. The 18 kDa translocator protein (TSPO) is upregulated in inflammatory disorders and can be targeted by positron emission tomography (PET) radioligands. Using the novel TSPO-PET radioligand [18F]GE-180, we sought to qualify its use in a longitudinal study of RRMS patients receiving natalizumab treatment.

Methods: The first two RRMS patients of our ongoing larger natalizumab study underwent 90-minute dynamic PET scans with [18F]GE-180 (average injected dose, ID, 183.9 ± 3.1 MBq),T_2 and T_1-weighted pre and post-contrast MRI sequences. The patients were then treated with natalizumab, before undergoing follow-up scans 14 weeks later (ID 183.3 ± 0.3 MBq). Baseline/follow-up EDSS scores were 3.0/4.0 for patient 1 and 3.5/3.5 for patient 2. PET images were co-registered to T_1 MR images and an ROI approach to quantification was employed. Metabolite-corrected arterial input functions (AIF) were generated; total volumes of distribution, V_T, were estimated with compartmental modelling from regions of interest (ROIs) including frontal lobe grey matter (GM) remote from MR-defined lesions, thalamus and MS lesions. A simplified approach; standardised uptake values (SUV) were also calculated from 60-90 minute data.

Results: [18F]GE-180 exhibits reversible binding. For plasma input functions with the one tissue compartment model (1TCM), V_T estimates were generally stable with coefficients of variation (COV) low. With the two tissue compartment, four rate constants model (2TCM), COV of V_T exceeded 100%, rendering its V_T unreliable. A gadolinium-enhancing (Gd) lesion in patient 1 had markedly increased [18F]GE-180 signal, with V_T in the lesion more than 400% higher than GM. Non-enhancing lesions had V_T estimates which were similar in magnitude to the thalamus. After three months of treatment, GM, thalamus and non-enhancing lesions V_T were relatively unchanged, while V_T in the lesion decreased by 52%. SUVs of patient 1 at baseline were higher in the lesion than GM and thalamus. Post-treatment, the SUV of the lesion decreased by 28% and non-enhancing lesions decreased by 9%, while other regions remained relatively unchanged. In patient 2, who showed no Gd-enhancing lesions on MRI, baseline V_T in lesions was similar to GM and thalamus V_T. Post-treatment, a decrease in V_T was observed across regions. SUVs were highest in the thalamus at baseline, while post-treatment values again showed a decrease in all regions.

Conclusion: In this preliminary analysis of two patients, a greater reduction of [18F]GE-180 V_T than of SUV was seen in a Gd-enhancing lesion following 3 months of natalizumab treatment, suggesting the potential usefulness of this imaging agent in the early assessment of this therapy. Data from 8 further patients will be analysed prior to the presentation of this abstract, and included in the results.

References:
1.Filippi M*, et al.* Neurology. 1994;44:635-41. 2. Brex PA*, et al.* N Engl J Med. 2002;346:158-64.

	Region	Patient 1			Patient 2		
		T1 Gd-enhancement	1TCM V_T	SUV 60-90 minutes	T1 Gd-enhancement	1TCM V_T	SUV 60-90 minutes
Pre-treatment	GM left	×	0.14 ± 0.02	0.43	×	0.07 ± 0.01	0.50
	GM right	×	0.14 ± 0.02	0.44	×	0.07 ± 0.01	0.53
	Lesions*	×	0.22 ± 0.04	0.47	×	0.10 ± 0.02	0.38
	Thalamus left	×	0.20 ± 0.04	0.53	×	0.08 ± 0.02	0.62
	Thalamus right	×	0.19 ± 0.04	0.52	×	0.09 ± 0.01	0.59
	Gd lesion	✔	0.74 ± 0.43	0.63	-	-	-
Post-treatment	GM left	×	0.15 ± 0.03	0.45	×	0.06 ± 0.01	0.31
	GM right	×	0.16 ± 0.03	0.47	×	0.06 ± 0.01	0.35
	Lesions*	×	0.21 ± 0.08	0.42	×	0.07 ± 0.02	0.24
	Thalamus left	×	0.19 ± 0.04	0.53	×	0.07 ± 0.02	0.39
	Thalamus right	×	0.21 ± 0.06	0.54	×	0.07 ± 0.02	0.39
	Gd lesion	✔	0.36 ± 0.18	0.45	-	-	-
Relative change	GM left	×	+6%	+5%	×	-20%	-38%
	GM right	×	+9%	+7%	×	-15%	-34%
	Lesions*	×	-4%	-9%	×	-34%	-36%
	Thalamus left	×	-3%	0%	×	-20%	-37%
	Thalamus right	×	+14%	+4%	×	-22%	-34%
	Gd lesion	✔	-52%	-28%	-	-	-

* Excluding Gd-enhancing lesion for patient 1

1-(4-[18F]Fluorobenzyl)-4-((tetrahydrofuran-2-yl)methyl)piperazine: a novel radiotracer for the sigma-1 receptors

Yingfang He[1], Fang Xie[1], Winnie Deuther-Conrad[2], Yiyun Huang[3], Jie Lu[1], Qian Yu[4], Jiajun Ye[1], Liang Wang[1], Jörg Steinbach[2], Peter Brust[2], Hongmei Jia[1*]

[1]Key Laboratory of Radiopharmaceuticals (Beijing Normal University), Ministry of Education, College of Chemistry, Beijing Normal University, Beijing, China, [2]Helmholtz-Zentrum Dresden-Rossendorf, Institute of Radiopharmaceutical Cancer Research/Department of Neuroradiopharmaceuticals, Leipzig, Germany, [3]PET Center, Department of Radiology and Biomedical Imaging, Yale University, New Haven, CT, [4]Department of Nuclear Medicine, Xuanwu Hospital, Capital Medical University, Beijing, China

Objectives: The sigma-1 (σ_1) receptors represent a distinct class of intracellular "ligand-operated receptor chaperones".[1] Increasing evidence suggests that the σ_1 receptors are involved in various human diseases including depression, schizophrenia, Alzheimer's disease, and neuroinflammation.[2] Herein we report the design, synthesis and evaluation of 1-(4-[18F]fluorobenzyl)-4-((tetrahydrofuran-2-yl)methyl)piperazine ([18F]**1**) as a potent PET imaging probe for mapping σ_1 receptors in the living brain.

Methods: Among a new series of disubstituted piperazine derivatives with binding selectivity for σ_1 receptors, compound **1** was identified as a candidate for radiolabeling. [18F]**1** was synthesized using a one-pot, two-step radiolabeling procedure (Scheme 1). The biological properties of the radioligand were determined in biodistribution and inhibition studies in ICR mice. Effect of P-glycoprotein (P-gp) on the delivery and binding, as well as the *in vivo* metabolic stability of the ligand were also investigated.

Results: *In vitro* competition binding assays showed that compound **1** exhibited nanomolar affinity for σ_1 receptors ($K_i(\sigma_1)$ = 3.70 ± 0.02 nM) and good subtype selectivity ($K_i(\sigma_2)$ = 213.4 ± 13.4 nM; $K_i(\sigma_2)/K_i(\sigma_1)$ = 58). [18F]**1** was prepared in 20-30% isolated radiochemical yield with radiochemical purity of >95% and specific activity of 54-86 GBq/μmol (n = 3). The log D value of [18F]**1** was determined to be 0.76 ± 0.01. Biodistribution studies in mice revealed very high uptake of [18F]**1** in the brain (%ID/g of 12.8 ± 0.8, 11.2 ± 0.9, 10.6 ± 1.3, 8.3 ± 0.7, 5.4 ± 0.6, respectively, at 2, 15, 30, 60 and 120 min after injection). The brain-to-blood ratios were high (22, 21, 20 and 14, respectively, at 15, 30, 60 and 120 min after injection). Pretreatment with the selective σ_1 ligand SA4503 (5 μmol/kg, iv) at 5 min prior to tracer injection significantly reduced the radiotracer uptake in the brain (by 79%, 88% and 86%, respectively, at 15, 30 and 60 min after injection, $p <$ 0.001) and other organs known to express σ_1 receptors, indicating the binding specificity of [18F]**1** *in vivo*. Administration of the P-gp inhibitor cyclosporine A (50 mg/kg, iv) before tracer injection induced slight increases of activity concentrations both in the blood and brain at 2 min after tracer injection. However, the difference in brain-to-blood ratio between the control and treated groups was small and not significant ($p >$ 0.05), suggesting that [18F]**1** is unlikely a substrate for P-gp. At 30 min after injection, multiple polar radiometabolites were detected in the liver, with 50% intact parent tracer. At the same time point the parent tracer accounted for ~98% of the radioactivity (n = 2) in the mouse brain, indicating no entry of radioactive metabolites into the brain.

Conclusions: These results suggest that [18F]**1** displayed high levels of uptake and specific binding in the mouse brain. Further investigation is warranted to determine the imaging characteristics of this novel radiotracer, and to assess its potential to image the σ_1 receptors in the living brain.

References:
[1] Hayashi, T.; Su, T.-P. *Cell* **2007**, *131*, 596. [2] Maurice, T.; Su, T.-P. *Pharmacol. Ther.* **2009**, *124*, 195.
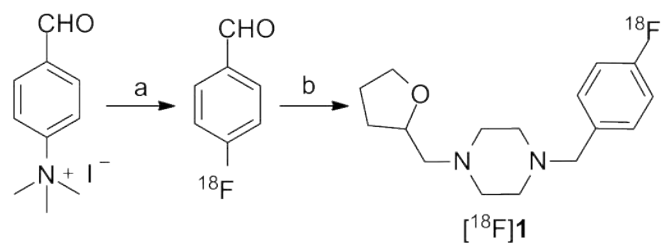
Scheme 1. Synthesis of the radiotracer [^{18}F]**1**. Reagents and conditions: (a) [^{18}F]F$^-$, K$_{2.2.2}$, K$_2$CO$_3$, DMSO, 140 $^\circ$C, 2.5 min; (b) 1-tetrahydrofurfuryl-piperazine, NaBH$_3$CN, CH$_3$COOH, DMSO, 110 $^\circ$C, 10 min.

PET/MR Imaging of morphine-induced mu-opioid receptor desensitization

Hsiao-Ying Wey[1], Jacob M. Hooker[1], Michael Placzek[1,2], Bruce R. Rosen[1], Joseph Mandeville[1]

[1]*A.A. Martinos Center for Biomedical Imaging, Massachusetts General Hospital, Charlestown, MA, USA,* [2]*McLean Hospital, Belmont, MA, USA*

Objectives: μ-Opioid receptor (MOR) agonists are the most effective analgesics for pain. However, the development of opioid tolerance results in less effective pain relief and prompts an increase in the dose needed over time. MOR agonists-induced receptor desensitization is a pivotal mechanism leading to opioid tolerance (1). Recent *in vitro* studies showed that desensitized MORs have an increased affinity for agonist binding (2). Therefore, it is anticipated that MOR agonists-induced desensitization and drug-radiotracer competition result in an increase and a decrease in PET binding potential signal, respectively. The purpose of this study is to measure morphine-induced MOR desensitization *in vivo* using simultaneous PET/MRI.

Methods: PET/MRI images were acquired from two macaques (male, ~12 kg) using a 3T Siemens BrainPET and an 8-channel coil. Animals were anesthetized with isoflurane and ventilated. PET/MR images were acquired from each animal using a μ-opioid selective radiotracers, [11C]carfentanil (~8 mCi; specific activity: ~3 mCi/nmol), given as a bolus-infusion. PET data were stored in list mode and binned into 1-min frames. CBV-fMRI data were obtained following an iron oxide (Feraheme, 10 ug/kg, i.v.) injection (3). Graded doses of an MOR agonist, morphine (baseline, 0.2, 0.5, and 1.0 mg/kg) were given intravenously at 35 min post radiotracer administration. PET data was analyzed for binding potentials referenced to a non-displaceable compartment (BP_{ND}) using the simplified reference tissue model (4). A gamma-variant function was used to model the PET and fMRI temporal response to drug challenge. Changes in fMRI signal were converted to CBV changes (3).

Results: Baseline TACs show that PET signal reached a steady-state with bolus/infusion of [11C]carfentanil (Fig 1a). TACs of the reference tissue are comparable between baseline and morphine scans. Apparent increases in TACs in high-binding regions following morphine injection (Fig 1a) was observed, suggesting a potential increase in receptor affinity. The largest BP_{ND} increases were observed in the thalamus, basal ganglia, amygdala, and the brainstem (Fig 1b). Percent increases in BP_{ND} (defined as $(BP_{ND,drug} - BP_{ND,baseline})/BP_{ND,baseline} \times 100\%$) is about 26% at 0.2 mg/kg, 41% at 0.5 mg/kg, and 49% at 1.0 mg/kg. We observed negative morphine-induced CBV changes as expected (-3.1% at 0.2 mg/kg, -1.5% at 0.5 mg/kg, and -1.1% at 1.0 mg/kg) because MOR is inhibitory. Dose-dependent changes in BP_{ND} and CBV were found between 0.2 mg/kg and 0.5 mg/kg of morphine, but a dose of 0.5 mg/kg and 1.0 mg/kg caused similar BP_{ND} and CBV responses.

Discussion and Conclusions: In this study, we demonstrated an increase in PET BP_{ND}, which potentially reflects morphine-induced MOR desensitization. An increased in PET BP_{ND} following MOR agonist challenges cannot be attributed to drug-radiotracer competition. In addition, morphine is known to be deficient to internalize MORs. Because [11C]carfentanil is an agonist radiotracer, it is possible to detect a change in affinity. With the help of simultaneously collected fMRI data, it is possible to quantify the amount of morphine-induced MOR desensitization *in vivo*. Additional experiments are ongoing to complete the dose-response study that will allow us to fit a PET/MRI model to quantitatively differentiate competition vs. desensitization.

References:
(1) Williams JT, et al. Pharmacological Reviews. 2013. (2) Birdsong WT, et al. J Neurosci. 2013. (3) Mandeville JB. NeuroImage. 2012. (4) Lammertsma AA, et al. NeuroImage. 1996.
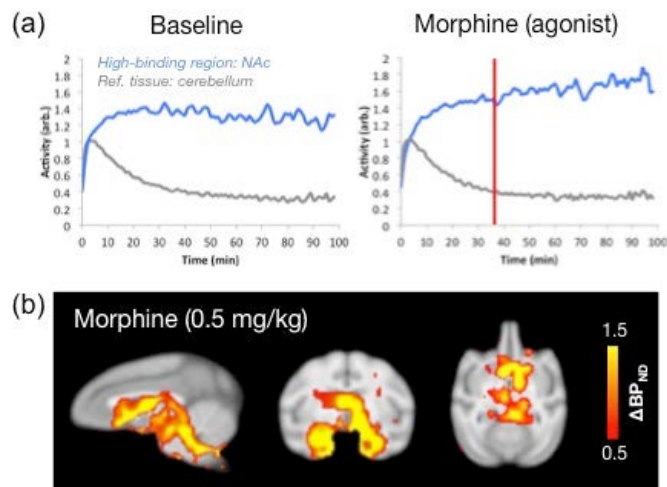
Figure 1. (a) Example time-activity curves (TACs) from a baseline and a morphine challenge scan from the same animal (TACs were normalized to the peak activity of the reference tissue). Red line indicates when morphine (0.5 mg/kg) was given intravenously. (b) Increases in BP_{ND} ($BP_{ND,drug}$-$BP_{ND,baseline}$) were found in thalamus, caudate, putamen, hypothalamus, amygdala, and the brainstem.

Simultaneous acquisition of GABA$_A$ receptor binding potential by [^{18}F]Flumazenil-PET and GABA by magnetic resonance spectroscopy

Lawrence K Fung[1], Meng Gu[2], Christoph Leuze[2], Trine Hjoernevik[2,3], Bin Shen[2], Jun-Hyung Park[2], Samantha Levine[2], Dawn Holley[2], Jae Ho Jung[5], Byung Chul Lee[4], Sang Eun Kim[4], Mehdi Khaligi[6], Praveen Gulaka[2], Greg Zaharchuk[2], Jennifer McNab[2], Andrew Quon[2], Daniel Spielman[2], Frederick T Chin[2]

[1]Psychiatry & Behavioral Sciences and [2]Radiology, Stanford University, Stanford, California, USA, [3]The Intervention Centre, Oslo University Hospital & Norwegian Medical Cyclotron Centre, Oslo, Norway, [4]Seoul National University Bundang Hospital, Seoul, Korea, [5]BioImaging Korea, Seoul, Korea, [6]GE Healthcare

Introduction: The major inhibitory system in the brain, the GABAergic system, is hypothesized to be abnormal in various neurodevelopmental disorders. Few studies have explored the GABA$_A$ receptor distribution by positron emission tomography (PET) or GABA levels by magnetic resonance spectroscopy (MRS) in neurodevelopmental disorders. Simultaneous acquisition of both PET and MRS data has not been possible until recently.

Objectives: This pilot study aims at demonstrating the feasibility of simultaneous acquisition of GABA$_A$ receptor binding potentials by PET (with [^{18}F]Flumazenil ([^{18}F]FMZ) as radiotracer) and GABA levels by MRS in normal human volunteers.

Methods: _Participants._ Healthy volunteers aged 18-45 consented according to the local IRB. _Image acquisition._ Subjects were scanned on GE SIGNA PET/MR (Waukesha, WI). PET data were acquired in list mode (0-30min; 50-65min p.i), dynamically reconstructed into 18 time-frames (4×15s, 2×30s, 3×1min, 2×2.5min, 4×5min; 3×5min) and corrected for photon attenuation using both scanner-specific 32-channel headcoil correction and a MR-measured head atlas-based attenuation correction maps. During PET data acquisition, a series of MR structural sequences were acquired, including (a) T1-weighted MP-RAGE sequence, (b) T2-weighted fast-spin-echo sequence. For the MRS measurement of GABA, MEGA-PRESS was performed on the left dorsolateral prefrontal cortex with a voxel size of 22cc and TE/TR=68/2000ms, 4.4min acquisition time.[1] _Image and data analysis_. The dynamic PET and structural MR data were normalized to MNI (Montreal Neurological Institute) space (PMOD 3.7, Switzerland). Time-activity curves were extracted using pre-defined volumes-of-interest (VOIs) based on the Hammers atlas[2]. A reference tissue model (Ichise model; MRTM0) was used to calculate binding potentials (BP$_{ND}$) with pons as the reference region[3]. Mean values between the two subjects for each VOIs were calculated. The MEGA-PRESS edited spectrum was obtained by subtracting the editing OFF spectrum from the editing ON spectrum. GABA level was estimated from the integrated 3ppm peak area in the edited spectrum divided by the Cre peak area.

Results: We have successfully acquired [^{18}F]FMZ-PET, MRS, and structural MRI data concurrently with a simultaneous PET/MR imaging system in two healthy male volunteers (both age 31). The Figure (a, b and c) shows selected axial PET, MR, and fused PET/MR brain images of one healthy volunteer. Highest uptake was observed in the neocortical regions (mean BP$_{ND}$ 4.0) and limbic system (BP$_{ND}$ 3.6), intermediate in the cerebellum (BP$_{ND}$ 2.6), thalamus (BP$_{ND}$ 1.8), and basal ganglia (BP$_{ND}$ 1.8), and low uptake in the brainstem (BP$_{ND}$ 0.2). The MEGA-PRESS edited spectrum is shown in Fig. (f), with the GABA+ peak at 3 ppm (J-coupled to GABA spins at 1.9ppm and coedited macromolecules) and combined glutamate+glutamine (Glx) peaks at 3.75ppm clearly observed. The estimated GABA/Cre ratio is 9.7%, in agreement with the level measured using MEGA-PRESS on healthy human subjects. The _in vivo_ data shown in Fig. (e) and (f), demonstrate that the GABA signal is readily detected on our 3.0T PET/MR scanner.

Conclusions: We have successfully acquired [^{18}F]FMZ-PET and MR data concurrently with our PET/MR imaging system in two healthy volunteers. We will proceed with implementing this protocol in patient populations with neurodevelopmental disorders in the near future.

References:
1. Mullins PG, McGonigle DJ, O'Gorman RL, Puts NA, Vidyasagar R, Evans CJ, Cardiff Symposium on MRSoG, Edden RA. Current practice in the use of MEGA-PRESS spectroscopy for the detection of GABA. _Neuroimage._ 2014;86:43-52; 2. Hammers A, Allom R, Koepp MJ, Free SL, Myers R, Lemieux L, Mitchell TN, Brooks DJ, Duncan JS. Three-dimensional maximum probability atlas of the human brain, with particular reference to the temporal lobe. _Hum Brain Mapp._ 2003;19(4):224-247; 3. Odano I, Halldin C, Karlsson P,

Varrone A, Airaksinen AJ, Krasikova RN, Farde L. [18F]flumazenil binding to central benzodiazepine receptor studies by PET--quantitative analysis and comparisons with [11C]flumazenil. *Neuroimage.* 2009;45(3):891-902.
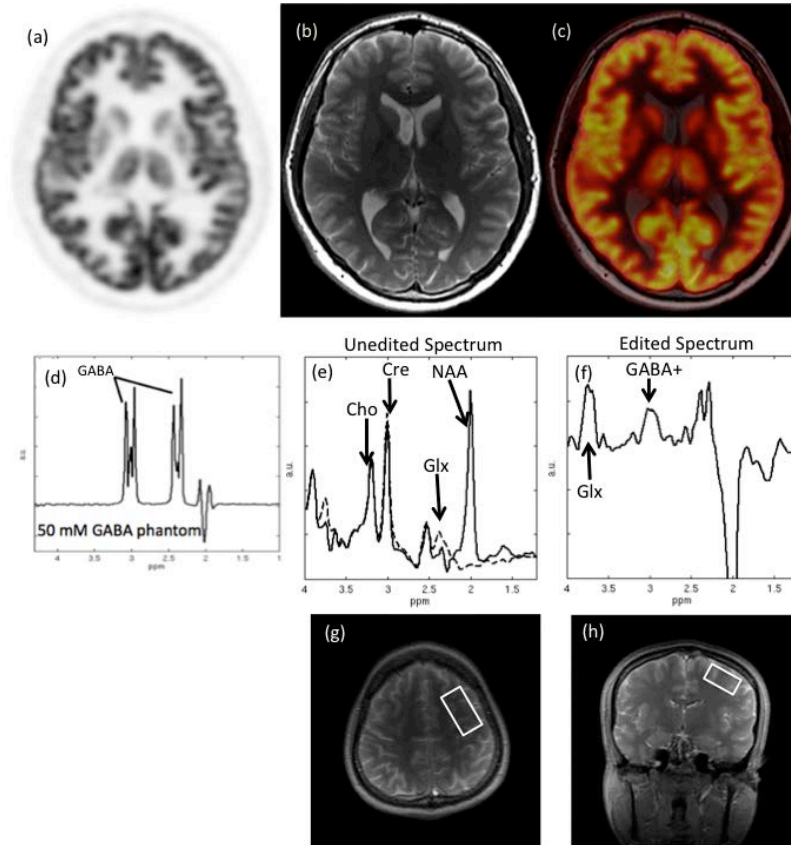
Figure: Selected transverse PET (a), MR (b), and fused (c) PET/MR images of a 31-year-old male healthy volunteer. PET data were reconstructed with attenuation correction. GABA-edited spectra from (d) 50 mM GABA phantom and (e,f) *in vivo* 20 cc (1.5cm°—3.6cm°—4.3cm) voxel at the dorsolateral prefrontal cortex (DLPFC). Oblique axial (g) and coronal (h) images showing the DLPFC voxel size and location.

Simultaneous PET and fMRI during deep brain stimulation of the ventral tegmental area

Christin Sander[1], John Arsenault[1,2], Hsiao-Ying Wey[1], Jacob Hooker[1], Joseph B. Mandeville[1], Wim Vanduffel[1,2], Bruce Rosen[1]

[1]A.A. Martinos Center for Biomedical Imaging, Massachusetts General Hospital, Charlestown, MA, USA,
[2]Laboratory of Neuro- and Psychophysiology, Medical School, Katholieke Universiteit, Leuven, Belgium

Introduction: Deep brain stimulation (DBS) through chronically implantable neurostimulation electrodes is used clinically as a symptomatic therapy in movement disorders, and has been shown to affect reinforcement learning and motivation[1]. Despite its success, the neurophysiological mechanisms underlying the efficacy of DBS remain a subject of debate. The goal of this study was to perform DBS during PET/fMRI in order to shed light on the dynamics of dopaminergic, metabolic and functional signature with the ventral tegmental area (VTA) as a stimulation target.

Methods: A microstimulation DBS electrode (consisting of 23 microwires) was implanted unilaterally in the right VTA of a baboon. Following recovery from surgery, the animal underwent 12 anesthetized imaging sessions with simultaneous PET/fMRI during electrode stimulation (200 ms pulses, 100 Hz, applied every 8, 16 or 30 s for 0.95 min at 2 microelectrodes). This stimulation period was interleaved with 0.85 or 1.7 min of rest and repeated for a total of 10-30 min. The radiotracer [^{11}C]raclopride was administered as a bolus+infusion to detect within-scan signal changes due to stimulation, and one session employed continuous infusion of [^{18}F]FDG, or fPET[3]. [^{11}C]raclopride TACs were analyzed with the SRTM[2], with a dynamic binding parameter[4]. Iron oxide was administered and fMRI data were converted to cerebral blood volume (CBV) for quantification. Data from multiple imaging sessions were analyzed using a mixed effects model.

Results: fMRI results showed a robust activation in the VTA (see figure, left), nucleus accumbens and caudate on the side of the implant (right), both in single and group analyses. Alterations in stimulation patterns affected CBV magnitude, with 16 s stimulation trains showing the largest CBV signal change at 5.4%. With [^{11}C]raclopride, up to 15% changes from baseline BP_{ND} were observed in single sessions in subregions of the striatum but no significant effects were observed in the group analysis. A representative TAC (top right) shows only small differences between the right (implanted side) and left caudate during 3x10min stimulation blocks (gray areas). With [^{18}F]FDG infusion, a significant change was observed in the right VTA, consistent with stimulation in this area. The corresponding TAC (bottom right) and model fit shows increased uptake in the VTA area, but not in caudate.

Discussion: This study shows the feasibility for doing concurrent deep brain microstimulation with combined PET and fMRI acquisitions. Significant CBV signal changes occur in regions consistent with dopaminergic projections from the VTA, but PET signal changes due to stimulation did not reach significance. Although a single stimulation could increase dopamine levels by several times its baseline levels[5], we did not observe a robust signal change with [^{11}C]raclopride. This result may reflect the limited temporal resolution of PET in relation to small and intermittent changes in dopamine. Interestingly, [^{18}F]FDG showed small but detectable changes in the VTA due to stimulation, suggesting a spatial mismatch between fMRI and metabolic activity. More extensive exploration of DBS parameters, together with augmenting raclopride displacement by pharmacologically blocking dopamine reuptake, can clarify the molecular underpinnings of VTA stimulation and its relationship to fMRI in this paradigm.

References:
[1] Arsenault et al., *Current Biology,* 2014. [2] Lammertsma et al. *NeuroImage* 1996. [3] Villien et al. *NeuroImage* 2014. [4] Sander et al., *Neuropsychopharmacology* 2015. [5] Schluter et al. *PLOS ONE* 2014.
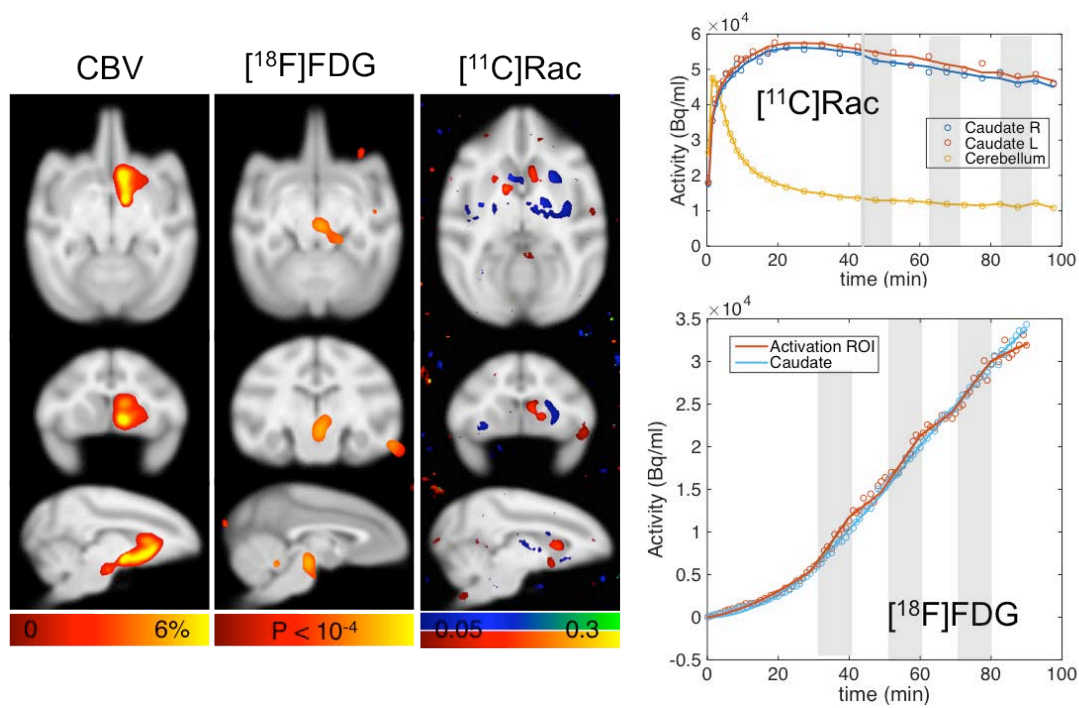
Figure legend: *Left*: Voxelwise maps showing changes in CBV signal in VTA, nucleus accumbens and caudate. The voxelwise maps from FDG-PET and raclopride-PET show changes in BP_{ND} before and after DBS stimulation. Data are from 12 imaging sessions and analyzed with a mixed effects model. fMRI maps are windowed by a P-value map with $P<10^{-5}$, FDG maps with $P<10^{-4}$. *Right*: Representative TACs from a single session for raclopride (B+I) and FDG infusion, with gray bars indicating stimulation blocks.

O-028

Investigating the dopaminergic response to music with simultaneous PET-MR imaging and the dopamine D1 receptor ligand [11C]SCH23390

Thomas H. Fritz[1,2], Swen Hesse[3,4], Michael Rullmann[1,3,4], Johanna Girbardt[5], Julia Luthardt[3], Simon Kaller[3], Christin Y. Sander[6], Marianne Patt[3], Philipp M. Meyer[3], Thies Jochimsen[3], Peter Werner[3], Georg-Alexander Becker[3], Kjell Nagren[7], Henryk Barthel[3], Arno Villringer[1], Osama Sabri[3,4]

[1]Max Planck Institute for Human Cognitive and Brain Sciences Leipzig, Germany, [2]Institute for Psychoacoustics and Electronic Music (IPEM) Gent, Belgium, [3]Department of Nuclear Medicine, University of Leipzig Leipzig, Germany, [4]University of Leipzig, IFB Adiposity Diseases, Leipzig, Germany, [5]Saxonian Hospital Altscherbitz, Neurology, Schkeuditz, Germany, [6]A.A. Martinos Center for Biomedical Imaging, Boston, MA, USA, [7]Department of Nuclear Medicine; PET and Cyclotron Unit; Odense University Hospital; Odense, Denmark

Introduction: The D2 dopamine (DA) receptor (D2R) system has previously been shown to relate to peak emotions and an anticipation of reward associated with music listening, using PET and the D2R antagonist [11C]raclopride. In accordance with the putative role of the striatum in music processing we aimed at investigating the D1 dopamine receptor (D1R) system and functional connectivity during music stimulation. These results shall add complementary information about phasic DA activity mediated via D1R.

Methods: Using PET-MRI (mMR Biograph, Siemens) and the D1R-selective antagonist [11C]SCH23390 we investigated 15 healthy volunteers (7 females, aged 33 ± 13yrs) on two different days where on each day they were measured once in a neutral setting and once while listening to one of two different music compilations. The music compilations were identical except with regard to their consonance/dissonance, and accordingly their pleasantness. The music excerpts comprised classical music that were rated as pleasant by participants, or their unpleasantly manipulated dissonant counterparts (the same music played simultaneously a tritone lower and a semitone higher in pitch). After 10 min of music listening PET images were acquired (90-min list mode acquisition) after a 90-sec bolus infusion of [11C]SCH23390 while simultaneously measuring fMRI (2 x 20 min EPI (TR=2s), followed by 4 min T1 MPRAGE sequences) during continued music stimulation. PET data were corrected for attenuation (using Dixon VIBE sequences) and motion (SPM8). After stereotactical normalization, parametric binding potential (BPnd) data were calculated using MRTM2 with the cerebellar cortex as the reference region for both SPM and VOI analyses, based upon an individual MR region segmentation of coregistered imaging data (PMOD 3.2). D1R PET BPnd data was obtained from a striatal VOI to calculate the first Eigenvariate of the EPI beta values across all striatal voxels for the duration of the initial 5 min of measurement. This time series was then implemented within the same single-subject general linear model as an additional non-interacting regressor, and analyzed for a positive whole brain correlation (enhanced connectivity) with the striatal seed region. To compare D1-related differences for pleasant vs. unpleasant music stimulation, the statistical maps representing the connectivity of each individual striatal seed were entered into a random effects group-level two-sample t-test, together with the individual BPnd values from the same striatal VOI. This allowed for an assessment of the functional connectivity of the striatum in relation to the individual striatal BPnd.

Results: Striatal BPnd during music listening (regardless of whether the music was pleasant or unpleasant) was significantly lower compared with BPnd in the neutral condition (1.27±0.29 vs. 1.31±0.31; P=0.03; paired t-test) (Figures-A-C). In the seed-based analysis, the striatum showed a higher functional connectivity (T=6.45) with the left dorsolateral prefrontal cortex when listening to pleasant music compared to unpleasant music (P<0.001, uncorrected; Figure-D).

Conclusions: The present data suggest that the D1R/ligand system is sensitive to music stimulation, independent of its valence. Furthermore, we observed a valence-specific effect in the fronto-striatal connectivity depending on the individual striatal D1R availability.
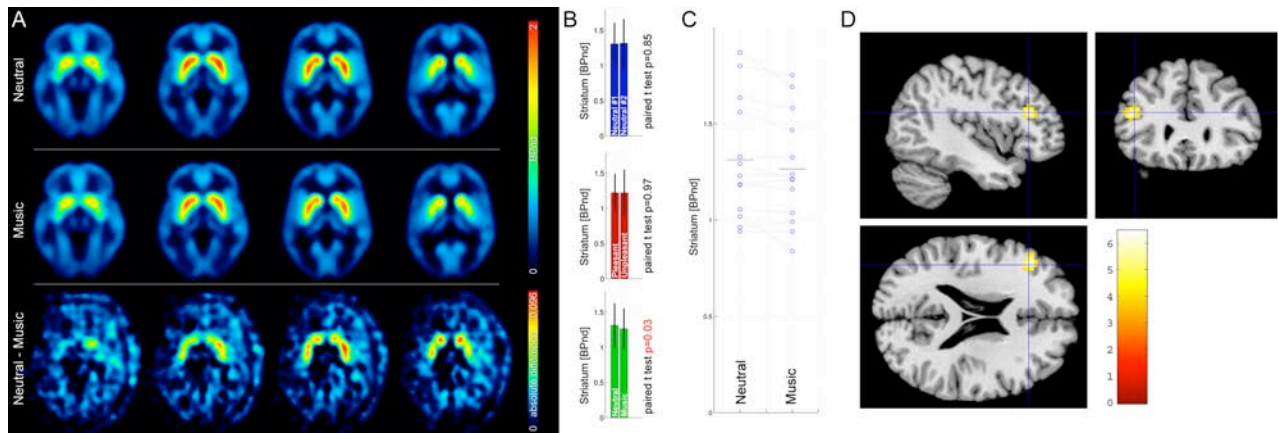
A, Averaged binding potential (BPnd) maps from the scan during in the neutral condition (no stimulation; upper row), during music stimulation (middle row), and the BPnd difference maps (lower row). B, Mean striatal BPnd from both neutral scans (upper row), from pleasant vs. unpleasant (middle row) showing no differences whereas striatal BPnd in neutral vs. music (lower row and C, individual values) indicates a significant reduction of BPnd during stimulation. D, Area with increased functional connectivity with the striatum (fMRI analysis) during pleasant compared to unpleasant music, depending on individual striatal BPnd.

Estimation of D2 receptor upregulation following repeat dose antagonist administration

Eugenii A. Rabiner[1,2], Roger N Gunn[1,3]

[1]Imanova Center for Imaging Sciences, London, UK, [2]Center for Neuroimaging Sciences, King's College, London, UK, [3]Division of Brain Sciences, Imperial College, London, UK

Introduction: Dopamine-D2 receptor (D2R) upregulation of up to 200%, after prolonged antagonist occupancy is well recognised [1] [2] {Ginovart, 2009 #2386}), with the result that determination of drug affinity from repeat dose PET occupancy studies suffers from potential bias.   Differences between antipsychotic D2R affinity assessed in healthy volunteers (typically performed following single dose (SD) administration) and patients (following repeat dose (RD) administration) are commonly reported. The most parsimonious explanation for these differences is the bias induced by ignoring D2R upregulation during repeat dose experiments, rather than any disease related differences in D2R affinity. We present a method to detect target upregulation in repeat-dose PET data, and apply it to existing data to explain discrepancies between SD and RD affinity estimates.

Methods: In the presence of receptor upregulation, the measured occupancy (Occ^M) can be described by Model-U:

$$O^M = \frac{[Drug] - EC_{50}\frac{Drug]}{[Drug] - EC_{50}}(U_{max}-1)}{[Drug] + EC_{50}}$$

where *[Drug]* is the plasma concentration of the drug at the time of the PET scan, EC_{50} is the plasma concentration of drug associated with 50% occupancy of the target, and U_{max} is the maximal fractional upregulation of the baseline receptor number when the target is fully occupied. When $U_{max} = 1$, Occ^M can be described by the standard occupancy model (Model-S)

$$O^M = \frac{[Drug]}{[Drug] + EC_{50}}$$

We applied Model-U to published [11C]raclopride PET occupancy data examining the relationship between D2R occupancy and the plasma concentration of the novel antipsychotic JNJ-37822681, following SD and RD administration [3, 4].   We fitted the combined SD and RD data, assuming a common EC_{50} and a $U_{max} = 1$ for the SD but not for the RD data, and compared the estimated parameters to those derived from Model-S fitted separately to SD and RD data.

Results: The EC_{50} from Model-S fits to SD and RD data were similar to those reported previously (see below). Model-U estimated an EC_{50} almost identical to the EC_{50} derived from the Model-S fit to the SD data, and D2R upregulation of ~150%. In this evaluation we made a biologically sensible assumption that no upregulation is present in SD data. To test this assumption, we also fitted the SD and RD data to a model assuming a common EC_{50} but allowing a $U_{max} \neq 1$ for both RD and SD data. The resultant parameters - $EC_{50} = 14.3$ ng/ml (5.6 – 23.0), $U_{max}^{RD} = 1.62$ (1.05-2.20) and $U_{max}^{SD} = 1.10$ (0.53-1.67), were consistent with this assumption.

	Model-S ($U_{max}=1$)		Model-U	
	EC_{50} (ng/ml)	U_{max}	EC_{50} (ng/ml)	U_{max}
SD	15.7 (13.5 – 18.0)	NA	15.7 (13.6 -17.8)	NA
RD	26.8 (23.3 – 30.3)	NA		1.53 (1.31 – 1.75)

Conclusions: We present a practical method to evaluate target upregulation in RD occupancy PET experiments, and demonstrate that discrepancies between RD and SD EC_{50} estimates are likely to be artefactual, due to the bias induced in RD data by ignoring the effects of target upregulation. The model we have developed can be extended to include cases where the maximal occupancy achievable is < 100%, and this produces similar results. Our findings prompt a re-evaluation of RD occupancy data to assess the biases induced by ignoring upregulation effects.

References:
1. Lee, T., Nature, 1978. **274**(5674): p. 897-900. 2. Tarazi, F.I., Psychopharmacology, 2008. **198**(1): p. 103-111. 4. Schmidt, M.E., Psychopharmacology, 2012. **224**(4): p. 549-557. 5. Te Beek, E.T., Journal of Psychopharmacology, 2012. **26**(8): p. 1128-1135.

O-030
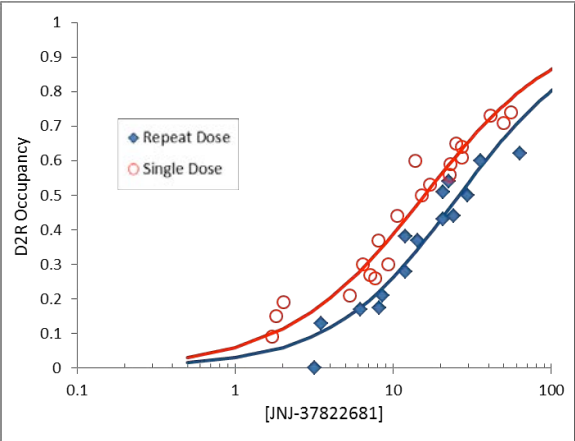
Molecular imaging of the glutamatergic and dopaminergic abnormalities in the quinpirole rat model for obsessive compulsive disorder

S.Servaes[1], D. Glorie[1], D. Thomae[1,2], J. Verhaeghe[1], S. Stroobants[1,2], S. Staelens[1]

[1]*Molecular Imaging Center Antwerp, University of Antwerp, Antwerp, Belgium,* [2]*Department of Nuclear Medicine, University Hospital Antwerp, Antwerp, Belgium*

Aims: Obsessive-compulsive disorder is a chronic, incapacitating, early onset psychiatric disorder that is characterized by obsessions and compulsions to reduce the associated anxiety. Convergent evidence has shown that both dopamine and glutamate are of importance in the pathophysiology of obsessive-compulsive disorder [1, 2]. We investigated this interplay by means of molecular imaging of the quinpirole sensitisation rat model for obsessive-compulsive disorder.

Methods: A total of 16 Sprague Dawley rats underwent μPET/CT baseline scans with both [^{11}C]-ABP-688 (ABP) and [^{11}C]-Raclopride (RAC) to first assess glutamatergic and dopaminergic systems respectively at baseline. Hereafter the animals were divided into a control group and a quinpirole group, receiving twice weekly an injection with respectively either saline or quinpirole (a D2 agonist). Each of these injections was paired with an open field test of 30 minutes, which was started 15 minutes after the injection of either saline or quinpirole. The behaviour was monitored through video tracking. After the 10th injection and associated open field test in week 5, animals were scanned again with both biomarkers to evaluate changes in both the dopaminergic and glutamateric systems.

Results: The quinpirole group displayed a strong increase in locomotor activity (+383 %; 48.41 ± 6.67 m versus 233.81 ± 23.64 m) and visiting frequency of one specific location (+699 %; 14 ± 2.79 versus 111.9 ± 13.02).
Volume-of-interest-based analysis (Fig. 1 panel A) revealed a decrease ($p < 0.001$) in the binding potential of RAC in the striatum of quinpirole animals compared to control (-52.59% ± 3.83%), which was confirmed by a voxel-based analysis. The binding potential of ABP was higher ($p < 0.05$) in the striatum (10.36% ± 4.09%), the anterior cingulate cortex (13.26% ± 4.01%) and the amygdala (24.36% ± 6.86%) in the quinpirole animals compared to the control group at the follow-up time point (Fig. 1 panel B).

Conclusions: Animals chronically treated with quinpirole show compulsive behaviour manifesting in an increased visiting frequency and an increased locomotor activity.   Our imaging data shows that both glutamatergic and dopaminergic systems are affected in regions closely associated with the CSTC-circuit. More specifically, glutamatergic differences were present in regions of the limbic system, hinting towards a dysfunctional working memory and error processing, both known to be affected in obsessive-compulsive disorder.

References:
1. Graybiel AM, Rauch SL (2000) Toward a neurobiology of obsessive-compulsive disorder. Neuron 28:343–347. 2. Pittenger C (2015) Glutamatergic agents for OCD and related disorders. Curr Treat Options Psychiatry 2:271–283.

A RACLOPRIDE

Base

Follow-up

B ABP-688

Base

Follow-up

Striatum

BP_{ND}

2.39±0.07 2.47±0.15 2.23±0.08 1.06±0.03

***
**

Base SAL Base QP Follow-up SAL Follow-up QP

Striatum

BP_{nd}

2.67±0.07 2.76±0.13 2.47±0.05 2.73±0.09

*

Base SAL Base QP Follow-up SAL Follow-up QP

Anterior Cingulate Cortex

BP_{nd}

2.29±0.09 2.41±0.11 2.18±0.04 2.46±0.08

*

Base SAL Base QP Follow-up SAL Follow-up QP

Amygdala

BP_{nd}

1.64±0.05 1.72±0.08 1.51±0.03 1.76±0.06

* *

Base SAL Base QP Follow-up SAL Follow-up QP

Hippocampus

BP_{nd}

1.98±0.05 2.04±0.11 1.92±0.03 2.10±0.06

Base SAL Base QP Follow-up SAL Follow-up QP

O-031

Further characterizing brain receptor occupancy with ITI-007: results from a PET study in patients with schizophrenia

Dean Wong[1], Robert E Davis[2], Yun Zhou[1], Weiguo Ye[1], Cedric O'Gorman[2], Jelena Saillard[3], James R. Brasic[1], Lorena Gapasin[1], Michal Weingart[2], Robert Litman[3], Sharon Mates[2], Kimberly E Vanover[2]

[1]Johns Hopkins University, School of Medicine, [2]Intra-Cellular Therapies, Inc, New York, NY, [3]CBH Health Rockville, MD

Antipsychotic medications for schizophrenia approved in the USA, have some dopamine D2 receptor occupancy (D2RO), but exhibit different threshold levels.   Most are antagonists, and have demonstrated efficacy with about 65 – 80% striatal D2RO, while D2RO >80% has been associated with the development of side effects.   Dopamine receptor partial agonists e.g., aripiprazole, a pre- and post- synaptic partial agonist, shows efficacy with higher (>80%) D2RO.   Clozapine is an exception to essentially all antipsychotics in current use, with efficacy associated with D2RO <50%.

ITI-007 is a first-in-class dopamine receptor phosphoprotein modulator (DPPM), acting as a presynaptic partial agonist and postsynaptic antagonist at D2 receptors.   This allows for reduced release of dopamine presynaptically compared to presynaptic antagonists along with blockade postsynaptically for more efficient reduction of dopaminergic signaling at D2 receptors.

ITI-007 also has 5-HT2A receptor antagonism, 5-HT transporter (SERT) inhibition, and acts as a partial agonist at D1 receptors. ITI-007 also indirectly increases phosphorylation of NMDA GluN2B receptor subunits via modulation of an intracellular signaling pathway downstream of D1 receptor activation. This unique pharmacology is associated with more efficient dopamine modulation leading to antipsychotic efficacy at relatively low D2RO.

PET data obtained in healthy volunteers (Clinical trial ITI-007-003) showed ITI-007 (10–40 mg) was safe and well tolerated with long-lasting and dose-related RO with >80% RO at 10 mg of cortical 5-HT2A receptors and ~12% D2RO. ITI-007 (40 mg) resulted in peak D2RO of 39% and 33% of SERT. Sixty mg was projected to have approximately 50% D2RO.

This study was designed to determine the striatal D2RO of ITI-007 in patients with schizophrenia at the 60 mg dose previously shown as efficacious in reducing psychosis without motoric disturbances.

Methods: Patients with stable schizophrenia were washed off their antipsychotic medications. After a drug-free period of at least 2 weeks, patients received a baseline scan followed by administration of 60 mg ITI-007 orally once daily for two weeks and subsequent post-treatment scans.   [11C] raclopride given IV bolus and images over 90 min on HRRT were obtained for each PET scan.   Parametric images of BPND were by SRTM with spatially-constraint and RO from % change.

Results: The mean (+/- SD) striatal D2RO was 39% + 12%, 34% + 8, 19% + 10% and 7% + 7% at 1, 3, 7.5 and approximately 24 hour post dosing of ITI-007. ITI-007 was considered safe and well tolerated. The most frequent adverse events that were considered to be at least possibly due to study drug were mild sedation and predominantly mild headache.

Discussion: Thus, ITI-007 demonstrates relatively low striatal D2RO at the efficacious daily dose of 60 mg compared to almost all efficacious antipsychotics to date.   It is more clozapine-like given its efficacy at low D2RO.   Yet, ITI-007 demonstrates a highly favorable safety profile, with lesser liability for D2 mediated side effects, such as motoric side effects and hyperprolactinemia.   Together, ITI-007 represents an exciting new treatment for schizophrenia.

Figure: Baseline (upper) and 1 h post-dose (lower) scans illustrating ~40% striatal D2RO at 60 mg ITI-007.
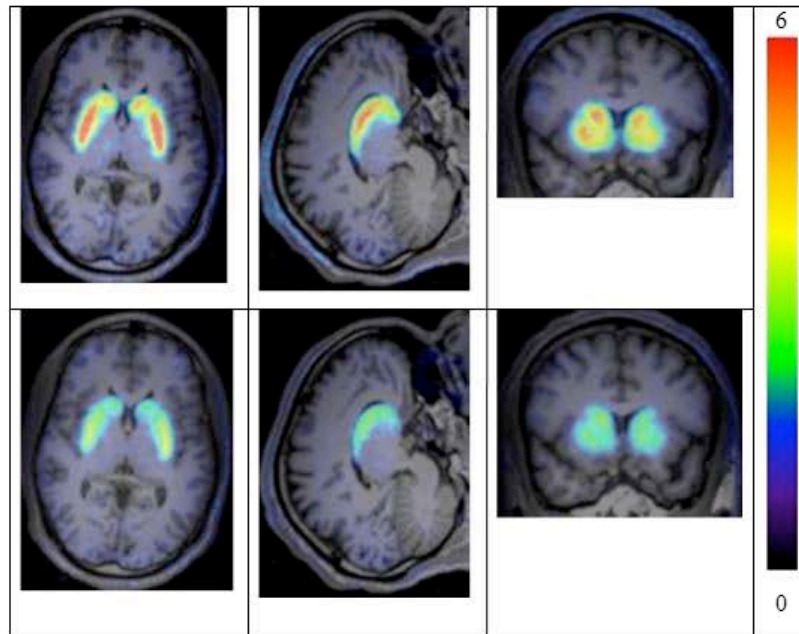
Spatial independent component analysis of [11C](+)PHNO PET reveals altered D2/D3 receptor networks in cocaine use disorder

Patrick D. Worhunsky[1], David Matuskey[1], Jean-Dominique Gallezot[1], Edward C. Gaiser[1], Nabeel Nabulsi[1], Gustavo A. Angarita[1], Vince D. Calhoun[2], Robert T. Malison[1], Marc N. Potenza[1], Richard E. Carson[1]

[1]Yale University, New Haven, CT, [2]University of New Mexico, Albuquerque, NM

Objectives. Both dopamine type 2 and type 3 receptors (D_2R/D_3R) appear critical to addictive disorders such as cocaine use disorder (CUD). [11C](+)PHNO is a D_3R-preferring agonist with regional binding reflective of local concentrations of both D_2R and D_3R [1], allowing for simultaneous imaging of D_2R/D_3R not possible using other D_2-like receptor radioligands (e.g., [11C]raclopride). However, as D_2R and D_3R are both expressed in many basal ganglia structures central to addiction (e.g., ventral striatum, pallidum), assessing potential alterations of specific receptor subtypes in these regions is challenging. We investigated the application of spatial independent component analysis (ICA) to identify subsystems of D_2R/D_3R in parametric [11C](+)PHNO PET images. ICA is a data-driven, higher-order statistical procedure that 'un-mixes' a measured signal into its maximally independent 'sources' [2]. Given the unique mixed-signal nature of [11C](+)PHNO and mixture-separating capabilities of ICA, we expected to identify D_2R-related and D_3R-related sources of BP_{ND}, or 'networks' of receptor availability. We also hypothesized that the intensity of these networks (i.e., how strongly a source contributes to the total mixture) would be consistent with evidence of upregulated D_3R [3] and downregulated D_2R in CUD [4].

Methods. 26 individuals with CUD and 26 age- and sex-matched healthy comparison (HC) participants completed [11C](+)PHNO PET scans (Siemens High Resolution Research Tomograph; HRRT) and MR imaging (Siemens 3T Trio). Dynamic PET data were reconstructed with corrections using the MOLAR algorithm [5]. Parametric images of [11C](+)PHNO BP_{ND} were computed using a simple reference tissue model (SRTM2) with the cerebellum as reference, registered into standard space using unified segmentation of the MR image in SPM12 (Wellcome Trust Centre for Neuroimaging), and smoothed with a 4mm FWHM Gaussian kernel. ICA was performed using the source-based morphometry utility of the GIFT Toolbox (v2.0e; http://mialab.mrn.org/software/gift) to explore D_2R/D_3R systems using a network-based, source-separation approach. Spatial composition of identified networks were compared to regional fractions of D_2R and D_3R of [11C](+)PHNO BP_{ND} [1], and individual network intensities were investigated for between-group differences and association with years of cocaine use.

Results. ICA identified three sources of [11C](+)PHNO BP_{ND} (striatopallidal, pallidonigral, and mesoaccumbens networks; Figure 1) that represent networks of brain regions displaying coherent variation in receptor availability. Spatial intensities of the striatopallidal network were strongly correlated with fractions of D_2R [11C](+)PHNO BP_{ND} (r=0.89, p=0.008), and the sum of the pallidonigral and mesoaccumbens networks were strongly correlated with D_3R fractions of [11C](+)PHNO BP_{ND} (r=0.90, p=0.005). There was a main effect of group on source intensities ($F_{3,48}=4.28$, p=0.009). CUD participants displayed reduced intensity of the striatopallidal network ($t_{50}=2.58$, p=0.013) that was negatively correlated with years of cocaine use (r=0.39, p=0.048), and greater intensity of the pallidonigral network ($t_{50}=2.03$, p=0.047) that was positively correlated with years of use (r=0.40, p=0.042).

Conclusions. The current study extends previous research of dopamine receptors in CUD, demonstrating the ability of ICA to separate sources of D_2R/D_3R availability measured with [11C](+)PHNO. Identified networks are consistent with dopamine circuitry and regional differences reported in CUD.
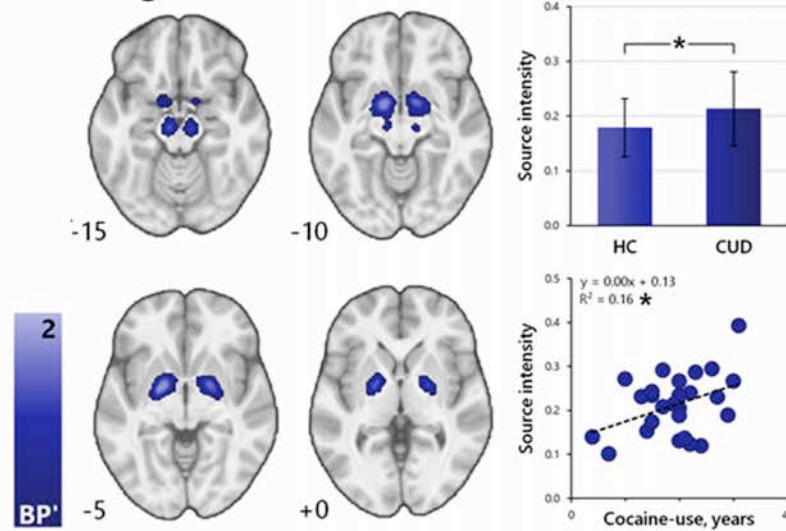
References.
[1] Searle GE, et al. *Neuroimage* 68, 119-132 (2013). [2] Calhoun VD, Liu J, & Adalı TA. *Neuroimage* 45, S163-S172 (2009). [3] Matuskey D, et al. *Drug and Alcohol Dependence* 139, 100-105 (2014). [4] Volkow N, et al. *Nature* 386, 830-833 (1997). [5] Carson RE, et al. *Nuclear Science Symposium Conference Record* 5, 3281-3285 (2003).
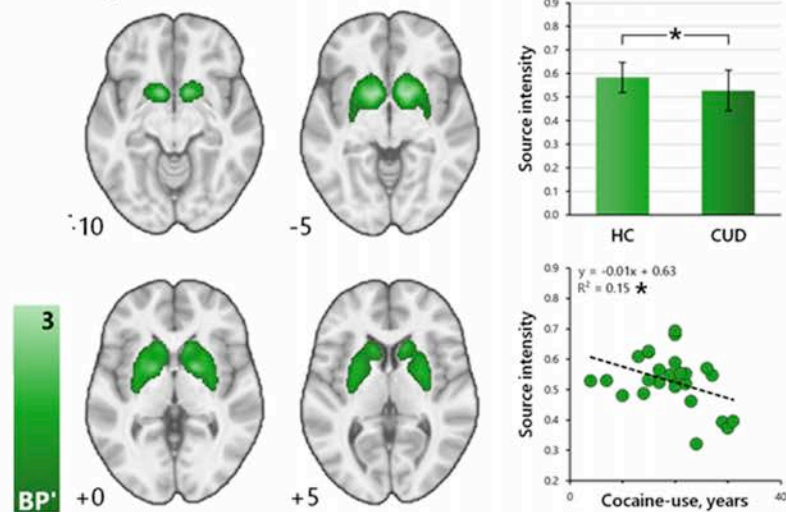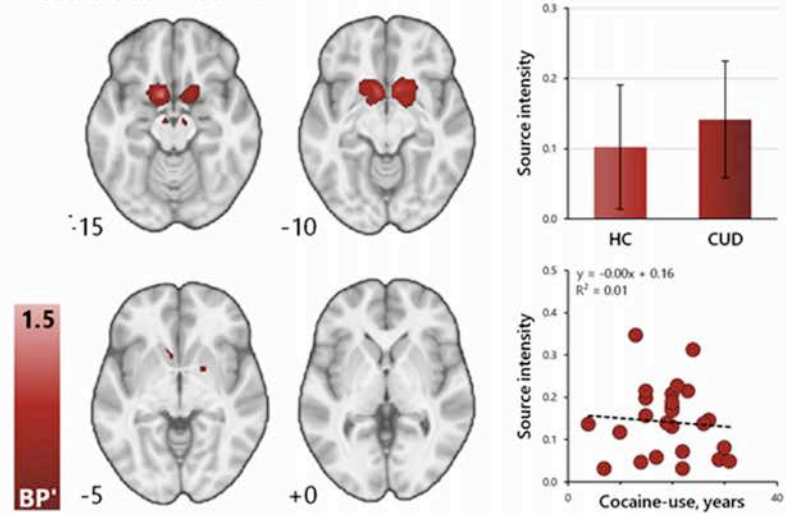
Figure 1. ICA-identified source networks of [^{11}C]PHNO BP_{ND}. Bar graphs display mean source network intensity for CUD and HC groups (error bars indicate SD) and scatter plots display relationships between years of cocaine use and source network intensity in CUD participants. *p<0.05.

Structural connectivity and striatal [11C]raclopride availability in social drinkers and nontreatment-seeking alcoholics

EJ Chumin[1,2], ME Halcomb[1], JA Contreras[1,2], M Džemidžić[1,5], J Goñi[1,3,4], KK Yoder[1,2,6]

[1]Center for Neuroimaging, Department of Radiology and Imaging Sciences, Indiana University School of Medicine, Indianapolis, IN, [2]Stark Neurosciences Research Institute, Indiana University School of Medicine, Indianapolis, IN, [3]Weldon School of Biomedical Engineering, Purdue University, West Lafayette, IN, [4]School of Industrial Engineering, Purdue University, West Lafayette, IN, [5]Department of Neurology, Indiana University School of Medicine, Indianapolis, IN, [6]Department Psychology, Indiana University Purdue University at Indianapolis, Indianapolis, IN

Introduction: The striatal dopamine system plays a role in cognitive processes underlying addiction. Corticostriatal innervation likely modulates striatal dopaminergic activity; as such, understanding the relationship between these connections and dopamine is important for the study of addiction. Diffusion-weighted imaging (DWI) allows characterization of *in vivo* human structural brain connectivity. Use of DWI with dopaminergic PET may shed light on structure-function relationships that may be altered in alcoholism and other addictions. Recent work suggests that corticostriatal projections may define local dopamine function (Tziortzi, 2014). However, we know little about how the properties of corticostriatal connections relate to dopamine tone. Additionally, no research has studied this in the context of alcoholism. We examined how the degree of corticostriatal structural connectivity (SC) relates to [11C]raclopride (RAC) binding potential (BP). We hypothesized that the strength of corticostriatal SC would relate with RAC BP, and that these relationships would differ between social drinkers (SD) and nontreatment-seeking alcoholics (NTS).

Methods: Ten SD (38.6±12.1 years old; 6M/4F) and 12 NTS (40.8±10.3 years old; 9M/3F) received a baseline RAC PET scan (Siemens mCT), a DWI scan, and a structural MRI (Siemens 3T Skyra). NTS subjects met DSV-IV criteria for alcohol dependence. Each participant's gray matter was parcellated into 278 functionally-defined regions of interest (ROIs) based on Shen 2013. DWI data were processed for tensor estimation and tractography. The primary variable of interest was "shortest path distance (SPD)" between any two regions of interest, as defined by Hagmann 2008. SPD is an index of distance between two target ROIs, which depends on the number of intermediate ROIs and the relative integrity of the projections along the path. Directly connected ROIs will have smaller SPD than those that are indirectly connected. We analyzed a subset of ROIs likely corresponding to corticostriatal projections (Haber, 2006). Cortical regions included ventromedial, dorsolateral, medial prefrontal, orbitofrontal, anterior cingulate, and other prefrontal cortical areas. Striatal parcellations (accumbens, head/tail of the caudate, and putamen) were also used to generate time-activity curves of RAC PET data. BP was estimated with MRTM with cerebellar gray matter as the reference region. Pearson's *r* tested for significant correlations between BP and SPD for a given data pair (e.g., L accumbens BP vs. L accumbens-L prefrontal cortex SPD). Fisher's *r*-to-*z* transformation was used to test for group differences in *r* of the BP:SPD pairs that were significantly related.

Results: Significant correlations of BP:SPD are presented by group in the attached figure. The spatial pattern of correlations differed between SD and NTS, and several BP:SPD associations differed significantly between groups. Most of the detected BP:SPD correlations were positive.

Conclusions: Positive relationships between RAC BP and SPD could indicate that longer, more indirect pathways may result in lower dopamine levels. Alternatively, higher striatal D_2 availability may be related to inefficient indirect neuronal communication. More work is needed to clarify and define relationships between SC and RAC BP, and to learn how group differences may inform our understanding of the neurophysiology of alcoholism.

References:
Hagmann, P., Cammoun, L., Gigandet, X., Meuli, R., Honey, C. J., Wedeen, V. J., & Sporns, O. (2008). Mapping the Structural Core of Human Cerebral Cortex. PLoS Biol, 6(7), e159. doi:10.1371/journal.pbio.0060159; Jarbo, K., & Verstynen, T. D. (2015). Converging structural and functional connectivity of orbitofrontal, dorsolateral prefrontal, and posterior parietal cortex in the human striatum. J

Neurosci, 35(9), 3865-3878. doi:10.1523/JNEUROSCI.2636-14.2015; Shen, X., Tokoglu, F., Papademetris, X., & Constable, R. T. (2013). Groupwise whole-brain parcellation from resting-state fMRI data for network node identification. Neuroimage, 82, 403-415. doi:http://dx.doi.org/10.1016/j.neuroimage.2013.05.081; Tziortzi, A. C., Haber, S. N., Searle, G. E., Tsoumpas, C., Long, C. J., Shotbolt, P., . . . Gunn, R. N. (2014). Connectivity-based functional analysis of dopamine release in the striatum using diffusion-weighted MRI and positron emission tomography. Cereb Cortex, 24(5), 1165-1177. doi:10.1093/cercor/bhs397

Group	BP:SC pair	SD r	SD p		NTS r	NTS p	Group Differences in r	
							z	p
Social Drinkers $n = 10$	L accum151: L accum151- L vmPFC170	0.68	0.031	NTS $n = 12$	0.34	0.279	0.94	0.35
	L accum151: L accum151- L vmPFC182	0.83	0.003		0.20	0.525	1.96	0.05
	R caud body25: R caud body25- R ACC27	0.68	0.032		0.05	0.872	1.55	0.12
	R accum114: R accum114- R mvPFC22	-0.73	0.016		0.46	0.133	-2.83	0.005
Nontreatment-seeking alcoholics $n = 12$	L put149: L put149- L ACC152	-0.72	0.008	SD $n = 10$	0.05	0.877	-1.90	0.058
	R put128: R put128- R dlPFC20	0.75	0.005		0.30	0.396	1.32	0.19
	R caud tail52: R caud tail52- R PFC131	0.63	0.029		0.30	0.402	0.86	0.39
	R caud tail52: R caud tail52- R dlPFC20	0.62	0.033		0.18	0.619	1.08	0.28
	R caud tail52: R caud tail52- R dlPFC88	0.73	0.007		-0.25	0.489	2.35	0.018
	R accum114: R accum114- R dlPFC20	0.60	0.04		-0.09	0.807	1.55	0.12

SD: social drinkers; NTS: nontreatment-seeking alcoholics; L: left; R: right; accum: accumbens; caud: caudate; put: putamen; ACC: anterior cingulate cortex; m: medial; d: dorsal; dl: dorsolateral; PFC: prefrontal cortex; OFC: orbitofrontal cortex. Region numbers indicate Shen (2013) parcellation label designations.

O-034

Sex differences in dorsolateral prefrontal cortex dopamine release and the relationship to tobacco smoking treatment outcomes

Yasmin Zakiniaeiz[1], Ansel T. Hillmer[2], Laura Goetz[3], Evan D. Morris[1,2,4,5], David Matuskey[2,4], Nabeel Nabusi[2], Yiyun Henry Huang[2], Sherry McKee[4], Kelly P. Cosgrove[1,2,4]

[1]Interdepartmental Neuroscience Program, Yale University, New Haven, CT, [2]Department of Radiology and Bioimaging, Yale University, New Haven, CT, [3]Yale College, Yale University, New Haven, CT, [4]Department of Psychiatry, Yale University, New Haven, CT, [5]Department of Biomedical Engineering, Yale University, New Haven, CT

Introduction: Sex differences exist in the behavioral and molecular mechanisms underlying tobacco smoking. In particular, men tend to smoke for the reinforcing effects of nicotine, whereas women tend to smoke to regulate stress and mood (Cosgrove, 2014, J Neurosci). While the mesolimbic dopamine (DA) system drives the reinforcing effects of tobacco smoking, the mesocortical DA system—including the dorsolateral prefrontal cortex (dlPFC)—is critical for inhibitory control and working memory function, which are both compromised by stress. Guanfacine is an alpha2-adrenergic agonist that is known to enhance inhibitory control and to reduce prefrontal cortical DA release, which we can measure with PET and the radiotracer [11C]FLB 457. The goals of this study were to investigate sex differences in amphetamine-induced cortical DA release in tobacco smokers and to examine whether the magnitude of DA release could predict subsequent guanfacine treatment outcomes.

Methods: Twenty-two tobacco smokers (9 females) participated in two [11C]FLB 457 PET scans on the same day before and 3 hours after administration of amphetamine (0.4-0.5mg/kg PO). Same day scans did not differ in injected activity (349.48±45.14 MBq baseline, 325.51±72.81 MBq post-amphetamine, p=0.145) or injected mass (0.40±0.15 μg baseline, 0.46±0.14 μg post-amphetamine, p=0.092). Subjects abstained from smoking overnight. Male (M) and female (F) groups were matched for age (M:34.54±9.61, F:34.56±10.45 years old, p=0.997), cigarettes smoked per day (M:13.00±5.32, F:12.22±5.36, p=0.740), and years of smoking (M:15.85±6.36, F: 14.67±7.35, p=0.692). After their first PET scan, all subjects participated in a guanfacine treatment trial for 3 weeks (3 mg PO, daily). Toward the end of the 3 weeks of guanfacine administration, all subjects participated in a smoking lapse self-administration paradigm following a psychological stressor (McKee, 2011, J Psychopharmacol), modeling the ability to resist smoking (i.e. latency to start smoking). We collected self-administration behavioral outcomes including time lapsed before the first cigarette. PET data were analyzed with SRTM using the cerebellum as a reference region to measure amphetamine-induced changes in [11C]FLB 457 binding potential (BP) in dlPFC. The percent fractional change in binding potential (%ΔBP) before and after amphetamine, an indirect measure of dopamine release, was calculated as %ΔBP=(1−ΔBP$_{Amphetamine}$/ΔBP$_{Baseline}$)*100. The difference in %ΔBP was compared between male and female smokers in the dlPFC.

Results: Preliminary analyses suggested that female smokers show a smaller amphetamine-induced DA binding change in dlPFC (%ΔBP=3.61±4.17%) than male smokers (%ΔBP=18.26±5.91%), p=0.08 (Figure 1A). For female smokers on guanfacine, preliminary data also indicate that smaller amphetamine-induced DA changes were associated with shorter time (less ability) to delay smoking in the self-administration paradigm following stressful imagery, p=0.026 (Figure 1B). This relationship was not found in male smokers.

Conclusions: Initial analyses of this ongoing study suggest that female smokers may have a blunted amphetamine-induced DA response compared to male smokers in the dorsolateral prefrontal cortex. Preliminary data suggest that the more blunted this response, the greater the inability to delay smoking after guanfacine treatment. This finding is consistent with previous literature showing that a blunted amphetamine-induced DA response in cocaine-dependent patients was predictive of poorer treatment outcomes (Martinez, 2011, Am J Psychiatry).
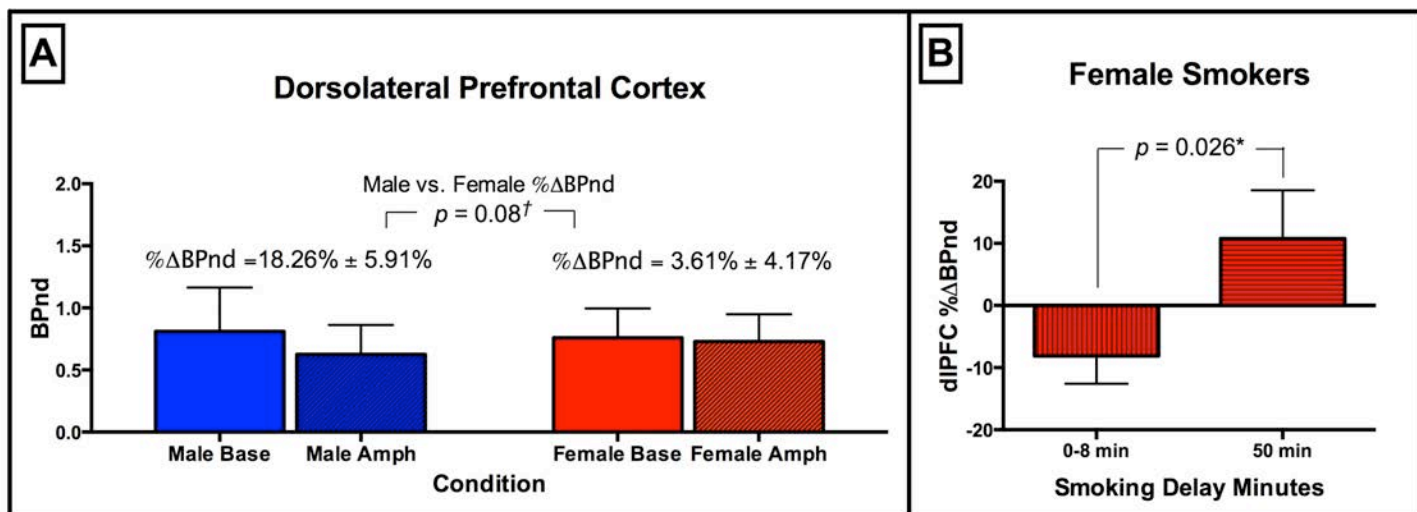
A. Average binding potential (BP) values in the dorsolateral prefrontal cortex (dlPFC) is shown for 13 male smokers (blue bars) and 9 female smokers (red bars) at baseline and after administration of amphetamine. The percent fractional change in binding potential (%ΔBP) is shown above the bars. There was a trend for a difference in %ΔBP between males and females (p=0.08, two-tailed). **B.** Average dlPFC %ΔBP is shown for female smokers with short (0-8 minutes) and long (50 minutes) smoking delay times following a stressful personalized script after three weeks of guanfacine treatment. The %ΔBP was significantly different between short and long smoking delay time groups among female smokers (p=0.026, two-tailed). Error bars display SEM.

O-035

Quantification strategies for [^{18}F]AV1451 tau binding

Andreas Hahn[1], Martin Schain[2], Maria Erlandsson[3], Petter Sjölin[3], Gregory M James[1], Olof T Strandberg[2], Douglas Hägerström[4], Rupert Lanzenberger[1], Jonas Jögi[5], Tomas G Olsson[3], Ruben Smith[6], Oskar Hansson[2,7]

[1]*Department of Psychiatry and Psychotherapy, Medical University of Vienna, Austria,* [2]*Clinical Memory Research Unit, Department of Clinical Sciences, Malmö, Lund University, Sweden,*
[3]*Department of Radiation Physics, Skåne University Hospital, Lund, Sweden,* [4]*Department of Clinical Neurophysiology, Skåne University Hospital, Lund, Sweden,* [5]*Department of Clinical Physiology and Nuclear Medicine, Skåne University Hospital, Lund, Sweden,* [6]*Department of Neurology, Skåne University Hospital, Lund, Sweden,* [7]*Memory Clinic, Skåne University Hospital, Malmö, Sweden di Milano; Italy*

Objectives: Aggregation of hyperphosphorylated tau is a major neuropathological characteristic of Alzheimer's disease and other neurodegenerative disorders [1, 2]. Here, we evaluated different quantification procedures for tau imaging in humans with [^{18}F]AV1451 (formerly T807) using arterial input function models, reference region models and simplified ratio methods.

Methods: Fifteen subjects were included: 4 healthy controls (HC 75±3.8 years), 6 patients with Alzheimer's disease (AD, 64.8±14.7 years), 2 with cortico basal syndrome (CBS, 66.5±0.7 years) and 3 with progressive supranuclear palsy (PSP, 74.3±5.8 years). PET measurements with [^{18}F]AV1451 (injected dose = 5.58±1.42 MBq/kg) were carried out on a GE Discovery 690 PET/CT scanner, lasting for 180min with 2x20min measurement breaks. For arterial input functions, blood samples were taken during the scan and radioactive metabolites were determined by HPLC analysis. Ten regions of interest (ROIs: 5 cortical, 4 subcortical, 1 cerebellum) were taken from atlases in FSL. ROIs were transformed to individual PET space by normalization of the corresponding structural MRI.
Quantification was carried out with one-, two- and three tissue compartment models (TCM) with and without coupling K_1/k_2 as well as the Logan plot. Using the cerebellum as reference region [3, 4], the simplified reference tissue model 2 (SRTM2) and the Logan reference plot were applied. Finally, simplified methods were calculated for various 20min time intervals. These included standard uptake values (SUV = activity ROI / injected dose / body weight) and SUVR ratios to cerebellum (activity ROI / activity cerebellum).

Results: 2TCM gave poor fits for 2 or more ROIs in 8 subjects and coupling K_1/k_2 yielded even worse fits for 3 subjects (figure 1a-b). Using the 3TCM improved the fits in these 3 subjects, but no improvement was noticed in the remaining subjects. Accordingly, standard errors of V_S exceeded 50% in 45 and 105 ROIs (out of 150) for 2TCM and 3TCM, respectively. In contrast, the invasive Logan plot showed excellent goodness of fit (R^2>0.993) and parameter identifiability (V_T standard error < 5%).
SRTM2 (R^2=0.92) and Logan reference plot (R^2=0.99) showed strong agreement as compared to the invasive Logan plot. Shortening the scan time gave good correspondence until 100min for the Logan reference plot (R^2=0.91). Similarly, SUVR 80-100min showed good agreement with the invasive Logan plot (R^2=0.93), which marginally increased for longer scan durations. SUV reached moderate agreement only at later time points (R^2=0.82 for 120-140min).
In HC, kinetics and Logan plot V_T were almost identical between cortical ROIs and cerebellum (figure 1), but cerebellar V_T was slightly higher in HC than patients. In AD, increased binding was observed for temporal, occipital, parietal, cingulate and frontal cortices as well as the hippocampus when using Logan plot (figure 1c), reference models and SUVR.

Conclusions: Since compartment models were not able to describe the kinetics adequately, the Logan plot represented the best invasive model. Assuming that the cerebellum contains no specific tau binding [3, 4], non-invasive alternatives provided robust estimates of tau binding. Furthermore, SUVR may offer potential clinical applicability with a static scan from 80-100min.

References:
[1] Dani M, et al. 2015. Tau imaging in neurodegenerative diseases. Eur J Nucl Med Mol Imaging [Epub ahead of print]; [2] Giacobini E, et al. 2013. Alzheimer disease therapy – moving from amyloid-beta to tau. Nat Rev Neurol 9: 677-686; [3] Marquie M, et al. 2015. Validating novel tau positron emission tomography tracer [18F]AV1451 (T807) on postmortem brain tissue. Ann Neurol 78: 787-800; [4] Herrmann M, et al. 1999. ELISA-quantitation of phosphorylated tau protein in the Alzheimer's disease brain. Eur Neurology 42: 205-210.
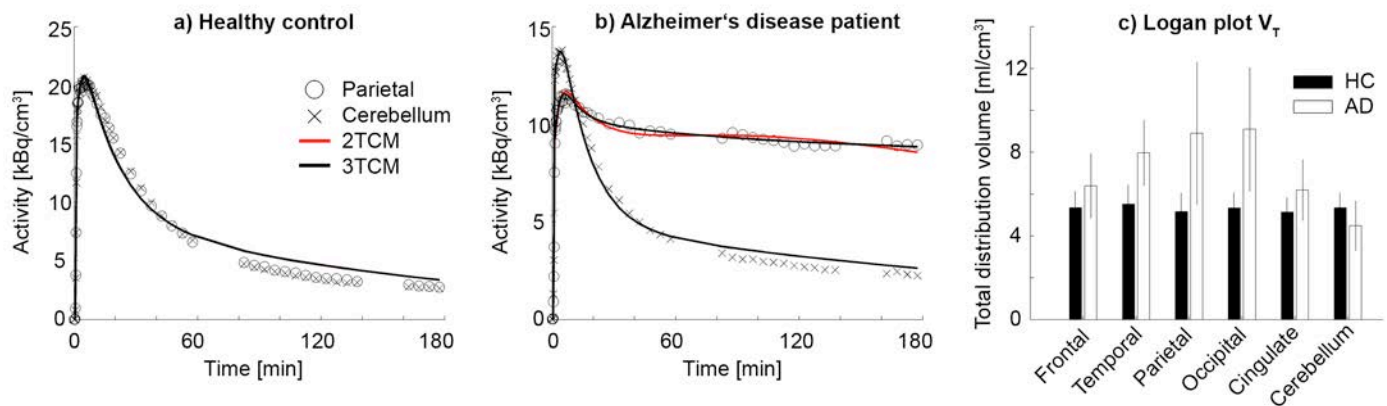
Figure 1: Time activity curves and compartment modeling results in a healthy subject (a) and a patient with Alzheimer's disease (b). 2TCM did not yield acceptable fits in cortical regions and the cerebellum for several subjects (a, note that 2TCM and 3TCM were virtually identical). 3TCM improved the fits only in few cases (b). Increased binding of [18F]AV1451 was found in cortical brain regions for AD patients for invasive Logan plot V_T (c) as well as reference models and SUVR.

Imaging Aβ and tau in early stage Alzheimer's sisease with [18F]AV45 and [18F]AV1451

Azadeh Firouzian[1], Alexander Whittington[2], Graham Searle[1], Ivan Koychev[3], Simon Lovestone[3], Roger N. Gunn[1,2,4]

[1]Imanova Ltd, London, UK, [2]Department of Medicine, Imperial College London, London, UK, [3]Department of Psychiatry, University of Oxford, Oxford, UK, [4]Department of Engineering   Science, University of Oxford, Oxford, UK

Introduction: Alzheimer's disease (AD) is a progressive neurodegenerative disorder that is associated with the accumulation of amyloid-β (Aβ) and hyperphosphorylated tau proteins which can be imaged by PET using tracers including [18F]AV45 (Aβ) and [18F]AV1451 (tau) [1].   We used dynamic PET data from the MRC Pilot Deep and Frequent Phenotyping Study (a multi-centre non-interventional feasibility study) to assess simplified static acquisitions and the relationship between Aβ and tau signals.

Materials and Methods: 15 subjects with early clinical AD (Mini Mental State Examination (MMSE)) score of 20 - 29), men and women aged 50 to 85 years underwent a T1-weighted MRI structural scan and two dynamic PET scans, one with [18F]AV45 (0-60min, 150±24MBq) and one with [18F]AV1451 (0-120min, 163±10MBq) to measure Aβ and tau respectively.

The dynamic PET images were motion corrected using a mutual information co-registration algorithm. The associated MRI data enabled nonlinear registration of the CIC atlas [2] into each subject's dynamic PET space and generation of regional time-activity data (TACs). The Simplified Reference Tissue Model (SRTM) [3], with cerebellum grey matter as reference region, was applied to the regional TACs to estimate the binding potential (BP_{ND}) values and a time stability analysis was performed to asses the impact of scan duration. Regional standard uptake values (SUV_r) with respect to cerebellum grey were also obtained for a range of 20min scan windows to investigate static acquisition outcome measures and their relationship to SRTM BP_{ND}. All image processing and kinetic analysis was performed in MIAKAT™ [4]. Furthermore, the relationship between regional Aβ and tau BP_{ND} estimates was investigated.

Results: All 15 subjects successfully completed the 60min Aβ PET scans and 10 out of 15 subjects completed 120min tau PET scan with the other 5 completing at least 60min. For all subjects, SRTM with cerebellum grey matter as reference region successfully described the [18F]AV45 and [18F]AV1451 TACs (Fig1. a,b). Time stability analysis of mean regional SRTM BP_{ND} values for [18F]AV45 (ranging -0.1-0.5) showed that it became stable for scan durations of ~35 min and for [18F]AV1451 (ranging -0.2-0.4) for scan durations of ~80 min. Time stability analysis of mean regional SUVr values showed that it became stable for scan windows of ~30-50min for [18F]AV45 and ~80-100min for [18F]AV1451. The relationship between these two measures started to plateau for scan windows of ~40-60min for [18F]AV45 and ~90-110 min for [18F]AV1451 (Fig 1c).

Additionally, strong correlation was found between some regional Aβ and tau signals (Fig.1d). In particular Aβ signal in thalamus was highly correlated with tau signal in thalamus (R^2 = 0.87, $p < 0.0005$), hippocampus (R^2 = 0.86, $p < 0.0005$) and striatum (R^2 = 0.80, $p < 0.005$).

Conclusions: In conclusion, short static PET scans at appropriate time windows provide SUVr values in good agreement with SRTM BP_{ND} values. Furthermore, in this early AD population Aβ levels in thalamus were highly correlated with tau uptake in thalamus, hippocampus and striatum.

References:
[1] R. H. Mach, "New Targets for the Development of PET Tracers for Imaging Neurodegeneration in Alzheimer Disease," *J. Nucl. Med.*, vol. 55, no. 8, pp. 1221–1224, 2014. [2] A. C. Tziortzi, G. E. Searle, S. Tzimopoulou, C. Salinas, J. D. Beaver, M. Jenkinson, M. Laruelle, E. A. Rabiner, and R. N. Gunn, "Imaging dopamine receptors in humans with [11C]-(+)-PHNO: Dissection of D3 signal and anatomy," *Neuroimage*, vol. 54, no. 1, pp. 264–277, 2011. [3] A. A. Lammertsma and S. P. Hume, "Simplified reference tissue model for PET receptor studies.," *Neuroimage*, vol. 4, no. 3 Pt 1, pp. 153–8, 1996. [4] www.miakat.org
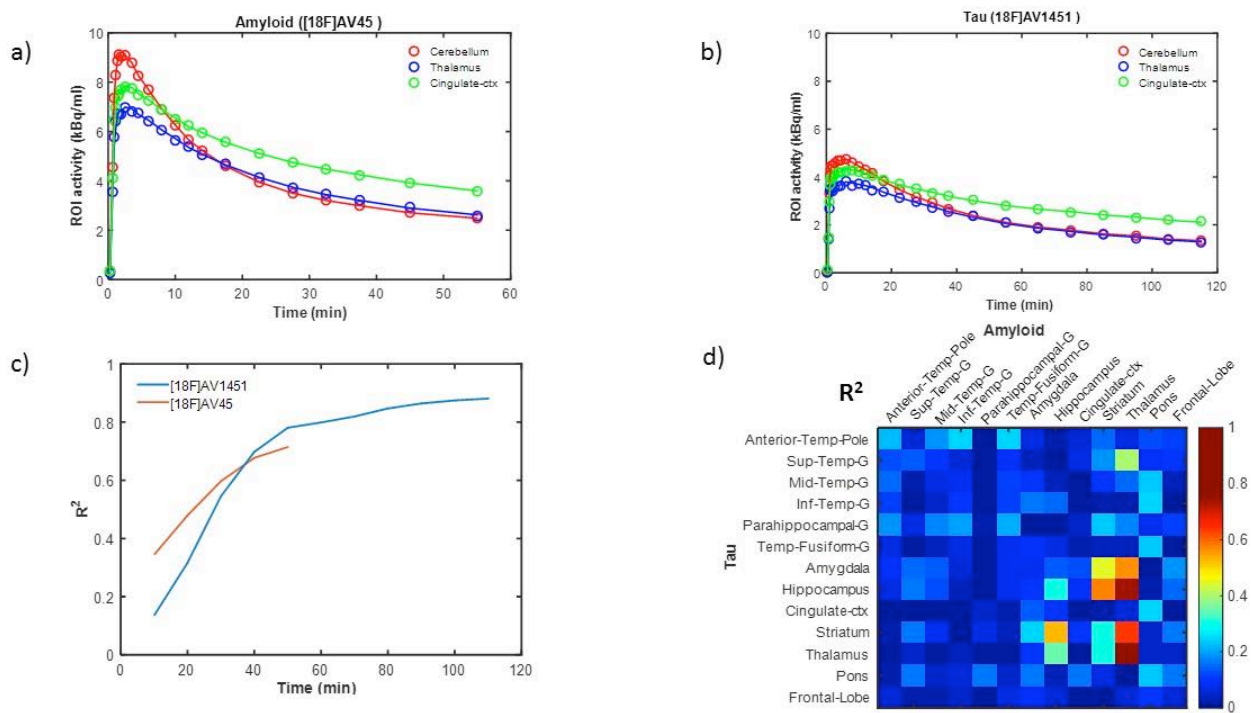
Figure 1: *Example of SRTM model fits (solid line), with cerebellum grey as the reference region, for a) [18F]AV45 (Ab) and b) [18F]AV1451 (tau). c) The coefficient of determination (R^2) between regional SRTM BP_{ND} and SUV_r values (plotted against the mid 20min SUV window time). d) The coefficient of determination (R^2) between regional Ab and tau SRTM BP_{ND} values (R^2).*

Longitudinal [11C]PiB PET study of amyloid-B accumulation in Down syndrome

PJ Lao[1], TJ Betthauser[1], JC Price[2], WE Klunk[2], PD Bulova[2], SL Hartley[1], R Hardison[2], RV Tumuluru[2], D Murali[1], CA Mathis[2], AD Cohen[2], TE Barnhart[1], D Tudorascu[2], DA Devenny[3], SC Johnson[1], BL Handen[2], BT Christian[1]

[1]University of Wisconsin-Madison, Departments of Medical Physics, Psychiatry, Medicine-Geriatrics and Waisman Center, [2]University of Pittsburgh, Department of Psychiatry, Medicine, Radiology, and Epidemiology Data Center, [3]New York State Institute for Basic Research in Developmental Disabilities

OBJECTIVE: Adults with Down syndrome (DS) are an at-risk population for the development of Alzheimer-like neuropathology that begins as early as the fourth decade and precedes cognitive decline. Longitudinal studies of the early changes of Alzheimer's disease (AD) in the DS population demonstrate the magnitude, distribution, and spread of amyloid-β plaques, providing insight into the link between Alzheimer-like neuropathology and clinical symptoms of dementia.

METHODS: As part of our ongoing longitudinal project including 80 nondemented adults with DS (age=30-53 yrs), 48 subjects have completed two cycles of [11C]PiB PET imaging with 3.0±0.7 years between scans. Standard uptake value ratio (SUVR) images were created using data 50-70 min post-injection and cerebellar gray matter as reference region. Parametric maps for the rate of change in SUVR per year were created for each participant. The mean rate of change (DSUVR/Δtime) was calculated for anterior cingulate, frontal cortex, parietal cortex, precuneus, striatum, temporal cortex defined by atlas-derived masks in standardized space. Subjects were classified as PiB positive if at least one ROI had a mean SUVR above its positivity threshold. Two-tailed one sample t-tests were used to test the null hypothesis that the rate of change is equal to zero on a ROI basis, and linear regression models were used to test the significance of predictors of baseline age or SUVR on the rate of change in SUVR without partial volume correction. A Bonferroni correction was applied to correct for multiple comparisons ($\alpha_{Bonferroni}$ = 0.0083).

RESULTS: There is a significant positive rate of change in PiB SUVR across all ROIs (P<0.008). Baseline PiB SUVR are significantly associated with the rate of change in PiB SUVR for all ROIs except the striatum, even after adjusting for age (Figure 1). Some PiB positive individuals appeared to have a slower rate of change in the striatum, an effect not observed in other investigated ROIs. Consistent with our previous findings that amyloid-β accumulation begins in the striatum in DS (Lao et al., 2015), similar to that in autosomal dominant AD (Klunk et al., 2007), it is possible that this would be the first brain region to reach amyloid-β plaque saturation. With dichotomized PiB SUVR as PiB positive or PiB negative, the PiB positive group demonstrated a higher rate of change than the PiB negative group in all ROIs except the striatum. Interestingly, age is a strongly significant predictor for PiB SUVR at baseline as well as follow-up in all ROIs, yet baseline age is not a significant predictor for the rate of change in PiB SUVR between scans.

CONCLUSIONS: There is evidence for an increase in PiB binding in nondemented adults with DS from baseline to follow-up scans, which is higher in subjects with elevated PiB SUVR at baseline. While the magnitude of PiB SUVR is correlated to age, the rate of change of PiB SUVR is only correlated to baseline PiB SUVR. These findings suggest that a disease-related process drives the rate of amyloid-β accumulation beyond what is expected from normal aging.
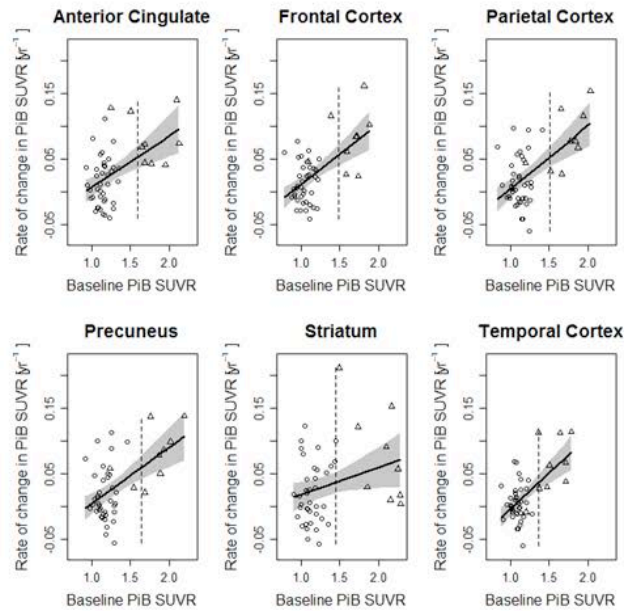
Region of Interest	All subjects	PiB negative	PiB positive
	Regression parameter and 95% Confidence Interval for the Effect of baseline SUVR on ΔSUVR/Δtime [yr⁻¹]	Mean and 95% Confidence Interval for one-sample t-test on ΔSUVR/Δtime [yr-1]	Mean and 95% Confidence Interval for one-sample t-test on ΔSUVR/Δtime [yr-1]
Anterior Cingulate	0.078, (0.038, 0.118)	0.014, (0.002, 0.025)	0.081, (0.051, 0.111)
Frontal Cortex	0.093, (0.056, 0.131)	0.012, (0.002, 0.022)	0.078, (0.043, 0.112)
Parietal Cortex	0.096, (0.059, 0.134)	0.014, (0.001, 0.026)	0.080, (0.046, 0.113)
Precuneus	0.096, (0.057, 0.134)	0.017, (0.004, 0.030)	0.077, (0.044, 0.110)
Striatum	0.041, (0.002, 0.081)	0.020, (0.005, 0.034)	0.077, (0.021, 0.133)
Temporal Cortex	0.110, (0.068, 0.152)	0.005, (-0.004, 0.013)	0.061, (0.027, 0.095)

Figure 1. An unadjusted regression line between the rate of change in PiB SUVR and baseline PiB is shown as the solid line with the gray shaded region representing a 95% confidence interval. The dotted line represents the PiB positivity threshold for that region of interest, with PiB positive subjects denoted by triangles. Note the low rates for subjects with high baseline in the striatum, which indicates the rate of change slows down in PiB positive subjects in this region. The table lists the regression parameter and 95% confidence interval for all subjects, and the mean and 95% confidence interval for two-tailed one-sample t-tests for determining if the rate was significantly different from zero for PiB negative and PiB positive subjects.

Spatiotemporal distribution of β-amyloid in AD results from heterogeneous regional carrying capacities

Alex Whittington[1,2], David J. Sharp[1], Roger N. Gunn[1,2,3]

[1]Imperial College London, [2]Imanova Ltd, [3]University of Oxford

Objective: β-amyloid (Aβ) is one of two pathological hallmarks of Alzheimer's Disease (AD) and its heterogeneous spatiotemporal distribution has been studied extensively *ex vivo.* We apply mathematical modelling to longitudinal and cross-sectional Aβ PET imaging data in order to investigate competing theories of Aβ spread in AD.

Methods: Cross-sectional [^{18}F]AV45 PET SUVr images for 723 subjects (125AD, 184LMCI, 243EMCI and 171HC) from the ADNI database, calculated using grey matter cerebellum as a reference region, were nonlinearly registered into stereotactic space. The CIC anatomical atlas[1] was then applied to calculate SUVr values for 119 cortical and subcortical regions.   The mean cortical SUVr was used to calculate where each individual resides chronologically in the disease process by fitting to a functional form for mean cortical SUVr obtained from longitudinal PET Aβ data[2].   This yielded a dataset with 723 time-points representing Aβ accumulation at the population level.
A 4-parameter logistic growth model was used to model the longitudinal regional accumulation of Aβ,

$$SUVr(t) = NS + \frac{K}{1 + e^{\, r(t - T_{50})}}$$

where K is the local Aβ carrying capacity, NS is tracer non-specific binding, r is the growth rate and T_{50} is the time of half maximal Aβ accumulation.   Sixteen model configurations were investigated in order to identify whether each of these parameters was constant across the brain (global) or different for each region (local). The most parsimonious model, determined using Akaike Information Criterion (AIC), was subsequently fitted at the voxel level to derive parametric maps of NS and K (with r and T_{50} fixed to the global values identified from the regional analysis).

Results: The chronological Aβ data showed strong coherence in all regions providing good evidence that there is a stereotypical regional spatiotemporal distribution at the population level.   AIC determined the most parsimonious model to have local K and NS and global T_{50} and r. This model accurately described the data in all regions (Figure 1A). Voxelwise fitting of this model produced parametric images of NS and K (Figure 1B). The highest carrying capacities were obtained in the cingulate and frontal cortices consistent with the regional analysis. The NS image was consistent with the known non-specific binding of [^{18}F]AV45 to white matter.

Conclusion: Chronological *in vivo* Aβ PET data at the population level can be accurately modelled using a 4-parameter logistic equation where the carrying capacity and non-specific binding vary across the brain and the growth rate and time of half maximal concentration are constant.   These results support the hypothesis that the process of regional accumulation of Aβ originates at the same time with the same growth rate for all regions. The model suggests that the distribution in Aβ results from different regional carrying capacities, rather than variable spreading of Aβ from a small number of seed regions.   Further, we propose that the estimation of a single outcome measure from Aβ PET scans defined as Aβ load,

$$A\beta_L = \frac{SUVr - NS}{K}$$

$A\beta_L$ can easily be calculated for individual Aβ PET scans using the template images generated for NS and K with linear regression.

References*:*
1. Tziortzi, A. C. *et al.* Imaging dopamine receptors in humans with [11C]-(+)-PHNO: Dissection of D3 signal and anatomy. *Neuroimage* **54,** 264–277 (2011). 2. Jack, C. R. J. *et al.* Brain β-amyloid load approaches a plateau. *Neurology* **80,** 890–896 (2013).

A bispecific antibody-based PET radioligand for imaging of amyloid-beta protofibrils

Dag Sehlin[1], Xiaotian T Fang[1], Linda M Cato[1], Greta Hultqvist[1], Johanna Fälting[2], Gunnar Antoni[3,4], Lars Lannfelt[1], Stina Syvänen[1]

[1]*Department of Public Health and Caring Sciences, Uppsala University, Uppsala, Sweden,* [2]*BioArctic Neuroscience AB, Stockholm, Sweden,* [3]*Department of Medicinal Chemistry, Preclinical PET Platform, Uppsala University, Uppsala, Sweden,* [4]*Uppsala University Hospital PET-centre, Uppsala, Sweden*

Background and Aim: The aim of this study was to develop an antibody-based radioligand for PET imaging of soluble aggregates of amyloid-beta, i.e. protofibrils, which are suggested to cause neurodegeneration in Alzheimer's disease [1, 2]. Antibodies are highly specific for their target protein, but their large molecular size have restricted their use at PET ligands for brain targets. In the present study we constructed a bispecific ligand with affinity for the transferrin receptor (TfR) and amyloid-beta protofibrils. The binding to TfR enabled receptor mediated transcytosis across the blood-brain barrier of the bispecific ligand. To our knowledge this is the first time an antibody ligand has been used successfully for imaging of a target inside the brain [3].

Methods: A $F(ab')_2$ fragment of the humanized variant of amyloid-beta protofibril selective antibody mAb158 [4], $F(ab')_2$-h158, was chemically fused with a TfR antibody (8D3, [5]) and the fusion protein was analyzed with ELISA for retained binding to amyloid-beta protofibrils and TfR. Brain uptake of the ^{125}I radiolabelled fusion protein and $F(ab')_2$-h158 was first studied *ex vivo* in the tg-ArcSwe mouse model of AD [6, 7]. The fusion protein was then labeled with ^{124}I and used for PET imaging of amyloid-beta protofibrils in AD and wild-type mice of different ages. A subset of mice were also scanned with [^{11}C]PIB. The SUV$_{ratio}$, using cerebellum as a reference region, was compared to amyloid-beta levels measured post mortem in brain tissue.

Results: The fusion protein retained its binding properties for both amyloid-beta protofibrils and TfR and displayed a 15-fold higher brain uptake compared to mAb158 three days post injection in AD mice. There was also a clear difference between AD mice and wild type mice in brain concentrations of the bispecific ligand. PET imaging confirmed the *ex vivo* result, showing a high signal in >12 months old AD mice. The SUV$_{ratio}$ increased with age in AD mice, while it was low in wild type mice of all ages. The SUV$_{ratio}$ correlated with levels of amyloid-beta protofibrils while no correlation was found with total brain levels of amyloid-beta (i.e. reflecting amyloid-beta plaque load) suggesting that the PET signal was specific for protofibrils.

Conclusions: This study shows for the first time *in vivo* PET images of soluble amyloid-beta protofibrils. Soluble amyloid-beta correlates better with Alzheimer's disease severity than insoluble plaques, which are the target of the currently used PET ligand Pittsburgh compound B (PIB). Thus, the new radioligand, holds great promise to become an important tool for determining disease stage and potential treatment effects in Alzheimer's disease. In a longer perspective, the use of bispecific fusion proteins as PET ligands may enable imaging of other proteins involved in neurodegenerative diseases for which imaging agents are completely lacking today.

References
1. H. Fukumoto, T. Tokuda, T. Kasai, N. Ishigami, H. Hidaka, M. Kondo, D. Allsop, M. Nakagawa, High-molecular-weight beta-amyloid oligomers are elevated in cerebrospinal fluid of Alzheimer patients. FASEB J 24, 2716-2726 (2010).
2. T. J. Esparza, H. Zhao, J. R. Cirrito, N. J. Cairns, R. J. Bateman, D. M. Holtzman, D. L. Brody, Amyloid-beta oligomerization in Alzheimer dementia versus high-pathology controls. *Ann Neurol* 73, 104-119 (2013).
3. D. Sehlin, X.T. Fang, L. Cato, G. Antoni, L. Lannfelt, S. Syvänen, Antibody-based PET imaging of amyloid-beta in mouse models of Alzheimer's disease. Accepted for publication in *Nature Communications* (2016).
4. H. Englund, D. Sehlin, A. S. Johansson, L. N. Nilsson, P. Gellerfors, S. Paulie, L. Lannfelt, F. E. Pettersson, Sensitive ELISA detection of amyloid-beta protofibrils in biological samples. J Neurochem 103, 334-345 (2007).
5. K. Kissel, S. Hamm, M. Schulz, A. Vecchi, C. Garlanda, B. Engelhardt, Immunohistochemical localization of the murine transferrin receptor (TfR) on blood-tissue barriers using a novel anti-TfR monoclonal antibody. Histochem Cell Biol 110, 63-72 (1998).
6. A. Lord, H. Kalimo, C. Eckman, X. Q. Zhang, L. Lannfelt, L. N. Nilsson, The Arctic Alzheimer mutation facilitates early intraneuronal Abeta aggregation and senile plaque formation in transgenic mice. Neurobiol Aging 27, 67-77 (2006).

7. O. Philipson, P. Hammarstrom, K. P. Nilsson, E. Portelius, T. Olofsson, M. Ingelsson, B. T. Hyman, K. Blennow, L. Lannfelt, H. Kalimo, L. N. Nilsson, A highly insoluble state of Abeta similar to that of Alzheimer's disease brain is found in Arctic APP transgenic mice. Neurobiol Aging 30, 1393-1405 (2009).
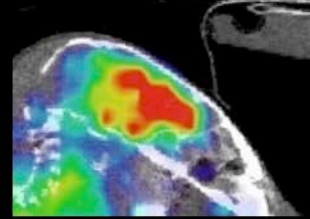
PET images acquired with a bispecific mAb-based ligand: Accumulation of the ligand in the brain increases with progression of pathology in a mouse model of AD
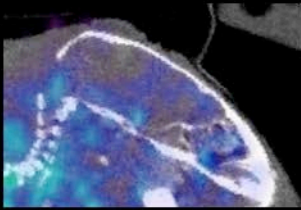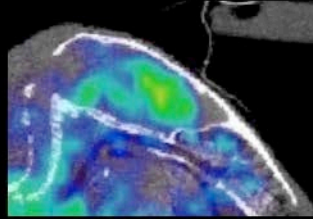
8 months   12 months   18 months

Use of ^{11}C-UCB-J as a biomarker for synaptic density: an in vivo/in vitro validation study

Sjoerd J. Finnema[1], Tore Eid[2], Ronnie Dhaher[2], Ming-Kai Chen[1], Shu-fei Lin[1], Evan Baum[1], Daniel Holden[1], Nabeel Nabulsi[1], Yiyun Huang[1], Richard E. Carson[1]

[1]PET Center, Yale University, New Haven, CT, [2]Department of Laboratory Medicine, Yale University, New Haven, CT

Introduction: Synaptic changes have been implicated in numerous brain disorders, including Alzheimer's disease and epilepsy. ^{11}C-UCB-J is a recently developed PET ligand for quantitative measurement of synaptic vesicle glycoprotein 2A (SV2A) in primates[1]. SV2A is located in the membrane of synaptic vesicles, similar to synaptophysin (SYN), and is ubiquitously present in the brain. SYN has been extensively studied as a biomarker for synaptic density using immunochemical techniques. Here we evaluated, in the nonhuman primate brain, the relationship of regional variations in brain density between SV2A and SYN by western blot analysis. The *in vitro* and *in vivo* SV2A binding of ^{11}C-UCB-J were also compared using a homogenate binding assay and PET, respectively.

Methods: One baboon was studied with ^{11}C-UCB-J in a Siemens Biograph mCT PET system. After completion of the PET scan, the baboon was euthanized, the brain harvested and sectioned, and tissue was frozen at -80°C. Tissue samples from 12 brain regions were obtained and analyzed with western blot analyses for SV2A and SYN, as well as homogenate binding assays with ^{11}C-UCB-J to allow for direct comparison of regional SV2A density (B_{max}) to the *in vivo* PET measure of volume of distribution (V_T). Regional V_T values were estimated with the arterial input function using the one-tissue compartment model.

Results: Western blot analyses demonstrated strong and specific SV2A and SYN signals in all gray matter regions, and weak/absent signals in the white matter (centrum semiovale). The correlation between SV2A and SYN was linear across all gray matter regions examined (SYN=1.177*SV2A-11934, R^2=0.88) (Fig A). In the homogenate binding assays, ^{11}C-UCB-J bound to a homogeneous population of binding sites with a K_i of 6.8 ± 1.3 nM, which is comparable to previously reported values in humans (6-7 nM)[1, 2]. The regional SV2A density ranged between 0.20 – 20.7 pmol/mg protein or 7 – 953 pmol/mL brain tissue. There was a good correlation between regional *in vitro* B_{max} values and the corresponding SV2A optical density (SV2A OD = 1098*B_{max}) (Fig B). The *in vitro* B_{max} values also correlated well with the *in vivo* V_T values measured with PET (V_T = 0.94*B_{max} + 9.25, R^2 = 0.84) (Fig C).

Conclusions: Our data validate the hypothesis that ^{11}C-UCB-J binding to SV2A may be interpreted as a measure of synaptic density. Regional differences in ^{11}C-UCB-J V_T measured with PET are related to differences in SV2A densities. The suitability of ^{11}C-UCB-J as a biomarker of synaptic density is currently being examined in a variety of disorders including Alzheimer's disease.

References:
1. Nabulsi, N., et al. J Nucl Med (2016); 2. Mercier, J., et al. ChemMedChem 9, 693-8 (2014).

A Y = 1.177*X - 11934
SYN (Optical density unit) vs SV2A (Optical density unit)

B Y = 1098*X - 0.0
SV2A (Optical density unit) vs SV2A (B_{max}, pmol/mg protein)

C Y = 0.9360*X + 9.251
SV2A (V_T) vs SV2A (B_{max}, pmol/mg protein)
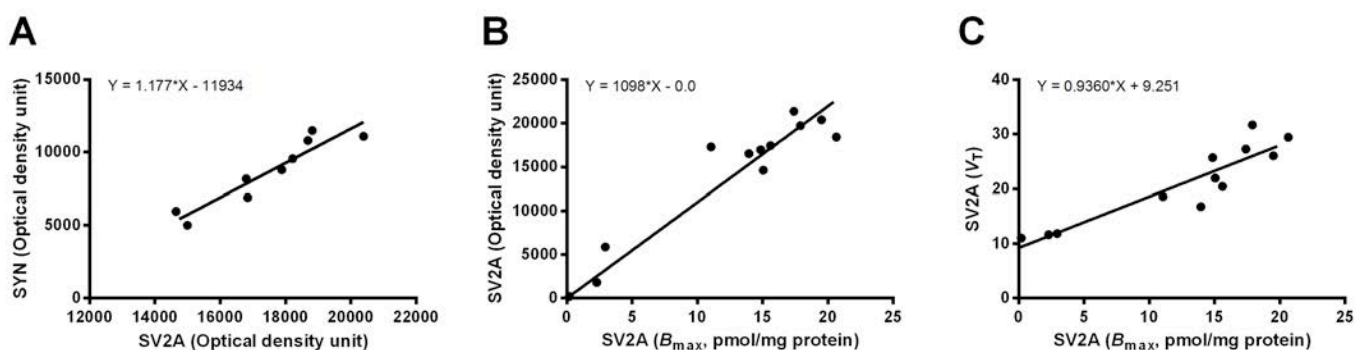
Simultaneous PET and microdialysis for estimation of unbound drug concentrations in brain

Sofia Gustafsson[1], Jonas Eriksson[2], Olof Eriksson[2], Margareta Hammarlund-Udenaes[1], Gunnar Antoni[2], Stina Syvänen[3]

[1]Department of Pharmaceutical Biosciences, Translational PKPD, Uppsala University, Uppsala, Sweden,
[2]Department of Medicinal Chemistry; Preclinical PET Platform, Uppsala University, Uppsala, Sweden,
[3]Department of Public Health and Caring Sciences, Uppsala University, Uppsala, Sweden

Background and Aim: Methods to investigate drug concentrations in the human brain are highly limited. Hence, there is a need to optimize the read-out of techniques like PET, with high translational applicability from rodents to man for studying neuropharmacokinetics, especially in the early development of drugs aimed for targets within the central nervous system. Both bound and free radioligand, as well as radiolabelled metabolites contributes to the PET signal. However, according to the free drug hypothesis, it is the unbound drug concentration that drives the pharmacodynamics. The aim of the present study was to investigate the possibility of translating total concentrations, obtained by small-animal PET imaging, to unbound concentrations, resembling those measured in the interstitial fluid by simultaneous microdialysis sampling.

Methods: Simultaneous PET scanning and microdialysis sampling was performed in rats throughout a 60 min infusion of [N-m$ethyl$-^{11}C]oxycodone in combination with isotopically unmodified oxycodone and during a 60 min follow up period after the end of infusion. The acquired PET concentrations were converted into unbound concentrations by compensating for brain tissue binding and brain intracellular distribution, using the unbound volume of distribution in brain ($V_{u,brain}$), and compared to microdialysis measurements of unbound concentrations. The PET scanning protocol was also repeated with two potential metabolites, [^{11}C]carbon dioxide and [^{11}C]formaldehyde.

Results: A good congruence between PET data acquired with [N-m$ethyl$-^{11}C]oxycodone corrected for intracellular distribution and microdialysis measurements of oxycodone was observed throughout the infusion (0-60 min). However, an accumulating divergence between the two methods was observed and got more pronounced during the elimination phase (60-120 min), most likely due to the accumulation of radiolabeled metabolites. It was also shown that after 60 min of [^{11}C]carbon dioxide and [^{11}C]formaldehyde infusion, the brain-to-blood radioactivity concentration ratio was 1.0 and 1.5, respectively, strongly indicating their significant contribution to the measured PET signal.

Conclusion: In conclusion, the study showed that PET can be used in combination with *in vivo* determined $V_{u,brain}$ to translate non-invasively measured total drug concentrations into pharmacologically active unbound concentrations as long as the study is designed to avoid a large contribution of radiolabeled metabolites, for example using a continuous infusion of the radiolabeled drug.
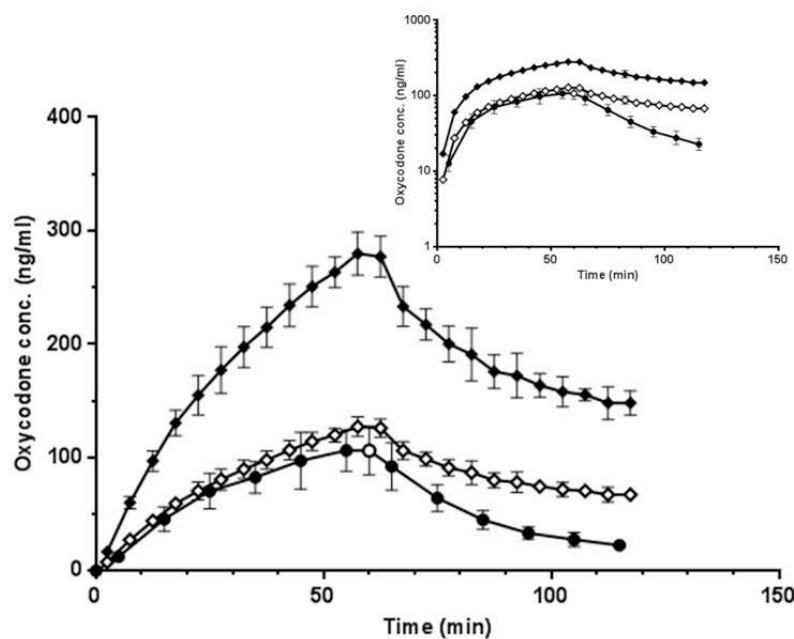
Concentration-time profiles of oxycodone total PET concentrations (filled diamonds), $V_{u,brain}$ transformed PET concentrations (open diamonds) and unbound microdialysis concentrations (filled circles) in rats receiving a 60 min constant rate infusion of [N-methyl-^{11}C]oxycodone in combination with a therapeutic dose of oxycodone, in the combined PET and microdialysis experiment (n=4). The linear graph illustrates the time dependent deviation between the microdialysis and PET unbound drug concentrations in brain and the logarithmic graph (insert) more clearly shows the half-life differences of PET and microdialysis data during the elimination phase. The data is presented as mean ± S.D.

[^{18}F]JNJ42259152 binding to PDE10A is altered in the presence of cyclic AMP

Maarten Ooms[1], Sofie Celen[1], Alfons Verbruggen[1], Koen Van Laere[2], Guy Bormans[1]

[1]*Laboratory for Radiopharmacy, KU Leuven, Belgium,* [2]*Division of Nuclear Medicine, KU Leuven and University Hospital Leuven, Belgium*

Objectives: PDE10A is an enzyme which is responsible for the hydrolysis of cAMP and cGMP. The enzyme is uniquely distributed with predominant expression in the medium spiny neurons of striatum. Since PDE10A regulates excitability of these dopaminergic neurons it plays an important role in the regulation of motor, reward and cognitive processes. Despite the interest in PDE10A as a drug and PET imaging target, not much is known about the regulation of PDE10A enzyme activity. Several contradictory reports have been published about the activation of PDE10A by cAMP. In order to clarify these contradictions, we aimed to further investigate the role of cAMP in the regulation of PDE10A activity and PDE10A PET imaging. Here, we used the PET radioligand [^{18}F]JNJ42259152, to investigate alterations in PDE10A binding secondary to changes in cAMP levels.

Materials & Methods: A striatum homogenate binding assay was developed to determine K_D and B_{max} of [^{18}F]JNJ42259152 *in vitro*. Homogenate binding was assessed in the presence of increasing concentrations of cAMP (0, 1, 10 and 100 μM). *In vivo* alterations in striatal cAMP levels in rats were induced by single dose injections with JNJ49137530 (10 mg/kg) or rolipram (10 mg/kg), selective inhibitors of PDE2 and PDE4 respectively. The effect of the induced cAMP alterations on PDE10A binding was assessed by comparing [^{18}F]JNJ42259152 microPET studies after treatment to [^{18}F]JNJ42259152 microPET studies acquired at baseline conditions prior to treatment.

Results: *In vitro* binding affinity of [^{18}F]JNJ42259152 was higher in the presence of cAMP compared to baseline conditions (K_D = 3.17 ± 0.91 nM with 10μM cAMP versus K_D = 6.62 ± 0.7 nM at baseline). No significant changes in B_{max} values could be detected in the presence of different concentrations of cAMP. Inhibition of PDE4 using rolipram significantly increased [^{18}F]JNJ42259152 binding 5 and 60 min after rolipram administration. Additionally, administration of JNJ49137530 significantly increased PDE10A binding potential (BP_{ND} = 2.74 ± 0.22 versus 2.05 ± 0.16 at baseline).

Conclusions: We successfully evaluated the effect of alterations in cAMP levels on [^{18}F]JNJ42259152 binding to PDE10A. In vitro striatum homogenate binding showed increased affinity of [^{18}F]JNJ42259152 for PDE10A in the presence of cAMP, suggesting a role for cAMP in the allosteric regulation of PDE10A. In vivo inhibition of PDE2 and PDE4 significantly increased [^{18}F]JNJ42259152 binding potentials. This further adds proof to the hypothesis that cAMP stimulates PDE10A activity. Finally, our data show a profound interaction between several PDEs in striatum. Further structural analysis of activated and native state PDE10A will be needed to fully confirm the mechanism of the activation by cAMP.

Baseline

BP$_{ND}$

0   3.5

Rolipram
5 min prior

O-043
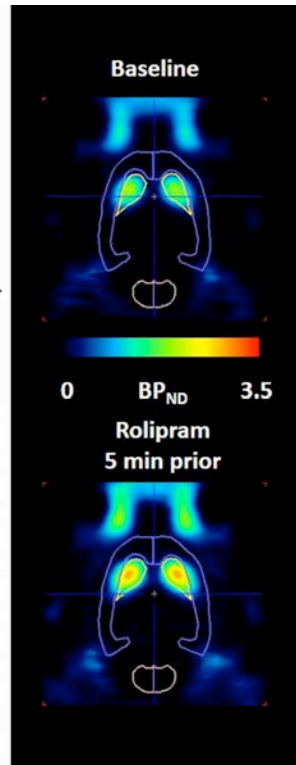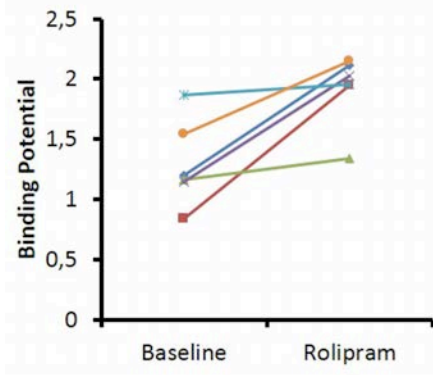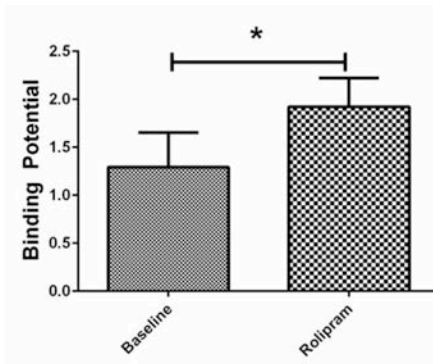
PET/fMRI imaging of inhibitory and excitatory signaling in the serotonin receptor system

EE Verwer[1], DW Wooten[1], JB Mandeville[2], NJ Guehl[1], Y Petibon[1], JM Hooker[2], G El Fakhri[1], NM Alpert[1], MD Normandin[1]

[1]Gordon Center for Molecular Imaging, Massachusetts General Hospital / Harvard Medical School, Boston, MA, USA, [2]A.A. Martinos Center for Biomedical Imaging, Massachusetts General Hospital, Charlestown, MA, USA

Introduction: Simultaneous PET/MR imaging allows for concurrent measurement of receptor occupancy (with PET) and neurovascular response (with fMRI) and thereby yields complementary information that can aid in investigating receptor systems and characterizing novel drugs. We recently demonstrated the utility of this paradigm in concurrent PET/fMRI studies involving administration of dopamine receptor agonists and antagonists. In the current study, we use PET/fMRI to examine the effect of agonist and antagonist drugs on the serotonin (aka 5-hydroxytryptamine, or 5-HT) system, in particular investigating the prominent 5-HT_{1A} and 5-HT_{2A} receptor subtypes. We hypothesize that agonist drugs targeting the excitatory 5-HT_{2A} receptor should raise metabolic demand and consequently lead to increases in CBV, whereas those targeting the inhibitory 5-HT_{1A} receptor should reduce metabolic demand leading to decreases in CBV, and vice versa for antagonist drugs.

Methods: Sixteen scans were obtained from two rhesus macaques on a simultaneous PET/MR system. For studies of 5-HT_{1A} using the agonist 8-OH-DPAT (2 mg/kg; dosage previously shown to produce ~75% receptor occupancy (*1*)) or antagonist mefway (10 μg/kg; dosage previously shown to produce >90% receptor occupancy (*2*)), fMRI data were acquired with iron oxide contrast enhanced echo-planar imaging to assess change in CBV. For studies using the 5-HT_{2A} agonists NBOH-2C-CN and DOI (10-50 μg/kg) or antagonist MDL100907 (10 μg/kg), simultaneous fMRI and [^{11}C]MDL100907 PET imaging was performed to assess change in CBV and receptor occupancy, respectively. For the antagonist drugs data were also acquired under conditions of elevated serotonin levels, achieved by administering the antagonist 30 min after i.v. fenfluramine (5 mg/kg over 5 min). These studies were performed because the functional response to antagonist drugs depends on the amount of endogenous serotonin signaling available to attenuate. If endogenous serotonin is low this may impose a floor effect impeding detection of the antagonist-induced response.

Results: The 5-HT_{1A} agonist 8-OH-DPAT caused strong cortical *decreases* in CBV (>20%; peak response), whilst the 5-HT_{1A} antagonist mefway *increased* CBV (>8%) under conditions of elevated endogenous serotonin levels. The 5-HT_{2A} agonists DOI and NBOH-2C-CN caused strong cortical *increases* in CBV (>30%), even at low receptor occupancies (<23%), whilst the antagonist MDL100907 *decreased* CBV (>10%) at PET measured occupancy >90%. At normal endogenous serotonin levels, none of the antagonists produced measurable changes in CBV despite near saturation of receptors. Patterns of CBV responses across the brain were generally in very good agreement with the spatial distribution of the receptors targeted by the challenge drug.

Conclusions: Our findings are in agreement with predictions regarding the receptor subtypes. Even at low occupancies, the 5-HT_{2A} agonists caused a strong excitatory response, whilst the 5-HT_{1A} agonist elicited a strong inhibitory response. The opposite was observed for the antagonists, despite near saturating occupancies, but only at elevated endogenous serotonin levels. This suggests that the fMRI response they elicit is from competing serotonin away from the receptor. These findings support the validity of using simultaneous PET/fMRI imaging to model pharmacological action in the serotonergic system in future studies.

References:
1. Milak MS, Severance AJ, Ogden RT, et al. Modeling considerations for 11C-CUMI-101, an agonist radiotracer for imaging serotonin 1A receptor in vivo with PET. J Nucl Med. 2008;49:587-596. 2. Wooten DW, Hillmer AT, Moirano JM, et al. Measurement of 5-HT(1A) receptor density and in-vivo binding parameters of [(18)F]mefway in the nonhuman primate. J Cereb Blood Flow Metab. 2012;32:1546-1558.
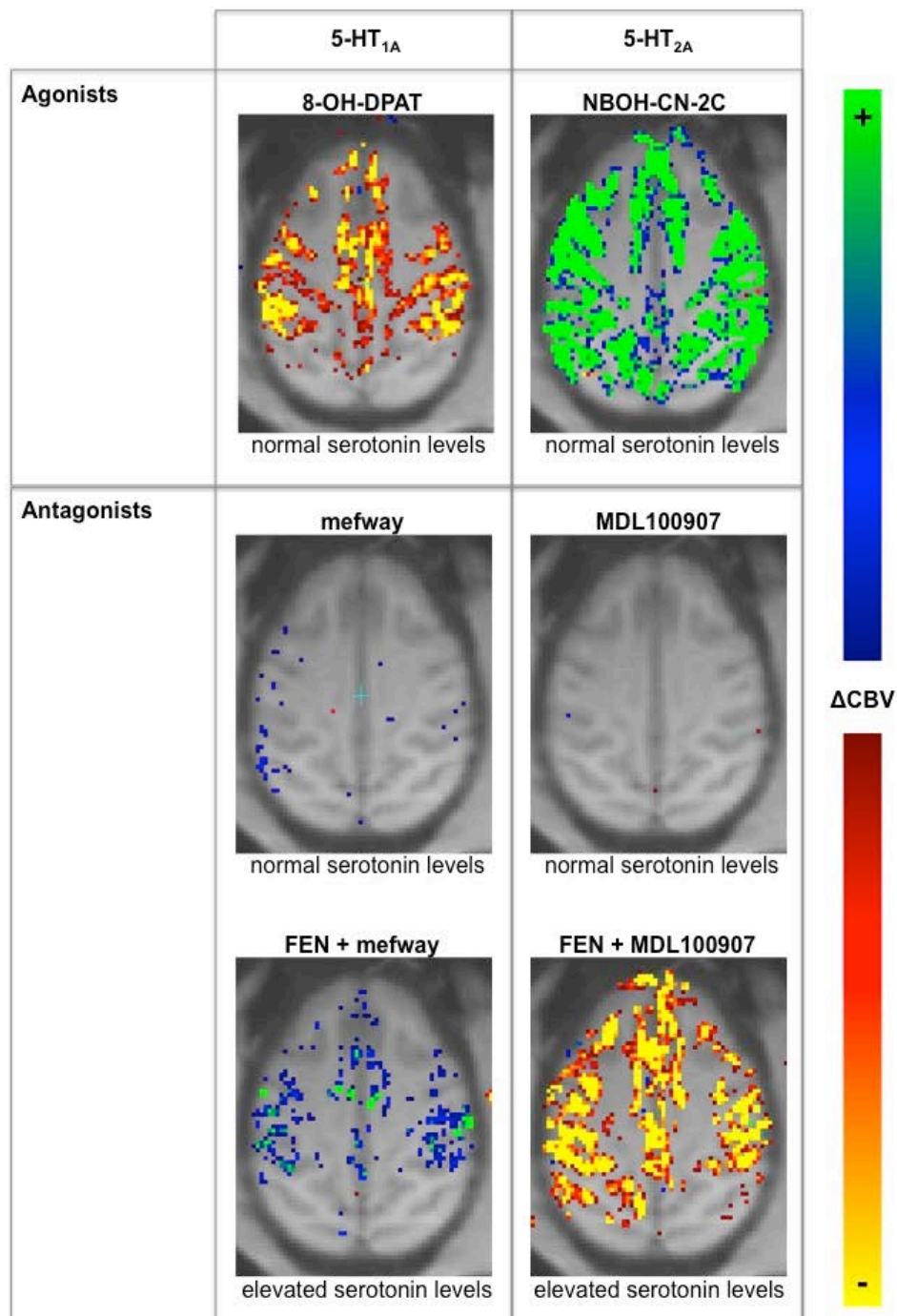
Figure 1. CBV response due to inhibitory 5-HT$_{1A}$ (left) and excitatory 5-HT$_{2A}$ (right) receptors stimulated by receptor subtype-specific agonist and antagonist drugs. Antagonist drug response was assayed under both normal and elevated endogenous serotonin levels, the latter achieved by administering fenfluramine (FEN).

Pharmacological functionality of 5-HT1BR compounds can be measured with simultaneous PET-MR

Hanne D. Hansen[1], Christin Y. Sander[2], Jacob Hooker[2], Bruce Rosen[2], Joseph Mandeville[2], Gitte M. Knudsen[1]

[1]Neurobiology Research Unit and NeuroPharm, Copenhagen University Hospital, Rigshospitalet, Copenhagen, Denmark, [2]A.A. Martinos Center for Biomedical Imaging, Massachusetts General Hospital, Charlestown, MA, USA

Rationale: Pharmacological functional MRI (phMRI) studies can make a significant contribution to our understanding of drug-effects on brain functions. Combining phMRI with the molecular specificity of PET provides the means for investigating occupancy and efficacy of drugs simultaneously. Here, we explore the concept of using simultaneous PET-MR for evaluation of drug function using the 5-HT_{1B} receptor specific partial agonist (AZ10419369)[1] and antagonist (GR127935)[2] as our pharmacological tools.

Methods: Three rhesus macaque monkeys underwent simultaneous PET/MR (Siemens Trio-3T with BrainPET insert) imaging with [^{11}C]AZ10419369 administered as bolus-infusion. Experiments were performed with within-scan challenges of cold AZ10419369 (0.88-36.2 µg/kg, n=9) or GR127935 (200 µg/kg, n=2). Relative changes in cerebral blood volume (CBV) were measured with 2D echo-planar imaging after injection of an iron oxide contrast agent. After radioligand injection, simultaneous PET and fMRI were acquired for 120 minutes. PET data were analyzed using ESRTM[3], and occupancy was measured as the relative difference between the BP_{ND} before and after the pharmacological challenge.

Results: Following the administration of different doses of the partial agonist AZ10419369 at 57 ± 7.4 min after the injection of the radioligand, a dose-dependent decrease in BP_{ND} in the occipital cortex (5-HT_{1B}R high binding region) was measured. The associated and simultaneously measured CBV changes in the occipital cortex were biphasic in shape, with a short decrease in CBV followed by a prolonged increase in CBV. The changes in CBV were strongest in 5-HT_{1B}R rich regions such as the occipital cortex and the basal ganglia, however strong changes were also observed in the thalamus, suggesting functional connectivity between the regions. The positive change in CBV, adjusted for the animals' age-decreasing BP_{ND}, also showed dose-dependency (Figure 1). By contrast, although administration of the antagonist GR127935 resulted in high 5-HT_{1B}R occupancy (53 and 72 %, n=2), CBV changes were not detected. When we pre-administrated either GR127935 (200 µg/kg, n=2) or AZ10419369 (36.2 µg/kg, n=1) leading to approximately 70 % occupancy, CBV changes elicited by the partial agonist (AZ10419369, 5 µg/kg) 60 min later were substantially diminished. That is, pharmacological blockade of 5-HT_{1B}R impaired the agonist-induced CBV response

Conclusion: We here show that 5-HT_{1B}R acting drugs with pharmacologically distinct characteristics elicit specific profiles in the brain's hemodynamic response. This approach can probably be applied to other systems including, e.g., enzymatic activity or other neurotransmitter systems. Combined simultaneous PET-MRI opens for the possibility of testing novel drug compounds for their blood-brain barrier passage, their brain occupancy and their functionality, based upon the hemodynamic response.

References:
1. Maier, D.L*., et al.* [N-methyl-3H3]AZ10419369 binding to the 5-HT1B receptor: in vitro characterization and in vivo receptor occupancy. *J Pharmacol Exp Ther* **330**, 342-351 (2009). 2. Skingle, M*., et al.* GR127935: a potent and selective 5-HT1D receptor antagonist. *Behav Brain Res* **73**, 157-161 (1996). 3. Zhou, Y*., et al.* An extended simplified reference tissue model for the quantification of dynamic PET with amphetamine challenge. *Neuroimage* **33**, 550-563 (2006).
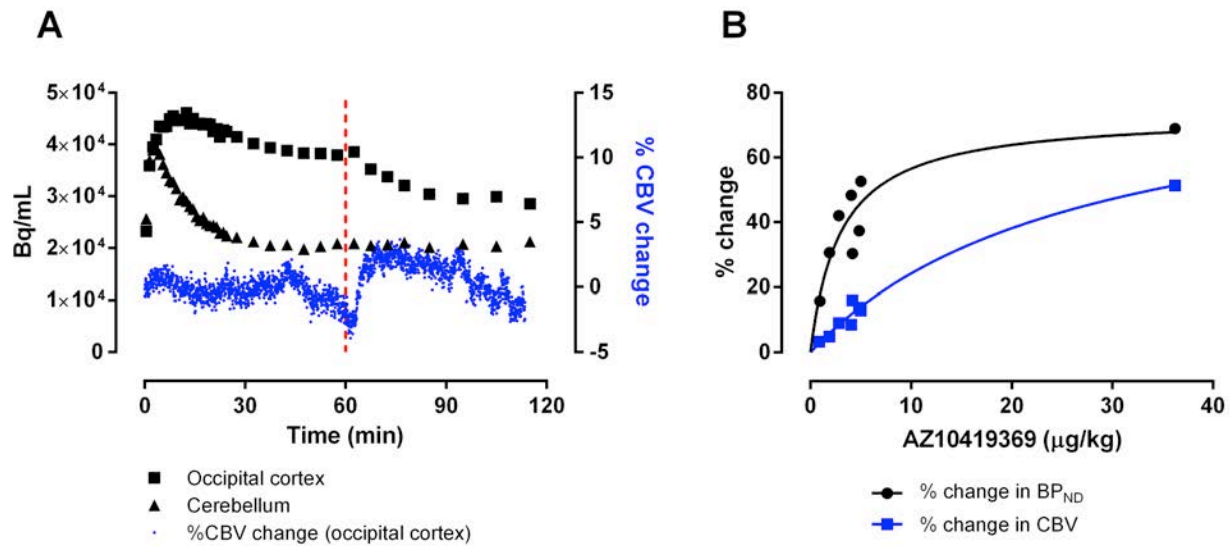
Figure 1: A) Time-activity curves of [^{11}C]AZ10419369 in the occipital cortex and cerebellum (black symbols) and for the changes in CBV (blue symbols). A within-scan challenge of AZ10419369 (5 µg/kg) was given 60 min after radioligand injection (red line). **B)** Quantified % changes in BP$_{ND}$ (black) and CBV (blue) in the occipital cortex for different doses of AZ10419369.

Imaging the imidazoline2 binding site with the novel PET ligand ^{11}C-BU99008 in humans: pharmacological characterisation

RJ Tyacke[1], J Myers[1], S Turton[1], A Venkataraman[1], I Mick[1], J Ramada-Magalhaes[2], H Chong[2], S Mos[2], J Passschier[2], EA Rabiner[2,3], RN Gunn[2,4], CA Parker[1,5] and DJ Nutt[1]

[1]Centre for Neuropsychopharmacology, Division of Brain Sciences, Imperial College London, UK, [2]Imanova Ltd, London, UK, [3]Centre for Neuroimaging Sciences, King's College, London, UK, [4]Centre for Restorative Neuroscience, Division of Brain Sciences, Imperial College London, UK, [5]Experimental Medicine Imaging, GlaxoSmithKline, UK

The density of the Imidazoline$_2$ binding sites (I$_2$BS) is changed in variety of neuropsychiatric disorders[1].   I$_2$BS are thought to be mainly located on glial cells and are implicated in the regulation of glial fibrillary acidic protein (GFAP)[2]. This has prompted interest in I$_2$BS and Imidazoline$_2$ ligands in neurodegenerative and neuroinflammatory conditions where glia function is altered (e.g. Alzheimer's Disease, Glial Tumors and Parkinson's Disease.   The development of a positron emission tomography (PET) ligand for these sites would prove valuable in the understanding of such disorders. We have previously identified and evaluated ^{11}C-BU99008 as a putative I$_2$BS PET ligand in preclinical species [3,4].   We present the first *in vivo* evaluation and characterisation of this ligand in healthy human volunteers using competition experiments to determine ^{11}C-BU99008 specificity and selectivity.

Methods: Dynamic PET imaging with arterial blood sampling was performed in 8 healthy male volunteers (age 52±8). Each subject had either 2 or 3 PET scans including a baseline (n=8), post dosing with the mixed I$_2$BS/α_2-adrenoceptor drug, Idazoxan (n=8; 20, 40, 60 and 80mg) and post dosing with the mixed irreversible MAO$_{A/B}$ inhibitor, Isocarboxazid (n=4; 50mg). PET scans were acquired for 120 min on a Siemens PET Biograph and reconstructed into 29 frames (8x15, 3x60, 5x120, 5x300, 7x600 s) using filtered back-projection. Dynamic images were corrected for motion using a mutual information co-registration algorithm with frame 16 as the reference. Associated T1 MRI data enabled nonlinear registration of the CIC atlas generation of regional time-activity data. The 2-tissue compartmental was identified as the most appropriate model (see Myers, et al., this meeting) and used to derive regional volumes of distribution (V$_T$) estimates. All image processing and kinetic analysis was performed in MIAKAT™ (www.miakat.org). Competition data were analysed using the occupancy plot to derive non-displaceable and specific binding.

Results: Brain uptake of ^{11}C-BU99008 was good with reversible kinetics and a heterogeneous distribution consistent with known I$_2$BS expression.   The regional uptake in humans correlated well to that seen pre-clinically in pig[3] (r=0.70; P<0.05) and primate[4] (r=0.84; P<0.05).   Uptake was highest in: nucleus accumbens (128.5 mL·cm^{-3}), globus pallidus (122.2 mL·cm^{-3}) and striatum (107.4 mL·cm^{-3}); intermediate in the insular cortex (63.9 mL·cm^{-3}), and cingulate cortex (61.5 mL·cm^{-3}); and lowest in the occipital cortex (50.4 mL·cm^{-3}) and cerebellum (44.6 mL·cm^{-3}). The uptake was dose-dependently reduced by pre-treatment with Idazoxan throughout the brain, with an average block across all regions of ~60% (V$_T$ = ~30 mL·cm^{-3}) at the highest dose (80 mg). These data indicate that there is no suitable reference tissue for this ligand. Non-displaceable distribution volume was calculated as 20.8±11.8 mL·cm^{-3}, and BP$_{ND}$ therefore varied between 1 and 6 in the target regions. The ED$_{50}$ for Idazoxan was calculated as 33.1 mg. Uptake was not blocked by pre-treatment with the MAO inhibitor, Isocarboxazid.

Conclusions: These data show that ^{11}C-BU99008 is a selective and reproducible PET ligand for the study of the I$_2$BS in vivo in humans.

References:
1. Garcia-Sevilla, J.A., P.V. Escriba, and J. Guimon, Imidazoline receptors and human brain disorders. Ann N Y Acad Sci, 1999. **881**: p. 392-409. 2. Olmos, G., et al., The effects of chronic imidazoline drug treatment on glial fibrillary acidic protein concentrations in rat brain. Br J Pharmacol, 1994. **111**(4): p. 997-1002. 3. Kealey, S., et al., Imaging imidazoline-I2 binding sites in porcine brain using

11C-BU99008. J Nucl Med, 2013. **54**(1): p. 139-44. 4. Parker, C.A., et al., Evaluation of 11C-BU99008, a PET Ligand for the Imidazoline2 Binding Sites in Rhesus Brain. J Nucl Med, 2014. **55**(5): p. 838-44.
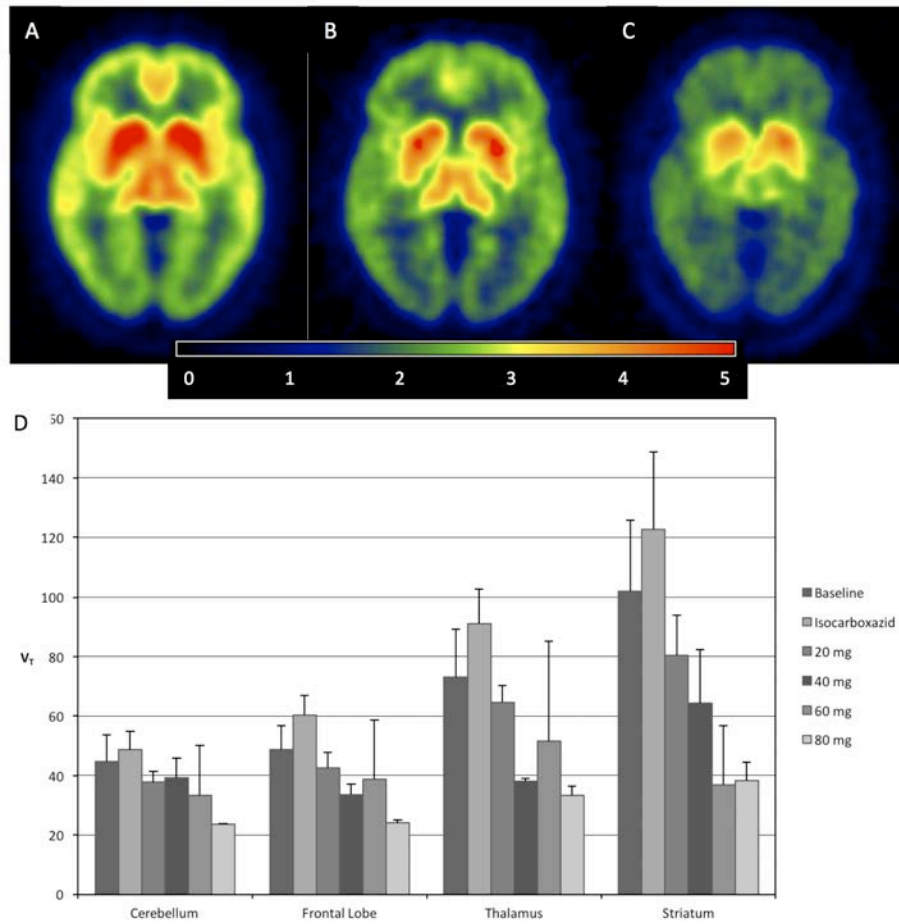
SUV Images of ^{11}C-BU99008 in human brain. Panel A: baseline uptake, panel B: reduction in binding post low dose Idazoxan (20mg) and panel C: high dose of Idazoxan (80mg). Panel D shows the dose-dependent reduction in V_T after competition with Idazoxan and no change following dosing with Isocarboxazid.

Glycine transporter 1 occupancy by PF-03463275 in healthy and schizophrenia subjects measured with ^{18}F-CFPyPB PET imaging

Mika Naganawa[1], Mohini Ranganathan[2], Nabeel Nabulsi[1], Ming-Qiang Zheng[1], Shu-Fei Lin[1], Yiyun Huang[1], John H. Krystal[2], Deepak Cyril D'Souza[2], Richard E. Carson[1]

[1]PET Center, Yale University, New Haven, CT, USA , [2]Department of Psychiatry, Yale University, New Haven, CT, USA

Objectives: Deficits in *N*-methyl-*D*-aspartate (NMDA) function are thought to contribute to cognitive impairments in schizophrenia (SZ). Enhancing NMDA receptor (NMDA-R) function via the glycine site may reduce cognitive deficits. Glycine transporter-1 (GlyT1) inhibitors raise glycine levels, increasing occupancy at the high-affinity co-agonist site of NMDA-R and enhance NMDA-R function. The purposes of this study were to 1) develop modeling methodology for the GlyT1 tracer ^{18}F-CFPyPB (aka ^{18}F-MK6577) and 2) characterize the relationship between the dose/blood level of the GlyT1 inhibitor PF-03463275 and brain GlyT1 occupancy (TO) in healthy control (HC) and SZ subjects.

Methods: Subjects (13 HC and 20 SZ) were assigned to 4 treatment groups based on a combination of placebo and 1 or 2 selected doses (10, 20, 40, and 60 mg). Subjects received PF-03463275 or placebo twice daily for 7 days in a double-blind randomized manner. On day 6 of each period, each subject underwent a PET scan with ^{18}F-CFPyPB (176±10 MBq) on the HRRT with metabolite-corrected input function measurement. Regional time-activity curves (TACs) were generated for 13 regions of interest (ROIs). Kinetic analysis of 90-min TACs was performed with one-tissue and two-tissue compartment models (1TC, 2TC) and multilinear analysis-1 (MA1) to quantify distribution volume (V_T). TO was calculated using the occupancy plot. For the subjects without V_T values at a placebo scan (due to a lack of blood data), the extension of the occupancy plot was applied, by comparing two scans at different occupancies with the dose normalized by body weight or drug concentration. Two occupancy plots for each subject were simultaneously calculated with a common V_{ND}. ID_{50} and IC_{50} were calculated using a single-site occupancy model.

Results: The MA1 model adequately described regional TACs and produced stable kinetic parameters. In the placebo scans, regional V_T (mL/cm^3) values were highest in the pons, midbrain, and cerebellum white matter (4.3-5.0) and lowest in cortical regions (1.9-2.0) and caudate (1.9). The SZ group showed 8% higher V_T values than the HC group, but the differences were not statistically significant. Dose-dependent reductions in V_T values were observed in all regions. The average V_{ND} estimate was 0.84 mL/cm^3, and BP_{ND} values ranged from 1.1 to 4.7. The relationship between the normalized dose and TO exhibited an ID_{50} (mg/kg) of 0.26, 0.38, and 0.18 for all subjects, HC, and SZ, respectively (Figure 1). The IC_{50} values (ng/mL) estimated from a relationship between drug levels and TOs were 12.3, 13.6, and 10.8 for all subjects, HC, and SZ, respectively (Figure 1). While the ID_{50} value from HC group was significantly higher than that from SZ group (P=0.0004), IC_{50} values were not significantly different (P=0.19), which suggests that discrepant occupancy levels between HC and SZ groups resulted from the differences in plasma PF-03463275 concentrations.

Conclusions: ^{18}F-CFPyPB kinetics are described well by MA1, and V_T values were reduced by PF-03463275 in a dose-dependent manner. At the same dose level, the SZ group displayed a higher occupancy than the HC groups, which is attributed to the differences in plasma drug concentrations between the groups.
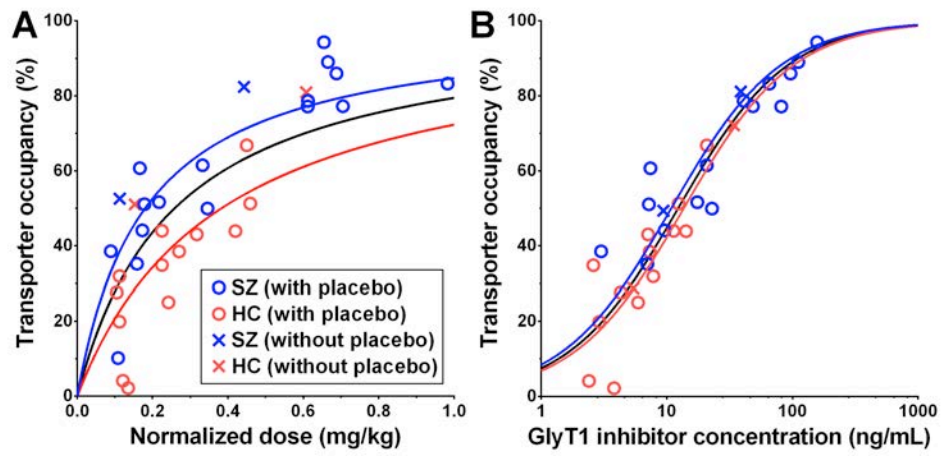
Figure 1: Relationship between transporter occupancy and inhibitor (A) dose and (B) concentration. The symbols of circles and crosses indicate the transporter occupancy estimated with and without a placebo scan, respectively. Three fits are shown: all subjects (black curve), schizophrenia subjects (blue curve), and healthy controls (red curve).

Decreased extra-striatal dopamine D2 receptor availability over human adulthood using [^{11}C]-FLB457

Vijay A[1], Crawford J[1], Seaman K[1], Morris ED[1], Samanez-Larkin G[1]

[1] Yale University, New Haven, CT, USA

Objectives: The effect of aging on dopamine receptor density has been well-characterized (1, 2), primarily in the striatum (3-5). Aging has been shown to impact dopaminergic function and dopamine decline in the striatum has been associated with poorer processing speed and cognitive task performance (6). However, execution of these tasks relies on cortical and frontostriatal regions of the brain and very few studies have measured cortical dopamine across adulthood. To image dopamine receptors in extrastriatal regions with PET, one must employ a high affinity tracer. Our goal in the present study was to use PET with the high affinity dopamine tracer, [^{11}C]-FLB457, to evaluate age effects on dopamine receptor availability in adult humans, *in vivo*, in 12 extra-striatal regions of interest (ROI).

Methods: 11 human subjects aged from 28 to 74 (6 males, 5 females) were scanned on the Siemens High Resolution Research Tomograph (HRRT) with [^{11}C]-FLB457, a high-affinity D2 receptor ligand (8). Tracer was administered as a bolus (8.94 ± 1.77 mCi) and data were acquired dynamically for 90 min. Partial volume correction was applied to all PET images (9). Time-activity curves were extracted for extra-striatal regions and data were fitted with the simplified reference tissue model (SRTM) using the cerebellum as the reference region to obtain regional binding potential (BP_{ND}). Regional BP_{ND} values were compared across age cohorts.

Results: BP_{ND} values in all extra-striatal regions showed a decrease of [^{11}C]-FLB BP_{ND} with age. The decrease of D2 receptor binding was 11% [r = -0.82, p<0.002] per decade in the thalamus, 9% in the ventromedial prefrontal cortex [r = -0.50], 8% in anterior cingulate[r = -0.40], hippocampus [r = -0.43] and orbitofrontal cortex [r = -0.52], 7% [r = -0.44] in temporal cortex, superior lateral frontal gyri (LFG) [r = -0.42] and inferior LFG [r = -0.44], 6% [r = -0.35] in parietal cortex, and 5% [r = -0.35] in the amygdala and medial LFG [r = -0.35].

Conclusions: This reports demonstrates a consistent decline of D2 receptor availability with increasing age in extrastriatal regions. The decline in the thalamus reached significance. Previous studies have shown a similar decline of dopamine receptors with age in extra-striatal regions using FLB. These previous studies, however, examined a smaller range of ROIs. Our findings are preliminary steps in understanding the effects of age-related changes in the dopamine system on key cortical fronto-striatal functions such as cognition, motivation and decision making.

References:
1. Inoue M, Suhara T, Sudo Y, Okubo Y, Yasuno F, Kishimoto T, et al. (2001): Age-related reduction of extrastriatal dopamine D 2 receptor measured by PET. Life sciences. 69:1079-1084.
2. Kaasinen V, Vilkman H, Hietala J, Någren K, Helenius H, Olsson H, et al. (2000): Age-related dopamine D2/D3 receptor loss in extrastriatal regions of the human brain. Neurobiology of aging. 21:683-688.
3. Rinne JO, Hietala J, Ruotsalainen U, Säkö E, Laihinen A, Någren K, et al. (1993): Decrease in human striatal dopamine D2 receptor density with age: a PET study with [11C] raclopride. Journal of Cerebral Blood Flow & Metabolism. 13:310-314.
4. Ishibashi K, Ishii K, Oda K, Kawasaki K, Mizusawa H, Ishiwata K (2009): Regional analysis of age-related decline in dopamine transporters and dopamine D2-like receptors in human striatum. Synapse. 63:282-290.
5. Wang Y, Chan GL, Holden JE, Dobko T, Mak E, Schulzer M, et al. (1998): Age-dependent decline of dopamine D1 receptors in human brain: A PET study. Synapse. 30:56-61.
6. manLars B□, Ginovart N, Dixon RA, Wahlin T-BR, Wahlin ī, Halldin C, et al. (2000): Age-related cognitive deficits mediated by changes in the striatal dopamine system. American Journal of Psychiatry. 157:635-637.
7. Delforge J, Bottlaender M, Loc'h C, Guenther I, Fuseau C, Bendriem B, et al. (1999): Quantitation of extrastriatal D2 receptors using a very high-affinity ligand (FLB 457) and the multi-injection approach. Journal of Cerebral Blood Flow & Metabolism. 19:533-546.
8. Giovacchini G, Lerner A, Toczek MT, Fraser C, Ma K, DeMar JC, et al. (2004): Brain incorporation of 11C-arachidonic acid, blood volume, and blood flow in healthy aging: a study with partial-volume correction. Journal of Nuclear Medicine. 45:1471-1479.

Figure 1. Normalized BP_{ND} versus age for three regions of interest. The decrease of BP_{ND} with age in the thalamus is significant.

P-002
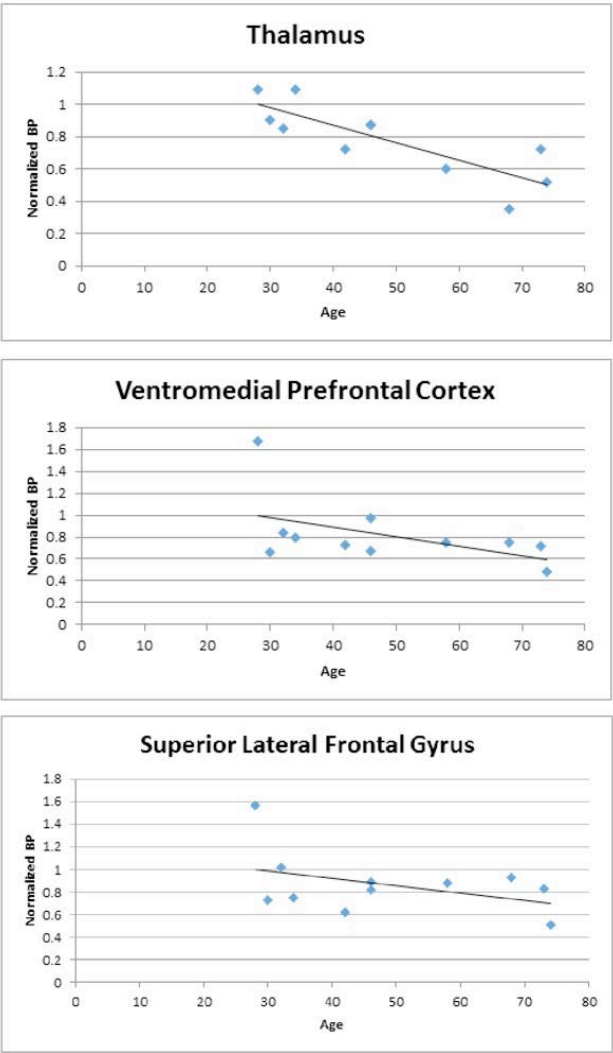
Effects of sex hormone treatment on olfactory perception and serotonergic neurotransmission

Kranz GS[1], Kaufmann U[2], Mitterhauser M[3], Vanicek T[1], Hienert M[1], Gryglewski G[1], Nics L[3], Vraka C[3], Wadsak W[3], Kasper S[1], Lanzenberger R[1]

[1]Department of Psychiatry and Psychotherapy, [2]Department of Obstetrics and Gynecology, [3]Department of Biomedical Imaging and Image-guided Therapy, Division of Nuclear Medicine, Medical University of Vienna, Austria

Introduction: Evidence suggests that women outperform men in core aspects of odor perception [1]. While sex hormones are discussed in moderating this effect, studies provided conflicting results so far. Research in rodents unveiled the mechanisms by which serotonin controls the processing of olfactory information [2]. Moreover, serotonergic neurotransmission is modulated by sex hormones, as indicated by positron emission tomography (PET) [3]. Here, our aim was to explore the effects of sex hormone treatment in female-to-male (FtM) and male-to-female (MtF) transsexuals and the association between serotonin transporter (5-HTT) binding, a marker of serotonin transmission, and odor perception.

Methods: 13 FtM and 19 MtF transsexuals of whom data were already published elsewhere [3, 4] were measured before start of hormone treatment, after one, and after four months of treatment start. FtM received testosterone undecanoate (and in two cases additionally lynestrenol). MtF received either cyproterone acetate (14 participants) or triptorelin acetate (4 participants). Additionally they received estradiol either transdermally or oral. PET measurements were performed using a GE Advance full-ring scanner in 3D mode. Dynamic PET scans started simultaneously with a bolus injection of [^{11}C]DASB measuring brain radioactivity in a series of 50 consecutive time frames. The non-displaceable binding potential (BP$_{ND}$) [5] was quantified using the multilinear reference tissue model in six ROIs and the cerebellar gray matter as reference region. The Sniffin' Sticks test battery was used to measure olfactory perception at the day of each PET scan. The battery consists of three subtests to measure absolute odor sensitivity, odor discrimination and odor identification.

Results: Results revealed higher odor sensitivity in FtM compared to MtF transsexuals (main effect of group, F=8.47, p=0.005; linear mixed models analysis). There was no effect of hormone treatment on odor perception in both groups (main effect of time, p>0.05) and no interactions between group and time (p>0.05). However, odor sensitivity correlated positively with free estradiol index in MtF transsexuals at baseline (r=0.63, p=0.024) and odor identification correlated negatively with free androgen index after one (r=-0.91, p=0.012) and four months (r=-0.84, p=0.018) of testosterone treatment in FtM transsexuals. Moreover, positive correlations between regional 5-HTT binding and odor perception were present after one month of hormone treatment in MtF transsexuals (olfactory cortex, r=0.71, p=0.018; orbitofrontal cortex, r=0.71, p=0.018; hippocampus, r=0.745, p=0.006).

Conclusion: This study is the first to investigate the effects of high-dose cross sex hormone treatment in transsexuals on odor perception and the relationship between serotonergic neurotransmission and olfactory performance in humans. The study confirms higher odor perception in genetic females compared to genetic males. However, one and four months of sex hormone treatment seem to have no significant effect on olfactory perception (when investigating common odorants as used in the Sniffin' Sticks test). Still, sporadic correlations between 5-HTT binding, sex hormones and olfactory perception do not preclude a serotonergic modulation of olfactory perception and may indicate a role of serotonin in mediating the relationship between olfactory perception and hormonal fluctuations. Investigating hormone effects on olfactory perception of sex-specific biological odorants should be considered in future research.

Disclosure: The authors report no conflicts of interest

References:

1. Hummel, T., G. Kobal, H. Gudziol, and A. Mackay-Sim, Normative data for the "Sniffin' Sticks" including tests of odor identification, odor discrimination, and olfactory thresholds: an upgrade based on a group of more than 3,000 subjects. Eur Arch Otorhinolaryngol, 2007. **264**(3): p. 237-43.
2. Petzold, G.C., A. Hagiwara, and V.N. Murthy, Serotonergic modulation of odor input to the mammalian olfactory bulb. Nat Neurosci, 2009. **12**(6): p. 784-91.
3. Kranz, G.S., W. Wadsak, U. Kaufmann, M. Savli, P. Baldinger, et al., High-Dose Testosterone Treatment Increases Serotonin Transporter Binding in Transgender People. Biol Psychiatry, 2015. **78**(8): p. 525-33.
4. Kranz, G.S., A. Hahn, P. Baldinger, D. Haeusler, C. Philippe, et al., Cerebral serotonin transporter asymmetry in females, males and male-to-female transsexuals measured by PET in vivo. Brain Struct Funct, 2014. **219**(1): p. 171-83.
5. Innis, R.B., V.J. Cunningham, J. Delforge, M. Fujita, A. Gjedde, et al., Consensus nomenclature for in vivo imaging of reversibly binding radioligands. J Cereb Blood Flow Metab, 2007. **27**(9): p. 1533-9.

Tariquidar is an inhibitor and not a substrate of P-glycoprotein

Lora D. Weidner[1,3], King Leung Fung[2], Pavitra Kannan[1,3], Janna K. Moen[2], Jeyan S. Kumar[2], Jan Mulder[3], Robert B. Innis[1], Michael M. Gottesman[2], and Matthew D. Hall[2]

[1]*Molecular Imaging Branch, National Institute of Mental Health, Bethesda, Maryland, USA*; [2]*Laboratory of Cell Biology, Center for Cancer Research, National Cancer Institute, Bethesda, Maryland, USA;*[3]*Karolinska Institutet, Department of Neuroscience, Stockholm, Sweden*

Background: Since its development, tariquidar (TQR) has been widely regarded as one of the more potent inhibitors of P-glycoprotein (P-gp), an efflux transporter of the ATP-binding cassette transporter family. A third-generation inhibitor, TQR exhibits high affinity for P-gp, although it is also a substrate of another ABC transporter, breast cancer resistance protein (BCRP). Recently, the results of several rodent PET imaging studies have questioned the mechanism by which [11C]TQR interfaces with P-gp, suggesting that TQR is a substrate for P-gp instead of a noncompetitive inhibitor. Therefore, we investigated TQR and its interaction with human and mouse P-gp to determine if TQR is a substrate of P-gp *in vitro*.

Methods: We used multiple *in vitro* transporter assays including cytotoxicity, flow cytometry, accumulation, ATPase, and transwell assays in cell lines expressing human or mouse P-gp. BCRP cell lines, including a newly generated BCRP cell line for transwell assays, were used as a positive control that demonstrates TQR-mediated transport. Confocal microscopy was used to demonstrate accumulation of tariquidar in lysosomes.

Results: Cytotoxicity and flow cytometry assays proved TQR to be a potent inhibitor of both human (IC_{50} = 74 nM) and mouse (IC_{50} = 150 nM) P-gp. Accumulation assays showed increased binding of [3H]TQR to P-gp expressing cells compared to parent cells, which was reversible with the addition of 'cold' TQR. Consistent with inhibitor-like behavior, the ATPase activity of P-gp decreased with increasing concentrations of TQR. In addition, no difference was observed in the uptake of TQR in P-gp-expressing cells before and after inhibition as compared to BCRP-expressing cells. Transwell assays confirmed these findings, showing no appreciable transport of [3H]TQR across a P-gp-expressing monolayer before or after inhibition, while BCRP-mediated transport could be reversed with BCRP-specific inhibitors.

Conclusion: Based on our results, we conclude that TQR is a potent inhibitor of both human and mouse P-gp and shows no signs of being a substrate at the concentrations tested. These *in vitro* data further support our position that the *in vivo* uptake of [11C]TQR into the brain can be explained by its high affinity binding to P-gp and by it being a substrate of BCRP, followed by amplification of the brain signal by ionic trapping in acidic lysosomes. This finding is of particular importance given the use of [11C]TQR in PET studies to measure the density of P-gp *in vivo*.

P-004

In vitro equilibrium partitioning in blood cells to measure plasma free fraction of PET radioligands

Sami S. Zoghbi, Aneta Kowalski, Cheryl L. Morse, Masahiro Fujita, Victor W. Pike, Robert B. Innis

National Institutes of Health, Bethesda, MD 20892, USA

Background: Ultrafiltration is the most common method of determining plasma free fraction (f_P) for brain PET radioligands (ratio of free concentration to free plus protein-bound concentrations). This fast centrifugally-driven method separates free radioligand in plasma from that equilibrated with the protein-bound radioligand. However, ultrafiltration is vulnerable to errors when a radioligand that should have passed into the filtrate is adsorbed to some portion of the ultrafiltration apparatus. Here, we propose the use of a distinctly different 'cell method' to validate ultrafiltration f_P measurements. This method is based on that earlier developed for tritiated compounds and has been compared with results obtained from classic equilibrium dialysis (*Biopharm Drug Dispos*; **5**:281, 1984), which is often viewed as the 'gold standard' method for measuring f_P. Here we describe a novel cell method for measuring radioligand f_P that uses membranes of intact blood cells as surrogates for a synthetic dialysis membrane to equilibrate and separate free from protein-bound radioligand.

Methods: Measurements of f_P were done simultaneously for [11]C-(*R*)-rolipram, ^{11}C-PBR28, and ^{11}C-FPEB by ultrafiltration and cell method. Concentrations of the ultrafiltrates (cpm/mL) were determined volumetrically and gravimetrically. By monitoring their specific concentrations (cpm/mL), specific sites of adsorption to the ultrafiltration apparatus were localized after incubating (30 min) disassembled components of the ultrafiltration apparatus with radioligands in media that mimicked solutions produced during f_P determinations. Cell-f_P was determined in vitro by incubating whole blood and PBS-washed blood cells with radioligand in microcentrifuge tubes at room temperature until equilibration (30 min). Cell-f_P was the ratio of radioactivity concentration in buffer supernate (free) normalized by hematocrit-corrected cell partitioning to that of the normalized plasma concentration (free plus protein-bound).

Results: [11]C-(*R*)-rolipram and ^{11}C-PBR28 demonstrated minimal adsorption to the ultrafiltration apparatus, and values for f_P were similar between the two methods (^{11}C-rolipram ultrafiltration f_P 4.47±0.25 (n=3), cell-f_P 4.55±0.46 (n=3); ^{11}C-PBR28 ultrafiltration f_P 2.67±0.18 (n=3), cell-f_P 2.56±0.36 (n=3)). However, f_P values for ^{11}C-FPEB differed by 40% between the two methods (ultrafiltration f_P 5.60±0.04 (n=3), cell-f_P 8.55±0.13 (n=3)); notably, with the ultrafiltration method, 16% was due to adsorption only to the collection cup. Other adsorptive surfaces included the polycarbonate surfaces and the filter membrane, which accounted for the remaining difference of 24%. Fewer surfaces were involved in the cell method; only one type of microcentrifuge tube was used and it showed no measurable radioligand adsorption.

Conclusion: This study implemented a novel cell method – analogous to the 'gold standard' of equilibrium membrane dialysis – to quickly measure f_P for short-lived PET radioligands. Like equilibrium membrane dialysis, the cell method was less prone to misleading loss of radioligand through surface adsorption. The cell method may become the reference against which other methods are evaluated for potential confounds.

Table 1. The average ± SD (n=3) values of plasma free fraction (f_p) and their percent coefficient of variations (COV) as measured simultaneously with the ultrafiltration and cell method for nine separate participants.

Radioligand	Participant	Ultrafiltration f_P (%)	COV (%)	Cell-f_P (%)	COV (%)	Difference (%)
[11]C-(R)-Rolipram						
	A	*5.58 ± 0.48	8.6	*5.56 ± 0.27	4.9	− 0.36
	B	*3.83 ± 0.22	5.7	*4.04 ± 0.43	10.6	5.48
	C	*4.01 ± 0.06	1.5	*4.06 ± 0.67	16.5	1.25
[11]C-PBR28						
	D	*2.62 ± 0.14	5.3	*2.63 ± 0.08	3.0	0.38
	E	*2.87 ± 0.26	9.1	*2.53 ± 0.19	7.5	−11.8
	F	*2.53 ± 0.14	5.5	*2.52 ± 0.82	32.5	−0.40
[11]C-FPEB						
	G	†5.45 ± 0.04	0.7	†8.61 ± 0.08	0.9	58.0
	H	†6.36 ± 0.05	0.8	†9.20 ± 0.08	0.9	44.7
	I	†4.98 ± 0.04	0.8	†7.83 ± 0.22	2.8	57.2

SD = Standard deviation; f_p = plasma free fraction; COV = coefficient of variations   *Not significantly different, 2-tailed paired t-test; $P > 0.051$. †Significantly different, 2-tailed paired t-test; $P < 0.05$.

PET Imaging of Pituitary Vasopressin 1b Receptor with a Novel Radiotracer ^{11}C-TASP0410699 in Monkeys and Humans

Mika Naganawa[1], Daniel Holden[1], Nabeel Nabulsi[1], Shu-Fei Lin[1], Shannan Henry[1], Ming-Rong Zhang[2], Tetsuya Suhara[2], Kazumi Koga[3], Yiyun Huang[1], Richard E. Carson[1]

[1]Yale University, PET Center, New Haven, CT, United States; [2]National Institute of Radiological Science, Chiba, Japan; [3]Taisho Pharmaceutical, Saitama, Japan

OBJECTIVES: Arginine vasopressin (AVP) is a hormone, which is synthesized in the hypothalamus and stored in the posterior pituitary. AVP is a primary regulator of hypothalamus-pituitary-adrenal (HPA) axis activity. Vasopressin receptors are categorized into at least three subtypes (V_{1a}, V_{1b}, V_2). Among these subtypes, the V_{1b} receptor regulates HPA axis activity, and is a potential target for the treatment of neuropsychiatric diseases, such as depression and anxiety. ^{11}C-TASP0410699 is a novel PET radiotracer with high affinity and selectivity for the V_{1b} receptor, which is highly expressed in the pituitary. The purpose of this study was to evaluate the binding profile of ^{11}C-TASP0410699 in the pituitary of monkeys and humans and examine test-retest variability.

METHODS: ^{11}C-TASP0410699 was produced in >95% RCP (n = 25) by alkylation of the pyridinolate precursor with [11]CH_3I followed by RP-HPLC purification. Head PET scans with ^{11}C-TASP0410699 were conducted for 2 h in two rhesus monkeys with metabolite-corrected arterial blood measurement. Each monkey was anesthetized and underwent two PET scans on the same day to measure the reproducibility of binding parameters. Six control-blocking studies were also performed in the same two monkeys. A specific blocking drug was administered by a bolus-plus-infusion paradigm. Six healthy human subjects participated in test-retest protocol (two scans on the same day, test: 618±134 MBq, retest: 519±196 MBq). A pituitary region of interest (ROI) was determined as the 80 voxels (~50 mm^3) in monkey and the 400 voxels (~700 mm^3) in human with the highest values on a summed image to generate a time-activity curve (TAC). TACs were analyzed with one- and two- tissue compartment (1TC and 2TC) models and multilinear analysis 1 (MA1) to calculate distribution volumes (V_T). Test-retest variability (TRV) was computed as $\{V_T(\text{test})-V_T(\text{retest})\}/\{V_T(\text{test})+V_T(\text{retest})/2\}$.

RESULTS: In monkeys and humans, the tracer uptake pattern was similar. The tracer showed high uptake in the pituitary and no uptake in any brain regions (Figure 1). Uptake peaked at approximately 5 min, and was followed by moderate clearance. In all studies, the 2TC model provided better fits than the 1TC model in terms of Akaike Information Criterion. The MA1 V_T estimates were very similar to the 2TC V_T estimates. TRV of V_T was good: -1±8% (2TC) and 0±16% (MA1) in monkey and -1±17% (2TC) and -2±14% (MA1) in human. In humans, reducing the size of the ROI produced unstable V_T estimates from the 2TC model in a few cases. The mean TRV of V_T from a half-sized region (200 voxels) was not different from that of the full-sized region (-3±20%, MA1). In monkeys, a blocking drug reduced ^{11}C-TASP0410699 V_T in a dose-dependent fashion, and showed that 70% of baseline uptake was specific binding.

CONCLUSIONS: We successfully conducted *in vivo* imaging and quantification of pituitary V_{1b} receptor binding using a novel radiotracer ^{11}C-TASP0410699. Evaluation in monkeys and humans indicated that ^{11}C-TASP0410699 displayed substantial specific binding and good reproducibility of V_T. This tracer is suitable for specific binding measurement of the pituitary V_{1b} receptor in humans.
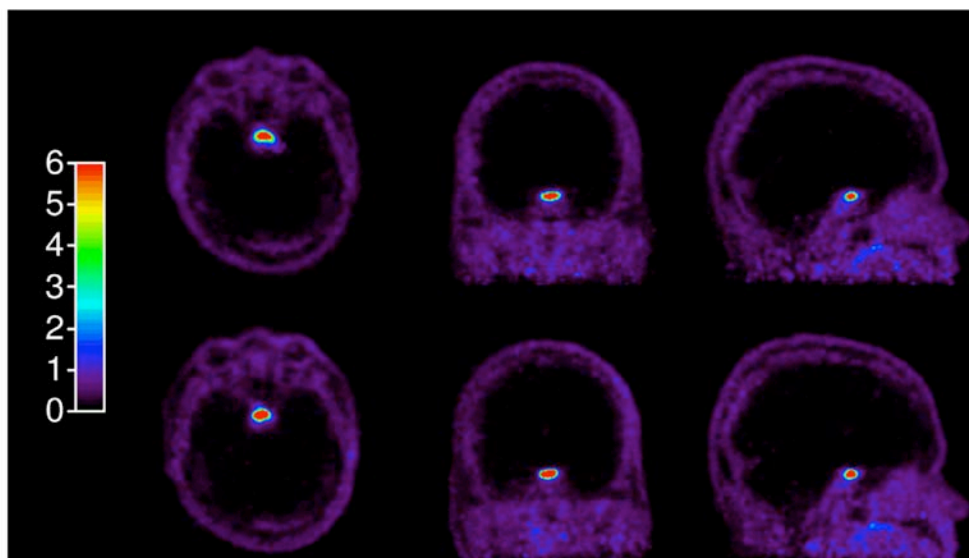
Figure 1. Test and retest human PET images summed from 30 min to 120 min after injection of ^{11}C-TASP0410699. Activity is expressed as SUV.

Molecular Connectivity: A Novel Biomarker for Major Depression

Rajapillai L. I. Pillai[1], Christine DeLorenzo[1], Maria A. Oquendo[2], J. John Mann[2], Ramin V. Parsey[1]

[1]*Stony Brook University Dept. of Psychiatry,* [2]*Columbia University Medical Center Dept. of Psychiatry;*

Background: The majority of brain PET research has focused on outcome measures in individual regions. However, by exploring the relationships between binding potential (BP_F) in *different* regions, we can learn more about effects across brain areas, such as common neurotransmission effects. The Dorsal Raphe Nucleus (DRN) is the principal source of serotonin innervation for the brain; serotonin 1A ($5\text{-}HT_{1A}$) autoreceptor BP_F in this region is elevated in patients with Major Depressive Disorder (MDD). This elevation is much greater in males. Examining $5\text{-}HT_{1A}$ autoreceptors on the DRN, which regulate serotonin transmission, in relation to post-synaptic $5\text{-}HT_{1A}$ receptors in other regions of the brain, may provide insight into serotonergic pathway disruptions. To explore this relationship, we delineated the DRN using a thresholding technique on an average PET image derived from scans of 52 healthy controls from a separate study using the $5\text{-}HT_{1A}$ antagonist [^{11}C]-WAY100635. From this average image, two high WAY binding regions (see figure) were identified: one in the olfactory sulcus (OLFS, blue) and one in perihippocampal cortex (PHC, red). As these regions are physiologically, rather than anatomically, defined by high $5\text{-}HT_{1A}$ binding activity, they are ideally suited to examine post-synaptic receptors. We aimed to examine the relationship between $5\text{-}HT_{1A}$ BP_F in the DRN, OLFS, and PHC, and how this relationship differs between healthy controls and patients with MDD.

Methods: 41 male subjects (25 healthy controls, 16 with MDD) were imaged with [^{11}C]-WAY100635. Arterial samples were collected and an input function was calculated using the interpolated unmetabolized fraction of tracer and total counts. PET emission data was coregistered to structural MRI and regions of interest (ROIs) were hand-drawn on the MRI based on atlases and published reports, aside from DRN, OLFS, and PHC as mentioned previously. ROI data were fit to a constrained two-tissue compartment model with cerebellar white matter as a reference region. Correlations between BP_F in atlas and manual regions and in the DRN were calculated and compared between control and MDD groups.

Results: In DRN and bilateral OLFS and PHC, BP_F was significantly higher in male subjects with MDD compared to controls (p<0.05—see figure). Much lower correlations were seen between the DRN and bilateral OLFS and PHC in MDD relative to healthy controls. This difference reached significance in right PHC ($r_{control}$ = 0.86, r_{MDD} = 0.54, p = 0.045) and trended towards significance in other regions. In addition, exploratory analysis revealed lower correlations in MDD across the brain in all regions, with significance reached in left amygdala ($r_{control}$ = 0.88, r_{MDD} = 0.60, p = 0.049).

Conclusions: In males with MDD, $5\text{-}HT_{1A}$ BP_F is greater across ROIs. However, this increase appears dependent on brain region, suggesting a change in regional serotonergic pathways. To reflect the neurochemical implications of this, we term BP_F coherence between regions Molecular Connectivity. This measure may prove to be a valuable biomarker, as it provides data about neurotransmission as well as binding. By applying this method to other transmitters in other disorders, we may uncover more about their underlying pathologies.
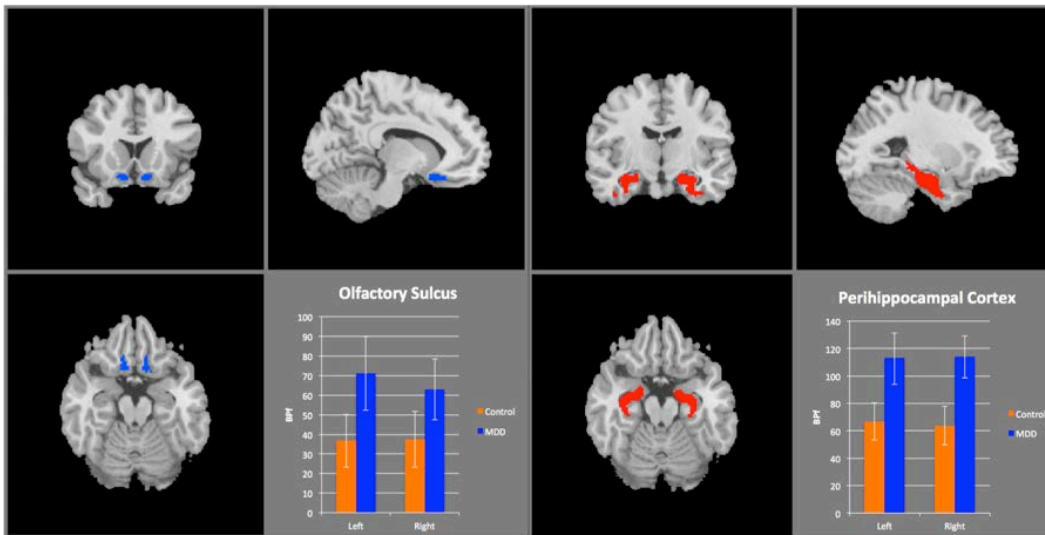
Figure: Two regions physiologically defined by high serotonin 1A binding potential: the olfactory sulcus (left) and perihippocampal cortex (right). Both regions have significantly higher binding potential in depressed subjects than in control subjects.

P-007

Identification of PET Ligands for Brain Imaging of Huntingtin Aggregates

Christopher Brown[1], Suzanne Bent[3], Galina Bursow[3], Daniel Clark-Frew[1], Samuel Coe[1], Afshin Ghavami[3], Paul Giles[1], Samantha Green[1], Jenny Häggkvist[5], Christer Halldin[5], David Hallet[1], Sarah Hayes[1], Todd Herbst[6], Frank Herrmann[2], Manuela Heßmann[2], Peter Johnson[1], Vinod Khetarpal[6], Thomas Krulle[1], Richard Marston[1], Matthew Mills[1], Michael Olsen[3],Laura Orsatti[4], Michael Prime[1], Sabine Schaertl[2], Vladimir Stepanov[5], Marie Svedberg[5], Glauco Tarozzo[2], Katarina Varnäs[5], Andrea Varrone[5], Celina Zerbinatti[2], Ignacio Munoz-Sanjuan[6], Ladislav Mrzljak[6], Jonathan Bard[6], John Wityak[6], and Celia Dominguez[6].

[1]Evotec (UK) Ltd, 114 Innovation Drive, Milton Park, Abingdon, UK, OX14 4SA, [2]Evotec AG, Manfred Eigen Campus, Essener Bogen 7, 22419 Hamburg, Germany, [3]PGI PsychoGenics Inc., 100 Philips Parkway, Montvale, NJ 07645, USA, [4]IRBM, IRBM Science Park S.p.A., Via Pontina Km 30,600 - 00071 Pomezia (RM) Italy. [5]Karolinska Institutet, Department of Clinical Neuroscience, Centre for Psychiatric Research, Karolinska Hospital, S-17176 Stockholm, Sweden. [6]CHDI Management/CHDI Foundation, 6080 Center Drive, Suite 100, Los Angeles, CA 90045, USA

Despite the initiation of huntingtin lowering clinical trials, biomarkers that can be used to assess target engagement and evaluate disease modification are currently lacking. A PET ligand that binds mutant HTT aggregates (mHTT) in both pre-clinical HD models and human subjects would allow changes in aggregate load in different brain regions over time to be monitored, and assist with translation from pre-clinical to clinical studies. An ideal PET ligand would penetrate the blood brain barrier and enter brain cells, bind mHTT aggregates with sufficient affinity to provide a signal over background noise, show little binding (signal) in non-diseased brain, be selective over other misfolded proteins, such as beta amyloid, and have suitable brain kinetics, metabolic profile and chemical structure for labelling with ^{11}C or [18]F.

Here we summarize our strategy to develop PET ligands directed to mHTT aggregates and highlight progress made during lead optimization. We will present data from a radioligand binding assay developed to detect binding to recombinant HTT aggregates, brain homogenate binding data that indicate low non-displaceable binding and highlight compounds with improved performance in autoradiography (ARG) using HD mouse brains. Binding selectivity data over beta amyloid binding in an ARG mouse AD model will be presented. In addition, we will show how translational analysis of *in vivo* and *in vitro* metabolite profiles can be used to design a PET labelling strategy with predicted minimal brain exposure of radiolabeled metabolites in humans. Finally, we will disclose results from mouse Q175 µPET studies using novel PET ligands which may be suitable for pre-clinical HD studies.

Radiosynthesis and microPET evaluation of a novel ^{11}C-labeled bispyridyl-carbamoylindole derivative as 5-HT$_{2C}$ receptors imaging agent

Fanxing Zeng,[a,*] Ronald J. Voll,[a] Jonathon A. Nye,[a] Jiyoung Mun,[a] Leonard L. Howell[b]   Mark M. Goodman [a,b]

[a]*Department of Radiology and Imaging Sciences, Emory University, 1841 Clifton Road NE, Atlanta, GA 30329*
[b]*Yerkes National Primate Research Center, Emory University, 954 Gatewood Road NE, Atlanta, GA 30329*

Objectives: The serotonin 5-HT$_{2C}$ receptor (5-HT$_{2C}$R) is abundantly expressed throughout the central nervous system, and is involved in a variety of neuroendocrine and neurobehavioral processes. Evidence from animal models, postmortem tissues, and molecular neuroscience studies suggests that dysfunction of 5-HT$_{2C}$R has been implicated in a number of significant neurological and psychiatric disorders, and 5-HT$_{2C}$R has been identified as a target for the treatment of obesity, depression, anxiety, drug abuse, schizophrenia and Parkinson's disease. However, a direct relationship between 5-HT$_{2C}$R physiology and brain diseases has proven difficult to establish due to an inability to accurately quantify 5-HT$_{2C}$R density and functional status in vivo. As of now, there are no selective antagonist radiotracers for visualization of the 5-HT$_{2C}$R in vivo, and the ligands available for in vitro autoradiography are nonselective. As part of an ongoing research project in our laboratories to develop 5-HT$_{2C}$R imaging agents using PET, we developed a novel ^{11}C-labeled bispyridyl-carbamoylindole derivative, [^{11}C]6-methyl-1*H*-indole-3-carboxylic acid [6-(2-methyl-pyridine-3-yloxy)-pyridine-3-yl]-amide (**1**). We report here the radiosynthesis and microPET evaluation of (**1**) as a prospective PET antagonist radioligand for 5-HT$_{2C}$R.

Methods: (**1**) and its corresponding boronate precursor (**2**) were synthesized via multi-step synthetic approaches. In vitro competition binding assays of (**1**) were conducted by NIMH Psychoactive Drug Screening Program (PDSP). [^{11}C]**1** was synthesized by palladium catalyzed cross-coupling of (**2**) with [11]CH$_3$I in NMP using palladium complex generated *in situ* from Pd$_2$(dba)$_3$ and (*o*-CH$_3$C$_6$H$_4$)$_3$P together with K$_2$CO$_3$ followed by HPLC purification.   Log P of **1** was measured between 1-octanol and phosphate buffer at PH 7.4. In vivo regional brain uptake of [^{11}C]**1** was determined in rhesus monkeys with a Siemens MicroPET Focus 220 scanner. Blocking study with a dose of 0.3 mg/kg and 0.1 mg/kg of SB-242084, respectively, was conducted to assess the in vivo specific binding to 5-HT$_{2C}$R.

Results: (**1**) displayed a high affinity for 5-HT$_{2C}$R (Ki = 1.6 nM) and a high selectivity over 5-HT$_{2A}$R (Ki > 1500 nM) and 5-HT$_{2B}$R (Ki = 113 nM).   [^{11}C]**1** was obtained in an average 24% decay-corrected radiochemical yield (n = 6) with a radiochemical purity of >98% and a specific activity of 0.6-1.2 Ci/μmol. (**1**) displays moderate lipophilicity with a log P7.4 of 2.54. After injection of [^{11}C]**1**, high binding was observed in the choroid plexus, the region with the highest density of 5-HT$_{2C}$R, whereas the bindings in all other brain regions were low.   Administration of a dose of 0.3 mg/kg of the 5-HT$_{2C}$R antagonist SB-242084 resulted in the reduction of 70-75% specific [^{11}C]**1** binding in the choroid plexus.

Conclusions: A new 5-HT$_{2C}$R imaging agent [^{11}C]**1** was successfully prepared. [^{11}C]**1** was suitable for detecting 5-HT$_{2C}$R in the choroid plexus of the primate brain. Structural modification of **1** will be conducted in order to increase binding affinity and brain penetration.

[11C]1

White arrows depict choroid plexus

[11C]1 + SB-242084
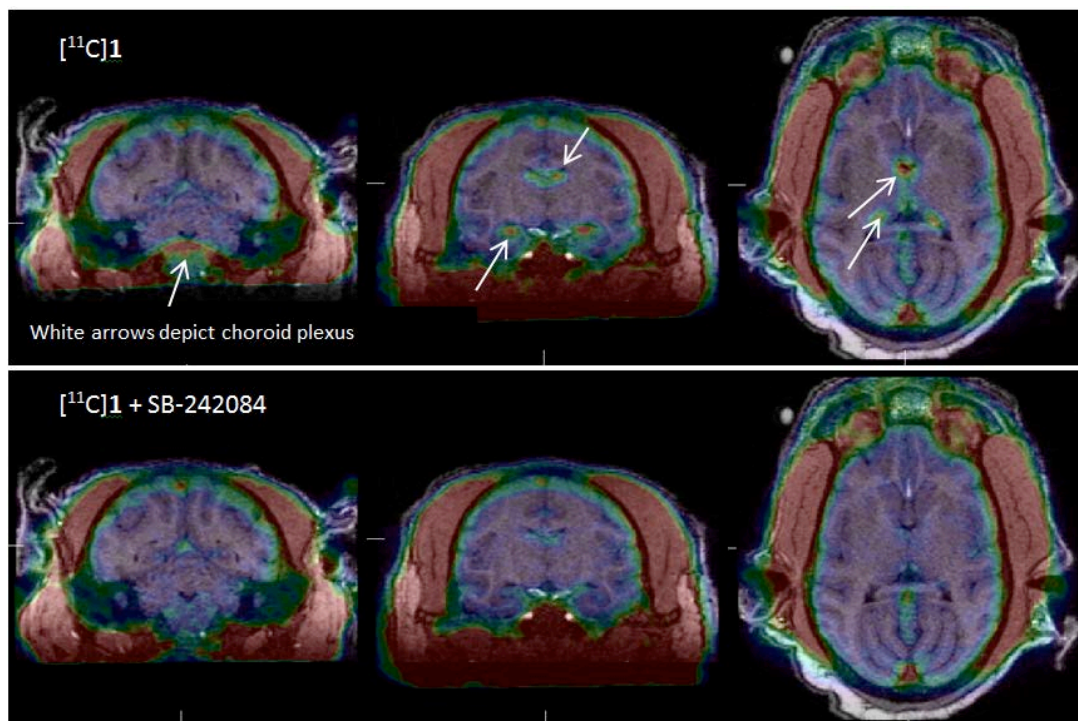
Drug Assessment in Small Animal Brain by 3D Tomographic Imaging of Positron Planar Imaging System

HIROYUKI OHBA, Ph.D.*, TAKASHI OKAMOTO**, HIDEO TSUKADA, Ph.D*.

*Central Research Laboratory, Hamamatsu Photonics, Hamamatsu, Shizuoka 434-8601, Japan; **Electron Tube Division, Hamamatsu Photonics, Iwata, Shizuoka 438-0193, Japan*

In last decades, PET becomes a practical tool in clinical field, and also plays an important role in pharmaceutical research to assess novel drugs in pre-clinical field. Various type of small animal PET systems have been developed for pre-clinical measurements, however, they still have several problems such as high system price, high running cost, and low throughput of data acquisitions. Positron planar imaging system (PPIS), which can measure real-time planar projection images of PET probes in living animals, was developed to fulfill the low system price, low running cost, and high throughput for positron imaging [1]. The developed system (PPIS-4800, Hamamatsu Photonics, Japan) has a arm with a pair of detector units placed in an opposite position (Figure 1(A)). In planar mode measurements, real-time images are periodically obtained every 5 sec, and time activity curves (TACs) in ROIs are also determined simultaneously.

Recently, we improved this PPIS system to achieve a tomographic image by manual step-wise rotation of the detector arm. The 3D mode of PPIS is useful to view a volumetric distribution of PET probe in small animal, however, the PET probe concentration is dynamically changed during step-wise rotation of the detector arm. So, we apply the Bolus plus Infusion method (B/I), which can achieve the equilibrium state of PET probe concentration [2,3]. In B/I, a part of volume of PET probe solution in a syringe is injected first, and continuous infusion is started simultaneously. PPIS measures a TAC placed on a target region using the planar mode. When TAC is reached in equilibrium state, PPIS is switched to the 3D measurement mode (Figure 1(B)). 3D tomographic image is reconstructed by 4 directions data around the object (Figure 1(C)). The system resolution is about 2mm.

In an application of drug assessment, the drug assessed is administered after the end of the first 3D mode acquisition. After the administration, PPIS is switched to the planar mode to detect the second equilibrium state of TAC. When TAC is reached in the second equilibrium state, 3D mode measurement is performed again. The drug is assessed quantitatively by the difference in the radioactivities of the first and the second 3D images. We tested the 3D mode brain imaging combined with B/I method in rats using [^{11}C]raclopride, and assessed the inhibition of [^{11}C]raclopride binding to dopamine D$_2$ receptors by cold-raclopride at doses of 3, 10, and 100 µg/kg. B/I protocol was set 1mL bolus and 0.8 mL/h infusion in all experiments. The first equilibrium was achieved 30 min after scan start and the second one was reached within 10 min after the administration of cold-raclopride at 60 min. Ratios of striatum to cerebellum, which were proportional to the binding potential of [^{11}C]raclopride binding to dopamine D$_2$ receptor were changed in a dose dependent manner.

These results suggest that the 3D imaging using PPIS become a useful tool for pharmaceutical researches especially for the assessment of the developing drug subjecting small animals.

References:
[1] Uchida H, et al. Nucl Instr Meth Phys Res. A. 2004;516:564-574.
[2] Carson, R. E., et al. J Cereb Blood Flow Metab. 1993:13, 24-42.
[3] Ohba H, et al. J Cereb Blood Flow Metab. 2012;33:85-90.
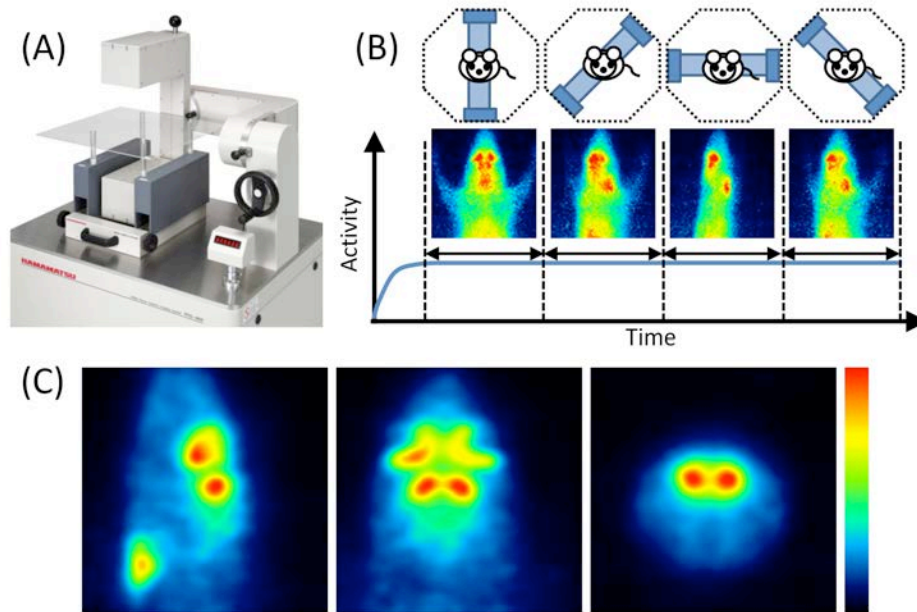
Figure Captions:

Figure 1 : Planar Positron Imaging System (PPIS-4800).

(A) Distance of a pair of detector units is 30 cm. An angle of the arm is fixed at an arbitrary angle. Small animals are placed on a plastic plate, and coincidences of gamma rays are measured to produce a projection image on a focal plane with FOV of 112mm × 200 mm in planar mode.（B）3D mode measurement is performed using step-wise rotation of the detector arm under the condition of the equilibrium state in small animal brain produced by B/I approach. (C) 3D tomographic image focused on a rat striatum normalized by the cerebellum radioactivity concentration of [11C] Raclopride.

In vivo PET imaging with [11C]PE2I and [11C]raclopride to evaluate striatal dopaminergic dysfunction in mild focal ischemia rats

N. Imamoto[1], S. Momosaki[1], M. Ito[1], H. Yamato[1], H. Iimori[1], H. Sumiyoshi[1], K. Morimoto[1], T. Watabe[2], E. Shimosegawa[2], J. Hatazawa[2], K. Abe[1,2]

[1]Shionogi & Co., Ltd., OSAKA, Japan, [2]Osaka University Graduate School of Medicine, OSAKA, Japan

Objectives: Striatal dopaminergic neural transmission is closely related to motor function after ischemic damage. The chronological changes of dopamine system such as dopamine D1 and D2 receptor after ischemia/reperfusion that induce cerebral infarction have been reported in rat. Furthermore, it has been also reported that progressive increase in apomorphine-induced circling behaviors appears from 7 days after mild focal ischemia that doesn't induce cerebral infraction. It indicated that dopaminergic imbalance was occurred even mild focal ischemia. In the present study, the chronological changes of dopamine transporter (DAT) and D2 receptor (DA D2 receptor) in the rat striatum by using [11C]PE2I and [11C]raclopride PET and circling behavior induced by amphetamine were investigated from 1 to 14 days after mild ischemia.

Methods: Mild focal ischemia of rats was induced by middle cerebral artery occlusion (MCAO) for 20 minutes. MCAO rats underwent PET using [11C]PE2I and [11C]raclopride on day 1, 2, 7 and 14 after reperfusion. Regions of interest (ROI) were defined for left (ipsilateral side) and right (contralateral side) striatum, and cerebellum. The binding potential (BP_{ND}) was calculated using cerebellum as the reference region. Moreover, amphetamine-induced circling behaviors were also performed at 1, 2, 7 and 14 days after reperfusion. In addition, HE staining to investigating the neuronal loss was performed at 2, 7 and 14 days after reperfusion.

Results: [11C]PE2I binding to DAT was significantly increased in the ipsilateral side of the striatum at 1 and 2 days after MCAO, and it reached a peak on day 1 (day 1: 153%, day 2: 144% of contralateral side). On day 7 and 14 after MCAO, there were no significant changes. On the other hand, [11C]raclopride binding to DA D2 receptor didn't change at 1 and 2 days after MCAO. On day 7 and 14 after MCAO, [11C]raclopride binding was significantly decreased on the ipsilateral side of the striatum (day 7: 62%, day 14: 49% of contralateral side). Moreover, amphetamine-induced circling behavior to the contralateral direction was significantly increased at 1 and 2 days after MCAO. Although this behavior was once disappeared on day 7, amphetamine-induced circling behavior to the ipsilateral direction was significantly increased on day 14. The progressive neuronal loss was observed from 7 days after reperfusion onward.

Conclusions: We consider that the amphetamine-induced circling behavior at the early phase might be induced by the change of dopaminergic neural transmission, while that at the late phase might be due to the neuronal loss. DAT and DA D2 receptor PET imaging might be useful to predict the dopaminergic dysfunction after mild focal ischemia.

Functional PET/MR Discloses Gender Differences in Color Processing in Mice

Philip C. Njemanze[1], Mathias Kranz[2], Peter Brust[2]

[1]*Chidicon Medical Center, International Institutes of Advanced Research Training, Neurocybernetic Flow Laboratory, Owerri, Nigeria.* [2]*Helmholtz-Zentrum Dresden-Rossendorf, Institute of Radiopharmaceutical Cancer Research, Department of Neuroradiopharmaceuticals, Leipzig, Germany.*

OBJECTIVES: Color processing is a central component of human vision. There has been much debate about the existence of color vision in animals. Mice have two types of cone pigments, one with a peak sensitivity at about 510 nm, and the other with a peak at 370 nm in the ultraviolet range. Most studies of color vision have used behavioral experiments, and hence uncertainties remain whether the two cone types yield color vision. Since PET has been used to measure changes of rCBF of rhesus monkeys performing color discrimination we have hypothesized that FDG-PET combined with anatomical MR can be used to study color processing in mice. Here we demonstrate gender differences in color processing in mice.

METHODS: Ten anaesthetized CD-1 mice were repeatedly injected on different days with 12 MBq ^{18}F-FDG and subjected in random order to separate monocular stimulation of the left and right eye with white, blue and yellow lights, respectively, for 20 min using gelatin-(Wratten)-filters affixed within a viewing device (Chromatoscope) specially designed for small animals. The SUV of ^{18}F-FDG was determined at 27.5, 32.5, 37.5 and 42.5 min p.i. in the whole cortex and in the left and right visual cortex. Data were analyzed with MANOVA and t-test.

RESULTS: In both genders no hemispheric differences are revealed in dark baseline condition and during stimulation with white light of either eye. Male mice have 13-16% higher SUV ($p< 0.001$) than female mice in the cortical area, right and left visual cortex in dark baseline condition and during stimulation with white, blue and yellow lights through the right eye but not the left. In **male** mice, the SUV was **higher** in the **left** visual cortex (1.53 ± 0.08) during **Blue** stimulation through the **right** eye compared to the right visual cortex (1.47 ± 0.10, $p<0.05$) (Fig. left) while the SUV **did not differ** during **Blue** stimulation through the **left** eye. Conversely, in **female** mice, the SUV was **higher** in the **right** visual cortex (1.34 ± 0.08) during **Blue** stimulation through the **left** eye compared to the left visual cortex (1.30 ± 0.11, $p<0.01$) (Fig. right) while there was **no change** during stimulation with **Blue** through the **right** eye. **Yellow** stimulation through the **right** eye revealed hemispheric differences only in **female** mice, while **Yellow** stimulation through the **left** eye revealed hemispheric differences only in **male** mice.

CONCLUSION: The experimental setup using FDG-PET combined with anatomical MR is suitable to study color processing in mice. As previously has been shown for human in a functional transcranial Doppler study (Njemanze 2011) gender differences in the perception of blue and yellow colors appear to exist also in rodents. In both species Blue provided the highest stimulation. In opposite to human the visual cortex in male mice revealed higher metabolism than in female.

REFERENCE

Njemanze PC. Gender-related differences in physiologic color space: a functional transcranial Doppler (fTCD) study. Exp. Transl Stroke Med. 2011; 3: 1.

MALE

visCtxL visCtxR

A

B

SUV
1.4

0

C

D

FEMALE

visCtxL visCtxR

A

B

SUV
1.4

0

C

D
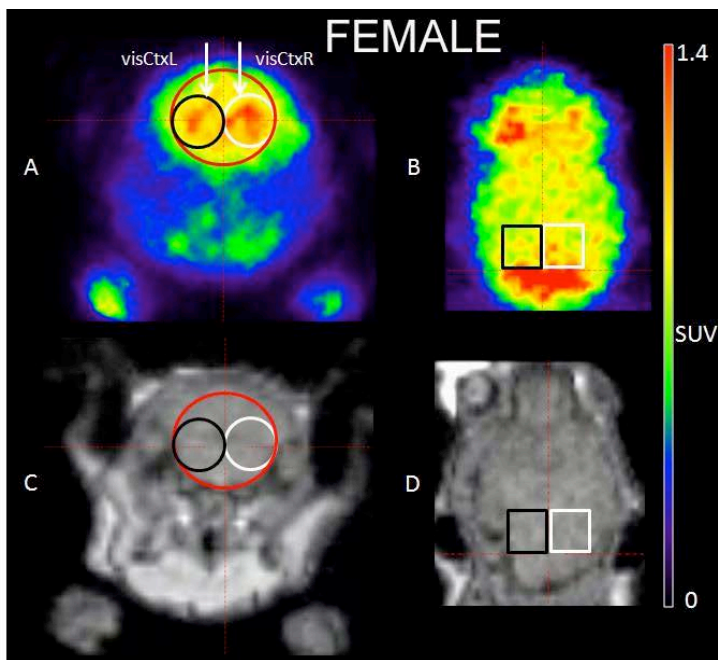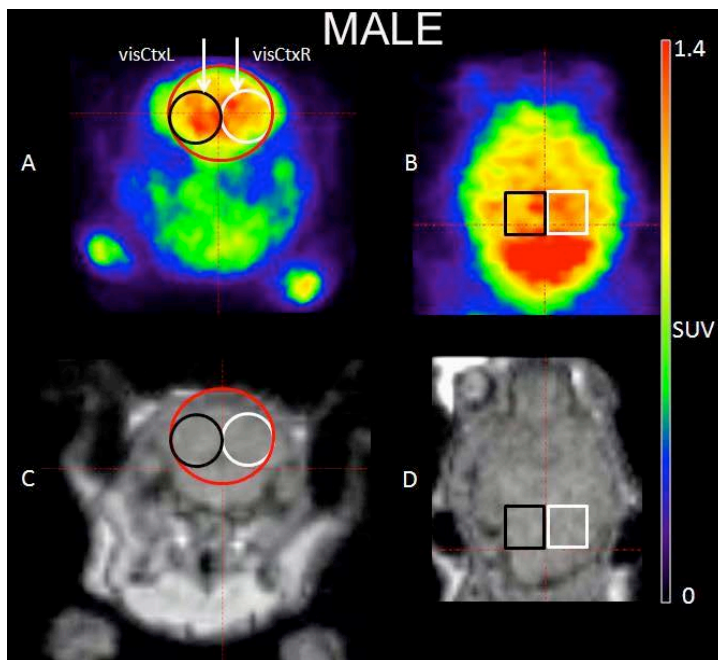
Animal PET/MR with the new radioligand [18F]AQ28A demonstrates the involvement of phosphodiesterase 10A in energy homeostasis

M. Kranz[1], M. Hankir[2], W. Deuther-Conrad[1], S. Wagner[1], R. Teodoro[1], S. Fischer[1], B. Wenzel[1], W.K. Fenske[1], P. Brust[2]

[1]Helmholtz-Zentrum Dresden-Rossendorf, Institute of Radiopharmaceutical Cancer Research, Department of Neuroradiopharmaceuticals, Leipzig, Germany. [2]Universität Leipzig, Integrated Research and Treatment Centre Adiposity Diseases, Leipzig, Germany.

OBJECTIVES: Cyclic nucleotide phosphodiesterases (PDEs) are enzymes that cleave the phosphodiester bond in the second messenger molecules cAMP and cGMP. PDE10A is dual-specific and mainly expressed in the striatum, a brain region which coordinates a great variety of cognitive functions, including motor and action planning, decision-making, motivation, reinforcement, and reward perception. Knock-out mice provided evidence for involvement of PDE10A in the regulation of energy balance as shown by their resistance to diet induced obesity (DIO). Therefore, we have used the novel selective radioligand [^{18}F]AQ28A [1] to investigate the expression of PDE10A in the striatum and brown adipose tissue (BAT) of lean, diet-induced (DIO) and leptin-deficient genetically obese mice. As BAT activation could previously be visualized by using [^{18}F]FDG [2], we also assessed whether inhibition of PDE10A modulates BAT activity.

METHODS: Isoflurane-anaesthetized female mice were injected with either [^{18}F]AQ28A (11±3 MBq) or [^{18}F]FDG (14±2 MBq) and subjected to 1 h PET/MR (Mediso nanoScan®). After co-registration of the dual modality image data volumes of interest (striatum, hypothalamus, interscapular BAT and muscle) were drawn manually with reference to the structural MRI data using ROVER software (ABX, Radeberg).The selectivity of [^{18}F]AQ28A towards PDE10A was investigated by baseline (n=3) and blocking (n=3) experiments with the PDE10A inhibitor MP-10 (5 mg/kg). Another set of animals was provided over 16 weeks either with standard food (lean, n=5) or high-fat high-sugar diet (DIO, n=5) and received [^{18}F]AQ28A PET/MR thereafter. A further group of lean mice (n=10), which was overnight fasted and housed under thermoneutral conditions, received either i.p. injection of MP-10 (n=5) or vehicle (n=5) followed 30 min later by 1 h [^{18}F]FDG PET/MR. Thereafter the mice were sacrificed and striatum, hypothalamus and BAT were collected. Relative mRNA expressions of PDE10A, thermoregulatory genes and the indirect neuronal activity marker *Fos* were analyzed by real-time qPCR.

RESULTS: PDE10A selectivity of [^{18}F]AQ28A was proven by blocking with MP-10 (SUV$_{15min}$ striatum baseline/blocking: 1.02±0.19/0.54±0.08; p<0.01). A 7-fold higher mRNA expression of PDE10A in striatum compared to hypothalamus was found (p<0.001). Acute pharmacological inhibition of PDE10A altered cAMP levels (p<0.01) and thermoregulatory gene and *Fos* expression in striatum (p<0.05), but not in hypothalamus. DIO resulted in ~60% and 80% higher PDE10A expression (p<0.05) in striatum and BAT, respectively, accompanied by an increased SUV of [^{18}F]AQ28A in both targets (p<0.05)(Fig.). Acute administration of MP-10 to lean mice resulted in significantly higher FDG uptake by BAT (SUV$_{55min}$: 0.40±0.01) compared to vehicle administration (SUV$_{55min}$: 0.25±0.02; p<0.01).

CONCLUSION: Distinct alterations of gene expression together with significant changes of PDE10A availability and of glucose metabolism in BAT after PDE10A inhibition reveal a novel thermoregulatory role for PDE10A. The data suggest that PDE10A inhibitors offer the potential to treat obesity by increasing thermogenesis and reducing hedonic feeding through recruiting striatal and BAT circuits.

REFERENCES:
[1] Wagner, S., et al. *Eur J Med Chem* 2016 107;97.
[2] Gnad, T.;…;Kranz, M.;…Pfeifer, A. *Nature*. 2014 18;516

Striatum

Lean   DIO

BAT

0 ▬▬▬▬▬▬▬ 3

SUV

PDE10A

2.5
2.0
1.5
1.0
0.5

relative mRNA

*

Lean   DIO

3.0

2.0

1.0

relative mRNA

*

Lean   DIO
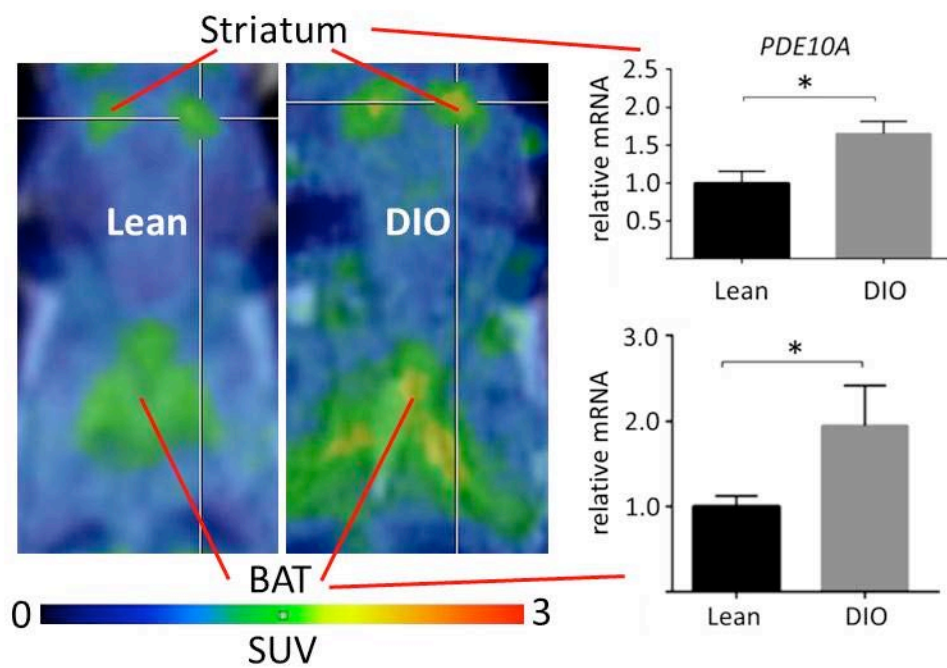
Parametric methods for dynamic [^{11}C]phenytoin PET studies

Syahir Mansor[1*], Ronald Boellaard[1,2], Maqsood Yaqub[1], Femke E Froklage[2], Anke de Vries[1], Esther DM Bakker[1], Rob A Voskuyl[3], Lothar A Schwarte[4], Joost Verbeek[1], Albert D Windhorst[1],   Adriaan A Lammertsma[1]

[1]*Department of Radiology & Nuclear Medicine, VU University Medical Center, Amsterdam, The Netherlands;* [2]*Department of Nuclear Medicine and Molecular Imaging,University Medical Center Groningen, Groningen, The Netherlands;* [3]*Department of Neurology, Stichting Epilepsie Instellingen Nederland (SEIN), Heemstede, The Netherlands;* [4]*Department of Anaesthesiology, VU University Medical Center, Amsterdam, The Netherlands*

Purpose: The purpose of this study was to assess the quantitative performance of various parametric methods for analysing [^{11}C]phenytoin kinetics.

Methods: Within a test-retest design, 6 healthy subjects underwent two 60 min dynamic [^{11}C]phenytoin scans at baseline on the same day. The administered activity of ^{11}C-Phenytoin was 345 ± 54 (mean ± standard deviation (SD)) MBq with a specific activity of 72 ± 27 MBq·µmol^{-1} .A metabolite corrected arterial input function was obtained using continuous arterial sampling in combination with 7 discrete samples. For various scan durations, parametric images were generated using Logan plot analysis, a basis function method (BFM) and spectral analysis (SA). Neuro-anatomic regions of interest were generated using PVELab analysis together with a coregistered T1w MRI scan. Regional averaged parametric distribution volume (V_T) and rate of influx (K_1) values were compared with those obtained from non-linear regression (NLR) analysis of time activity curves. In addition, both global and regional test-retest (TRT) variabilities were determined for parametric K_1 and V_T values.

Results: The plasma to whole blood ratio was relatively constant over time, ranging from about 1.3 to 1.4. The parent fraction of ^{11}C-Phenytoin in plasma slowly decreased to 79±4% at 60 minutes, while non-polar and polar metabolite fractions increased from 2.3±2.1% and 2.1±1.8% at 2.5 minutes to 16.1±3.1% and 4.4±2.2% at 60 minutes, respectively. Bias, as compared to NLR, in V_T was less than 5% for all parametric methods. For K_1, SA showed a negative bias of 16%. Mean TRT variabilities of V_T and K_1 were <10% for all methods and the lowest for BFM (<5%) as shown in Table 1. Shortening the scan duration to 45 minutes provided similar V_T and K_1 values with comparable TRT performances as those derived from 60 minutes data.

Conclusion: Among the various parametric methods tested, BFM provided parametric V_T and K_1 values with the smallest bias compared to NLR data. In addition, it showed a TRT variability <5%, also for shorter scan durations.

References:
(1) Svarer C, Madsen K, Hasselbalch SG, et al. MR-based automatic delineation of volumes of interest in human brain PET images using probability maps. *Neuroimage.* 2005; 24:969-979.

Table 1. The summary of TRT repeatibility between test and retest data and correlation between various parametric methods compare to NLR.

	Mean TRT (%)	correlation (R^2)	slope	intercept	correlation (R^2)	slope
Logan V_T test	-1.759	0.8116	0.7869	0.1453	0.7768	0.9482
Logan V_T retest		0.8702	0.8952	0.053	0.8665	0.9531
BFM V_T test	-0.589	0.7862	0.8418	0.1026	0.7716	0.9557
BFM V_T retest		0.7315	0.8319	0.1048	0.7174	0.9464
SA V_T test	0.396	0.8326	0.8929	0.0595	0.828	0.9589
SA V_T retest		0.8364	0.9435	0.0134	0.8361	0.9581
BFM K_1 test	-1.29	0.9732	0.8388	0.0074	0.9179	1.0347
BFM K_1 retest		0.9206	0.8127	0.0083	0.8518	1.0304
SA K_1 test	-1.516	0.8916	0.7501	0.0039	0.8744	0.8523
SA K_1 retest		0.8482	0.7366	0.0046	0.825	0.8557

P-014

Six Novel Mutant Huntingtin Binding Radioligands: Evaluation in Non-Human Primate and in the zQ175 Mouse Model of Huntington´s Disease

Jenny Häggkvist[1], Vladimir Stepanov[1], Marie Svedberg[1], Lenke Tari[1], Katarina Varnäs[1], Miklós Tóth [1], Akihiro Takano[1], Nahid Amini[1], Sangram Nag[1], Andrea Varrone[1], Christer Halldin[1], Daniel Clark-Frew[2], Samuel Coe[2], Paul Giles[2], Samantha Green[2], David Hallet[2], Sarah Hayes[2], Peter Johnson[2], Thomas Krulle[2], Richard Marston[2], Matthew Mills[2], Chris Brown[2], Michael Prime[2], Vinod Khetarpal[3], Todd Herbst[3], Ignacio Munoz-Sanjuan[3], Celia Dominguez[3], Andrew Wood[3], Ladislav Mrzljak[3], John Wityak[3], and Jonathan Bard[3]

[1]*Karolinska Institutet, Department of Clinical Neuroscience, Centre for Psychiatric Research, Karolinska Hospital, S-171 76 Stockholm, SWEDEN;* [2]*Evotec (UK) Ltd, 114 Innovation Drive, Milton Park, Abingdon, UK, OX14 4SA;* [3]*CHDI Management/CHDI Foundation 6080 Center Drive, Suite 100, Los Angeles, CA 90045*

Huntington's disease (HD) is a neurodegenerative genetic disorder, characterized by progressive loss of medium spiny neurons in the striatum. Huntington's disease is caused by the expansion of CAG repeats in the huntingtin (HTT) gene. The CAG-expansion causes accumulation of mutant HTT protein (mHTT), which is associated with the loss of neurons leading to development of motor dysfunction, emotional disturbances, psychiatric symptoms and cognitive deficits. Today, there is strong evidence that lowering mHTT would be a potential therapeutic strategy for HD. Therefore, specific biomarkers for mHTT are of great value in order to be able to assess the efficacy of novel experimental therapies aimed at lowering mHTT.

In the present study, we examined the properties of six new potential mHTT binding radioligands, [11C]CHDI-00481562, [11C]CHDI-00484210, [11C]CHDI-00483578, [11C]CHDI-00482879, [11C]CHDI-00482927 and [11C]CHDI-00485180 PET in healthy non-human primates (NHP) as well as in vitro autoradiography (ARG) and small animal PET imaging in the zQ175 knock-in mouse model (heterozygous and homozygous animals).

All radioligands entered the brain in NHP as well as in WT and zQ175 mice. In the NHP, rapid kinetics and low non-specific binding was observed for [11C]CHDI-00484210, whereas [11C]CHDI-00481562 showed slow distribution to brain (T_{max}=7.5 min). The remaining tracers displayed comparable in vivo kinetic profiles in the NHP.
In mice, all radioligands showed an initial uptake between 200-300 % SUV. [11C]CHDI-00484210 showed the most rapid washout from the brain and had also the lowest background binding in WT animals. All the other radioligands showed similar in vivo kinetics. The binding of the radioligands, as measured by % SUV and AUC, was lowest in WT, moderate in heterozygous zQ175 and highest in homozygous zQ175 animals.
To compare the different radioligands, the AUC ratio between zQ175 and WT were calculated by dividing the average AUC for Het and Hom zQ175 respectively with the average AUC for the WT. [11C]CHDI-00485180 and [11C]CHDI-00482879 showed the highest binding as expressed by AUC, as well as the highest binding ratio both in heterozygous and homozygous animals. The results from the PET-imaging studies in rodents were confirmed in vitro by autoradiography.

Taken together, this preclinical evaluation of novel mHTT binding radioligands in NHP and in zQ175 mouse brain suggests that several of these radioligands are potential candidates, with [11C]CHDI-00482879, [11C]CHDI-00482927 and [11C]CHDI-00485180 being the top three candidates, for study as PET imaging agents in HD patients.

P-015

Synergistic PET/MRI combination for Partial Volume Correction in myelin imaging

Elisabetta Grecchi[a], Mattia Veronese[a], Benedetta Bodini[b,c], Daniel García-Lorenzo[b], Bruno Stankoff[b,c,d] and Federico E Turkheimer[a]

[a]Centre for Neuroimaging, Institute of Psychiatry, Psychology and Neuroscience King's College London, London, UK; [b]Sorbonne Universités, UPMC Univ Paris 06, UMR S 1127, and CNRS UMR 7225, and ICM, F-75013, Paris, France; [c]Service Hospitalier Fréderic Joliot, SHFJ, I2BM-DSV, CEA, Orsay, France; [d]APHP Hôpital Saint-Antoine, Paris, France

[11C]PIB PET was originally developed for amyloid imaging and has been recently repurposed to quantify myelination and demyelination in multiple sclerosis (MS) (1,2). The potential of PET in myelin imaging however is somewhat limited by its low resolution with resulting significant partial volume effects that deteriorate the accuracy of the quantification of white matter lesions. In previous work, we have used the wavelet transform and synergistic statistical models to combine structural (MR or CT) (3,4) images to improve the resolution of PET images in brain and whole-body applications. Here we demonstrate a similar approach that is specific to [11C]PIB PET/MR. The resulting approach is called Multiresolution–Multimodal Resolution-Recovery (MM-RR).

Our previous synergistic technologies for PET/MR and PET/CT data used structural information in combination with anatomical atlases to correct PET data for resolution effects. The MM-RR technique takes also advantage of the multiresolution property of the wavelet transform; it combines the [11C]PIB-PET specificity to myelin basic protein and its poor resolution with the high-resolution of MR. The algorithm models the relationship between MR and PET signals at low resolution scales and uses this model to insert high-resolution MR coefficients into the PET image after appropriate scaling and de-noising.

The performance of MM-RR was evaluated with a data set comprising [11C]PIB PET and MR T1 and T2 images of healthy control subjects (n=10) and MS patients (n=20). Images were evaluated qualitatively and quantitatively in term of image contrast, ROIs quantification comparison and influence of partial volume correction (PVC) in lesion quantification.
For the healthy control group, the MM-RR PET showed an increase of 5.7% in white-matter (WM) uptake while the grey-matter (GM) uptake remained constant resulting in 31% white/gray matter contrast. In the patient group, MM-RR PET images showed sharper lesions contour, uptake decrease in lesions of 5% and increase in perilesion up to 5% when compared to Standard PET. The difference in lesion uptake between standard PET and MM-RR PET was bigger for smaller lesions while the two modalities gave comparable results for bigger lesions, thus indicating effective and specific PVC.

We conclude that the MM-RR methodology generates [11C]PIB PET images with improved quantitative and qualitative properties as well as superior lesion delineation. The methodology is particularly indicated for the newly introduced PET/MR scanners and will further benefit in the future from the use of myelin specific MR sequences (e.g. MTR, mcDESPOT).

References
1. Stankoff B et al. Imaging central nervous system myelin by positron emission tomography in multiple sclerosis using [methyl11C]2(4methylaminophenyl)6hydroxybenzothiazole. *Annals of neurology.* 2011
2. Veronese M et al. Quantification of [11C]PIB PET for imaging myelin in the human brain: a test–retest reproducibility study in high-resolution research tomography. *Journal of Cerebral Blood Flow & Metabolism.* 2015
3. Shidahara M et al. Functional and structural synergy for resolution recovery and partial volume correction in brain PET. *Neuroimage.* 2009
4. Grecchi E et al. Multimodal Partial Volume Correction–Application to 18F-Fluoride PET/CT bone metastases studies. *Journal of Nuclear Medicine.* 2015

A)

	GM		NAWM		Perilesions		T2-w lesions		Black Holes		Gad + lesions	
	1.09 ± 0.01	1.10 ± 0.10	1.25 ± 0.06	1.33 ± 0.06	1.13 ± 0.05	1.19 ± 0.06	1.00 ± 0.05	0.96 ± 0.04	0.90 ± 0.12	0.7 9 ± 0.13	1.14 ± 0.08	1.08 ± 0.09

Standard PET

High Resolution PET

B)

MRI   Standard Resolution PET   High Resolution PET
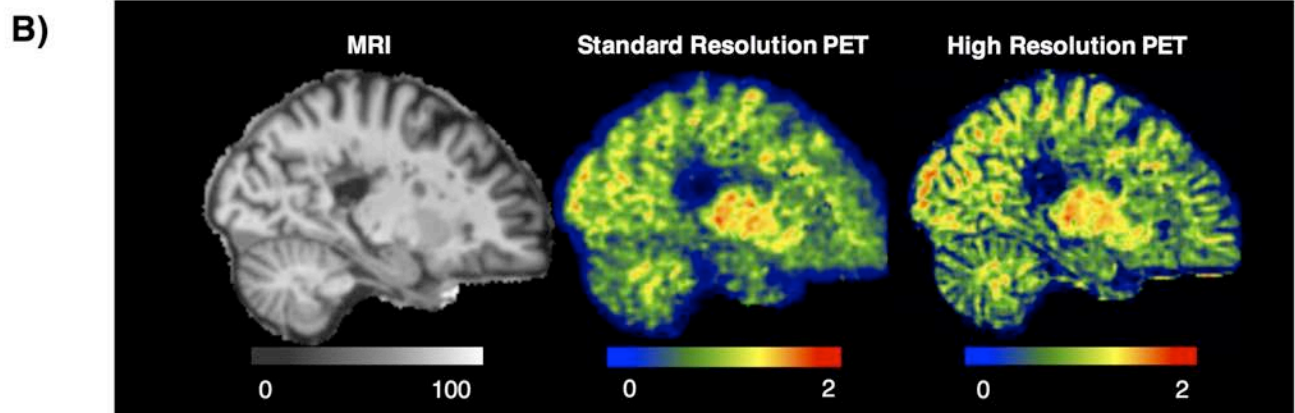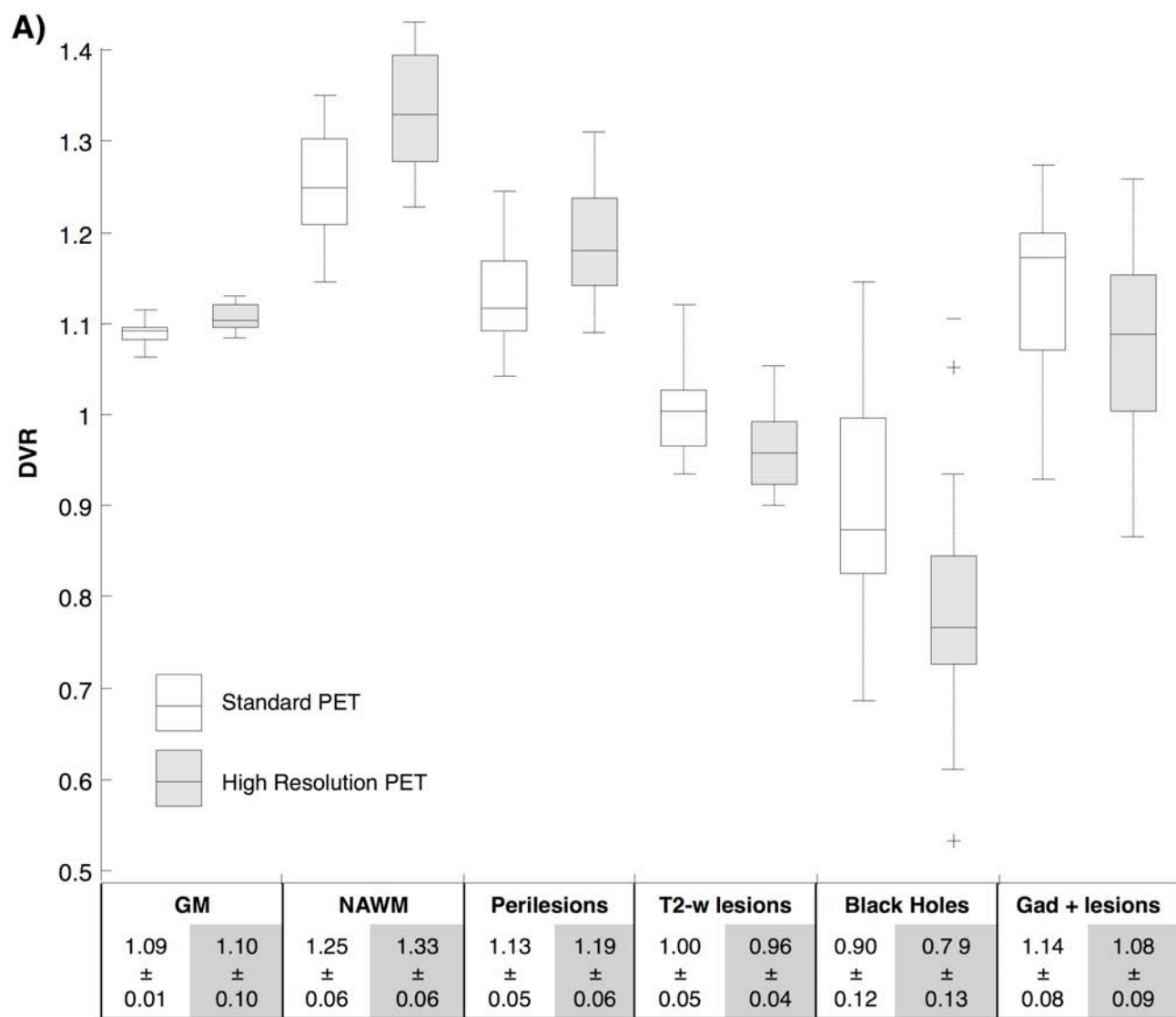
PET Imaging of the Receptor for the Advanced Glycation Endproducts

Brian P. Cary[1], Allen F. Brooks[1], Lindsey R. Drake[2], Maria V. Fawaz[1,2], Timothy J. Desmond[1], Phillip Sherman[1], Carole A. Quesada[1] and Peter J. H. Scott[1,2]

[1] *Division of Nuclear Medicine, Department of Radiology, University of Michigan Medical School, Ann Arbor, Michigan 48109, United States;* [2] *The Interdepartmental Program in Medicinal Chemistry, University of Michigan, Ann Arbor, Michigan 48109, United States*

Objectives: The receptor for advanced glycation endproducts (RAGE) is a 35 kDa transmembrane receptor and a member of the immunoglobulin superfamily of cell surface molecules. RAGE is heavily implicated in Alzheimer's disease (AD) where it is thought to mediate transport of peripheral amyloid-β (Aβ) across the blood-brain barrier (BBB). Although the exact mechanism of transport is unknown, it has been proposed that RAGE initiates a neuroinflammatory response, which alters junctions through the Ca^{2+}–calcineurin pathway, and causes an increase in the influx of Aβ into the brain. PET radiotracers that can be used to quantify CNS RAGE will aid in elucidating the complexity of this receptor, including its dynamic relationship with Aβ in early stages of AD. An increase in RAGE could therefore be a prodromal biomarker of AD, and we hypothesize that PET radiotracers for RAGE could detect AD prior to the onset of amyloid aggregation. The goal of this project is the development and evaluation of small molecule PET radiotracers for RAGE.

Methods: Radiotracers are labeled with fluorine-18 using an automated synthesis module. For example, [18F]RAGER (**2**) (based upon FPZ-ZM1 (**1**), a known RAGE inhibitor, [1]) was synthesized (44 ± 10 mCi radiochemical yield (2.9% nondecay corrected based upon 1.5 Ci of [18F]fluoride), excellent radiochemical purity (>99%), and high specific activity (3740 ± 495 Ci/mmol); n = 6). The synthesis of 2nd generation analogs employs the same radiofluorination method. Evaluation of the radiotracers is being conducted using pre-clinical PET imaging (rodents and non-human primates) as well as autoradiography with post-mortem AD brain tissue samples. Radiotracer metabolism is evaluated in rodents and primates, either *in vivo* through analysis of blood samples, or using *in vitro* liver microsome experiments. Metabolic profiling is conducted using HPLC or LCMS.

Results: We recently reported the initial synthesis and evaluation of [18F]RAGER (**2**), a small molecule PET radiotracer for RAGE (Kd = 15 nM) [2], which showed specific binding in AD brain samples that colocalized with RAGE identified by immunohistochemistry, CNS penetration in rodent and non-human primate, and increased uptake in areas of the brain known to express RAGE (e.g. the hippocampus). The first generation radiotracer represented initial proof-of-concept and a promising first step toward quantifying CNS RAGE activity using PET. However, there were high levels of nonspecific binding *in vitro*, attributed to its high log P (3.5), and rapid metabolism of [18F]RAGER in rat liver microsome studies. Therefore, synthesis and evaluation of second-generation radiotracers, such as **3**, with lower log P and improved imaging properties, is ongoing. Radiosyntheses, pharmacological challenge studies to investigate specific binding, and studies investigating rodent and primate metabolism pathways for these new radiotracers will be reported in this presentation.

Conclusions: [18F]RAGER and its analogs represent the first class of brain penetrant small molecule PET radiotracers for the receptor for advanced glycation endproducts. Lead optimization is ongoing to identify a candidate radiotracer for translation into clinical imaging studies.

References:
[1] Deane *et al*., *J. Clin. Invest.* **2012**, *122*, 1377; [2] Cary *et al*., *ACS Chem. Neurosci.*, **2016**, ASAP (DOI: 10.1021/acschemneuro.5b00319).
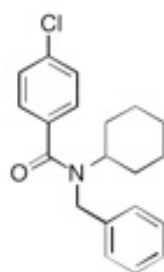
1
FPZ-ZM1
Ref [1]
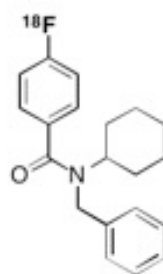
2
[¹⁸F]RAGER
Ref [2]
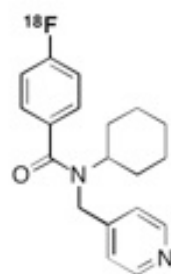
3
(2nd Generation
Analog)
This work

Test-retest properties of [11C]Arachidonic Acid brain incorporation measurements

Francesca Zanderigo[1,2], Yeona Kang[3], Dileep Kumar[1], Anastasia Nikolopoulou[3], Paul D. Mozley[3], Paresh J. Kothari[3], David Schlyer[3], Stanley I. Rapoport[4], Maria A. Oquendo[1,2], Shankar Vallabhajosula[3], J. John Mann[1,2,5], M. Elizabeth Sublette[1,2]

[1]Department of Molecular Imaging and Neuropathology, New York State Psychiatric Institute, New York, NY, USA; [2]Department of Psychiatry, Columbia University, New York, NY, USA; [3]Department of Radiology, Weill Cornell Medicine, New York, NY, USA; [4]National Institute on Aging, Bethesda, MD, USA; [5]Department of Radiology, Columbia University, New York, NY, USA

Introduction. Arachidonic acid (AA) is a second messenger involved in phospholipase A2-mediated signal transduction[1]. Positron Emission Tomography (PET) can quantify the regional brain incorporation rate K* (μL•min^{-1}•mL^{-1}) of [11C]AA[2-5]. However, reproducibility of K* measurements remains undetermined. We assessed test-retest properties of K* measurements using data from subjects imaged twice. We also investigated effects of using a noninvasive estimation of input function, and population-based metabolite correction.

Materials and Methods. Five healthy volunteers underwent two 60-minute PET scans with [11C]AA approximately 6 weeks apart. [11C]AA was synthesized as reported[6] and infused intravenously for 3 minutes at a constant rate. Arterial blood samples were concurrently collected to measure arterial plasma tracer radioactive counts. In 3 of the scans, the fraction of unchanged [11C]AA in plasma was determined using a basic extraction followed by acid extraction in the presence of heptane. PET images were motion-corrected, and average time-activity curves automatically extracted in 10 regions of interest (ROIs). Correction for tissue concentration of [11C]CO$_2$ was not performed as its contribution to the variance is minimal[2]. For each scan, an image-derived input function (IDIF) was calculated as reported[7]. At the ROI level, K* was estimated using the irreversible model proposed for [11C]AA[2], with arterial blood data or IDIF as input function. Input function curves were corrected for the fraction of plasma unchanged [11C]AA using published values[2] or individual measured values (when available). Reproducibility of K* was calculated using the percent difference (PD) (absolute difference between test and retest values divided by their average).

Results. Figure 1(A) shows the effect of using an IDIF: K* estimates are close to those using arterial input data for 6 out of 10 scans; in scans 2, 4, 5, and 6, IDIF underestimates the peak of the blood-based input function, most likely due to insufficient partial volume correction, and overestimates K*. Figure 1(B) shows the effect of using published population-based metabolite fraction values instead of individually measured values: K* estimates using individual values are very close to those using published values in the 3 scans with data available. In Figure 1(C), PD values obtained using IDIF are quite similar to values obtained using arterial blood data (PD values are reported in order of decreasing ROI size): there is no evidence that values are different between the two methods, as two-sample t-tests, region by region, yield p-values ranging from 0.383 to 0.921. Mean test-retest differences range from ~7 to 16%.

Conclusion. Our results suggest that it is feasible to use [11C]AA to monitor within-subject changes in K* over a six-week period, such as before and after treatment, although reproducibility appears to be less adequate in the hippocampus. Moreover, these data support the use of IDIF and a population-based metabolite correction in future studies with [11C]AA instead of performing invasive arterial blood sampling, and metabolite assays. Additional characterization studies underway in an expanded dataset are investigating the relation between [11C]AA K* and metabolic rates of glucose consumption using [18F]FDG images acquired in the same subjects.

References:
[1] Rapoport SI, Neurochemical research, 1999; 24: 1403-1415.
[2] Giovacchini G et al., Journal of cerebral blood flow and metabolism, 2002; 22: 1453-1462.
[3] Esposito G et al., NeuroImage, 2007; 34: 1342-1351.
[4] Thambisetty M et al., Journal of cerebral blood flow and metabolism, 2012; 32: 676-684.
[5] Esposito G et al., Journal of nuclear medicine, 2008; 49: 1414-1421.
[6] Chang MC et al., Brain research, 1997; 755: 74-83.
[7] Kang Y et al., Society of Nuclear Medicine and Molecular Imaging, Baltimore, Maryland, Journal of nuclear medicine; 2015: 152.

K* estimates using IDIF versus arterial blood data

A

y = 1.614x - 0.541
R² = 0.983

y = 1.338x + 0.293
R² = 0.978

y = 1.198x + 0.005
R² = 0.998

y = 1.066x - 0.602
R² = 0.990

y = 0.907x + 0.382
R² = 0.977

y = 1.188x + 0.027
R² = 0.999

y = 1.049x - 0.428
R² = 0.998

y = 0.977x - 0.144
R² = 0.999

y = 1.010x + 0.187
R² = 0.972

y = 1.195x - 0.691
R² = 0.960

K* using IDIF and published population-based metabolite values

K* using arterial blood data and published population-based metabolite values

K* estimates using individual versus population-based metabolite values

B

y = 1.025x + 0.061
R² = 1.000

y = 0.979x + 0.028
R² = 1.000

y = 0.947x + 0.097
R² = 0.999

K* using arterial blood data and individually measured metabolite values

K* using arterial blood data and published population-based metabolite values

TEST	RE-TEST
scan 1	scan 3
scan 2	scan 4
scan 5	scan 6
scan 7	scan 9
scan 8	scan 10

Test-retest K* percentage differences in ROIs

C

- using arterial blood data and published population-based metabolite values
- using IDIF and published population-based metabolite values

Percentage difference for K* across test-retest pairs

temporal, gray matter cerebellum, parietal, occipital, orbital, white matter cerebellum, cingulate, thalamus, hippocampus, dorsal caudate

Striatal and extrastriatal ^{123}I-FP-CIT binding in multiple system atrophy and progressive supranuclear palsy

Juho Joutsa[1,2,3], Marko Seppänen[4], Tommi Noponen[4], Valtteri Kaasinen[1,2,3]

[1]Turku PET Centre, University of Turku, Turku, Finland; [2]Division of Clinical Neurosciences, Turku University Hospital, Turku, Finland; [3]Department of Neurology, University of Turku, Turku, Finland; [4]Department of Nuclear Medicine, Turku University Hospital, Turku, Finland

Introduction: ^{123}I-FP-CIT SPECT can be used to aid differential diagnosis between neurodegenerative parkinsonism syndromes and conditions that are not associated with dopaminergic defects. However, it is not known if the method is useful in the differentiation of idiopathic Parkinson's disease (PD) from other, more aggressive parkinsonism syndromes, such as progressive supranuclear palsy (PSP) or multiple system atrophy (MSA).

Methods: Patients with clinical diagnoses of PSP and MSA were searched from our database of 563 patients scanned with ^{123}I-FP-CIT SPECT at Turku University Hospital during years 2007-2012. Eight patients with the clinical diagnosis of probable MSA (5 MSA-P and 3 MSA-C) and 13 with probable PSP were identified. As PSP patients were older compared to MSA patients (72 vs 62 year, p=0.02), separate groups of demographically and clinically comparable PD patients served as controls (n=16 and n=26, respectively). Striatal ^{123}I-FP-CIT binding was analyzed using semiquantitative region-of-interest analysis. Separate voxel-by-voxel analysis was used over the entire brain (SPM8).

Results: PSP patients had 18.8% lower caudate nucleus binding (p=0.03) and 20.3% lower caudate-to-posterior putamen ratio (p=0.02) compared to PD patients. In voxel-based analyses, patients with PSP had lower binding in the midbrain, caudate nuclei, thalamus, ventral striatum, insula and prefrontal cortex compared to patients with PD (cluster-level P_{FWE}<0.001, Figure). There were no significant differences between MSA and PD patients or between PSP and MSA patients.

Discussion: ^{123}I-FP-CIT SPECT shows reduced binding in the midbrain, thalamus and frontostriatal regions in PSP compared to PD patients with matched age, sex and symptom duration. Striatal binding defects in PSP likely reflect losses in dopamine transporter whereas extrastriatal also serotonin transporter. The results indicate that PSP is associated with a more widespread degeneration of monoaminergic pathways than the degeneration seen in PD.

P-019
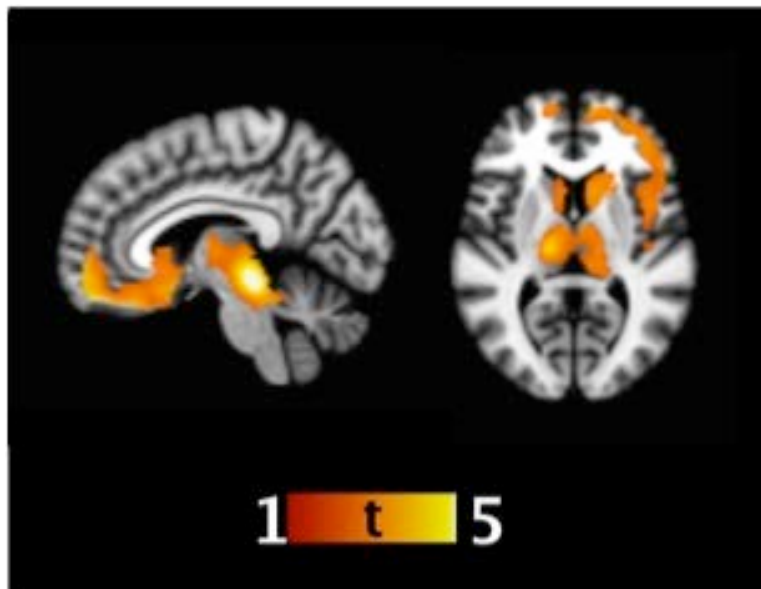
Preliminary evidence of a TSPO polymorphism genotype-disease interaction in manifest Parkinson's and subjects at risk

V Sossi[1], R Mabrouk[1], M Walker[1], N Heffernan[1], J Mackenzie[1], K Dinelle[1], M Sacheli[1], M Farrer[1], Jan Aasly[2], Z Wszolek[3], Q Miao[1,4], M Adam[4], AJ Stoessl[1]

[1] *University of British Columbia, Vancouver, BC, Canada;* [2] *NTNU, Trondheim, Norway;* [3] *Mayo Clinic, Jacksonville, FL, USA;* [4] *TRIUMF, Vancouver, BC, Canada*

Objectives. To investigate evidence of neuroinflammation in subjects with sporadic Parkinson's disease (PD) and asymptomatic PD LRRK2 mutation carriers.

Background. Increased neuroinflammation is hypothesized to be a potential disease initiating or disease promoting factor in neurodegeneration. Published imaging studies performed in PD subjects show controversial results. A possible confound may be due to the use of different tracers that are currently used to investigate neuroinflammation. While all tracers bind to the 18-kDa Translocator Protein (TSPO), their binding affinity varies. Most importantly, it was shown that using any second generation TSPO ligand, subjects can be classified into high, medium and low affinity binders (HAB, MAB, LAB) with the affinity state determined by TSPO polymorphism. HAB and LAB express a single binding site for TSPO either with high or low affinity, while MAB express a mixture of the two. The difference in relative affinities is tracer dependent. ^{11}C-PBR28, which is one of the most commonly used tracers, has a very large difference in the binding affinity for the two sites (K_{IH}= 3.4nM, K_{IL}=188nM)(*1*).

Methods. The study included 12 HABs and 14 MABs. **MAB**: 4 subjects were healthy controls (HC) (age 44±16, mean, std; range 24-63), 6 were subjects with PD (age 67±14; range 48-86, disease duration 5 ± 4 yrs; range 1 - 10) and 4 were unaffected LRRK2-mutation carriers (age 48± 11; range 37-61). **HAB:** 5 HC (age 65 ±14; range   47-80), 4 PD (age 55 ± 6; range   48-62; disease duration 5 ± 1 yrs; range 4-6) and 3 unaffected mutation carriers (age 57 ± 9 yrs; range 49-67). All subjects were injected with 20 mCi of [^{11}C]-PBR28 and dynamic PET scans were performed for 90 minutes. Time-averaged images from 30 min intervals of scanned data (60-90 min) were calculated and converted into standard uptake value (SUV) images. SUV values were cross-validates with plasma input Logan derived V_T values for a subset of subjects, including HAB and MAB, where plasma data were available.

Results. Very good correlation was obtained between the V_T and SUV values (R^2 = 0.83, p<0.001) indicating that in these populations SUVs are likely a reliable quantitative measure. The overall results were very different between the MABs and HABs.   For the MAB, the SUV values were significantly elevated in all brain regions for the asymptomatic mutation carriers compared to controls (p < 0.0001) (figure 1). All but one PD subject also exhibited elevated SUV values (p=0.05 after correction for age). No difference was observed between HAB groups in any brain region.

Discussion and conclusion. The MAB results show a significant and diffuse increase in neuroinflammation in subjects at increased risk for PD indicating that neuroinflammation may precede overt disease and continue (although in a more variable way) once disease is manifest. However the HAB did not show similar findings. While the reason for the difference is at present unclear and these finding may be limited by the low number of subjects, similar differences may partially explain different findings existing in the literature.

References:
1.   Guo Q, Owen DR, Rabiner EA, Turkheimer FE, Gunn RN. Identifying improved TSPO PET imaging probes through biomathematics: The impact of multiple TSPO binding sites in vivo. Neuroimage. 2012;60:902-910.
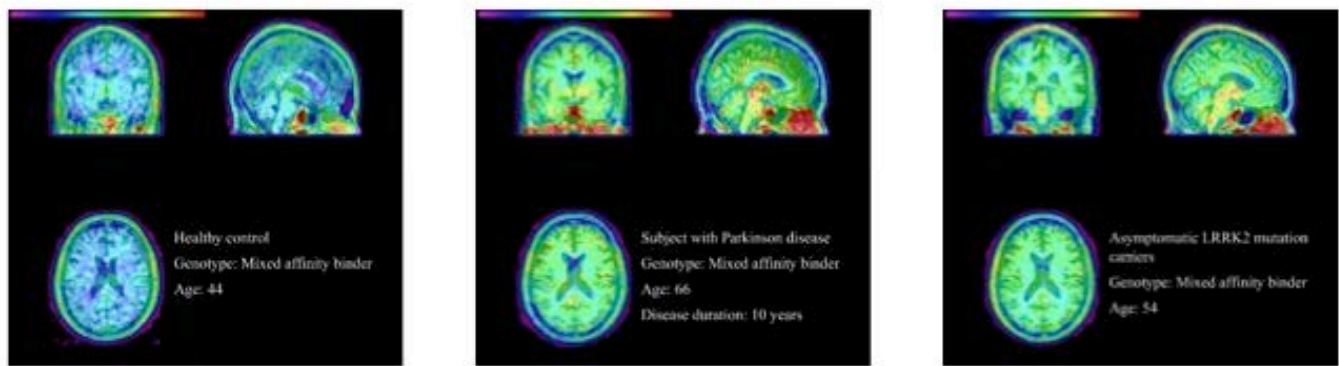
Figure 1- Caption. SUV parametric images for a healthy control, a PD subject and a LRRK2 mutation carrier. Images are scaled to the same maximum.

P-020

Preclinical characterization and initial clinical results for [18F]MK-6240, a PET tracer with high selectivity and sensitivity for neurofibrillary tangles (NFTs)

Eric D Hostetler[1], Abbas M Walji[1], Zhizhen Zeng[1], Patricia Miller[1], Idriss Bennacef[1], Cristian Salinas[1], Talakad G Lohith[1], Marie Holahan[1], Kerry Riffel[1], Liza Gantert[1], Hyking Haley[1], Mona Purcell[1], Wenping Li[1], Aileen Soriano[1], Brett Connolly[1], Paul Coleman[1], Jing Li[1], Aimie Ogawa[1], Serena Xu[1], Xiaoping Zhang[1], Elizabeth Joshi[1], Joseph Della Rocca[1], Joel Schachter[1], David Hesk[1], David J Schenk[1], Florestina Telan-Choing[1], Cyrille Sur[1], Arie Struyk[1], Ruben Declercq[2], Tom Reynders[2], Sofie Celen[3], Guy Bormans[3], Kim Serdons[4], Michel Koole[4], Jan de Hoon[4], Rik Vandenberghe[4], Koen Van Laere[4], Jeffrey L Evelhoch[1]

[1]Merck & Co., Inc., USA; Merck Sharp & Dohme (Europe) Inc., Belgium; [3]KU Leuven, Belgium; [4]UZ Leuven, Belgium

Objectives: Alzheimer's Disease (AD) is a terminal neurodegenerative disease with no effective disease-modifying treatments. To facilitate the discovery of novel therapeutics, biomarkers are needed that provide confidence in the therapeutic mechanism prior to large investments in clinical efficacy trials. The abundance of postmortem neurofibrillary tangles (NFTs) has been histopathologically correlated with disease progression and cognitive decline. Development of a PET tracer with high specificity and sensitivity for NFTs may provide a useful tool to determine if novel therapeutic candidates are able to modify the progression of NFTs as an indicator of disease progression in patients.

Methods: Log D was determined from the octanol/water partition coefficient at pH 7.4. In vitro binding studies were performed with [3H]MK-6240 in human AD and non-AD brain homogenates and slices which were characterized by immunohistochemistry for amyloid plaque and NFT abundance. Nondisplaceable binding (NDB) was defined by self-block or by block with T808, a structurally dissimilar NFT ligand. [18F]MK-6240 was prepared in high specific activity by nucleophilic displacement of a nitroarene precursor with [18F]KF/K2.2.2. [18F]MK-6240 PET studies were performed in anesthetized rhesus monkeys and in healthy human volunteers.

Results: MK-6240 was identified as a high affinity (K_D = 0.3 nM in NFT-rich AD brain homogenate), moderately lipophilic (Log D = 3.3), highly selective (K_i > 10 uM in plaque-rich NFT-poor AD brain homogenate) ligand for NFTs. In vitro binding studies with [3H]MK-6240 in human NFT-rich AD brain homogenates and slices provided similar levels of high displaceable binding whether NDB was defined by self-block or the structurally diverse NFT ligand T808, demonstrating the high sensitivity and selectivity of MK-6240 binding for NFTs. Furthermore, in vitro binding studies with [3H]MK-6240 in non-AD brains showed no displaceable binding. [18F]MK-6240 PET studies in rhesus monkey showed high, homogeneous tracer distribution in the brain which cleared rapidly. In self-block PET studies, no change in regional [18F]MK-6240 V_T values were observed, providing further evidence of selectivity for NFTs. In human whole-body PET studies, [18F]MK-6240 was safe and well-tolerated with excellent brain penetration, rapid clearance, and favorable radiation dosimetry.

Conclusion: [18F]MK-6240 is a promising PET ligand for quantification of NFTs and warrants continued evaluation in healthy elderly subjects and AD patients.

P-021

PET imaging of translocator protein detects inflammation after traumatic brain injury

Masahiro Fujita[1], L Christine Turtzo[2], Christian N. Shenouda[3], Emily R. Fennell[1], John A. Butman[4], Dzung L. Pham[3], Sarah Yang[3], Sami S. Zoghbi[1], Cheryl L Morse[1], Mohammad B. Haskali[1], Victor W. Pike[1], Ramon R. Diaz-Arrastia[3], Robert B. Innis[1], Lawrence L. Latour[2]

[1]National Institute of Mental Health, [2]National Institute of Neurological Disorders and Stroke, [3]Center for Neuroscience and Regenerative Medicine, [4]National Institutes of Health Clinical Center, Bethesda, MD, USA.

Objectives: Neuroinflammation is a secondary injury after traumatic brain injury (TBI) relevant to patient outcome. Magnetic resonance imaging (MRI) can identify foci of primary injury but cannot differentiate secondary inflammatory response. We investigated whether positron emission tomography (PET) imaging of translocator protein (TSPO) detects neuroinflammation in TBI patients—either around the primary site or in remote areas—that are not detectable by MRI.

Methods: Twenty-five TBI subjects (49 ± 15 years, 5F/20M) with TBI-related MRI changes were studied; eight subjects had a PET scan within approximately three months of injury and 17 after approximately three months of injury. Four of the eight subjects with an initial PET scan within three months had a follow-up PET scan two to 14 months later. The lowest Glasgow Coma Scale rating for each subject was 14±3. Among those subjects who had an initial PET scan within three months, extra-axial lesions (i.e., subdural and subarachnoid hemorrhage) were prominent on MRI in three subjects, microhemorrhage and diffuse axonal injury (DAI) were prominent in two subjects, and contusion was prominent in three subjects. Among the 17 subjects scanned more than three months post-injury, extra-axial lesions were prominent in seven, microhemorrhage/DAI was prominent in five, and contusion was prominent in five. Among the seven subjects scanned three months post-injury with extra-axial-prominent lesions, two had large hemorrhages expanding to one hemisphere that required surgical drainage. TSPO was measured as V_T using ^{11}C-PBR28 and metabolite-corrected arterial input function.

Results: PET and MRI showed markedly different findings in some but not all subjects. One of two subjects with large subdural hematoma showed a widespread ~20% TSPO increase compared with the contralateral side despite not having MRI-visible lesions in brain parenchyma at the time of PET (Fig. 1). This subject with increased TSPO showed MRI-contrast enhancement of the meninges in the injured hemisphere at the time of PET, suggesting persistent extra-axial inflammation. Changes in TSPO were undetectable in the other subjects with smaller extra-axial hemorrhages. TSPO around microhemorrhage/DAI showed time-related changes undetectable by MRI. Of the two subjects with microhemorrhage/DAI who had PET scans at two time points within less than three months, one showed an approximately 15% increase of TSPO at two weeks but not at three months (Fig. 2); the other showed increased TSPO over time. No subjects with microhemorrhage/DAI who had a PET scan six months to three years after injury showed detectable TSPO increases, indicating that TSPO increases in microhemorrhage/DAI are temporal. Regardless of the time since injury, larger contusion lesions tended to show greater increases in TSPO.

Conclusions: The complexity of TBI is reflected in these diverse findings, and some may be more relevant to secondary inflammation than others. We found that inflammation can be detected with TSPO in some, but not all, patients in areas both close to and remote from the regions of focal injury. Therefore, PET imaging of TSPO may identify patients in whom post-traumatic brain inflammation is a significant component of tissue response to injury that cannot be identified by MRI alone.

Fig. 1

FLAIR
1 day

FLAIR
10 mo.

PET
12 mo.
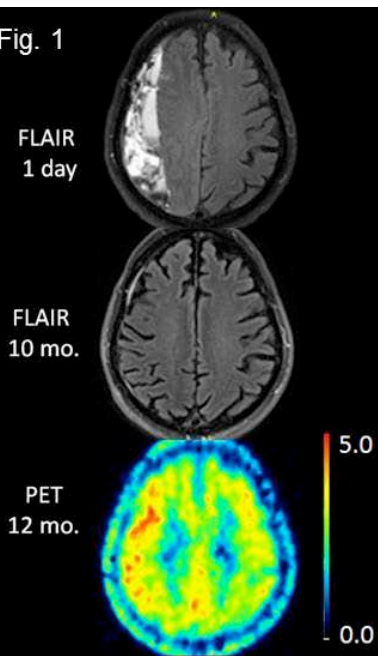
Fig. 2a

Axial

GRE 1 day
PET 13 days

GRE 96 days
PET 92 days

b
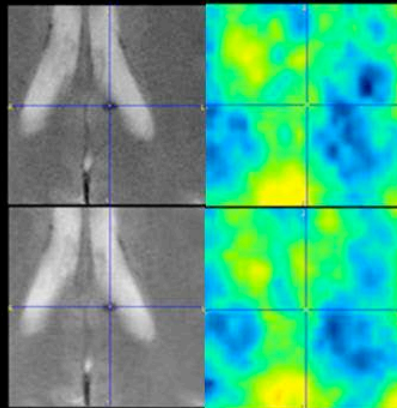
Saggital
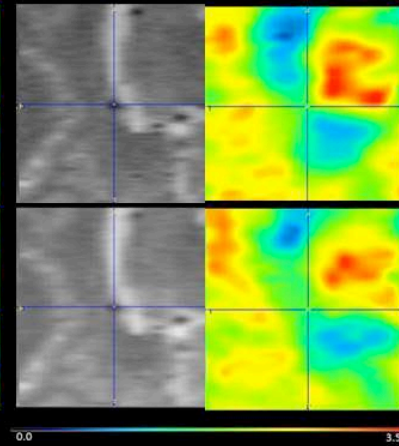
Olfactory Neuron Population Monitoring in Neurodegenerative Disease: Toward Human Translation of a PET Imaging Agent

Genevieve Van de Bittner[1], Misha Riley[1], Luxiang Cao[2], Janina Ehses[1], Hsiao-Ying Wey[1], Ramesh Neelamegam[1], Mark Albers[2], Jacob Hooker[1]

[1]Department of Radiology, Athinoula A. Martinos Center for Biomedical Imaging, Massachusetts General Hospital, Harvard Medical School, Charlestown, MA, USA; [2]Department of Neurology, Massachusetts General Hospital, Harvard Medical School, Charlestown, MA, USA

Background: Olfactory dysfunction is an early, detectable sign of several neurodegenerative diseases and is associated with cognitive decline in aging. We have developed a PET imaging tool, [11C]neuroflux, which specifically binds the mature olfactory sensory neurons (OSNs), which mediate the sense of smell, and quantifies the steady-state OSN population. Applied to longitudinal imaging, [11C]neuroflux provides a measurement of OSN population flux, or the net change in the neuron population over time. We hypothesize that in neurodegenerative disease [11C]neuroflux may elucidate the underlying biological etiology of olfactory dysfunction, measure the severity of OSN loss, and provide an imaging tool for monitoring therapeutic efficacy.

Methods: To begin assessment of this hypothesis, we have gathered data from rodent models and non-human primates, and we will commence first-in-human studies in early 2016. In a proof of concept model, [11C]neuroflux was applied to imaging OSN neurodegeneration during normative aging in rats. Beginning at 5 months of age, rats were monitored via [11C]neuroflux imaging every three months until death. To assess [11C]neuroflux in neurodegenerative disease, the murine rTg4510 tauopathy model was scanned at an early-symptomatic stage (3.7 months) and a severe neurodegeneration stage (7 months). To address the clinical aspects of our hypothesis, we first adapted [11C]neuroflux to fluorine-18 PET imaging to provide a more widely-accessible imaging agent. [18F]Neuroflux has been administered to rhesus macaque following treatment with vehicle or a dose of non-radiolabeled [18F]neuroflux.

Results: [11C]Neuroflux imaging during aging identifies individual-specific rates of OSN population flux and reveals the presence of OSN neurodegeneration beginning at approximately 12 months, or middle age. Ongoing longitudinal aging studies with intermittent [11C]neuroflux imaging aim to compare the magnitude and rate of OSN loss with individual lifespan. [11C]Neuroflux imaging was additionally applied to the rTg4510 tauopathy model, which develops a severe neurodegenerative phenotype with concomitant negative effects on memory and behavior. Significant reductions in neuroflux binding, 17% ($P < 0.05$) at 3.7 months and 34% ($P < 0.005$) at 7 months, were found in the rTg4510 animals relative to age-matched controls, identifying a novel, early-stage OSN neurodegeneration phenotype. Finally, the translational potential of neuroflux was assessed through administration of [18F]neuroflux to rhesus macaque, demonstrating a maintained binding to the olfactory sensory neurons across species.

Conclusions: Neuroflux exhibits sensitive detection of neurodegeneration in rodent models of aging and tauopathy. The stratification of healthy and tauopathy animals at 3.7 months, prior to significant cortical neurodegeneration, positions neuroflux uniquely for the assessment of the global OSN population in patients early-stage neurodegenerative disease. The translation of [18F]neuroflux to imaging patients with neurodegenerative disease is further supported by specific binding of [18F]neuroflux to OSNs in a non-human primate specie. Over the next several months, [18F]neuroflux will undergo first-in-human trials, laying the groundwork for clinical research studies in patient populations.

Brain Areas Associated with Cognitive Impairment in Small Vessel Disease: A Diffusion Tensor Imaging and [18F]FDG PET Study

Min-Jeong Kim[1,2], Kyoung-Min Lee[2], Young-Don Son[3], Hyeon-Ae Jeon[4], Sejin Yoo[5], Young-Bo Kim[3], Zang-Hee Cho[3]

[1]*Molecular Imaging Branch, National Institute of Mental Health, National Institutes of Health, Bethesda, MD, USA;* [2]*Department of Neurology, Seoul National University Hospital, Seoul, Republic of Korea;* [3]*Neuroscience Research Institute, Gachon Medical School, Incheon, Republic of Korea;* [4]*Department of Neuropsychology, Max Planck Institute for Human Cognitive and Brain Sciences, Leipzig, Germany;* [5]*Interdisciplinary Program in Cognitive Science, Seoul National University, Seoul, Republic of Korea*

Objectives: Cerebral small vessel disease (SVD)—which presents on magnetic resonance imaging (MRI) as subcortical white matter hyperintensities, lacunar infarcts, and microbleeds—significantly contributes to cognitive decline in old age, although it is commonly observed in the normal elderly population as well. The specific brain areas linked to cognitive impairment, and the associated mechanism of action, remains unclear. Several hypotheses have been suggested regarding the pathophysiology of SVD, including disruption of the limbic circuit or cholinergic pathways, interruption of cortico-subcortical connection, and altered cortical blood flow [1]. This study sought to compare the affected brain areas between those with and without cognitive impairment in SVD subjects; subcortical areas were evaluated via diffusion tensor imaging (DTI) and cortical areas by [18F]Fluorodeoxyglucose (FDG) PET. We also sought to investigate the association between relevant cortical and subcortical areas in order to identify the most feasible hypothesis.

Methods: Twenty-nine SVD subjects with MRI data available were included in the study; 10 healthy subjects without SVD were included as a normal control group. Subjects with SVD were classified into two groups based on their cognitive assessment results: 17 subjects had cognitive impairment (SVD-CI) and 12 subjects had no cognitive impairment (SVD-NCI). Mean age of SVD-CI, SVD-NCI, and normal control group was 73.5, 65.6, and 67.1 years, respectively, and there was no significant difference of gender distribution among the groups. All subjects underwent DTI, [18F]FDG PET, and 3-dimensional T1 MRI. On DTI, fractional anisotropy (FA) was compared between the groups on a whole brain basis using tract-based spatial statistics (TBSS). [18F]FDG PET data were also compared between the groups by voxel-based analysis with MRI co-registration. Both comparisons were adjusted for age, sex, and education level. Tracts-of-interest (TOIs) were selected on the basis of significant TBSS results, and the averaged FA in each TOI was defined as the representative value. Cortical areas with significant associations were delineated between each FA of TOI and [18F]FDG uptake.

Results: Compared to SVD-NCI subjects, SVD-CI subjects showed significantly decreased FA values in the cingulum, corona radiata, superior longitudinal fasciculus, and, partly, in the inferior longitudinal fasciculus. SVD-CI subjects also had significantly lower [18F]FDG uptake in the dorsolateral prefrontal, orbitofrontal, and medial frontal cortices, perisylvian cortices, and lateral inferior temporal cortices compared to SVD-NCI subjects. These areas showed considerable overlap with the distribution of cortical areas, showing significant correlations between [18F]FDG uptake and representative FAs of each TOI.

Conclusion: In SVD subjects, the major differences between those with and without cognitive impairment were observed along the well-known cortical and subcortical cholinergic pathways [2]. In addition, cortical and subcortical areas showed significant correlation as observed via DTI and [18F]FDG PET. These findings support the notion that cognitive impairment due to SVD will be mainly attributable to ischemic damage and disconnection of subcortical cholinergic fibers and concomitant secondary dysfunction in the fronto-temporal cortices.

References:
[1] Menon U et al., Int Rev Neurobiol 2009; 84: 21-33; [2] Selden NR et al., Brain 1998; 121: 2249-57
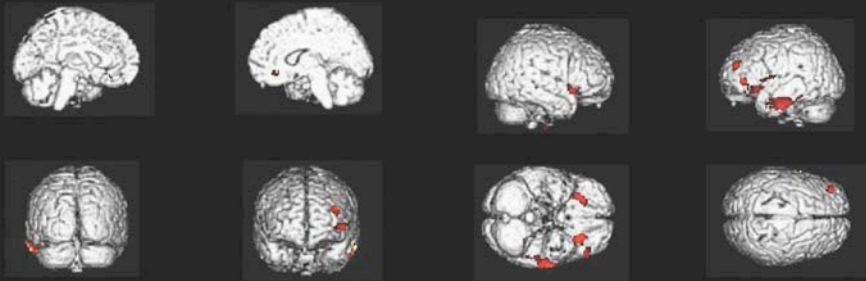
Figure. Voxel-wise comparison of fractional anisotropy (A) and [¹⁸F]FDG uptake (B) between SVD-NCI and SVD-CI groups. (A) The results are superimposed on the fiber skeleton (Green color). Red and yellow colors mean significant difference. SVD-NCI, small vessel disease with no cognitive impairment; SVD-CI, small vessel disease with cognitive impairment.

Serotonin 1B receptor binding is associated with trait anger and level of psychopathy in violent offenders

Sofi da Cunha-Bang[1,2] , Liv V. Hjordt[1,2], Erik Perfalk[1,2], Vincent Beliveau[1,2], Camilla Bock[3], Szabolcs Lehel[4], Carsten Thomsen[5], Dorte Sestoft[6], Claus Svarer[1], Gitte Moos Knudsen[1,2]

[1] *Neurobiology Research Unit and Center for Integrated Molecular Imaging, Rigshospitalet, Copenhagen, Denmark.* [2] *Faculty of Health and Medical Sciences, University of Copenhagen, Denmark.* [3] *The Danish Prison and Probation Service, Anstalten Herstedvester, Denmark.* [4] *PET and Cyclotron Unit, Rigshospitalet, Copenhagen, Denmark.* [5] *Department of Radiology, Rigshospitalet, Copenhagen, Denmark.* [6] *Ministry of Justice, Clinic of Forensic Psychiatry, Copenhagen, Denmark.*

Background: The involvement of serotonin in aggression has traditionally been attributed to impaired prefrontal serotonergic inhibitory control of emotional reactions to provocations in antisocial individuals. However, it is unclear which specific serotonergic receptors are involved in the effects. A large body of preclinical research support a specific role of serotonin 1B receptors (5-HT_{1B}) in aggression and impulsivity, but this has never been evaluated in humans. Given that knockout of 5-HT_{1B} increase aggression in mice, we hypothesized that individuals with high levels of aggression would have reduced 5-HT_{1B} binding compared to non-aggressive controls, and that 5-HT_{1B} binding would be inversely correlated with measures of aggression, anger and psychopathy.

Methods: Nineteen incarcerated violent offenders and 24 healthy control non-offenders were included and examined with positron emission tomography, using the radioligand [^{11}C]AZ10419369 for quantification of cerebral 5-HT_{1B} binding. Level of psychopathy was assessed using the Psychopathy Checklist-Revised (PCL-R) in violent offenders, and all participants completed self-report measures of trait anger, trait aggression and trait psychopathy. We focused on 3 brain regions of interest (ROIs); the anterior cingulate cortex, orbitofrontal cortex (OFC) and striatum, as they have consistently shown structural and or functional abnormalities in violent and aggressive individuals. Voxel-based analysis was performed to evaluate possible effects in non-hypothesized regions. Group comparisons in 5-HT_{1B} binding were evaluated using unpaired t-tests and associations were evaluated in multiple linear regression analyses with scale measures as outcome variables and regional 5-HT_{1B} binding as the predictive variables, adjusting for age, group status, intelligence quotient and injected mass/kg bodyweight.

Results: Interactions between group and 5-HT_{1B} binding within the striatum significantly predicted trait anger ($p=0.01$) and trait psychopathy ($p=0.05$). In the violent offender group striatal 5-HT_{1B} binding was positively associated with self-reported trait anger ($p=0.002$, fig. 1A), trait psychopathy ($p=0.01$, fig. 1B) and with level of psychopathy (PCL-R, $p=0.03$, fig. 1C). Whole-brain voxel-wise analysis in the violent offenders confirmed the positive correlation between 5-HT_{1B} binding and trait anger in the caudate (cluster size: 178 voxels, z: 4.65, $p<0.05$ corrected, x=14 y=18 z=4) and OFC (cluster size: 183 voxels, z: 4.09, $p<0.05$ corrected, x=36 y=42 z=-8). We found no group differences in 5-HT_{1B} binding in the ROIs or in the voxel-based analysis.

Conclusions: Our data demonstrate for the first time in humans a specific involvement of 5-HT_{1B} binding in anger and psychopathy. The findings markedly support the involvement of serotonin in aggression, and suggest that striatal 5-HT_{1B} binding reflects symptom severity in individuals with pathological aggression. 5-HT_{1B} putatively represent a molecular target for development of pharmacological anti-aggressive treatments.

1A

1B

1C
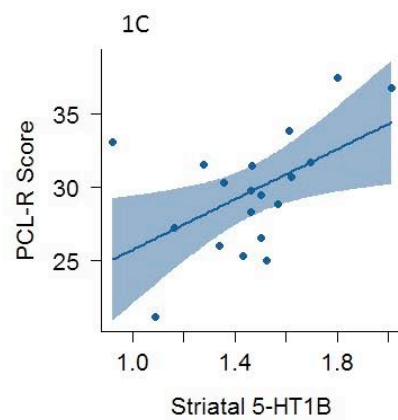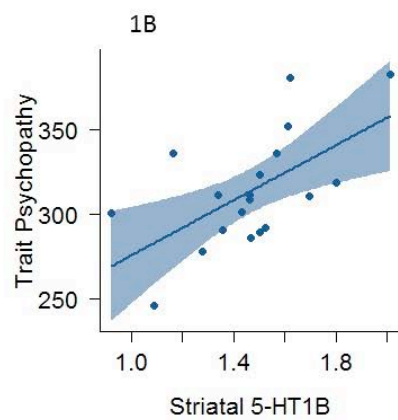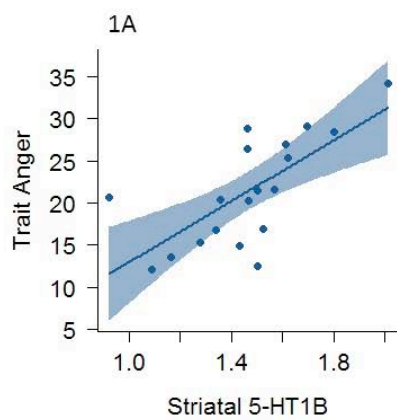
Circadian pattern of the metabotropic glutamate receptor 5 in the rat brain

David Elmenhorst[1], Kristina Mertens[1], Tina Kroll[1], Angela Oskamp[1], Johannes Ermert[2], Eva-Maria Elmenhorst[3], Franziska Wedekind[1], Simone Beer[1], Heinz H. Coenen[2] and Andreas Bauer[1]

[1] Institute of Neuroscience and Medicine, INM-2, Forschungszentrum Jülich, Jülich, Germany; [2] Institute of Neuroscience and Medicine, INM-5, Forschungszentrum Jülich, Jülich, Germany; [3] Institute of Aerospace Medicine, German Aerospace Center, Cologne, Germany

In psychiatric disorders like depression the subtype 5 of the metabotropic glutamate receptor (mGluR5) is a recent topic of research. It is involved in synaptic plasticity and it has been shown that mGluR5 availability in the human brain is increased after sleep deprivation. This study investigated in a rat model if mGluR5 availability underlies a circadian variation.

Its density was determined in a counterbalanced order at 6 different daytimes in 11 adult Sprague Dawley rats during a 7am/7pm light/dark cycle. MGluR5 availability was quantified by using the radioligand [^{11}C]ABP688 and small animal positron emission tomography (PET). [^{11}C]ABP688 cerebral uptake was computed in nine volumes of interest by the use of a reference tissue model.

Between the different circadian times significant differences in the binding potential (BP_{ND}) were found in cortex, cingulate cortex, amygdala, caudate-putamen and nucleus accumbens. Post hoc statistical analysis of the respective time points revealed significant changes in BP_{ND} between the start of light-on phase (7am) and the second third of the light-on phase (3pm) in caudate-putamen.

This study reveals that mGluR5 availability is elevated during the sleep or light-on phase of rats by approximately 10%. The pattern of glutamatergic receptor expression observed (nadir of mGluR5 at the end of the dark phase) is anticyclical to the circadian changes of glutamate levels reported in the literature. A possible explanation besides receptor plasticity could be that endogenous glutamate blocks the radioligand binding.

[^{11}C]AZ10419096 - a full antagonist PET radioligand for imaging 5-HT$_{1B}$ receptors

Anton Lindberg[1], Magnus Schou[2], Sangram Nag[1], Akihiro Takano[1], Charles S. Elmore[3], Victor W. Pike[4], Christer Halldin[1]

[1]Karolinska Institutet, Department of Clinical Neuroscience, Centre for Psychiatric Research, Karolinska University Hospital, Stockholm, Sweden; [2]Personalised Healthcare and Biomarkers, Innovative Medicines and Early Development Biotech Unit, AstraZeneca Translational Science Centre at Karolinska Institutet, Stockholm, Sweden; [3]Isotope chemistry, Enabling Services, Drug Safety and Metabolism, AstraZeneca; [4]Intramural Research Program, National Institute of Mental Health, NIH, Bethesda, Maryland, USA

Background: Among reported radioligands for imaging the serotonin (5-HT) 1b receptor with positron emission tomography (PET) [1,2], [^{11}C]AZ10419369 has demonstrated sensitivity to elevated endogenous 5-HT levels in the monkey brain [3]. Interestingly, although originally referred to as an antagonist, [^{11}C]AZ10419369 appears to be a partial agonist at the 5-HT$_{1B}$ receptor (antagonist GTPγS effect 48%; agonist GTPγS effect 53%). In relation to this updated view on the intrinsic activity of AZ10419369, we herein aimed to explore how the intrinsic activity of a 5-HT$_{1B}$ receptor radioligand affects its sensitivity to endogenous 5-HT.   Thus, from a library of over 3000 compounds, we identified the high-affinity full antagonist AZ10419096 (antagonist GTPγS effect 190%; 5-HT$_{1B}$ IC_{50}: 2 nM) as a prospective PET radioligand for the 5-HT$_{1B}$ receptor.

Methods. N-Desmethyl-AZ10419096 was prepared in high purity by demethylation of AZ10419096.   [^{11}C]AZ10419096 (938 ± 283 MBq) was obtained by rapid methylation of the N-desmethyl compound with [^{11}C]methyl triflate (Fig. 1A), followed by HPLC purification and formulation for intravenous injection.   [^{11}C]AZ10419096 (169 ± 9 MBq; 528 ± 230 GBq/μmol) was administered to two cynomolgus monkeys (4–7.75 kg) in baseline PET experiments and regional brain radioactivity was recorded over 120 min.   Venous blood was sampled at different times during the PET measurements for HPLC analysis of radioligand metabolites in plasma.   5-HT$_{1B}$ receptor-poor cerebellum was used as a reference region for PET data analysis with a simplified reference tissue model (SRTM).

Results.   Following intravenous injection of [^{11}C]AZ10419096, radioactivity in monkey brain rapidly reached a maximum of ~ 1.75 SUV (3% I.D.).   After this initial peak there was a heterogeneous distribution of radioactivity within brain with higher radioactivity observed in regions known to be rich in the 5-HT$_{1B}$ receptor (Fig. 1B).   Thus, higher radioactivity was observed in the cortex, thalamus and striatum than in the cerebellum (Fig. 1C–1E).   Differences in radioactivity between 5-HT$_{1B}$ receptor-rich regions and cerebellum peaked by 40 min and the ratios of binding in these regions to that in cerebellum ranged from 1.2 in caudate to 3 in occipital cortex, corresponding to BP_{ND} values from SRTM of 0.38 and 1.19, respectively.   Thirty minutes after injection, 60% of the radioactivity in plasma corresponded to parent and the observed radiometabolites were more polar than [^{11}C]AZ10419096.

Conclusions.   [^{11}C]AZ10419096 is a promising full antagonist PET radioligand for imaging brain 5-HT$_{1B}$ receptors and merits further characterization and evaluation for sensitivity to endogenous serotonin.

References:
[1] Finnema S.J. *et al*. Synapse 64:573-577 (2010).
[2] Nabulsi N. Nucl. Med. Biol. 37:205-214 (2010).
[3] Finnema S.J. *et al.* J. Cerebr. Blood Flow Metab. 32: 685-695 (2012).
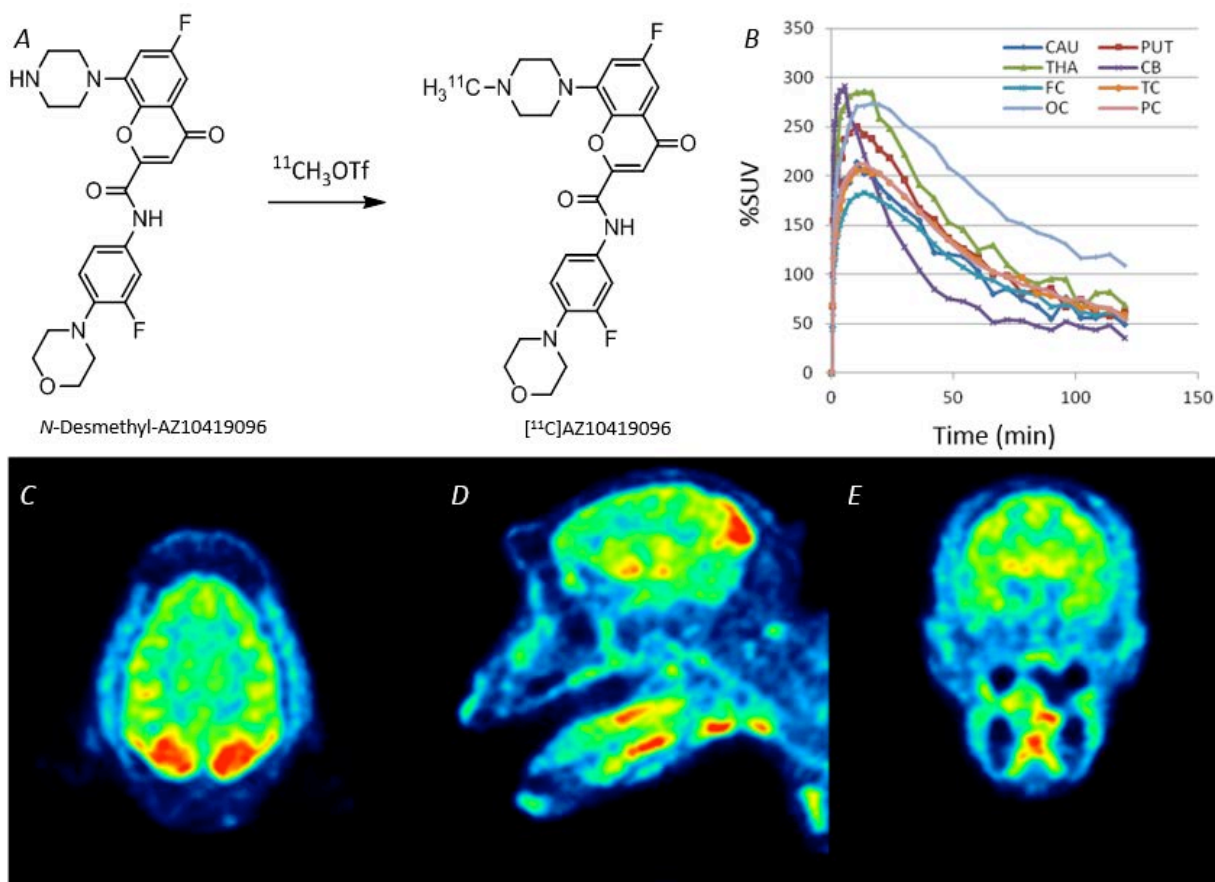
Figure 1. (A) Labelling scheme for [^{11}C]AZ10419096. (B) Regional time-activity curves, (CAU: caudate, PUT: putamen, THA: thalamus, CB: cerebellum, FC: frontal cortex, TC: temporal cortex, OC: occipital cortex, PC: parietal cortex.). (C–E) PET Summation image (9-93min), (C) Horizontal view, (D) Sagittal view, (E) Frontal view.

Dopamine and opioid neurotransmission in behavioral addictions: A comparative PET study in pathological gambling and binge eating

Joonas Majuri[1,2], Juho Joutsa[1,2], Jarkko Johansson[1], Kati Alakurtti[1,3], Riitta Parkkola[3], Tuuli Lahti[4], Hannu Alho[4], Eveliina Arponen[1], Sarita Forsback[1], Valtteri Kaasinen[1,2]

[1]Turku PET Centre, University of Turku, Turku, Finland, [2]Division of Clinical Neurosciences, Turku University Hospital, Turku, Finland, [3]Department of Radiology, Turku University Hospital, Turku, Finland, [4]Department of Health, Unit of Tobacco, Alcohol and Gambling, National Institute for Health and Welfare, Helsinki, Finland

Background: The term 'behavioral addictions' refers to a group of heterogeneous conditions that are characterized by compulsive pursuit of rewards through repetitive behavioral patterns. Although these disorders share many clinical features with drug addictions, they show strikingly large variation in their behavioral phenotypes (e.g. pathological gambling [PG] and binge eating disorder [BED]). Whether different behavioral addictions result from neurobiologically similar mechanisms has importance not only in the classification of these disorders, but in their pharmacological treatment efforts. Therefore, the aim of this study was to investigate neurobiological similarities and differences in patients with PG and BED.

Methods: Fifteen patients with PG, seven patients with BED and seventeen healthy age-matched volunteers were scanned with [^{11}C]carfentanil and [^{18}F]fluorodopa PET using a Siemens high-resolution research tomograph (HRRT). Freesurfer software was used to define regions of interest (ROIs) using T1-weighted MR images. Binding potentials relative to non-displaceable binding (BP_{ND}) for [^{11}C]carfentanil and K_i values for [^{18}F]fluorodopa were calculated using the occipital cortex as the reference region. Parametric images were normalized to the Montreal Neurological Institute (MNI) space and analyzed voxel-by-voxel over the entire brain using general linear model in SPM8. Cluster-level family-wise error (FWE) corrected P-values less than 0.05 were considered statistically significant.

Results: [^{11}C]Carfentanil BP_{ND} in the nucleus accumbens was 29.7% lower in BED compared to PG and 34.4% lower in BED compared to controls (p<0.001). [^{18}F]Fluorodopa K_i in the nucleus accumbens was 19.7% lower in BED compared to PG (p=0.001) and 20.4% lower compared to controls (p<0.001). Using [^{11}C]carfentanil, BED patients showed binding losses also extrastriatally in several cortical brain regions whereas differences in [^{18}F]fluorodopa uptake were restricted to the nucleus accumbens and the putamen when compared to controls. PG patients showed only slightly reduced [^{11}C]carfentanil BP_{ND} in the anterior cingulate compared to controls and no differences in [^{18}F]fluorodopa uptake. The results remained the same when only women and non-smokers were included in analyses. Voxel-by-voxel analyses confirmed the findings by showing clearly reduced tracer bindings in BED in similar areas as in ROI comparison (Figure, left: BED vs. controls with [^{11}C]carfentanil, right: BED vs. controls with [^{18}F]fluorodopa).

Conclusions: There are substantial neurotransmitter differences between BED and PG. Compared to PG patients, BED patients show widespread losses of mu-opioid receptor binding together with more regionally limited dopaminergic defects. These differences can be detected particularly in structures of the brain reward system, such as the nucleus accumbens. The results suggest fundamental neurobiological differences between phenotypically different behavioral addictions.
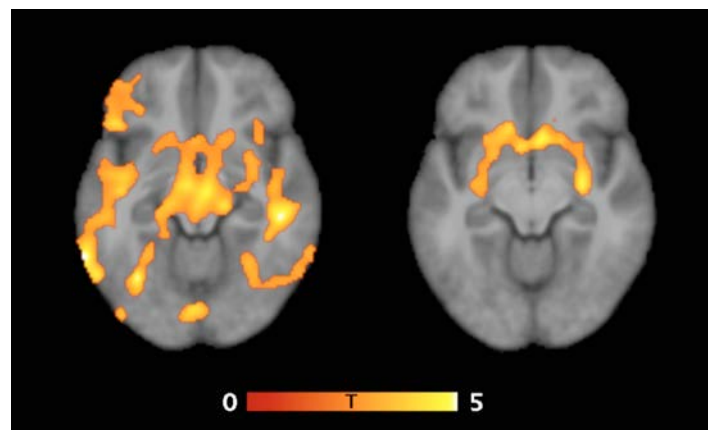
PET imaging of increased amyloid-beta accumulation in two mouse models of traumatic brain injury

Stina Syvänen[1], Dag Sehlin[1], Greta Hultqvist[1], Xiaotian T Fang[1], Lars Lannfelt[1], Anna Erlandsson[1] and Fredrik Clausen[2]

[1]Department of Public Health and Caring Sciences, Uppsala University, Uppsala, Sweden; [2]Department of Neuroscience, Uppsala University, Uppsala, Sweden

Background: It is well established that there is an epidemiological association between traumatic brain injury (TBI) and the development of neurodegenerative diseases such as Alzheimer's disease (AD) later in life. One pathological hallmark of the AD brain is insoluble plaques mainly consisting of amyloid-beta (*Aβ)* fibrils. However, *Aβ* aggregation starts with the formation of soluble aggregates that gradually increase in size. In addition it appears that the amount of these soluble aggregates, e.g. oligomers and protofibrils, rather than the amount of plaques, correlate with disease stage and that oligomers/protofibrils are neurotic and eventually cause the neurodegeneration observed in AD [1-2].

Objective: The aim of the study was to investigate the effect of TBI on the accumulation of *Aβ* protofibrils using PET in two mouse models of TBI.

Methods: Mice, tg-ArcSwe, harbouring the *Arctic (AβPP E693G)* and *Swedish (AβPP KM670/671NL)* AβPP mutations were subjected to either controlled cortical impact (**CCI**) or midline fluid percussion injury (**mFPI**) at the age of 3 months. Untreated tg-ArcSwe littermates were kept as controls. Spatial learning and memory was investigated 6 months after injury using the Morris water maze (MWM) test (four learning trials per day for four days). PET imaging using a radiolabeled antibody-based ligand targeting *Aβ* protofibrils [3] was performed 1-2 weeks later. Mice were then euthanized and the brain was isolated for post mortem analysis of *Aβ* levels and immunohistochemcial analysis of inflammation markers.

Results: Mice subjected to either mFPI or CCI performed significantly worse in the MWM test than controls. CCI mice tended to find the platform faster than mFPI mice. PET imaging revealed higher brain concentrations of the *Aβ* binding PET-ligand in mFPI and CCI mice compared with controls, especially in cortical regions. *Ex vivo* autoradiography confirmed the PET findings. Immunohistochemistry reveal co-localisation of *Aβ* and inflammation marker GFAP expressed by reactive astrocytes.

Conclusion: In order to prevent the onset of neurodegeneration following TBI, a better understanding of the cellular and molecular mechanisms triggering the first steps of the disease is highly desirable. Our data demonstrates that *Aβ* protofibrils are present in the brain in higher amounts in TBI subjected than in untreated tg-ArcSwe mice and that PET imaging can be used to detect this accelerated accumulation. Furthermore, the levels of *Aβ* protofibrils are correlated with cognitive function measured by MWM.

References

1. H. Fukumoto, T. Tokuda, T. Kasai, N. Ishigami, H. Hidaka, M. Kondo, D. Allsop, M. Nakagawa, High-molecular-weight beta-amyloid oligomers are elevated in cerebrospinal fluid of Alzheimer patients. FASEB J 24, 2716-2726 (2010).
2. T. J. Esparza, H. Zhao, J. R. Cirrito, N. J. Cairns, R. J. Bateman, D. M. Holtzman, D. L. Brody, Amyloid-beta oligomerization in Alzheimer dementia versus high-pathology controls. *Ann Neurol* **73**, 104-119 (2013).
3. D. Sehlin, X.T. Fang, L. Cato, G. Antoni, L. Lannfelt, S. Syvänen, Antibody-based PET imaging of amyloid-beta in mouse models of Alzheimer's disease. Accepted for publication in *Nature Communications* (2016).

Sensitivity of the α$_4$β$_2$*-Nicotinic Acetylcholine Receptor Radioligand (-)-[^{18}F]Flubatine to Acetylcholine Levels in Humans: Comparison of Bolus and Bolus Plus Infusion Paradigms.

Hillmer AT[1,2], Esterlis I[1,2,3], Gallezot JD[2], Bois F[2], Zheng MQ[2], Nabulsi N[2], Lin SF[2], Huang Y[2], Sabri O[5], Carson RE[1,2], Cosgrove KP[1,2,3,4]

[1]Department of Radiology and Biomedical Imaging, Yale University School of Medicine, New Haven, CT; [2]Yale PET Center, Yale University School of Medicine, New Haven, CT; [3]Department of Psychiatry, Yale University School of Medicine, New Haven, CT; [4]Department of Neurobiology, Yale University School of Medicine, New Haven, CT; [5]Department of Nuclear Medicine, University of Leipzig, Leipzig, Germany

Background: PET imaging techniques measuring changes in synaptic acetylcholine can provide new insight into the pathophysiology underlying neuropsychiatric disorders associated with altered acetylcholine function, such as substance abuse disorders, schizophrenia, and Alzheimer's disease. The goal of this work was to assess the binding sensitivity of the PET radioligand (-)-[^{18}F]flubatine (also called (-)-[^{18}F]NCFHEB), which is specific to α$_4$β$_2$*-nicotinic acetylcholine receptors, to changes in acetylcholine levels induced by the acetylcholinesterase inhibitor physostigmine. This was assessed with two experimental designs: a two-scan bolus radiotracer injection design (before and after physostigmine administration) and a single-scan design using bolus plus constant infusion (B/I) of radiotracer.

Methods: Healthy human subjects (n=13) were imaged with (-)-[^{18}F]flubatine PET, including arterial blood sampling to measure the metabolite-corrected parent input function. Time-activity curves were extracted from cerebellum, caudate, putamen, hippocampus, and frontal, occipital, parietal, and temporal cortices for analysis. The first set of scans (n=6) acquired PET data for 150 min immediately following bolus injection of 181± 77 MBq (-)-[^{18}F]flubatine. Scans were acquired at baseline (scan 1) and post-drug (scan 2; 1.5 mg physostigmine was given over 60 min, starting 5 min before radiotracer injection). Free-fraction corrected total distribution volumes (V_T/f_P) were evaluated with compartment modeling and graphical analysis techniques. Physostigmine-induced changes in V_T/f_P were estimated as $\Delta V_T/f_P=[V_T/f_{P(Baseline)}-V_T/f_{P(Physo)}]/V_T/f_{P(Baseline)}$. The second set of scans (n=7) acquired PET data for 210-240 min during B/I administration of 244±58 MBq (-)-[^{18}F]flubatine given with K_{bol}=360 min. A 1.5 mg physostigmine dose was administered over 60 min, starting 125 min after the initiaion of radiotracer administration. V_T/f_P values were evaluated with equilibrium analysis from 90-120 min (baseline) and 210 min (post-drug) to estimate $\Delta V_T/f_P$.

Results: Small reductions in (-)-[^{18}F]flubatine binding were found. In the bolus paradigm, $\Delta V_T/f_P$ ranged from 0.8±5.7% in caudate to 4.6±5.2% in parietal cortex (Fig. 1A); these differences were not statistically significant. In the B/I paradigm, larger reductions were found, with $\Delta V_T/f_P$ ranging from 0.0±5.3% in hippocampus to 6.5±4.9% in frontal cortex (Fig. 1B), with a significant effect in parietal cortex (p=0.048) and trends in frontal and occipital cortices (p<0.1). These results are summarized in Fig. 1C.

Conclusion: We observed decreases in (-)-[^{18}F]flubatine V_T/f_P after physostigmine administration in cortical regions using a single-scan B/I paradigm. This logistically straightforward paradigm indicates the sensitivity of (-)-[^{18}F]flubatine binding to extracellular acetylcholine fluctuations and could be extended to models of neuropsychiatric disorders.

A: Physostigmine-Induced Competition with Bolus Paradigm

Cerebellum — Baseline / Post-Physo

Frontal Cortrex — Baseline VT/fP / Physostigmine

Striatum — Baseline VT/fP / Physostigmine
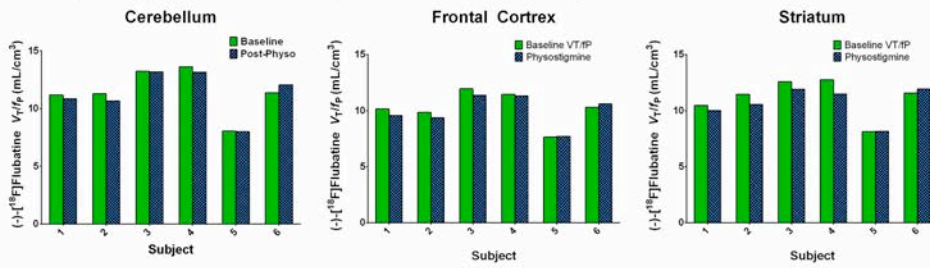
B: Physostigmine-Induced Competition with Bolus-Constant-Infusion Paradigm

Cerebellum — Baseline VT/fP / Physostigmine

Frontal Cortex — Baseline VT/fP / Physostigmine

Striatum — Baseline VT/fP / Physostigmine
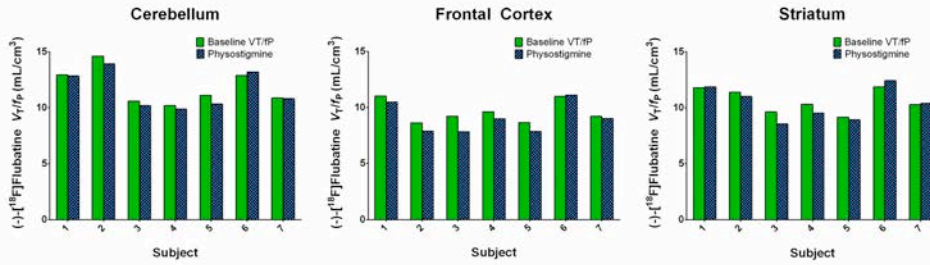
C: Paradigm Comparison

	$\Delta V_T/f_P$	
	Bolus	B/I
Caudate	0.8 ± 5.7%	2.7 ± 5.6%
Cerebellum	1.1 ± 4.0%	2.8 ± 2.5%
Cingulate	1.3 ± 3.6%	4.8 ± 4.4%
Frontal	2.2 ± 3.6%	6.5 ± 5.0%
Hippocampus	1.1 ± 6.2%	0.0 ± 5.3%
Occipital	3.7 ± 7.0%	4.8 ± 4.4%
Parietal	4.6 ± 5.2%	6.3 ± 4.1%
Putamen	4.0 ± 4.9%	3.2 ± 4.6%
Temporal	2.3 ± 4.6%	5.1 ± 3.4%

Figure Legend: A) V_T/f_P measured with a two-scan bolus paradigm for each subject (n=6) in cerebellum, frontal cortex, striatum, and thalamus. B) V_T/f_P measured with a B/I paradigm for each subject (n=7) in cerebellum, frontal cortex, and striatum. For A and B, bars with solid green fill are baseline V_T/f_P while hatched blue fill is physostigmine V_T/f_P. C) Comparison of physostigmine induced (-)-[18F]flubatine $\Delta V_T/f_P$ with bolus (n=6) and B/I (n=7) designs. Values are mean ± standard deviation.

Relation between serotonin 1A receptor binding and gray matter volume in the healthy brain and in major depressive disorder

Francesca Zanderigo[1,2], Binod Thapa Chhetry[1,2], Spiro Pantazatos[1,2], Harry Rubin-Falcone[1,2], R. Todd Ogden[1,2,3], Gregory Sullivan[1,2], Maria A. Oquendo[1,2], J. John Mann[1,2,4]

[1]Department of Molecular Imaging and Neuropathology, New York State Psychiatric Institute, New York, NY, USA; [2]Department of Psychiatry, Columbia University, New York, NY, USA; [3]Department of Biostatistics, Columbia University, Mailman School of Public Health, New York, NY, USA; [4]Department of Radiology, Columbia University, New York, NY, USA

Introduction. Serotonin plays a trophic role in brain development and adult neurogenesis[1] and 5-HT$_{1A}$ receptors may mediate this role[2,3]. MRI and PET studies have respectively identified gray matter volume (GMV) loss[4,5] and 5-HT$_{1A}$ receptor binding alterations[6,7] in major depressive disorder (MDD). The relation between 5-HT$_{1A}$ receptors and GMV has been investigated *in vivo* only in healthy controls (HC)[8]. We investigated this relationship separately for HC and MDD patients.

Materials and Methods. Forty HC and 47 MDD patients underwent 1.5T T1-weighted MRI and [^{11}C]WAY100635 PET scan with measurement of metabolite-corrected arterial input function and tracer plasma free fraction. MRI images were bias-corrected, segmented, and normalized to Montreal Neurological Institute (MNI) space using DARTEL[9]. Gray matter segments were multiplied by the measure of warped/unwarped structures derived from the normalization step, and the modulated GMV images smoothed. PET images were motion-corrected and time activity curves extracted in 13 regions of interest (ROIs)[6]. Distribution volumes (V_T) were estimated using a two-tissue constrained compartment model[6] at the ROI-level and basis pursuit[10] at the voxel-level; binding potential BP_F was then calculated using cerebellar white matter as the reference region. BP_F images were normalized to MNI space, smoothed, and mean centered. At both ROI- and voxel-level, within each group we performed a regression analysis[11] (BP_F, independent variable; GMV, dependent variable) with age, gender, and total intracranial volume as covariates. Same analyses were repeated with raphe BP_F as independent variable.

Results. In HC, 5-HT$_{1A}$ BP_F is positively associated with GMV across most regions. At ROI-level, correlation is statistically different from zero in occipital cortex (r = 0.444, p = 0.006) and hippocampus (r = 0.334, p = 0.043); voxel-wise, positive correlations are observed in supramarginal gyrus and dorsolateral prefrontal cortex (p<0.05, FDR-corrected). Similar positive associations are observed in MDD, with correlations statistically different from zero in temporal lobe at ROI-level (r = 0.483, p = 0.001), and parietal cortex, supramarginal gyrus and dorsolateral prefrontal cortex at voxel-level (p<0.05, FDR-corrected). Raphe autoreceptor BP_F tended to predict lower cortical GMV in HC and greater GMV in MDD: Figure 1(A) (ROI-level) shows scatter plots between raphe BP_F and GMV (adjusted values) for temporal and parahippocampal gyrus. Exploratory voxel-level results are consistent: Figure 1(B) shows clusters where raphe BP_F/GMV correlations are moderated by diagnosis (orbitofrontal cortex, temporal lobe and parahippocampal gyrus, p<0.01 uncorrected, k>10).

Conclusion. Our results using BP_F confirm previous findings in HCs using BP_{ND}[8], namely that 5-HT$_{1A}$ binding is positively correlated with GMV in HC across most brain regions. We extended these findings to MDD. However, in contrast with[8], we found that raphe autoreceptor BP_F is mostly negatively correlated with postsynaptic GMV, in line with the 5-HT$_{1A}$ raphe autoreceptors role in inhibiting serotonin neuron firing and release. In HCs more autoreceptor binding would favor less serotonin release and less trophic effect. In contrast, in MDD raphe BP_F tends to be positively correlated with postsynaptic GMV, perhaps indicating a failure of the trophic effect at the postsynaptic receptor level due to impaired signal transduction, as we have previously reported in cortex.

References:
[1] Daubert EA, Condron BG, *Trends in neurosciences*, 2010; 33: 424-434.
[2] Borroto-Escuela DO et al., *Biochemical and biophysical research communications*, 2015; 463: 180-186.
[3] Pittenger C, Duman RS, *Neuropsychopharmacology*, 2008; 33: 88-109.

[4] Goodkind M et al., *JAMA psychiatry*, 2015; 72: 305-315.

[5] Depping MS et al., *Journal of affective disorders*, 2015; 174: 650-657.

[6] Parsey RV et al., *Biological psychiatry*, 2010; 68: 170-178.

[7] Drevets WC et al., *Nuclear medicine and biology*, 2007; 34: 865-877.

[8] Kraus C et al., *NeuroImage*, 2012; 63: 1091-1098.

[9] Ashburner J, *NeuroImage*, 2007; 38: 95-113.

[10] Gunn RN et al., Journal of cerebral blood flow and metabolism, 2002; 22: 1425-1439.

[11] Casanova R et al., *NeuroImage*, 2007; 34: 137-143.
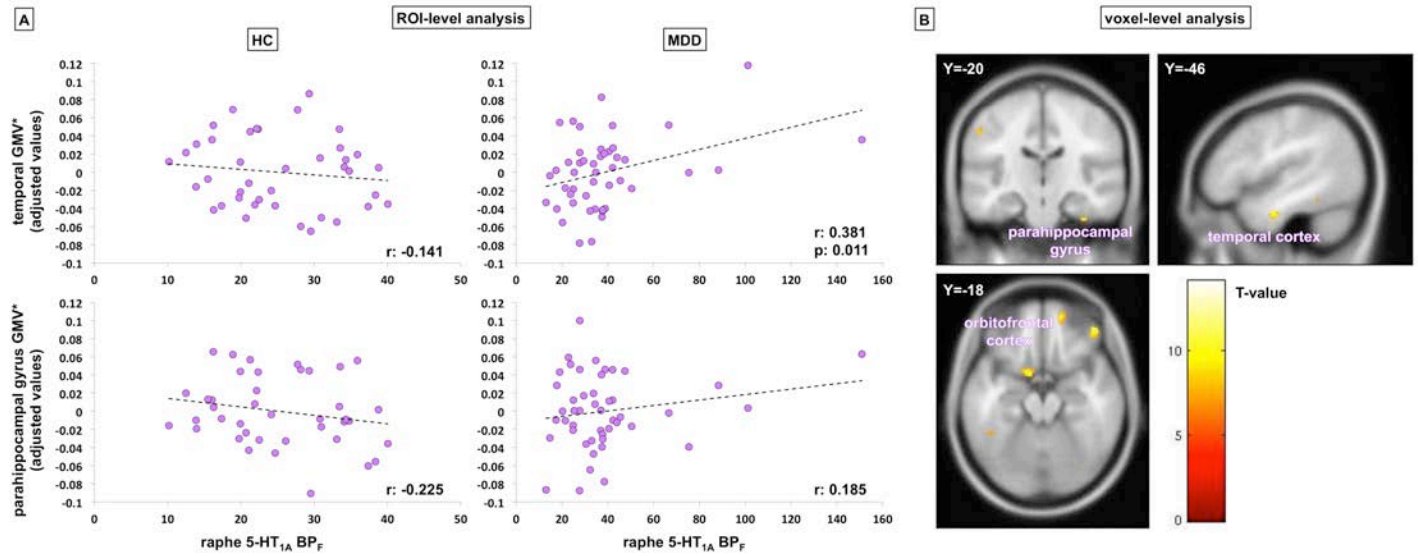
In vivo measurement of Phosphodiesterase 10A (PDE10A) enzyme occupancy following single oral dose administration of PF-02545920 in healthy subjects. A positron emission tomography (PET) study

Andrea Varrone[1], Marielle Delnomdedieu[2], Anton Forsberg[1], Sridhar Duvvuri[2], Patrik Fazio[1], Ching-Ray Yu[3], Per Stenkrona[1], Adam Ogden[2], William David[4], Nabil Al-Tawil[5], Ottavio Vitolo[2], Nahid Amini[1], Sangram Nag[1], Christer Halldin[1].

[1]Karolinska Institutet, Stockhom, Sweden; [2]Pfizer Neuroscience&Pain Research Unit, Cambridge, MA USA; [3]Pfizer Global Innovative Pharma, New York, NY USA; [4]Mass General Hospital, Boston, MA USA; [5]Karolinska Trial Alliance, Stockholm, Sweden.

Introduction. Phosphodiesterase 10A (PDE10A) is an enzyme highly enriched in the medium-sized spiny neurons of the striatum and is a primary target of interest in Huntington´s disease (HD). PDE10A is involved in the regulation of the cytoplasmic levels of cAMP and cGMP and in the signaling within the basal ganglia circuitry. Recent positron emission tomography (PET) studies reported a reduction of striatal PDE10A ranging from 50 to 70% for HD subject in Stage 1-2. Pre-clinical studies suggest that inhibition of PDE10A might improve corticostriatal connectivity in transgenic HD mouse models. Therefore, PDE10A inhibition might represent a treatment strategy to improve corticostriatal function in HD. PF-02545920 is a highly selective PDE10A inhibitor being developed for the symptomatic treatment of HD.

Aim. The aim of this PET study was to measure the enzyme occupancy of PF-02545920 after a single oral dose in healthy volunteers.

Methods.   Male healthy volunteers (age 48±4 years) underwent 2 PET measurements with the PDE10A radioligand [18F]MNI-659. 2 doses were assessed with up to 4 subjects receiving 20 mg and 3 subjects 10 mg of PF-02545920. Arterial blood sampling was performed to obtain a metabolite-corrected plasma input function for the quantification of [18F]MNI-659 binding to PDE10A. Region of interest (ROI) analysis was done using the Automated Anatomical Labeling template. [18F]MNI-659 binding was quantified using Logan graphical analysis. The primary outcome measure was the total distribution volume (V_T) in caudate and putamen. Binding potential (BP_{ND}) was calculated as V_T in target ROI / V_T in reference region (cerebellum) - 1.   The percentage of PDE10A enzyme occupancy (EO%) with PF-02545920 was assessed with two different methods. In Method 1, the occupancy was calculated using the formula: EO%=($BP_{ND\ BASELINE}$ - $BP_{ND\ DRUG}$)/ $BP_{ND\ BASELINE}$ * 100. In Method 2, the occupancy was estimated from the slope of the revised Lassen´s plot as $V_{T\ BASELINE}$ - $V_{T\ DRUG}$ = EO%$_{DRUG}$ ($V_{T\ BASELINE}$ - V_{ND}).

Results. One subject in the 20 mg cohort was considered a biological outlier based on V_T values and was excluded from the final analysis. The range for PDE10A occupancy in the striatum (N=3) was 45-63% with 20 mg PF-02545920 and 14 -27% with 10 mg PF-02545920 (Method 1). With Method 2, the range of occupancy (N=3) was 46-55% with 20 mg PF-02545920 and 15-37% with 10 mg PF-02545920 (Method 2). Corresponding Mean EO% and SD are shown in Table 1.

Conclusions. Single doses of 10 mg or 20 mg of PF-02545920 were generally well tolerated in healthy male volunteers. The enzyme occupancy values of PF-02545920 obtained using [18F]MNI-659 PET were in the expected range based on the results of simulations in a non-human primate EO model (27-42% at 10 mg, 42-59% at 20 mg). The enzyme occupancy could be reliably estimated based on the calculation of binding potential (BP_{ND}) values from the distribution volumes, using the cerebellum as reference region. The single dose of 20 mg of PF-02545920 provided ~50% occupancy of PDE10A, which could be sufficient for efficacy measurement in clinical trials in HD.

Table 1.

PDE10A % enzyme occupancy (mean±SD) after single oral dose administration of PF-02545920.

EO%	PF-02545920 20 mg (n=3)		PF-02545920 10 mg (n=3)	
Region	**Method 1**	**Method 2**	**Method 1**	**Method 2**
Caudate	51.7 ± 10.8	-	20.1 ± 9.4	-
Putamen	51.8 ± 9.6	-	21.9 ± 5.4	-
Striatum	51.8 ± 10.0	51.8 ± 5.3	21.3 ± 6.7	28.1 ± 12.0

A fully automated in-loop [^{11}C]carboxylation and gentle metal-free reduction method to prepare [^{11}C]-(+)-PHNO

J.W. Hicks* and M.S. Kovacs

Department of Medical Biophysics, Western University and Lawson Health Research Institute, London, Ontario, Canada

Objective: The radiolabeled dopamine (DA) receptor agonist [^{11}C]-(+)-PHNO and PET have been employed to index DA release in a number of neurological and psychiatric disorders.[1] Agonist radioligands binding solely to the active or high affinity state DA receptors are reputed to provide higher sensitivity to changes in synaptic DA.[2] Furthermore, [^{11}C]-(+)-PHNO possesses a 20-fold preference for D_3 over D_2 receptor subtype.[3] Unfortunately, current production methods are hampered by elongated synthesis time and are prone to failure. Efficient and reliable radiosynthetic procedures are integral components in the intricate organization of expensive and coordinated clinical studies, therefore we endeavored to improve the preparation of [^{11}C]-(+)-PHNO on a commercial automated synthesis module without the use of harsh reductive metals.

Method: Building upon the Vienna group's [^{11}C]carboxylation of a Grignard in a loop method,[4] the number of reactors was reduced to one, thereby permitting the use of a GE TRACERLab FX$_{C-Pro}$. [^{11}C-*carboxyl*]propionyl chloride is produced in the loop and added to (+)-HNO in the reactor to form an [^{11}C-*carboxyl*]amide intermediate. The amide was reduced using tri(pentafluorophenyl)borane and polymethylhydrosiloxane. Following HPLC purification, [^{11}C]-(+)-PHNO was formulated for human injection and tested for quality control. Production was completed in adherence to Good Manufacturing Practice (GMP).

Results: Prior to reduction with lithium aluminum hydride (LiAlH$_4$), time consuming reactor cooling (80 ^{0}C to -15 ^{o}C) was required. Cooling was eliminated by use of a Lewis acid hydrosilylation reaction to reduce the amide intermediate to [^{11}C]-(+)-PHNO. Furthermore, substitution of air- and water-stable reductants for LiAlH$_4$ reduced to number of failed reactions caused by premature quenching.

Conclusion: A combination a loop carboxylation and gentler amide reduction using the atmospherically stable hydrosilylation reagents has reduced the total radiosynthesis time and increased the reliability. With radioligand in hand, a clinical study is underway investigating differential expression of DA receptors between patients with Alzheimer's disease and dementia with Lewy bodies (DLB).

References:
1. Cumming, P. *Imaging Dopamine*. (Cambridge University Press, 2009).
2. Willeit, M. *et al.* High-Affinity States of Human Brain Dopamine $D_{2/3}$ Receptors Imaged by the Agonist [^{11}C]-(+)-PHNO. *Biol. Psychiatry* 59, 389–394 (2006).
3. Tziortzi, A. C. *et al.* Imaging dopamine receptors in humans with [^{11}C]-(+)-PHNO: dissection of D3 signal and anatomy. *NeuroImage* 54, 264–277 (2011).
4. Rami-Mark, C. *et al.* Reliable set-up for in-loop ^{11}C-carboxylations using Grignard reactions for the preparation of [*carbonyl-*^{11}C]WAY-100635 and [^{11}C]-(+)-PHNO. *Appl. Radiat. Isot.* 82, 75–80 (2013).

Building a normal database for brain translocator protein imaged using ^{11}C-PBR28

S.Paul, JS.Liow, S.Mabins, Sami.S.Zoghbi, RN.Gunn*, William C.Kreisl, Erica M. Richards, P.Zanotti-Fregonara§, CL.Morse, JS.Hong, A.Kowalski, VW.Pike, RB.Innis, M.Fujita

*Intramural Research Program, National Institute of Mental Health, Bethesda, Maryland, USA; *Division of Brain Sciences, Department of Medicine, Imperial College, London,UK; Imanova, Centre for Imaging Sciences, London, UK; §INCIA UMR-CNRS 5287, Université de Bordeaux, Bordeaux, France*

Objectives: Neuroinflammation plays an important role in a number of brain disorders, and translocator protein (TSPO) has been widely used as an imaging target to detect such inflammation. Over the past several years, ^{11}C-PBR28 has been used by several PET centers to image TSPO. This study sought to build a normal database of TSPO imaged with ^{11}C-PBR28, which could be used to compare patient data, to estimate specific binding of ^{11}C-PBR28 in high- (HABs) and mixed-affinity binders (MABs), and to study the effect of potential contributors to neuroinflammation, i.e., aging and obesity, in healthy subjects.

Methods: ^{11}C-PBR28 scans in 45 healthy subjects (20 HABs and 25 MABs, 20F/25M, age: 41.4±17.4 years) with known affinity type were retrospectively analyzed in a standard manner. Seventy-eight volumes of interest (VOIs) were defined based on high resolution magnetic resonance imaging (MRI) by PNEURO/PMOD, which uses segmentation, spatial normalization, and Hammers' N30R83 maximum probability atlas. In each scan, total distribution volume (V_T) and V_T normalized to plasma free fraction (f_P) were measured via unconstrained two compartment model, Logan plot, and Ichise multilinear analysis (MA1) using metabolite-corrected arterial input function. V_{ND} or V_{ND}/f_P was estimated by the polymorphism plot (1) using differences in V_T or V_T/f_P between HABs and MABs. Correlations between V_T or V_T/f_P and age or body mass index (BMI) were examined by including data from both HABs and MABs, controlling for affinity type (i.e., partial correlation). Multiple comparison correction was applied by controlling the false discovery rate.

Results: The two-compartment model did not identify V_T well in 18% of datasets with SE >10%. Logan plot identified V_T well in all datasets with no outliers. V_T by MA1 was 8±27% higher across the 78 VOIs than that of Logan plot, possibly due to underestimation by Logan plot. However, V_T of MA1 had some outliers; in 11% of 78 VOIs SD/mean across subjects was greater than 0.75. Because Logan plot provided the most reliable binding measures of the three methods, further analyses were performed using V_T and V_T/f_P obtained by this method. The Logan plot gave V_T and V_T/f_P of 2.9±0.8 and 91±37, respectively, for MABs, and 3.6±1.0 and 120±41 for HABs across 78 VOIs. V_T and V_T/f_P were fairly uniform throughout brain regions; highest binding was in brain stem, with moderate amount of binding in most cerebral cortices (Table). The polymorphism plot estimated V_{ND} as 1.52 (95% CI 0.86-1.97) and V_{ND}/f_P as 49 (95% CI 32-61). Specific-to-nondisplaceable ratio (BP_{ND}) was 1.41±0.21 and 0.90±0.13 in HABs and MABs, respectively. Binding potential normalized to plasma free fraction (BP_F) was 71±41 and 42±37 mL·cm^{-3} in HABs and MABs, respectively. No significant correlation was observed between V_T or V_T/f_P and age or BMI.

Conclusions: Logan plot provided reliable binding measurements in all 78 areas of Hammers' maximum probability atlas and provided data for normal TSPO distribution. HABs showed 1.6 and 1.4 fold greater levels of specific binding than MABs, based on V_T and V_T/f_P, respectively. Age and BMI had no effect on ^{11}C-PBR28 binding levels.

References:
1) Owen DR, Guo Q, Kalk NJ, Colasanti A, Kalogiannopoulou D, Dimber R, et al. Determination of [(11)C]PBR28 binding potential in vivo: a first human TSPO blocking study. J Cereb Blood Flow Metab 2014; 34:989-94.

Regional ^{11}C-PBR28 binding values in healthy controls

	Whole brain	Cerebellum	Brain Stem	Frontal Cortex	Temporal Cortex	Thalamus	Hippocampus
V_T							
HAB	3.6±1.00	3.9±1.0	4.4±1.3	3.7±1.1	3.7±1.0	4.3±1.3	3.7±0.9
MAB	2.9±0.8	3.0±0.79	3.4±1.0	3.0±0.8	2.6±0.7	3.1±0.9	2.7±0.6
V_T / f_P							
HAB	120±41	128±45	144±55	122±45	122±35	142±51	122±41
MAB	91±37	92±37	105±43	93±40	83±34	97±40	86±33

V_T: distribution volume; HAB: high-affinity binder; MAB: mixed-affinity binder

Higher translocator protein (TSPO) availability, a marker of neuroinflammation, in posttraumatic stress disorder

Robert H. Pietrzak, PhD, MPH[1,4], Irina Esterlis, PhD[1,3,4], Ansel Hillmer, PhD[2,3], David Matuskey, MD[1,2,3], Nabeel Nabulsi, PhD[2,3], Jim Ropchan[3], Yiyun Huang, PhD[2,3], Richard E. Carson, PhD[2,3], Steven M. Southwick, MD[1,4], John H. Krystal, MD[1,4], and Kelly P. Cosgrove, PhD[1-4]

[1]Department of Psychiatry, Yale University; [2]Department of Radiology and Biomedical Imaging, Yale University; [3]Yale PET Center, Yale University; [4]National Center for PTSD, West Haven CT VAMC

Background: Posttraumatic stress disorder (PTSD) is associated with elevated rates of physical and other mental health conditions. The immune system is responsible for maintaining health, which includes mounting a response to physical (e.g., virus, injury) and psychological (e.g., stress) insults, as well as modulating the progression of neurodegenerative disorders such as Alzheimer's disease. All of these—physical health conditions, psychological distress, and neurodegenerative disorders—are more prevalent in individuals with PTSD. While some studies have documented peripheral immune system abnormalities in PTSD, no study has evaluated the role of the neuroimmune system in this disorder. In the healthy immune system, the response of the central nervous system to an insult or damage is mediated by the activation of microglia, which carry out repair functions. However, excessive microglial activation can lead to neuronal dysfunction and damage through the release of inflammatory cytokines and other mediators, and may contribute to neurodegeneration, which is associated with PTSD. The goal of the current study was to determine whether individuals with PTSD have higher levels of activated microglia compared to matched controls.

Methods: Six individuals with PTSD and 6 age-, sex-, race/ethnicity- and TSPO genotype-matched, trauma-exposed healthy controls (HC) participated in one MRI and one PET scan with the radiotracer [^{11}C]PBR28, which binds to translocator protein (TSPO), a marker of microglial activation. Arterial blood sampling was done for each PET scan to measure the metabolite-corrected parent input function for use in kinetic analysis of PET data to derive regional volume of distribution (V_T). PTSD diagnosis was determined using the Clinician-Administered PTSD Scale for DSM-5. The PTSD group included 5 women and 1 man with a mean age of 33.3 years (SD=9.3, range=21-48); 3 Caucasian; 2 African-American, and 1 Hispanic individual; and the index traumas included 3 robbed at gunpoint; 2 witnessed attempted murder of husband; and 1 sexual assault.

Results: Relative to the HC group, the PTSD group had markedly higher global (30.4% higher) and regional (16.2% to 50.3% higher) [^{11}C]PBR28 V_T values (**Figure**). The magnitude of the global difference was large (Cohen d=0.9) and was most pronounced in the amygdala (50.3% higher; d=1.4), hippocampus (35.7% higher; d=1.1), and thalamus (39.7% higher; d=1.1).

Conclusions: Results of this preliminary study suggest that PTSD is associated with higher levels of activated microglia than is found in controls, indicated by higher levels of TSPO binding measured with [^{11}C]PBR28. The most pronounced elevations in TSPO availability were evident in brain regions implicated in the pathophysiology of PTSD, specifically the amygdala, hippocampus, and thalamus. Taken together, these initial findings suggest that pharmacotherapies targeting the neuroimmune system may have a role in treating PTSD.
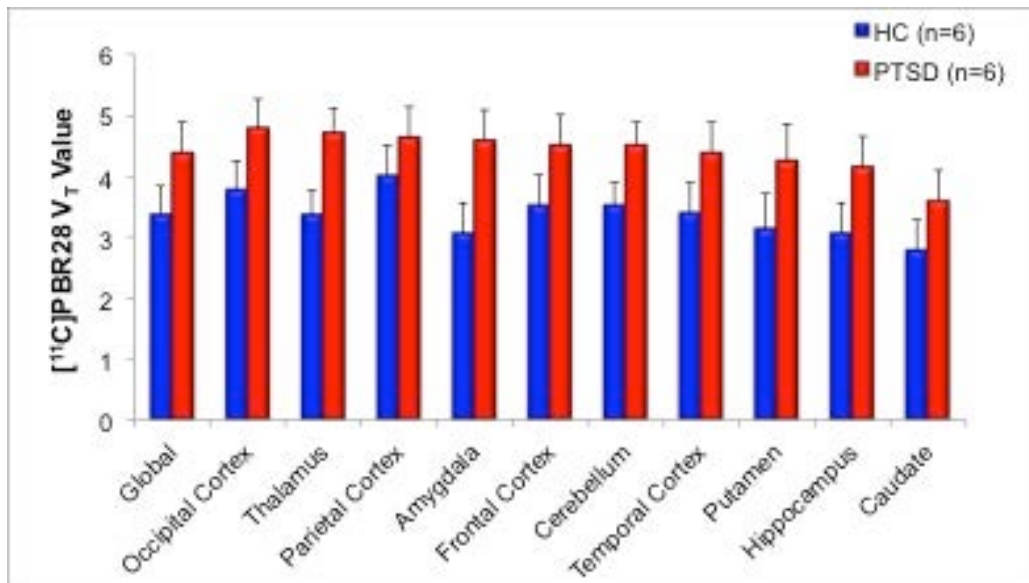
Figure Legend. Global and regional [^{11}C]PBR28 V_T values (mean±SEM) in 6 healthy controls (HC) and 6 participants with posttraumatic stress disorder (PTSD).

Screening of 31 Amyloid PET Radioligands with Clinical Usefulness Criterion by Biomathematical Modelling Approach using in-silico data

YH. Nai[1], M. Shidahara[2], C. Seki[3], H. Watabe[1]

[1]CYRIC, Tohoku University, Sendai, JAPAN, [2]Tohoku University School of Medicine, Sendai, JAPAN, [3]National Institute of Radiological Sciences, Chiba, JAPAN.

Background: We have developed a biomathematical model to predict clinical SUVR of amyloid PET tracers with great potential [1]. By means of the proposed model, we attempted to screen the clinical usefulness of amyloid tracers, which is defined as the tracer's ability to detect the amyloid load to diagnose individual subject accurately.

Purpose: We proposed a screening methodology of amyloid PET radioligands without any in vivo PET scans, based on in-silico data and a biomathematical model, as well as clinical usefulness index (CUI), which is defined to judge the power of the tracer to distinguish pathological groups in clinical PET scans. A total of 31 (13 clinically applied, 18 candidate) tracers were used for evaluation based on CUI.

Proposed framework (Figure 1) requires 4 main steps: *1*) **Generation of input parameters**: In-silico volume (V_x), lipophilicity (MLogP), plasma free fraction (f_p) and tissue free fraction (f_{ND}) [1] and in-vitro K_D for each tracer and fixed B_{avail} for Healthy Control (HC), Mild Cognitive Impaired (MCI), severe Alzheimer's Disease (AD) conditions of 4nM, 20nM and 50nM respectively (Figure 1B), *2*) **Prediction of Kinetic Partameters**: K_1, k_2, BP_{ND} (Figure 1B) for each tracers using the amyloid prediction model [1, 2], *3*) **Generation of TACs:** 1000 Time activity curves (TACs) with noise for both target and reference regions, with population realizations by varying K_1 by 10%, k_2 by 20% and B_{avail} by 80%, 35% and 20% in HC, MCI, AD respectively, and calculate the corresponding 1000 SUVRs in HC, MCI and AD each, to simulate clinical SUVR distribution situations in the 3 subject groups (Figure 1C), and *4*) **Evaluation of CUI**: CUI was computed using 3 evaluation strategies (Figure 1D) – Receiver Operating Characteristics (ROC), Power and Sample Size (PSS) and SUVR ratios of MCI/HC & AD/MCI for all tracers.

Evaluation Methods: ROC analysis was carried out using Matlab (The MathWorks, US))by comparing 1000 SUVR datasets of HC vs MCI and MCI vs AD, and the output Area under ROC (Az) was used for tracer evaluation. **PSS** analysis was carried out using G*Power (Universitat Kiel, Germany) [3], with one-tail-t-test for 2 independent means, to determine required sample size at α = 0.05, β = 0.95 and effect size (Es), which was used for tracer evaluation. **SUVR ratios (Sr)** of MCI vs HC and AD vs MCI were calculated by dividing the averaged SUVR values of each subject groups respectively. The outcome evaluation measurements for HC vs MCI, MCI vs AD, from ROC, PSS and SUVRr were averaged to obtain $\overline{Az}$, $\overline{Es}$, $\overline{SUVRr}$, which were then combined together to determine clinical usefulness index,

$$CUI = \overline{Az} \times \overline{Es} \times \overline{SUVRr}.$$

Results: ROC, PSS and SUVRr evaluated different properties among 31 the amyloid tracers, which when combined together enhanced clinical usefulness index of the tracer, resulting in a broad range of indexes of 0.10 to 5.62 (Figure 1E). Hence, allowing for clearer differentiation of poorer tracers from potential clinically-applicable tracers and clinically applied tracers.

Conclusions: Screening methodology of Amyloid PET radioligands using CUI showed potential in evaluating tracers.

References:
1. Arakawa Y. et al., EANM, OP162, 2015.
2. Guo Q. et al., JNM, 50(10):1715-23, 2009
3. Faul, F. et al., BRM, 39, 175–191, 2007
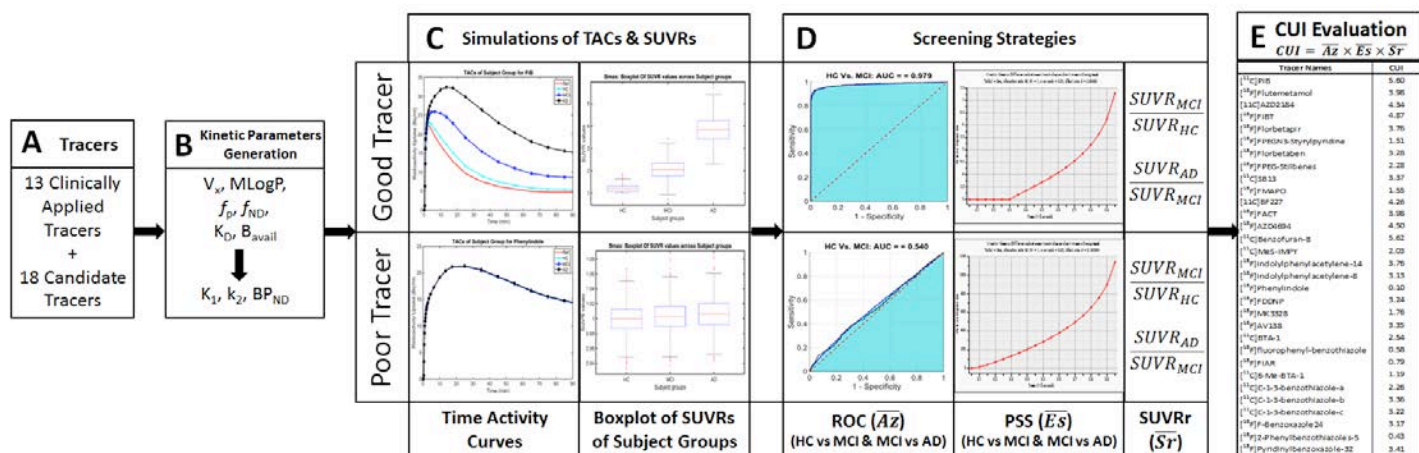
Figure 1: Schematic flow of proposed framework: (A) 31 compounds, (B) Generation of kinetic parameters, (C) Simulations of TACs & SUVRs by biomathematical modelling, (D) Evaluation of tracers by 3 strategies, and (E) Clinical Usefulness Index (CUI) of 31 tracers.

Direct Reconstruction of Parametric Images: Evaluation Across Tracers and Count Levels

Mary Germino[1], Jianhua Yan[2], Richard E. Carson[1]

[1]*Department of Biomedical Engineering, Yale University, New Haven, CT, USA;* [2]*Department of Nuclear Medicine, First Hospital of Shanxi Medical University, Taiyuan, Shanxi, China*

Purpose. Parametric images are typically obtained from dynamic PET data by reconstructing images at multiple time frames, then fitting a kinetic model to each voxel time activity curve (TAC). An alternative method, "direct reconstruction," produces parametric images directly from raw data by incorporating the kinetic model into the reconstruction algorithm. Because the image-domain noise distribution is difficult to model, direct reconstruction, using the Poisson model, can achieve lower-variance parameter estimates than the indirect method. In this work, we studied the noise-reduction benefit of direct reconstruction compared to the indirect method for parametric imaging of the human brain, for two tracers, at multiple count levels.

Methods. This study uses two previously acquired 2-hour list mode datasets from the HRRT with the tracers [^{11}C]AFM (serotonin transporter) and [^{11}C]UCB-J (synaptic vesicle glycoprotein 2A). The 1-tissue compartment (1T) model describes the kinetics of both tracers. Input functions were measured from arterial blood samples. List mode data were down-sampled to three count levels (5,10, and 20% of total counts) by applying a repeating sequence of 50-ms gates. Five replicates at each count level were reconstructed for each tracer by the direct and indirect methods. All reconstructions used 4 iterations of 20 subsets and included event-by-event motion correction using measurements of the Polaris Vicra tool. Direct reconstructions were performed using a previously published algorithm (PMOLAR-1T), newly extended to incorporate event-by-event motion correction. Indirect reconstructions used 17 frames; parametric images were obtained by fitting the 1T model to each voxel TAC using the basis function method with weights based on noise equivalent counts. Distribution volume (V_T) images were computed as K_1/k_2. Voxelwise mean and coefficient of variation (COV) were computed across replicates for each case, and summarized regionally.

Results. Primary results for V_T are shown in the Figure. Mean V_T at iteration 2 was similar across count levels for the direct method but increased substantially for indirect at lower counts, with best agreement between indirect and direct at the 20% count level. This trend continued at later iterations e.g., at the 20% count level for AFM (UCB-J), indirect mean V_T increased by 59% (56%) and direct mean V_T did not change between iteration 3 and 4. This suggests that the indirect method suffers from noise-induced bias at low counts.

Mean K_1 estimates were similar between direct and indirect, and across count levels and iteration (all differences <8%). Direct reconstruction provided lower noise images for both tracers, and this difference became larger at lower counts. At iteration 2, the percent reduction in V_T COV provided by direct reconstruction compared to indirect ranged from 45%-67%, with the greatest percent reduction at the 5% count level. Direct COV at the 5% count level approximately matched indirect COV at the 20% count level. Direct reconstruction reduced K_1 COV by 27-46% at iteration 2, with greatest percent reduction at the 5% count level.

Conclusion. Direct reconstruction provides a substantial reduction in image noise compared to the indirect method, which becomes more pronounced as count level is reduced.

[¹¹C]AFM	Direct V_T Mean		Indirect V_T Mean	
20% counts				
5% counts				
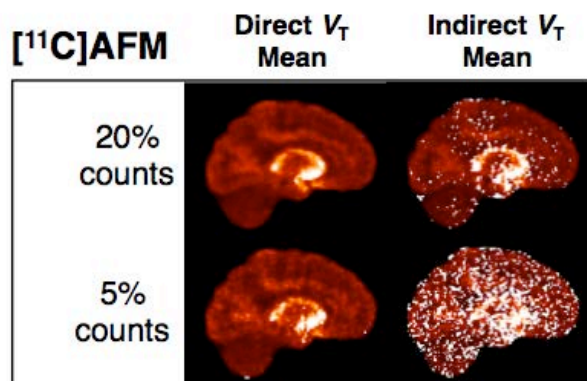
	Direct V_T		Indirect V_T	
	Mean	COV	Mean	COV
20%	15	11%	17	23%
10%	15	15%	36	41%
5%	15	22%	81	66%

[¹¹C]UCB-J	Direct V_T Mean		Indirect V_T Mean	
20% counts				
5% counts				
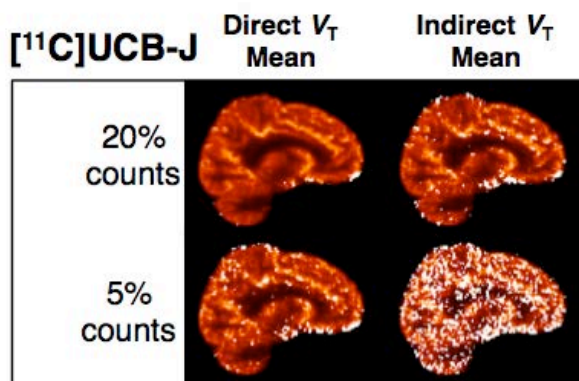
	Direct V_T		Indirect V_T	
	Mean	COV	Mean	COV
20%	25	12%	28	22%
10%	25	18%	51	40%
5%	29	28%	120	69%

Images show mean distribution volume (V_T) across replicates by the direct and indirect methods at two count levels for two tracers. Tables give mean regional results in the frontal lobe (AFM) or gray matter (UCB-J) across three count levels. All results are shown for iteration 2.

Biomathematical Modelling Approach Using In-Silico Data to Predict Clinical SUVR in Amyloid PET Imaging

YH. Nai[1], M. Shidahara[2], Y. Arakawa[2], C. Seki[3], H. Watabe[1]

[1]Cylotron RadioIsotope Center (CYRIC), Tohoku University, Sendai, JAPAN, [2]Tohoku University School of Medicine, Sendai, JAPAN, [3]National Institute of Radiological Sciences, Chiba, JAPAN.

Background: There is an increasing use of amyloid imaging to diagnose Alzheimer's disease (AD) conversion but there are only a few clinical amyloid tracers available due to poor conversion of in-vitro or preclinical results to clinical use, long drug translation cycle and poor binding properties of tracer to amyloid fibrils.

Purpose: In order to predict clinical SUVR of amyloid PET radioligands, we proposed a biomathematical model using in-silico data by extending the model for CNS tracers, developed by Guo et al [2]. Evaluation of the proposed model was carried out by comparing predicted K_1, k_2, BP_{ND} and SUVR against clinically observed values from literatures.

Methods: Kinetic parameters, K_1, k_2 and BP_{ND} were derived using lipophilicity (LogP), McGowan Volume (V_x), plasma free fraction (f_p), tissue free fraction (f_{ND}), dissociation constant (K_D) and concentration of binding sites (B_{avail}). Lipophilicity, Moriguchi logP (MLogP) and V_x were calculated based on the tracer's chemical structure using commercially available software (dproperties, Affinity Science corp). f_p and f_{ND} were extrapolated from correlation relationships between f_p -f_{ND} and f_{ND}-CLogP from Wan and Maurer's datasets [3, 4] for CNS drug compounds. K_D was extracted from literatures [1]. Fixed B_{avail} values of 4nM and 50nM were applied for Healthy Control (HC), and severe AD conditions respectively. Time activity curves (TACs) were generated for both target and reference regions using one-tissue compartmental model with arterial plasma input function of [11C]BF227 in HC, with the calculated kinetic parameters. Standardized uptake value ratios (SUVR) for each condition were obtained by dividing the area under the simulated TACs of target region over that of the reference region. Linear correlations between calculated and clinically observed kinetic parameters of K_1, k_2 and BP_{ND} from literatures were also carried out. Simulated SUVRs values were compared with clinically observed SUVR values of 10 clinical tracers: [11C]PIB, [11C]BF-227, [11C]AZD2184, [11C]SB-13, [18F]FACT, [18F]Florbetapir, [18F]Flutemetamol, [18F]Florbetaben, [18F]AZD4694, and [18F]FDDNP, by means of linear correlation to determine the suitability of the model developed.

Results: Good correlations between predicted and clinically observed K_1 and k_2 values of R^2 = 0.71 and 0.81 in AD and R^2 = 0.71 and 0.78 in HC respectively were obtained (Figure 1A and 1B). Average correlations between predicted and clinically observed BP_{ND} of R^2 = 0.55 (Figure 1C) and between predicted and clinically observed SUVR values of R^2 = 0.54 were observed in AD, with slight over-prediction for [11C]PiB (Figure 1D).

Conclusions: Despite variations in data extracted from literatures due different imaging and analysis protocols across various institutions and the use of only in-silico input data, relatively good correlation between predicted SUVR and clinically observed SUVR values was obtained. The in-silico biomathematical model showed potential in predicting SUVR values for amyloid PET tracers.

References:
1. Arakawa Y. et al., EANM OP162, 2015.
2. Guo Q. et al, JNM, 50(10):1715-23, 2009.
3. Wan H. et al, JMC, 50:4606–4615, 2007.
4. Maurer T.S. et al., DMD, 33, 175–181, 2004.
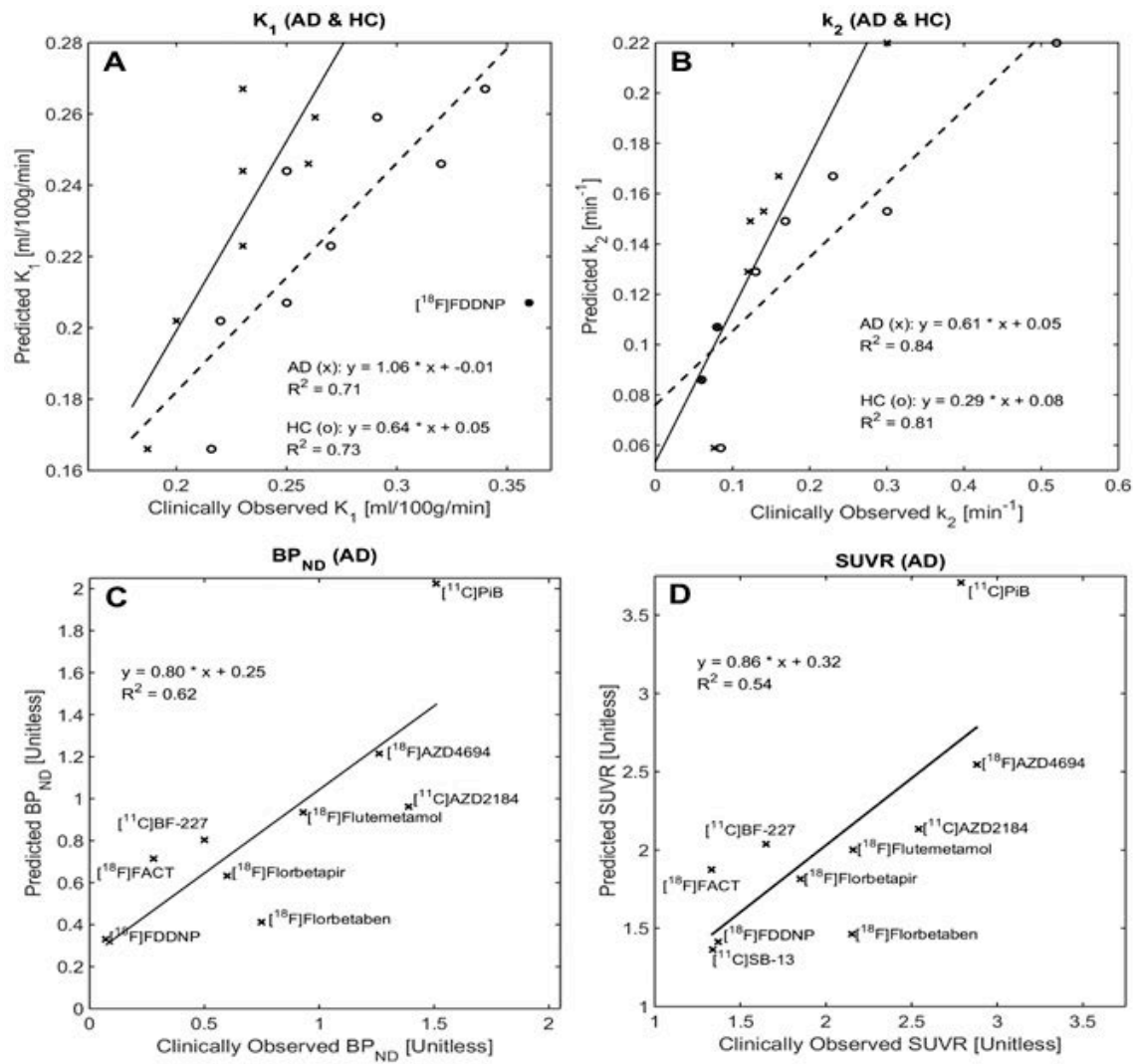
Figure 1: Comparison between clinically observed and predicted (A) K_1 (AD & HC), (B) k_2 (AD & HC) and (C) BPND (AD only) for 8 tracers, and (D) SUVR (AD only) for 10 tracers. For K1 (AD) correlation, FDDNP was excluded as an outlier.

Acute and subsequent effects of transcranial direct current stimulation on the dopaminergic transmission in healthy humans

Clara Fonteneau[a,b,c,d,e], Frédéric Haesebaert [a,b,c,d,e], Jérome Redouté [f], Didier Le Bars[f], Nicolas Costes [f], Jérome Brunelin [a,b,c,d,e], Marie-Françoise Suaud-Chagny [a,b,c,d,e]

[a] INSERM, U1028, Lyon Neuroscience Research Center, ΨR2Team, Lyon, F-69000, France; [b] CNRS, UMR5292, Lyon Neuroscience Research Center, ΨR2Team, Lyon, F-69000, France; [c] University Lyon, F-69000, France; [d] University Lyon 1, Villeurbanne, F-69000, France ; [e] Centre Hospitalier Le Vinatier, F-69000, France ; [f] CERMEP—Imagerie du vivant, Lyon, France

Bifrontal transcranial direct current stimulation (tDCS), applied over the dorso-lateral prefrontal cortex (DLPFC), is associated with improvement of depressive symptoms and cognitive functions. Despite an increasing use in clinical settings, acute and subsequent neurobiological effects of tDCS are far from being completely understood. Some offline imaging reports suggest that tDCS neurobiological effects are not restricted to the brain areas located under the electrodes, but spread through distributed cortical networks functionally connected with the targets and reach subcortical areas, such as dopaminergic areas. A recent fMRI study suggests subcortical effects of bifrontal tDCS including modulations in the caudate nucleus. Moreover, some offline studies suggest that cortical stimulation by other approaches, such as transcranial magnetic stimulation may evoke a subcortical dopamine release in the nucleus accumbens following a single session applied over the left DLPFC (Brunelin et al, *Schizophr Res*, 2011). However, the effect of bifrontal tDCS on dopaminergic transmission is still unknown as well as if this effect is specifically distributed across subcortical dopaminergic areas.

Objectives: The aim of this study is to test, in healthy subjects, the effect of a single-session of bifrontal tDCS with the anode over the left DLPFC and the cathode over the right DLPFC on the subcortical dopaminergic transmission. These effects are explored online by positron emission tomography (PET) using dopaminergic D2 subtype receptor availability via [^{11}C]raclopride binding.

Methods: At the end, 30 healthy subjects randomly assigned in two groups (active, n = 15 vs sham, n=15) will receive at rest a single-session of either active or sham bifrontal tDCS during a PET scan of 100-minute duration. The tracer, [^{11}C]raclopride, is administered intravenous, using a bolus-plus-continuous-infusion method. The stimulation starts 40 minutes after the injection of the tracer, lasts 20 minutes, and is set at 2mA in active mode. PET scans are preceded by an anatomical MRI scan to control subject anatomy, electrode position and define the regions of interest (ROI). Extracellular dopamine concentration is assessed using simple pseudo-equilibrium 5-min ratios of ROI to cerebellum activities (B/F ratio). To investigate the changes induced by tDCS, variations of B/F ratio are calculated before, during and after the stimulation in the right and left nucleus accumbens, caudate nucleus, putamen and precentral gyrus.

Results: Preliminary results show that tDCS modulates B/F ratio specifically in the nucleus accumbens. During the stimulation, the effects observed tend to be opposite in the left and right nucleus accumbens.

Conclusion: These results suggest that tDCS rapidly impacts subcortical dopaminergic transmission specifically in the nucleus accumbens.

Neurophysiological impact of a fronto-temporal tDSC in healthy subjects: A multimodal PET-MR imaging approach

Clara Fonteneau [a,b,c,d,e], Frédéric Haesebaert [a,b,c,d,e], Marjorie Villien [f], Jérome Redouté [f], Didier Le Bars [f], Nicolas Costes [f], Jérome Brunelin [a,b,c,d,e], Marie-Françoise Suaud-Chagny [a,b,c,d,e],

[a] INSERM, U1028, Lyon Neuroscience Research Center, ΨR2Team, Lyon, F-69000, France ; [b] CNRS, UMR5292, Lyon Neuroscience Research Center, ΨR2Team, Lyon, F-69000, France ; [c] University Lyon, F-69000, France ; [d] University Lyon 1, Villeurbanne, F-69000, France ; [e] Centre Hospitalier Le Vinatier, F-69000, France ; [f] CERMEP—Imagerie du vivant, Lyon, France

Fronto-temporal transcranial direct current stimulation (tDCS), with anodal stimulation over the left dorsolateral prefrontal cortex and cathodal stimulation over the left temporo-parietal junction, has been reported to reduce treatment-resistant auditory hallucinations, negative symptoms and insight of the illness in schizophrenia. Despite an increasing use in clinical settings, acute and subsequent effects of fronto-temporal tDCS are far from being completely understood. The few imaging and computational reports available suggest that fronto-temporal tDCS effects are not restricted to the brain areas located under the electrodes, but spread through distributed cortical networks functionally connected with the targets and reach subcortical areas, such as dopaminergic areas. Overall, these studies suggest that tDCS modulates functional connectivity within and across resting-state networks and brain activity. However, these effects are currently described at different levels depending on the imaging technique used. Finally, effects of the stimulation applied online are rarely inspected.

Objectives: According to the hypothesis that fronto-temporal tDCS modulates brain activity, connectivity and dopaminergic transmission, the aim of this project is to reveal the combined neurobiological impact of an online single session of fronto-temporal tDCS in a unique experiment by developing a simultaneous multimodal imaging approach (PET-MR). The online implementation of the stimulation will allow deciphering changes induced during and after stimulation compared to baseline levels.

Methods: As a first step, before investigating patients with schizophrenia, 30 healthy subjects will be randomly assigned in two groups (active, n=15 vs sham, n=15) and will receive a single-session of either active or sham fronto-temporal tDCS during a simultaneous PET and MR scan of 110-minutes duration. The stimulation will start 40 minutes after the injection of the tracer, last 30 minutes and be set at 1 mA in active mode.
The distributed changes will be explored at rest through:
• Specific and localized dopaminergic transmission evaluated by PET using dopaminergic D2 subtype receptor availability via [^{11}C]raclopride binding. The tracer will be administered intravenous, using a bolus-plus-continuous-infusion method. A simple pseudo-equilibrium 5-min ratio of region of interest (right and left nucleus accumbens, caudate nucleus, putamen) to cerebellum activities provided an assessment of extracellular dopamine concentration before, during and after tDCS.
• Spontaneous functional connectivity assessed by resting state functional MRI (rs-fMRI, three 13 min scans before, during and after tDCS).
• Brain activity assessed by cerebral blood flow quantitatively and directly measured by pseudo-continuous arterial spin labelling (pCASL, three 6 min scans before, during and after tDCS).
• Connectivity assessed by diffusion tensor imaging (DTI, two 10 min scans before and after tDCS).

Results: With the first subjects included in the study, image analysis protocols are being developed independently for each modality in order to establish correlations. Also, the combination of these modalities is being considered.

Conclusion: Our unique approach will create a coherent ensemble, which is a mandatory and critical step to understand the mechanisms of action of tDCS. Moreover, in the long run, we expect that it will provide an imaging biomarker essential to improve our understanding of the "normal brain" and deficient mechanisms underlying schizophrenia as well as neurological disorders.

Towards Development of [11C]THK-5351 – A Potential Novel Carbon-11 Tau Imaging PET Tracer

Vladimir Stepanov [a], Marie Svedberg [a], Zhisheng Jia [a], Raisa Krasikova [a],[b], Laetitia Lemoine [c], Nobuyuki Okamura [d], Shozo Furumoto [d], Bengt Långström [e], Agneta Nordberg [c], Christer Halldin [a]

[a] Karolinska Institutet, Department of Clinical Neuroscience, Center for Psychiatric Research, Stockholm, Sweden; [b] N.P. Bechterva Institute of Human Brain, Russian Academy of Science, St.-Petersburg, Russia; [c] Karolinska Institutet, Department of Neurobiology, Center for Alzheimer Research, Stockholm, Sweden; [d] Department of Pharmacology, Tohoku University School of Medicine, Sendai, Japan; [e] Department of Chemistry, Uppsala University, Uppsala, Sweden

Due to the rise in the number of patients with dementia the imperative for finding new diagnostic and treatment options becomes ever more pressing. While significant progress has been made in PET imaging of Aβ aggregates both *in vitro* and *in vivo*, there are limited PET radioligands available for selectively imaging Tau protein aggregates. Given the significant role Tau plays in many neuropathologies's having a selective PET imaging agent for Tau would afford great opportunities both for basic neurological research as well as better diagnostics, disease progression monitoring and treatment option evaluation. Based on the work of Harada, Okamura *et al* from Tohoku University, Japan (J Nucl Med 2015 doi:10.2967/jnumed.115.164848) on selective fluorine-18 Tau tracers, and in particular the [18F]THK-5351, we explored the carbon-11 version - [11C]THK-5351. There are a few advantages carbon-11 labeling may provide over fluorine-18 label, such as lack of radiodefluorination, possibility of imaging the same subject with repeated injection on the same day and lesser radiation burden on the patients in clinical studies. In parallel, THK-5351 was also labeled with tritium, [3H]THK-5351, for *in vitro* autoradiography (ARG) application.

The 2-steps carbon-11 labeling (Figure 1-A) was conducted starting with di-protected enantiomerically pure precursor - tert-butyl 5-(6-((2S)-3-fluoro-2-(tetrahydro-2H-pyran-2-yloxy)propoxy)quinolin-2-yl)pyridin-2-ylcarbamate, which was reacted with [11C]MeI, obtained via reaction of [11C]methane with elemental iodine, using DMF as the reaction solvent and NaH as base (300 seconds at 50 ^{o}C), followed by deprotection with trifluoroacetic acid (300 seconds at 70 ^{o}C). The resulting [11C]THK-5351 - (S)-1-fluoro-3-(2-(6-([11C]methylamino)pyridin-3-yl)quinolin-6-yloxy)propan-2-ol - was purified on HPLC using Waters XBridge 250×10 mm column, with acetonitrile/ammonium formate as mobile phase, concentrated on SPE cartridge and reconstituted in sterile saline-ethanol mixture, followed by sterile filtration. [11C]THK-5351 was produced in sufficient yield - 1900±355 MBq, high specific radioactivity - 361±119 GBq/µmol and radiochemical purity >99.8% (N=3) for further use in pre-clinical and clinical studies. Tritium labeling (Figure 1-B) and purification of [3H]THK-5351 was conducted using similar approach, with commercially-obtained [3H]MeI (Amersham, USA), resulting in [3H]THK-5351 with RCP >99.8% and specific radioactivity of 1.3 GBq/µmol (35 Ci/mmol).

For evaluation of usefulness of [3H]THK-5351 for ARG imaging of Tau binding sites in post-mortem human brain tissue cortical sections from one AD patient and one control subject were thawed and pre-incubated in Tris HCl (50 mM) at pH 7.4. Slides were then incubated at 0.5 nM [3H]THK-5351 in Tris HCl buffer for 60 min. 20 µM cold THK5351 was used to block specific binding. After incubation the slides were washed in ice-cold Tris HCl 50 mM, pH 7.4, followed by a brief wash in distilled water. The slides were exposed to phosphor imaging plates (Fujifilm Plate BAS-TR2025, Fujifilm, Tokyo, Japan), plates were then scanned on a Fujifilm BAS-5000 phosphor imager (Fujifilm, Tokyo, Japan). [3H]THK-5351 binding density was higher in the AD patient compared to the control subject, the binding that was completely displaced by the addition of unlabeled THK5351 resulting in a specific [3H]THK-5351 binding of 100% (Figure 1-C).
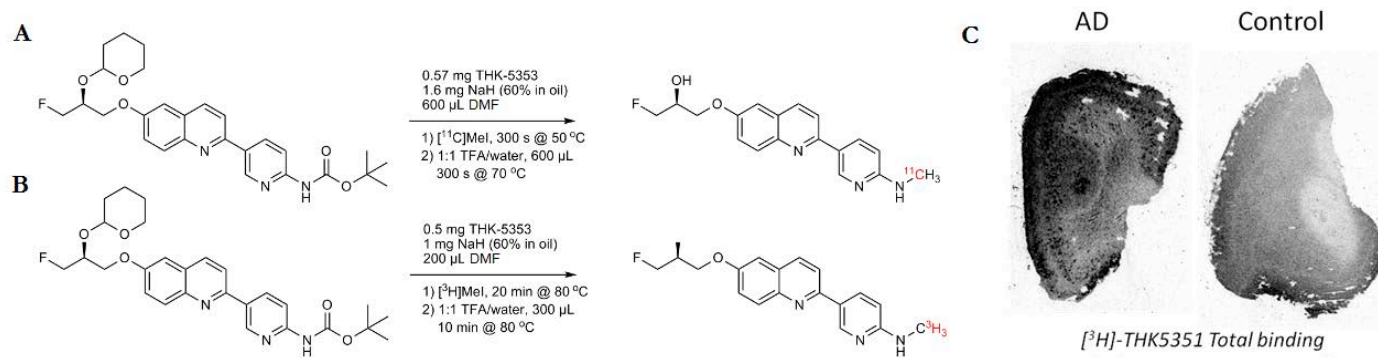
Figure 1. The 2-steps labeling of [^{11}C]THK-5351 (A) and [^{3}H]THK-5351 (B), respectively. ARG of post-mortem human brain tissue from AD patient and control (C).

Investigation of Parkinson's Disease Related Covariance Pattern in the Serotonergic System using [11C]-DASB/PET

J Fu[1], N Vafai[2], E Shahinfard[2], N Heffernan[2], J McKenzie[2], R Mabrouk[1], I Klyuzhin[1], AJ Stoessl[2], V Sossi[1]

[1]Department of Physics and Astronomy, University of British Columbia, Vancouver, B.C., Canada V6T 1Z1; [2]Pacific Parkinson's Research Centre, University of British Columbia, Vancouver, B.C., Canada V6T 2B5

We used PET imaging with [11C]-3-amino-4-(2-dimethylaminomethylphenylsulfanyl)- benzonitrile (DASB) and analysis based on statistical regional covariance model, namely the Scaled Subprofile Model (SSM) [1,2], to investigate whether a Parkinson's disease (PD) related pattern could be identified for the serotonergic system. We also explored if the asymptomatic LRRK2 mutation carriers would exhibit a different pattern compared to healthy control (HC) and subjects with manifest PD.

We studied 12 LRRK2 unaffected mutation carriers, 9 HC, and 18 PD subjects (11 subjects with sporadic PD (sPD), 7 with LRRK2 mutation- associated PD (gPD)). We applied SSM analysis on the DASB non-displaceable binding potentials (BP_{ND}) evaluated in 45 pre-defined regions of interest. The BP_{ND} was obtained using the Reference Tissue Model with cerebellum used as reference [3].

The Akaike Information Criterion-based [4] combination of two principal components (PCs) accounting for 27% of the total variance was found to yield a highly significant separation between the HC and PD groups. The spatial pattern was comprised of a relatively decreased binding in Caudate, Putamen, and Pedunculopontine Nucleus, and relatively preserved binding in Hypothalamus and Hippocampus in PD compared to HC. The individual subject scores for this covariance pattern were significantly higher for PD compared to HC ($p<0.01$), and significantly correlated with the age of disease onset ($p=0.03$). No correlation was found between subject scores and any other measured clinical variables. No significant difference between age- and disease severity- matched sPD and gPD subjects ($p=0.12$) was observed. The pattern was validated using cross-validation and bootstrapping.

PD subjects also showed a significantly different covariance pattern compared to unaffected mutation carriers ($p<0.01$) using a combination of PCs (31% of the total variance). This covariance pattern was comprised of a relatively decreased binding in Hypothalamus, Substantia Nigra, Pedunculopontine Nucleus, and Ventral Tegmental Area, and relatively preserved binding in Anterior Cingulate, Dorsolateral Prefrontal Cortex, Orbitofrontal Cortex, and Posterior Cingulate in PD compared to unaffected mutation carriers.

Absolute BP_{ND} values suggested an increased binding in Hypothalamus and Hippocampus ($p<0.05$) in unaffected mutation carriers compared to HC, but no difference was found in the covariance pattern between the two groups.

These findings, although obtained with a small number of subjects, suggest that the serotonergic system may be affected by PD in a specific pattern. sPD and gPD subjects appear to exhibit the same brain pattern once disease is established. The findings are consistent with previous reports that early and established PD subjects exhibit a significantly reduced binding in Caudate and Putamen compared to HC ($p<0.01$) [5], and that PD subjects with depression have significantly increased binding in Hypothalamus and Posterior Cingulate compared to age matched-PD subjects without depression [6]. The unaffected mutation carriers exhibit higher BP_{ND} values in several regions, but do not exhibit a PD related pattern, which indicates that either such increase is of compensatory nature or is a characteristic of this specific mutation. These initial results will be confirmed by including more subjects into the analysis.

References

1. Moeller, J. R., et al. "Scaled subprofile model: a statistical approach to the analysis of functional patterns in positron emission tomographic data."*Journal of Cerebral Blood Flow & Metabolism* 7.5 (1987): 649-658.
2. Eidelberg, D. "Metabolic brain networks in neurodegenerative disorders: a functional imaging approach." *Trends in neurosciences* 32.10 (2009): 548-557.

3. Gunn, RN., et al. "Parametric imaging of ligand-receptor binding in PET using a simplified reference region model."*Neuroimage* 6.4 (1997): 279-287.

4. Akaike, H. "An information criterion (AIC)." *Math Sci* 14.153 (1976): 5-9.

5. Politis, M., et al. "Staging of serotonergic dysfunction in Parkinson's disease: an in vivo 11 C-DASB PET study." *Neurobiology of disease* 40.1 (2010): 216-221.

6. Politis, M., et al. "Depressive symptoms in PD correlate with higher 5-HTT binding in raphe and limbic structures." *Neurology* 75.21 (2010): 1920-1927.

DASB-PDRP regional weights PD vs Control
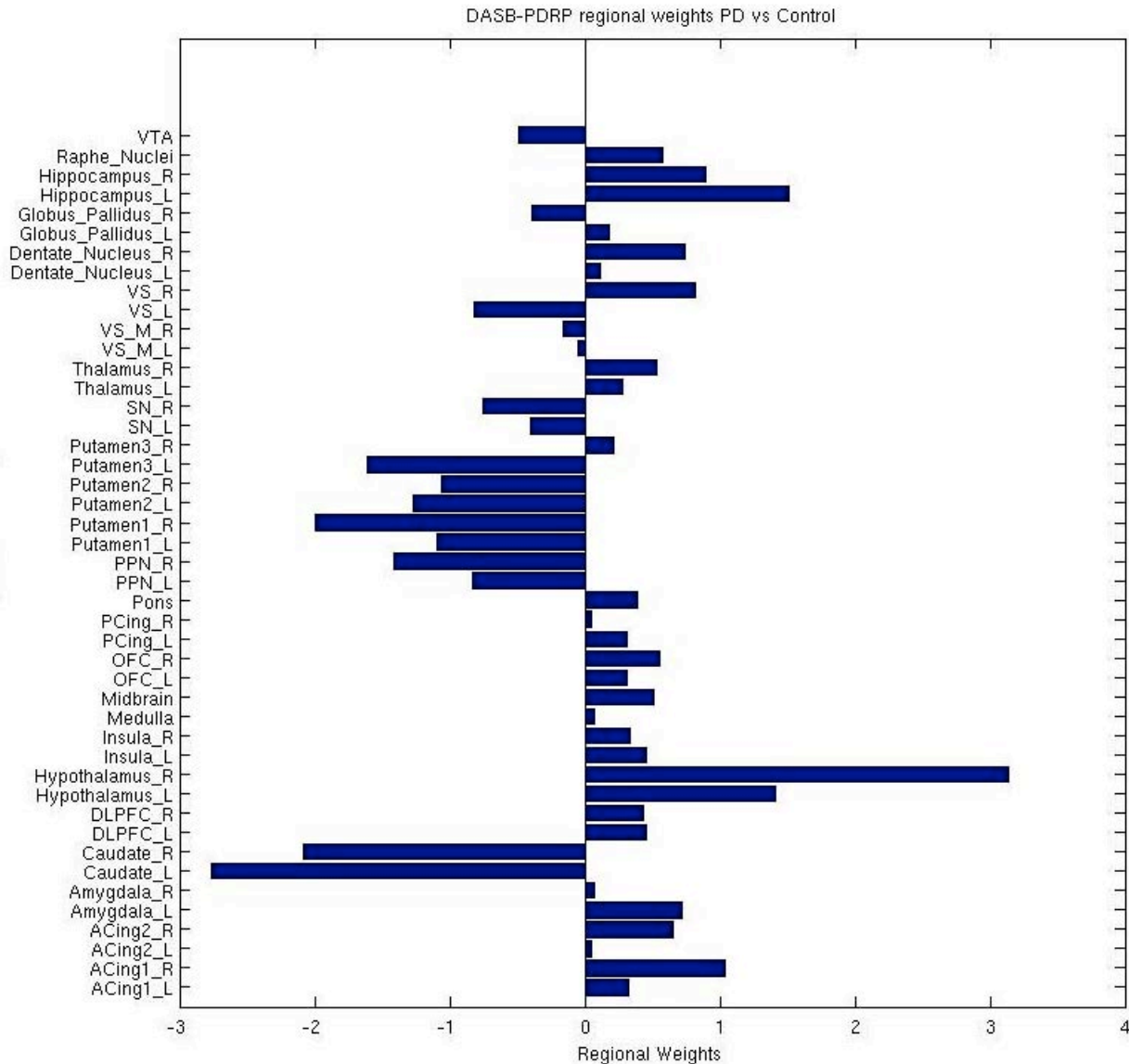
Regional weights represent the contribution from each brain region to DASB PD related pattern (PDRP). Regions with weights greater than 1 have relatively preserved binding, and regions with weights less than -1 have relatively decreased binding in PD subjects compared to healthy controls.

Polyunsaturated Fatty Acid Associations with Serotonin Transporter Binding in Major Depressive Disorder Assessed with [11C]DASB PET

M. Elizabeth Sublette[1,2], Manesh Gopaldas[1,2,3], Francesca Zanderigo[1,2], Harry Rubin-Falcone[1,2], Thomas B. Cooper[1,2,4], Maria A. Oquendo[1,2], Gregory Sullivan[1,2], J. John Mann[1,2,5]

[1]Department of Molecular Imaging and Neuropathology, New York State Psychiatric Institute, New York, New York, USA ; [2]Department of Psychiatry, Columbia University, New York, New York, USA; [3]Herbert Wertheim College of Medicine, Florida International University, Miami, Florida, USA; [4]Nathan S. Kline Institute for Psychiatric Research, Orangeburg, New York, USA ; [5]Department of Radiology, Columbia University, New York, New York, USA

Background: Low serotonin transporter (5-HTT) binding[1] and imbalances in polyunsaturated fatty acids (PUFAs)[2] have been implicated in major depressive disorder (MDD). Using positron emission tomography (PET) with [11C]DASB, we studied relationships between 5-HTT binding and plasma PUFA levels in MDD patients and healthy volunteers (HV). Since lower n-3 (omega-3) PUFAs relative to n-6 PUFAs are seen in MDD, we hypothesized that docosahexaenoic acid (DHA, 22:6n-3) would correlate positively and arachidonic acid (AA, 20:4n-6) would correlate negatively with 5-HTT binding, with a more pronounced effect in MDD. Eicosapentaenoic acid (EPA, 20:5n-3) was a control as it occurs in low levels in the brain.

Methods: MDD patients (*n*=23) with a score of at least 16 on the Hamilton Depression Rating Scale (HDRS-17) and HV (*n*=8) had fasting blood drawn on the day of [11C]DASB PET. Plasma PUFAs were quantified using direct transesterification and gas chromatography. In the MDD group, the binding potential (BP_{ND}) of [11C]DASB was calculated for 12 brain regions of interest (ROIs) as $BP_{ND} = V_T - V_{ND}/V_{ND}$ (V_T = volume of distribution, V_{ND} = nonspecific binding in the ROI, estimated using a novel hybrid deconvolution approach (HYDECA)[3] that combines deconvolution[4] and simultaneous search across regions[5] to estimate V_{ND} without relying on any reference region). Correlations were studied between PUFA levels (*ln*-transformed to correct distributional skew) and BP_{ND}, and regression models were employed to study effects of PUFA levels and BP_{ND} on HDRS-17 scores. Effects of diagnostic group (MDD vs. HV) were explored by including group as a covariate in linear regression models with BP_{ND} as outcome measure, and AA as predictor. For these analyses, BP_{ND} values were calculated using the simplified reference tissue model (SRTM) with the cerebellar gray matter as a reference region (due to missing blood data among HV).

Results: In MDD, correlations with 5-HTT binding were negative for all PUFAs in all 12 ROIs. Significant correlations were seen for AA (see Figure) in all ROIs (*p*-values ranging from 0.001 – 0.029 with a trend in hippocampus, *p*=0.098) except orbital cortex (*p*=0.468). BP_{ND} predicted depression severity in the amygdala and ventral striatum (*p*=0.02), associations that were strengthened (*p*=0.002 – 0.004) by inclusion of AA but not DHA, EPA, sex, or age in the models. In the full sample, both AA and diagnostic group had significant main effects on BP_{ND} in anterior cingulate, temporal cortex, ventral striatum, and caudate, and a trend in dorsolateral prefrontal cortex.

Conclusions: Our hypothesis of differential directionality of n-3 vs. n-6 PUFA correlations with 5-HTT binding was not supported; group effects on correlations between AA and BP_{ND} were observed, but must be replicated, given the small size of the HV sample. The most significant results were negative correlations between plasma AA and 5-HTT binding. These AA findings are consistent with a cascade previously observed in 5-HTT-deficient mice, which have elevated extracellular 5-HT that stimulates cytosolic phospholipase A2 (via binding to $5-HT_{2A/2C}$ receptors) and thereby increases the release of AA from membrane phospholipids[6].

References

1. Selvaraj S, et al. Psychopharmacology (Berl). 2011;213(2-3):555-62.
2. Lin PY, et al. Biol Psychiatry. 2010;68(2):140-7.
3. Zanderigo F, et al. XXVIIth International Symposium on Cerebral Blood Flow, Metabolism and Function & XIIth International Conference on Quantification of Brain Function with PET. Vancouver, Canada. 2015.
4. Zanderigo F, et al. J Cereb Blood Flow Metab. 2015;35(8):1368-79.
5. Todd O R, et al. Neuroimage. 2015;108:234-42.
6. Basselin M, et al. Neuropsychopharmacology. 2009.

Correlations Between Serotonin Transporter Binding and Plasma Arachidonic Acid in MDD

combined Pearson's *r*=0.4578
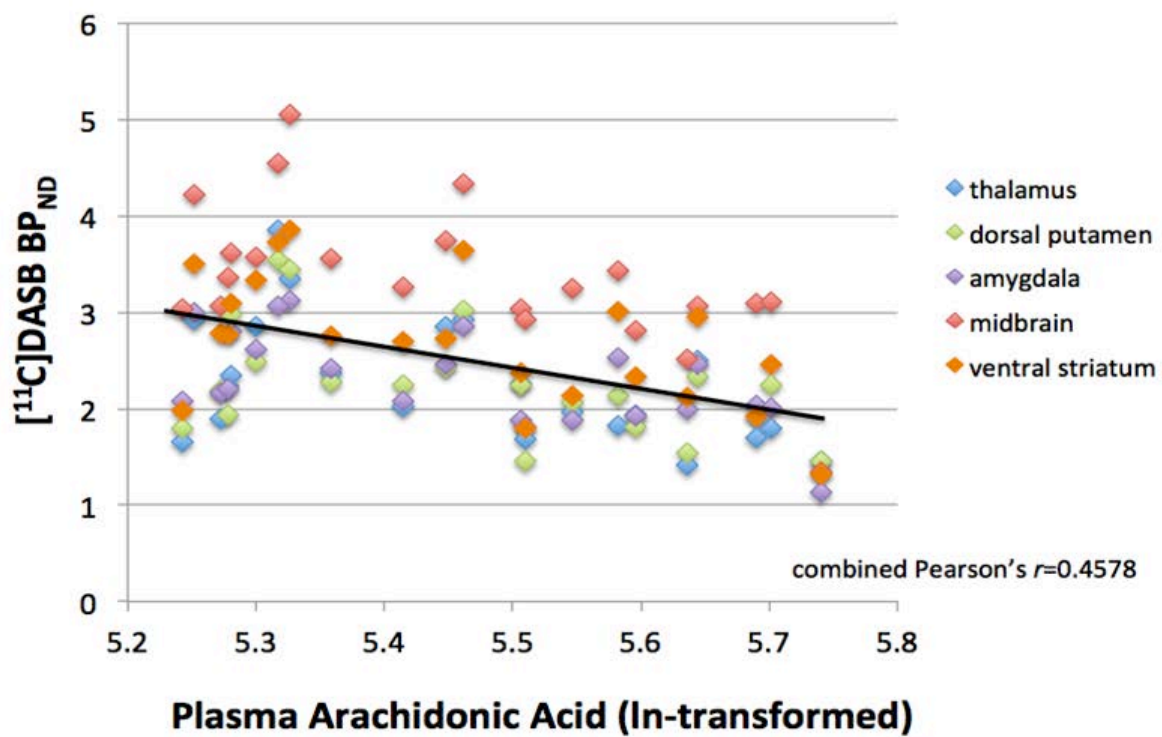
Relevance of distribution of 5-HT$_{2A}$ and dopamine D$_2$ receptors in human cerebral cortex using a cluster analysis

T. Ishii[1,2], M. Yamada[1], Y. Kimura[1], Y. Takado[1], K. Takahata[1], S. Kitamura[1], M. Kubota[1], S. Moriguchi[1], H. Ito[1], M. Ichise[1], Y. Okubo[2], T. Suhara[1]

[1]*Molecular Imaging Center, National Institute of Radiological Sciences, Chiba, Japan;* [2]*Department of Neuropsychiatry, Nippon medical school, Tokyo, Japan*

Background: Serotonin 2A receptors (5-HT$_{2A}$) and dopamine D$_2$ receptors are intimately related to the pathophysiology of depression. PET studies in depression revealed that 5-HT$_{2A}$ receptor density in the cerebral cortex was decreased in patients with major depressive disorder [1]. Electroconvulsive therapy decreased D$_2$ receptor binding in the rostral AC in major depressive disorder patients [2]. Although, there were a large number of studies investigating distribution of 5-HT$_{2A}$ receptor and dopamine D$_2$ receptors separately, little is known about the relevance of distribution of the two receptors in the cerebral cortex. In the present study, we investigated the relevance of distribution of 5-HT$_{2A}$ receptor and dopamine D$_2$ receptor in human cerebral cortex using PET and a cluster analysis.

Methods: PET scans were performed on seven healthy volunteers with [18F]Altanserin and [11C]FLB 457. Binding potential (*BP*) was calculated for 84 cerebral cortical regions defined by Automated Anatomical Labeling. A correlation matrix was calculated between *BP* of [18F]Altanserin and [11C]FLB457, which was made of 84 x 84 regional pairs. The relevance of distribution with 5-HT$_{2A}$ and dopamine D$_2$ receptors was investigated by bi-clustering of regional pairs on the correlation matrix, using an iterative signature Algorithm (ISA) implemented in the BicAT (The Biclustering Analysis Toolbox, Eidgenössische Technische Hochschule, Zürich).

Results: Four clusters were extracted from the correlation matrix between *BP* of [18F]Altanserin and [11C]FLB457 in the cerebral cortical regions. The extracted clusters were divided into two groups. The clusters in the first group consisted of the correlation between 5-HT$_{2A}$ receptor *BP* of bilateral hippocampus and parahippocumpus and dopamine D$_2$ receptor *BP* of a broad regions in the cerebral cortex ($r = 0.46 \pm 0.15$, mean ± SD). The clusters in the second group consisted of the correlation between 5-HT$_{2A}$ receptor *BP* of temporal and occipital cortex and dopamine D$_2$ receptor *BP* of a broad regions in the cerebral cortex ($r = 0.41 \pm 0.17$).

Conclusions: We found that density of 5-HT$_{2A}$ receptor in two groups of regions were positively correlated to the density of dopamine D$_2$ receptors of a broad regions in the cerebral cortex. It may indicate functional and/or developmental relevance of the two receptors in those regions.

References:

[1]Messa C, et al. 5-HT(2A) receptor binding is reduced in drug-naive and unchanged in SSRI-responder depressed patients compared to healthy controls: a PET study. *Psychoparmacology*. 2003 Apr;167(1):72-8.

[2]Saijo T, et al. Electroconvulsive Therapy Decreases Dopamine D2 Receptor Binding in the Anterior Cingulate in Patients With Depression: A Controlled Study Using Positron Emission Tomography With Radioligand [11C]FLB 457. *J Clin Psychiatry* 71:6, June 2010

Cerebral 5-HT release correlates with [11C]AZ10419369 PET measures of 5-HT1B receptor binding in the pig brain

Louise M Jørgensen[1,2], Pia Weikop[3,4], Claus Svarer[1], Ling Feng[1], Sune H. Keller[5], Gitte M Knudsen[1,2]

[1]*Neurobiology Research Unit, Rigshospitalet, Copenhagen, Denmark;* [2]*Faculty of Health and Medical Sciences, University of Copenhagen, Denmark;* [3]*The Laboratory of Neuropsychiatry, Department of Neuroscience and Pharmacology, University of Copenhagen, Denmark;* [4]*Psychiatric Centre Copenhagen, University of Copenhagen, Denmark;* [5]*Department of Clinical Physiology, Nuclear Medicine and PET, Rigshospitalet, University of Copenhagen, Copenhagen, Denmark.*

Objectives: Several studies have investigated PET radioligands for their ability to be displaced by endogenously released 5-HT, but the outcomes in humans have not convincingly shown the expected effect of pharmacological interventions supposed to increase brain interstitial 5-HT[1]. Two recent studies in humans, however, suggest that when a selective 5-HT reuptake inhibitor (SSRI) is given, the PET radioligands [11C]CUMI-101[2] (a 5-HT$_{1A}$ receptor ligand) and [11C]AZ10419369[3] (a 5-HT$_{1B}$ receptor ligand) show *increased* binding. This unexpected finding has been interpreted as being caused by the autoreceptor function, with 5-HT$_{1A}$ and 5-HT$_{1B}$ stimulation inhibiting 5-HT release. By contrast, a recent combined PET and microdialysis study in pigs showed that a high dose of the SSRI escitalopram was associated with a robust increase in cerebral interstitial 5-HT levels as well as a decrease in binding of the 5-HT$_{2A}$ agonist receptor ligand [11C]Cimbi-36[4]. The apparently conflicting outcomes may be due to differences in how pharmacological challenges affect synaptic 5-HT levels, but so far, no studies investigated the effect of clinically relevant doses of escitalopram on brain interstitial 5-HT levels.

The aim of the present study was to measure the effect of different pharmacological interventions on cerebral 5-HT by microdialysis and to correlate the change in interstitial 5-HT to the change in BP$_{ND}$ of [11C]AZ10419369 by PET. Here, we simultaneously measured pharmacologically induced changes in 5-HT levels in the medial prefrontal cortex (mPFC) and cerebral [11C]AZ10419369 binding in pigs.

Methods: Ten Danish Landrace pigs had implanted microdialysis probes bilaterally in the mPFC from which extracellular fluid were collected during PET scanning and subsequently analyzed off-line for 5-HT with HPLC. The pigs went through two separate scanning sessions; on both occasions they were given an IV bolus injection of [11C]AZ10419369 and were subsequently scanned for 120 minutes in the HRRT PET scanner. 56.5 min after the first radioligand injection, a saline injection was given and 56.5 min after the second radioligand injection, either escitalopram (0.28 mg/kg, N=5) or the potent 5-HT releaser fenfluramine (0.5 mg/kg, N=5) was given. The extended SRTM was used for quantification of BP$_{ND}$ before and after the saline/drug intervention. The mean increase in brain 5-HT level relative to baseline in response to the intervention was computed as well as the change in BP$_{ND}$.

Results: Whereas saline injection did not change 5-HT levels, escitalopram intervention was associated with a mean (SEM) increase in brain interstitial fluid 5-HT level of 163±35% and fenfluramine with a mean increase of 292±39 %. Neocortex [11C]AZ10419369 BP$_{ND}$ remained unaltered after saline injection (-1%) but was decreased by escitalopram (-6%) and fenfluramine (-13%), Figure 1.

Conclusions: We here show, firstly, that acutely administered escitalopram in clinically relevant doses induces an acute increase in the cerebral interstitial fluid concentration of 5-HT in the brain; an effect that is almost doubled with fenfluramine. Secondly, we demonstrate that the cerebral binding of the 5-HT$_{1B}$ receptor antagonist [11C]AZ10419369 decreases in proportional response to these interventions. In conclusion, [11C]AZ10419369 binding is sensitive to acute changes in 5-HT levels, although less sensitive as compared to [11C]Cimbi-36[4]

References
1. Paterson LM, Tyacke RJ, Nutt DJ, Knudsen GM. Measuring endogenous 5-HT release by emission tomography: promises and pitfalls. *J Cereb Blood Flow Metab*. 2010;30(10):1682-1706. doi:10.1038/jcbfm.2010.104.
2. Selvaraj S, Turkheimer F, Rosso L, et al. Measuring endogenous changes in serotonergic neurotransmission in humans: a [11C]CUMI-101 PET challenge study. *Mol Psychiatry*. 2012;17(12):1254-1260. doi:10.1038/mp.2012.78.

3. Nord M, Finnema SJ, Halldin C, Farde L. Effect of a single dose of escitalopram on serotonin concentration in the non-human and human primate brain. *Int J Neuropsychopharmacol*. 2013;16(07):1577-1586. doi:10.1017/S1461145712001617.

4. Jørgensen LM, Weikop P, Villadsen J, et al. Cerebral 5-HT release correlates with [11C]Cimbi36 PET measures of 5-HT2A receptor occupancy in the pig brain. *J Cereb Blood Flow Metab*. January 2016:0271678X16629483. doi:10.1177/0271678X16629483.
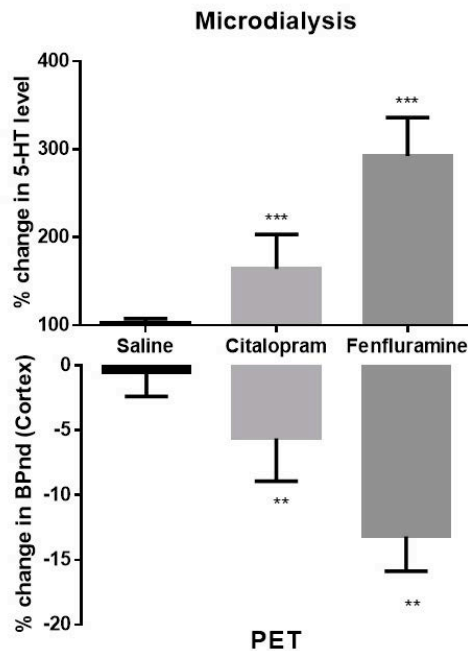
Figure 1.

Relative increase in the interstitial cerebral 5-HT level compared to baseline (100 %) as measured by microdialysis in the PFC and the corresponding relative decrease in BPnd as measured by PET in the neocortex in the three conditions following a within-scan pharmaceutical challenge of saline, 0.28 mg/kg escitalopram and 0.5 mg/kg fenfluramine. The changes as measured by both PET and microdialysis were significant (Kruskal-Wallis test) with *** ($p<0.001$) and ** ($p<0.01$).

Effects of common anesthesia on [18F]flumazenil binding to the GABA$_A$ receptor.

Mikael Palner[1,3], Corinne Beinat[1], Sam Banister[1], Francesca Zanderigo[4], Jun Hyung Park[1], Lawrence Fung[2], and Frederick T. Chin[1]

Departments of Radiology[1] and Psychiatry & Behavioral Sciences[2], Stanford University School of Medicine, Stanford, California, USA; [3]Neurobiology Research Unit, Rigshopitalet, Copenhagen, Denmark; [4]Department of Molecular Imaging and Neuropathology, New York State Psychiatric Institute and Columbia University

Imaging studies in humans can typically be performed without anesthetization of the subject, but imaging in younger people, especially when mentally challenged with fragile X syndrome, anxiety or schizophrenia, have required the use of anesthesia or anxiolytics to prevent motion artifacts in the acquired images. It has been shown that most volatile general anesthetics, including isoflurane, propofol, and pentobarbital, affect GABA$_A$ receptors. The aim of this study was to determine the effects of the common anesthesia, isoflurane, ketamine and dexmedetomidate on [18F]flumazenil binding to the GABA$_A$ receptors in mice, prior to a translational study in individuals with fragile X syndrome.

We used a combination of [18F]flumazenil PET and *ex vivo* brain dissection to compare the binding under four anesthetic/anxiolytic conditions in mice: isoflurane-anesthetized, ketamine/dexmed-etomidate-anesthetized, dexmedetomidate-treated, and awake. PET images were acquired as 60-minute dynamic scans in the anesthetized conditions, and as 10-minute static scans under brief isoflurane anesthetics in the dexmedetomidate-treated and awake condition. The brain was dissected and plasma and whole blood samples collected at 60 minutes post injection in all conditions. Semi-quantitative kinetic analysis of the volume of distribution was carried out as group estimates using either an image derived input function from the heart or the *ex vivo* measured whole blood radioactivity.

PET imaging under the four test conditions (see figure) clearly visualize the effect on [18F]flumazenil binding (n=4 per group). At 25 minutes, the isoflurane-anesthetized mice (A) had above 20% ID/g in the high-binding regions of frontal cortex (FC) and hippocampus (HC) while there were 7% ID/g in the same areas in the ketamine/dexmedetomidate-anesthetized mice (B) and 4% ID/g in the dexmedetomidate-treated (C). We found less than 2% ID/g in the same areas in the awake mice (D). This effect was even more pronounced at 60 minutes post-injection where the awake mice were devoid of any detectable [18F]flumazenil in the brain whereas the isoflurane anesthetized mice still showed significant binding (approximately 10% ID/g). Isoflurane and dexmedetomidate alone significantly increased the [18F]flumazenil distribution volumein the hippocampus while ketamine/dexmedetomidate decreased the [18F]flumazenil distribution volume in the frontal cortex, compared with the awake condition.

Each anesthetic affected the uptake and binding of [18F]flumazenil in some way compared with the awake condition. These results emphasize the importance of carefully designing and controlling the experimental conditions when imaging GABA$_A$ receptors in combination with anesthetics or anxiolytics.
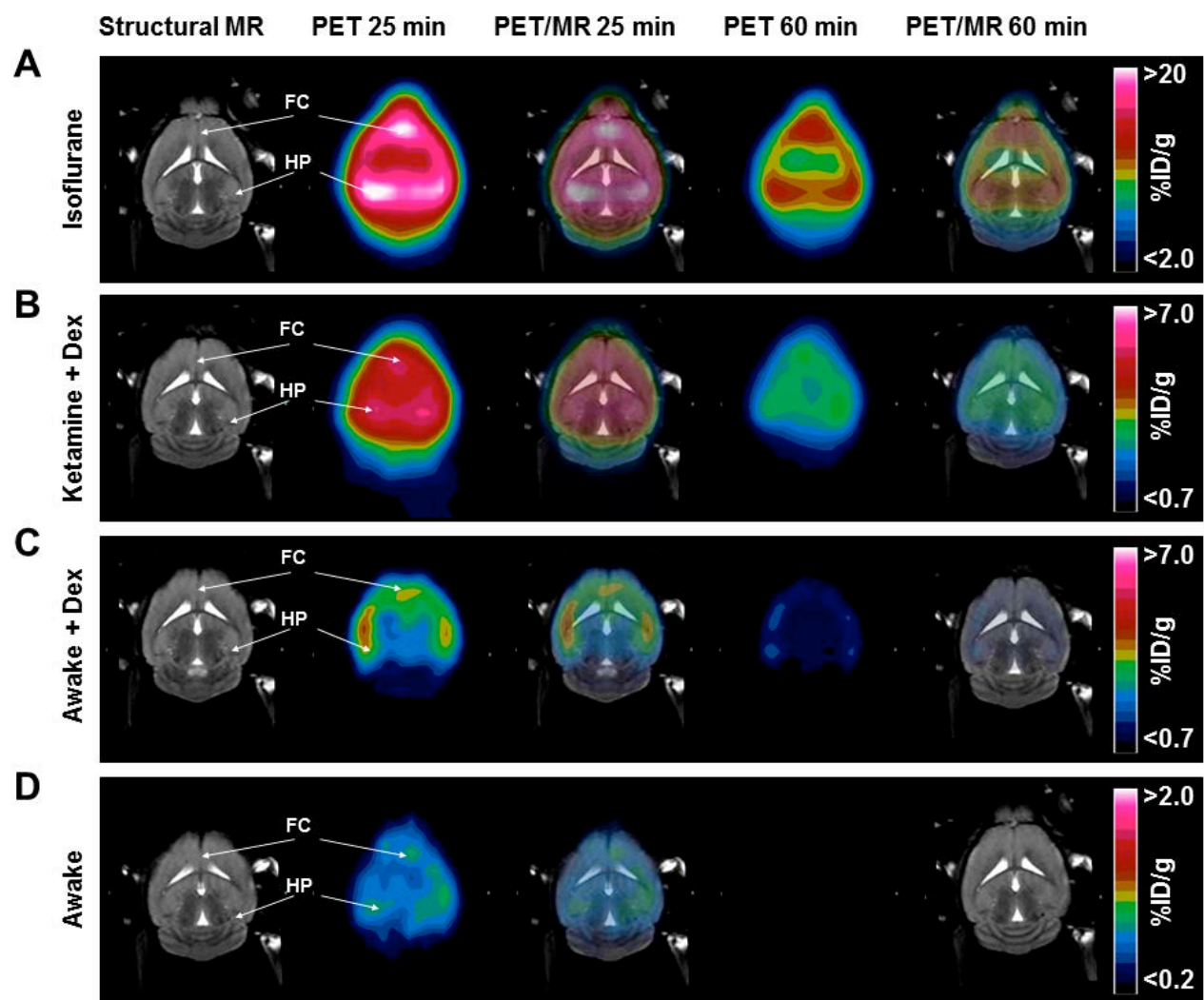
[^{18}F]flumazenil PET images of the GABA$_A$ receptor in four different anesthetic conditions. Extracted images from a 60 minute dynamic scan using (A) isoflurane or (B) ketamine/dexmedetomidine and from a 10 minute static scans using isoflurane of (C) dexmedetomidine treated or (D) awake mice. Note that the scalebare are different for the different anesthetic conditions to better accommodate the dynamic range in the individual images.

Evaluation of reference region approaches for quantification of phosphodiesterase 10A binding with [11C]Lu AE92686 in the cynomolgus monkey brain

Kai-Chun Yang[1], Vladimir Stepanov[1], Nahid Amini[1], Stefan Martinsson[1], Akihiro Takano[1], Jacob Nielsen[2], Christoffer Bundgaard[3], Benny Bang-Andersen[3], Sarah Grimwood[4], Christer Halldin[1], Lars Farde[1], Sjoerd J. Finnema[1, 5]

[1]*Karolinska Institutet, Department of Clinical Neuroscience, Stockholm, Sweden;* [2]*H. Lundbeck A/S, Division of Synaptic Transmission, Valby, Denmark;* [3]*H. Lundbeck A/S, Discovery Chemistry and DMPK, Valby, Denmark;* [4]*Pfizer Inc., Neuroscience Research Unit, Cambridge, MA, USA;* [5]*Yale University, Department of Radiology and Biomedical Imaging, New Haven, CT, USA*

Objectives: Phosphodiesterase 10A (PDE10A) is a potential therapeutic target for neuropsychiatric disorders. The density of this intracellular enzyme is high in striatum, globus pallidus and substantia nigra, but low in cerebellum [1]. The novel high affinity positron emission tomography (PET) radioligand [11C]Lu AE92686 has previously been validated for imaging of striatal PDE10A in the human [2] and monkey brain [2,3]. The aim of this study was to further validate the cerebellum as a reference region for quantification of [11C]Lu AE92686 in monkey brain by pretreatment studies with unlabelled Lu AE92686 or the PDE10A inhibitor MP-10.

Methods: The study was approved by the Animal Research Ethical Committee of the Northern Stockholm region and all experiments were performed according to the 'Guidelines for planning, conducting and documenting experimental research of Karolinska Institutet'. A total of 8 PET measurements were performed on a High Resolution Research Tomograph (HRRT) in 2 cynomolgus monkeys, including 4 baseline measurements and 4 subsequent PET measurements after pretreatment with Lu AE92686 (0.5 mg/kg and 2.0 mg/kg) or MP-10 (1.5 mg/kg, n = 2). Arterial blood was collected to determine a metabolite-corrected arterial input function, plasma free fraction (f_P) and drug plasma concentrations. Five target regions: putamen, caudate nucleus, ventral striatum, globus pallidus and substantia nigra as well as cerebellum were delineated on MRI. Volumes of distribution (V_T) were estimated by Logan plot analyses. Binding potential (BP_{ND}) values were obtained by Logan plot analyses and the simplified reference tissue model (SRTM). An attempt to estimate the affinity of Lu AE92686 for PDE10A (K_i) and regional PDE10A density (B_{max}) was made using the baseline and pretreatment measurements with Lu AE92686. The K_i value was estimated by a hyperbolic function [4] using the free fraction of the plasma level of Lu AE92686 and corresponding occupancy levels estimated by the occupancy plots. Regional B_{max} values were derived according to the equation $B_{max} = K_i \times [(V_T - V_{ND})/ f_P]$.

Results: At baseline, the V_T/f_P values for the cerebellum were 8.6 ± 2.5 (n = 4). There was no significant effect (4.8 ± 15.4 %, P = 0.55) of pretreatment by Lu AE92686 or MP-10 on the V_T/f_P values. There was a close correlation between the BP_{ND} values obtained by Logan plot analyses and SRTM, respectively (Pearson r = 0.96, P < 0.0001). The estimated K_i was 3.0 nM and the regional B_{max} values ranged from 108.4/43.4 nM (substantia nigra) to 704.2/451.5 nM (putamen) and were comparable to the literature [5].

Conclusions: The results of the present pretreatment study support the use of cerebellum as a reference region for quantification of [11C]Lu AE92686 binding to PD10A in striatum as well as the substantia nigra.

References:
[1] Nishi et al, Front Neuroanat, 2011; [2] Kehler et al, J Nucl Med, 2014; [3] Yang et al, ISCBFM, 2015; [4] Farde et al, Psychopharmacology, 1989; [5] Hwang et al, Nucl Med Biol, 2015.
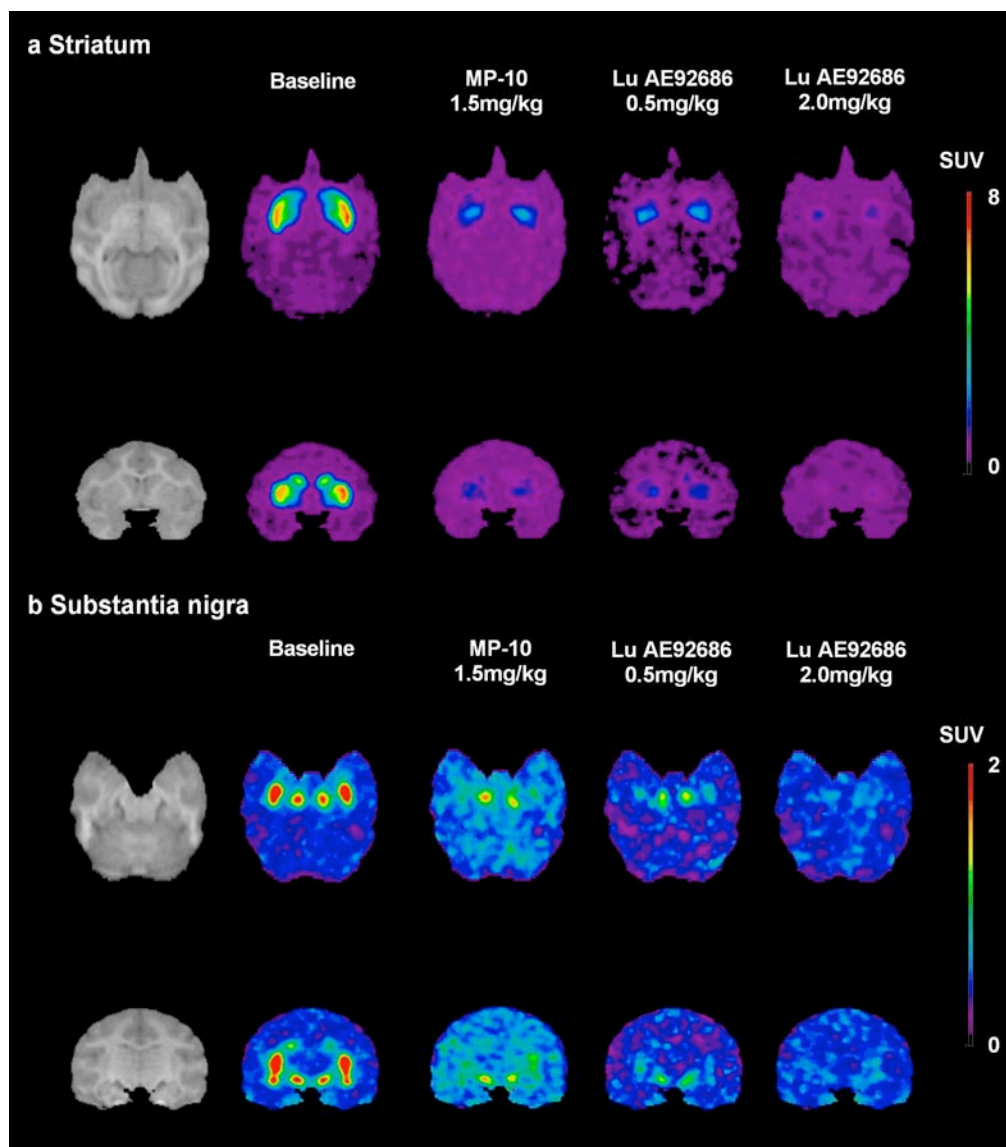
Fig 1. MR images and corresponding coregistered PET summation images (average of frames from 9 to 123 min) showing [^{11}C]Lu AE92686 binding in the NHP brain at baseline (mean of 3 measurements) and at 3 pretreatment conditions at the level of striatum (a) and substantia nigra (b).

A unified framework for the automatic blood data modelling in dynamic PET studies

Matteo Tonietto[1], Gaia Rizzo[1], Mattia Veronese[2] and Alessandra Bertoldo[1]

[1]*Department of Information Engineering, University of Padova, Padova, Italy;* [2]*Department of Neuroimaging, Institute of Psychiatry, King's College London, London, UK*

Introduction: In dynamic PET studies, arterial input function (AIF) requires correction for radiometabolites and data fitting to describe time-continuous activity of the tracer in blood. The first correction is performed by fitting a data model to a series of sparse Plasma Parent fraction (PPf) measurements. Corrected AIF is then fitted with another mathematical function to obtain a noise-free time-continuous estimation of the system input.

Objectives: In this work we propose a unified and fully automated framework for the blood data modelling and radiometabolite correction of PET AIFs. The method aims to be radioligand independent and applicable to both continuous and discrete blood sampling.

Methods: In [1] we demonstrated that modelling PET AIF as a linear and time-invariant system was superior to standard models for a wide range of radioligands. The general mathematical framework to describe AIF can be formulated as follows:

$$AIF(t) = h_p(t) \otimes u(t) \quad \text{with} \quad h_p(t) = \sum_{i=1}^{N} A_i \left(e^{-\lambda_i(t-t_0)} - e^{-\lambda_2(t-t_0)} \right) \quad \text{and} \quad u(t) = \begin{cases} 0 & t < 0 \vee t \geq T \\ 1 & 0 \leq t < T \end{cases}$$

where $h_p(t)$ is the system impulse response (described by a sum of N exponential functions with exponents λ_i and coefficients A_i), $\otimes$ is the convolution operator, and $u(t)$ is the system input (tracer injection of duration T). Extending the same approach to the appearance of radiometabolites in plasma (Cmet), it results:

$$Cmet(t) = h_{met}(t) \otimes AIF(t) \quad \text{with} \quad h_{met}(t) = \sum_{j=1}^{M} B_j \left(e^{-\beta_j(t-t_0)} - e^{-\beta_2(t-t_0)} \right)$$

where $h_{met}(t)$ is the metabolite system impulse response (described by a sum of M functions with exponents β_j and coefficients B_j). Both AIF and Cmet models can be estimated using a basis function approach [2]: a grid of 1000 λ_i (from 0.0001 to 10 min^{-1}) and 200 β_j (from 0 to 1 min^{-1}) are used to generate the corresponding components of h_p and h_{met}. The number of relevant components (N and M) and the corresponding coefficients are estimated from the data using a non-negative least squares estimator. The positive constrain on the coefficients A_i and B_j is motivated by previous studies [1,3].

However, what is measured in practice is the total activity in plasma $C_{tot}(t) = AIF(t) + C_{met}(t)$ and the $PPf(t) = \frac{AIF(t)}{AIF(t) + C_{met}(t)}$. The method thus starts with a linear interpolation of the measured PPf and it proceeds by iteratively fitting the AIF and the Cmet models. At each iteration both Ctot and PPf models are updated until convergence of the weighted residuals sum of squares.

This method was tested on two datasets with manual blood samples: [11C]PIB (n°=10) and [11C]WAY-100635 (n°=16), and two datasets with automatic samples [11C]-(+)-PHNO (n°=1) and [11C]PBR28 (n°=21). Details on the protocols can be found in [4-7].

Results: Weighted residuals analysis was in agreement with measurement error assumptions (i.e. random and standard normal distributed). Overfitting was not observed. M was on median 2 in all dataset, and N was on median 5 in the automatic sampled dataset and 4 in the manual cases. Figure shows fits of Ctot and PPf for one representative subject per dataset.

Conclusions: The method proposed appears to be flexible and robust enough to correctly model the kinetics of various radioligands across different measurements modalities (automatic vs manual) in a fully automated way.

References:
[1] Tonietto et al. (2015) *IEEE EMBC.*
[2] Cunningham et Jones (1993) *J. Cereb. Blood Flow Metab.*
[3] Feng et al. (1993) Int. J. Biomed. Comput.
[4] Devanand et al. (2010) J. Geriatr. Psychiatry Neurol.

[5] Parsey et al. (2000) J. Cereb. Blood Flow Metab.
[6] Suject available from MIAKAT (http://www.miakat.org/)
[7] Bloomfield et al. (2015) *Am. J. Psychiatry.*
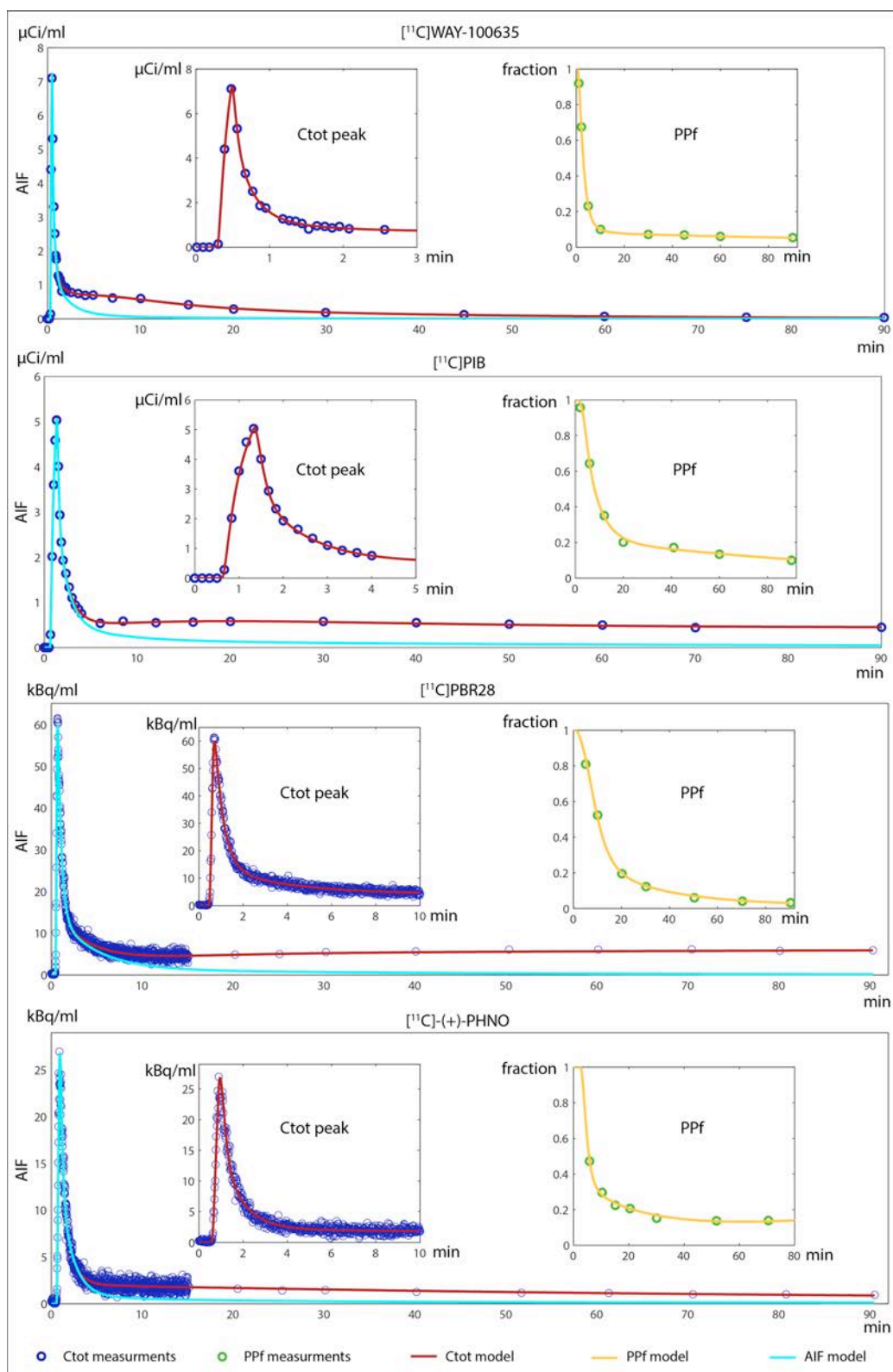
Legend: Figure shows the results obtained with one representative subject for each dataset. Circles denote measured blood data while solid lines represent model fits.

Population-based input function for 5HT$_{2A}$R agonist [11C]Cimbi-36 PET

Ling Feng[1], Anders Ettrup[1], Claus Svarer[1], Brice Ozenne[1,3], Agnete Dyssegaard[1], Lars H. Pinborg[1,2], Gitte M Knudsen[1,2]

[1]Neurobiology Research Unit, Rigshospitalet, Copenhagen, Denmark. [2]Faculty of Health and Medical Sciences, University of Copenhagen, Denmark. [3]Department of Biostatistics, University of Copenhagen, Denmark

Introduction: The first-in-human study of the 5HT$_{2A}$R agonist [11C]Cimbi-36 validated different kinetic models and found that reference tissue models underestimated non-displaceable binding potential (BP$_{ND)}$) by ~20% as compared to indirect calculation from V$_T$s of two-tissue compartment model (2TCM) [1]. Although the bias was found to be predictable, the inaccuracy of simplified reference tissue model (SRTM) estimation may be questionable in characterizing receptor occupancy, especially when high drug dose was administrated, due to larger change of bias between baseline and blocking/challenged conditions [2]. Population-based input function (PBIF) has been used for quantitative neuroimaging of many tracers to replace full arterial blood sampling [3]. Therefore, here we investigated the feasibility of PBIF for [11C]Cimbi-36.

Methods: Data was previously reported in detail [1,4]. Twenty-nine healthy volunteers (23.0±5.1 years, 15 males) were PET scanned for 2h after [11C]Cimbi-36 bolus injection. Arterial input function was measured in all scans and to evaluate the test-retest variability, 8 volunteers were rescanned.

Each metabolite-corrected plasma (real) input functions (RIF) normalized by injected dose per body weight were fitted with linear interpolation before the peak and with a triexponential function after the peak, then they were shifted in time to have a common peak time. PBIF was created by averaging these functions at the same time grid. PBIF was individualized by applying a leave-one-out procedure and was scaled by two blood samples, selected by Pearson's correlation to area under the curve (AUC) of RIFs.

BP$_{ND}$ was calculated for 17 ROIs as $V_T^{Target}/V_T^{Cerebellum} - 1$, where V$_T$s were modeled by both 2TCM (with 5 parameters) and Logan analysis using PBIF and RIF respectively. BP$_{ND}$ values from different models and IFs were compared using a linear mixed effect model with random effect on subjects and ROIs. Intra-class correlation coefficient (ICC) was calculated to evaluate the test-retest variability.

Results: PBIF curves were scaled by blood samples at 10 and 70 min. The scaled PBIF represented the shape of RIF well, except for a large difference in the peak height, and occasional differences in the tail shape. Nevertheless, AUC of the RIF was well estimated with a ratio PBIF/RIF of 1.02±0.07(n=29). Logan analysis utilizes the AUC rather than the exact shape of IF, thus it is an appropriate model to use with PBIF. Furthermore, using RIF Logan analysis estimated BP$_{ND}$ with only 1.8±1.7% difference (p=0.293) compared to 2TCM. BP$_{ND}$ estimates using three methods are shown in Figure 1. Logan analysis with PBIF resulted in 0.4±2.2% lower BP$_{ND}$ values (p=0.85) compared to 2TCM with RIF, and this difference is much smaller than the underestimation of 17.2±1.6% (p<0.001) with SRTM [1].

Test-retest variability increased from 4.7% using 2TCM with RIF to 6.6% using Logan analysis with PBIF, and ICC across 17 ROIs changed from 0.72±0.21 [4] to 0.73±0.16, none were significant.

Conclusion: We conclude that use of PBIF can accurately quantify BP$_{ND}$s for [11C]Cimbi36 without a full arterial input function, but limited to two blood samples. We are currently searching for alternatives to scale PBIF and will investigate the possibility of using PBIF in occupancy studies.

References:
1. Ettrup et al. *J Cereb Blood Flow Metab.* 2014;34(7):1188-96.
2. Salinas et al. *J Cereb Blood Flow Metab.*2015;35:304-311.
3. Takikawa et al. *Radiology* 1993;188(1):131-6.
4. Ettrup et al. *NeuroImage* 2016(in press).
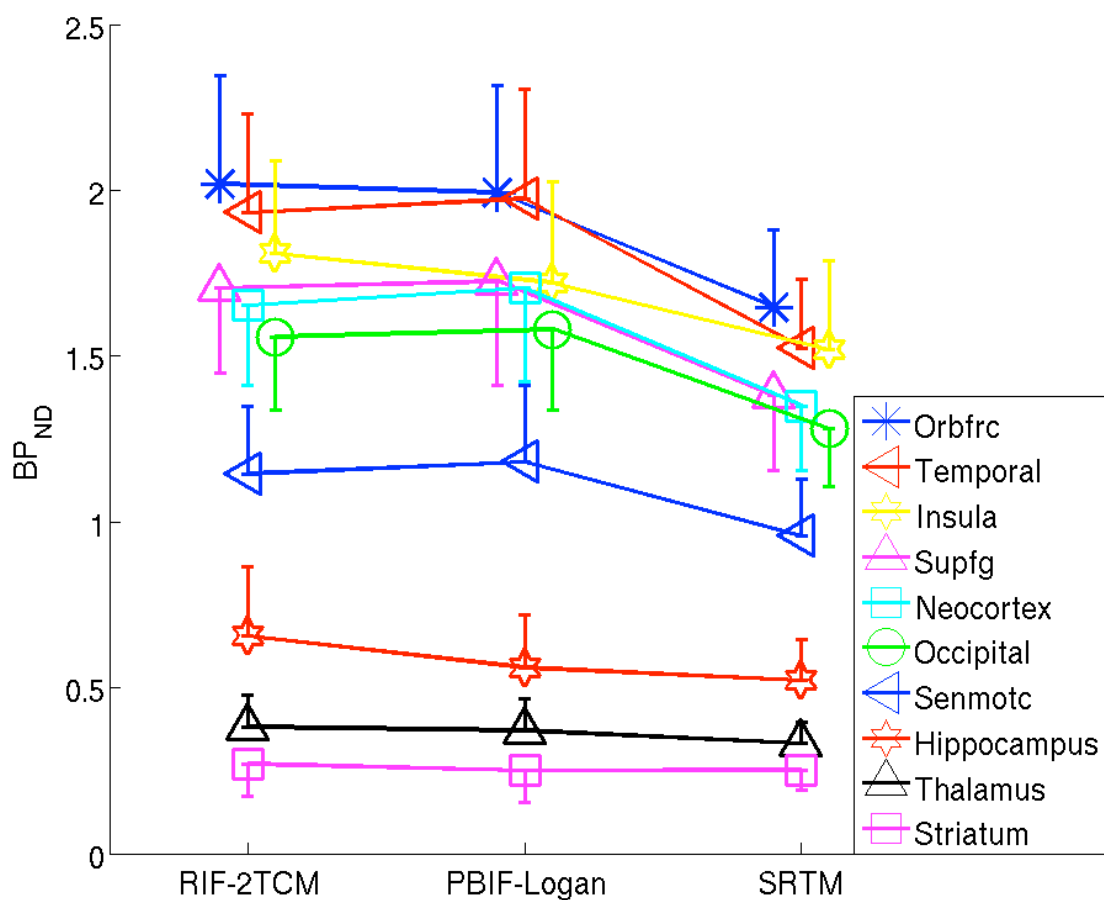
Figure 1 BP_{ND} (mean and one-direction standard deviation) of 10 ROIs using different modeling approaches and input functions. RIF-2TCM: 2 tissue compartment modeling using real input function; PBIF-Logan: Logan analysis using population-based input function; SRTM: simplified reference tissue model using cerebellum as the reference region.

Network analysis of brain PET data: application to cross-sectional studies

Mattia Veronese[a,*], Lucia Moro[b,*], Gaia Rizzo[b], Paul Expert[a], Wasim Khan[a], Alessandra Bertoldo[b] and Federico E Turkheimer[a]

[a]*Centre for Neuroimaging Sciences, IoPPN, King's College London, London, UK;* [b]*Department of Information Engineering, Padova University, Padova, Italy*
Equal contribution

Introduction: Analysing brain structural and functional imaging data using network theory is becoming increasingly popular in modern neuroimaging [1], where graphs can be used to represent anatomical and functional relations between different cerebral areas. Unfortunately, network-based approaches are not applicable to PET individual data, due to their limited temporal resolution (i.e. a single set of kinetic parameters per PET scan).
In this work we present a network-based approach for brain PET studies using population-based covariance matrices, with the aim to explore topological tracer kinetics differences in PET cross-sectional investigations.

Methods: PET connectivity matrices were defined by measuring the linear correlations between individual parameter estimates at region of interest (ROI) level, using both synthetic and measured PET data. These matrices were then translated into networks, with ROIs and cross-correlations becoming respectively the nodes and the weights of the links of the networks. Three graph metrics (strength, pagerank centrality, and clustering coefficient) were calculated for each network using the brain connectivity toolbox [2]. Several statistical tests (Wilcoxon Rank-Sum, Ansari-Bradley, Welch's t-test and F-test) were then implemented to test differences between networks, with and without the use of permutation. Krzonowski's test was also applied to compare network principal components [3].
All the methods were tested in term of false positive rates and sensitivity to population size, by generating random subgroups of subjects derived from the same homogenous population.
Finally, network differences in two case-control studies were investigated, including a [18F]FDG dataset of 80 healthy controls and 76 Alzheimer's disease (AD) subjects [4] and a [18F]FDOPA PET dataset of 10 healthy controls and 15 patients with schizophrenia [5].

Results: Simulations showed that permutation tests significantly contribute to reduce false positive rates, independently from the type of network metric under analysis. Large population sizes (>20 subjects per group) are recommended. The most interesting results were obtained for the [18F]FDG study, where several metrics for the control network were significantly different from the AD group ones (Figure A). In the [18F]FDOPA study, no significant differences were found between healthy controls and patients with schizophrenia after permutation tests, although the two networks appear qualitatively different (Figure B). This might be due to the low number of subjects included in the analysis.

Conclusions: Network-based methods can be applied to brain PET studies allowing the topological analysis of the tracer kinetics. This information can be used to understand how the biological function target of the PET radiotracer is organised across brain regions. The proposed method is complementary to standard PET analysis, where cross-sectional mean differences of tracer kinetics are generally the only outcomes. Further studies are required to explore the biological interpretability of network metrics in the PET domain.

References
[1] Bullmore ET and Sporns O, "Complex brain networks: graph theoretical analysis of structural and functional systems", Nat Rev Neurosci, 2009.
[2] Rubinov M and Sporns O, "Complex network measures of brain connectivity: Uses and interpretations", NeuroImage, 2010.
[3] Krzanowski WJ, "Permutational tests for correlation matrices", Stat. Comput., 1993.
[4] Jagust WJ et al., "The Alzheimer's Disease Neuroimaging Initiative Positron Emission Tomography Core", Alzheimer's & Dementia, 2010.
[5] McGowan S et al., "Presynaptic dopaminergic dysfunction in schizophrenia: A positron emission tomographic [18F]fluorodopa study" Arch. Gen. Psychiatry, 2004.
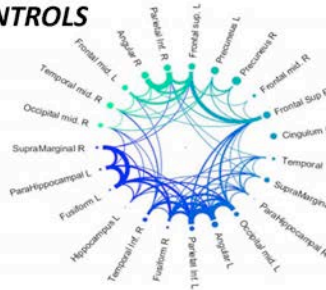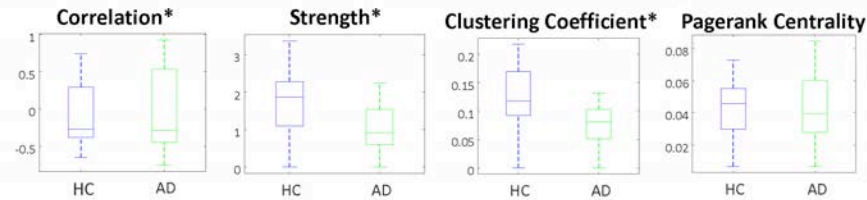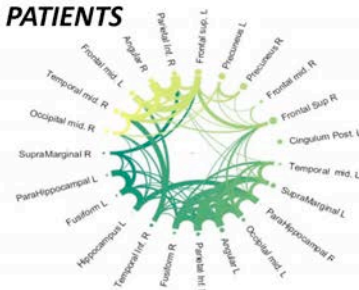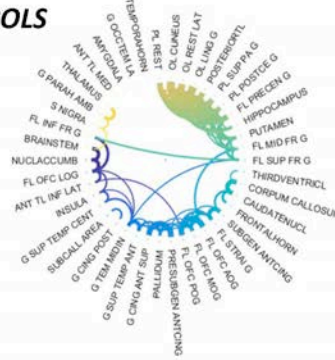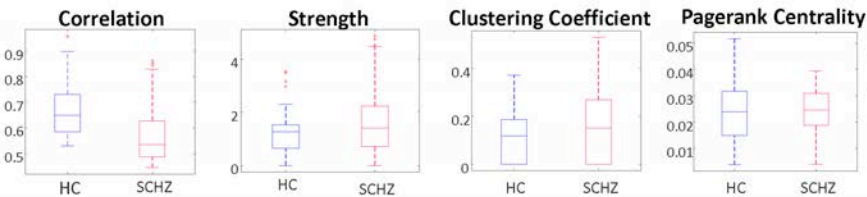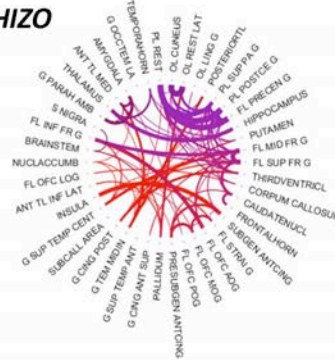
Network-based PET cross-sectional analysis of [18F]FDG brain PET data (panel A, healthy controls vs. AD patients) and [18F]FDOPA brain PET data (panel B, healthy controls vs. patients with schizophrenia). Both PET-based population network (circular diagrams) and network metrics (box plots) are reported. * indicates p-value <0.05.

Measuring task-specific glucose metabolism with constant infusion of [^{18}F]FDG

Hahn A[1], Gryglewski G[1], Nics L[2], Hienert M[1], Rischka L[1], Ganger S[1], Vraka C[2], Silberbauer L[1], Sigurdardottir H[1], Vanicek T[1], Hartenbach M[2], Wadsak W[2], Mitterhauser M[2], Hacker M[2], Kasper S[1], Lanzenberger R[1]

[1] Department of Psychiatry and Psychotherapy, Medical University of Vienna, Austria; [2] Department of Biomedical Imaging and Image-guided Therapy, Division of Nuclear Medicine, Medical University of Vienna, Austria

Objectives: The assessment of task-specific glucose metabolism with [^{18}F]FDG previously required two separate scans or double-injection protocols. We extend a recently introduced approach [1] to obtain baseline and task-specific glucose metabolism in a single scan with constant infusion of [^{18}F]FDG.

Methods: Eighteen healthy subjects (24.1±4.3 years, 8 female) underwent one scan with [^{18}F]FDG (3MBq/kg) constant infusion (36ml/h) using a combined PET/MR system (Siemens mMR). Fifteen of those were additionally measured twice with a PET system (GE Advance), one scan with constant infusion, the other with bolus application for comparison. Arterial blood sampling was carried out automatically for 3min and manually thereafter. For the 60min bolus scan, subjects kept eyes closed. For both 95min infusion scans, subjects opened their eyes (10-20min and 60-70min) or repeatedly tapped the right thumb to the fingers (35-45min and 85-95min).

PET/MR attenuation correction was done with low dose CT. PET images were corrected for head motion, normalized to MNI-space and smoothed. For the bolus scan, quantification of the influx constant (Ki) and cerebral metabolic rate of glucose (CMRGlu) was carried out with the Patlak plot in PMOD3.703. For constant infusion scans, we employed a two-step procedure. First, time activity curves (TACs) were fitted with a general linear model using regressors for baseline metabolism, eye and finger conditions and motion parameters. Baseline regressor was defined as average across all gray matter voxels. Task regressors were defined as linear ramp functions with slope=1 during the task and slope=0 otherwise (Fig.1b). Second, the Patlak plot served for quantification of Ki and CMRGlu. Here, multiplication of the baseline regressor with beta-values from the GLM gives regionally specific TACs for baseline metabolism. Further, task-specific changes in metabolism are directly proportional to changes in the slope of the TAC and hence proportional to changes in Ki. This procedure enables assessment of baseline and task-specific metabolism in a single GLM and a single measurement.

During PET/MR, resting-state functional MRI was simultaneously acquired for rest and tasks (5min each, TE/TR=30/2440ms). Preprocessing included slice-timing and motion correction, normalization, smoothing, regression against confounding signals (white matter, cerebrospinal fluid, motion) and band-pass filtering [2]. Functional connectivity was computed from seed regions with increased glucose metabolism.

Results: Baseline metabolism from constant infusion matched with bolus application (test-retest variability CMRGlu=0.5±24.5%) [3]. In contrast, the previous method [1] underestimated metabolism by -41.4±24.9%.

Task-specific glucose metabolism increased in the left precentral (t=10.2 and t=12.0 for PET and PET/MR, respectively) and calcarine cortices (t=10.9 and t=11.3, p<0.05 FWE-corrected, Fig.1c-d). Decreased metabolism was observed in default mode network regions (p<0.05 FWE-corrected).

Compared to rest, functional connectivity decreased between pre- and paracentral cortices during finger tapping as well as between calcarine and middle/inferior temporal cortices during eyes open (p<0.05 FWE-corrected, Fig.1e-f).

Conclusions: In addition to baseline metabolism, the approach enables quantification of temporally and regionally specific glucose metabolism during different tasks with a single measurement. Task-specific decreases in functional connectivity seem to reflect regions with no task-relevant contribution. Such combinations offer novel strategies for the investigation of task-specific brain function in health and disease.

References

[1] Villien et al. 2014. Dynamic functional imaging of brain glucose utilization using fPET-FDG. NeuroImage 100: 192-199.

[2] Hahn et al. 2015. Individual diversity of functional brain network economy. Brain Connectivity 5: 156-165.

[3] Schmidt et al. 1996. Cerebral glucose metabolism during pharmacological studies: test-retest under placebo conditions. Journal of Nuclear Medicine 37: 1142-1149.
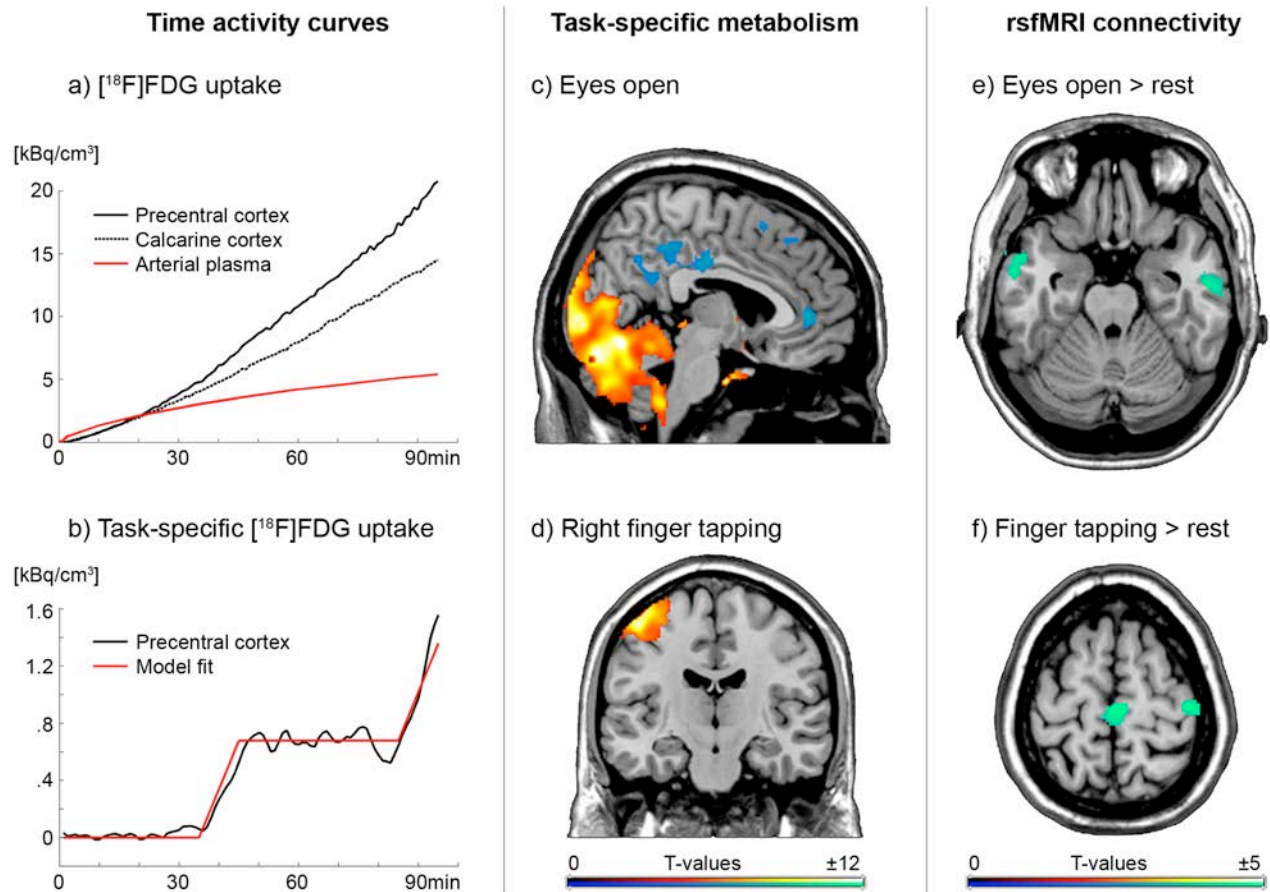
Figure 1: Group analyses averaged across all subjects. a) Time activity curves for the precentral and calcarine cortices as well as the plasma arterial input function. b) Task-specific time activity curve in the precentral cortex after subtracting baseline and motion activity. c-d) Significant task-specific glucose metabolism during the eyes open condition and right finger tapping (p<0.05 FWE-corrected). e-f) Using the calcarine and precentral cortices as seed regions, decreased functional connectivity emerged between eyes open vs rest and finger tapping vs rest, respectively (p<0.05 FWE-corrected). Axial images are in neurological convention, i.e., left is left.

Quantification and Comparison of Intranasal and Intravenously administered [^{18}F]-FDG in rats

N. Singh, D. Cash, M. Veronese, C. Simmons, T. Sementa, A. Gee, F. Turkheimer

King's College London, London, UK

Objectives: To develop the methodology to determine how drugs administrated intranasally access the brain. There is a surge in the use of the intranasal route of administration for peptides, drugs and even ribonucleic acid targeting the brain. However, how these molecules access the brain remains disputed. Some propose a direct pathway from the nose to the brain; others suggest that brain access occurs via the blood. The aim of this study was to use [^{18}F]-Fludeoxyglucose (FDG) to develop a methodology to calculate and compare the brain concentration of [^{18}F]-FDG when administered intranasally versus intravenously.

Methods: Femoral venous and arterial cannulae were surgically placed and rats were administered [^{18}F]-FDG either via the intranasal or the intravenous routes. The rats were scanned for on a Mediso NanoPET scanner and blood samples were collected at discrete intervals. Brain to blood concentration ratios were calculated for both administration routes. We hypothesize that if there is a direct nose to brain pathway, the brain to blood ratios should be higher via intranasal administration compared to the intravenous route.

Results: The brain blood ratio was not significantly different between the two groups (Figure 1) at the different time points measured. This suggests that FDG accesses the brain via the blood rather than directly through the nose.

Ratio of Brain to Blood concentration of [^{18}F]-FDG
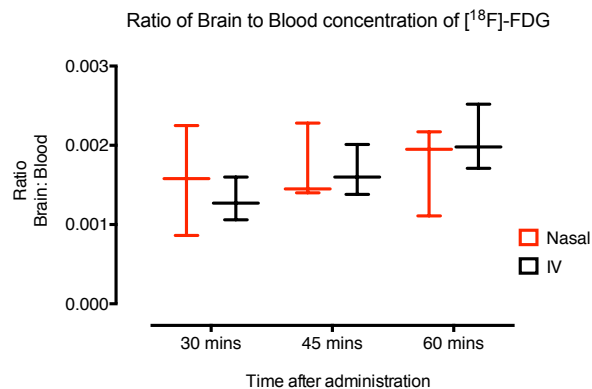
Conclusions: We hypothesized that if there exists a direct nose to brain pathway, it should result in an increase in brain:blood ratio. This is because in addition to the blood, there is another nasal component contributing to the total [^{18}F]-FDG concentration in the brain. However, in this study we did not find any increase in [^{18}F]-FDG brain concentration when given nasally compared to intravenously. Hence, we conclude that in case of FDG at least, there is no direct nose to brain pathway in rats. However, this methodology can be translated into people to test whether or not other molecules such as oxytocin, insulin, etc can access the brain when given intranasally.

Inverse correlation between insulin sensitivity and insulin-stimulated cerebral glucose influx rate using whole body PET-MR

Kerstin Heurling[1], Emil Johansson[1,2], Stanko Skrtic[3], Jan Eriksson[4], Mark Lubberink[1,5], Håkan Ahlström[1], Joel Kullberg[1]

[1]Uppsala University, Department of Surgical Sciences, Section of Radiology, Uppsala, SWEDEN; [2]Centre for Clinical Research Sormland-Uppsala Universitet, Eskilstuna, SWEDEN; [3]AstraZeneca R&D & Dept of Medicine, Sahlgrenska Academy at Gothenburg University, Gothenburg, SWEDEN; [4]Uppsala University, Department of Medical Sciences, Uppsala, SWEDEN; [5]Uppsala University Hospital, Uppsala, SWEDEN

OBJECTIVES: Decreased cerebral glucose metabolism has been shown in pre-diabetical and type 2 diabetes (T2D) patients, measured using [^{18}F]fluorodeoxyglucose ([^{18}F]FDG) PET[1]. However, an insulin-induced elevation of whole brain glucose metabolism has been demonstrated in patients with impaired glucose tolerance, and to a lesser extent in healthy subjects[2]. The aim of the present work was to examine the voxel-wise correlations between the "gold standard" measurement of insulin sensitivity; the hyperinsulinemic euglycemic clamp measured total body glucose disposal rate (M-value), and the insulin-stimulated cerebral glucose influx rate.

METHODS: Ten subjects underwent whole body imaging with [^{18}F]FDG (average dose 330 MBq) on an integrated Signa PET/MR (GE Healthcare). Five subjects were healthy volunteers (average age 64 years, BMI: 27) and five had a diagnosis of T2D (average age 59 years, BMI: 29). PET imaging was performed as one 10 min dynamic thorax-scan starting at the time of injection followed by six serial total body scans with 30 s per bed position (5 min per total body scan). PET images were corrected for attenuation using a built-in MR-based attenuation correction. Parametric whole body images of glucose influx constant (K_i) were calculated using the Patlak method with a plasma corrected ascending aorta image derived input function. The image segment containing the brain was extracted and spatially normalized using a PET driven template registration in SPM8.

Insulin sensitivity was estimated under steady state clamp condition during the PET/MRI acquisition, as the M-value normalized to fat-free mass [$mg \cdot kg^{-1} \cdot min^{-1}$]. The clamp procedure was performed with a constant infusion of insulin (56 $mU \cdot m^{-2} \cdot min^{-1}$) and a glucose infusion adjusted to maintain a steady state plasma glucose level of 5.6 mmol/L. Whole-brain as well as voxel-wise correlations between K_i and M-values were calculated as voxel-wise t statistics.

RESULTS: Whole-brain K_i demonstrated a negative correlation with M-values (Pearson's r = -0.839, p = 0.002). The voxel-wise analysis revealed significant correlation at $p < 0.05$ in large portions of the cortex. In particular areas, correlations were reached with $p < 0.001$, such as anterior cingulate and precuneus. The voxel-wise correlations did not hold for correction for multiple comparisons.

CONCLUSIONS: A significant inverse correlation was observed between glucose influx rates and insulin sensitivity, primarily in cortical areas of the brain, as measured during insulin stimulation. Our findings are in line with the previously demonstrated insulin-stimulated increase in cerebral glucose metabolic rate in subjects with impaired glucose tolerance. Further studies are required to confirm and refine these findings.

REFERENCES
1. Baker, L. D. et al. Insulin resistance and Alzheimer-like reductions in regional cerebral glucose metabolism for cognitively normal adults with prediabetes or early type 2 diabetes. Arch Neurol 68, 51–57 (2011).
2. Hirvonen, J. et al. Effects of insulin on brain glucose metabolism in impaired glucose tolerance. Diabetes 60, 443–447 (2011).
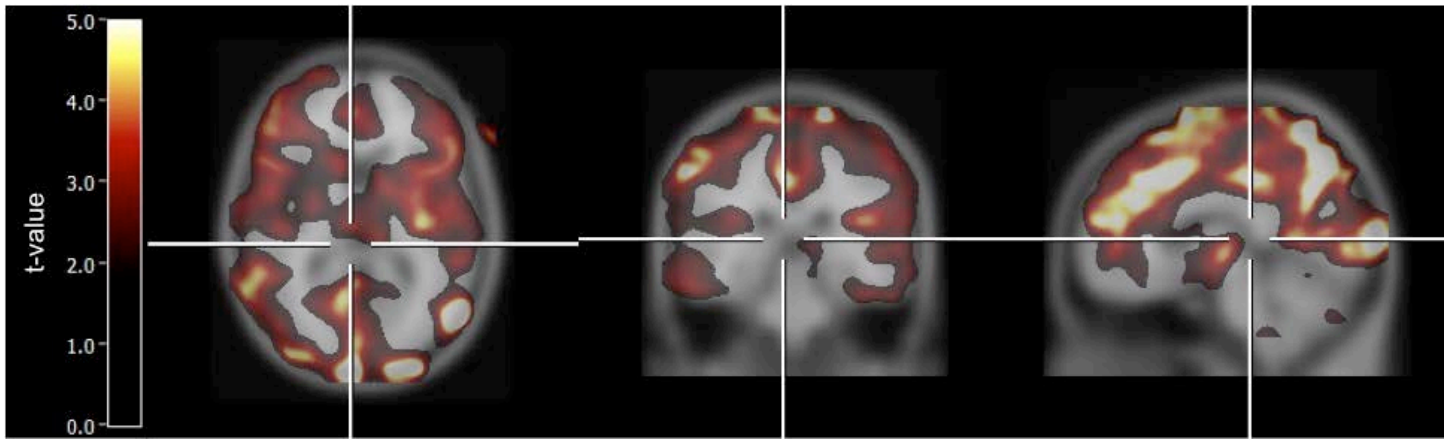
Figure 1. Voxel-wise t statistic values for the negative correlation between K_i and M-value during insulin stimulation (uncorrected for multiple comparisons, $p<0.05$).

Development of [11C]PF-367 for PET neuroimaging of glycogen synthase kinase-3

Steven Liang[1], Marc Normandin[1], Eli Livni[1], Nicolas Guehl[1], Dustin Wooten[1], Thomas Lee Collier[1], Georges El Fakhri[1], Ravi. Kurumbail[2] and Neil Vasdev[1,*]

[1]*Gordon Center of Medical Imaging, Division of Nuclear Medicine and Molecular Imaging, Massachusetts General Hospital & Department of Radiology, Harvard Medical School, Boston, MA, USA;* [2]*Pfizer Worldwide Research and Development, Groton Laboratories, Eastern Point Road, Groton, CT, USA.*

Objectives: Dysregulation of glycogen synthase kinase 3 (GSK-3) is implicated in the pathogenesis of neurological diseases, with recent interests focused on its phosphorylation of tau protein. PET radiotracers for this kinase have remained elusive because of inadequate potency, selectivity and/or brain penetration. In the present study, we discovered a novel GSK-3 inhibitor and conducted PET-CT studies in nonhuman primates with its 11C-isotopologue.

Methods: The lead compound, *N*-(3-(1H-1,2,4-triazol-1-yl)propyl)-5-(3-chloro-4-methoxyphenyl)oxazole-4-carboxamide; PF-367) was discovered by high throughput screening and evaluated in an array of *in vitro* and *in vivo* assays. [11C]PF-367 was labeled by reaction of the phenolic precursor in TBAOH/DMF with [11C]CH$_3$I. Dynamic PET scans in rhesus monkeys (7-8kg) were acquired for 120 minutes and included arterial sampling with radiometabolite correction for estimation of the [11C]PF-367 arterial input function. Baseline scans were performed in which high specific activity [11C]PF-367 was administered and blocking scans included [11C]PF-367 plus 0.1mg/kg of PF-367.

Results: We have identified PF-367 as a highly potent inhibitor of GSK-3 and demonstrated its efficacy in modulation of tau phosphorylation *in vitro* and *in vivo.* PF-367 was equipotent towards both known GSK-3 isoforms (GSK-3α and GSK-3β) with IC$_{50}$ values of 10.0 and 9.0 nM, respectively. Based on functional and competitive binding assays against a wide panel of protein kinases, we have shown that PF-367 represents the most selective inhibitor of GSK-3 to date (>450-fold selective over 240 kinases). A single dose (50 mg·kg^{-1}, subcutaneous) of PF-367 showed a rapid 76% reduction of pTau levels in the brain and 92% reduction of phospho-glycogen synthase (pGS) in skeletal muscle one hour post-administration in rats. Whereas the kinetics of PF-367 binding in brain tissues are too fast for an effective therapeutic agent, the pharmacokinetic profile of PF-367 is ideal for discovery of radiopharmaceuticals for GSK-3 in the central nervous system. [11C]PF-367 was synthesized in >5% uncorrected yield relative to [11C]CO$_2$ with specific activity >2 Ci/μmol (n>10). *In vivo* assessments of [11C]PF-367 (log$D_{7.4}$ = 2.14) kinetics were performed to determine brain penetration and displaceable specific binding. [11C]PF-367 showed good brain penetration (1 SUV; standardized uptake value) with similar uptake immediately after radiotracer injection in baseline and blocking experiments, and as predicted, blocking experiments showed a more rapid clearance of [11C]PF-367 due to reduced availability of binding sites and resulted in lower brain concentrations at later. Preliminary kinetic analyses indicate regional reductions in displaceable specific binding of approximately 30%.

Conclusions: We have identified PF-367 as a highly potent inhibitor of GSK-3 and demonstrated the efficacy in modulation of tau phosphorylation *in vitro* and *in vivo* with excellent bioavailability. Based on functional and competitive binding assays against a wide panel of protein kinases, we have shown that PF-367 represents one of the most selective inhibitor of GSK-3 that has been reported to date. PET imaging studies confirm that [11C]PF-367 readily crosses the blood-brain barrier and that [11C]PF-367 has favorable characteristics warranting further evaluation as a PET tracer for *in vivo* imaging of GSK-3. Development of other radiotracers based on PF-367 and related scaffolds for imaging GSK-3 are underway.

Synthesis and Preliminary PET Imaging Studies of [11C-Carbonyl]-Carbamates and Ureas for Imaging Monoacylglycerol Lipase

Lu Wang[1], Wakana Mori[2], Ran Cheng[1], Joji Yui[2], Akiko Hatori[2], Longle Ma[1], Yuji Nagai[2], Benjamin H. Rotstein[1], Neil Vasdev[1], Ming-Rong Zhang[2] and Steven H. Liang[1],*

[1] Gordon Center of Medical Imaging, Division of Nuclear Medicine and Molecular Imaging, Massachusetts General Hospital & Department of Radiology, Harvard Medical School, Boston, MA, USA; [2] Molecular Imaging Center, National Institute of Radiological Sciences, Chiba, Japan

Objectives: Monoacylglycerol lipase (MAGL) is a 33 kDa member of the serine hydrolase superfamily that preferentially degrades 2-arachidonoylglycerol to arachidonic acid in the endocannabinoid (eCB) system. Inhibition of MAGL represents a possible therapeutic approach for the treatment of eCB disorders, such as drug addiction and anxiety, as well as neurodegenerative diseases, including PD, AD and multiple sclerosis. Unlike several fatty acid amide hydrolase (FAAH)-targeting PET radiotracers in human use, there is an unmet need for probing MAGL in clinical research and drug development studies of this central enzyme. Herein we described our medicinal chemistry efforts to identify new potent and selective MAGL inhibitors, radiolabeling and in vivo evaluation of novel [11C-*carbonyl*]-labeled carbamate and ureas in rodents and preliminary PET imaging studies in non-human primate (NHP).

Methods: Eleven sulfonamido carbamates / ureas were synthesized and evaluated in MAGL / FAAH / cannabinoid receptors (CB1/CB2) competitive binding assays (Fig. A). The most promising compounds, namely a novel MAGL inhibitor, *N*-((1-(1*H*-1,2,4-triazole-1-carbonyl)piperidin-4-yl)methyl)-4-chlorobenzenesulfonamide (TZPU), and the known inhibitor 1,1,1,3,3,3-hexafluoropropan-2-yl 4-(((4-chlorophenyl)sulfonamido)methyl)piperidine-1-carboxylate (SAR127303), were radiolabeled with carbon-11. Ex vivo biodistribution and in vivo PET imaging studies in rodents were carried out to determine their brain permeability and specificity. [11C]SAR127303 was advanced for preliminary PET neuroimaging studies in nonhuman primate.

Results: Two equipotent and selective MAGL inhibitors, TZPU and SAR127303 were identified (IC_{50} = 35.9 nM and 39.3 nM, respectively; no significant FAAH inhibition, no CB1 and CB2 receptors agonism and antagonism @ 30 μM). [11C]TZPU and [11C]SAR127303 were radiolabeled in 3.1% and 35% uncorrected yields, relative to $^{11}CO_2$, respectively (Fig. B). PET imaging of [11C]TZPU in rats showed a limited brain uptake (0.4 SUV) and no significant washout during the scan. Pretreatment with TZPU (1 mg/kg) resulted in a 50% reduction in the accumulation of radioactivity in the brain, indicating certain modest specificity of [11C]TZPU (Fig. C). [11C]SAR127303 demonstrated high whole brain uptake (1.7 SUV) and no significant clearance during the scan (Fig. D). Pretreatment studies with SAR127303 (1 mg/kg) or KML29 (3 mg/kg) remarkably decreased the brain uptake (ca. 40-50% reduction). Blocking studies with a potent FAAH inhibitor, URB597 (3 mg/kg), showed no effect towards the uptake and distribution as predicted for this selective MAGL radiotracer. Ex vivo biodistribution studies of [11C]SAR127303 in mice was consistent with the distribution of MAGL (Fig. E), as high expression in the brown adipose tissue, adrenal glands, liver, brain and kidneys has been previously observed.[1] In particular, [11C]SAR127303 showed characteristic high uptake (> 10 %ID/g) in brown adipose tissue, which has the most abundant MAGL expression in rodents. [11C]SAR127303 crossed the blood-brain barrier (*ca.* 1 SUV) in NHP and reached plateau after 20 min without a significant clearance (Fig. F). The distribution of [11C]SAR127303 was heterogeneous with the highest uptake in the occipital cortex, followed by striatum, cerebellum, hippocampus, and the lowest uptake in pons, consistent binding with the distribution of MAGL.

Conclusion: [11C]SAR127303 shows promise as a proof-of-concept radiotracer for neuroimaging of MAGL. Further studies of [11C]SAR127303 are warranted and radiotracers based on this scaffold are underway development.

References:
[1] Karlsson M et al. *J Biol Chem.* 1997; 272: 27218-23.

A. Medicinal chemistry efforts

X — (aryl with substituents)
Aryl groups with different substituents
Different linkers
Leaving group
Various leaving groups
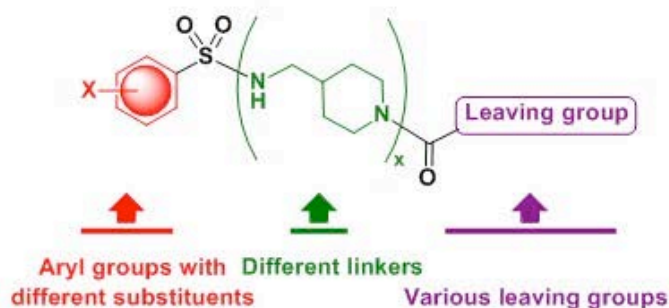
B. Carbon-11 labeled lead compounds

[^{11}C]TZPU
IC$_{50}$ = 39.3 nM (hMAGL)

[^{11}C]SAR127303
IC$_{50}$ = 35.9 nM (hMAGL)
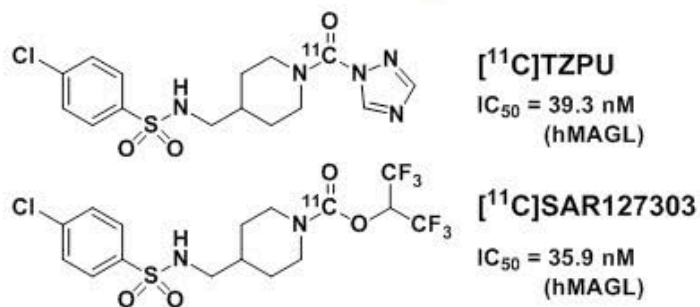
C. Time-activity curves of [^{11}C]TZPU in rat brain

- baseline
- TZPU (blocking)
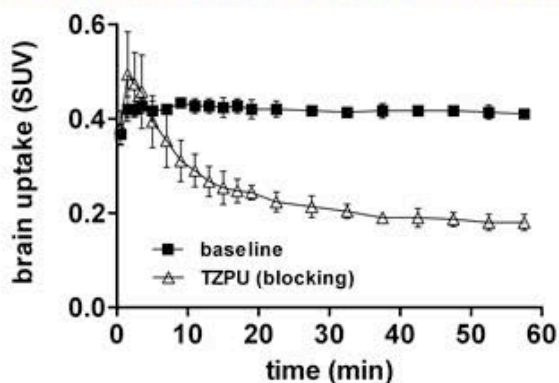
D. Time-activity curves of [^{11}C]SAR127303 in rat brain

- baseline
- KML29 (blocking)
- SAR127303 (blocking)

E. Ex vivo biodistribution of [^{11}C]SAR127303 in mice

1 min, 5 min, 30 min
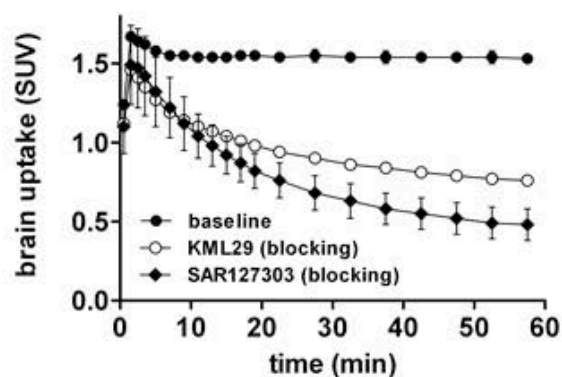
blood, heart, lungs, liver, pancreas, spleen, adrenal glands, kidneys, small intestine, testes, muscle, brain, white adipose, brown adipose
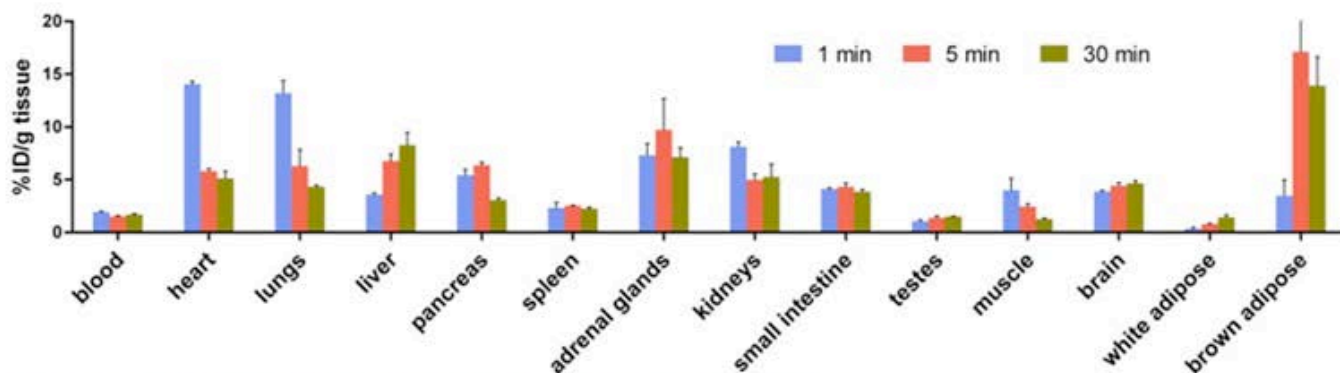
F. PET imaging studies of [^{11}C]SAR127303 in nonhuman primate

0.3 SUV 0.9

- occipital cortex
- cerebellum
- pons
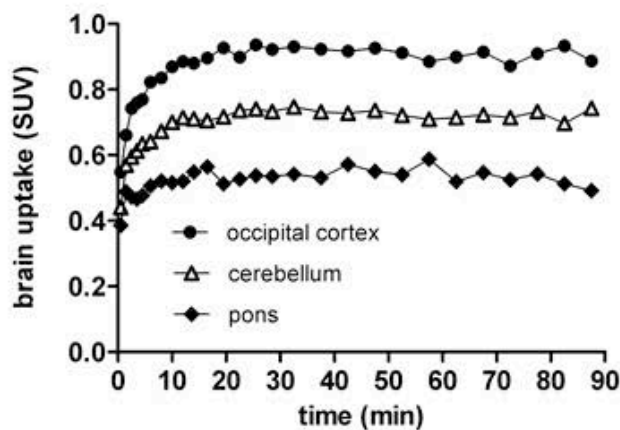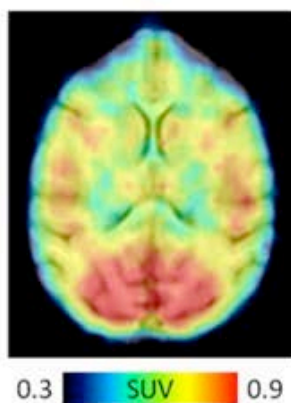
Exploring multi-scale brain functional dynamics and cerebral protein synthesis measured with L-[1-^{11}C]leucine PET

Hellyer, PJ [1], Barry, E [1]*, Pellizzon, A [2]*, Veronese, M [1], Rizzo, G [2], Tonietto, M [2], Bertoldo, A [2], Turkheimer, FE [1]

1Centre for Neuroimaging Sciences, King's College London; 2Department of Information Engineering, University of Padova, Italy

*These authors contributed equally to the work presented in this abstract.

Introduction: In recent years, graph theory seems to be the most appealing way to model and investigate brain connectivity, yet theoretical measures do not have a straightforward biological interpretation. Recently, L-[1-^{11}C]leucine PET has been used to objectively measure in vivo protein synthesis in the cortex [1]. However, the relationship between regional protein synthesis and on-going neural dynamics is unclear. We use a graph theoretical approach [2], to examine the relationship between functional connectivity (measured using fMRI) and the rate of cerebral protein synthesis (rCPS).

Methods: We used resting state functional MRI (R-fMRI) from 20 healthy subjects (Age: 23-33) derived from the Human Connectome Project 'FIX' pipeline [3]. R-fMRI was filtered in a broad frequency band between 0.001 and 0.3 Hz. Functional connectivity (FC) matrices were generated using three different brain anatomical atlases (AAL [4], Craddock 200 [5], and Freesurfer [6]). Group level FC matrices were then thresholded in order to maximize cost-efficiency [7], before calculating graph theoretical measures (Clustering Coefficient, Local Efficiency, and Strength), using the Brain Connectivity Toolbox [8]. Age matched L-[1-^{11}C]leucine and [^{18}F]FDG PET templates were derived from previously published studies [2] and were segmented using the same parcellation schemes as the MRI data.

Results: Using a filter-bank approach, we firstly demonstrated a significant relationship between protein turnover (measured using L-[1-^{11}C]Leucine PET) and graph theoretical measures of functional connectivity. Moreover, this relationship was significantly modulated by temporal scale, where dynamics with a temporal frequency of 0.06-0.12 Hz were producing stronger correlations (Figure). To assess how these relationships may be driven simply by enhanced metabolism within hub-regions in the brain, we performed similar analysis using [^{18}F]FDG binding patterns. Whilst some relationship between FDG binding and graph theoretical measures was present, when included as a covariate in the relationship between L-[1-^{11}C]Leucine and functional connectivity, there remained a significant relationship between protein turnover and graph theoretical measures. Results were consistent for the different atlases.
We also used a sliding window approach to split R-fMRI scans into shorter consecutive time-series, and found that protein synthesis was inversely correlated with the variability of theoretical network measures, suggesting greater stability in hub regions.

Conclusion: With this work we demonstrate using a combined fMRI and PET approach that cerebral protein synthesis has a strong relationship to neural dynamics at the macroscopic scale. The association between the two appears to be dependent to the temporal scale of fMRI signal, and independent from tissue metabolism.

References:

1. Veronese M *et al.* Use of spectral analysis with iterative filter for voxelwise determination of regional rates of cerebral protein synthesis with L-[1-11C]leucine PET. JCBFM, 2012.
2. Bullmore E *et al.* Complex brain networks: graph theoretical analysis of structural and functional systems. *Nat Rev Neurosci.,* 2009.
3. Van Essen D *et al.* The WU-Minn Human Connectome Project: An Overview. N*euroimage,* 2013.
4. Tzourio-Mazoyer N *et al.* Automated Anatomical Labeling of activations in SPM using a Macroscopic Anatomical Parcellation of the MNI MRI single-subject brain. *NeuroImage,* 2001.
5. Craddock RC *et al.* A whole brain fMRI atlas generated via spatially constrained spectral clustering. *Hum Brain Mapp.,* 2012.
6. Fischl B FreeSurfer. *Neuroimage,* 2012.
7. Bassett DS *et al.* Cognitive fitness of cost-efficient brain functional networks. *PNAS,* 2009.
8. Rubinov M *et al.* Complex network measures of brain connectivity: Uses and interpretations. *NeuroImage, 2010.*
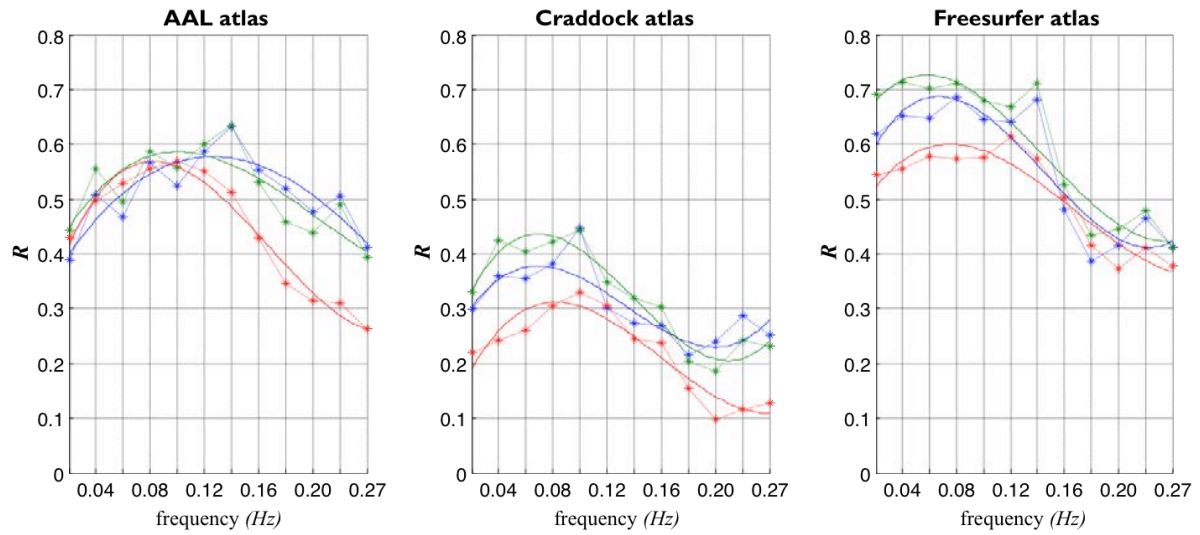
Figure: Correlations between R-fMRI network measures and rate of cerebral protein synthesis, as function of BOLD signal frequency. Results are shown for Clustering Coefficient (blue), Local Efficiency (green) and Strength (red) in three different anatomical atlases: Automated Anatomical Labeling (AAL), Craddock 200 and Freesurfer. Solid lines represent the 3rd degree polynomial interpolation of data points.

Exploring Feature-Based Approaches to Assess Neuroinflammation in Patients with Parkinson's disease: a PBR28 PET Imaging Study

R Mabrouk[1], I Klyuzhin[2], E Shahinfard[1], N Vafai[1], J Fu[2], S Blinder[1], M Walker[4], A Rahmim[3], V Sossi[1,2]

[1]Pacific Parkinson's Research Centre, UBC, Vancouver, B.C., Canada, V6T 2B5; [2]Department of Physics and Astronomy, University of British Columbia, Vancouver, BC, V6T 1Z1; [3]Department of Radiology, Johns Hopkins University, Baltimore, MD 21287; 4 Radiation Physics & Protection, Oxford University Hospitals NHS Foundation Trust, Oxford, OX3 7LE, UK.

Objective. To investigate the ability of texture features extracted from PET regions of interest (ROIs) to assess microglial activation known to be a biomarker of neuroinflammation.

Background. Microglial activation is a hallmark of Neuroinflammation and hence an increase in microglia activity levels creates clusters around the injured site within the brain regions. We hypothesize that textural descriptors of $[^{11}C]$-PBR28 PET binding in these regions, which are independent of the overall region size and magnitude, are able to generate similar or added information relative to standard uptake value (SUV) outcome analysis.

Methods. Participants included 4 healthy controls (HC) (age 44±16, mean, std, range 24-63) and 6 subjects with Parkinson's disease (PD) (age 67±14, mean, std, range 48-86; disease duration 5±4, mean, std, range 1-10). All subjects were mixed affinity binders (MAB). A 19.7±1.2 mCi dose of $[^{11}C]$-PBR28 was intravenously injected and dynamic PET scans were performed for 90 minutes. Time-averaged images were reconstructed from data acquired between 60 and 90 minutes post-injection and were converted to SUV images. 48 MRI derived ROIs were placed on the SUV images, and the mean SUVs were calculated for these ROIs. SUV values were binned into a standard gray level grid to define the distribution of co-occurring values in a gray level co-occurrence matrix (GLCM). 13 texture metrics were derived from the GLCM. Correlations between dependent variables, SUV or GLCM-derived metrics, were made against disease duration (DD) and age, utilizing both univariate linear regression against each variable, and multivariate linear regression considering both DD and age. Metric values were then compared to mean SUV values across the ROIs in terms of their ability to discriminate between groups using the t-test.

Results. From the 13 GLCM-derived metrics, two texture metrics, namely CONTRAST and HOMOGENEITY depicted significant correlation with DD for most regions, though this was reduced to a trend when adjusting for age. SUV, however, showed significant correlation with AGE but was also reduced to a trend when adjusting for DD. For example in the putamen, with simple linear regressions, a significant correlation of CONTRAST with DD (R^2 = 0.78, p = 0.01) was found, but not with AGE (R^2 = 0.34, p = 0.22), and this was similarly the case for correlation of HOMOGENEITY with DD (R^2 = 0.76, p = 0.02) and AGE (R^2 = 0.30, p = 0.14). SUV was found to have only a trend with DD (R^2 = 0.54, p = 0.09), but correlate significantly with AGE (R^2 = 0.69, p = 0.04).
HC and PD groups were discriminated moderately using CONTRAST and HOMOGENEITY metrics in the whole brain (CONTRAST$_{HC}$ = 222±29, CONTRAST$_{PD}$ = 487±242, p<0.05; HOMOGENEITY$_{HC}$ = 0.16±0.007, HOMOGENEITY$_{PD}$ = 0.12±0.02, p<0.05), and were strongly discriminated using SUV (SUV$_{HC}$ = 0.52±0.04, SUV$_{PD}$ = 0.80±0.12, p<0.001).

Conclusion. Data from more subjects are required to fully characterize the behaviour of texture metrics. However these preliminary results suggest that GLCM-derived metrics applied to $[^{11}C]$-PBR28 PET may provide disease related information and could serve as an auxiliary tool for tracking of disease and for quantitation. This would be of particular relevance to this tracer as no suitable tissue input function is universally possible to enable conventional kinetic modeling.
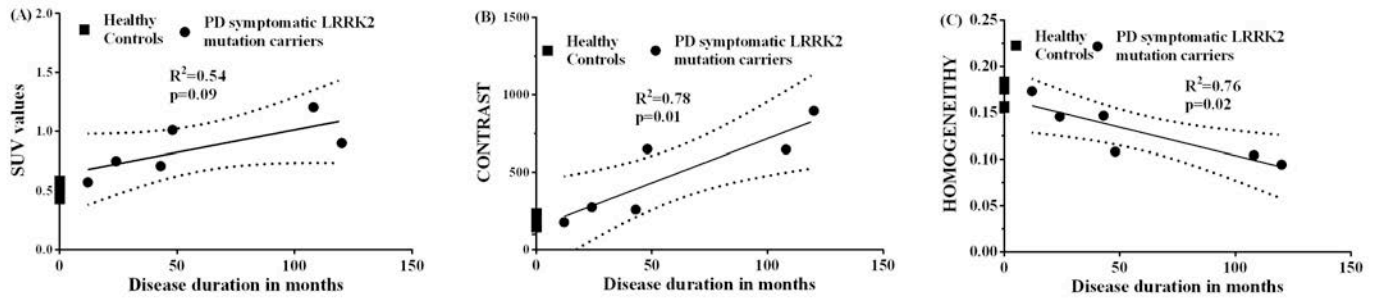
Figure 1

Figure 1. Correlation of ROI based metrics with disease duration in the Putamen. A) Mean SUV values had only a trend towards statistical significance. B) and C) show a significant increase and decrease of CONTRAST and HOMOGENEITY metrics with disease duration. This can be attributed to the deficit of neurons in Putamen triggering the neuroinflammation process and distorting the homogeneity of the region.

Evaluation and correction of bias introduced by the use of automated whole-blood measurements in ^{11}C-PBR28 studies

Jean-Dominique Gallezot[1], Qi Guo[2], Eugenii A Rabiner[2], Roger N Gunn[2] and Richard E Carson[1]

[1]Yale University, New Haven, CT, USA; [2]Imanova, London, United Kingdom.

INTRODUCTION: ^{11}C-PBR28 is used to study neuroinflammation by imaging TSPO, a protein overexpressed in activated microglia. With ^{11}C-PBR28, the arterial input function must be measured. When using an automated blood counter (ABC) to measure the whole blood (WB) radioactivity curve during the first minutes after injection, no early plasma data are available, and it must be inferred from WB data. However, for ^{11}C-PBR28, the relationship between plasma and WB changes rapidly in early samples (See Figure), due to uptake and specific binding in blood cells[1], so the early phase of this relationship is complex. The objective of this study was to evaluate the biases induced by the use of an ABC, and to evaluate methods to correct these biases.

METHODS: Brain scans and arterial data were collected from 4 patients. Arterial data were collected using fast manual sampling (FMS), and WB and plasma radioactivity were measured for all samples. First, the WB curve was fitted with various compartmental models taking into account blood cells (BC) and/or ^{11}C-PBR28 metabolites. Next, an experimental protocol using an ABC was simulated with limited early plasma data (i.e., 2 samples, 3- and 5-min). Plasma values were then estimated based on a Linear extrapolation of the WB to plasma ratio (ABC-L method), or based on the selected WB Compartmental model (ABC-C, method). Brain curves were fitted using the two-tissue compartment model, (with a fixed vascular fraction of 0.05 mL blood/cm^3 tissue) using either the input function obtained with FMS, or one of the two input functions obtained with methods ABC-L and ABC-C. The error introduced by the use of an ABC were computed as $p_{ABC-x}/p_{FMS} - 1$ (x=L or C) for each parameter of interest p (V_T, K_1).

RESULTS: The WB to plasma radioactivity ratio was 0.66±0.03 at t<1 min, peaked at 0.96±0.21at ~6.5 min, and decreased monotonically to 0.72±0.07 at t=120 min. Among all tested WB models, the one providing the best fit to 0-120 min of data had 2 BC compartments for unchanged ^{11}C-PBR28 and none for metabolites (See Figure), suggesting that ^{11}C-PBR28 slowly enters BCs, but that its metabolites do not. If only 0-15 min of data were fitted, a simpler 1 BC compartment model ignoring the difference between parent and metabolized ^{11}C-PBR28 accurately fitted the WB curve. This simpler model was used for the ABC-C method. When using the ABC-L method, the influx rate constant K_1 is overestimated by 22%±16%, but volume of distribution V_T had minimal bias: 2%±4%. When using the ABC-C method, K_1 bias was reduced to -3%±9% and V_T bias remained low: 1%±5%.

CONCLUSION: Based on kinetic modeling, the relationship between plasma and WB radioactivity concentration can be explained by a slow entry of ^{11}C-PBR28 into BCs. When using ABC data, K_1 is clearly overestimated, but V_T is unaffected. Further work is needed to validate the correction for K_1 estimates for historical ABC datasets. For future studies, FMS is the most suitable method to measure ^{11}C-PBR28 input functions.

REFERENCES:

Guo et al., BrainPET 2015 abstract 151
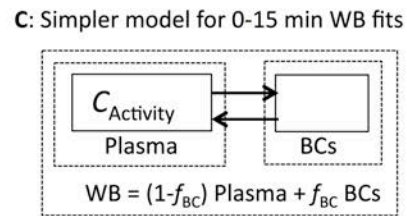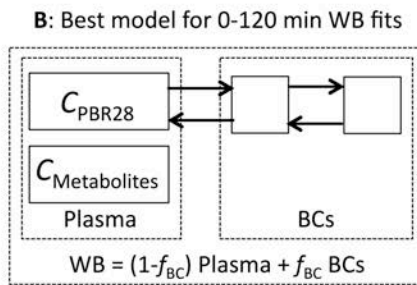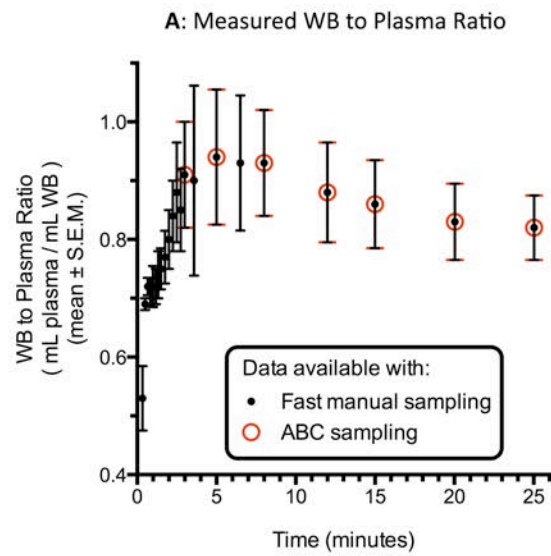
A: Measured WB to Plasma Ratio

WB to Plasma Ratio
(mL plasma / mL WB)
(mean ± S.E.M.)

Data available with:
• Fast manual sampling
○ ABC sampling

Time (minutes)

B: Best model for 0-120 min WB fits

C_{PBR28}

$C_{Metabolites}$

Plasma

BCs

WB = $(1-f_{BC})$ Plasma + f_{BC} BCs

C: Simpler model for 0-15 min WB fits

$C_{Activity}$

Plasma

BCs

WB = $(1-f_{BC})$ Plasma + f_{BC} BCs

Positron Emission Tomography Quantification of Serotonin Transporter Binding in Posttraumatic Stress Disorder

Manesh Gopaldas[1,2,3], Jeffrey M. Miller[1,2], R. Todd Ogden[1,2,4], Francesca Zanderigo[1,2], Harry Rubin-Falcone[1,2], Gregory Sullivan[1,2], Maria A. Oquendo[1,2], J. John Mann[1,2,5]

[1]*Department of Molecular Imaging and Neuropathology, New York State Psychiatric Institute, New York, New York, USA;* [2]*Department of Psychiatry, Columbia University, New York, New York, USA;* [3]*Herbert Wertheim College of Medicine, Florida International University, Miami, Florida, USA;* [4]*Department of Biostatistics, Columbia University, New York, New York, USA;* [5]*Department of Radiology, Columbia University, New York, New York, USA*

Background: The serotonergic system is implicated in posttraumatic stress disorder (PTSD)[1] and mood disorders[2,3] which are often comorbid. Few studies have considered the effects of their comorbidity on serotonergic abnormalities. Using positron emission tomography (PET) and [^{11}C]DASB radiotracer, we compared serotonin transporter (5-HTT) binding in volunteers who were healthy (HV) or had PTSD with and without current comorbid mood disorders. We hypothesized low 5-HTT binding in PTSD, with even greater deficits in those with PTSD and current comorbid mood disorders.

Methods: PTSD patients (*n*=22) and HV (*n*=32) underwent PET scanning with [^{11}C]DASB. Eight PTSD patients had no current mood disorder and 14 had a current comorbid major depressive disorder (MDD) or bipolar disorder. Binding potential (BP_F) of [^{11}C]DASB was calculated as (V_T - V_{ND})/f_P, where V_T is the tracer volume of distribution (obtained using likelihood estimation in graphical analysis[4]), and V_{ND} the tracer nonspecific binding, in the region of interest (ROI). V_{ND} was estimated using a hybrid deconvolution approach[5] that combines deconvolution[6] and simultaneous search across regions[7] to estimate V_{ND} without relying on any reference region. We examined seven ROIs (anterior cingulate cortex, amygdala, dorsolateral prefrontal cortex, hippocampus, medial prefrontal cortex, midbrain, and orbitofrontal cortex) implicated in PTSD[1,8–11].

Results: There was a trend toward lower 5-HTT BP_F in individuals with PTSD (with and without current comorbid mood disorders) compared to HV considering all ROIs simultaneously (*p*=0.070). A region-by-diagnosis interaction was observed (*p*=0.045), indicating that this group effect varied across regions. Post-hoc testing in individual ROIs was significant in amygdala (*p*=0.0251) and midbrain (*p*=0.0069), with a trend in orbitofrontal cortex (*p*=0.0587).

There was a difference in 5-HTT binding considering three groups simultaneously: PTSD with a current mood disorder, PTSD without current mood disorder, and HV (*p*=0.031). In pairwise contrasts, PTSD with current comorbid mood disorder had lower binding than HV (*p*=0.012) and a trend for lower binding compared with PTSD without current comorbid mood disorder (*p*=0.056). No difference in 5-HTT BP_F was seen between PTSD patients without current comorbid mood disorder and HV (*p*=0.9522).

Neither PTSD severity nor depression severity was related to 5-HTT binding (*p*=0.97 and *p*=0.95 respectively). In HV, history of past trauma exposure did not influence 5-HTT binding (*p*=0.93).

Conclusions: Low 5-HTT binding was seen in PTSD with current comorbid mood disorders. 5-HTT binding in PTSD without current mood disorders was comparable to binding in HV. This suggests that low 5-HTT binding in PTSD is driven by a current comorbid mood disorder. Since most PTSD patients without a current mood disorder had a remitted mood disorder, this suggests a depression state-dependent abnormality in mood disorders. Our results also indicate that low 5-HTT binding is region specific, with the greatest differences seen in the midbrain and amygdala, two brain areas where we previously reported low 5-HTT binding in MDD alone. These findings suggest that other serotonergic or non-serotonergic pathways are more likely to be related to the pathophysiology of PTSD.

References
1. Sullivan, G. M., R. T. Ogden, et al. (2013). Higher in vivo serotonin-1a binding in posttraumatic stress disorder: a PET study with [11C]WAY-100635. Depress Anxiety 30(3): 197-206.
2. Miller, J. M., N. Hesselgrave, et al. (2013). Positron emission tomography quantification of serotonin transporter in suicide attempters with major depressive disorder. Biol Psychiatry 74(4): 287-295.

3. Miller, J. M., B. A. Everett, et al. (2016). Positron emission tomography quantification of serotonin transporter binding in medication-free bipolar disorder. Synapse 70(1): 24-32.
4. Ogden, R. T. (2003). Estimation of kinetic parameters in graphical analysis of PET imaging data. Statistics in Medicine 22: 3557-3568.
5. Zanderigo F, Ogden RT, Mann J. (2015). Hybrid deconvolution approach for model-free estimation of non-specific binding in PET studies without requiring a reference region. XXVIIth International Symposium on Cerebral Blood Flow, Metabolism and Function & XIIth International Conference on Quantification of Brain Function with PET. Vancouver, Canada.
6. Zanderigo F, Parsey RV, Ogden RT. (2015). Model-free quantification of dynamic PET data using nonparametric deconvolution. Journal of cerebral blood flow and metabolism: official journal of the International Society of Cerebral Blood Flow and Metabolism. 35:1368-1379.
7. Ogden RT, Zanderigo F, Parsey RV. (2015). Estimation of in vivo nonspecific binding in positron emission tomography studies without requiring a reference region. NeuroImage 108:234-242.
8. Huang, M. X., K. A. Yurgil, et al. (2014). Voxel-wise resting-state MEG source magnitude imaging study reveals neurocircuitry abnormality in active-duty service members and veterans with PTSD. Neuroimage Clin 5: 408-419.
9. Fredrikson, M. and V. Faria. (2013). Neuroimaging in anxiety disorders. Mod Trends Pharmacopsychiatri 29: 47-66.
10. Ahs, F., A. Frick, et al. (2014). Human serotonin transporter availability predicts fear conditioning. Int J Psychophysiol.
11. Murrough, J. W., Y. Huang, et al. (2011). Reduced amygdala serotonin transporter binding in posttraumatic stress disorder. Biol Psychiatry 70(11): 1033-1038.
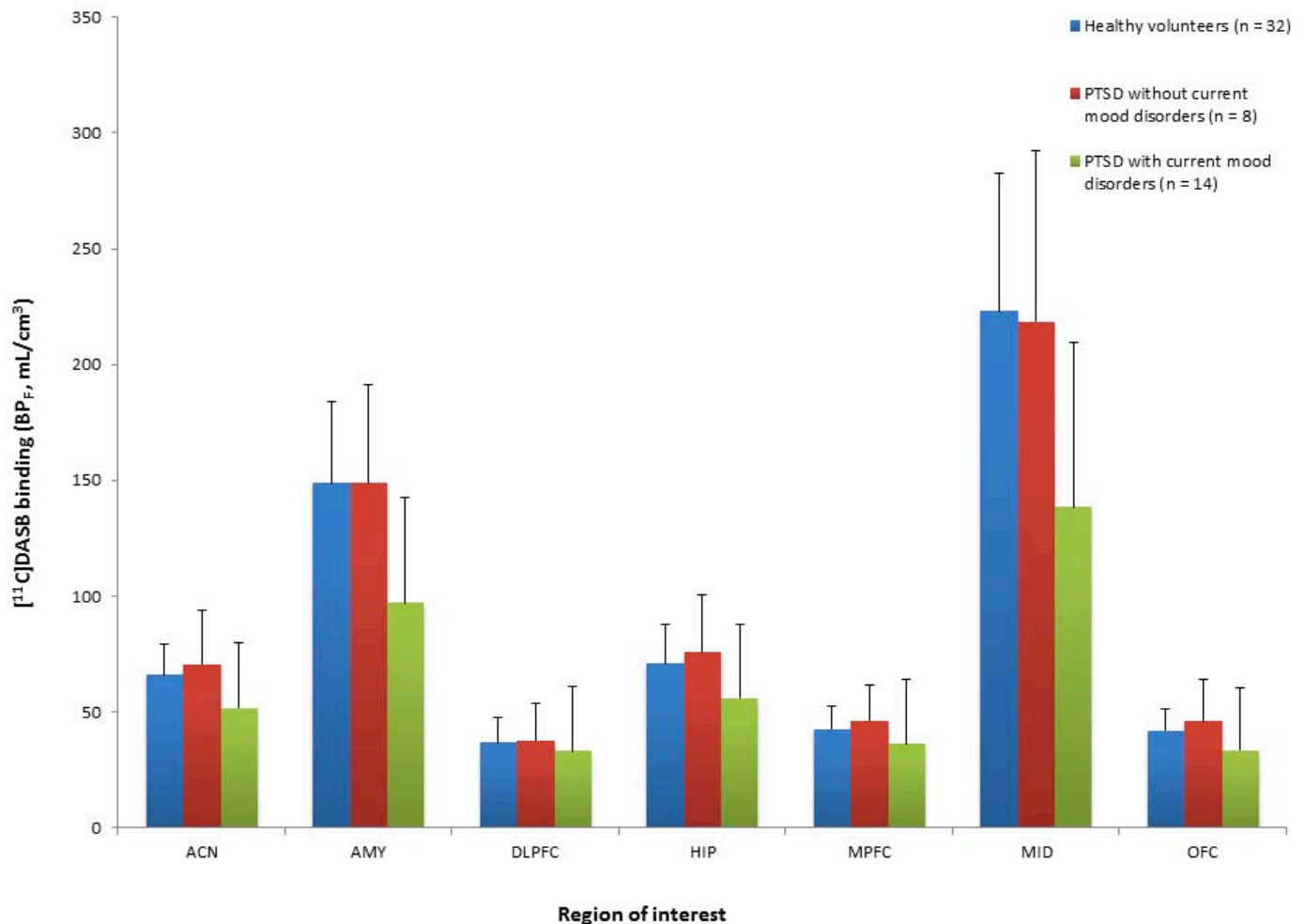
Enhancement of the Raphe Nuclei in [11C]WAY-100635 PET data with a Gradual Point Spread Function Maximum Likelihood Expectation Maximization Reconstruction Approach

Nandita Joshi[1], Arthur Mikhno[2], Christine DeLorenzo[1], Ramin V. Parsey[1]

[1] *Stony Brook University, Stony Brook, NY, USA;* [2] *Columbia University, New York, NY, USA*

OBJECTIVES: The raphe is the principal site of the serotonergic system responsible for regulation of serotonin release throughout the brain. It is a cluster of nuclei, each ~5 mm in diameter [1], which is close to resolution of PET scanners, and therefore vulnerable to partial volume error (PVE). With Filtered Back Projection (FBP) and Maximum Likelihood Expectation Maximization (MLEM) reconstruction approaches, the nuclei are difficult to identify because their signal is corrupted by noise and PVE. Incorporating a point-spread function (PSF) within MLEM (i.e. PSF-MLEM) improves image resolution of PET data, but at the expense of ringing and over-enhancement artifacts, and convergence issues [2]. The objective of this study is to evaluate the recovery of the raphe signal with a novel Gradual PSF MLEM (GPSF-MLEM) image reconstruction approach [3] designed to suppress PSF artifacts, improve image resolution, reduce PVE, and provide quantitative signal recovery.

METHODS: MRI, PET and arterial input function data were obtained for 35 subjects from a previous study [4]. The [11C]WAY-100635 PET data, acquired over 120 minutes on an ECAT HR+ were reconstructed with FBP and GPSF-MLEM, using the Software for Tomographic Image Reconstruction (STIR) framework [5]. GPSF-MLEM was initialized with 20 iterations of MLEM, and 380 iterations with the PSF gradually decreasing from 10mm to 4.5mm isotropic FWHM. The reconstructed images were motion corrected and coregistered with the MRI, using a PET derived atlas for the raphe [6], and a manually drawn dorsal pre-frontal cortex (DPFC) [4] region for comparison. Time-activity curves were modeled using a 2-tissue compartment constrained (2TCC) model (cerebellar white matter reference) with a metabolite corrected arterial input function. The performance of GPSF-MLEM relative to FBP was assessed both visually on MR coregistered PET scans and quantitatively with BP_F.

RESULTS: The raphe is distinctly identifiable on all GPSF-MLEM reconstructed PET scans. In a short 5-minute PET acquisition, compared to FBP images that show high binding voxel clusters in the brain stem, GPSF-MLEM demonstrates enhanced signal and contrast that enable delineation of the raphe nuclei (Figure 1). The linear regression of GPSF-MLEM against FBP BP_F for the raphe and the DPFC resulted in r-squared values of 0.86 and 0.99 with slope(intercept) of 1.32(7.65) and 1.23(1.02), respectively (p<0.001 for both). The bootstrapped error of the BP_F estimates for the raphe using FBP and GPSF-MLEM were mean(STD) 6.79(5.45) and 6.16(5.76), respectively. The difference in errors was not statistically significant (p=0.64).

CONCLUSION: GPSF-MLEM provides substantial visual enhancement of the raphe nuclei in existing PET data. The lower GPSF-MLEM versus FBP BP_F correlation in the raphe, as compared to the larger DPFC region, suggests a region size dependent signal recovery pattern with GPSF-MLEM that is consistent with partial volume correction. GPSF-MLEM may provide benefits for quantification of raphe and other regions by improving signal recovery, kinetic modeling, and identification of smaller structures in existing PET images. Further validation of GPSF-MLEM, comparison to other reconstruction approaches, and application to additional scanners and tracers is the subject of future work.

REFERENCES:
1. Kranz, G.S., et al. *Challenges in the differentiation of midbrain raphe nuclei in neuroimaging research*. Proceedings of the National Academy of Sciences of the United States of America, 2012. **109**, DOI: 10.1073.
2. Rahmim, A., J. Qu, and V. Sossi, *Resolution modeling in PET imaging: Theory, practice, benefits, and pitfalls.* The International Journal of Medical Physics Research and Practice, 2013. **40**(6).
3. Mikhno, A (2015), *Non-invasive and cost-effective quantification of Positron Emission Tomography data* (Doctoral dissertation), Columbia University in the City of New York.
4. Kaufman, J., et al., Quantification of the Serotonin 1A Receptor Using PET: Identification of a Potential Biomarker of Major Depression in Males. Neuropsychopharmacology, 2015. **40**: p. 1692-1699.
5. Thielemans, K., et al., *STIR: Software for Tomographic Image Reconstruction Release 2*, Physics in Medicine and Biology, **57** (4), 2012 pp.867-883.

6.   DeLorenzo, C., et al., Prediction of Selective Serotonin Reuptake Inhibitor Response Using Diffusion-Weighted MRI. Frontiers in Psychiatry, 2013. **4**(5).
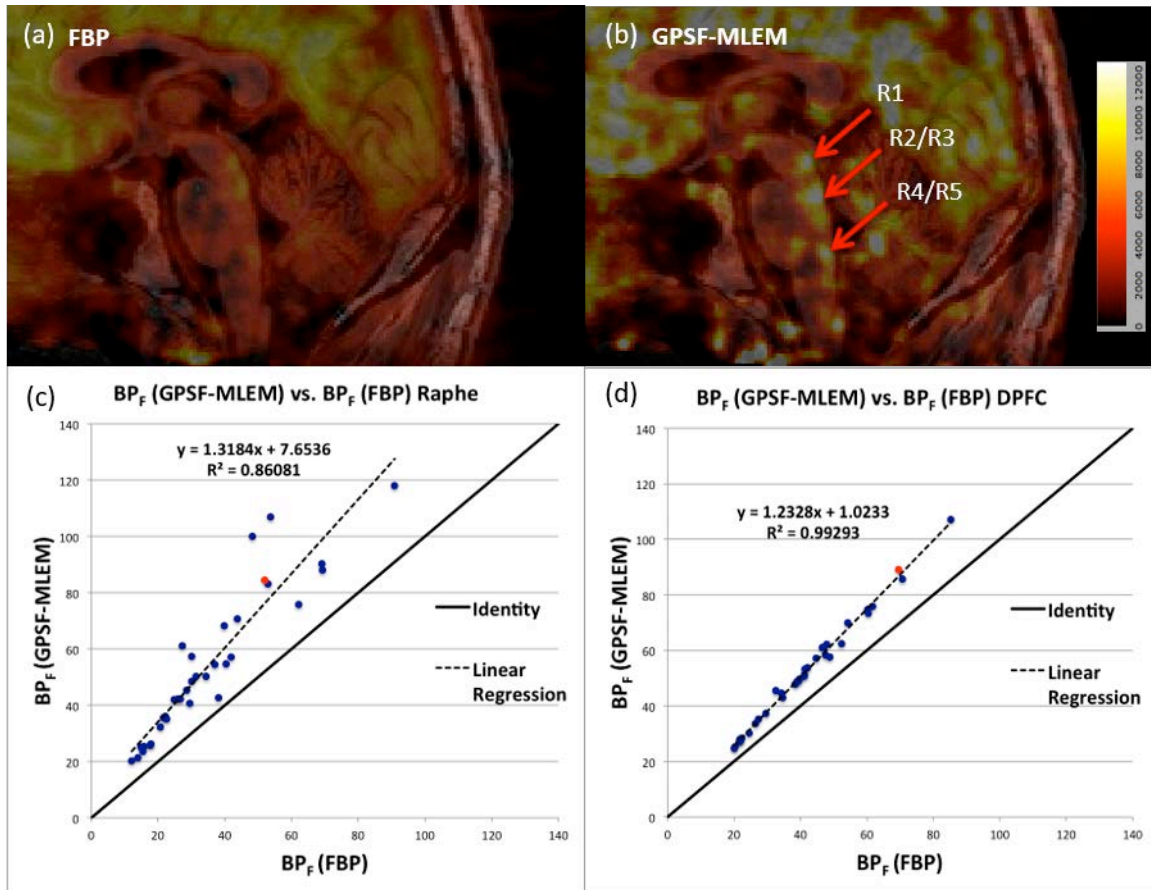
Figure 1: MR coregistered 5-minute [^{11}C]WAY-100635 PET acquisition (10-15min window) of a scan where visually the raphe nuclei were the most enhanced with (b) GPSF-MLEM as compared to (a) FBP. The colorbar shows the intensity of raw counts. Scatter plots and linear regression statistics of GPSF-MLEM against FBP derived BP_F for (c) raphe and (d) DPFC. Red marker in the scatter plots indicates the scan shown in (a)-(b) with BP_F values FBP/GPSF-MLEM of 52.0/84.5 for the raphe and 69.6/89.2 for DPFC. DPFC = Dorsal Pre-Frontal Cortex, R1 = Dorsal Raphe Nucleus, R2 = Median Raphe Nucleus, R3 = Nucleus Raphe Magnus, R4 = Nucleus Obscuris, R5 = Nucleus Pallidis

P-060

Hemispheric differences in the relationship of serotonin transporter availability and hippocampal volumes in the human brain

[1]Yuan Hwa Chou, [2]Jiing-Feng Lirng,

Department of [1]Psychiatry and [2]Radiology, Taipei Veterans General Hospital, Taipei, Taiwan

Hippocampus and serotonin transporter (SERT) comes from two totally distinct systems but share a similar function, regulation of mood. Reduction of hippocampal volumes has been consistently reported in patient with major depressive disorder (MDD). Meanwhile, alteration of SERT, which terminates the serotonin action, has been implicated in the pathophysiology of MDD. However, the study of the functional and structural relationship between hippocampus and SERT was still limited. The aim of this study was to examine their relationship in the human brain. Six-four healthy subjects were recruited. All participants examined with 1.5T high-resolution magnetic resonance imaging. Image was analyzed by two different methods: manual and FreeSurfer. Manual method was applied to analyze the longitudinal axis of hippocampal volumes, which included head, body and tail body. FreeSurfer was used to analyze the volumes of hippocampal subfields. ^{123}I-ADAM with single-photon emission computed tomography was applied for SERT imaging. Regions of interest included the midbrain, thalamus, caudate and putamen. Linear regression analysis was applied for the association of SERT and hippocampus. When took into account of age, sex and educational levels, SERT in the midbrain was associated with left total hippocampal volume ($R2=0.15$, adjusted $R2=0.10$, $F=2.68$, $p=0.04$), mainly contributed by body ($\beta=0.33$, $t=2.66$, $p=0.01$) and tail ($\beta=0.31$, $t=2.55$, $p=0.013$), but not right total hippocampal volume. In contrast, SERT in the thalamus was significantly associated with right total hippocampal volume ($R^2=0.15$, adjusted $R^2=0.09$, $F=2.57$, $p=0.04$), mainly contributed by head ($\beta=0.32$, $t=2.5$, $p=0.02$) but not left total hippocampus. There was no significant association between SERT and subfields of hippocampus. In conclusion, our results suggest that the association of serotonergic system and hippocampus is different in hemispheres. A further study to test this idea in MDD is warrant.

Key words: hippocampus, serotonin transporter, SPECT

Increased ^{18}F-DPA714 binding in genotyped Parkinson patients compared to healthy volunteers

Sonia Lavisse[1,2], Catriona Wimberley[3], Mickaël Labit[4,5], Claire Leroy[3], Claire Thiriez[6], Luce Dauphinot[7,8], Daniel García-Lorenzo[7,8], Philippe Hantraye[1,2], Bruno Stankoff[7,8], Michel Bottlaender[3,5], Philippe Remy[1,2,6,9]

[1]CEA-DSV-I2BM, MIRCen, Fontenay-aux-Roses, France; [2]CNRS-UMR9199, Universités Paris-Sud and Paris-Saclay, Fontenay-aux-Roses, France; [3]Laboratoire Imagerie Moléculaire In Vivo (IMIV), CEA, Inserm, Univ Paris Sud, CNRS, Université Paris Saclay, CEA-SHFJ, 91400 Orsay, France; [4] CATI Multicenter Neuroimaging Platform, France; [5]CEA-DSV-I2BM, Neurospin, Gif-sur-Yvette, France; [6]Centre Expert Parkinson, Neurology Department, CHU Henri Mondor, AP-HP, Créteil, France; [7]Institut du Cerveau et de la Moelle épinière, Inserm-U1127 and Sorbonne University, UPMC-UMRS-1127, Paris, France; [8]CNRS-UMR7225, Paris, France; [9]Paris-Est University, Créteil, France

Introduction: Activated microglia has been found in human post-mortem studies of idiopathic Parkinson's disease ([1]). This neuroinflammatory activation can be studied using PET imaging and tracers targeting the TSPO which are selectively overexpressed by activated microglia and astrocytes. Previous studies in Parkinson's Disease reported either increased ^{11}C-PK11195 binding in the midbrain ([2]) or in the pons and basal ganglia ([3]) while no evidence of increased binding was found using ^{18}F-FEPPA ([4]). The ^{18}F-DPA714 tracer has shown high specificity for TSPO in non-human primates and was quantified in healthy genotyped volunteers ([5], [6]). Using this tracer, we examined Parkinson patients and healthy volunteers with reference-region-based quantification using either the cerebellum grey matter or a region determined by a supervised cluster analysis (SCA), previously validated (*submitted*) on heathy volunteers with arterial sampling.

Methods: Patients (n=12, UPDRS 13-29; 66.3±6.5 years) and healthy volunteers (n=20; 59.1± 11.6 years) were enrolled. Genetic analysis to genotype the polymorphism in the TSPO gene revealed 7/8 mixed-affinity binders (MAB), 3/11 high-affinity binders (HAB) and 2/1 low-affinity binders in patients and volunteers, respectively. PET data were acquired on a HRRT scanner for 90 minutes after injection of 197.8 ± 14.7 MBq ^{18}F-DPA714.
SUV images (60-90min) were calculated and a Regions of Interest (ROI)-based approach was performed using the AAL atlas including 90 cortical and subcortical ROIs on the T1-weighted individual MRI. Grey matter of the cerebellum was used to extract $SUVr_{Cerv}$ for each region and subject. A SCA based on four kinetic classes ([7]) was conducted in each subject to extract a reference region (Ref_{SCA}). Subsequent $SUVr_{SCA}$ values were compared to $SUVr_{Cerv}$. Finally, a Logan analysis was computed to extract BP_{ND} estimates using either grey matter cerebellum (BP_{Cerv}) or Ref_{SCA} (BP_{SCA}) as the reference region.

Results: Since only the MAB group was of comparable number, MABs were considered for primary investigation. In this group, $SUVr_{Cerv}$ and $SUVr_{SCA}$ were higher in patients compared to volunteers in all regions from +3.9% (and 0.4%) in temporal cortex up to +83% (and + 176% for $SUVr_{SCA}$) in substantia nigra (SN). Difference was significant in bilateral SN (p=0.0017) and with $SUVr_{SCA}$ in the globus pallidus (p=0.035), the parietal cortex (p=0.047) and the putamen (p=0.043) as well.
Similarly, BP_{SCA} in patients were higher than BP_{SCA} in volunteers in all regions from +8% in the thalamus up to +243% in the striatum (p=0.034). BP_{Cerv} were poorly identified and we could not accurately compare patients and volunteers. $SUVr_{Cerv}$, $SUVr_{SCA}$ and BP_{SCA} in the substantia nigra did not correlate with disease severity (UPDRS scores).

Conclusion: The SCA appeared to be a more accurate reference region than the cerebellum to analyze ^{18}F-DPA714 PET data in healthy volunteers and patients in the absence of arterial blood sampling.
In the substantia nigra and in the putamen, $SUVr_{SCA}$ images showed a significant higher ^{18}F-DPA714 binding in Parkinson patients compared to healthy volunteers. Logan analysis confirmed the increased PET binding in the substantia nigra and putamen of patients. Inclusions are still ongoing and should enable further analysis in both MAB and HAB subjects.

REFERENCES
1. Hirsch EC, Vyas S, Hunot S. Neuroinflammation in Parkinson's disease. *Parkinsonism Relat Disord.* 2012;18 Suppl 1:S210-212.
2. Ouchi Y, Yoshikawa E, Sekine Y, et al. Microglial activation and dopamine terminal loss in early Parkinson's disease. *Ann Neurol.* 2005;57:168-175.

3.   Gerhard A, Pavese N, Hotton G, et al. In vivo imaging of microglial activation with [11C](R)-PK11195 PET in idiopathic Parkinson's disease. *Neurobiol Dis.* 2006;21:404-412.

4.   Koshimori Y, Ko JH, Mizrahi R, et al. Imaging Striatal Microglial Activation in Patients with Parkinson's Disease. *PLoS One.* 2015;10:e0138721.

5.   Lavisse S, Garcia-Lorenzo D, Peyronneau MA, et al. Optimized Quantification of Translocator Protein Radioligand (1)(8)F-DPA-714 Uptake in the Brain of Genotyped Healthy Volunteers. *J Nucl Med.* 2015;56:1048-1054.

6.   Lavisse S, Inoue K, Jan C, et al. [18F]DPA-714 PET imaging of translocator protein TSPO (18 kDa) in the normal and excitotoxically-lesioned nonhuman primate brain. *Eur J Nucl Med Mol Imaging.* 2015;42:478-494.

7.   Yaqub M, van Berckel BN, Schuitemaker A, et al. Optimization of supervised cluster analysis for extracting reference tissue input curves in (R)-[(11)C]PK11195 brain PET studies. *J Cereb Blood Flow Metab.* 2012;32:1600-1608.

P-062

In Vivo Characterization of ^{11}C-BU99008 in Humans - A Novel PET ligand for the Imidazoline$_2$ Binding Site

Myers JFM[1], Tyacke RJ[1], Turton S[1], Venkataraman A[1], Mick I[1], Hill S[2], Chong H[2], Mos S[2], Passchier J[2], Rabiner EA[2&3], Parker CA[1&4], Gunn RN[2&5], & Nutt DJ[1]

[1] *Centre for Neuropsychopharmacology, Division of Brain Sciences, Imperial College London, UK;* [2] *Imanova Ltd, London, UK;* [3] *Centre for Neuroimaging Sciences, King's College, London, UK;* [4] *Experimental Medicine Imaging, GlaxoSmithKline, UK;* [5] *Centre for Restorative Neuroscience, Division of Brain Sciences, Imperial College London, UK*

The imidazoline$_2$ binding sites (I$_2$BS), are expressed in glia, are thought to be implicated in the regulation of glial fibrillary acidic protein and the availability of a PET ligand for this target would be important for the investigation of neurodegenerative and neuroinflammatory diseases. ^{11}C-BU99008 has previously been identified as a putative PET radioligand for I$_2$BS and shown to have specificity and selectivity for this target in primates[1]. Here we present the first in vivo characterisation of this PET radioligand in humans and assess its test-retest reproducibility.

14 healthy male volunteers (age 54±7 years) underwent dynamic PET imaging with ^{11}C-BU99008 (309±14 MBq, 2.59±2.52 μg) and arterial sampling. 5 of these subjects had a retest scan after 1 week. PET scans were acquired for 120 min on a Siemens PET Biograph and reconstructed into 29 frames (8x15, 3x60, 5x120, 5x300, 7x600 s) using filtered back-projection. Dynamic images were corrected for motion using a mutual information co-registration algorithm with frame 16 as the reference. Associated T1 MRI data enabled nonlinear registration of the CIC atlas into the space of each subject's dynamic PET data and the generation of regional time-activity data. Arterial plasma input functions corrected for metabolites were generated and tracer compartmental modelling techniques (1 Tissue Compartmental Model (1TC) and 2 Tissue Compartmental Model (2TC)) were applied with a fixed 5% blood volume to derive the outcome measure V_T (regional total distribution volume) and assess test-retest reliability. All image processing and kinetic analysis was performed in MIAKAT™ (www.miakat.org).

[11]C-BU99008 was metabolised such that 10% of the parent radioligand remained in plasma at 120 min. The radioligand showed a rapid uptake and heterogeneous distribution consistent with the known expression of I$_2$BS. Akaike model selection criteria indicated that the 2TC was preferred over 1TC (see Figure 1C). Estimates of the delivery rate constant K_1 (=0.79±0.18 mL·cm^{-3}·min^{-1}: 2TC) were high indicating a high extraction for the tracer. V_T estimates were broadly similar with 1TC and 2TC with highest values obtained in the striatum (2TC V_T = 113±20 mL·cm^{-3}), medium frontal lobe uptake (2TC V_T = 55±9 mL·cm^{-3}) and lowest uptake in cerebellum (2TC V_T = 47±7 mL·cm^{-3}).

The intersubject % coefficient of variation was between 14% and 18% in every region. Test-retest reliability was good with 2TC %VAR (=2(T-R)/(T+R)) < 10% in the key target regions of interest (Figure 1C).

In summary, ^{11}C-BU99008 in human PET studies demonstrates good brain delivery, reversible kinetics, heterogeneous distribution and specific binding signal consistent with I$_2$BS distribution. Test-retest reliability was best for 2TC with target regions of interest showing a %VAR <10%.

References:
1. Parker, C.A., et al., Evaluation of 11C-BU99008, a PET Ligand for the Imidazoline2 Binding Sites in Rhesus Brain. J Nucl Med, 2014. **55**(5): p. 838-44.
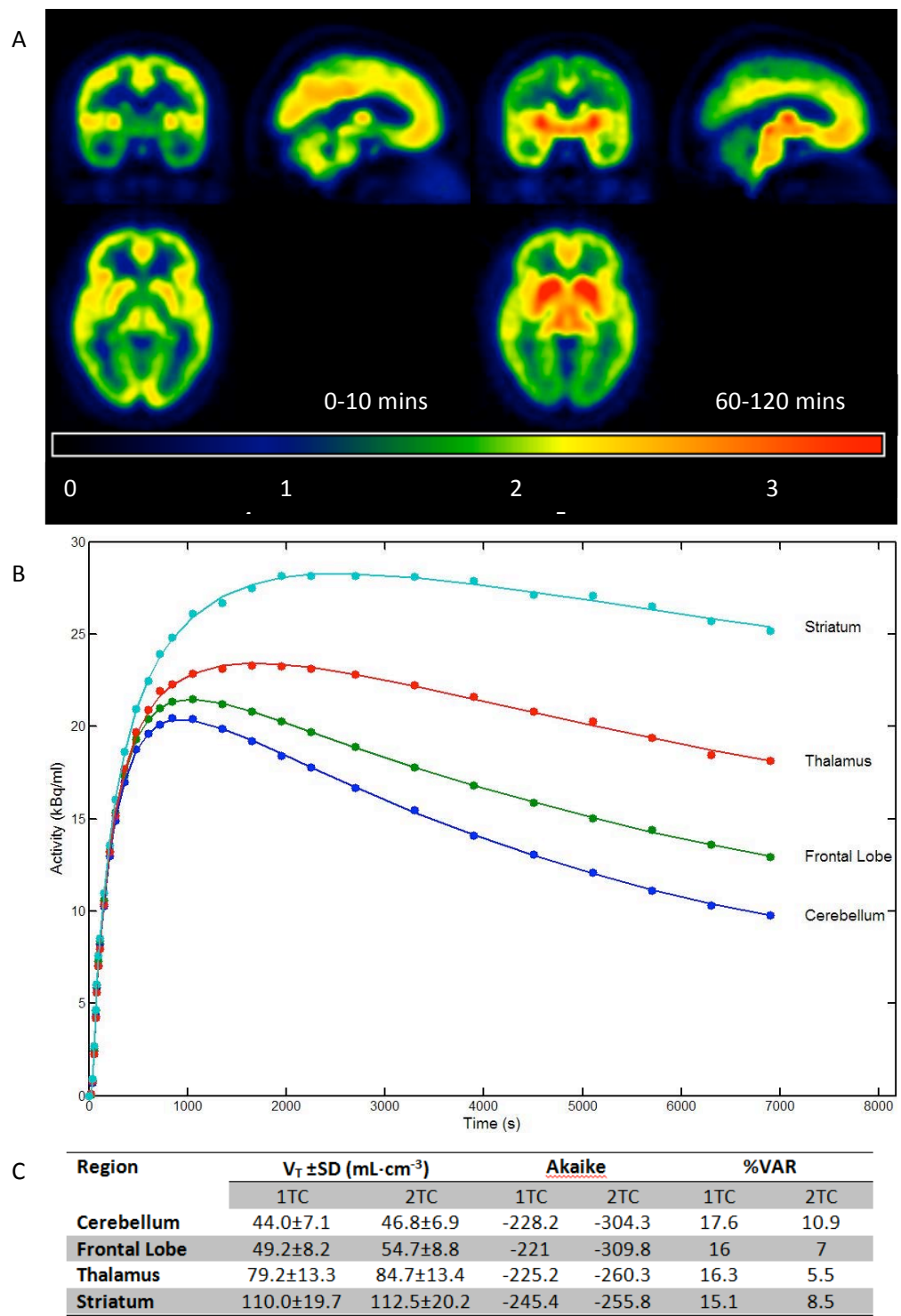
Figure 1: (A) SUV images of early (0-10 mins, left) and late (60-120 mins, right) to show uptake and retention of
[11]C-BU99008. (B) Time-activity curves and 2TC model fits in four regions of interest. (C) Table to show binding
parameters and test-retest reliability for 2TC.

Imaging buprenorphine brain kinetics and target engagement using ^{11}C-buprenorphine PET in nonhuman primates: quantitative correlation to pharmacological MRI data

Sylvain Auvity, Claire Leroy, Sébastien Goutal, Irène Buvat, Michel Bottlaender, Fabien Caillé, Nicolas Tournier

Imagerie Moléculaire In Vivo, IMIV, CEA, Inserm, CNRS, Univ. Paris-Sud, Université Paris Saclay, CEA-SHFJ, Orsay, F-91400, France

CONTEXT: The high variability of response to opioid drugs between individuals and the development of opioid tolerance complicate the management of chronic pain in patients. Combined PET and pharmacological MRI (phMRI) is an appealing strategy to study the neuropharmacological parameters that control the variability of response to opioid drugs. Buprenorphine, a partial μ-opioid receptor (MOR) agonist, is a widely prescribed analgesic drug. ^{11}C-buprenorphine was proposed as a PET probe to study MOR density in monkeys, using cerebellum as reference region (1). phMRI experiments using a cerebral blood volume (CBV)-based approach have recently determined the differential activation of brain regions elicited by the systemic administration of an analgesic dose of buprenorphine (0.03 mg/kg i.v.) in awake macaques (2). The aim of this study is to determine the kinetic parameters that predict the differential hemodynamic response to buprenorphine between brain regions.

METHODS: Four macaques underwent an anatomical T1-weighted MRI and two ^{11}C-buprenorphine PET imaging (~221±24 MBq i.v, 90 min). A first PET acquisition was performed for baseline condition, whereas the second was co-injected with of an analgesic dose of buprenorphine (BUP, 0.03 mg/kg). MR images were normalized onto a macaque T1-MR template (3) and matrix were applied to the co-registered dynamic PET images so that all PET images were superimposed on 24 brain regions from an common atlas. Regional ^{11}C-buprenorphine brain kinetics were measured in each region for both conditions (Baseline and BUP) with SUV_{90min} and BP_{ND} using cerebellum as reference region and the Simplified Reference Tissue Model . PET-derived outcome parameters were $SUV_{90min\ baseline}$, $SUV_{90min\ BUP}$, $BP_{ND\ baseline}$, $BP_{ND\ BUP}$, ΔSUV (=$SUV_{90min\ baseline}$ - $SUV_{90min\ BUP}$), ΔBP_{ND} (= $BP_{ND\ baseline}$ − $BP_{ND\ BUP}$) and target engagement TE (= ($BP_{ND\ baseline}$ − $BP_{ND\ BUP}$) / $BP_{ND\ baseline}$). Regional PET-derived parameters were plotted as a function of the quantitative phMRI data ($\Delta rCBV$), obtained from a published (open access) study (2).

RESULTS: Baseline brain uptake of ^{11}C-buprenorphine was consistent with reported MOR density (1) and was displaced by BUP co-injection suggesting specific binding to the brain. $SUV_{90min\ baseline}$ was maximal in the following regions: putamen>caudate>thalamus>amygdala and did not correlate to $BP_{ND\ baseline}$ (amygdala>putamen>caudate>thalamus) (r=0.017). Conversely, $SUV_{90min\ BUP}$ was well correlated to $BP_{ND\ BUP}$ (r=0.61, p=0.0012). There was no significant correlation between MRI-derived $\Delta rCBV$ and $BP_{ND\ baseline}$ (r=0.13), $BP_{ND\ BUP}$ (r=0.36), ΔBP_{ND} (r=0.054) or TE (r=0.065). We found a significant correlation between $\Delta rCBV$ and $SUV_{90min\ baseline}$ (r=0.51, p= 0.015), $SUV_{90min\ BUP}$ (r=0.44, p=0.04) or ΔSUV (r=0.48, p=0.02).

DISCUSSION: The differential hemodynamic response to buprenorphine between brain regions is preferentially predicted by the regional uptake of ^{11}C-buprenorphine, estimated either in the presence or the absence of co-injected BUP. We show that CBV-based phMRI signal is not predicted by the estimated BUP interaction with its target (TE, ΔBP_{ND}) or ^{11}C-buprenorphine target availability ($B_{max}=BP_{ND}\times K_d$), assuming a constant affinity (K_d) of MOR for buprenorphine. The parameters that control the phMRI response to BUP do not solely restrict to the occupation/availability of neuroreceptors and may involve other neurokinetic processes that influence buprenorphine regional uptake and hemodynamic response.

References

1. Shiue CY, Bai LQ, Teng RR, Arnett CD, Dewey SL, Wolf AP, et al. A comparison of the brain uptake of N-(cyclopropyl[11C]methyl)norbuprenorphine ([11C]buprenorphine) and N-(cyclopropyl[11C]methyl)nordiprenorphine ([11C]diprenorphine) in baboon using PET. Int J Rad Appl Instrum B. 1991;18(3):281–8.
2. Seah S, Asad ABA, Baumgartner R, Feng D, Williams DS, Manigbas E, et al. Investigation of cross-species translatability of pharmacological MRI in awake nonhuman primate - a buprenorphine challenge study. PloS One. 2014;9(10):e110432.
3. Rohlfing T, Kroenke CD, Sullivan EV, Dubach MF, Bowden DM, Grant KA, et al. The INIA19 Template and NeuroMaps Atlas for Primate Brain Image Parcellation and Spatial Normalization. Front Neuroinformatics. 2012;6:27.

11C-buprenorphine

Baseline

Buprenorphine 0.03 mg/kg

0.5   SUV   1.3

0.5   SUV   1.3
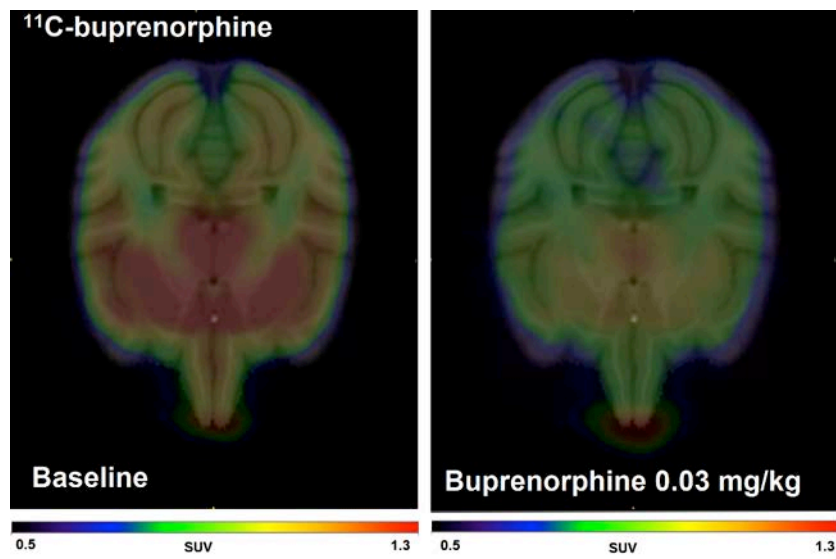
Partial volume effect on brain PET in relation to MR-derived cortical thickness measures.

Keisuke Matsubara[1], Masanobu Ibaraki[1], Tetsuya Maeda[2] and Toshibumi Kinoshita[1]

[1] *Department of Radiology and Nuclear Medicine, Research Institute for Brain and Blood Vessels – Akita, Akita, Japan;* [2] *Department of Neurology, Research Institute for Brain and Blood Vessels – Akita, Akita, Japan*

Introduction: Partial volume effect (PVE) due to limited spatial resolution of PET causes spill-over of signals from an interested region. Degree of the spill-over depends on object size and morphological change of the interested object. For example, atrophy in cerebral cortex reduces apparent radioactivity by spill-over of the PET signal. Region-based partial volume correction (PVC) has been proposed and widely utilized in brain PET study. However, few studies have investigated dependency on object size in PET measurement corrected with region-based PVC. We aimed to investigate the PVE in brain PET in terms of correlation with cortical thickness derived from MR images.

Methods: [^{18}F]FDG PET scans for 30 minutes were performed with five healthy volunteers (HV) and 27 patients with Parkinson's disease (PD), including ten without any cognitive impairment (PD non-cognitive; PDNC), nine with mild cognitive impairment (MCI) and eight with dementia (PD with dementia; PDD). The acquired PET images were smoothed with 6-mm full-width at half maximum (FWHM) Gaussian filter to reduce noise in PET measurements. Final spatial resolution of acquired images was 7.5 mm FWHM. The PET images were corrected for PVE with geometric transfer matrix (GTM), region-based PVC method (Rousset et al., 1998), with 7.5 mm FWHM Gaussian kernel as point spread function.
Thin-sliced three-dimensional MR T1 images for the all subjects were also acquired. Regions of interest (ROIs) for each subject were automatically extracted from the T1 image with FreeSurfer software package (Fischl et al., 2004), and merged to 19 regions. The extracted ROIs were utilized for PVC with GTM. Cortical thickness in each cortical ROI was calculated with FreeSurfer (Fischl and Dale, 2000). Single regression analysis between the calculated cortical thickness and standardized uptake value (SUV), normalized with global mean, was implemented to investigate the dependency on cortical thickness.

Results: Normalized SUV without PVC in parietal and temporal cortex correlated with cortical thickness significantly among all subjects [$r = 0.369$, $p = 0.038$ in parietal cortex; $r = 0.535$, $p = 0.002$ in temporal cortex]. No significant and inter-subject correlation between PVE-corrected SUV and the cortical thickness was observed.
In one HV and one PDNC subjects, negative and inter-regional correlations between SUV without PVC and cortical thickness were observed [$r = -0.742$ in the HV subject and -0.859 in the PDNC patient (see also Figure)]. These negative correlations are inconsistent with expectation that spill-over at smaller object induces larger reduction in PET signal. Regional SUV with PVC in 17 of the subjects were also negatively correlated with cortical thickness [$r = -0.950$ to -0.711].

Conclusions: The results reveal dependency on cortical thickness in SUV due to PVE, and indicate that PVC can remove the dependency. The unexpected negative and inter-regional correlations between the SUV and cortical thickness may reflect existence of error in calculation of cortical thickness and extraction of cortical regions. The findings indicate that PVC can be useful to correct the spill-over with morphological change such as atrophy, however, we should pay attention to validity of extracted cortical regions.

References:
Fischl, B., Dale, A.M., 2000. Measuring the thickness of the human cerebral cortex from magnetic resonance images. Proc. Natl. Acad. Sci. 97, 11050–11055. doi:10.1073/pnas.200033797
Fischl, B., Kouwe, A. van der, Destrieux, C., Halgren, E., Ségonne, F., Salat, D.H., Busa, E., Seidman, L.J., Goldstein, J., Kennedy, D., Caviness, V., Makris, N., Rosen, B., Dale, A.M., 2004. Automatically Parcellating the Human Cerebral Cortex. Cereb. Cortex 14, 11–22. doi:10.1093/cercor/bhg087
Rousset, O.G., Ma, Y., Evans, A.C., 1998. Correction for Partial Volume Effects in PET: Principle and Validation. J. Nucl. Med. 39, 904–911.

Figure Inter-regional correlation between cortical thickness and SUV without (left) and with PVC (right) in one PDNC patient.

P-065
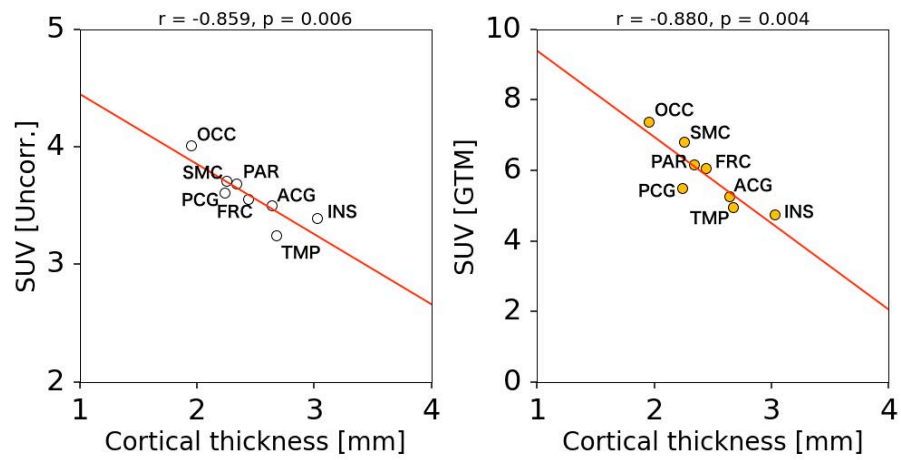
Image fusion using a novel multi-modal imaging marker

Takayuki Ose[1,2], Hiroshi Watabe[2], Joonas Autio[1], Nobuyoshi Tanki[1], Ami Igesaka[3], Hisashi Doi[3], Yasuhiro Wada[4], Takuya Hayashi[1]

[1] Functional Architecture Imaging Unit, RIKEN Center for Life Science Technologies, Kobe, JAPAN; [2] Cyclotron Radioisotope Center (CYRIC), Tohoku University, Sendai, JAPAN; [3] Labeling Chemistry Team, RIKEN Center for Life Science Technologies, Kobe, JAPAN; [4] Pathophysiological and Health Science Team, RIKEN Center for Life Science Technologies, Kobe, JAPAN

Objectives: Multi-modal fusion analysis may crucially depend on accuracy of image registration. However, the procedure of registration can sometimes yield poor results because structural information is often unclear in some modalities. The purpose of this study was to establish a novel radioisotope-free multi-modal imaging marker and the marker-based registration system. We designed a multi-modal marker using a material containing Tungsten solution which has a high imaging contrast in Computed Tomography (CT), Positron Emission Tomography Transmission scan (PET/Tx), and in Magnetic Resonance Imaging (MRI), and assessed here its capability as an imaging marker in a maker-based registration system.

Methods: A proposed marker contained Tungsten (W) solution, which has a high density per unit volume thus causing absorption of radio wave (X or gamma ray), as well as a magnetic property that shortens the relaxation time and causes the contrast in the MRI.
We investigated the contrast to noise ratio (CNR) in various concentrations of the W solution in each of CT, PET/Tx and MRI, and compared with those of other material solutions known to have contrast in MRI (Mn, Ni, Cu, and Gd). We also evaluated the identification and registration accuracy of the novel marker using a 5-marker phantom in which five markers were placed pentagonally on the rigid plate in known dimensions (Fig (a)). The distance between a pair of markers was measured using images of CT, PET/Tx and MRI, as well as by using optical system (Polaris, NDI), and the distance bias was plotted against modalities. A transformation matrix for registration and its error was evaluated using the root-mean square deviation of the marker distances between images (MRI-CT or MRI-PET/Tx) in a point-based registration based on Kabsch algorithm (Kabsch W 1976) (Fig (b, c)). The transformation of images was applied using the registration matrix using FSL FLIRT. Finally, we performed animal experiments using this marker in MRI and ^{11}C-raclopride PET and performed marker-based registration to evaluate its applicability in comparison with software-based registration.

Results: All of known contrast agents (Mn, Ni, Cu and Gd) had high MR CNR only at a low density concentration (<1.1g/mL), and any of them did not show high CNR in CT and PET/Tx. In contrast, the solution of W showed high MR SNR even at a high density concentration (~3.0g/mL), thus also yielding high CNR in CT and PET/Tx as well. The distance bias in images was 0.44 ± 0.33 mm, 0.15 ± 0.06 mm, and 0.16 ± 0.17 mm in MRI, CT and PET/Tx, respectively. Registration error was 0.34mm (MRI and CT) and 0.56 mm (MRI and PET/Tx). We also confirmed accurate registration between ^{11}C-raclopride PET and MR images, allowing us to calculate partial-volume corrected cortical binding potential (Fig (d)).

Conclusions: Our results indicate that the novel marker containing a solution of W had high CNR enough to identify the locations in three kinds of imaging modalities (MRI, CT and PET/Tx) and may be applicable to in vivo studies of brain imaging.
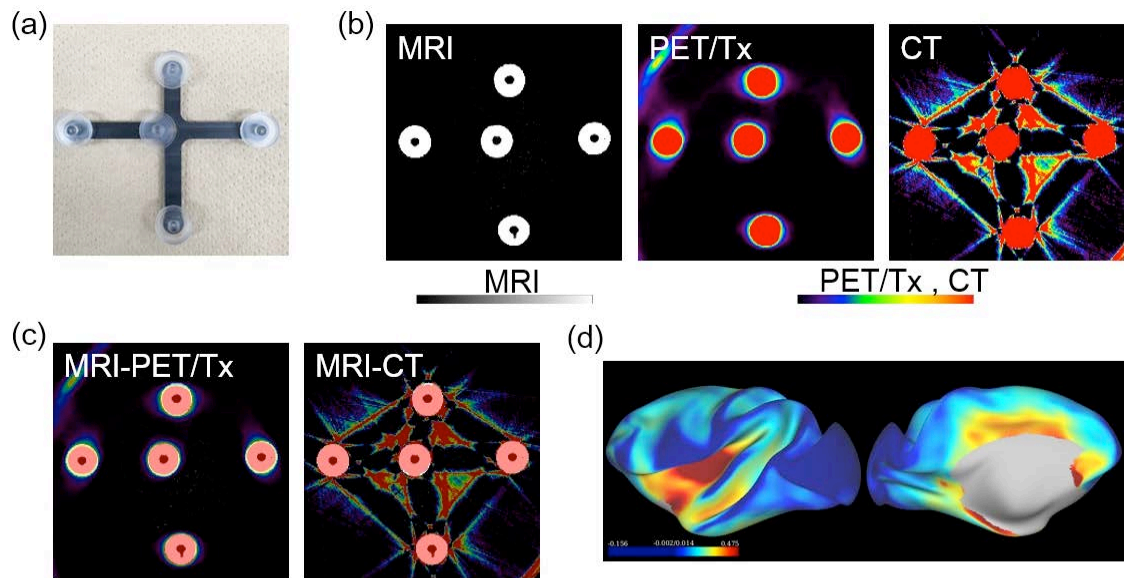
(a) Photograph of a 5-marker phantom. (b) MRI, PET/Tx and CT images of 5-marker phantom. (c) Images of MRI overlaid on PET/Tx (MRI-PET/Tx) and on CT (MRI-CT) after a marker-based registration. (d) Macaque brain cortical surface mapping of binding potential of [^{11}C] raclopride, obtained after preprocessing of the marker-based registration between MRI and PET and partial volume correction of PET data.

A head-to-head comparison of two different ^{11}C-labelling positions of Cimbi-36

A. Johansen[1], H.D. Hansen[1], N. Gillings[2], L. Feng[1], C. Svarer[1], G.M. Knudsen[1]

[1]Neurobiology Research Unit, Rigshospitalet, COPENHAGEN, Denmark, [2]PET & Cyclotron Unit, Rigshospitalet, COPENHAGEN, Denmark

Objectives: [11C]Cimbi-36 (Figure 1A) was recently validated as a 5-HT$_{2A}$ receptor agonist PET radioligand in humans[1]. The Cimbi-36 structure contains three methoxy groups which are amenable to ^{11}C-labelling. We have established that the major metabolic pathway for Cimbi-36 is by demethylation of the methoxy group on the 5-position followed by rapid glucuronidation[2]. Thus the main radiometabolite of [11C]Cimbi-36 (N-(2-[**[11]C-OCH$_3$**]methoxybenzyl)-2,5-dimethoxy-4-bromophenethylamine) is the glucuronide conjugate (M2) (Figure 1C), whereas the major radiometabolite of [11C]Cimbi-36_5 (N-(2-methoxybenzyl)-2-dimethoxy-5-**[^{11}C-OCH$_3$**]methoxy-4-bromophenethylamine (Figure 1B)) is a group of highly polar compounds (M1). Here we compare [11C]Cimbi-36 and [11C]Cimbi-36_5 in healthy volunteers, evaluating which radioligand yields the best signal to noise ratio.

Methods: Six female healthy volunteers were included (mean age 23.2 ± 3.3 years). Each received two 120 minutes dynamic PET scans following intravenous injection of [11C]Cimbi-36 and [11C]Cimbi-36_5, respectively. Venous blood samples were used to determine the radiometabolic profiles of the radioligands using radio-HPLC, and to measure radioactivity in plasma and whole blood using a well counter. The non-displaceable binding potentials (BP$_{ND}$s) of [11C]Cimbi-36 and [11C]Cimbi-36_5 were calculated with the simplified reference tissue model using cerebellum as the reference region as previously described[1].

Results: Standard uptake values (SUV) showed that compared to [11C]Cimbi-36, [11C]Cimbi-36_5 was associated with higher uptake in both the neocortex and cerebellum (Figure 1E). Neocortical BP$_{ND}$ of [11C]Cimbi-36 was 1.38 ± 0.07 whereas for Cimbi-36_5 it was 1.18 ± 0.14. The mean of absolute differences was 0.20 ± 0.09 (p < 0.003). We propose the lower BP$_{ND}$ of [11C]Cimbi-36_5 was caused by the polar M1 metabolites, resulting from 5'-demethylation, which were the major radiometabolites of [11C]Cimbi-36_5 (Figure 1D). These are likely to comprise [11C]methanol, [11C]formaldehyde, [11C]formic acid and/or [11C]carbon dioxide/bicarbonate. Both methanol, formaldehyde and carbon dioxide/bicarbonate cross the blood brain barrier (BBB)[3,4,5] and other cell membranes. The fact that a lower ratio of radioactivity concentration in plasma relative to whole blood was observed for [11C]Cimbi-36_5 compared to [11C]Cimbi-36 (Figure 1F), suggests that a part of these polar radioactive metabolites enter the erythrocytes, and thus corroborate our hypothesis that these radiometabolites cross the BBB. In the brain these radiometabolites increase the non-specific binding and decrease the signal-to-noise ratio, which is identified by the lower BP$_{ND}$ of [11C]Cimbi-36_5.

Conclusions: Changing the ^{11}C-labelling position of Cimbi-36, and thus the radiometabolic profile, significantly decreased the neocortical BP$_{ND}$ of [11C]Cimbi-36_5 as compared to [11C]Cimbi-36 in humans. [11C]Cimbi-36 is thus the superior radioligand for future 5-HT$_{2A}$ receptor agonist studies. Our data also show that the common notion that polar radiometabolites are unlikely to cross the blood-brain barrier is questionable.

References:
1 Ettrup A *et al.* Serotonin 2A receptor agonist binding in the human brain with [11C]Cimbi-36. J. Cereb. Blood Flow & Metab. 2014; 34: 1188–1196. 2 Leth-Petersen S et al. Metabolic Fate of Hallucinogenic NBOMes. Chem. Res. Toxicol. 2015; 29: 96-100. 3 Raichle ME et al. Blood-brain barrier permeability of ^{11}C-labeled alcohols and ^{15}O-labbeled water. Am J Physiol. 1976; 230: 543-552. 4 Shields A et al. Contribution of labeled carbon dioxide to PET imaging of carbon-11-labeled compounds. J nucl med 1992; 33: 581–4. 5 Shcherbakova L, et al. Permeability of the blood-brain barrier for intravascular formaldehyde. B Exp Biol Med 1986; 102: 1553–1554.
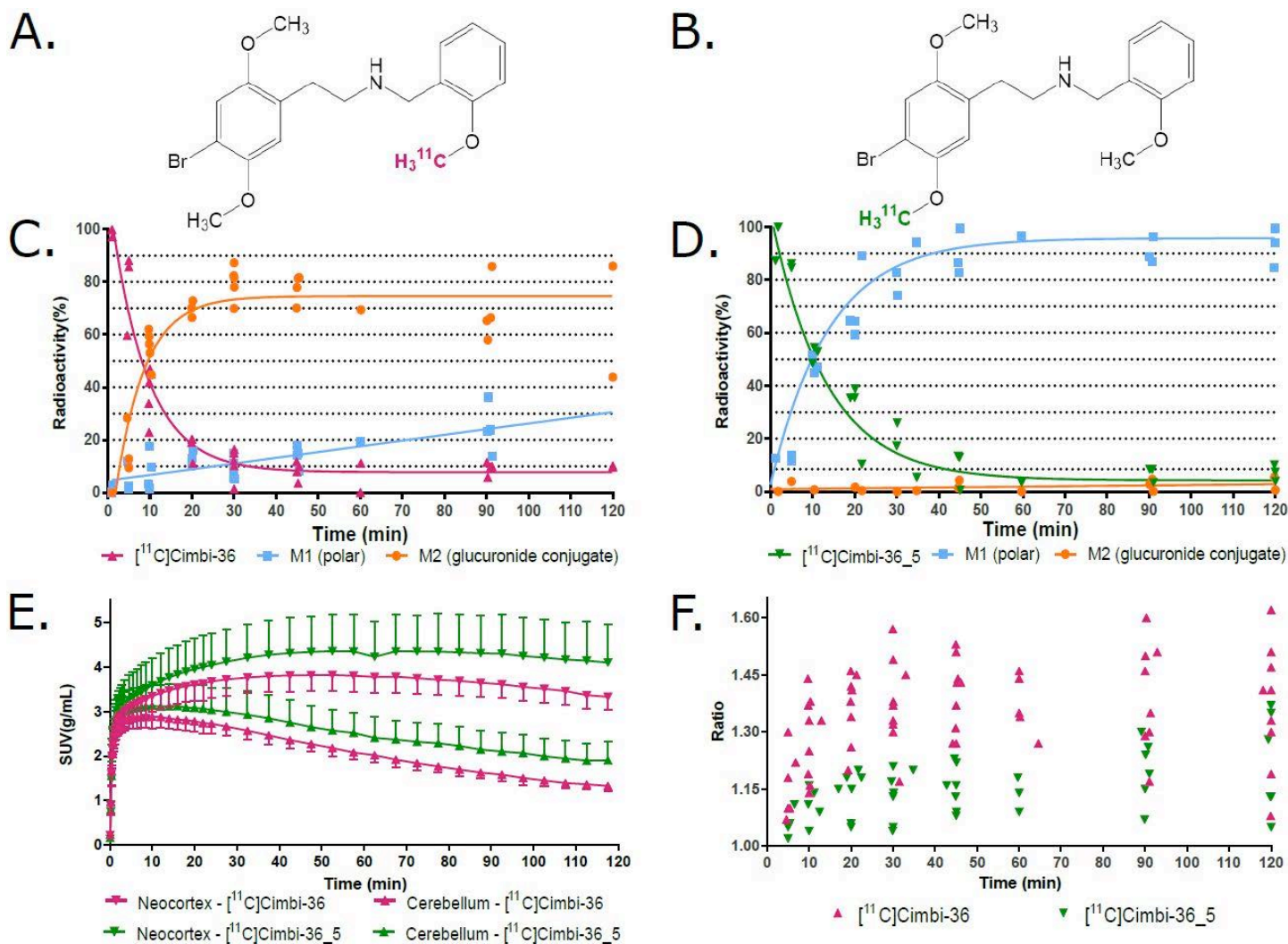
Figure 1. Chemical structures and labelling positions for [11C]Cimbi-36 (A) and [11C]Cimbi-36_5 (B) and corresponding radiometabolite profile for the two radioligands in plasma (C, D respectively). Standard uptake values in neocortex and cerebellum (E) shows that [11C]Cimbi-36 yields a less noisy signal. (F) Ratio of radioactivity concentration in plasma relative to whole blood. In all figures pink denotes [11C]Cimbi-36 and green represents [11C]Cimbi-36_5.

Image-derived approach software to estimate binding parameters and images of dopamine transporters in non human primate brain using [^{18}F]FE-PE2I

Ikuo Odano [1,2], Andrea Varrone [1], Tetsuo Hosoya [3], Kazuya Sakaguchi [4], Balázs Zoltán Gulyás [1,5], Krishna Ghosh [5], Changtong Yang [5], Parasuraman Padmanabhan [5], Ilonka Guenther [6], Wang Zhimin [5], Raymond Serrano [6], G. Nevil Chimon [7], Lars Farde [1] and Christer Halldin [1,5]

[1] *Psychiatric Section, Department of Clinical Neuroscience Karolinska Institutet, Stockholm, Sweden;* [2] *Division of Molecular Imaging Sciences, Sendai Medical Imaging Center. Sendai, Japan;* [3] *Department of Quality Assurance, QMS Group, FUJIFILM RI Pharma Co., Ltd. Tokyo, Japan;* [4] *Department of Medical Engineering and Technology, School of Allied Health Sciences, Kitasato University, Tokyo, Japan;* [5] *Lee Kong Chian School of Medicine, Nanyang Technological University (NTU), Singapore;* [6] *Duke-NUS Medical School, Laboratory for Translational and Molecular Imaging, Singapore;* [7] *Singapore Radiopharmaceuticals Pte Ltd., Singapore*

Introduction: Dopamine transporter (DAT) imaging using positron emission tomography (PET) is a well-established tool to evaluate dopaminergic function in neurodegenerative and psychiatric disorders. Recently we proposed a new PET radioligand, [^{18}F]FE-PE2I, which has suitable affinity and selectivity for dopamine transporters. The purpose of the present study was to examine the accuracy of a software program, automated receptor imaging system (ARIS), which enables the calculation of binding parametric images and the estimation of binding parameters of [^{18}F]FE-PE2I.

Methods: The method for ARIS is based on image-driven and voxel-based approach, including two reference tissue models: simplified reference tissue model (SRTM) and non-invasive graphical approach (Logan DVR approach). The software program runs on the Windows platform and analyzes dynamic PET data sets. The procedure is semi-automatic and not time-consuming, and provides robust binding parameters. Parametric images and binding parameters were obtained from non-human primate PET studies for DAT binding with [^{18}F]FE-PE2I, and values of binding potential derived from parametric images were compared with those obtained by ROI-based numerical approaches using conventional time activity curves. Kinetic analysis with 2TCM using arterial plasma input was also applied for validation.

Results: Binding potential images obtained by SRTM and by Logan DVR approach are shown in Figure. Binding potential values obtained using ARIS were in good agreement with those obtained by the ROI-based numerical approaches. Since parametric images obtained by Logan DVR approach were less nosy than those obtained by SRTM, Logan DVR approach was preferable. However Logan DVR approach tended to underestimate binding potential values in DAT rich regions.

Discussion: We found that the proposed image-derived and voxel-based approach, ARIS, provides high quality binding parametric images and robust parametric values. Binding potential values obtained are in good agreement with those obtained by the ROI-based numerical approaches, demonstrating that ARIS software is a useful tool for transporter binding studies with [^{18}F]FE-PE2I and PET.
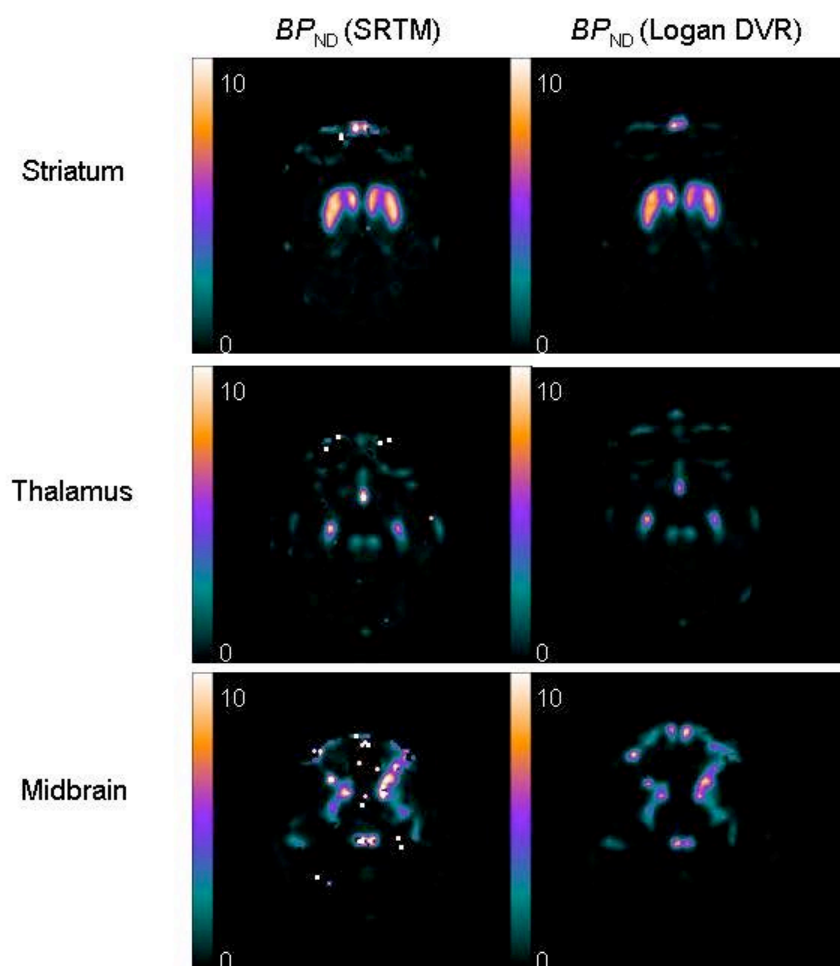
Figure. Binding potential images of $[^{18}F]$FE-PE2I at the level of the striatum, the thalamus and the midbrain of a representative non human primate. The images were obtained by SRTM and by Logan DVR approach using ARIS software.

In vivo comparison of 18F-T807 in the normal rat brain and in various rat models of sporadic and familial tauopathy using PET

N. Van Camp[1-2], E. Diguet[3], D. Chéramy[3], K. Cambon[1-2], M. Guérif[3], L. Eymin[1-2], Y. Bramoullé[1-2], M. d'Orange[1-2], M.Guillermier[1-2], G. Auregan[1-2], C. Joséphine[1-2], N. Dufour[1-2], M.-C. Gaillard[1-2], Anne-Marie Chollet[3], A.P. Bemelmans[1-2], P. Hantraye-[1-2]

[1] Commissariat à l'Energie Atomique et aux Energies Alternatives (CEA), Département des Sciences du Vivant (DSV), Institut d'Imagerie Biomédicale (I2BM), MIRCen, F-92260 Fontenay-aux-Roses, France; [2]Centre National de la Recherche Scientifique (CNRS), Université Paris-Sud, Université Paris-Saclay, UMR 9199, Neurodegenerative Diseases Laboratory, F-92260 Fontenay-aux-Roses, France; [3] Institut de Recherches Servier, DRD-RDNPS, 125 chemin de ronde, 78 290 Croissy sur Seine, France.

Introduction: Validation of radioligands specifically interacting with pathological tau-proteins is challenging due to the existence of different tau isoforms and the co-existence of tau with other protein aggregates, such as amyloid-β deposits. A high *in vivo* selectivity and affinity of the tau ligands is thus required. ^{18}F-T807 seemed to fulfill these conditions with a selectivity 25 fold higher for Tau aggregates than amyloid-β and no white matter retention; though recently some undefined off-target binding has been reported.

We created a rat model of tauopathy by intracerebral injection of AAV vectors that overexpress either the human mutant h1N4R-P301L-Tau or the WT h1N4R together with a pro-aggregating peptide. Histological staining on these models showed that the rat brains were positive for pathological Tau-aggregation as soon as one month after vector induction. This model allows the evaluation of the binding characteristics of Tau-ligands in an *in vivo* setting in the absence of any other confounding pathological protein aggregate. In addition, as Tau-aggregation is only induced after vector induction, the off-target, or non-specific, uptake of the ligand can be evaluated in the same, healthy brain before vector injection.

Methodology: 16 rats underwent successively T_2-weighted MR-imaging on an 11.4T Bruker scanner and a ^{18}F-T807 PET scan on a FOCUS220 scanner, before being injected with either one of two vectors. One month after surgery, all animals underwent the same imaging procedure and were sacrificed after the last PET scan. 3 control sham groups have been included in the study and are subjected to the similar imaging and handling procedures: one group (n=3) has not undergone any surgery between the two imaging sessions; another group has been injected with PBS; and the last group has been injected with a vector encoding GFP. PET images are co-registered to the corresponding T_2-weighted MR-images, and used for segmentation of anatomical regions of interest. ^{18}F-T807 uptake is expressed in SUV ratios, relative to the cerebellar uptake. After imaging, brains are immunostained for the detection of early (AT8), and late (AT100) tau pathology and amyloid-b deposition; in addition CSF samples will be analyzed for the presence of soluble Tau. In vitro data will finally be correlated to the *in vivo* PET data.

Results: In the healthy rat brain, ^{18}F-T807 showed a homogeneous brain distribution without any retention in myelin-rich regions. Surprisingly a global increased brain uptake of ^{18}F-T807 was observed in both rat models of tauopathy, which showed an important and progressive AT8 immunoreactivity but restricted to only the injected regions. PET imaging and analysis are still ongoing on the 3 control groups to define the test-retest variability and non-specific *off-target* binding.

Conclusion: We choose ^{18}F-T807 to evaluate Tau-pathology in viral vector induced models. We demonstrated increased radioligand binding, which was however not restricted to the Tau-overexpressing brain regions. Correlative PET-histological analyses are still ongoing to assess the ability of these ligands to detect post-translational and conformational changes in tau protein species.

Changing Hardware: Quantification of H$_3$ Receptor Radioligand [11C]GSK189254 in Human Brain Revisited.

Rusjan PM[1,2], Sabioni P[1,2], Di Ciano P[1,2], Mansouri E[1,2], Houle S[1,2], Wilson AA[1,2], Boileau I[1,2], Leveillé A[3], Capet M[3], Duvauchelle T[3], Schwartz JC[3], Le Foll B[1,2]

[1]*PET Centre. CAMH. Toronto. ON. Canada;* [2]*University of Toronto. ON. Canada;* [3]*Bioprojet, Paris, France*

PET is the gold standard to investigate brain chemistry in living humans. While accurate quantification relies on robust kinetic modelling, limitations still exist to translate the use of a radioligand to a new environment such as different scanner, radiochemistry suite or quantification hardware (eg ABSS). [11C]GSK189254 is a H$_3$ receptor antagonist which showed favorable selectivity and uptake in vivo human brain[1]. Total distribution volume (V_T), estimated with the 2 Tissue Compartment Model (2TCM), was the preferred quantification parameter. Unusual high values of K_1 was purported to arise from dispersion in a long arterial line. The suggested implementation of the 2TCM required including dispersion as a variable within the kinetic equation, and coupling V_{nd} and k_4 across regions of interest (ROIs) [1]. In the present work, we revised the quantification of [11C]GSK189254 with a different experimental setup.

Methods: Five healthy subjects (age:19-32) were scanned in a High Resolution Research Tomograph (HRRT) for 90 min after receiving an i.v. bolus injection of [11C]GSK189254 (337±51 MBq, 2.7±0.4 µg). Subjects were scanned twice within 33±16 days in the placebo condition, and 3 hours after an oral dose (40 mg) of the H$_3$ inverse agonist Pitolisant. Automatic arterial sampling was effected with an ABSS, Model #PBS-101(Veenstra Instruments) using a PTFE line (100 cm, ⌀=1 mm) at a rate of 350 mL/hour for the first 7.25 min. Manually collected blood samples were centrifuged and radioactive metabolites assayed using a solid-phase cartridge method. ROIs were automatically delineated on a co-registered MRI[2]. (c.f with methods in [1]).

Results: A Hill function describe the slow metabolization (ca. 5-10% after 90 min) when the radiochemistry purity was >99%. Input function was not different between blocked and unblocked conditions. Dispersion was estimated 5±2 sec using the beginning of the head curve[3] (cf. ~40sec in [1]). Time-activity curves (TACs) in the blocked condition showed a peak (2.5-3.1 SUV) followed by a washout (1.2-2.7 SUV at the end of the scan). The TACs did not show washout at any time in the baseline. Overall, an unconstraint 2TCM fitted the TACs better than a 1TCM. K_1 values were 0.29±0.06 ml/cm^3/min. Explicit inclusion of dispersion as previously proposed was not necessary. Frequently V_T in the baseline condition did not present identifiability in striatal areas. Regional V_T values in the baseline (ranging from 10 to 60 ml/cm^3) were lower than in[1]. Lassen plots presented excellent linearity and the Pitolisant occupancies (83±11%) were robust to the subset of ROI chosen. V_{nd} calculated from Lassen plot was 3.6±2.0 ml/cm^3. Coupling V_{nd} between ROIs, or fixing V_{nd} in the baseline condition to the value from the blocked scan did not impact on the occupancy estimations.

Conclusion: Data acquisition in a different environment (i.e. scanner/hardware) may require to adjust the optimal method for quantification of radioligands. The new protocol for [11C]GSK189254 acquisition helps to overcome some of the methodological challenges previously identified. Despite the lack of washout of the TACs in the baseline condition, the [11C]GSK189254 can give robust occupancies. Potential mass effects are under investigation.

References:
1. Ashworth S et al. J Nucl Med. 2010 Jul;51(7):1021-9
2. Rusjan PM et al, Psychiatry Res. 2006 Jun 30;147(1):79-89
3. Rusjan PM et al, J Cereb Blood Flow Metab. 2011 Aug;31(8):1807-16

Quantitative measurement of 5HT6 and 5HT2A Occupancy by SYN120 using [11C]GSK215083 and Dynamic Modeling of PK-RO Relationships

Dean F Wong[1], Hiroto Kuwabara[1], Uwe Meya[2], James Brasic[1], Ann Neale[2], William Willis[1], Emily Gean[1], Lesley Pickford[2], Anil Mathur[1], Cristian Salinas[3], Graham Searle[3], Stephen Bandak[2], Maria Thomas[1], Eugenii A Rabiner[3,4], Roger N Gunn[3,5]

Johns Hopkins University, Baltimore (JHU)1, Biotie2, Imanova Ltd, London, UK3, King's College, London, UK4, Imperial College London, London, UK5

Treatments for Alzheimer's disease (AD) including anticholinergic and anti-amyloid have been mixed and disappointing. One novel approach includes dual antagonism of the 5HT6 and 5HT2a receptor, which in preclinical models demonstrates greater pro-cognitive activity than antagonism at either receptor alone. Target engagement with such a dual antagonist, SYN120 (pKi 9.6 5HT6; pKi 7.8 5HT2A) was evaluated with PET using [11C]GSK215083 at 3 and 27 hours following a single oral dose (10 – 300 mg) in 9 healthy male subjects aged 18 – 54 yrs. Dynamic PET scans were carried out on a High Resolution Research Tomograph (HRRT) at JHU for 90 min following an IV bolus of [11C]GSK215083 (injected dose: 680 + 33 MBq, injected mass:1.4 + 0.48 ug). Radial arterial blood was collected during all PET scans and a metabolite corrected arterial plasma input function generated.

Four tracer kinetic models using arterial input were employed including 1 tissue (1TCM), 2 tissue unconstrained (2TCM-UC), constrained to K1/k2 of the cerebellum (2TCM-C) and Plasma Reference Graphical Analysis (PRGA) to derive outcome measures of VT and BPND. 5HT6 receptor occupancy (RO) was obtained from caudate and putamen, and 5HT2A RO from the frontal cortex. The plasma SYN120 PK data was fitted to a first order absorption elimination model and the RO data was then fitted to direct and indirect PK-RO models (Abanades et al, 2011; Salinas et al, 2013). The indirect model accounts for a dynamic lag between plasma and target receptor bound concentrations of the drug. VT in cerebellum was not changed between baseline and post-dose scans enabling its use as a reference region. Akaike Information Criteria supported 2TCM-C over 1TCM. However, both 2TCM models yielded outliers (defined as: VT>10 mL/mL; BPND > 5; eg, 5.5% of regions were outliers 2TCM-UC), and showed higher inter-subject variations than PRGA. PRGA plots from 40 minutes onwards showed excellent linearity (R2 > 0.97 in all regions). Therefore, PRGA was selected as the method for estimating BPND and calculating RO.

For PK-RO modeling, model selection criteria identified the indirect PK-RO model (parameters: Emax, koff and EC50) as the optimal model for the 5HT6 data (putamen: Emax of 86% and SYN120 EC50 of 6.9 ng/ml). A direct relationship with a floating Emax was identified as the optimal model for the 5HT2 data (frontal cortex: Emax of 69% and SYN120 EC50 of 78.7± 22.6 ng/ml). Thus, the in vivo SYN120 selectivity ratio for 5HT6:5HT2A was ~12.5. The fitted PK-RO models where then applied to SYN120 PK simulations to demonstrate that 80% RO at 5HT6 and 5HT2a would be achieved by 4.5 mg and 93 mg repeated daily dosing respectively.

In summary, this demonstrates the value of multiple measures of RO at different time points along with the application of PK-RO models to quantify target engagement of SYN120 at the 5HT6 and 5HT2A receptor in the human brain.

Age and BMI related findings using the PET tracer [11C]PBR28 in healthy volunteers

Rohit Gudepu[1], Venkatesh Sreeram[1], Jean-Dominique Gallezot[1], Brian Pittman[2], Christine M. Sandiego[1], Nabeel Nabulsi[1], Yiyun Huang[1], Ming-Kai Chen[1], Irina Esterlis[1,2], Richard E Carson[1], Kelly Cosgrove[1,2], David Matuskey[1,2]

[1]Department of Radiology and Biomedical Imaging, Yale University, New Haven, CT 06520; [2]Department of Psychiatry, Yale University, New Haven, CT 06519

Background: [11C]PBR28 is a positron emission tomography (PET) tracer that measures the 18 kDa translocator protein (TSPO), a putative neuroinflammatory marker. TSPO is a transmembrane protein involved in a variety of routine cellular functions (e.g., mitochondrial cholesterol transport) and is located in a variety of tissues like microglial and adipose cells. The human brain normally contains low TSPO expression, whereas increased expression is seen in neuroinflammatory and neurodegenerative disorders and has been shown to be derived primarily from activated microglia. Aging studies have employed different TSPO tracers and although there have been mixed results, the majority have shown no significant increase in neuroinflammation with age (Debruyne et al., 2003; Kreisl et al., 2013; Yasuno et al., 2008; Suridjan et al., 2014; Kumar et al., 2012). To date, however, limited data are available on the effect of body mass index (BMI) on TSPO binding in humans (Hannestad et al., 2013; Setiawan et al., 2015). Our study sought to evaluate potential age and BMI related changes in activated microglial cells *in vivo* measured with [11C]PBR28 PET in the human brain.

Materials and Methods: Twenty-five healthy volunteers (9 females, 16 males; age range 19-55, BMI range 20-37) were scanned with [11C]PBR28 using a High Resolution Research Tomograph (HRRT). Based on the known effects of TSPO genotype on [11C]PBR28 binding, high affinity binders (HABs; N=13) or mixed affinity binders (MABs; N=12) (Guo et al., 2012) were included in the current work. Both groups were examined separately and then together after being genotype-adjusted. Regions of interest (ROIs) were mapped from Montreal Neurological Institute (MNI) template space to PET space to compute tissue time-activity curves (TACs). TACs were analysed based on the multilinear analysis (MA1) model, using the metabolite-corrected arterial plasma activity curve as input function to estimate the volume of distribution (V_T, ml/cm^3) in each ROI. Global brain uptake was assessed and consisted of the average V_T across the amygdala, anterior cingulate cortex, caudate, hippocampus, hypothalamus, pallidum, putamen, thalamus, and the frontal, occipital, parietal, and temporal cortices.

Results: Global brain [11C]PBR28 uptake did not show a significant correlation with age in the HABs (r= -0.378, p= 0.20), MABs (r= 0.323, p= 0.30), or genotypically adjusted whole cohort (r= -0.064, p= 0.76). No individual ROIs were found to be significant with age. BMI and [11C]PBR28 V_T globally showed no correlations in the HABs (r= -0.381, p= 0.19), but a negative correlation was seen in MABs (r= -0.63, p= 0.02) and the genotypically adjusted whole cohort (r= -0.44, p= 0.03). All individual ROIs were significant or near-significant in the latter two analyses (not corrected for multiple comparisons).

Conclusion: In accordance with the majority of the previous studies examining TSPO, our current results suggest there are no significant age-related changes in neuroinflammatory markers as measured by [11C]PBR28 binding. A significant decrease was found, however, in the brain globally with [11C]PBR28 V_T and BMI in the MAB and genotypically adjusted cohort. Given the importance of TSPO on lipid and cholesterol metabolism, these novel results warrant further studies for validation.

References:

1. Debruyne, J.C., Versijpt, J., Van Laere, K.J., De Vos, F., Keppens, J., Strijckmans, K., Achten, E., Slegers, G., Dierckx, R.A., Korf, J., De Reuck, J.L., 2003. PET visualization of microglia in multiple sclerosis patients using [11C]PK11195. European Journal of Neurology 10, 257-264.
2. Guo, Q., Owen, D.R., Rabiner, E.A., Turkheimer, F.E., Gunn, R.N., 2012. Identifying improved TSPO PET imaging probes through biomathematics: The impact of multiple TSPO binding sites in vivo. Neuroimage 60, 902-910.
3. Hannestad, J., DellaGioia, N., Gallezot, J.D., Lim, K., Nabulsi, N., Esterlis, I., Pittman, B., Lee, J.Y., O'Connor, K.C., Pelletier, D., Carson, R.E., 2013. The neuroinflammation marker translocator protein is not elevated in individuals with mild-to-moderate depression: a [(1)(1)C]PBR28 PET study. Brain Behav Immun 33, 131-138.
4. Kreisl, W.C., Jenko, K.J., Hines, C.S., Hyoung Lyoo, C., Corona, W., Morse, C.L., Zoghbi, S.S., Hyde, T., Kleinman, J.E., Pike, V.W., McMahon, F.J., Innis, R.B., the Biomarkers Consortium, P.E.T.R.P.T., 2013. A genetic polymorphism for translocator protein

18 kDa affects both in vitro and in vivo radioligand binding in human brain to this putative biomarker of neuroinflammation. Journal of Cerebral Blood Flow & Metabolism 33, 53-58.

5. Kumar, A., Muzik, O., Shandal, V., Chugani, D., Chakraborty, P., Chugani, H.T., 2012. Evaluation of age-related changes in translocator protein (TSPO) in human brain using 11C-[R]-PK11195 PET. Journal of Neuroinflammation 9, 1-11.

6. Setiawan, E., Wilson, A.A., Mizrahi, R., et al., 2015. ROle of translocator protein density, a marker of neuroinflammation, in the brain during major depressive episodes. JAMA Psychiatry 72, 268-275.

7. Suridjan, I., Rusjan, P.M., Voineskos, A.N., Selvanathan, T., Setiawan, E., Strafella, A.P., Wilson, A.A., Meyer, J.H., Houle, S., Mizrahi, R., 2014. Neuroinflammation in healthy aging: A PET study using a novel Translocator Protein 18 kDa (TSPO) radioligand, [18F]-FEPPA. Neuroimage 84, 868-875.

8. Yasuno, F., Ota, M., Kosaka, J., Ito, H., Higuchi, M., Doronbekov, T.K., Nozaki, S., Fujimura, Y., Koeda, M., Asada, T., Suhara, T., 2008. Increased Binding of Peripheral Benzodiazepine Receptor in Alzheimer's Disease Measured by Positron Emission Tomography with [11C]DAA1106. Biological Psychiatry 64, 835-841.

Investigating Simultaneous Estimation for the Full Quantification of [11C]ABP688 PET Data

Samantha Rossano[1,2], Francesca Zanderigo, PhD.[3], Ramin Parsey, MD, PhD.[1], Christine DeLorenzo, PhD.[1,3]

[1]Stony Brook University Departments of Psychiatry and [2]Biomedical Engineering, Stony Brook University, Stony Brook, NY; [3]Department of Molecular Imaging and Neuropathology, New York State Psychiatric Institute and Columbia University, New York, NY

Introduction: Full quantification of PET data requires the placement of an arterial line for continuous arterial sampling in order to measure an arterial input function (AIF). Simultaneous Estimation (SIME) can be used to impute the AIF using PET data and a single arterial blood sample. SIME has been investigated for application with several PET tracers [1] and upgraded to use with no required blood sample for two tracers [2, 3]. Therefore SIME has the potential to provide full PET quantification with reduced burden on subjects. The purpose of this study is to investigate the performance of SIME with [11C]ABP688, a PET tracer that binds to the metabotropic glutamate receptor, subtype 5 (mGluR5) [4], and a single arterial sample.

Methods: Arterial radioactive counts and metabolite values were collected for 15 subjects during a PET scan with [11C]ABP688. The total Volume of Distribution (V_T) of the tracer [5] was calculated via kinetic analysis of the time activity curves assuming a two-tissue compartment model and using both the traditional quantification with AIF and the SIME algorithm with a single sample of arterial input data. Four time points were considered for the blood sample: 4, 12, 30, and 60 minutes after tracer injection. V_T values calculated using SIME in ten regions of interest (amygdala, anterior cingulate, dorsal caudate, dorsal putamen, cerebellum, hippocampus, medial prefrontal cortex, orbital prefrontal cortex, parietal lobe, ventral striatum) were plotted against the values obtained using the fully-sampled AIF in each study, and the correlation and regression analysis obtained. Additionally, their percent differences (PD) were calculated as PD= |(V_T (full AIF) − V_T (SIME))|/(V_T (full AIF))*100.

Results: The lowest PD value corresponds to SIME using the arterial sample from the 12-minute time point: the average (+/- one standard deviation) PD is 19.97% (+/- 18.01%) across the 15 subjects. The second lowest PD value corresponds to SIME using the sample at 30 minutes, with an average PD of 67.81% (+/- 16.31%). The results of the regression analysis of the 12- and 30- minute results shows a high correlation between measures from SIME compared to the corresponding measures from AIF, though with a bias (Figure 1).

Discussion and Conclusion: Results suggest that SIME may cause a bias in outcome measure estimation for [11C]ABP688 with respect to the quantification with fully-sampled AIF. However, using SIME with arterial samples at certain time points provides estimates that are highly correlated. Future work will include further optimization of SIME for [11C]ABP688 (e.g., different model for the input function, optimized boundaries for the free-parameters, potential bias prediction), as well as investigation of the possibility of replacing the single arterial blood sample with a venous blood sample.

References:
1. Ogden, R.T., et al., J Cereb Blood Flow Metab, 2010. 30(4): p. 816-26.
2. Zanderigo, F., R.T. Ogden, and R.V. Parsey,   J Cereb Blood Flow Metab, 2015. 35(1): p. 148-56.
3. Mikhno, A., et al., IEEE J Biomed Health Inform, 2015.
4. DeLorenzo, C., et al., J Cereb Blood Flow Metab, 2011. 31(11): p. 2169-80.
5. Innis, R.B., et al., J Cereb Blood Flow Metab, 2007. **27**(9): p. 1533-9.P-073
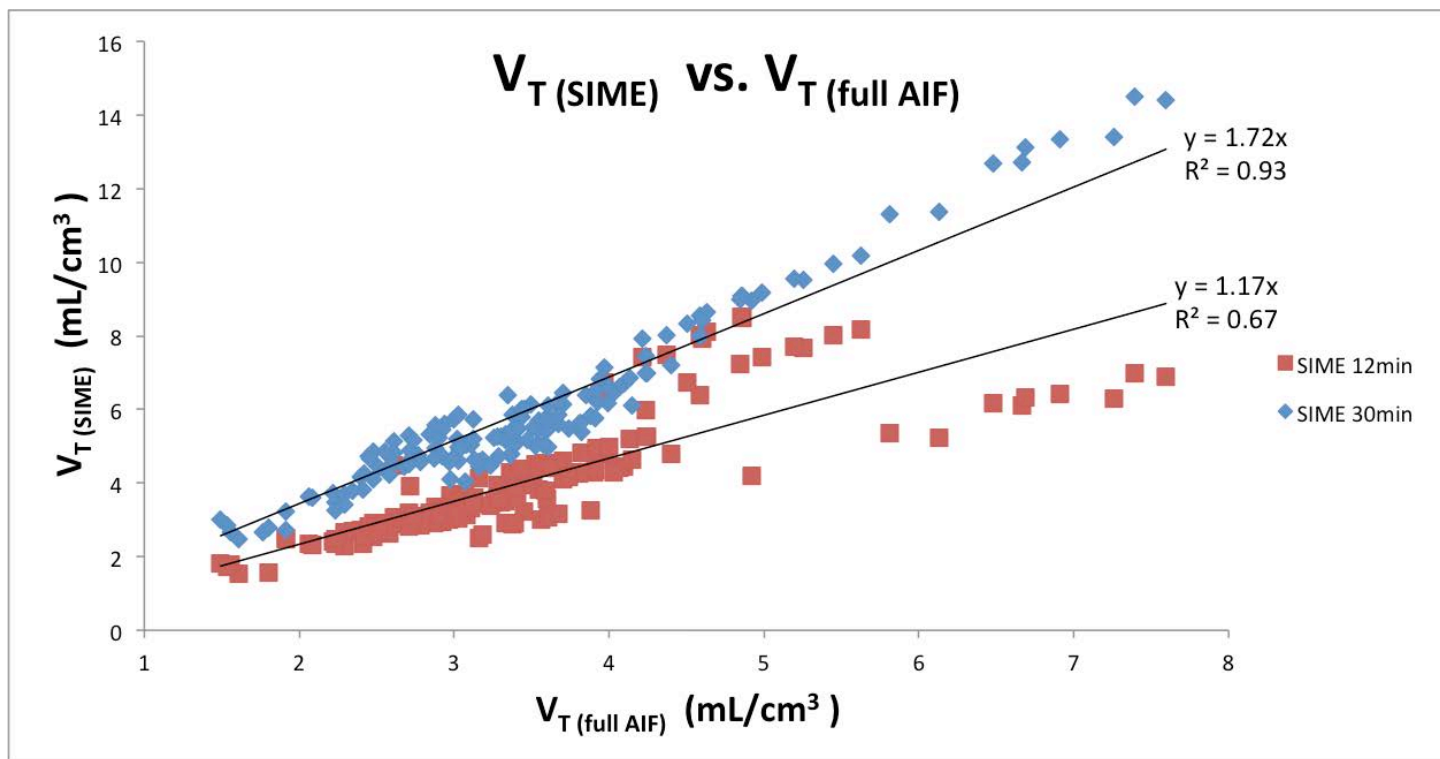
Figure 1: V_T values estimated with SIME using a single arterial samples acquired at either 12 (red) or 30 (blue) min vs. V_T values calculated with full arterial sampling for all regions across all subjects.

Optimal timing of tau pathology imaging using [^{18}F]THK5317

Mark Lubberink[1,3], My Jonasson[1,3], Anders Wall[1,4], Konstantinos Chiotis[5], Laure Saint-Aubert[5], Gunnar Antoni[2,4], Agneta Nordberg[5]

[1]*Department of Surgical Sciences and* [2]*Pre-clinical PET platform, Uppsala University, Uppsala, Sweden;* [3]*Medical Physics and* [4]*PET Centre, Uppsala University Hospital, Uppsala, Sweden;* [4]*Department of Neurobiology, Care Sciences and Society, Karolinska Insitutet, Stockholm, Sweden;* [5]*Department of Geriatric Medicine, Karolinska University Hospital, Stockholm, Sweden*

Rationale: Use of tau imaging in clinical practice for diagnostic purposes, study of disease progression and evaluation of drug treatment effects with PET is facilitated by short static scans and simplified analysis methods. Previous studies, however, have shown a poor correlation between static standardized uptake value ratio (SUVR) at various late time intervals and binding potential BP$_{ND}$ based on dynamic scans with [^{18}F]THK5317 in AD patients[1]. The optimal time for assessment of SUVR is at peak specific binding, or transient equilibrium (TE), when theoretically SUVR-1 equals BP$_{ND}$. The aim of the present work was to determine time to TE for various brain tissues and the optimal time window, including at TE for each individual tissue, for measurement of SUVR of [^{18}F]THK5317.

Methods: Data from seven AD patients and five healthy controls (HC) were used. Each subject underwent a 90 min dynamic PET scan after injection of 3 MBq/kg [^{18}F]THK5317 on an ECAT Exact HR+ scanner. Volumes of interest (VOIs) were placed using a probabilistic atlas (PVElab). DVR-1 values were calculated using the reference Logan method (30-90 min) with cerebellar grey matter as reference tissue. For each VOI, the time at which TE occurred was determined as the peak of the specific binding curve, calculated by subtraction of the cerebellum TAC from the VOI TAC. SUVR-1 was calculated for all VOIs at their respective TE time (SUVR$_{TE}$-1) and for 7 different 20 min intervals between 10 and 90 min p.i.. Correlation and agreement between SUVR values and DVR-1 were calculated by linear regression and Bland-Altman analysis.

Results: In AD patients, TE was reached first in putamen, at 18±3 min, and last in sensorimotor cortex at 48±19 min (mean±SD). In HC, TE was reached first in putamen and temporal cortex, at 17±4 min, and last in sensorimotor and occipital cortex at 81±6 and 83±6 min. In AD, TE in temporal cortex was reached at 24±3 min. Mean time to TE across the whole brain was 29±4 min in AD and 40±5 min in HC (p<0.05). Over all regions and subjects, SUVR$_{20-40}$-1 correlated best with DVR-1 for both HC and AD (R^2 0.98 for both) and showed the lowest mean bias for all fixed interval SUVR (3% and 4%, respectively). Use of SUVR$_{TE}$-1 resulted in somewhat lower correlations with DVR-1 (R^2 0.87 and 0.86 in HC and AD), but in the smallest bias (-0.1%) in AD patients.

Conclusion: The highly varying time to TE across the brain and between AD and HC groups complicates the definition of a static scan interval. Overall, [^{18}F]THK5317 SUVR-1 values correlated and agreed best with DVR-1 values for the 20-40 min interval, both in AD and HC. Although use of SUVR values at TE for each individual VOI leads to better agreement with DVR-1 in AD patients, correlation with DVR-1 was worse than for SUV$_{20-40}$ and SUVR at an early fixed interval is preferred in terms of feasibility and robustness. SUVR$_{20-40}$ allows for optimal semi-quantitative assessment of tau pathology a single clinically feasible 20 min scan.

References:

1. Jonasson et al, J Nucl Med 2016
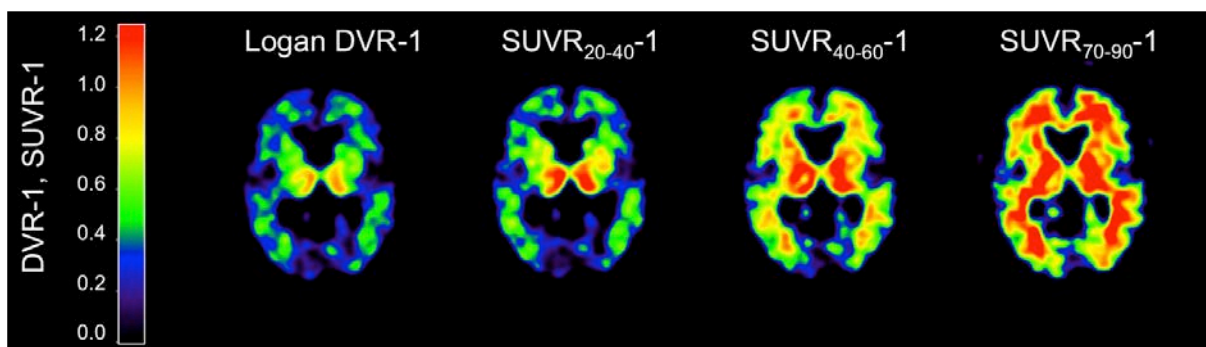
[^{18}F]THK5317 Logan DVR-1 and SUVR-1 images for the 20-40, 40-60 and 70-90 min intervals in a typical AD patient.

Development and initial preclinical evaluation of a novel dual P-gp and BCRP substrate

Verbeek J[1], De Cleyn M[2], Gijsen H[2], Sinha V[2], Mannaert E[2], Mannens G[2], Haspeslagh P[1], Dubois K[2], Schmidt M[2], Andres J.I[2], Koole M[3], Bormans G[1].

[1]Laboratory for Radiopharmacy KU Leuven, Belgium, [2]Janssen Research & development, Belgium, Spain & USA, [3]Nuclear medicine & Molecular imaging, University hospitals Leuven, Belgium.

Introduction: Currently potential CNS drugs are discarded in an early stage of development, if the compound appears to be a substrate for either P-gp (p-glycoprotein) and/or BCRP (breast cancer resistant protein), while it still might be reaching a pharmacologically relevant concentration in the brain. To obtain a better understanding, and to be able to discriminate early on in research, [11C]JVGB a dual P-gp and BCRP substrate was developed and preclinically evaluated *in vivo* for future comparison with early *in vitro* preclinical data.

Results/discussion: [11C]JVGB was synthesized by methylation of 1.3 µmol of its precursor with [11C]methyl triflate in the presence of 7 µmol K_2CO_3 in 0.5 mL DMF 4 minutes at 65 °C, to yield 44 ± 22% of [11C]JVGB with a specific activity of 118 ± 63 GBq/µmol.
Radiometabolite analysis of plasma from healthy Wistar rats (N=2), showed that 57 ± 12% of parent tracer was still intact 30 min p.i., thus showing moderate stability in vivo.
Next 34 ± 6 MBq of [11C]JVGB was administered in 4 groups of Sprague Dawley rats: P-gp knockout (KO), BCRP KO, P-gp/BCRP double KO and wild type rats (N=3 per group), and a PET scan was performed during 90 min, blood samples were taken at 10, 20 and 45 minutes after tracer injection. The brain uptake is shown in Figure 1, with a higher brain uptake for the P-gp/BCRP double knockout when compared to both single knockout groups and the wild-type group. The brain uptake 45 min after injection depicted in SUV is 0.32 ± 0.04 (P-gp KO) 0.23 ± 0.05 (BCRP KO), 0.70 ± 0.04 (P-gp KO/BCRP KO) and 0.22 ± 0.01 (wild type). The blood concentration depicted in SUV after 45 minutes is 0.63 ± 0.11, 0.55 ± 0.11, 0.69 ± 0.18 and 0.51 ± 0.07 for the P-gp KO, BCRP KO, P-gp KO/BCRP KO and wild type respectively, and shows no statistical significant differences, thus the higher brain uptake for the P-gp KO/BCRP KO is not due to a change of tracer influx, but due to the lack of both efflux transporters. When lacking only one transporter (P-gp or BCRP), the other transporter appears to be able to maintain a low brain concentration.

Conclusion: [11C]JVGB can be synthesized using [11C]methyl triflate in good yields, shows moderate *in vivo* stability and appears to be a substrate PET tracer for both P-gp and BCRP.
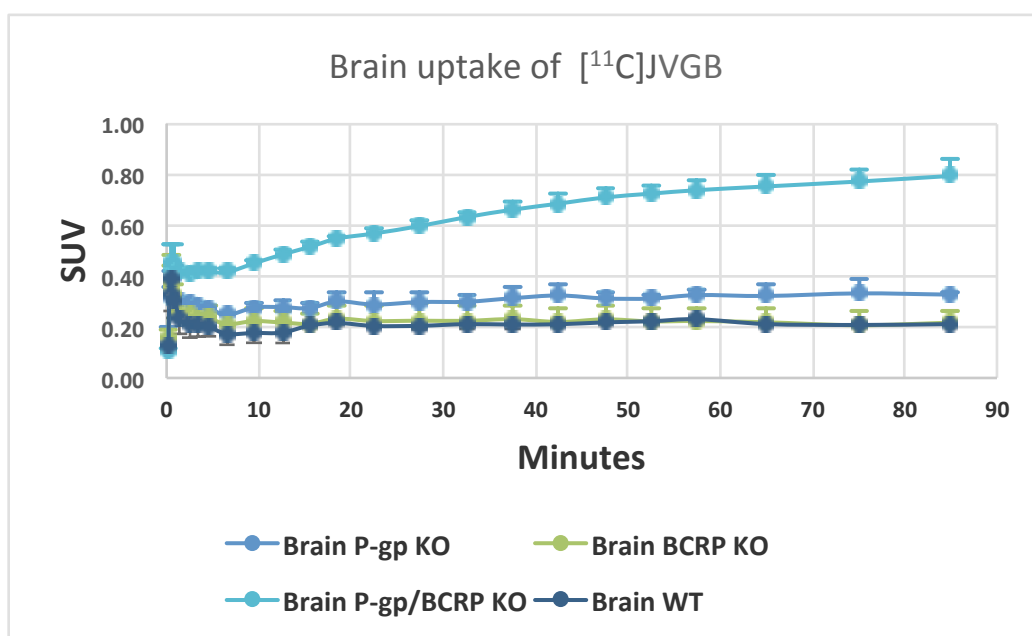
Figure 1: Brain uptake of [11C]JVGB in different groups of Sprague Dawley knockout rats (N=3).

The serotonin-1B receptor and personality: a positron emission tomography study in control subjects

Rosén G, Varrone A, Plavén-Sigray P, Borg J, Cervenca S, Varnäs K, Nord M, Tiger M, Farde L, Lundberg J.

PET-center, Dept Clin Neuroscience, Karolinska Institutet.

Background: The serotonin 1B receptor (5-HT$_{1B}$ receptor) has been suggested to be of central interest in the regulation of animal and human behavior. Briefly, studies in rodents suggest that a ubiquitous low expression of 5-HT$_{1B}$ receptors is associated with substance abuse, increased impulsive and aggressive behaviour and reduced social reward. Moreover, a low 5-HT$_{1B}$ receptor expression in the Nucleus Accumbens is coupled to impulsive behaviour and a low expression in the FC is coupled to aggressive behaviour[1–3].

Aims: The aim of this study was to examine the relationship between 5-HT$_{1B}$ receptor binding in the central nervous system and personality traits of healthy subjects, using positron emission tomography (PET) and the radioligand [11C]AZ10419369, and assessments of personality with the Swedish Universities Scales of Personality.

Materials and Methods: 35 subjects (F:M 13:22) were examined with the High Resolution Research Tomograph (HRRT) and the 5-HT$_{1B}$ receptor selective radioligand [11C]AZ10419369[4]. PET data acquisition time was 63 or 93 minutes. Injected dose was 285 – 424 MBq. The specific activity was >85 GBq/µmol. Regions of interest (ROIs) for frontal cortex (FC), putamen (PUT), ventral striatum (VSTR) and cerebellum, which was used as a reference region for the determination of nondisplaceable radioligand binding, were defined on magnetic resonance images (MRIs) using the automated anatomic labelling template[5]. MRI data were coregistered to PET data using SPM5. Specific radioligand binding was quantified using the Simplified Reference Tissue Model (SRTM)[6]. Binding Potential (BP$_{ND}$) was the parameter of interest. The personality was determined using the Swedish Universities Scales of Personality questionnaire[7]. In order to control for effects of age and sex, the regression was performed with a stepwise method. Predictors were included in the order of the significance level of the regression coefficient, starting with the most significant. Correlations between [11C] AZ10419369 BP$_{ND}$ and scores of the personality questionnaires were reported as adjusted R^2. The linear relationship between each predictor and the dependent variable was calculated and reported as standardized coefficient beta.

Results: The highest [11C] AZ10419369 BP$_{ND}$ was found in VSTR (mean=1.98, std SD=0.33, range=1.29) followed by FC (mean=1.58, SD=0.34, range=1.32) and PUT (mean=1.07, SD=0.16, range=0.73). Age was not normally distributed (kurtosis = -1,8). All other variables showed an acceptable normal distribution. Age and [11C]AZ10419369 binding in the frontal cortex and verbal trait aggression showed a positive relationship (standardized coefficient beta=0.270, P=0.044) as did binding potential in ventral striatum and impulsivity (standardized coefficient beta=0.263, P=0.048).

Conclusions: The results of this study are supported by previous studies in mice, although the relationship was opposite to the relationship that was found in this study. This could in part be explained by that the mice natural behaviour in these regards differs significantly from humans. The fact that PET-examination does not allow differentiation between hetero and auto receptors could also partially explain the differences, as they played different roles for the behavioural phenotype according to the data from mice studies. The interpretation of data should be cautious before a replication in a larger sample is reported.

References:
1.Crabbe, J. C. *et al.* Elevated alcohol consumption in null mutant mice lacking 5-HT1B serotonin receptors. *Nat. Genet.* **14,** 98–101 (1996).
2.Dölen, G., Darvishzadeh, A., Huang, K. W. & Malenka, R. C. Social reward requires coordinated activity of nucleus accumbens oxytocin and serotonin. *Nature* **501,** 179–184 (2013).
3.Nautiyal, K. M. *et al.* Distinct Circuits Underlie the Effects of 5-HT1B Receptors on Aggression and Impulsivity. *Neuron* **86,** 813–826 (2015).
4.Varnäs, K. *et al.* Quantitative analysis of [11C]AZ10419369 binding to 5-HT1B receptors in human brain. *J. Cereb. Blood Flow Metab. Off. J. Int. Soc. Cereb. Blood Flow Metab.* **31,** 113–123 (2011).

5.Tzourio-Mazoyer, N. *et al.* Automated anatomical labeling of activations in SPM using a macroscopic anatomical parcellation of the MNI MRI single-subject brain. *NeuroImage* **15,** 273–289 (2002).

6.Lammertsma, A. A. & Hume, S. P. Simplified reference tissue model for PET receptor studies. *Neuroimage* **4,** 153–8. (1996).

7.Gustavsson, J. P. *et al.* Swedish universities Scales of Personality (SSP): construction, internal consistency and normative data. *Acta Psychiatr. Scand.* **102,** 217–225 (2000).

Region	Model	Adjusted R² (predictor)	Std. Error of the estimate	Sig.	Standardized coefficient beta (predictor)	Significance	Tolerance
frontal cortex	1	0,56 (age)	0,23	< 0,001	-0,76 (age)	< 0,001	1,00
frontal cortex	2	0,60 (age and verbal trait agression)	0,22	< 0,001	-0,61 (age)	< 0,001	0,70
frontal cortex	2				0,27 (verbal trait agression)	0,044	0,70
ventral striatum	1	0,40 (age)	0,26	< 0,001	-0,65 (age)	< 0,001	1,00
ventral striatum	2	0,46 (age and impulsivity)	0,25	< 0,001	-0,61 (age)	< 0,001	0,98
ventral striatum	2				0,26 (impulsivity)	0,048	0,98

Table 1. Model summary with frontal cortex and ventral striatum as dependent variable. Description of the adjusted R2, standard error of the estimate and significance of two different models of the multiple regression. In both models [11C]AZ1041969 BPND in the frontal cortex was used as a dependent variable. In model 1 age was used as predictor. In model 2, age and verbal trait aggression were used as predictors. Description of the direction and magnitude of the relationship between [11C]AZ1041969 BPND in the frontal cortex and the predictors of two different models expressed as standardized coefficient beta.

Preclinical evaluation of the PDE2A tracer [^{18}F]PF-05270430 in healthy rats

Matusiak N[1], Coello C[1], Plisson C[1], Wells L.A[1], Smyth E[1] and Tang S-P[1]

[1]*Imanova Limited, Burlington Danes Building, Imperial College London, Hammersmith Hospital, Du Cane Road, London, W12 0NN (UK)*

Objectives: Inhibition of Phosphodiesterase 2A (PDE2A) activity has been shown to improve cognitive performance in aged and Alzheimer's disease preclinical models [1]. The ability to image PDE2A availability non-invasively *in vivo*, using radiolabelled synthetic inhibitors, would support drug discovery efforts. [^{18}F]PF-05270430 (4-(3-[^{18}F]fluoroazetidin-1-yl)-7-methyl-5-[1-methyl-5-[4-(trifluoromethyl)phenyl]pyrazol-4-yl]imidazo[5,1-f][1,2,4]triazine) is the only specific PDE2A tracer available for PET [2]. [^{18}F]PF-05270430 has been already evaluated in non-human primates (NHP) and humans [3]. Our aim was to investigate this radioligand in healthy rats and compare the results obtained to those of NHP and humans.

Methods: [^{18}F]PF-05270430 (n = 2) was prepared by direct radiofluorination of the corresponding tosyl precursor in DMSO at 120 ^{0}C for 10 min. After injection of [^{18}F]PF-05270430 (10.8 ± 2.35 MBq, 0.083 ± 0.025 μg), male Sprague Dawley rats (n = 3) received a dynamic scan for 90 min with arterial blood sampling and metabolite analysis. Regions of interest were manually drawn in the striatum, a high PDE2A expressing region [4], and the cerebellum to generate the time-activity curves. Tissue kinetics were modelled using a one-tissue (1TCM) and a two-tissue compartment model (2TCM) to estimate the regional volume of distribution (V_T). A reference region approach was also investigated using the simplified reference tissue model (SRTM). Based on the reported NHP and human data, the cerebellum was considered as a suitable reference region to generate the non-displaceable binding potential (BP_{ND}).

Results: HPLC-purified [^{18}F]PF-05270430 was obtained in high chemical and radiochemical purity. The mean specific activity of [^{18}F]PF-05270430 was 113 ± 16 GBq/μmol (n = 2) at the end of synthesis. The average yield at the end of the radiosynthesis was 537 ± 56 MBq (n = 2). The total synthesis time including purification and formulation was around 90 min from the end of cyclotron bombardment. No solid phase extraction purification prior to semi-preparative HPLC was required, as previously reported [2]. A moderate rate of metabolism (47 ± 6 % at 20 min p.i.) was obtained, which is similar to that observed in NHP (53 ± 18 % at 30 min p.i.) and humans (55 ± 8 % at 30 min p.i.) [3]. In healthy rats, the striatum showed higher tracer uptake than the cerebellum as depicted in Figure 1. The 2TCM provided a better fit than the 1TCM based on the Akaike information criteria. BP_{ND} values in the striatum were 0.68 ± 0.31 for 2TCM and 0.62 ± 0.22 for SRTM. Striatal BP_{ND} values obtained in the rat were similar to those seen in humans (BP_{ND} 0.6-0.8) and two-to three-fold lower than in NHP (BP_{ND} 1.5-2). A time-stability assessment of the V_T showed that a stable measurement was achieved by 60 min.

Conclusion: These results demonstrate that [^{18}F]PF-05270430 is a suitable PET ligand to quantify PDE2A in rat brain. SRTM shows promising results as compared to the gold-standard arterial input function 2TCM. Further validation will assess specific binding in the cerebellum by a displacement protocol. [^{18}F]PF-05270430 PET in rodents could be a useful tool for the pharmacological characterization and evaluation of novel PDE2A inhibitors.

References:
[1] Heckman PR, Wouters C, Prickaerts J. Curr Pharm Des. 2015, 21, 317-31.
[2] Zhang L, Villalobos A, Beck EM et al. J Med Chem. 2013, 56, 4568-79.
[3] Naganawa M, Nabulsi N, Waterhouse R. J Nucl Med. 2013, 54 (Suppt 2):201.
[4] Stephenson DT. Neuroscience. 2012, 226, 145-155.
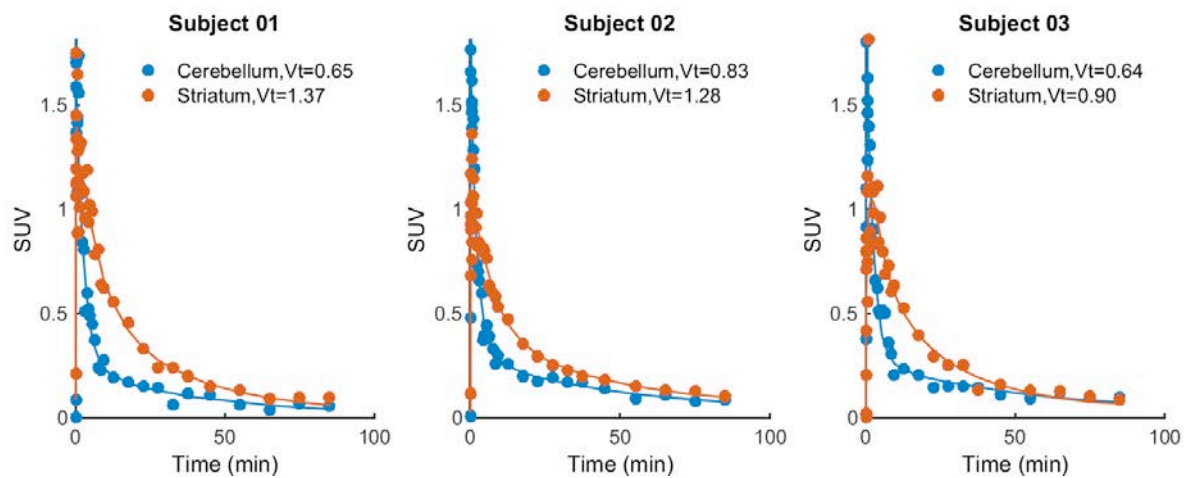
Figure 1: Striatum (red) and cerebellum (blue) time activity curves and 2TCM model fit of subjects 1 to 3. Volumes of distribution are reported in the legend for each ROI.

Association of Ventral Striatum Monoamine Oxidase-A Binding and Functional Connectivity in Antisocial Personality Disorder

Nathan J. Kolla, M.D., Ph.D.[1,2,3,4*], Katharine Dunlop, B.Sc.[4,5], Jonathan Downar, M.D., Ph.D.[3,4,5], Paul Links, M.D., M.Sc.[4,6], R. Michael Bagby, Ph.D.[1,3,7], Alan A. Wilson, Ph.D.[1,2,3,4], Sylvain Houle, M.D. Ph.D.[1,2,3], Fawn Rasquinha[1,2], Alexander I. Simpson, M.B.Ch.B.[3], Jeffrey H. Meyer, M.D., Ph.D.[1,2,3,4]

[1]CAMH Research Imaging Centre; [2]Campbell Family Mental Health Research Institute, CAMH; [3]Department of Psychiatry, University of Toronto; [4]Institute of Medical Science, University of Toronto; [5]University Health Network; [6]Department of Psychiatry, University of Western Ontario; [7]Department of Psychology, University of Toronto

*Corresponding author: Nathan J. Kolla, CAMH Research Imaging Centre, 250 College Street, Toronto, ON, Canada; phone: (416) 535-8501 ext. 34248; fax: (416) 979-6702; email: nathan.kolla@mail.utoronto.ca

Introduction: Impulsivity is a core feature of antisocial personality disorder (ASPD) that is associated with abnormal brain function and neurochemical alterations. The ventral striatum (VS) is a key region of the neural circuitry mediating impulsive behavior, and low monoamine oxidase-A (MAO-A) level in the VS has shown a specific relationship to the impulsivity of ASPD (Kolla et al., 2015). Because it is currently unknown whether phenotypic MAO-A markers can influence brain function in ASPD, we investigated VS MAO-A level and the functional connectivity (FC) of two seed regions, superior and inferior VS (VSs, VSi).

Methods: Nineteen impulsive ASPD males underwent [^{11}C] harmine positron emission tomography scanning to measure VS MAO-A V_T, an index of MAO-A density, and resting-state functional magnetic resonance imaging that assessed the FC of bilateral seed regions in the VSi and VSs. Subjects also completed self-report impulsivity measures, including the Barratt Impulsiveness Scale-11 (BIS-11) and the NEO Personality Inventory-Revised (NEO PI-R) impulsivity subscale.

Results: Results revealed functional coupling of the VSs with bilateral dorsomedial prefrontal cortex (DMPFC) that was correlated with VS MAO-A V_T ($r = 0.47$, $p = 0.04$), and functional coupling of the VSi with right hippocampus that was anti-correlated with VS MAO-A V_T ($r = -0.55$, $p = 0.01$). Additionally, VSs-DMPFC FC was negatively correlated with NEO PI-R impulsivity ($r = -0.49$, $p = 0.03$), as was VSi-Hippocampus FC with BIS-11 motor impulsiveness ($r = -0.50$, $p = 0.03$).

Conclusions: These results highlight an association of VS MAO-A level with the FC of striatal regions linked to impulsive behavior in ASPD and suggest that phenotype-based brain markers of ASPD have relevance to understanding brain function.

References: Kolla, N. J., Matthews, B., Wilson, A. A., Houle, S., Bagby, R. M., Links, P., . . . Meyer, J. H. (2015). Lower Monoamine Oxidase-A Total Distribution Volume in Impulsive and Violent Male Offenders with Antisocial Personality Disorder and High Psychopathic Traits: An [(11)C] Harmine Positron Emission Tomography Study. *Neuropsychopharmacology, 40*(11), 2596-2603. doi: 10.1038/npp.2015.106

Ventral Striatum Functional Connectivity Relates to Ventral Striatum Monoamine Oxidase-A Total Distribution Volume in Antisocial Personality Disorder
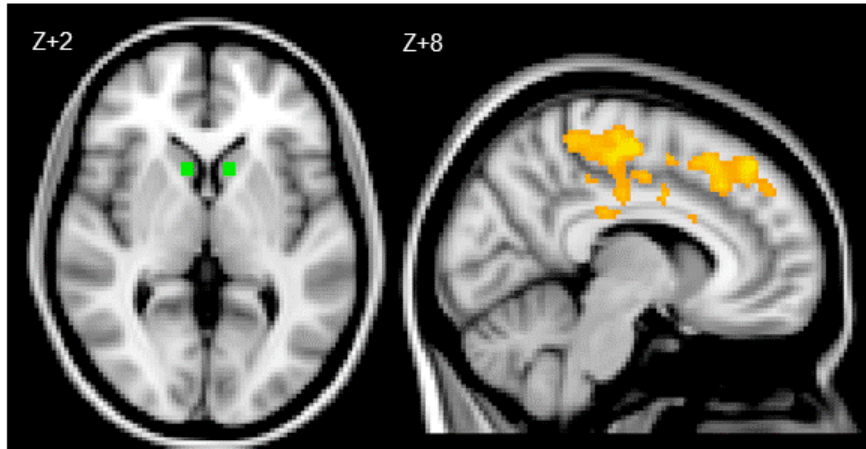
A. Dorsomedial prefrontal cortex (orange) functional connectivity with the superior ventral striatum seeds (green) is significantly correlated with ventral striatum monoamine oxidase-A total distribution volume.
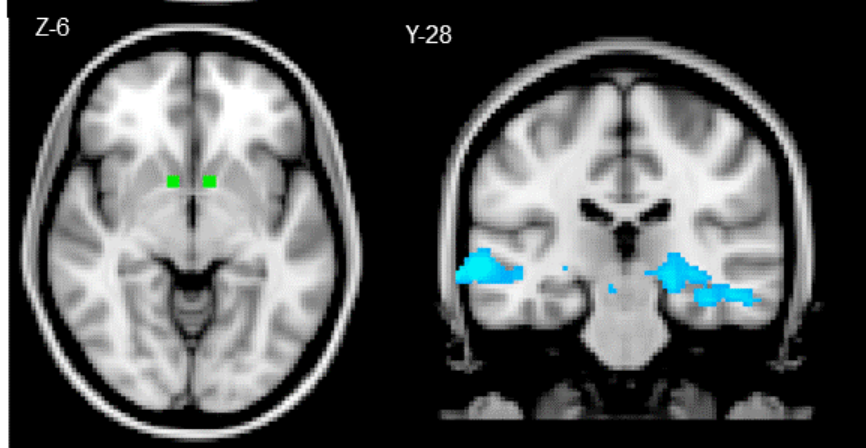
B. Right hippocampus (blue) functional connectivity with the inferior ventral striatum seeds (green) is significantly anti-correlated with ventral striatum monoamine oxidase-A total distribution volume.

Individuals Resilient to Seasonal Affective Disorder Downregulate their Cerebral Serotonin Transporter Binding in Winter

Brenda Mc Mahon[1,2], Martin Nørgaard[1], Claus Svarer[1], Sofie B. Andersen[1], Martin K. Madsen[1], William Baaré[3], Jacob Madsen[4], Vibe G. Frokjaer[1] and Gitte M. Knudsen[1,2]

[1] Neurobiology Research Unit, Rigshospitalet and Center for Integrated Molecular Brain Imaging, Section 6931, Blegdamsvej 9, 2100 Copenhagen, Denmark; [2] Faculty of Health and Medical Sciences, University of Copenhagen, Denmark; [3] Danish Research Centre for Magnetic Resonance, Centre for Functional and Diagnostic Imaging and Research, Copenhagen University Hospital Hvidovre, Kettegårds allé 30, 2650 Hvidovre, Denmark; [4] PET and Cyclotron Unit, Rigshospitalet, Blegdamsvej 9, 2100 Copenhagen, Denmark

Introduction: Cross-sectional ^{11}C-DASB PET studies including males and females have shown an inverse association between levels of the serotonin transporter (SERT) and daylight minutes, particularly in carriers of the short allele (S-carriers) of the serotonin transporter linked polymorphic region (5-HTTLPR). Gender may play a role since studies exclusively in males have failed to replicate these findings and seasonality, being characterized by low mood, reduced vigilance and increased appetite particularly affects women.

Methods: Twenty-three (13 women, age: 26±6 years) healthy S-carriers resilient to seasonality-associated symptoms were PET-scanned with ^{11}C-DASB both summer and winter in a randomized counterbalanced fashion. The non-displaceable binding potential (BP_{ND}) was obtained with the Multilinear Reference Tissue Model 2 (MRTM2) with cerebellum as reference region, in Freesurfer. Effects of season, sex and sex-by-season in raphé nuclei and in 17 grey matter projection areas (global BP_{ND}) was analyzed with two separate single-factor repeated measures ANOVA models. Global BP_{ND} was computed as ($\sum(BP_{NDx} * volxume_x))/ \sum volume_x$). A whole brain voxel-wise analysis was included to disclose brain local effects of season.

Results: Across all participants, raphé nuclei and global SERT binding were lower in winter compared to summer (raphé nuclei: F_{season} = 10.92, P = .003, global: F_{season} = 11.47, P = .003). In neither analysis did we detect a sex difference when season was not taken into account (raphé nuclei: F_{sex}: 0.56, P = .46 and global: F_{sex} = 0.37, P = .55). A significant sex-by-season interaction effect was found in global SERT binding ($F_{sex-by-season}$ = 5.54, P = .029), it was attributable to females showing a decrease in global SERT binding in the winter relative to summer, whereas males on average did not differ in winter and summer SERT levels. No sex-by-season interaction was found in raphé nuclei ($F_{sex-by-season}$ = 1.73, P = .20). The voxel-based analysis showed that the season effect was particularly pronounced bilaterally across the angular gyri (.0016 < $P_{corrected}$ < .00047), the middle frontal gyri (.0039 < $P_{corrected}$ < .00087) and across occipital cortices and the posterior inferior temporal cortices (.0066 < $P_{corrected}$ < .0001) (figure).

Conclusion: Our study suggests that global down-regulation of SERT levels in winter relative to summer promote resilience to winter-induced seasonal affective symptoms, possibly via increased serotonergic tone. This phenomenon was most pronounced in women.

Voxelwise paired t-test, corrected (n = 23)

LEFT

RIGHT
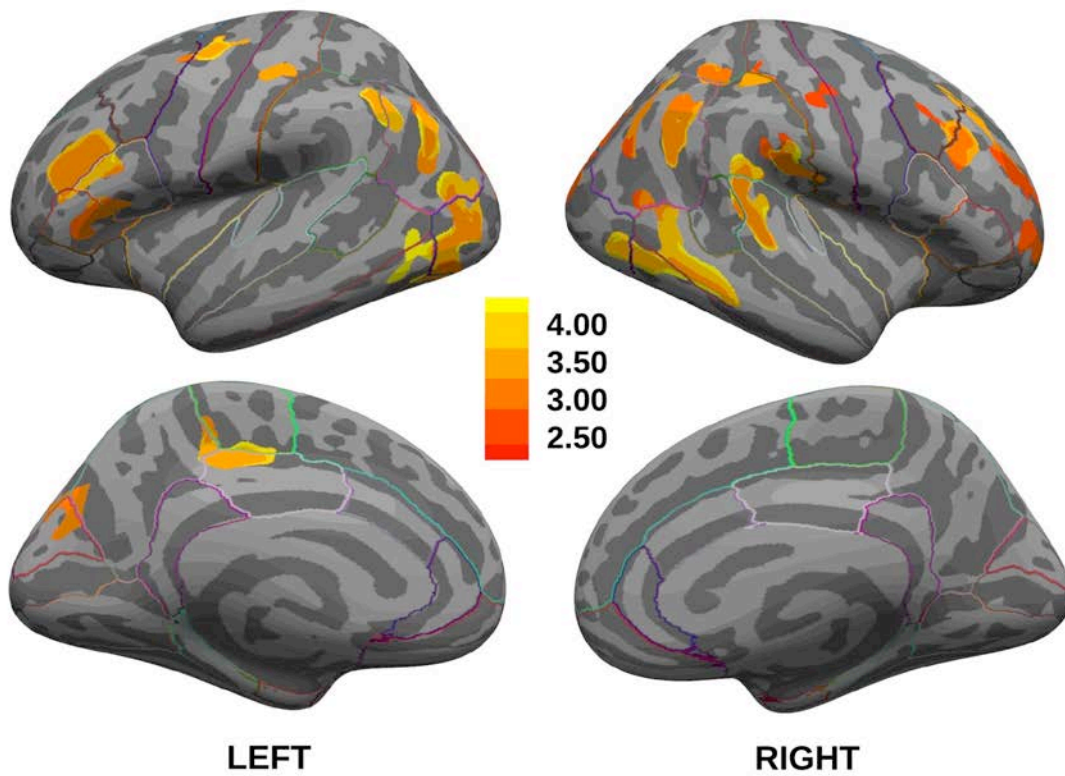
Figure. The univariate voxel-wise analysis depicted on the inflated brain. The map displays the t-values of clusters with significant changes in ^{11}C-DASB binding across seasons (summer - winter), corrected for multiple comparisons. The top row: represents the surface and the bottom row a mid-saggital cut.

Investigation of Tether-Bearing THK-523 Derivatives for Potential PET Radioligands for Neurofibrillary Tangles in Neurodegenerative Diseases

Lisheng Cai,[1*] Baoxi Qu,[2] Bryan T. Hurtle,[1] Ramon Diaz-Arrastia,[2] Sureshbabu Dadiboyena,[1] and Victor W. Pike[1]

[1]*Molecular Imaging Branch, National Institute of Mental Health, National Institutes of Health, Bethesda, MD 20892, USA.* [2]*Center for Neuroscience and Regenerative Medicine, Uniformed Services University of the Health Sciences, Bethesda, Maryland, USA.*

Introduction: Neurofibrillary tangles (NFTs) and β-amyloid plaques are the two hallmarks of Alzheimer's Disease [1]. We have identified two binding sites for ligands on NFTs, namely a THK-523 binding site and a distinct T807 binding site. The PET radioligand [18F]THK-523 suffers a number of limitations, such as troublesome radiodefluorination and low signal in brain due to low binding affinity. There remains a need for PET radioligands for imaging NFTs with a greater dynamic imaging range than [18F]THK-523. To address this need, we considered that extensions of the THH-523 structure by addition of tethers of various lengths might well unveil a secondary binding interaction, in addition to the primary interaction observed for THK-523, and thereby enhance ligand affinity.

Methods: We prepared several THK-523 derivatives with tethers composed of oxyethylene units of various number (1–6) and with a variety of terminal substituents, including a fluoro substituent with potential for labeling with fluorine-18. The synthetic strategy was based on commercially available 2-chloro-6-methoxyquinoline as starting material. Three binding assays using [3H]PIB, [3H]T807 and [3H]THK-523, respectively, were used to assess the binding of the derivatives to post mortem brain tissue homogenate.

Results: From only a small set of THK-523 derivatives, a few compounds (**1**, **7**, and **10**) emerged with high affinity (< 50 nM) and selectivity for the THK-523 binding site (Table 1). One compound, **4**, competes with both THK-523 site and PIB site, and none of the prepared compounds showed high affinity for the T-807 site, consistent with a 2-binding site model for NFTs. Compound **1** is of special interest because it has an affinity at least comparable with that of THK-523, with only slightly increased lipophilicity (+ 0.44 clogD units), and amenability to labeling with fluorine-18.
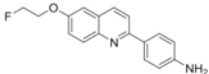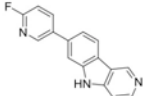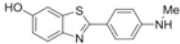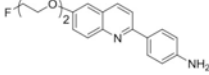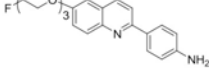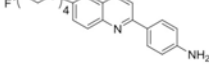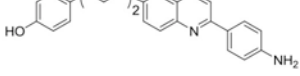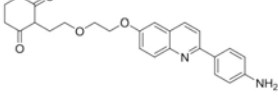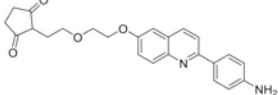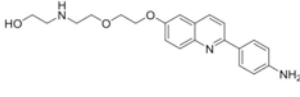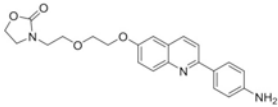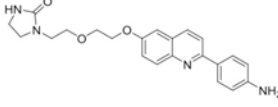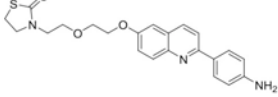
Conclusions: Tether addition to THK-523 was successful in generating compounds with high affinity and selectivity for the THK binding site, with potential for PET radioligand development.

References:
Selkoe, D.J. *Physiol. Rev.*, 2001, 81, 741 ;2. Chien, D.T. et al. *J. Alzheimer's. Dis.,* 2013, 34, 457.

Table 1. K_i values for ligands at three binding sites in AD brain homogenates.

Compound	Structure	Affinity (K_i, nM)		
		at THK-523 site	at T807 site	at PIB site
THK-523		51 ± 22	425 ± 383	> 1000
T807		> 1000	2.6 ± 0.7	> 1000
PIB		> 1000	> 1000	34 ± 3
1		37	> 1000	> 1000
2		> 1000	> 1000	> 1000
3		> 1000	> 1000	> 1000
4		48	> 1000	42
5		927	> 1000	674
6		> 1000	> 1000	> 1000
7		22	> 1000	> 1000
8		52	> 1000	> 1000
9		75	> 1000	> 1000
10		21	> 1000	> 1000

Note: K_i values are average of 5 measurements for THK-523, T807, and PIB. K_i values for other compounds are average of 2 measurements.

Simultaneous Estimation of Input Functions: A Functional Principal Components Analysis Approach

R. Todd Ogden[1,2], Harry Rubin-Falcone[2], Tao Sun[3], and Francesca Zanderigo[2,4]

[1]Department of Biostatistics, Mailman School of Public Health, Columbia University, New York, New York, U.S.A.; [2]Department of Molecular Imaging and Neuropathology, New York State Psychiatric Institute, New York, New York, U.S.A.; [3]Department of Biostatistics, University of Pittsburgh, Pittsburgh, Pennsylvania, U.S.A.; [4]Department of Psychiatry, Columbia University, New York, New York, U.S.A.

Introduction. In neuroreceptor mapping, methods for estimation of a radiotracer's volume of distribution and related binding measures require estimation of a metabolite-corrected input function. Such an input function is most commonly determined by drawing and analyzing a sequence of arterial blood samples that are collected during the scan, but this is an invasive procedure that requires significant effort. In the absence of arterial sampling data, it has been shown[1,2] that parameters of a patient-specific input function may be estimated reliably by fitting several regions simultaneously. By expressing the input function in terms of a small number of basis functions[3], it is possible to improve the efficiency of estimation of the input function parameters, and, thereby, also of binding measures that rely on a valid input function.

Methods. We performed a functional principal component analysis[4] (FPCA) based on a B-spline representation on existing data using two tracers: [11C]DASB and [18F]FDG. Interior knots were placed at 1.7min and 6min for [11C]DASB and at 4.5min and 5min for [18F]FDG. For each tracer we found that two principal components together account for more than 98% of the total variance and thus we reduced the dimensionality of the representation of the input function from 8 to 2. As with previous methods for recovering the input function with simultaneous estimation, we require one arterial blood sample to ensure identifiability. For each tracer considered, we first compared estimates of binding measures using only the spline representation of the input function (which corresponds to the maximal number of principal components) with those obtained using all arterial data. Finding good agreement, we next compared estimates of binding using the first two principal components and one arterial "anchor" point (at 50 minutes after injection for [11C]DASB and 40 minutes for [18F]FDG) with estimation using all available arterial data.

Results. While the principal component basis does not always capture the peak in the input function well, this seems to have minimal effect on estimation of binding measures. The figure shows the agreement across regions for 211 studies imaged with [11C]DASB. Despite using only a single plasma data point and a two-parameter representation of the input function, there is good agreement across the regions. To determine whether such a procedure is viable when fewer studies with full arterial data are available, we repeated the FPCA with only 25 subjects and found that the results do not change appreciably.

Conclusions. By effectively reducing the dimensionality of the representation of the input function using a basis derived from a spline-based FPCA, it is possible to reliably estimate measures of binding using only one sampled arterial data point. The performance of the method will depend on how well the input function can be approximated by a FPCA basis and how well its coefficients can be estimated from data from multiple regions. To apply and validate this approach with a new tracer, it would be necessary to have sufficient scans with full arterial sampling in order to obtain accurate estimates of the principal components.

References
[1] Wong KP, Feng D, Meikle SR, Fulham MJ (2001) Simultaneous estimation of physiological parameters and the input function—in vivo PET data. *IEEE Trans Inform Technol Biomed* 5:67–76
[2] Ogden RT, Zanderigo F, Choy S, Mann JJ, and Parsey RV (2010). Simultaneous estimation of input functions: An empirical study. *J Cereb Blood Flow Metab* 30: 816-826.
[3] Verhaeghe J, Deleye S, Amhaoul H, Stroobants S, Dedeurwaerdere S, and Staelens S (2013). Population derived principal component analysis based model for the [18F]PBR111 arterial input function in rats, in *Nuclear Science Symposium and Medical Imaging Conference (NSS/MIC)*, IEEE.
[4] Ramsay J and Silverman BW (2005). *Functional Data Analysis*. Springer: New York.

P-081
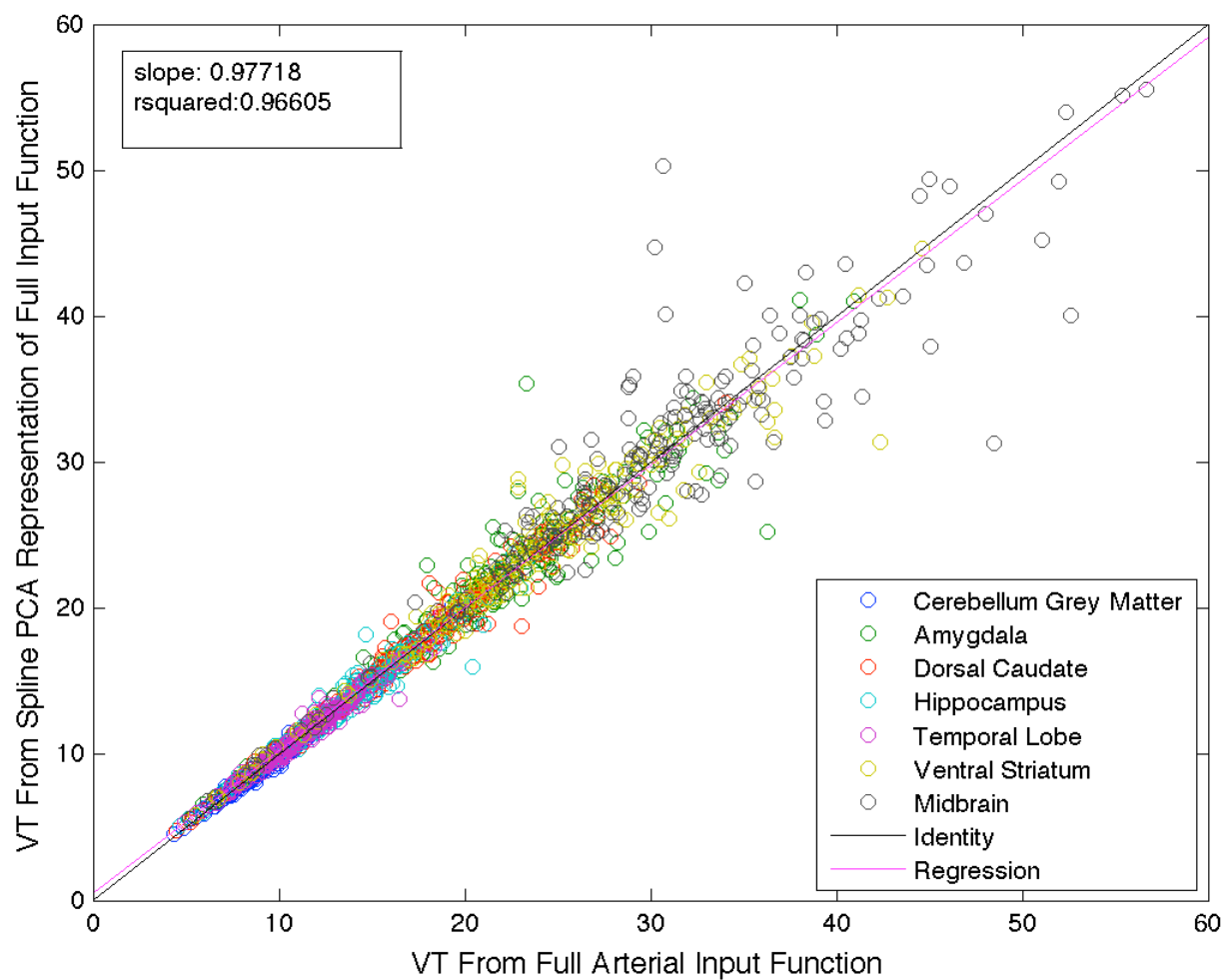
Comparison of Arterial and Venous Blood Sampling for Positron Emission Tomography with [11C]-CUMI-101

Samantha Rossano[1,2], Christine DeLorenzo[1,4,5], Ashwin Malhotra[1], Rajapillai L.I. Pillai[1], Brendan Zareno[1], Irina Esterlis[3], Shu-fei Lin[3], Michael Kapinos[3], Nabbel Nabulsi[3], Yiyun Huang[3], Richard E. Carson[3], Ramin V Parsey[1], Francesca Zanderigo[4,5]

Stony Brook University Departments of Psychiatry[1], Biomedical Engineering[2], Stony Brook University, Stony Brook, NY; Yale PET Center[3], Yale University, New Haven, CT; Department of Molecular Imaging and Neuropathology[4], New York State Psychiatric Institute, New York, NY, USA; Department of Psychiatry[5], Columbia University, New York, NY, USA

Introduction: Arterial input functions (AIFs) are acquired to calculate PET outcome measures such as BP_F. Numerous techniques have been developed to decrease the invasiveness and cost associated with arterial blood sampling. One such technique, Simultaneous Estimation (SIME), estimates a metabolite-corrected AIF based on the PET signal from several brain regions and a single arterial blood sample as an anchor point. SIME has proven effective for use with a number of tracers [1-3]. Although this method potentially decreases the invasiveness of an arterial line to a single arterial puncture, burden on the patient is still present. This burden can be further decreased if a single venous sample could replace the arterial sample. This study investigates the differences in tracer metabolite and radioactivity concentration derived from venous and arterial blood samples acquired during a PET scan with the serotonin-1A receptor (5-HT$_{1A}$R) tracer [11C]-CUMI-101 [4], for which SIME with one arterial sample acquired at 60 minutes had previously been validated [2]. Our study aims to determine whether SIME with a single venous blood sample can generate accurate binding estimates from the tracer.

Methods: Arterial and venous blood samples were collected at five time points (3, 12, 30, 60, and 90 minutes after tracer injection) for 16 subjects during a [11C]-CUMI-101 PET scan. The tracer metabolite and radioactivity concentration calculated from both arterial and venous samples were compared by ratio (venous/arterial), and the average and standard deviation of these ratios across all subjects were plotted for each of the five time points. The volume of distribution (V_T) derived from SIME using either a single venous (VEN) or arterial (ART) blood sample as an anchor was calculated in six subjects across 8 regions of interest (cerebellum, raphe, amygdala, entorhinal cortex, hippocampus, insula, posterior parahippocampal gyrus and temporal lobe). SIME-ART and SIME-VEN V_T values were compared to estimates obtained using the full AIF using correlation and regression analysis. Percent difference between SIME-ART and SIME-VEN V_T was compared to the percent difference in both ART to VEN radioactivity concentration and percent parent compound.

Results: The average VEN/ART ratio of plasma radioactivity concentration was 0.91 ± 0.09 (±SD) at 60 minutes after tracer injection, while the average VEN/ART ratio of parent fraction was 1.01 ± 0.02 across all time points considered (Figure 1a). The resulting V_T from SIME-ART and SIME-VEN are both linearly correlated with the corresponding V_T estimates from full AIF (Figure 1b, 1c), and with each other (Figure 1d). The differences in SIME-ART and SIME-VEN V_T estimates are not correlated with the differences observed between ART and VEN radioactivity and percent parent compound.

Conclusion: These results suggest that a venous blood sample may be used as an anchor for SIME with [11C]-CUMI-101. This can potentially decrease the invasiveness of blood data acquisition and analysis during a PET scan with this radiotracer. Further investigation includes expanding the cohort in which SIME with venous anchor is evaluated.

Figure 1: A (top): The average ratios (venous-derived/arterial-derived measures) of the percent parent compound (blue) and plasma radioactivity (red) are shown for 5 time points: 3, 12, 30, 60 and 90 minutes after tracer injection. Standard deviation across 16 subjects is shown by the error bars. **B-D:** The resulting Volume of Distribution V_T from full AIF vs. SIME with arterial blood data at 60 minutes after tracer injection (B), full AIF vs. SIME with venous blood data at 60 minutes after tracer injection (C), and SIME with arterial vs. SIME with venous blood data from 60 minutes after tracer injection (D), for 6 subjects across 8 ROIs. Identity line (red) shown for reference.

References:

1.   Ogden, R.T., et al., *Simultaneous estimation of input functions: an empirical study.* J Cereb Blood Flow Metab, 2010. **30**(4): p. 816-26.
2.   Zanderigo, F., R.T. Ogden, and R.V. Parsey, *Noninvasive blood-free full quantification of positron emission tomography radioligand binding.* J Cereb Blood Flow Metab, 2015. **35**(1): p. 148-56.
3.   Mikhno, A., et al., *Toward Non-invasive Quantification of Brain Radioligand Binding by Combining Electronic Health Records and Dynamic PET Imaging Data.* IEEE J Biomed Health Inform, 2015.
4.   Milak, M.S., et al., *In vivo quantification of human serotonin 1A receptor using 11C-CUMI-101, an agonist PET radiotracer.* J Nucl Med, 2010. **51**(12): p. 1892-900.

Figure 1: A (top): The average ratios (venous-derived/arterial-derived measures) of the percent parent compound (blue) and plasma radioactivity (red) are shown for 5 time points: 3, 12, 30, 60 and 90 minutes after tracer injection. Standard deviation across 16 subjects is shown by the error bars. **B-D:** The resulting Volume of Distribution V_T from full AIF vs. SIME with arterial blood data at 60 minutes after tracer injection (B), full AIF vs. SIME with venous blood data at 60 minutes after tracer injection (C), and SIME with arterial vs. SIME with venous blood data from 60 minutes after tracer injection (D), for 6 subjects across 8 ROIs. Identity line (red) shown for reference.

Quantification of tau pathologies with ^{11}C-PBB3 PET using reference tissue voxels extracted from brain cortical gray matter

Yasuyuki Kimura[1], Hironobu Endo[1,2], Masanori Ichise[1], Hitoshi Shimada[1], Chie Seki[1],
Yoko Ikoma[1], Hitoshi Shinotoh[1], Makiko Yamada[1], Makoto Higuchi[1], Ming-Rong Zhang[1], and Tetsuya Suhara[1]

[1]*Molecular Imaging Center, National Institute of Radiological Sciences, Chiba, Japan, 4-9-1 Anagawa, Inage-ku, Chiba, Chiba 263-8555, Japan;* [2]*Division of Neurology, Kobe University Graduate School of Medicine, Kobe, Japan 7-5-1 Kusunoki-cho, Chuo-ku, Kobe 650-0017 Japan*

Background. Quantitative imaging of tau pathologies would improve diagnostic accuracy of neurodegenerative tauopathies and facilitate evaluation of disease-modifying drugs targeting tau lesions in these diseases. Tau pathology can be quantified by positron emission tomography (PET) without arterial blood sampling when reference tissue devoid of target binding sites is available. The cerebellar cortex has been used as a reference region in analyses of tau PET data in Alzheimer's disease (AD). However, tau accumulation may occur in diverse brain regions including the cerebellar cortex in the other tauopathies such as progressive supranuclear palsy and corticobasal degeneration. This hampers selection of a distinctive reference region lacking binding of tau PET ligands. The purpose of this study was to validate a new method to quantify specific binding of a PET radioligand, ^{11}C-PBB3, to tau deposits using reference voxels extracted from the cortical gray matter, which have a low likelihood of containing tau accumulations.

Methods. ^{11}C-PBB3 PET data of seven mild AD patients (ADs) and 7 elderly healthy control subjects (HCs) acquired in a previous study was re-analyzed. As a standard method, we initially generated parametric images of binding potential (BP^*_{ND}) using reference tissue manually defined on the cerebellar cortex. We then plotted the distribution of voxel BP^*_{ND} data in the parametric image as a voxel frequency histogram, and extracted those cortical gray matter voxels that have a low likelihood of ^{11}C-PBB3 binding by defining a certain range of BP^*_{ND} values on the histogram. Finally, we used these voxels as reference tissue for generating new BP^*_{ND} parametric images.

Results. Reference tissue voxels defined by the histogram analysis spread throughout the cortical gray matter of AD and HC brains. The BP^*_{ND} values determined by our new method correlated very well with those estimated by the standard method (r^2 = 0.94), although the binding estimates by the current method were slightly higher by ~0.14 than those by the standard method.

Conclusions. We validated a new method enabling quantification of tau lesions that can accumulate in the cerebellum and other extensive brain areas. This method should be applicable to tau PET imaging for all tauopathy subtypes using tau PET ligands including ^{11}C-PBB3.
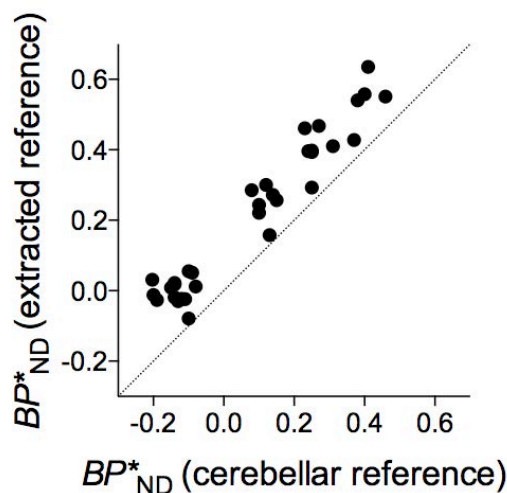
Target regions were defined as in a previous report
(Kimura et al. JNM 2015;56:1359)

Displacement studies of yohimbine binding in non-human primates

Alex Z. Kadhim[1*], Anna Schildt[1*], Steen Jakobsen[2], Vesna Sossi[3], Doris J. Doudet[1,2]

[1] Department of Medicine/Neurology, 2221 Wesbrook Mall,, Vancouver, BC Canada V6T 1Z3, Canada. [2] Department of Nuclear Medicine and PET-Centre, Aarhus University and Hospital, Nørrebrogade 44, Building 10G, 8000, Aarhus C, Denmark. [3] Department of Physics and Astronomy, 2221 Wesbrook Mall, Vancouver, BC, Canada.
*Equal contribution

Background: The role of the noradrenergic (NA) system in health and disease attracts significant attention but few tracers permit the in vivo its evaluation. In tracer dose, $[^{11}C]$yohimbine has been shown to be a selective tracer of the alpha2 adrenergic receptors but non selectively labels the 3 major subtypes, A, B and C. Challenge studies have demonstrated its sensitivity to changes in the concentrations of the endogenous ligand. We investigated the usefulness of the tracer as well as parameters that may affect its binding and determined the actual binding potential BP_{ND} in non-human primates (NHP).

Methods: Six normal rhesus monkeys (5 females, one male) each received 2-3 scans in a Siemens high resolution research tomograph (HRRT) with high specific activity yohimbine. In one or two of the scans, a pre-determined dose of cold yohimbine (from 0.005 to 0.03 mg/kg) was administered 10-15 min prior to the tracer. The free fraction was measured in a blood sample taken immediately prior to tracer injection. The PET scans were registered to a MR atlas of the rhesus monkey brain. Multiple volumes of interest in cortical and sub-cortical structures were placed on the normalized data and used to create regional time activity curves. A metabolite-corrected plasma activity curve was used to calculate the total volume of distribution V_T. Correction was performed for free fraction and yielded V_T/f_p. Lassen plots (Xaxis: V_T baseline; Yaxis: V_T base-$V_T$cold) were constructed which permitted the determination of V_{ND}. The binding potential BP_{ND} was obtained as $V_T/V_{ND}-1$.

Results: The tracer readily entered the brain. The free fraction was found to be relatively stable between animals and remained between 10 and 13% (i.e. higher than in healthy human subjects). Even low doses of cold yohimbine induced a non dose-dependent increase in free fraction to 18-22%. As has been reported in human subjects[2] but as opposed to pigs[1], the metabolism of the tracer varied among animals with slow and fast metabolizers. However, the metabolic pattern remained highly reproducible within subjects, independent of the dose of cold yohimbine administered. The V_{ND}, measured from the baseline and displacement studies from the highest dose of cold yohimbine varied from 1.6 to 2.3. Individual values were applied to individual animal to evaluate BP_{ND}.
In NHP brain, there was no clear area of non-specific binding. White matter regions showed the lowest V_T but suffered from significant partial voluming contamination, preventing them from being used as adequate regions of non-specific binding. The thalamus, cortex and striatum had the highest concentration of alpha 2 adrenergic receptor, cerebellum the lowest. The BP_{ND} spanned a large range, from 0.5 to 5 between animals. The highest dose of cold yohimbine induced a generalized decrease in yohimbine binding of up to 40-80% depending on the region and the subject.

Conclusions: This preliminary study suggests that yohimbine can be used as a tracer of the alpha 2 adrenergic receptors in non-human primates and may be useful to evaluate the role of NA in various animal models of neurodegenerative diseases. It however suggests a large variability between subjects of to date unknown origin.

References:
1. Jakobsen, S, Pedersen, K, Smith, DF, et al. Detection of alpha2 adrenergic receptors in brain of living pig with 11 C-yohimbine. Journal of Nuclear Medicine. 2006;47:2008.
2. Nahimi, A, Jakobsen, S, Munk, OL, et al. Mapping alpha2 adrenoceptors of the human brain with 11C-yohimbine. J Nucl Med. 2015 Mar;56(3):392.

Assessment of Microscale Thermophoresis as a binding assay method for the development of PET radioligands for misfolded proteins

Emily Fisher[1*], *Yanyan Zhao*[1*], Alexander Buell[3] , Gergley Toth[2], Franklin Aigbirhio[1]

1 – Molecular Imaging Chemistry Laboratory, Wolfson Brain Imaging Centre, Department of Clinical Neurosciences, University of Cambridge, Cambridge, CB2 0QQ, England; 2 – Institute of Organic Chemistry, Research Centre for Natural Science, Hungarian Academy of Science, Budapest, 1117, Hungary; 3 - Heinrich-Heine-Universität Düsseldorf, Institut für Physikalische Biologie, Universitätsstr.1, 40225, Düsseldorf
Equal contribution

Background: Neurodegenerative diseases such as Alzheimer's disease (AD) and Parkinson's disease (PD) share the pathological hallmark of misfolded proteins. During the progress of these diseases, proteins such as tau in AD, and alpha-synuclein (α-syn) in PD, form insoluble fibrils. Imaging these fibrillar proteins forms *via* positron emission tomography (PET) imaging would allow for improved understanding of how these diseases progress and may also allow for better assessment of new potential treatments. However, work in this field has been challenging due to lack of techniques for effectively measuring binding affinities between these protein fibrils and small molecules for the discovery of novel PET radioligands. In this work we have investigated the use of microscale thermophoresis (MST) as a novel method to overcome these challenges. MST is a promising new biophysical method for measuring biomolecular binding affinities, which exploits the phenomenon of thermophoresis – the directed movement of molecules along a temperature gradient.[1] The technique uses infra-red (IR) laser heating to induce a temperature gradient in capillary tubes whilst continually measuring fluorescence intensity to monitor the movement of labelled species within the capillaries. The potential major advantage of MST over other more common assay methods is the very low amounts of protein required for measurements – approximately 200 μL of solution at nM concentration per experiment.

Methods: A method to detect the interaction between an aggregated protein and compounds was developed using an MST instrument Nanotemper Monolith NT. 115. For tau fibrils; NT647-NHS dye was used to label the fibrils generated *in vitro*. Measurements were conducted using 25 nM protein with 0.05% Tween HEPES buffer. The unlabelled binding partner was then titrated to assess the interaction. Untreated Enhanced Gradient standard capillaries were used in each experiment using settings of 90-100% LED power and 40% MST power. For fibrillar α-syn; Alexa-647 dye was used to label the fibrils generated *in vitro*. Measurements were conducted using 500 nM protein with Tris buffer. The unlabelled binding partner was then titrated to assess the interaction. Standard capillaries were used in each experiment using settings of 20-90% LED power and 40% MST power.

Results: For tau fibrils, two compounds, thiazine red and lansoprazole were used as reference compounds as these have published K_d values of 18 nM[2] and 2.5 nM[3] respectively. In addition to these, two other test compounds, PBB3 and T807, also known to bind to tau fibrils were evaluating using MST.
For fibrillar α-syn, Pittsburgh Compound B (PiB) was used as a reference compound with a reported binding affinity of K_d = 10.07 nM[4]. We have also analysed SIL26, another compound with reported affinity for fibrillar α-syn.
The results of these experiments are listed in the table below.

Conclusion: The assessment with tau fibrils shows highly promising results with MST derived binding affinities comparable with published values. However, with α-syn there is more variation in results, highlighting that the type, form and preparations of the misfolded protein could be significant factors for obtaining consistent and accurate results. Work is on-going to determine and refine these factors. However, as the assay is quick and simple to perform with the major advantage that only very small quantities of protein are required, it shows great potential for future use in this difficult field.

References:
1. M. Jerabek-Willemsen, *et. al.*, *Journal of Molecular Structure*, 2014, **1077**, 101-113
2. Gu, J 2013. TU Darmstadt. Ph.D. Thesis.
2. Rojo LE, *et al.*, Journal of Alzheimer's, 2010, **19(2)**, 573-589
3. M.T. Fodero-Tavoletti, *et al.*, *J. Neurosci.*, 2007, **27**, 10365-10371

4. M. Maruyama, *et. al.*, *Neuron*, 2013, **17(6)**, 1094-1108

5. C.-F. Xia, *et. al.*, *Alzheimer's and Dementia*, 2013, **9(6)**, 666-676

6. X. Zhang, *et. al.*, *Applied Sciences*, 20114, **4**, 66-78

Tau fibrils			α-syn fibrils		
Compound	Literature K_d (nM)	MST K_d (nM)	Compound	Literature K_d (nM)	MST K_d (nM)
Thiazine Red	18	3.39 ± 0.8	PiB	10.07	573 ± 62.7
Lansoprazole	2.5	33.8 ± 8.4	SIL26	11.7-49.0[7]	129 ± 28.1
PBB3	2.5[5]	0.57 ± 0.05			
T807	14.6[6]	23.3 ± 4.9			

Automated single-step radiosynthesis of [18F]SIL26, a PET marker of misfolded proteins including fibrillar alpha-synuclein

Emily Fisher, Franklin Aigbirhio

1 – Molecular Imaging Chemistry Laboratory, Wolfson Brain Imaging Centre, Department of Clinical Neuroscience, University of Cambridge, CB2 0QQ, England

Background: The pathological hallmark of several neurodegenerative diseases, such as Parkinson's disease, is Lewy Bodies. Lewy Bodies are insoluble protein clumps containing primarily fibrillar alpha-synuclein (α-syn). As this occurs many years before any clinical symptoms arise, the ability to image fibrillar α-syn *via* PET imaging would have significant impact on early diagnosis and treatment of these diseases. It may also allow us to investigate mechanisms of disease progression and assist with identification of new targets for treatment. Herein, we describe the fully automated radiosynthesis of [18F]SIL26 – a radiotracer that has been shown to bind to fibrillar α-syn (K_i = 15.5 nM)[1]. However it has also been shown to show some non-selectivity with high binding affinities also to tau fibrils (125 nM) and Ab fibrils (103 nM). The previously reported radiosynthetic approach to produce this compound was multi-stepped and not automated (Scheme 1)[2], in order to use this radiotracer for an α-syn development programme, including preclinical imaging assessments, we required a method for large-scale radioactivity preparations.

Methods: The radiosynthesis was performed on a GE Healthcare F_X-F_N TRACERlab automated module according to the following procedure; precursor **[5]** was readily synthesised in six steps from commercially available starting materials to yield an air-stable product. **[5]** (1 mg, 2 μmol) was reacted with anhydrous no carrier added [18F]fluoride in DMSO (1 mL) at 117 °C for 15 minutes, before purification by prep-HPLC (MeCN:0.1 M Ammonium Formate pH 4.5 40:60), which showed a single radiolabelled product was formed during the reaction with excellent conversion from fluoride (Scheme 2).

Results: [18F]SIL26 was obtained in a single reaction step combining radiolabelling and N-deprotection 27.5 ± 3.3 % decay corrected radiochemical yield, calculated from [18F]fluoride eluted from cyclotron (n = 4) in 63 mins. Radiochemical purity of the product was >98% and good specific activity (~ 124 GBq/μmol) was obtained at end-of-synthesis (EOS). The identity of the radiolabelled product was confirmed using analytical HPLC by co-injection of unlabelled SIL26 (C18 Luna, MeCN:0.1 M Ammonium Formate pH 4.5 40:60, 1.5 mL/min, retention time = 7.7 min).

Conclusions: We have successfully developed an automated radiosynthetic method for large-scale radioactivity productions of [18F]SIL26 based on a single-step method, which also incorporates removal of the protective chemical group. The automated process has a total time from wet fluoride to formulated product of 63 mins, producing final radiochemical products of 0.14-2.02 GBq at EOS. This radiotracer is now being applied to *in vitro* and *in vivo* characterision of α-syn.

References:
1 – D.P. Bagchi, *et. al.*, *PLOS One*, 2013, **8(2)**, e55031
2 - X. Zhang, *et al.*, *Appl. Sci.*, 2014, **4**, 66-78

Scheme 1:
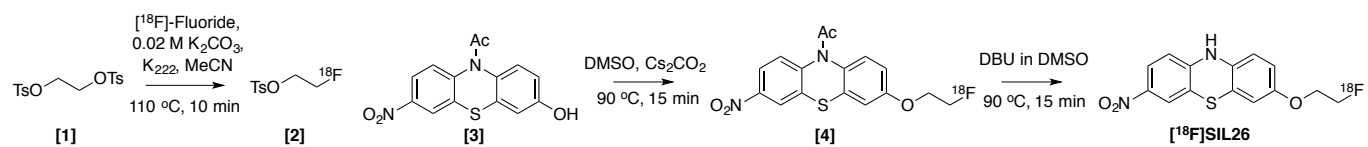
Scheme 2:
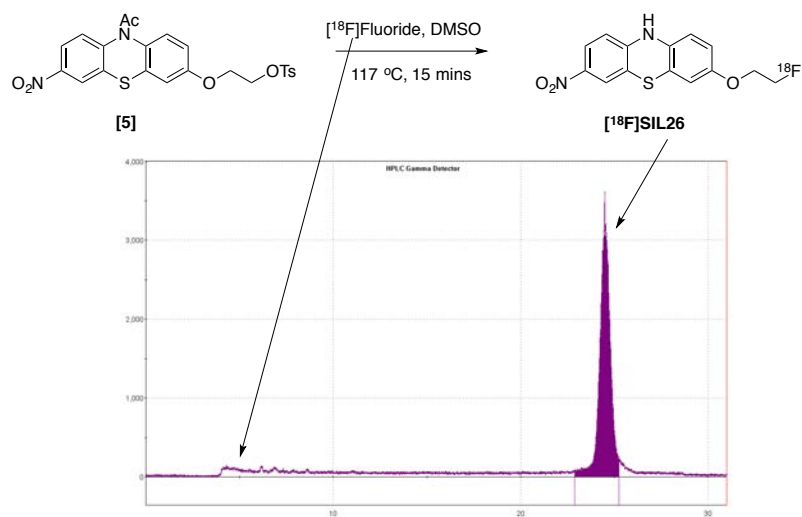
Kinetic Modeling of (+)-[18F]Flubatine Binding to Nicotinic α4β2* Acetylcholine Receptors in Human Brains

Georg A. Becker[1], Solveig Tiepolt[1], Marianne Patt[1], Julia Luthardt[1], Michael Rullmann[1], Swen Hesse[1], Stephan Wilke[1], Philipp M. Meyer[1], Henryk Barthel[1], Gudrun Wagenknecht[2], Alexander Höpping[3], Hermann-Josef Gertz[4], Jörg Steinbach[5], Peter Brust[5], Osama Sabri[1]

[1]Department of Nuclear Medicine, University of Leipzig, Leipzig, Germany; [2]Multimodal Image Processing, Central Institute ZEA-2 Electronic Systems, Forschungszentrum Jülich GmbH, Jülich, Germany; [3]Advanced Biochemical Compounds (ABX), Radeberg, Germany; [4]Department of Psychiatry, University of Leipzig, Leipzig, Germany; [5]Institute of Radiopharmaceutical Cancer Research, Helmholtz-Zentrum Dresden-Rossendorf, Research Site Leipzig, Germany

Objectives: Nicotinic α4β2* acetylcholine receptors (nAChR) are an important target for diagnostic neuroimaging because of their involvement e.g. in Alzheimer's and Parkinson's diseases, and nicotine addiction. The development of new PET tracers for these receptors is an active field of research. Here we present the PET quantification of the new nAChR-ligand (+)-[18F]Flubatine, an enantiomer of (-)-[18F]Flubatine, also known as (-)-[18F]NCFHEB, which is already used for clinical PET imaging of nAChRs.

Methods: After intravenous administration of 284.1±13.2 MBq (+)-[18F]Flubatine PET brain recordings were performed in 11 healthy non-smoking subjects (age 66.6±4.4 years) using an ECAT EXACT HR+ system in 3D-acquisition mode. 41 frames were acquired from 0-270 min post injection and motion corrected with SPM2. Kinetic modeling using 1- and 2-tissue compartment models (1TCM, 2TCM) with arterial input-function was applied to the volume of interest (VOI) based tissue time-activity curves (TACs) generated for 36 brain regions (anatomically defined via MRI co-registration). Time ranges from 0 to 90 and 0 to 270 min were investigated. Model-based receptor parameter was the total distribution volume V_T (ml/cm^{-3}). Metabolites in plasma were measured by radioactivity HPLC and the free fraction of (+)-[18F]Flubatine in plasma was determined by ultracentrifugation.

Results: The tracer showed high stability in vivo with more than 97% remaining as untransformed parent compound at 90 and 270 min. The free fraction in plasma was high and showed only small interindividual variations (0.86±0.02, n=11). Given the negligible amounts of metabolites present in plasma the arterial input function was not corrected for metabolites.
TACs of all 36 regions could be described with the 1- or 2TCM. V_T in all cortical regions could be reliably estimated from 90 min PET data. V_T increased with receptor density as expected. Using the 2TCM and 270 min PET data: Corpus callosum (V_T: 7.9±1.5, n=11), frontal cortex (10.8±1.2), pons (16.3±3.1), thalamus (41.3±8.7). For 90 min PET data the distribution volumes were very similar: Corpus callosum (V_T: 7.9±1.3), frontal cortex (10.3±1.4), pons (15.4±3.0), thalamus (41.0±9.0). The distribution volumes of the 1- and 2TCM were comparable. 1TCM: Frontal cortex (10.9±1.3, 270 min) and (10.2±1.4, 90 min).
The previously investigated enantiomer (-)-[18F]Flubatine showed very similar V_T in cortical structures e.g., frontal (10.4±1.3, n=12) but lower V_T in pons (12.4±1.9) and especially thalamus (27.6±4.2) (2TCM, 90 min; Sabri et al., 2015).

Conclusions: (+)-[18F]Flubatine has an optimal metabolic profile. The amount of metabolites is very low and no metabolite correction has to be applied to the arterial input function. The high V_T values in subcortical structures are favorable. Receptor parameters can be estimated with a 1- or 2TCM from 90 min PET data. If a model derived receptor parameter is used in a classification problem, e.g., distinguishing patients with Alzheimer's disease from healthy controls the bias-variance tradeoff problem associated with the simpler 1TCM (higher bias) and the more complex 2TCM (higher variance) has to be solved. The final decision which model should be used will be made on the basis of the PET data of both groups.

Reference:

Sabri O et al. (2015) Neuroimage 118:199-208
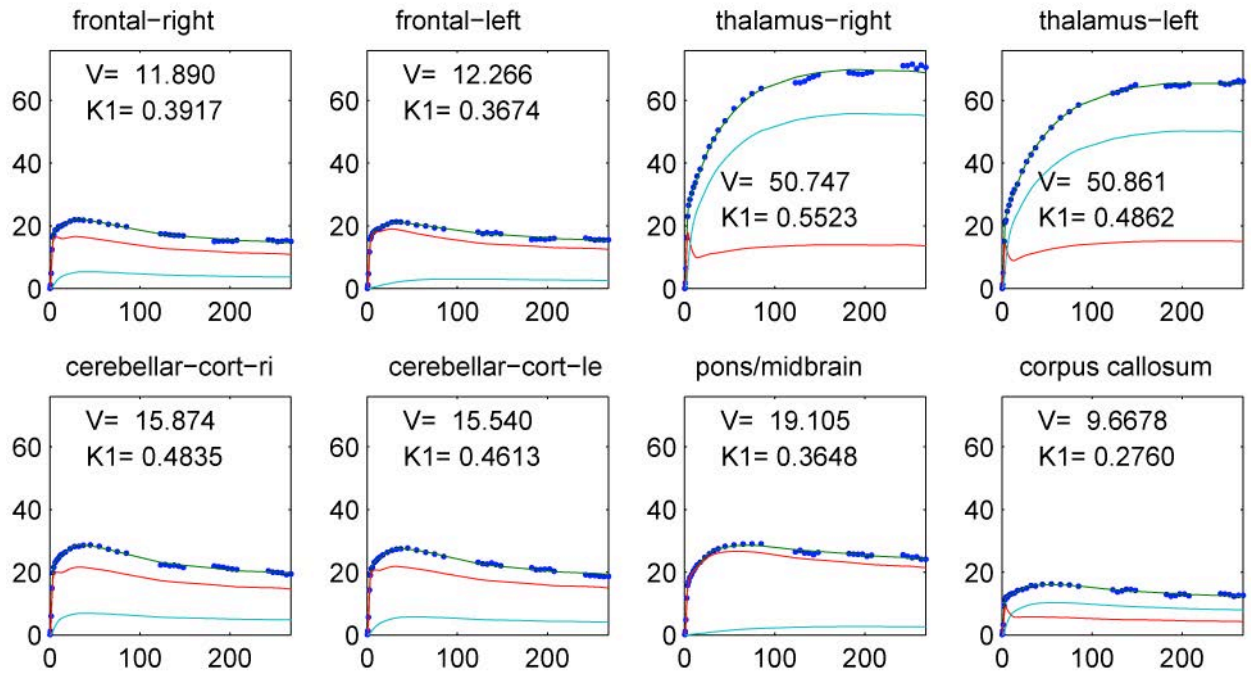
Figure Legend: 2TCM fits (270 min) in 8 brain regions. Abscissa: Time in min, ordinate: Activity (kBq/cm^3). Computed total tracer amount in tissue is presented but also the tracer amount in the non-displaceable and specific tissue compartment, the total distribution volume V and influx rate constant K_1.

Quantification of serotonin transporter occupancy during PET/MR hybrid imaging using bolus plus constant infusion of [11C]DASB

Gryglewski G[1], Hahn A[1], Klebermass E[2], Rischka L[1], Nics L[2], Sigurdardottir H[1], Philippe C[2], James GM[1], Silberbauer L[1], Kautzky A[1], Traub-Weidinger T[2], Hartenbach M[2], Wadsak W[2], Mitterhauser M[2], Prayer D[3], Hacker M[2], Kasper S[1], Lanzenberger R[1]

[1] Department of Psychiatry and Psychotherapy, Medical University of Vienna, Austria; [2] Department of Biomedical Imaging and Image-guided Therapy, Division of Nuclear Medicine, Medical University of Vienna, Austria; [3] Department of Biomedical Imaging and Image-guided Therapy, Division of Neuro- and Musculoskeletal Radiology, Medical University of Vienna, Austria

Objective: The goal of this pilot study was to validate PET/MR imaging methods to be used for the investigation of the efficacy of selective serotonin reuptake inhibitors (SSRIs) in clinical samples. Quantification using the equilibrium method with tracer bolus plus infusion application may enable the assessment of protein binding before and after drug challenge in a single measurement, hence reducing scanning time drastically.

Methods: 6 healthy subjects underwent two PET/MR (SIEMENS mMR) and two PET (GE advance) scans each. During PET/MR scans [11C]DASB was applied as bolus plus constant infusion, with bolus dose equivalent to 170 minutes of infusion, and scanning conducted for 120-140 minutes. Two PET scans were conducted after tracer bolus injection [1]. Double-blind application of 7.5mg citalopram or placebo over 7.5 minutes was performed 30 minutes before PET scans and 60 minutes after start PET/MR scans, respectively. Arterial blood samples were collected automatically for the first 3 minutes and manually at 1, 5, 10, 20, 40, 70 and every 10 minutes after drug challenge during PET/MR scans. for PET, and for PET/MR data. For PET scans, attenuation correction was performed using a ^{68}GE transmission scan and binding potentials (BP$_P$) were calculated using a two-tissue compartment model with K_1/k_2 fixed to that of cerebellar gray matter [2] in PMOD. For PET/MR scans, a low-dose CT recorded on a PET-CT scanner and coregistered to T_1-MPRAGE MRI (TE/TR = 4.2/2000ms, voxel size 1x1x1.1mm) was used for attenuation correction. Brain and plasma parent activities at equilibrium after drug challenge were averaged (after 105 minutes of scanning). BP$_P$ was calculated by subtracting the distribution volume of cerebellar gray matter (V$_{ND}$) from total distribution volumes [3]. BP$_{ND}$ was calculated by dividing BP$_P$ with V$_{ND}$. Occupancies were calculated as the relative decrease in BP between placebo and drug scans. Bias in measured occupancy was calculated as the relative difference compared to occupancy obtained using BP$_P$ in PET/MR.

Results: PET/MR and PET BP$_P$ highly correlated for each subject (r=0.87-0.96) and r=0.67 for all subjects and regions (n=5). Occupancies calculated using BP$_P$ were highly correlated between PET and PET/MR (r≥0.86 for each region investigated; r=0.90 for all regions and subjects, n=4 as one PET scan failed in 2 subjects each, see table). However, there was an average bias towards 22(±13)% lower occupancies in PET. While there was no systematic bias to occupancies obtained using BP$_{ND}$ compared to BP$_P$ (average= -0.03), correlation was only moderate (r=0.26-0.74) and variability of bias pronounced (22-88%).

Conclusions: The current results indicate that measurement of serotonin transporter occupancy using the equilibrium method in PET/MR is in high agreement with well validated kinetic quantification methods in PET [4]. The inclusion of blood data appears to be essential, as occupancies obtained using BP$_{ND}$ suffer from variable bias and slightly underestimate occupancies calculated using BP$_P$ [2]. The correlation of BP$_P$ between scanners might further benefit from a unified pipeline of attenuation correction.

References
[1] Hahn A et al. Hum Brain Mapp. 2014;35(8):3857-66.
[2] Parsey RV et al. Biol Psychiatry. 2006;59(9):821-8.
[3] Innis et al. J Cereb Blood Flow Metab. 2007;27(9):1533-9.
[4] Meyer et al. Am J Psychiatry. 2004;161(5):826-35.

Brain region	Occupancy PET/MR BP_P	Occupancy PET/MR BP_{ND}	Occupancy PET Bolus BP_P*	Occ. PET/MR BP_P vs. PET BP_P (r)*	Bias (±SD)	Occ. PET/MR BP_P vs. PET/MR BP_{ND} (r)	Bias (±SD)
Thalamus L	0.63±0.2	0.56±0.07	0.59±0.2	0.99	-0.16±0.10	0.55	-0.04±0.32
Thalamus R	0.62±0.24	0.56±0.12	0.57±0.18	0.98	-0.20±0.05	0.74	0.04±0.46
Putamen L	0.66±0.19	0.58±0.09	0.52±0.16	0.89	-0.26±0.09	0.43	-0.06±0.29
Putamen R	0.64±0.19	0.54±0.12	0.55±0.16	0.86	-0.20±0.10	0.29	-0.08±0.34
Nucleus Accumbens L	0.57±0.22	0.47±0.14	0.52±0.28	0.97	-0.27±0.29	0.35	-0.06±0.46
Nucleus Accumbens R	0.58±0.23	0.48±0.14	0.57±0.23	0.93	-0.07±0.14	0.42	-0.07±0.40
Nucleus Caudatus L	0.69±0.18	0.63±0.08	0.51±0.18	0.95	-0.31±0.09	0.55	-0.05±0.22
Nucleus Caudatus R	0.65±0.22	0.57±0.11	0.56±0.18	0.90	-0.22±0.10	0.46	-0.03±0.39
Amygdala L	0.63±0.24	0.53±0.11	0.48±0.21	0.92	-0.32±0.13	0.26	-0.03±0.48
Amygdala R	0.60±0.29	0.51±0.17	0.47±0.29	0.97	-0.34±0.22	0.66	0.05±0.50
Midbrain	0.54±0.24	0.42±0.07	0.57±0.22	0.98	-0.12±0.13	0.49	0.02±0.74

Values are given ± standard deviation where applicable. r, Pearson's correlation coefficient. *n=4 due to failure of 1 PET scan each in 2 subjects.

A high-resolution molecular imaging atlas of the human brain 5-HT system

Vincent Beliveau[1,2], Melanie Ganz[1], Ling Feng[1], Patrick M. Fisher[1], Claus Svarer[1], Douglas N. Greve[3,4], Gitte M. Knudsen[1,2]

[1]*Neurobiology Research Unit and Center for Integrated Molecular Brain Imaging, Rigshospitalet, Copenhagen, Denmark;* [2]*Faculty of Health and Medical Sciences, University of Copenhagen, Copenhagen, Denmark;* [3]*Athinoula A. Martinos Center for Biomedical Imaging, Department of Radiology, Massachusetts General Hospital, Boston, MA, USA;* [4]*Harvard Medical School, Boston, MA, USA*

Introduction: The serotonin (5-HT) system plays a central role in many brain functions and abnormal variations in the 5-HT receptors' distribution have been associated with several neuropsychiatric disorders. In vivo receptor distribution can only be studied with molecular imaging techniques such as PET, but image resolution often limits the investigation to regional analysis. Here, we combined high-resolution PET with structural MRI to generate high-precision human brain atlases for some of the major 5-HT receptors and its transporter (5-HTT). We also compared the atlases to autoradiography measurements [1] and mRNA levels [2,3] obtained from post-mortem human brains.

Methods: All data were from the Cimbi database. Only healthy volunteers aged between 18-45 years were included. High-resolution PET images (2mm in-plane) were acquired with a HRRT scanner using the following radioligands: [^{11}C]CUMI-101 (5-HT$_{1A}$, n=8), [^{11}C]AZ10419369 (5HT$_{1B}$, n=36), [^{18}F]Altanserin (5-HT$_{2A}$ antagonist, n=12), [^{11}C]Cimbi36 (5-HT$_{2A}$ agonist, n=29), [^{11}C]SB207145 (5-HT$_4$, n=59), and [^{11}C]DASB (5-HTT, n=100). Corresponding structural MRI were available for all subjects. PET images were reconstructed using a 3D-OSEM-PSF algorithm and motion corrected with AIR 5.2.5. Data was processed with FreeSurfer 5.3 using the regional, surface and volume stream. Surface and volume time activity curves (TACs) were transformed to common space and smoothed by 10 or 5 mm FWHM, respectively. Kinetic modeling (BP$_{ND}$) was performed using MRTM2 for all radioligands except [^{18}F]Altanserin, which was quantified using steady-state quantification (BP$_P$). For each target, the individual binding maps were averaged to create the final maps. Regional binding values were compared to autoradiography measurements and mRNA levels using linear regression.

Results: The average binding maps showed a good receptor/transporter distribution in accordance with literature values of regional densities as determined with autoradiography (R^2 between 0.34 and 0.83). The regression between mRNA and binding (figure 1A) indicated a strong association between mRNA levels and 5-HT$_{1A}$, 5-HT$_{2A}$ and 5-HT$_4$ (figure 1 B, D, E) but no significant association for 5-HT$_{1B}$ (C) and 5-HTT (A). A nonlinear (approximately log-linear) relationship was observed for the 5-HT$_{2A}$ binding (C-D); this relation appeared to be linear for cortical regions and was replicated with two different 5-HT$_{2A}$ receptor radioligands.

Conclusion: We here present high-resolution MR- and PET-based brain atlases of some important receptors and the transporter for the cerebral 5-HT system, to aid the neuroscientific community in future studies. The good correspondence between autoradiography and in vivo neuroimaging outcomes support the validity of these atlases. Finally, we have investigated the association between mRNA and binding and shown results which are in line with previous findings in animal models and humans [4–8]. The lack of association between mRNA and protein levels for 5-HT$_{1B}$ and 5-HTT may be due to the presynaptic localization of these targets, on nerve terminals in the 5-HT projection areas. Consistent with this, postsynaptic receptors (5-HT$_{1A}$, 5-HT$_{2A}$ and 5-HT$_4$) displayed a high correlation between mRNA levels and binding.
This new neuroimaging tool will be made publicly available to serve as an instrument for comparing related neuroscience modalities and as a comparative instrument to assess patients with brain disorders.

References:
[1] Varnäs, K., Halldin, C. and Hall, H. (2004) 'Autoradiographic distribution of serotonin transporters and receptor subtypes in human brain', *Human Brain Mapping*, **22**, 246–60
[2] French, L. and Paus, T. (2015) 'A FreeSurfer view of the cortical transcriptome generated from the Allen Human Brain Atlas', *Frontiers in Neuroscience*, **9**, 1–5
[3] Hawrylycz, M.J., Lein, E.S., Guillozet-Bongaarts, A.L., Shen, E.H., Ng, L., Miller, J.A. et al. (2012) 'An anatomically comprehensive atlas of the adult human brain transcriptome', *Nature*, **489**, 391–9

[4]   Pompeiano, M., Palacios, J.M. and Mengod, G. (1992) 'Distribution and cellular localization of mRNA coding for 5-HT1A receptor in the rat brain: correlation with receptor binding.', *The Journal of Neuroscience : The Official Journal of the Society for Neuroscience*, **12**, 440–53

[5]   López-Giménez, J., Vilaro, T.M., Palacios, J.M. and Mengod, G. (2001) 'Mapping of 5-HT2A receptors and their mRNA in monkey brain: [3H]MDL100,907 autoradiography and in situ hybridization studies', *Journal of Comparative Neurology*, **429**, 571–89

[6]   Varnäs, K., Hurd, Y.L. and Hall, H. (2005) 'Regional expression of 5-HT1B receptor mRNA in the human brain.', *Synapse*, **56**, 21–8

[7]   Vilaró, M.T., Cortés, R. and Mengod, G. (2005) 'Serotonin 5-HT4 receptors and their mRNAs in rat and guinea pig brain: distribution and effects of neurotoxic lesions.', *The Journal of Comparative Neurology*, **484**, 418–39

[8]   Zhou, F.C., Tao-Cheng, J.H., Segu, L., Patel, T. and Wang, Y. (1998) 'Serotonin transporters are located on the axons beyond the synaptic junctions: anatomical and functional evidence.', *Brain Research*, **805**, 241–54
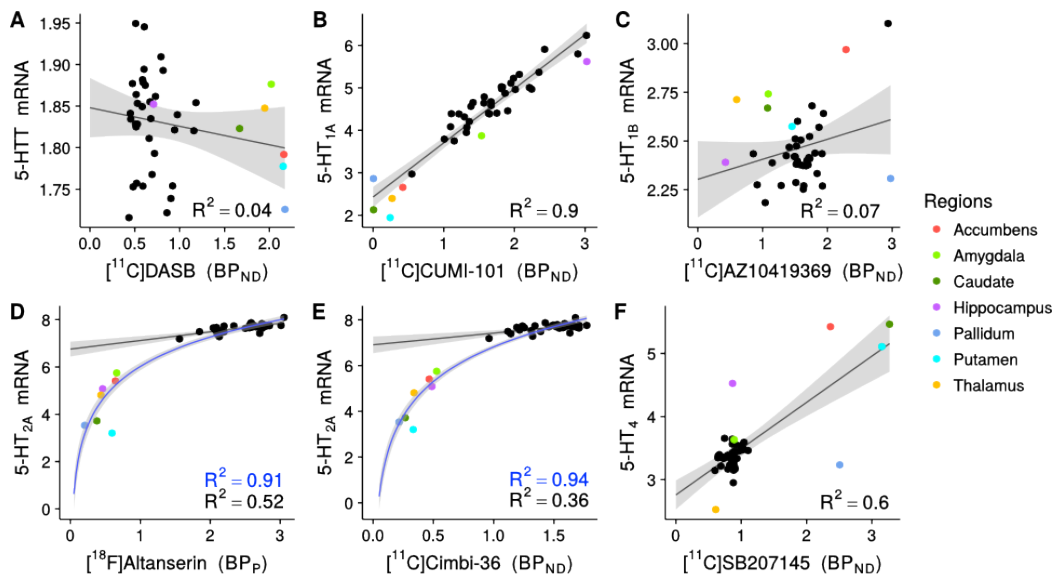
Figure 1. Association between mean regional binding values and mRNA levels for all radioligands. Cortical regions are shown in black and subcortical regions are shown in color. The regression line and associated R^2 are shown in black and the corresponding 95% confidence interval (CI) is shown in gray. Additionally, a log-linear regression (and the corresponding 95% CI and R^2) is shown in blue for panel D-E.

Comparison of zero-echo-time, head-atlas and [68]Ge-transmission attenuation correction for ^{11}C-PE2I-PET-MR dopamine transporter imaging

Joao M. Sousa[1], Lieuwe Appel[l], Stergios Papadimitriou[2], Dag Nyholm[2], Jens Sörensen[1], Torsten Danfors[1], Elna-Marie Larsson[1], Gaspar Delso[3], Florian Wiesinger[3], Håkan Ahlström[1], Mark Lubberink[1]

Departments of (1) Surgical Sciences and (2) Neurosciences, Uppsala University; (3) GE Healthcare.

Objectives: Incorporation of bone in MR-based attenuation maps in PET-MRI is a challenge because of the low proton density and fast decay time of bone tissue. The Dixon fat-water segmentation method, generally used for MR-based attenuation correction of PET data, does not allow for bone segmentation and omission of bone in attenuation maps affects the quantitative accuracy of PET data. The use of a CT-based head atlas, co-registered to and inserted into the individual patient's MR images, is one possibility to include bone tissue in attenuation maps of the head. The recent advent of zero-echo-time (ZTE) MR imaging, allowing for bone segmentation, has been shown to result in more anatomically accurate maps of bone tissue[1]. The aim of the present study was to assess the quantitative accuracy of head-atlas and ZTE-based attenuation correction in brain-PET-MR imaging by comparison to data corrected using a transmission scan with rotating [68]Ge rod sources, considered the gold standard for PET attenuation correction.

Methods: Five patients underwent 80 min PET scans using the specific dopamine transporter radioligand ^{11}C-PE2I (about 5 MBq/kg) on a time-of-flight integrated PET-MR scanner (Signa PET-MR). PET images were reconstructed using OSEM (2 iterations, 28 subsets, 5 mm Gaussian filter), applying three different attenuation correction methods: the standard head atlas-based method, a Dixon+ZTE-based attenuation map, and a co-registered [68]Ge-based transmission map acquired previously on an ECAT Exact HR+ scanner. The ZTE attenuation map was created by segmenting bone and air from a ZTE image and inserting these into the Dixon attenuation map. Volumes of interest were defined using a probabilistic template (PVElab) on T1-MRI images and transferred to all three PET images. Correlation and agreement between absolute radioactivity concentrations based on head-atlas and ZTE versus those based on [68]Ge correction in striatum, anterior and posterior cortical regions, limbic regions and cerebellum, as well as activity concentration ratios normalized to cerebellum, were assessed using regression and Bland Altman analysis.

Results: The table below shows correlation, slope of Deming regression, and bias of radioactivity concentrations in ^{11}C-PE2I PET images corrected with head-atlas and ZTE versus those corrected with [68]Ge attenuation correction. On average, the head-atlas method resulted in a positive bias ranging from 3.3% in limbic regions to 9.6% in posterior cortical regions, whereas ZTE showed a smaller negative bias ranging from -0.2% in striatum to -2.6% in posterior cortical regions. Correlation between ZTE-based and [68]Ge-based values in cortical regions was better than between head-atlas-based and [68]Ge-based values, and regression slopes were closer to 1 for ZTE in all regions. A paired t-test showed a significant overestimation in both anterior and posterior cortical regions using the head-atlas method, whereas no significant differences between ZTE-based and [68]Ge-based values were found. Normalisation of activity concentrations to cerebellum resulted in a considerably reduced bias in head-atlas based values, though still significant in posterior cortical regions.

Conclusion:
This study showed a high correlation and agreement between ^{11}C-PE2I PET images after ZTE and [68]Ge-based attenuation correction, whereas head-atlas attenuation correction resulted in a significant positive bias in cortical regions. ZTE appears to be an effective method for quantitatively accurate MR-based attenuation correction in PET-MR brain scans.

References:
[1]Delso et al, J Nucl Med 2015

	Head atlas				ZTE			
	R^2	Slope (CI)	Bias (CI)	t-test	R^2	Slope (CI)	Bias (CI)	t-test
STR	0.98	0.91 (0.79-1.02)	4.6 (-10.0 – 19.3)	ns	0.99	1.01 (0.92-1.09)	-0.2 (-10.8 – 10.4)	ns
ACR	0.76	0.71 (0.52-0.91)	6.6 (-18.2 – 31.3)	p<0.05	0.94	0.99 (0.87-1.11)	-1.9 (-12.5 – 8.7)	ns
PCR	0.54	0.72 (0.32-1.11)	9.4 (-18.4 – 37.1)	p<0.05	0.94	0.95 (0.81-1.09)	-2.6 (-12.5 – 7.3)	ns
LR	0.94	0.81 (0.71-0.91)	3.3 (-11.3 – 17.9)	ns	0.90	1.02 (0.84-1.19)	-1.2 (-17.0 – 14.7)	ns
CER	0.90	0.63 (0.25-1.01)	3.6 (-13.4 – 20.6)	ns	0.88	0.96 (0.31-1.61)	-1.0 (-14.0 – 11.9)	ns

STR: striatum; ACR: anterior cortical regions; PCR: posterior cortical regions; LR: limbic regions; CER: cerebellum

Quantitative image validation of PET-MR against stand-alone PET - A dynamic ^{11}C-PE2I PET study

Joao M. Sousa[1], Lieuwe Appel[l], Stergios Papadimitriou[2], Dag Nyholm[2], Jens Sörensen[1], Torsten Danfors[1], Elna-Marie Larsson[1], Håkan Ahlström[1], Mark Lubberink[1]

Departments of (1) Surgical Sciences and (2) Neurosciences, Uppsala University.

Objectives: For PET-MR, challenges incorporating bone in attenuation maps remain, which may affect quantitative accuracy of PET data. The stand-alone PET ECAT HR+ scanner, using rotating [68]Ge rod sources for attenuation correction, is often considered the gold standard for quantitative brain PET imaging. The aim of the present work was to compare quantitative measures of dopamine transporter availability and relative cerebral blood flow based on dynamic ^{11}C-PE2I-PET data acquired on a time-of-flight integrated PET-MR and a stand-alone PET scanner.

Methods: Six patients evaluated for Parkinsonism underwent two 80 min dynamic PET scans using the specific dopamine transporter radioligand ^{11}C-PE2I (about 5 MBq/kg). First they were investigated on a stand-alone PET scanner (ECAT HR+) and within 6 months they underwent a second investigation on a time-of-flight integrated PET-MR scanner (Signa PET-MR). ECAT images were reconstructed using OSEM (6 iterations, 8 subsets, 4 mm Hanning post-filter). PET-MR images were reconstructed using a resolution-matched protocol (OSEM; 2 iterations, 28 subsets, 5 mm Gaussian filter). PET-MR attenuation correction was based on a head atlas method. Both dynamic PET series were co-registered to T1-MRI images using SPM8. Volumes of interest were defined using a probabilistic template (PVElab) on the T1- MRI images and transferred to both sets of PET images. Binding potential (BP_{ND}), reflecting dopamine transporter availability, and relative cerebral blood flow (R_1) were derived from the PET images for a number of clinically relevant tissues using the simplified reference tissue model, with cerebellar grey matter as reference tissue. BP_{ND} in putamen, and R_1 in striatum as well as anterior cortical, posterior cortical, and limbic regions, were compared between both modalities using regression and Bland-Altman analysis.

Results: PET-MR BP_{ND} in putamen agreed well with stand-alone PET BP_{ND} (R^2 0.97), with a slope of 0.86 (CI 0.64-1.09) and intercept of 0.36 (CI -0.39 – 1.11), and no significant bias. PET-MR R_1 correlated best with stand-alone PET in striatum and limbic regions (R^2 0.95 and 0.89, respectively), with lower values in anterior and posterior cortex (R^2 0.70 and 0.45). A significant positive bias of PET-MR R_1 values was found in posterior cortex (bias 0.14, CI 0.02-0.25). Correlation plots are shown in Figure 1.

Conclusion:

This study showed a good agreement between the PET-MR and stand-alone PET for BP_{ND} in putamen and for R_1 in striatal and limbic regions. However, cortical regions presented relatively low correlations between R_1 values based on both modalities, which might be explained by the attenuation correction method. Besides extension of the number of patients, additional investigations assessing other attenuation correction methods for further improvement of the quantitative accuracy of dynamic PET-MR data are required.
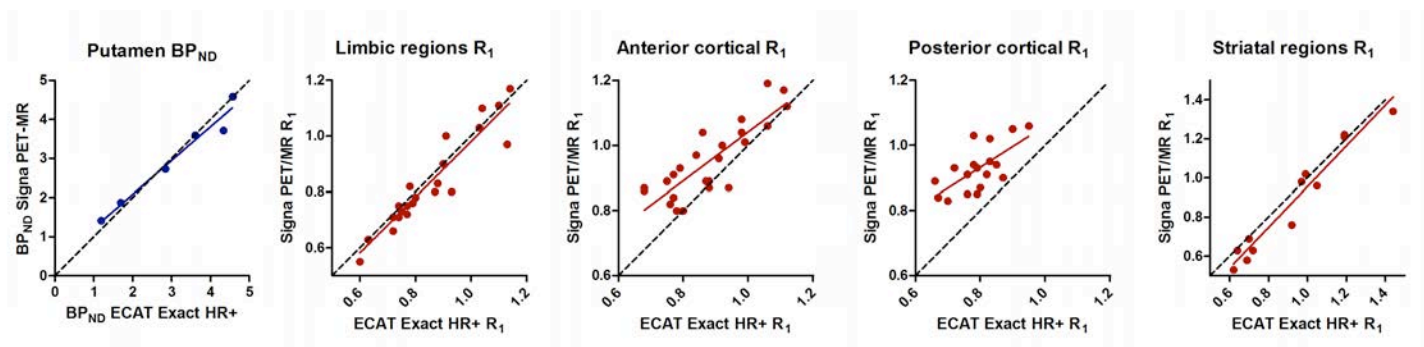
Figure 1 – PET-MR versus stand-alone PET BP_{ND} (left panel) and R_1 values. The black lines are lines of identity; the colored lines are regressions.

First-in-Human Dynamic PET Brain Imaging of [18F] Fluortriopride, a Dopamine D3 Receptor Selective Radiotracer

Jacob Dubroff[1], Robert Doot[1], Chris Ward[2], Jenny Cai[1], Hsiaoju Lee[1], Erin Schubert[1], Shihong Li[1], Catherine Hou[1], Regan Sheffer[1], Alexander Schmitz[1] and Robert Mach[1]

University of Pennsylvania, Perelman School of Medicine: [1] Department of Radiology, Division of Nuclear Medicine and Molecular Imaging; [2] Department of Anesthesiology and Critical Care

Background: The dopamine D3 receptor is thought to represent the principal neural substrate of the dopaminergic mesolimbic circuit, the primary reward pathway in the mammalian brain. D3 receptor dysfunction has been implicated in many diseases including drug addiction, Parkinson's disease, and schizophrenia. For these reasons, the dopamine D2-like receptors (i.e., D2/3 receptors) have been the most extensively studied CNS receptor with PET. There are 3 different radiotracers which have been largely used in these studies: [11C]raclopride, [18F]fallypride;, and[11C]PHNO. Raclopride and fallypride are nonselective dopamine D2/3 antagonists; raclopride has an affinity for D2 and D3 receptors in the low nM range, whereas fallypride has a sub-nM affinity for both receptors. Consequently, PET studies with [11C]raclopride and [18F]fallypride provide a measurement of the D2/3 binding potential. The sub-nM affinity for D3 receptors indicates that imaging studies with [18F]fallypride result in a higher labeling of D3 receptors than what is observed with [11C]raclopride. Although [11C]PHNO is recognized to be preferential for D3 (vs D2) receptors, it is not selective for D3. [18F]Fluortriopride (FTP) is a novel radioligand that demonstrates high specificity for D3 vs D2 receptors (>160-fold). In anesthetized non-human primates, [18F]FTP binding was sensitive to levels of endogenous dopamine but reflected the distribution of D3 receptors as determined by autoradiography (1,2). To further evaluate the applications of this radiotracer, we performed the described first-in-human studies.

Methods: Bilateral upper extremity IV access and left upper extremity arterial line access were obtained in 5 healthy adult volunteers (1 female and 4 males, ages 23-51, mean 32). Then, each underwent 2 hours of dynamic PET brain imaging following the intravenous administration of [F-18] FTP (7.0 mCi, 6.79-7.34). Dynamic venous and arterial sampling was performed with subsequent metabolite analysis. Each participant also underwent high resolution MRI T1 imaging with isotropic voxels for co-registration with the PET data.

Results: In all 5 of the healthy volunteers, [18F] FTP brain distribution reflects the same pattern observed in post mortem quantitative autoradiography (3) as well as non-human primate PET imaging (2). A representative transaxial brain image demonstrates [18F]FTP binding in caudate (A), putamen (B), and thalamus (C). Uptake also localizes to the choroid plexus (D). Metabolite analysis of arterial blood demonstrated a single polar metabolite with identical HPLC retention time to previously reported metabolite values in rat and nonhuman primates. This polar metabolite should not be able cross the blood brain barrier.

Conclusion: [18F] Fluortriopride PET brain distribution parallels that seen in prior human quantitative autoradiography and non-human primate PET studies. Higher uptake in the thalamus, a known D3 dopamine receptor rich region, relative to regions such as the caudate and putamen that have high levels of both D2 and D3 receptors (3) distinguishes it from other probes. These data warrant further investigation examining the effect of modulating endogenous dopamine as well as its behavior in disease states.

References:
1. Synapse. 2010 Jun;64(6):449-59; 2. Synapse. 2011 Aug;65(8):724-32; 3. PLoS One. 2012;7(11):e49483.
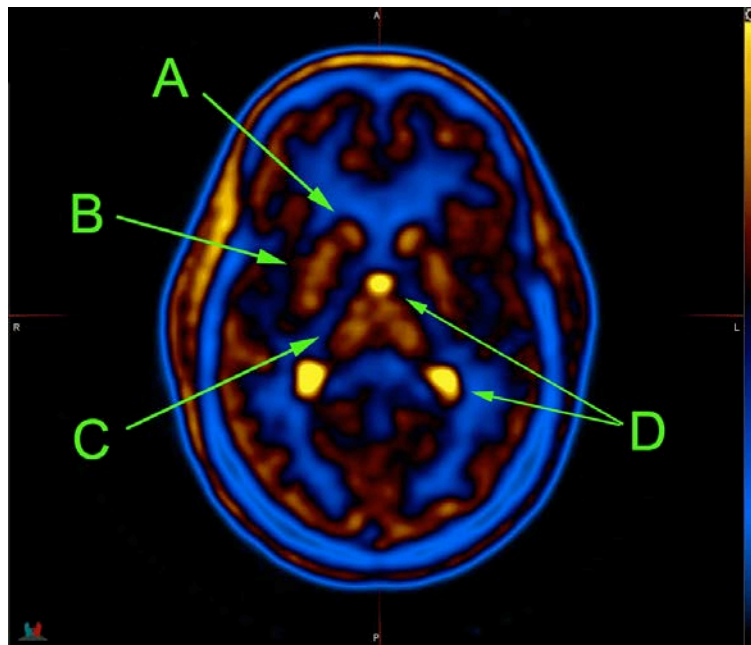
Reproducibility studies of [11C]-yohimbine using 2 different input functions

Alex Z. Kadhim[1*], Schildt A[1*], Steen Jakobsen[2], Vesna Sossi[3], Doris J. Doudet[1,2]

[1] *Department of Medicine/Neurology, 2221 Wesbrook Mall, Vancouver, BC, Canada V6T 1Z3, Canada;* [2] *Department of Nuclear Medicine and PET-Centre, Aarhus University and Hospital, Nørrebrogade 44, Building 10G, 8000, Aarhus C, Denmark;* [3] *Department of Physics and Astronomy, 2221 Wesbrook Mall, Vancouver, BC, Canada*
*Equal contribution

Aims: To determine the reproducibility [11C]-yohimbine as a PET tracer to image α2 adrenergic receptors in humans

Introduction: Noradrenaline plays important roles in many biological processes such as sleep, circadian rhythms, pain modulation and stress response as well as in neurodegenerative diseases and mood disorders. Yet, its exact role and function remain unclear. In this study, we sought to determine the reproducibility and stability of the binding of a new α2 adrenergic receptor tracer ([11C]-yohimbine) in healthy volunteers, using either a metabolite-corrected arterialized venous input or a white matter region as non-specific input for calculation of the total volume of distribution V_T or the binding potential BP_{ND} .

Methods: 4 healthy subjects were scanned twice using a Siemens high resolution research tomograph (HRRT). Each dynamic emission scan lasted 90 min from tracer administration and consisted of 17 frames of increasing duration. The subjects underwent T1-weighted MR imaging for registration purposes. PET images were registered to a standard MRI atlas using MNI tools. Volume of interest (VOIs) were applied to the normalized registered dynamic data and time activity curves in multiple cortical and subcortical (striatum, thalamus, hippocampus) regions, cerebellum and corpus callosum were created. Arterialized venous samples were collected throughout the scans for acquisition of a total time activity curve and measurement of free fraction. Yohimbine and metabolites were measured throughout each scan using high performance liquid chromatography (HPLC). The metabolite corrected curve was then used for Logan plot linear regression analysis to determine V_T.   Alternatively, the corpus callosum, a white matter region with the consistently lowest V_T, was used as a non-specific binding region to measure the distribution volume ratio (DVR) and BP_{ND} as DVR-1.

Results: The free fraction was consistent between subjects (9 ±0.02%) and stable between scans. As previously reported (Nahimi et al. 2015), metabolism between subjects was variable (including one low or non-metabolizer). There was however some subtle differences between the morning and afternoon scans with apparent faster metabolism (disappearance of the parent compound) in the 2nd, afternoon, scans, differences that will need to be investigated in a larger sample. Using the metabolite corrected input function, and in this small sample of subjects, the approximate test-retest reproducibility between scans 1 and 2 was 20-25%.
The binding potential BP_{ND} showed little variability between subjects and between cortical and subcortical regions (BP_{ND}: 0.2 to 0.5). The test-retest reproducibility was however highly reduced (8-12%) between scans in all regions.

Conclusion: As has been consistently reported for many tracers, the reproducibility was much reduced when a region of non-specific binding was used to measure the parameter of interest instead of a metabolite-corrected plasma input. While arterialized venous sampling (as opposed to arterial) was chosen to investigate the possibility to reduce burden and increase participation for clinical studies, the major hurdle remains the variability associated with HPLC measurement.   If further studies (including challenge studies) confirm the use of a white matter region as a feasible and reliable alternative to plasma input, yohimbine will prove a useful tracer for investigation of the α2 adrenergic receptors in humans and image changes in NA release (Landau et al. 2013).

In vivo comparison of [18F]-(S)THK5117 and [18F]-THK5351 in presymptomatic and symptomatic Alzheimer's disease

Tobey J Betthauser[1,2], Patrick J Lao[1,2], Dhanabalan Murali[1], Todd E Barnhart[1], Shozo Furumoto[3], Nobuyuki Okamura[4], Charles K Stone[5], Sterling C Johnson[6], Bradley T Christian[1,2]

[1] Department of Medical Physics, University of Wisconsin, Madison, WI, USA; [2] Waisman Laboratory for Brain Imaging and Behavior, University of Wisconsin, Madison, WI, USA; [3] Division of Radiopharmaceutical Chemistry, Tohoku University, Sendai, Japan; [4] Division of Radiopharmaceutical Neuroimaging, Tohoku University, Sendai, Japan; [5] Department of Medicine, University of Wisconsin, Madison, WI, USA; [6] Wisconsin Alzheimer's Disease Research Center, University of Wisconsin, Madison, WI, USA

Introduction: 18F-(S)THK5117 and 18F-THK5351 are tau specific PET radioligands for detection of Alzheimer's disease (AD) tau aggregates. In vivo studies with arterial blood sampling have validated the Logan reference tissue method (30-60 min) for (S)THK5117 binding estimation, and indicated SUVR overestimates white matter (WM) more than gray matter (GM) at late time points (70-90 min) (Jonasson, M, et al. 2016). Comparatively, THK5351 has been shown to have reduced WM uptake and faster kinetics (Okamura, N, er al. 2015). This work compares in vivo kinetics and binding characteristics of (S)THK5117 and THK5351 and reference based methods for estimating specific tracer binding.

Methods: Seventeen subjects were recruited from the Wisconsin Registry for Alzheimer's Disease and UW Alzheimer's Disease Research Center cohorts. Subjects were grouped ranging from cognitively normal to AD based on longitudinal neuropsychological evaluation and clinical diagnosis. Ninety minute dynamic THK5351 (N=11) and/or (S)THK5117 (N=14) PET scans were acquired on a Siemens ECAT HR+, along with T1w MRI on a GE Signa 750. Reconstructed PET data were coregistered to T1w MRI, and time activity curves (TACs) were extracted from cerebellar GM and 38 unilateral FreeSurfer derived ROIs. Standard uptake values (SUVs) and TACs normalized to maximum bolus signal (t = 2-4 min) were used to compare uptake and clearance in cerebellar GM. Using cerebellar GM as a reference region, target-to-reference ratios were used to assess kinetics, and specific binding was estimated using reference tissue methods (SUVR, Logan, MRTM2, SRTM). Binding estimates were compared by linear regression with Logan DVR (30-60 min, k_2 term removed). SUVR timing windows were assessed in 20 minute intervals centered at 30, 40, 50, 60, 70 and 80 min post injection.

Results: Compared to (S)THK5117, THK5351 cerebellar GM showed a 48±5% decrease in SUV after bolus passage (t>10 min) and more rapid clearance. Target-to-cerebellum ratios plateau faster in low and moderate binding regions with THK5351 and reach higher max values for GM ROIs and lower values for WM at the end of 90 minutes. Linearization of Logan plots occurs at t*=30 min for both THK5351 and (S)THK5117. Regression with Logan DVR showed agreement with MRTM2 (1.08xLogan-0.09,R^2=0.99) and SRTM (1.07xLogan-0.08,R^2=0.96) for THK5351, but less so for (S)THK5117 (MRTM2=1.11xLogan-0.05,R^2=0.93; SRTM=0.64xLogan+0.55,R^2=0.109) with SRTM failing to converge in 0.5% and 6.6% of ROIs for THK5351 and (S)THK5117, respectively. SUVR increasingly overestimated binding compared to Logan as the SUVR timing window was shifted later, though regression slope parameters were not significantly different for SUVR windows beyond 50-70 min for both radiotracers. Regression slopes were increasingly greater for WM compared to GM for (S)THK5117 as the SUVR window was further delayed, whereas the opposite was observed for THK5351.

Conclusions: Compared to (S)THK5117, THK5351 shows lower brain penetrance, more rapid cerebellar GM clearance, higher GM-to-WM signal, and increased signal in GM tau. Increased binding estimates for THK5351 indicate improved sensitivity for detecting AD tau, which may improve early detection. SUVRs are confounded by high WM binding with (S)THK5117, but are likely useful for THK5351. Studies comparing regional (S)THK5117 and THK5351 binding are ongoing.
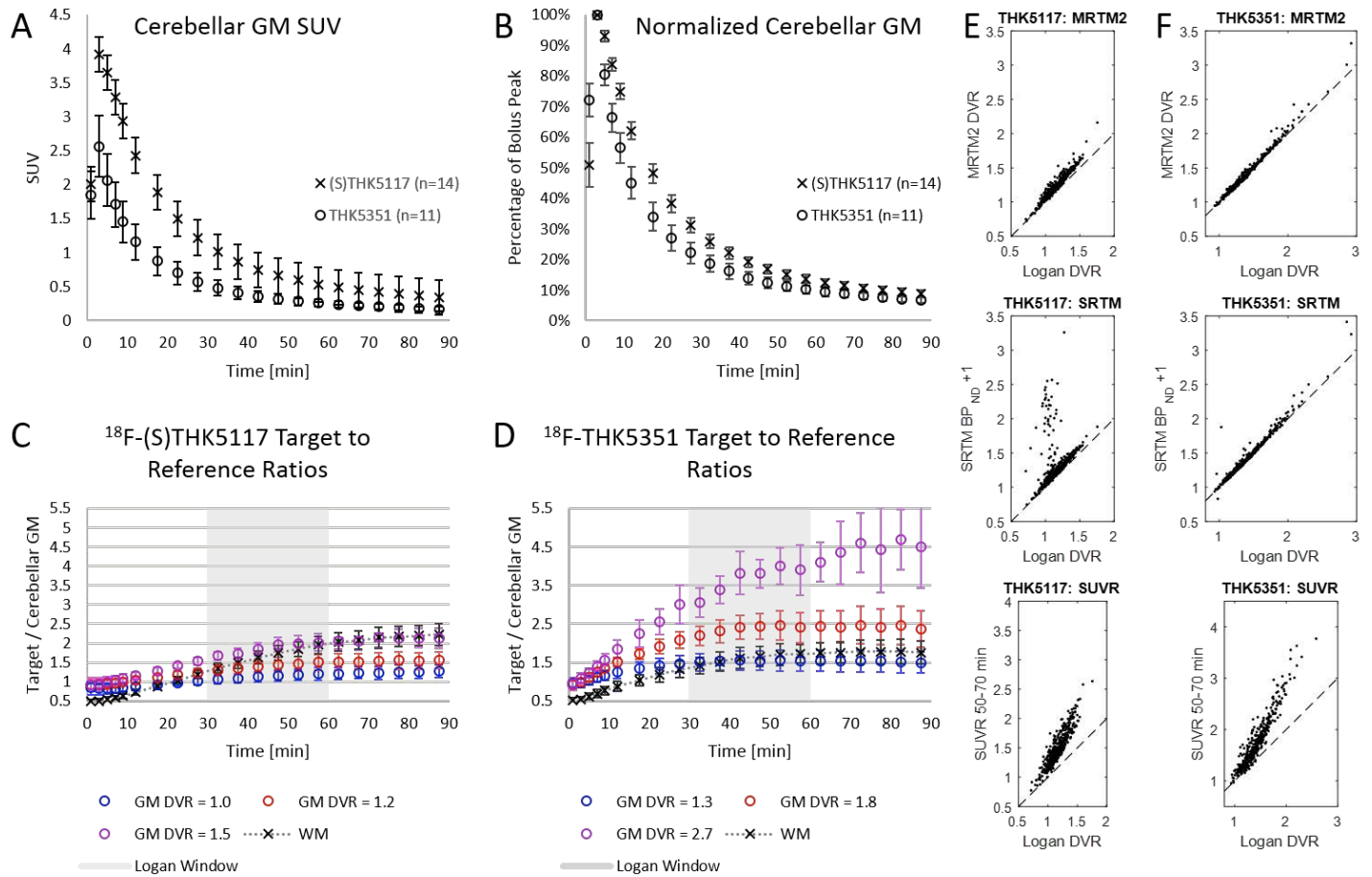
Figure 1: Comparison of in vivo (S)THK5117 and THK5351 kinetic properties in cerebellar gray matter (A and B), and in low, middle, and high binding gray matter and white matter ROIs (C and D). Compared to (S)THK5117, THK5351 shows reduced brain penetrance (A), faster clearance in cerebellar GM (B), more rapid kinetics in GM and WM and reduced WM signal relative to cortical GM (C and D). Low, middle and high binding regions represent the lower, middle, and upper third of ROI DVR values across all subjects and ROIs for each tracer. E and F scatter plots demonstrate concordance of binding estimates for various reference tissue methods with Logan DVR. The dashed line represents the identity line (x=y).

5-HT1A Binding in Depression With and Without Disturbed Thinking

Stephanie Mulhern[1], John Keilp[2], Zenas Ignobias[3], Jeffrey Miller[4], R. Todd Ogden[5], Matthew Milak[6], Maria Oquendo[7], Ramin Parsey[8], John Mann[9]

[1] Department of Psychiatry, Columbia University, College of Physicians and Surgeons, New York, New York, United States; [2] Department of Psychiatry, Columbia University, College of Physicians and Surgeons, New York, New York, United States; Molecular Imaging and Neuropathology Division, New York State Psychiatric Institute, New York, New York, United States; [3] Department of Psychiatry, Columbia University, College of Physicians and Surgeons, New York, New York, United States; [4] Department of Psychiatry, Columbia University, College of Physicians and Surgeons, New York, New York, United States; Molecular Imaging and Neuropathology Division, New York State Psychiatric Institute, New York, New York, United States; [5] Department of Biostatistics, Columbia University, Mailman School of Public Health, New York, New York, United States; Molecular Imaging and Neuropathology Division, New York State Psychiatric Institute, New York, New York, United States; [6] Department of Psychiatry, Columbia University, College of Physicians and Surgeons, New York, New York, United States; Molecular Imaging and Neuropathology Division, New York State Psychiatric Institute, New York, New York, United States; [7] Department of Psychiatry, Columbia University, College of Physicians and Surgeons, New York, New York, United States; Molecular Imaging and Neuropathology Division, New York State Psychiatric Institute, New York, New York, United States; [8] Department of Psychiatry, Stony Brook Medicine, Stony Brook, New York, United States; [9] Departments of Psychiatry and Radiology, Columbia University, College of Physicians and Surgeons, New York, New York, United States; Molecular Imaging and Neuropathology Division, New York State Psychiatric Institute, New York, New York, United States.

Introduction: The challenge of understanding the pathophysiology of major depressive disorder (MDD) partially stems from the pleomorphic nature of its clinical manifestations. We have demonstrated that MDD patients have elevated serotonin 1A (5-HT_{1A}) receptor binding across brain regions of interest (ROIs). Using fluorodeoxyglucose (^{18}F) positron emission tomography **(**FDG-PET), we previously found that depressed individuals presented with distinct patterns of resting glucose metabolic rate in association with *specific symptom factors* derived from the Beck Depression Inventory (BDI), including subjective depression, self-blame, and somatic complaints. In this study, we examined the relationship between 5-HT_{1A} binding in MDD and healthy volunteers (HV) and symptom factors derived from both the Hamilton Depression Rating Scale (HDRS) and the BDI.

Methods: We used [^{11}C]WAY100635 to quantify 5-HT_{1A} binding in a cohort of 106 unmedicated MDD patients in a current major depressive episode and 57 HV. We acquired a metabolite-corrected arterial input function and estimated binding potential (BP_F) in 13 *a priori* regions of interest using kinetic modeling with a 2-tissue compartment model and cerebellar white matter as reference region. Depression factors were derived from the HDRS and BDI as previously described{Grunebaum, 2005, 15923041}. The relationship between these depression factors and 5-HT_{1A} binding was evaluated using a linear mixed effects model (with sex and genotype as covariates, subject ID as a random effect and symptom factors and diagnoses as fixed effects).

Results: In the MDD group, we found a significant negative correlation between HDRS factor 3: disturbed thinking (comprising lack of insight, depersonalization, paranoia and obsessive compulsive thinking) and 5-HT_{1A} binding (p=0.0125). Depressed individuals with disturbed thinking (n=49) had lower levels of 5-HT_{1A} binding across all regions of interest compared to depressed individuals without disturbed thinking (n=57) and had levels comparable to healthy volunteers. No other symptom factor was related to 5-HT_{1A} binding.

Conclusions: These findings suggest a difference in the pathophysiology of MDD with and without disturbed thinking. MDD with disturbed thinking may be less dependent on serotonergic function, which if replicated in additional samples may be informative to physicians planning MDD treatment.

Estimation of [^{11}C]PBR28 non-displaceable binding without the use of a reference region

Pontus Plaven-Sigray[1], Martin Schain[1,2], Francesca Zanderigo[2,3], R. Todd Ogden[2,3,4], Karin Collste[1], Anton Forsberg[1], Christer Halldin[1], Lars Farde[1], Andrea Varrone[1] and Simon Cervenka[1]

[1]*Department of Clinical Neuroscience, Karolinska Institutet, Stockholm, Sweden;* [2]*Department of Molecular Imaging and Neuropathology, New York State Psychiatric Institute, New York, NY, USA;* [3]*Department of Psychiatry, Columbia University, New York, NY, USA;* [4]*Department of Biostatistics, Columbia University, Mailman School of Public Health, New York, New York, USA*

Objective: Estimation of non-displaceable binding potential (BP_{ND}) in PET studies relies on the existence of a brain region devoid of the target of interest. This requirement is not fulfilled for the Translocator Protein, which is expressed in immune cells throughout the brain. In studies using [^{11}C]PBR28, the two-tissue-compartment model (2TCM) is commonly used to estimate the distribution volume (V_T). However, as BP_{ND} relates the concentration of specifically bound radioligand to the non-displaceable concentration, theoretically this parameter should have higher sensitivity than V_T. Recently, a novel approach for estimation of the non-displaceable distribution volume (V_{ND}) without using a reference region has been described (1). Here, we applied this method to estimate [^{11}C]PBR28 distribution volume ratio (DVR) and BP_{ND}, and evaluated the reproducibility of these outcome measures using a test-retest dataset.

Methods: Eight healthy subjects (four females, four males, four mixed affinity binders and four high affinity binders) with a mean age of 23.8±3.3 years were examined twice using [^{11}C]PBR28 and the High-Resolution Research Tomograph. Grey matter (GM) V_T values were derived using the standard 2TCM and an arterial input function. V_{ND} for every individual examination was derived following the previously described procedure (1). In brief, the algorithm operates by identifying the V_{ND} that results in the lowest sum of squared residuals of fits across multiple regions. This is achieved by searching for the minimum in a grid consisting of a range of candidate V_{ND} values and their corresponding cost functions. GM DVR and BP_{ND} were calculated using the estimated V_{ND} values and V_T values derived from the standard 2TCM. Average absolute percentage differences (AAPD) were calculated for all parameters as a measure of reproducibility. Additionally, since DVR, BP_{ND} and V_T values have different means and are of different units, the outcome values were rescaled to have a mean of zero, in order to allow for comparison of AAPD between the different parameters.

Results and conclusion: For all 16 measurements, clear minima of the cost functions were observed, allowing for good identifiability of V_{ND} values. V_T and V_{ND} values were significantly correlated (r=0.8, df=14, p<0.001). Table 1 shows descriptive and test-retest statistics of the estimated outcome measures. Mean, standard deviation and range of the obtained V_{ND} values were similar to those previously described in a pharmacological blocking study with [^{11}C]PBR28 (2). AAPD for calculated BP_{ND} and DVR values were within acceptable range of reproducibility. Rescaled DVR and BP_{ND} values showed slightly lower AAPD compared to rescaled V_T values. The method evaluated in this study may be useful for estimation of DVR or BP_{ND} of [^{11}C]PBR28 and should be validated using blocking data.

References

1. Ogden RT, Zanderigo F, Parsey R V (2015): Estimation of in vivo nonspecific binding in positron emission tomography studies without requiring a reference region. *Neuroimage*. 108: 234–242.
2. Owen DR, Guo Q, Kalk NJ, Colasanti A, Kalogiannopoulou D, Dimber R, *et al.* (2014): Determination of [11C]PBR28 binding potential in vivo: a first human TSPO blocking study. *J Cereb Blood Flow Metab*. 34: 989–994.

Table 1. Descriptive and test-retest statistics of estimated parameters. Statistics for V_{ND} values from Owen et al. are extracted from the Figure 3C occupancy plot in Owen et al. (2014). For comparative reasons the estimated parameters were rescaled by subtracting the parameter mean from every individual value to create zero-centered scales, as shown in the *Centered* column.

	Mean (SD)	Range	CoV	Mean APD (SD)	Mean APD (SD) Centered*	Mean AND (SD)
V_{ND} Owen et al.	1.89 (0.65)	0.95-2.45	0.35	-	-	-
V_{ND} PET1	1.69 (0.76)	0.79-2.88	0.45	12% (15%)	35% (38%)	0.15 (0.10)
V_{ND} PET2	1.67 (0.78)	0.70-2.80	0.47			
V_T GM PET1	3.62 (1.94)	1.38-7.58	0.54	10% (14%)	47% (64%)	0.31 (0.31)
V_T GM PET2	3.80 (1.92)	1.42-7.71	0.51			
BP_{ND} GM PET1	1.17 (0.63)	0.70-2.27	0.54	19% (25%)	37% (47%)	0.21 (0.26)
BP_{ND} GM PET2	1.31 (0.54)	0.77-2.22	0.41			
DVR GM PET1	2.17 (0.63)	1.70-3.27	0.29	10% (14%)	37% (47%)	0.21 (0.26)
DVR GM PET2	2.31 (0.54)	1.77-3.22	0.23			

CoV=coefficient of variance; APD= Absolute percentage difference; AND=Absolute numerical difference; PET1=first examination; PET2=second examination; DVR is calculated as V_T/V_{ND}; BP_{ND} is calculated as V_T/V_{ND}-1

* Values were centered on their respective means and APD was then calculated.

Assessing the affect of image post processing on parameter estimates for [^{18}F]DPA-714 in the healthy human

Catriona Wimberley[1], Anthonin Reilhac[4], Marie-Anne Peyronneau[1], Simon Stute[1], Vincent Brulon[1], Claude Comtat[1], Sonia Lavisse[2,3], Claire Leroy[1], Philippe Remy[2,3,5,6], Bruno Stankoff[7,8], Michel Bottlaender[1,9], Irene Buvat[1]

[1]IMIV, Inserm, CEA, Paris-Sud Univ, Orsay, France; [2]MIRCen, CEA, Fontenay-aux-Roses, France; [3]CNRS-UMR9199, Univ Paris-Sud, Fontenay-aux-Roses, France; [4]CERMEP, Lyon, France; [5]Centre Expert Parkins, Neurology Department, CHU Henri Mondor, AP-HP, Créteil, France; [6]Paris-Est University, Créteil, France; [7]Institut du Cerveau et de la Moelle épinière, ICM, Paris, France; Inserm, U 1127, F-75013, Paris, France and Sorbonne University, UPMC Univ Paris 06, UMR S 1127, Paris, France; [8]CNRS, UMR 7225, F-75013, Paris, France; [9]Neurospin, CEA, Gif-sur-Yvette, France

Objectives: TSPO has been identified as a suitable marker for inflammation that may occur in neurodegenerative diseases and [18F]DPA-714 is one of several second generation TSPO tracers used in PET imaging. [18F]DPA-714 PET scans can be affected by partial volume effect and noise which can impact the estimates of the binding parameters. In this study, we investigated the impact of post reconstruction processing to remove noise and improve spatial resolution on parameter estimation of [18F]DPA-714 PET in healthy human subjects.

Methods: Eight healthy human subjects (5 high affinity binders, HAB, 3 mixed affinity binders, MAB) underwent [18F]DPA-714 PET on the HRRT scanner with arterial blood sampling[1]. The scans were reconstructed with AB-EMML with PSF modelling[2], and post-smoothing[3]. A 4D iterative deconvolution (5 iterations) and spatiotemporal regularisation process (ID-SR) were used for spatial resolution recovery and noise removal[4]. The two tissue compartmental model with an extra compartment included for vascular trapping (2TCM-1K) as described by Rizzo et al. 2014[5] (found as most appropriate in a parallel study) was applied with metabolite corrected arterial input function. The parameter estimates from the 2TCM-1K were compared with and without the ID-SR.

Results: Before the ID-SR, the regional estimates varied from 2.78 to 5.02 mL/cm3 for Vt and 1.50 to 5.79 for BPnd in HABs; from 2.09 to 3.77 mL/cm3 for Vt, and 0.85 to 4.01 for BPnd in MABs. After applying ID-SR, the regional parameter estimates varied from 2.36 to 3.72 mL/cm3 for Vt, and 1.71 to 2.11 for BPnd in HABs; from 1.94 to 3.20 mL/cm3 for Vt, and 1.02 to 1.25 for BPnd in MABs. The Vt and BPnd values were significantly lower (p<0.01) in MABs than HABs after applying ID-SR.
With the use of ID-SR, the parameter estimates were much better identified compared to without ID-SR, with average standard error (SE) value changing from 16% (before ID-SR) to 7% (after ID-SR) for Vt and from 49% to 23% for BPnd. The regional standard deviation for parameter estimates decreased for the HABs: Vt 60% to 55% and BPnd 77% to 51%. For the MABs, the standard deviation for Vt increased slightly from 12% to 14% but reduced for BPnd from 88% to 66%. The typical value for the vascular binding rate constant, kb, was reduced and more stable after ID-SR processing compared to before processing, at 0.19±0.09 (HAB) and 0.12±0.05 (MAB) compared to 0.61±1.08 (HAB) and 0.65±1.01 (MAB).

Conclusion: This study examined the impact that post processing of images can have on parameter estimate identifiability and variability. Applying the ID-SR to remove noise and recover spatial resolution improved the identifiability of all estimated parameters and reduced the variability of most parameters estimated (except where there was already a low level of variability).

References:
(1) Lavisse, S; Garcia-Lorenzo, D; Peyronneau, MA et al.; Optimized Quantification of Translocator Protein Radioligand [18F]DPA-714 Uptake in the Brain of Genotyped Healthy Volunteers; J Nucl Med. (2015), 56(7):1048-54.
(2) Van Slambrouck, K; Stute, S; Comtat, C et al.; Bias Reduction for Low-Statistics PET: Maximum Likelihood Reconstruction With a Modified Poisson Distribution, IEEE Transactions on Medical Imaging 34 (2015), 126-136.
(3) Stute, S and Comtat, C.; Practical considerations for image-based PSF and blobs reconstruction in PET; Physics in Medicine and Biology 58 (2013), 3849-3870.
(4) Reilhac, A; Charil A; Wimberley, C et al.; 4D PET iterative deconvolution with spatiotemporal regularization for quantitative dynamic PET imaging; Neuroimage (2015), 118:484-93

(5) Rizzo, G; Veronese, M; Tonietto, M et al.; Kinetic modeling without accounting for the vascular component impairs the quantification of [11C]PBR-28 brain PET data.; JCBFM (2014), 34(6):1060-9
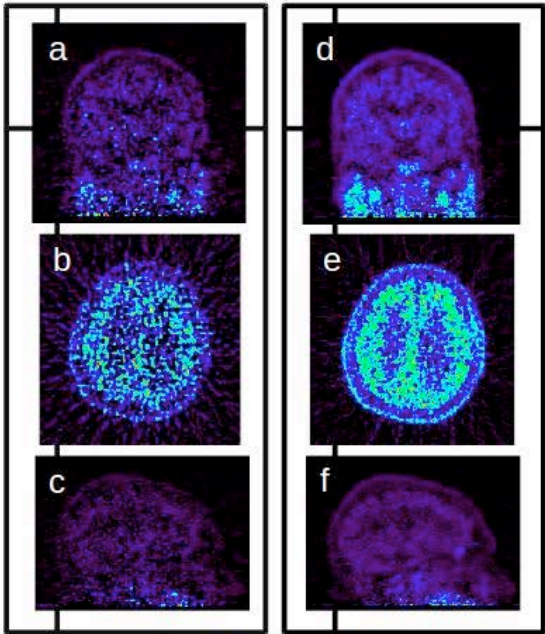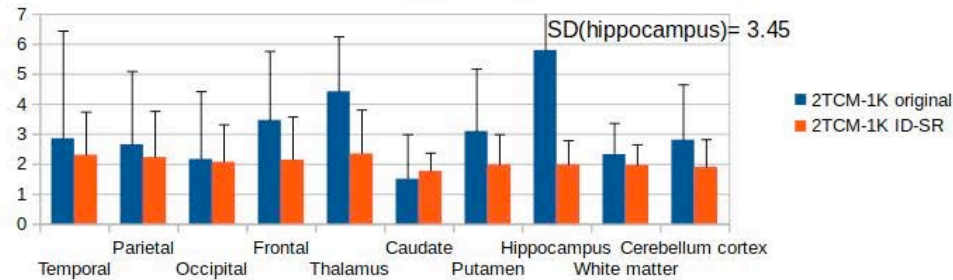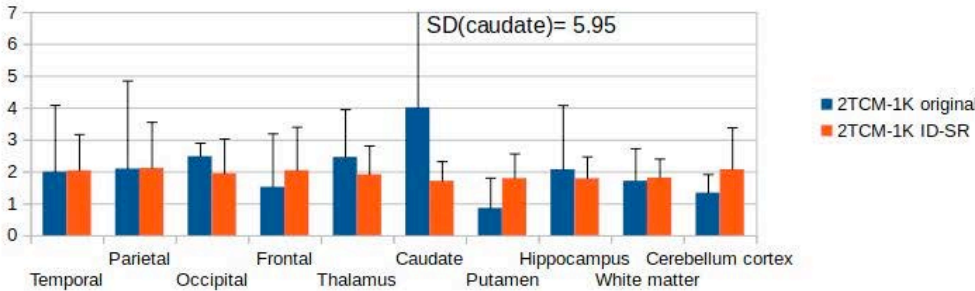

Figure i. a: PET of one patient, frame 20-25 mins 1. original AB-EMML reconstruction a). coronal, b). transverse and c). sagittal and d-f). after ID-SR processing in the same views.

ii. BPnd - HABs

SD(hippocampus)= 3.45

- 2TCM-1K original
- 2TCM-1K ID-SR

iii. BPnd - MABs

SD(caudate)= 5.95

- 2TCM-1K original
- 2TCM-1K ID-SR

Strategies to ensure quality, consistency and reproducibility of PET analysis

Graham E. Searle[1], Christopher Coello[1], Roger N. Gunn[1,2,3]

[1] *Imanova Ltd, London, UK ;* [2] *Department of Medicine, Imperial College London, London, UK ;* [3] *Department of Engineering Science, University of Oxford, Oxford, UK*

Introduction: Quantitative imaging analysis has historically required many human steps with several software packages and 'home brew' scripts to perform the analysis workflow from acquired data to end results. The software and workflow employed, along with their myriad options are often detailed in individuals' notebooks and neither controlled nor entirely reproducible. This can lead to inefficiency, inconsistency through human error, and end results which are difficult or impossible to reproduce later or extend by others to new data sets.

Independent replication has always been a cornerstone of science; modelling and data analysis are somewhat unique in that perfect replication is perfectly possible. This not only enables verification of results, but also the ability for others to build upon initial research, both in the extension of the methodology and its application. This is becoming ever-more important with the increase in shared databases (e.g. for large scale studies of neurodegeneration).

Here we discuss strategies to ensure the quality, consistency (intra- and inter-study) and reproducibility of PET data analysis, and introduce MIAKAT, a software package designed to support these strategies.

Methods

Choice of workflow: each research centre (and to an extent each individual) has their own preferences on the specifics of how PET neuroimaging data should be analysed, but there is a degree of convergence across the field. Examples include the definition of ROIs on a subject's MRI via nonlinear deformation of template and atlas images, subject motion correction for dynamic PET images, the standard methods for derivation of parent in plasma input functions from measured arterial data, and the application of a comprehensive set of compartmental and other modelling techniques. An example analysis workflow is depicted in Figure 1. This represents or approximates workflows currently employed by most of the top research centres.

Detailed descriptions: the workflow employed, together with the details of each step should be recorded in a manner which facilitates review and reproduction. This could include software configuration files, or simply a detailed breakdown of the processes performed, and could be made available as part of e.g. 'supplemental data' for a journal paper, or on researchers' own websites.

Software choices: several software packages are in use for analysis of PET neuroimaging data. Few are capable of running the entire analysis workflow from primary data through to end results. We have recently released MIAKAT, a MATLAB toolbox for analysis of PET neuroimaging data. MIAKAT enables users to use a standard workflow, with study specific refinements and options, and apply that consistently to all subjects within a study. The analysis performed is recorded, along with a QC audit trail, making it possible to review the data and analysis even years later, easily enabling the transfer of analysis workflows between studies or centres.

Summary: Quality, consistency and reproducibility of PET analysis are entirely attainable, and software tools exist to facilitate this. By effective use of these tools, the field can operate more efficiently and effectively, especially for analysis of large, shared and evolving datasets.

Figure 1: Standard analysis workflow

P-098
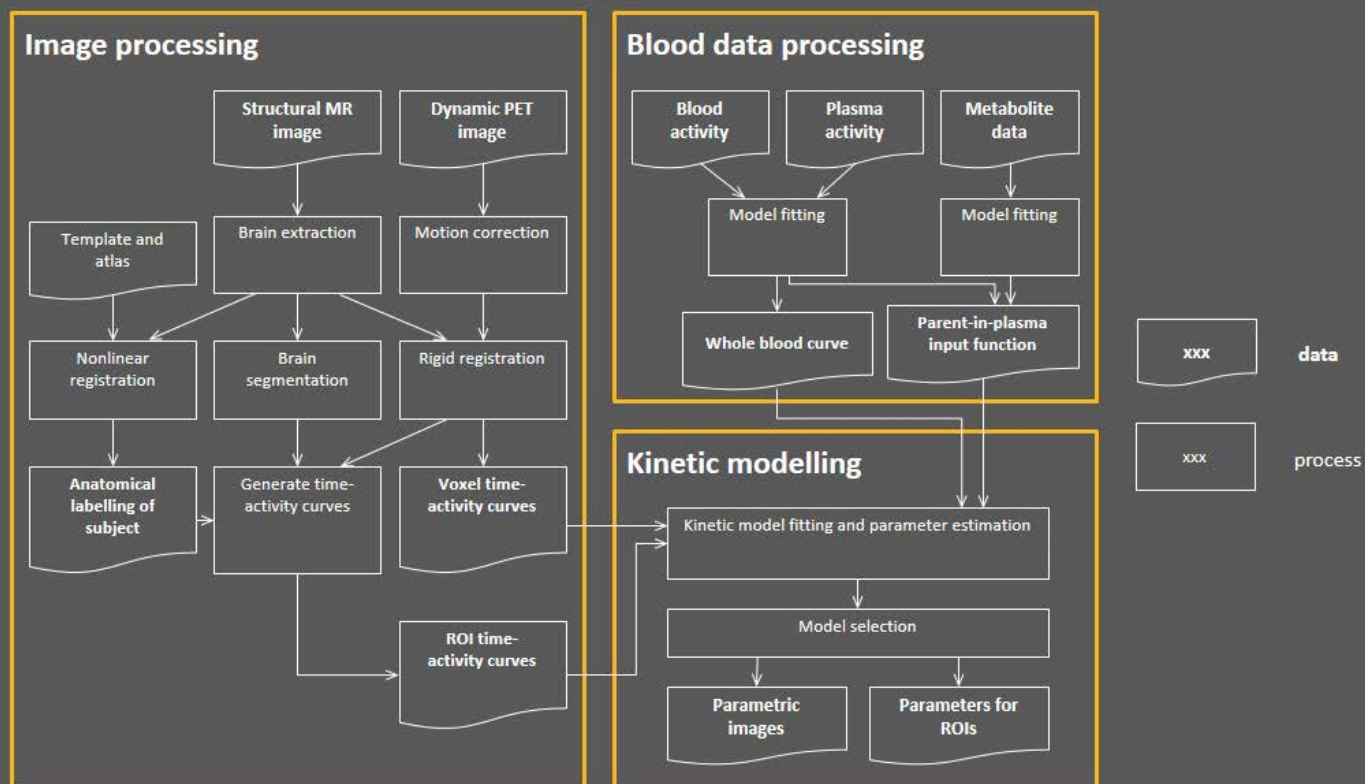
In vivo imaging of GABAa-receptor and serotonin transporter in high functioning autism

Max Andersson[1], Ämma Tangen[1], Jacqueline Borg[1,2], Johan Lundberg[1], Sven Bölte[2], Christer Halldin[1], Lars Farde[1]

[1]Department of Clinical Neuroscience, Karolinska Institutet, Stockholm, Sweden; [2] Department of Women's and Children's Health, Center of Neurodevelopmental Disorders (KIND), Karolinska Institutet, Stockholm, Sweden.

Objectives: In autism spectrum disorder (ASD), gene[1] and post mortem[2] studies indicate lower $GABA_a$ receptor expression, These observations   support the hypothesis that alterations in the GABA system cause a neuronal imbalance in excitatory/inhibitory systems affecting cortical maturation and cognitive and social functioning[3]. To this date only one small pilot study has compared   GABA receptor binding in vivo in ASD subjects compared to controls[4]. A role for the neurotransmitter serotonin (5-HT) in ASD has been suggested from numerous studies on peripheral markers[5], genetics[6] and in vivo brain imaging[7]. The serotonin transporter (5-HTT) is a primary mechanism for regulation of synaptic serotonin concentration in brain and has in one previous PET study been associated with lower social cognitive ability[7].
This case-control PET-study is conducted within the EU-AIMS framework (www.eu-aims.eu). The aim is to investigate putative alterations in the GABA and serotonin systems in vivo in ASD.

Methods: Fifteen subjects with high-functioning autism (11 men, age range 19-48 years, IQ >70) and 15 healthy control subjects matched for age, gender and IQ were examined with PET using the ECAT EXACT HR 47 system (Siemens Molecular Imaging) and the radioligands [^{11}C]flumazenil[8] and [^{11}C]MADAM[9], selective for the $GABA_a$ receptor and for the 5-HT transporter (5-HTT) respectively. Cortical and subcortical regions of interest (ROIs) were automatically delineated on previously acquired T1w MR images using the Freesurfer software and coregistered to PET data with SPM 5. Regional binding potential values (BP_{ND}) were calculated using the Simplified Reference Tissue Model[10]. Reference regions were delineated manually for calculation of [^{11}C]MADAM (cerebellum) and [^{11}C]flumazenil (pons) binding. Differences in mean BP_{ND} between groups for each ROI were evaluated using independent samples t-test.

Results: Mean injected radioactivity of [^{11}C]flumazenil was 329.6 MBq and 369.3 MBq of . [^{11}C]MADAM. There were no significant differences in injected or specific radioactivity between the groups.
 [^{11}C]MADAM BP_{ND} in the autism group was significantly lower in anterior cingulate cortex (p=.022), posterior cingulate cortex (p=.023), putamen (p=.020) and thalamus (p=.039).
Regional [^{11}C]flumazenil BP_{ND} was not significantly different for any of the regions examined. However, although differences were not statistically significant, BP_{ND} in the autism group was 10-20% lower   for all regions and a trend was obtained for   the posterior cingulate cortex (p=.090).

Preliminary conclusions and future planning: The findings from the examinations with [^{11}C]MADAM support the hypothesis of 5-HT involvement in ASD and confirms a previous finding regarding 5-HTT[7]. The results for [^{11}C]flumazenil binding did not confirm the hypothesis of GABA involvement in ASD.
For confirmatory purposes, future analysis of data at voxel level is planned as well as examination of the relationship between PET data and social cognitive performance.

References:
1.   Coghlan, S. *et al.* GABA system dysfunction in autism and related disorders: from synapse to symptoms. *Neurosci. Biobehav. Rev.* **36,** 2044–55 (2012).
2.   Oblak, A. L., Gibbs, T. T. & Blatt, G. J. Reduced GABAA receptors and benzodiazepine binding sites in the posterior cingulate cortex and fusiform gyrus in autism. *Brain Res.* **1380,** 218–28 (2011).
3.   Rubenstein, J. L. R. & Merzenich, M. M. Model of autism: increased ratio of excitation/inhibition in key neural systems. *Genes, Brain Behav.* **2,** 255–267 (2003).
4.   Mendez, M. A. *et al.* The brain GABA-benzodiazepine receptor alpha-5 subtype in autism spectrum disorder: a pilot [(11)C]Ro15-4513 positron emission tomography study. *Neuropharmacology* **68,** 195–201 (2013).
5.   Gabriele, S., Sacco, R. & Persico, A. M. Blood serotonin levels in autism spectrum disorder: a systematic review and meta-analysis. *Eur. Neuropsychopharmacol.* **24,** 919–29 (2014).
6.   Veenstra-VanderWeele, J. & Blakely, R. D. Networking in Autism: Leveraging Genetic, Biomarker and Model System Findings in the Search for New Treatments. *Neuropsychopharmacology* **37,** 196–212 (2012).

7. Nakamura, K. *et al.* Brain serotonin and dopamine transporter bindings in adults with high-functioning autism. *Arch. Gen. Psychiatry* **67,** 59–68 (2010).
8. Odano, I. *et al.* [18F]Flumazenil binding to central benzodiazepine receptor studies by PET: – Quantitative analysis and comparisons with [11C]flumazenil. *Neuroimage* **45,** 891–902 (2009).
9. Lundberg, J., Odano, I., Olsson, H., Halldin, C. & Farde, L. Quantification of 11 C-MADAM Binding to the Serotonin Transporter in the Human Brain. *J. Nucl. Med.* **46,** 1505–1516 (2005).
10. Lammertsma, A. A. & Hume, S. P. Simplified reference tissue model for PET receptor studies. *Neuroimage* **4,** 153–8 (1996).

		[^{11}C]flumazenil		[^{11}C]MADAM	
		BP_{ND} (mean±SD)	p	BP_{ND} (mean±SD)	p
orbitofrontal cx	control	6.33 ± 1.62	.376	0.20 ± 0.11	.466
	autism	5.84 ± 1.35		0.18 ± 0.07	
medial frontal cx	control	6.20 ± 1.46	.244	0.13 ± 0.08	.142
	autism	5.62 ± 1.22		0.09 ± 0.04	
fusiform cx	control	6.32 ± 1.55	.277	0.21 ± 0.10	.353
	autism	5.74 ± 1.30		0.18 ± 0.09	
anterior cingulate cx	control	6.81 ± 1.77	.235	0.35 ± 0.12	.022
	autism	6.12 ± 1.29		0.27 ± 0.06	
posterior cingulate cx	control	6.04 ± 1.24	.090	0.27 ± 0.10	.023
	autism	5.29 ± 1.12		0.19 ± 0.08	
caudate	control	2.35 ± 0.64	.415	0.64 ± 0.13	.057
	autism	2.16 ± 0.57		0.55 ± 0.12	
putamen	control	3.20 ± 0.86	.434	1.06 ± 0.16	.020
	autism	2.97 ± 0.72		0.91 ± 0.16	
thalamus	control	2.43 ± 0.48	.296	0.97 ± 0.13	.039
	autism	2.21 ± 0.63		0.87 ± 0.11	

table 1 [^{11}C]flumazenil and [^{11}C]MADAM BP_{ND} for selected regions in autism group and control group

Quantification of Cerebral Metabolism and Blood Flow in Multiple Sclerosis: A Comparison of [18F]FDG-PET and ASL-MRI

Elizabeth Bartlett[1], Christine DeLorenzo[1,2], John Gardus[2], Margaret Kasschau[3,4], Ramin V. Parsey[2,5], Lauren Krupp[3,4], Leigh Charvet[3,4]

[1]Department of Biomedical Engineering, Stony Brook University, Stony Brook, NY, USA; [2]Department of Psychiatry, Stony Brook Medicine, Stony Brook, NY, USA; [3]Department of Neurology, NYU Langone Medical Center, New York University Medicine, NY, NY, USA; [4]Department of Neurology, Stony Brook Medicine, Stony Brook, NY, USA; [5]Department of Radiology, Stony Brook Medicine, Stony Brook, NY, USA

Brain hypometabolism[1-6] and hypoperfusion[1, 2, 7-15] have been shown in multiple sclerosis (MS), compared to healthy controls (HCs). Specifically, deep grey matter (DGM) regions have been shown to have inflammation, demyelination, and neurodegeneration in MS patients.[16] A quantitative neuroimaging measure with high sensitivity to regional activity alterations is necessary to elucidate the biological mechanism by which DGM is affected in MS. This study investigates whether cerebral blood flow (CBF), computed from magnetic resonance imaging (MRI)-based, arterial spin labeling (ASL), and 18F-fluorodeoxyglucose positron emission tomography ([18F]FDG-PET) derived measures could, in combination, more precisely pinpoint dysregulated DGM brain regions in MS.

3D-GRASE pseudocontinuous ASL (pCASL) and [18F]FDG-PET were performed simultaneously on 6 relapsing-remitting MS (2 female, 4 male) patients and 9 (3 female, 6 male) HCs. Partial volume corrected CBF maps were generated from the pCASL data after motion-correction, coregistration, and smoothing. The 60-minute [18F]FDG-PET scans were binned into 26 frames, motion-corrected, and coregistered to the T1w MRI, allowing for probabilistic region of interest (ROI) labels to be warped onto each PET image. For each frame and ROI, a weighted average of activity within the region was computed to establish regional time activity curves. Region-wise (standardized uptake value) SUVs were calculated as previously described.[17] Simultaneous estimation (SIME), with a single venous sample, was employed to estimate a full AIF for the metabolic rate of glucose (MRGlu) calculation.[18]

Spearman's correlations indicated good correspondence between MRGlus and SUVs in the MS and HC cohorts in the 20 bilateral ROIs tested (r=0.89, p<0.001 and r=0.76, p<0.001, respectively). Correlations between SUVs and CBF in the MS and HC cohorts in the 15 ASL-specific bilateral ROIs tested (r=0.58, p<0.001 and r=0.41, p<0.001, respectively) were also significant.

Although no differences between the MS and HC cohorts were observed using SUVs or CBF in DGM ROIs (thalamus, dorsal caudate, dorsal putamen, and hippocampus), there was a diagnosis by sex interaction in pCASL-CBF ($p<0.001$). In *post-hoc* analyses, there was significant hypoperfusion in MS males, as compared to male HCs ($p=0.003$). When each ROI was analyzed individually, the only ROI with significant hypoperfusion was the dorsal caudate ($p=0.034$).

When SUVs and CBF values were analyzed together using a MANCOVA, the diagnosis by sex interaction persisted ($p<0.001$). In *post-hoc* analyses, there was a significant difference between males in the MS and HC groups in the hippocampus, thalamus, dorsal caudate, and dorsal putamen ($p<0.001$ in each ROI). Due to the limited sample size, *post-hoc* analyses were not performed for females.

These findings suggest that [18F]FDG-PET derived MRGlu is correlated with 3DGRASE-pCASL derived CBF values in MS and HCs. Additionally, pCASL-CBF may be more sensitive than [18F]FDG-SUVs to sex differences, which is reflected in the low correlations between CBF and SUVs. The use of [18F]FDG-PET derived measures, combined with pCASL-CBF, provides a more sensitive composite measure than either alone. This composite measure revealed significant differences in DGM regions in MS in the male cohort and thus, can be used to further elucidate the biology underlying the sex differences involved in MS disease progression.

References:

1. Brooks, D.J., et al., Studies on regional cerebral oxygen utilisation and cognitive function in multiple sclerosis. J Neurol Neurosurg Psychiatry, 1984. **47**(11): p. 1182-91.
2. Sun, X., et al., Clinical significance of reduced cerebral metabolism in multiple sclerosis: a combined PET and MRI study. Ann Nucl Med, 1998. **12**(2): p. 89-94.
3. Paulesu, E., et al., Functional basis of memory impairment in multiple sclerosis: a[18F]FDG PET study. Neuroimage, 1996. **4**(2): p. 87-96.
4. Bakshi, R., et al., High-resolution fluorodeoxyglucose positron emission tomography shows both global and regional cerebral hypometabolism in multiple sclerosis. J Neuroimaging, 1998. **8**(4): p. 228-34.
5. Bakshi, R., et al., Fatigue in multiple sclerosis and its relationship to depression and neurologic disability. Mult Scler, 2000. **6**(3): p. 181-5.
6. Roelcke, U., et al., Reduced glucose metabolism in the frontal cortex and basal ganglia of multiple sclerosis patients with fatigue: a 18F-fluorodeoxyglucose positron emission tomography study. Neurology, 1997. **48**(6): p. 1566-71.
7. Swank, R.L., J.G. Roth, and D.C. Woody, Jr., Cerebral blood flow and red cell delivery in normal subjects and in multiple sclerosis. Neurol Res, 1983. **5**(1): p. 37-59.
8. Lycke, J., et al., Regional cerebral blood flow in multiple sclerosis measured by single photon emission tomography with technetium-99m hexamethylpropyleneamine oxime. Eur Neurol, 1993. **33**(2): p. 163-7.
9. Papadaki, E.Z., et al., White matter and deep gray matter hemodynamic changes in multiple sclerosis patients with clinically isolated syndrome. Magn Reson Med, 2012. **68**(6): p. 1932-42.
10. Law, M., et al., Microvascular abnormality in relapsing-remitting multiple sclerosis: perfusion MR imaging findings in normal-appearing white matter. Radiology, 2004. **231**(3): p. 645-52.
11. Adhya, S., et al., Pattern of hemodynamic impairment in multiple sclerosis: dynamic susceptibility contrast perfusion MR imaging at 3.0 T. Neuroimage, 2006. **33**(4): p. 1029-35.
12. Varga, A.W., et al., White matter hemodynamic abnormalities precede sub-cortical gray matter changes in multiple sclerosis. J Neurol Sci, 2009. **282**(1-2): p. 28-33.
13. Inglese, M., et al., Deep gray matter perfusion in multiple sclerosis: dynamic susceptibility contrast perfusion magnetic resonance imaging at 3 T. Arch Neurol, 2007. **64**(2): p. 196-202.
14. Rashid, W., et al., Abnormalities of cerebral perfusion in multiple sclerosis. J Neurol Neurosurg Psychiatry, 2004. **75**(9): p. 1288-93.
15. Debernard, L., et al., Reduced grey matter perfusion without volume loss in early relapsing-remitting multiple sclerosis. J Neurol Neurosurg Psychiatry, 2014. **85**(5): p. 544-51.
16. Haider, L., et al., Multiple sclerosis deep grey matter: the relation between demyelination, neurodegeneration, inflammation and iron. J Neurol Neurosurg Psychiatry, 2014. **85**(12): p. 1386-95.
17. Kinahan, P.E. and J.W. Fletcher, Positron emission tomography-computed tomography standardized uptake values in clinical practice and assessing response to therapy. Semin Ultrasound CT MR, 2010. **31**(6): p. 496-505.
18. Ogden, R.T., et al., Simultaneous estimation of input functions: an empirical study. J Cereb Blood Flow Metab, 2010. **30**(4): p. 816-26.

P-100

In vivo histamine H1 receptor occupancy in human brain using [11C]doxepin: PET correlates with antihistamine sedative effects

James R. Brašić, M.D., M.P.H.[1], Wichana Chamroonrat, M.D.[2], Ana M. Catafau, M.D., Ph.D.[1], Ahmet S. Dogan, M.D.[1], Hiroto Kuwabara, M.D., Ph.D. [1], Kazuhiko Yanai, M.D., Ph.D.[3], Steven Offord, Ph.D.[4], Hayden Ravert, Ph.D.[1], John Hilton. D.Phil.[1*], Dean F. Wong, M.D., Ph.D.[1]

[1]Division of Nuclear Medicine and Molecular Imaging, The Russell H. Morgan Department of Radiology and Radiological Science, Johns Hopkins School of Medicine, Baltimore, Maryland, United States; [2]Nuclear Medicine, Ramathibodi Hospital, Bangkok, Thailand; [3]Department of Pharmacology, Tohoku University School of Medicine, Japan; [4]Otsuka America Pharmaceutical Inc., Princeton, New Jersey, United States;
*Deceased

INTRODUCTION: Although histamine H_1 receptor occupancy has been determined for individual antihistamines (Dogan, *et al.,* 2001a,b,c; Farré, *et al.,* 2014; Hiraoka, *et al.,* 2015; Kubo. *et al.,* 2011; Tashiro, *et al.,* 2006, Wong, *et al.,* 2000) and antipsychotics (Sato, *et al.,* 2015), differential effects merit clarification. We aimed to characterize H_1 receptor distribution and differences in regional occupancy by various antihistamines. We hypothesized that commonly used antihistamines demonstrate greater occupancy of H_1 receptors analogous to their observed sedative effects (Dogan, *et al.,* 2001a,b,c; Wong, *et al.,* 2000), in a hierarchy from least occupancy to greatest occupancy as follows: No antihistamine $\leq$ fexofenadine $\leq$ cetirizine $\leq$ diphenhydramine.

METHODS: Twenty healthy adult volunteers (13 males, 7 females, age 18-53 years, mean age 26.9 years) underwent positron emission tomography (PET) after the rapid intravenous administration of 259-296 mBq (7-8 mCi) of [11C]doxepin with 30 sequential image frames were acquired over 90 minutes with 35 slices (slice thickness: 4.25mm) reconstructed using filtered back-projection with a ramp-0.5 filter (matrix size: 128x128, pixel size 2mmx2mm). Although no dose was administered before baseline scans, doses of antihistamines were administered 90 min before the antihistamine scans. Radial arterial blood samples were obtained during the study for blood input function and for metabolite correction.

We obtained the nondisplaceable binding potential (BP_{ND}) (Innis, *et al.,* 2007) of [11C]doxepin which is considered to be proportional to the density of unoccupied receptors ($B_{max'}$) in various regions of the brain. First, volumes of interest (VOIs) of cortical regions were obtained automatically by Freesurfer (Fischl, *et al.,* 2004) and VOIs of subcortical regions were obtained automatically utilizing the subcortical segmentation tools of the software library of the Oxford Centre for fMRI of the Brain (Jenkinson, *et al.,* 2012; Patenaude, *et al.,* 2011; Woolrich, *et al.,* 2009), and refined manually using a locally developed VOI tool (VOILand) as needed.
Then, VOIs were transferred from MRI to PET space according to MRI-to-PET coregistration parameters obtained with the coregistration module (Ashburner and Friston, 2004) of Statistical Parametric Mapping (SPM12) (Wellcome Trust Centre for Neuroimaging, 2015), and applied to PET frames to obtain regional time (radioactivity) curves (TACs). Regional BP_{ND}s were obtained by the reference tissue graphical analysis (RTGA) (Logan, *et al.,* 1996, 2011) and the multilinear reference tissue with two parameters (MRTM2) (Ichise, *et al.,* 2003).

RESULTS: Diphenhydramine demonstrated much greater H_1 occupancy in the frontal, temporal, parietal, and occipital lobes, the fusiform and cingulate gyri, amygdala, and insula (See Figure).

CONCLUSION: The brain histamine H_1 receptor distribution found in this study is consistent with previous studies in humans, i.e., higher density in the cortex, moderate density in the basal ganglia, and lower density in the cerebellum and the pons. Additionally, the results confirm that H_1 receptor occupancy in human brain using [11C]doxepin PET correlates with sedative effects of antihistamines in a hierarchy from least occupancy to greatest occupancy as follows: No antihistamine $\leq$ fexofenadine $\leq$ cetirizine $\leq$ diphenhydramine.
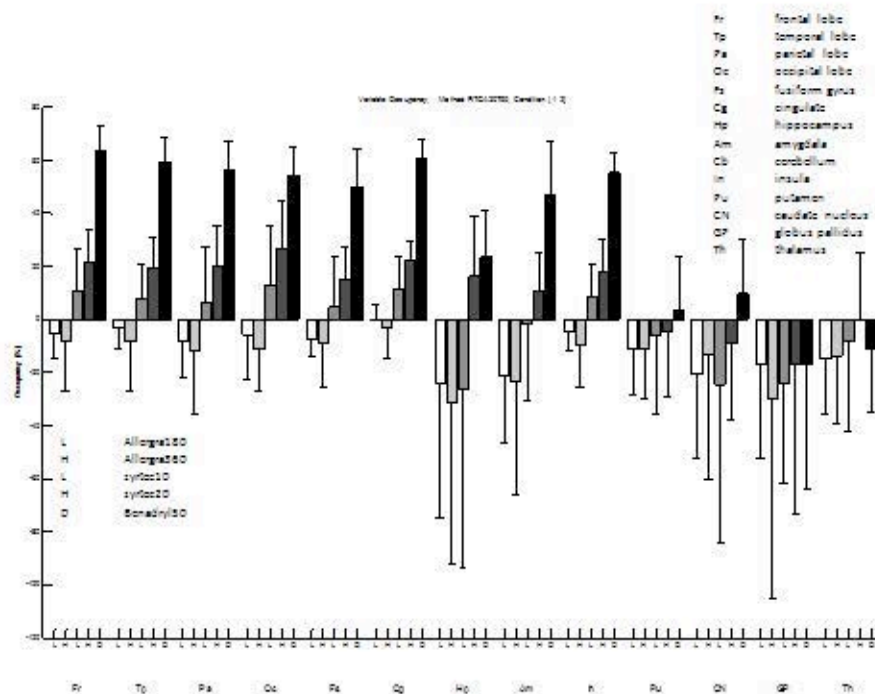
H1 histamine receptor occupancy as measured by positron emission tomography (PET) following the intravenous bolus administration of 259-296 mBq (7-8 mCi) of [^{11}C]doxepin to healthy adults. Ninety minutes before the start of the PET, each participant consumed an oral dose of an antihistamine. Occupancy (%) = 100 × (BP$_{ND(baseline)}$ – BP$_{ND(antihistamine)}$) / BP$_{ND(baseline)}$ is plotted on the ordinate. The regions of the brain are represented on the abscissa; for each region doses of antihistamines from left to right are as follows: 180 mg fexofenadine (Allegra), 360 mg fexofenadine (Allegra), 10 mg cetirizine (Zyrtec), 20 mg cetirizine (Zyrtec), and 50 mg diphenhydramine (Benadryl).

BP$_{ND}$ = nondisplaceable binding potential (Innis, et al., 2007)

TSPO PET reveals attenuation of neuro-inflammation after minocycline treatment during epileptogenesis

Pablo Bascuñana[1], Mirjam Brackhan[1,2], Johannes M. Postema[1], Tobias L. Ross[1], Frank M. Bengel[1], Marion Bankstahl[2], Jens P. Bankstahl[1].

[1]*Department of Nuclear Medicine, Hannover Medical School, Hannover (Germany);* [2]*Department of Pharmacology, Toxicology and Pharmacy, University of Veterinary Medicine, Hannover (Germany)*

Introduction: Evidence indicates that, after an insult, brain inflammation may contribute to epileptogenesis. The aim of this study was (1) to characterize the timeline of microglia activation after pilocarpine-induced status epilepticus (SE), and (2) to evaluate the effect of anti-inflammatory treatment with minocycline, using TSPO PET.

Methods: Epileptogenesis was initiated by pilocarpine-induced SE. The temporal profile of neuroinflammation was assessed in rats at 8 time points (n=4-8) over 16 weeks after SE performing [^{11}C]PK11195 PET imaging. Subsequently, additional rats were treated with either minocycline (25 mg/kg) or vehicle for 8 days starting 24 hours after SE and underwent [^{18}F]GE180 PET scans before SE (n=9), and at 7 and 14 days post SE (n=5-7 per time point and treatment group). Sixty-minute dynamic scans were performed in rats anesthetized with isoflurane for both tracers. Images were analyzed in Pmod software by comparing standardized uptake values (SUV), binding potential (BP$_{ND}$; simplified reference tissue model). In addition, statistical parametric mapping (SPM12) was used for comparing each time point to baseline. For treatment evaluation, volume of distribution (V$_t$; 2-tissue compartment model) was also calculated as the [^{18}F]GE180 dynamic images allowed for determination of an image-derived input function.

Results: Compared to baseline, [^{11}C]PK11195 uptake values were increased in epileptogenesis-associated brain regions at 48 hours after SE and peaked at 7 days after SE (up to 2.09-fold increase in uptake, $p < 0.05$). Interestingly, BP$_{ND}$ peaked later than uptake values, with maximal BP$_{ND}$ observed at 14 days in ventral hippocampus (0.96 ± 0.18; $p<0.05$). Uptake and BP$_{ND}$ remained above baseline values up to 3 weeks after SE. During anti-inflammatory treatment evaluation, elevated [^{18}F]GE180 uptake, BP$_{ND}$ and V$_t$ were observed at both investigated time points after SE in both groups. Minocycline treatment decreased the V$_t$ in the ventral hippocampus (3.72 ± 0.25 vs. 2.66 ± 0.53, $p < 0.05$) and entorhinal cortex (3.66 ± 0.32 vs. 2.77 ± 0.38, $p < 0.05$) at 1 week post SE, and in the piriform cortex at both time points compared to the vehicle-treated group (1 week: 3.58 ± 0.30 vs. 2.83 ± 0.33, $p < 0.05$; 2 weeks: 3.29 ± 0.04 vs. 2.54 ± 0.07, $p < 0.05$). No difference was found in SUV or binding potential.

Conclusions: The revealed time course of neuroinflammation after epileptogenic brain insult enables appropriate timing and evaluation of inflammation-targeting antiepileptogenic pharmacotherapy. Anti-inflammatory treatment with minocycline after SE moderately reduced epileptogenesis-associated brain inflammation.

Test-retest reproducibility of [11C]Ro15 4513, a PET ligand for GABA-A receptors containing alpha 5 subunits

Colm J. McGinnity[1, 2, 3], Daniela A. Riaño Barros[1, 2], Lula Rosso[1, 2], Mattia Veronese[4], Gaia Rizzo[5], Alessandra Bertoldo[5], Rainer Hinz[6], Federico E. Turkheimer[4], Matthias J. Koepp[7], Alexander Hammers[1, 2, 3, 8].

[1] Centre for Neuroscience, Department of Medicine, Imperial College London, London, UK; [2] MRC Clinical Sciences Centre Hammersmith Hospital, London, UK; [3] Division of Imaging Sciences & Biomedical Engineering, King's College London, London, UK; [4] Centre for Neuroimaging Sciences, Institute of Psychiatry, Psychology & Neuroscience, King's College London, London, UK; [5] Department of Information Engineering, University of Padova, Padova, Italy; [6] Wolfson Molecular Imaging Centre, University of Manchester, Manchester, UK; [7] Department of Clinical and Experimental Epilepsy, Institute of Neurology, University College London, UK, and Epilepsy Society, Chalfont St Peter, UK; [8] The Neurodis Foundation, CERMEP - Imagerie du Vivant, Lyon, France.

Introduction: Alteration of γ-aminobutyric acid "A" ($GABA_A$) receptor-mediated neurotransmission has been associated with a variety of neurological and psychiatric disorders. [11C]Ro15 4513 is a PET ligand with high affinity for α5-subunit-containing $GABA_A$ receptors, which are highly expressed in limbic regions of the human brain (Sur C et al., 1998). We quantified the test-retest reproducibility of measures of [11C]Ro15 4513 PET.

Methods: Five healthy males (median age 40 years, range 38–49 years) had a 90-minute PET scan on two occasions, after injection of a median dose of [11C]Ro15 4513 of 441 MBq. Metabolite-corrected arterial plasma input functions (ppIFs) were generated for all scans using Clickfit (*in-house* software).
We quantified regional uptake using MICK/MICKPM software (Hinz R, University of Manchester, Manchester, U.K.) by 12 methods: 1) Models requiring arterial ppIFs – reversible compartmental models with one and two tissue classes (2kbv; 4kbv), and Logan's graphical analyses (Logan J et al., 1990) applied to regional time-activity data and alternatively voxel-wise; 2) Model-free (spectral) analyses (Cunningham VJ and Jones T, 1993), applied to regional data and alternatively voxel-wise; 3) methods not requiring ppIFs – modified standardised uptake values (mSUV = (activity × [weight (kg) + 70]/2)/injected dose; Thie JA *et al.*, 2007) calculated for two intervals, and the simplified reference tissue model (SRTM) with brainstem or alternatively cerebellum as pseudo-reference regions, applied to regional data (Lammertsma AA and Hume SP, 1996) and alternatively voxelwise (Gunn RN *et al.*, 1997).
We sampled the mean values of the outcome parameters within six bilateral, non-reference grey matter regions-of-interest that had been delineated using MAPER (Heckemann RA et al., 2006, 2010). Percentage test-retest differences (t-rt), between-subject coefficients of variation (BS-CV), and intraclass correlation coefficients (ICC) were compared between methods, with particular interest in the hippocampus.

Results: The outcome measures were sensitive to weighting of frames. The SRTM with the brainstem yielded reliable data (median absolute t-rt 5% applied to regional data and voxelwise), but low median BS-CV (6% for both). Three methods that yielded reliable data (i.e. median t-rt < 10%) had median BS-CVs >7.5%; the SRTMs with the cerebellar pseudo-reference region, and SA applied at the voxel level (figure 1). The median absolute t-rt across regions among these methods was approximately 4-5% with interquartile ranges (iqr) of 2/3% – 5/7%; median BS-CV across regions was 8% -11%. The range of ICCs for the hippocampus was 0.89 – 0.95 (excellent); ICCs across regions were 0.71 (iqr 0.64 – 0.84; moderate – excellent) and 0.87 (0.74 – 0.93; good – excellent) for SRTM-cerebellum applied to regional data and voxelwise, respectively, and 0.89 (0.75 – 0.90; very good – excellent) for voxel-wise SA. The remaining methods yielded high median t-rt (>10%), however, the 4kbv model yielded a hippocampal ICC of 0.89.

Conclusion: Quantification of [11C]Ro15 4513 uptake shows moderate to excellent reproducibility with SRTM using the cerebellum, and very good to excellent reproducibility with voxel-wise SA which, however, requires a ppIF. Quantification of uptake in the α5 subunit-rich hippocampus is particularly reliable. Investigators should be mindful of the very low expression of the α5 subunit in the cerebellum (Pirker S *et al.*, 2000).

Spectral analysis

V_T: 0 — 18

SRTM cerebellum

BP_{ND}: -0.5 — 3.5
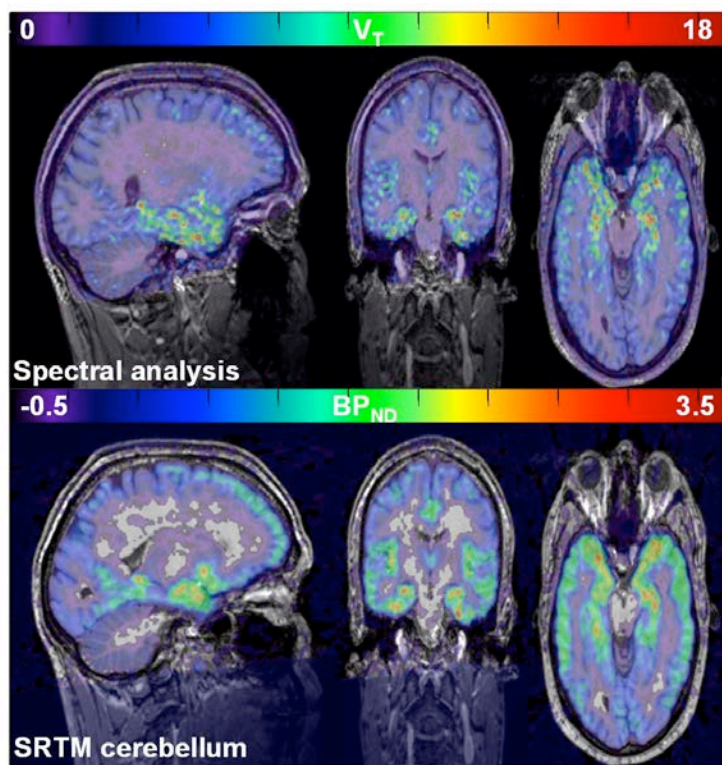
Simplifying [18F]GE-179 PET: are both arterial blood sampling and 90-minute acquisitions essential?

Colm J. McGinnity[1,2,3], Daniela A. Riaño Barros[1,2], William Trigg[4], David J. Brooks[5], Rainer Hinz[6], John S. Duncan[7], Matthias J. Koepp[7], Alexander Hammers[1,2,3,8]

[1] *Division of Brain Sciences, Department of Medicine, Imperial College London, London, UK;* [2] *MRC Clinical Sciences Centre, London, UK;* [3] *Division of Imaging Sciences and Biomedical Engineering, Faculty of Life Sciences & Medicine, King's College London, London, UK and The PET Centre, St. Thomas' Hospital, London, UK;* [4] *GE Healthcare plc, Amersham, UK;* [5] *Centre of Functionally Integrative Neuroscience, Aarhus University, Aarhus, Denmark;* [6] *Wolfson Molecular Imaging Centre, University of Manchester, Manchester, UK;* [7] *Department of Clinical and Experimental Epilepsy, UCL Institute of Neurology, London, UK, and Epilepsy Society, Chalfont St. Peter, UK;* [8] *The Neurodis Foundation, CERMEP - Imagerie du Vivant, Lyon, France.*

Introduction: The volume-of-distribution (V_T) of the NMDA receptor PET radioligand [18F]GE-179 has been previously quantified using arterial blood sampling and using 90-minute dynamic scans. A true reference region does not exist. Regarding voxelwise quantification of the uptake/distribution, we explored: 1) whether arterial blood sampling is avoidable, via the use of modified standardised uptake values (mSUVs; Thie JA *et al.,* 2007) or population-based input functions (PBIFs); and 2) whether shorter scans are feasible, i.e. can V_T be calculated over 60 rather than 90 minutes?

Methods: For 20 existing [18F]GE-179 datasets (McGinnity CJ *et al.*, 2014, 2015), we generated: 1) decay-corrected mSUVs over the intervals t = 30–59 minutes and t = 60–89 minutes (inclusive); 2) PBIFs for each participant by scaling the median parent plasma input function (ppIF) according to the radioactivity concentration in a blood sample (arterial plasma at t = 50 minutes); we used these PBIFs to generate [18F]GE-179 V_T images for t= 0–89 minutes via voxelwise spectral analysis (SA) 3) V_T images using original ppIF for t = 0–59 minutes. We sampled the means of the mSUV/V_T within seven bilateral regions-of-interest (ROIs). The relationships with V_Ts calculated over t = 0–89 minutes using the original ppIFs were quantified using Spearman's rank (ρ) correlation coefficient. Agreement between V_T estimates was assessed by Bland – Altman plot (Bland JM and Altman DG, 1986). We compared global and hippocampal V_T between groups using t = 0–59 and t = 0–89 minute estimates.

Results: MSUVs were moderately correlated with original ppIF-derived V_T estimates, particularly over the later interval: across ROIs the range of ρ was from 0.68 (hippocampi) to 0.77 (occipital lobes; all $p < 0.005$) for 60–89 minutes. V_Ts calculated using the PBIFs were moderately correlated with original ppIF-derived V_T estimates: the range of ρ was 0.71 (hippocampi) to 0.83 (occipital lobes/thalami; all $p < 0.001$). PBIF-based quantification was associated with increases in between-subject coefficient of variation in V_T (median 36%, range 32% – 37% for PBIF versus 23% (20% – 25%) for original ppIFs). V_Ts calculated over 60 minutes were very strongly correlated with original (t = 0 – 89 minutes; Figure 1) ppIF-derived V_Ts: the range of ρ was from 0.93 (thalami) to 0.99 (cerebelli/occipital lobes; all $p < 0.001$). A negative bias was observed (maximal in the hippocampus; median difference in V_T 1.76, i.e. 15.1%, Figure 1) without increase in BS-CV. Between-group differences in global V_T and alternatively in absolute hippocampal V_T remained statistically significant ($F(2, 13) > 17.0$, $p < 0.001$).

Conclusion: Whilst mSUVs and PBIF-derived V_Ts were moderately correlated with original V_T estimates, arterial blood sampling permits reduction of the scan duration to 60 minutes. Reduction in scan duration is associated with a negative bias, but appears unlikely to significantly reduce the power of between-groups comparisons. Based on the half-life of [18F], the relatively slow kinetics of the radioligand, and the correlation observed for t = 60 – 89 minutes, calculation of mSUVs over t = 90–120 minutes merits investigation.
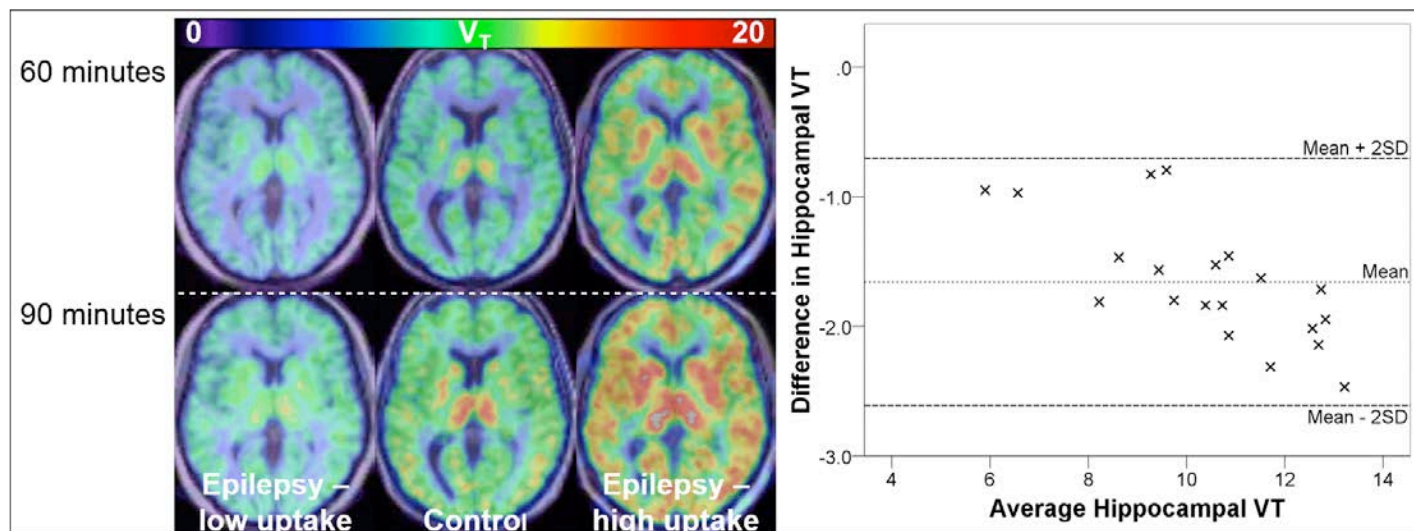
mGluR5 abnormalities in focal cortical dysplasia identified in vivo with [11C]ABP688 PET imaging

Jonathan M. DuBois[1]; Olivier G. Rousset, PhD[2]; Marie-Christine Guiot, MD[1,2];   Jeffery A. Hall, MD, MSc, FRCPS[1]; Andrew J. Reader, PhD[4,5]; Jean-Paul Soucy, MD, MSc[4,6]; Pedro Rosa-Neto, MD, PhD[1,4,7]; Eliane Kobayashi, MD, PhD[1]

[1]Department of Neurology and Neurosurgery, Montreal Neurological Institute, McGill University, Montreal, Canada; [2]Division of Nuclear Medicine and Molecular Imaging, Johns Hopkins University, Baltimore, United States of America; [3]Department of Pathology, McGill University, Montreal, Canada; [4]PET Unit, McConnell Brain Imaging Center, Montreal Neurological Institute, McGill University, Montreal, Canada; [5]Division of Imaging Sciences and Biomedical Engineering, King's College London, St. Thomas' Hospital, London, UK; [6]Bio-Imaging Group, PERFORM Centre, Concordia University, Montreal, Canada; [7]Translational Neuroimaging Laboratory, McGill Center for Studies in Aging, Douglas Mental Health University Institute, McGill University, Montreal, Canada

Metabotropic glutamate receptor type 5 (mGluR5) abnormalities have been described in tissue resected from epilepsy patients with malformations of cortical development, including focal cortical dysplasia (FCD)[1]. To determine if these abnormalities could be identified *in vivo,* we investigated mGluR5 availability in 10 patients with focal epilepsy and an MRI diagnosis of FCD using positron emission tomography (PET) and the radioligand [11C]ABP688.

[11C]ABP688 is a positron emission tomography (PET) tracer that binds selectively to the mGluR5 allosteric site with high selectivity and affinity[2]. In a previous study, we have demonstrated that [11C]ABP688   PET can depict regional differences in cortical concentrations of mGluR5[3]. [11C]ABP688 binding potential (BP_{ND}) comparisons were computed, using the cerebellar cortex as a reference region, between each patient and homotopic cortical regions in 33 healthy controls. FCD lesions were manually traced, and used to generate labels for the perilesional cortex and the cortex contralateral to the lesion. In addition to the region-of-interest (ROI) analysis, vertex-wise Z-score maps were generated to assess patient/control differences in [11C]ABP688 BP_{ND} across the entire cortex (significance level of $p < 0.05$, corrected for multiple comparisons).

Reduced [11C]ABP688 BP_{ND} in the FCD was seen in 6/10 patients with ROI-analysis and 5/10 patients using vertex-wise analysis. In the vertex-wise analysis, regions of reduced [11C]ABP688 BP_{ND} generally did not encompass the entire lesion. While extralesional abnormalities were also found in the majority of patients, systematic differences were not present in either the perilesional or contralateral cortices. Reduced FCD [11C]ABP688 BP_{ND} was found in 4/5 operated patients (mean follow-up: 66 months; Engel I).

We showed for the first time *in vivo* evidence of reduced mGluR5 availability in FCD. Reduced [11C]ABP688 BP_{ND} may indicate reduced mGluR5 tissue concentration or reduction of [11C]ABP688 affinity to mGluR5 (due to receptor internalization or conformational changes affecting the availability of its allosteric binding site). The results show focal mGluR5 abnormalities in FCD patients and raise the possibility that modulation of glutamatergic transmission via mGluR5 might contribute to intrinsic epileptogenicity attributed to FCD[4]. Future work is needed to determine the yield of [11C]ABP688 PET as a clinical imaging tool for detection of small or subtle cortical abnormalities.

References

1. Aronica E, Gorter JA, Jansen GH, van Veelen CW, van Rijen PC, Ramkema M *et al.* Expression and cell distribution of group I and group II metabotropic glutamate receptor subtypes in taylor-type focal cortical dysplasia. *Epilepsia* 2003; 44(6)**:** 785-95.
2. Elmenhorst D, Minuzzi L, Aliaga A, Rowley J, Massarweh G, Diksic M et al. In vivo and in vitro validation of reference tissue models for the mGluR(5) ligand [(11)C]ABP688. Journal of cerebral blood flow and metabolism : official journal of the International Society of Cerebral Blood Flow and Metabolism 2010; 30(8)**:** 1538-49.

3.   DuBois JM, Rousset OG, Rowley J, Porras-Betancourt M, Reader AJ, Labbe A *et al.* Characterization of age/sex and the regional distribution of mGluR5 availability in the healthy human brain measured by high-resolution [(11)C]ABP688 PET. *European journal of nuclear medicine and molecular imaging* 2016; 43(1)**:** 152-62.

4.   Palmini A, Gambardella A, Andermann F, Dubeau F, da Costa JC, Olivier A *et al.* Intrinsic epileptogenicity of human dysplastic cortex as suggested by corticography and surgical results. *Annals of neurology* 1995; 37(4)**:** 476-487.

5-HTT binding potential as a predictor of 8 week treatment remission in unipolar depression: a prospective PET study

Mala Ananth[1]; Christine DeLorenzo[2,3,4]; Jie Yang[5]; Jeffrey Miller[4]; J. John Mann[4]; Ramin Parsey[2,4]

[1]Department of Neurobiology and Behavior, Stony Brook University, Stony Brook, NY; [2]Department of Psychiatry, Stony Brook University School of Medicine, Stony Brook, NY; [3]Department of Biomedical Engineering, Stony Brook University, Stony Brook, NY; [4]Department of Psychiatry, Columbia University, College of Physicians and Surgeons, New York, New York, 10032; [5]Department of Family, Population, and Preventative Medicine, Stony Brook University Medicine Center, Stony Brook, NY

Introduction: Major Depressive Disorder (MDD) is a debilitating condition that affects over 14 million Americans[1]. Optimizing medication treatment is challenging, and often involves weeks of trial and error. Remission occurs in a minority of individuals following first-line antidepressant treatment (approximately 35 percent); treatment-specific predictors are therefore needed. Using PET imaging with a radiotracer specific for the serotonin transporter (5-HTT), [11C]McN5652, we have found that non-remission from MDD after 12 months of **naturalistic** treatment may be predicted by decreased midbrain and amygdalar binding[2]. Here, revisiting our hypothesis with a prospective study with standardized treatment for eight weeks, and with a PET tracer that has higher selectivity for 5-HTT as well as improved signal to noise[3,4], we investigated whether pre-treatment 5-HTT binding is predictive of subsequent remission.

Methods: 31 healthy controls (HC) and 25 medication free patients with MDD (male and female) were scanned using the 5-HTT tracer, [11C]DASB. MDD subjects then received eight weeks of standardized pharmacotherapy with the selective serotonin reuptake inhibitor escitalopram. The relationship between pretreatment binding and post-treatment clinical status was examined. [11C]DASB scans were acquired for 90 minutes after tracer injection, and arterial blood samples were collected to calculate the metabolite-corrected arterial input function. Time activity curves were fit with likelihood estimation in graphical analysis (LEGA)[5,6] and, with the arterial analysis, were used to calculate the outcome measure, V_T/f_P. Using this measure, estimated binding does not rely on a reference region[7]. Remission status was determined using the 24 item Hamilton Depression Rating Scale (HDRS-24)[8]. Remission was defined as a posttreatment HDRS score of less than 10 as well as ≥50% reduction in HDRS-24 score from baseline.

Results: A linear mixed effects model comparing group differences in two regions of interest (amygdala & midbrain) revealed a significant difference in amygdalar binding between HC and remitters (p=0.029, unadjusted), where remitters had lower amygdalar binding than controls. This result is not significant following Bonferroni correction for multiple comparisons (p=0.058). No differences were found in amygdalar binding between non-remitters and either remitters or HC (all p>0.05). No differences were found in midbrain binding between HC, remitters or non-remitters (all p>0.05). Additionally, we found no relationship between pretreatment amygdalar binding and post-treatment HDRS-24 score based on a linear mixed effects model adjusted for baseline HDRS-24 score.

Conclusions: Data suggests that decreased 5-HTT amygdalar binding should be examined further, and in conjunction with other measures, as a possible predictor of remission. The differences from our previous study may be attributed to improvements in 5-HTT selectivity due to the use of a superior tracer, standardized treatment, different time-point of assessing clinical outcome (8 weeks vs. 1 year), and the use of a different PET outcome measure. Follow-up studies with increased sample size, pre-and post-treatment scans, and standardized treatment are needed to further investigate changes in 5-HTT binding as a predictor of remission.

References

1. http://www.nimh.nih.gov/health/topics/depression/index.shtml
2. Miller, J.M., et al., *Serotonin transporter binding as a possible predictor of one-year remission in major depressive disorder.* J Psychiatr Res, 2008. **42**(14): p. 1137-44.
3. Wilson, A.A., et al., *In vitro and in vivo characterisation of [11C]-DASB: a probe for in vivo measurements of the serotonin transporter by positron emission tomography.* Nucl Med Biol, 2002. **29**(5): p. 509-15.
4. Szabo, Z., et al., *Comparison of (+)-(11C)-McN5652 and (11C)-DASB as serotonin transporter radioligands under various experimental conditions.* J Nucl Med, 2002. **43**(5): p. 678-92.
5. Ogden, R.T., Estimation of kinetic parameters in graphical analysis of PET imaging data. Stat Med, 2003. 22(22): p. 3557-68.

6. Parsey, R.V., R.T. Ogden, and J.J. Mann, Determination of volume of distribution using likelihood estimation in graphical analysis: elimination of estimation bias. J Cereb Blood Flow Metab, 2003. 23(12): p. 1471-8.
7. Parsey, R.V., et al., Acute occupancy of brain serotonin transporter by sertraline as measured by [11C]DASB and positron emission tomography. Biol Psychiatry, 2006. 59(9): p. 821-8
8. Hamilton, M., A RATING SCALE FOR DEPRESSION. J Neurol Neurosurg Psychiatry, 1960. 23(1): p. 56-62.

Interpreting the Simplified Reference Tissue Model: A Correction

James E. Holden

Dept. of Medical Physics, School of Medicine and Public Health University of Wisconsin–Madison

The noise-free time course of a macromolecule-binding tracer ligand can never be fitted by a one-tissue-compartment model. However, the simplified reference tissue model (SRTM),[1] which is based on the assumption of a single tissue compartment, both accurately describes binding ligand time–activity curves and provides estimates of distribution volume ratios (DVR) that compare well with those from other methods. I investigated this apparent contradiction using simulated data.

Methods: Multiple noise-free two-tissue-compartment time courses of one-hour duration were simulated with a wide range of rate constants (k_2=0.07–0.31/min, k_3=0.07–0.39/min, k_4=0.04–0.10/min). The resulting kinetics always comprised an early, rapidly clearing component and a slowly clearing component that was dominated by the bound compartment. Reference tissue time courses were calculated assuming R_1=1. The simulated data were then fitted with both the one-tissue-compartment plasma-input model and the SRTM

$$C(t) = P_1 C_R(t) + P_2 \exp(-P_3 t) \otimes C_R(t)$$

where $C(t)$ and $C_R(t)$ are the target and reference tissue time courses.

Results: The two model curves always differed (Figure 1A). That is, the SRTM did not reproduce the curve obtained from the one-tissue-compartment model. The fitted exponential parameter P_3 had a nearly constant relationship with the exponent of the two-compartment slow component ($P_3 \approx 0.9\alpha_1$, R^2=0.98) over the entire range of models fitted (Figure 1B). These results show, as discussed below, that the SRTM does not in fact behave as expected.

Discussion: The SRTM represents a one-compartment solution only if $P_1=P_2/(k_2'-P_3)$, where k_2' is the true tissue-to-plasma efflux rate constant for the reference tissue. However, the fitted P_1 was always larger than this value. Thus the SRTM solution equals the desired one-compartment solution plus a component proportional to the reference tissue time course $C_R(t)$. The fixed relationship between the fitted exponent P_3 and the two-compartment exponent α_1 implies that the convolution term of the SRTM is consistently being used to attempt to fit the slowly clearing component of the two-compartment solution, which is indeed a one-compartment solution. Given that the residual between the data and this estimate of the slowly clearing component resembles the rapidly clearing component, which in turn resembles $C_R(t)$, including more of the reference tissue time course than is needed for the one-compartment component will always improve the fit to the data. SRTM fits were excellent over the whole range of rate constants studied. In all cases, however, the SRTM DVR values were biased toward high values. Bias decreased as any of the three two-compartment rate constants increased in value. For k_4=0.10 and $k_2 > 0.12$, the bias was less than 2 percent. Nearly identical results were obtained as the shape of the plasma input function was varied. Finally, linearized SRTM[2] produced a similar pattern of positive DVR bias as the two-compartment rate constants were varied, but with smaller bias values relative to those from the convolution-based method.

References:

1. NeuroImage 1996; 4: 153–158; 2. NeuroImage 2003; 18: 975–989

A

Radioactivity concentraion

time (min)

data
one-comp. fit
SRTM

B

$P_3 = 0.88\alpha_1 + 0.0002 \qquad R^2 = 0.98$

P_3 vs α_1

P_3 (min^{-1})

$k_4 = 0.04$/min
$k_4 = 0.07$/min
$k_4 = 0.10$/min

α_1 (min^{-1})

$$\alpha_1 = \frac{k_2 + k_3 + k_4 - \sqrt{(k_2 + k_3 + k_4)^2 - 4k_2 k_4}}{2}$$
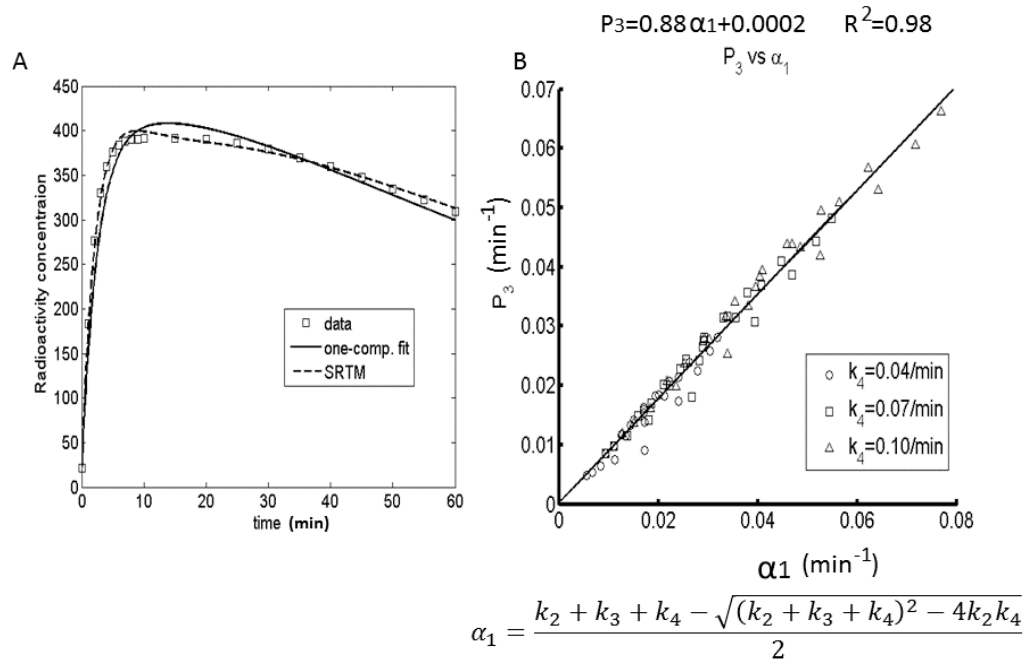
Evidence for neuroinflammation in Major Depressive Disorder and its association with suicidal thoughts: a [11C](R)-PK11195 study

Sophie E Holmes[1], Rainer Hinz[2], Jose M Anton-Rodriguez[3], Michael Green[4], Peter S Talbot[5]

[1]Yale University, [2]Wolfson Molecular Imaging Centre, University of Manchester, [3]Wolfson Molecular Imaging Centre, University of Manchester, [4]Wolfson Molecular Imaging Centre, University of Manchester, [5]Wolfson Molecular Imaging Centre, University of Manchester

Introduction: Major Depressive Disorder (MDD) is a debilitating disorder that affects millions of people worldwide. Despite its prevalence and burden to society, current antidepressant treatment is inadequate (1). It is vital that novel avenues of research are explored so that depression can be treated more effectively. Inflammation is a highly topical research area owing to mounting and converging evidence suggesting its involvement in MDD (2). Less clear is the involvement of inflammation in the brain. Neuroinflammation can be measured *in-vivo* using Positron Emission Tomography (PET) and radioligands that bind to the translocator protein (TSPO), which is upregulated on activated microglia. A recent study demonstrated TSPO upregulation in the ACC, PFC and insula of moderate to severely depressed patients who were off medication (3). However, in this study and in studies measuring peripheral inflammatory markers (4)(5) there seems to be a subset of patients with a heightened inflammatory state. Our study aimed to clarify the role of microglial activation in antidepressant-free moderate to severe depression and to address a key question: what is specific about those subjects showing a heightened inflammatory state?

Methods: Fourteen patients (7 males; age 31±12) in a major depressive episode of at least moderate severity (mean MADRS score 31±4; mean HAM-D score 20±3) and thirteen age and gender matched controls (7 males; age 33±11) underwent a 60 minute dynamic PET scan with [11C](R)-PK11195 using the High Resolution Research Tomograph (HRRT). Patients were antidepressant-naïve or -free for at least 6 months, were non-smoking, medically healthy and had no alcohol or substance misuse. As an exploratory analysis we compared binding potential (BP_{ND}) between patients with (n=9) and without (n=5) suicidal thoughts. A grey matter cerebellum input function was used to generate parametric maps of BP_{ND} using the SRTM (6). A maximum probability brain atlas (7) was applied to the parametric brain maps to give readouts from each ROI (ACC, PFC, insula and total cortical).

Results: A MANOVA including ACC, PFC, insula and total cortical binding indicated a significant main effect of group, with elevated [11C](R)-PK11195 binding in the MDD patients compared to controls ($F_{4, 22}$=4.6, *p*=0.008). Evaluating the selected regions, [11C](R)-PK11195 binding was significantly higher in the MDD patients compared to controls in the ACC ($F_{1, 25}$=6.0, *p*=0.022), with a 37% increase in BP_{ND}. Binding in PFC, insula and total cortical regions was increased by 20%, 17% and 26%, respectively, but these increases were not statistically significant. In relation to suicidal thoughts, there was significantly higher binding in the patients experiencing suicidal thoughts compared to those who were not ($F_{4,9}$=4.94, *p*=0.022), with a mean increase of 64% across all ROIs. BP_{ND} was significantly higher in total cortical regions, ACC ($F_{1, 12}$=11.71, *p*=0.005) and insula ($F_{1, 12}$=6.86, *p*=0.022) and reached trend significance in PFC ($F_{1, 12}$=3.58, *p*=0.083).

Conclusion: Our research provides evidence for the presence of microglial activation in MDD, specifically in the ACC, a key region involved in the pathophysiology of depression. Our findings are largely in line with the most recent PET study investigating neuroinflammation in MDD (3). Exploratory analysis suggests that the presence of suicidal thoughts may be one factor associated with increased microglial activation in MDD. If confirmed, it will be important to investigate whether interventions that reduce inflammation result in reduced suicidal thinking.

References:
1. Millan MJ, Goodwin GM, Meyer-Lindenberg A, Ove Ogren S (2015): Learning from the past and looking to the future: Emerging Perspectives For Improving The Treatment Of Psychiatric Disorders. *Eur Neuropsychopharmacol* 25: 599–656.
2. Kiecolt-Glaser JK, Derry HM, Fagundes CP (2015): Inflammation: Depression Fans the Flames and Feasts on the Heat. *Am J Psychiatry* 172: 1075–91.
3. Setiawan E, Wilson AA, Mizrahi R, Rusjan PM, Miler L, Rajkowska G, *et al.* (2015): Role of Translocator Protein Density, a Marker of Neuroinflammation, in the Brain During Major Depressive Episodes. *JAMA Psychiatry* 72: 268–275.
4. Howren MB, Lamkin DM, Suls J (2009): Associations of depression with C-reactive protein, IL-1, and IL-6: A meta-analysis. *Psychosom Med* 71: 171–186.

5. Dowlati Y, Herrmann N, Swardfager W, Liu H, Sham L, Reim EK, Lanctot KL (2010): A Meta-Analysis of Cytokines in Major Depression. *Biol Psychiatry* 67: 446–457.

6. Lammertsma AA, Hume SP (1996): Simplified reference tissue model for PET receptor studies. *Neuroimage* 4: 153–8.

7. Hammers A, Allom R, Koepp MJ, Free SL, Myers R, Lemieux L, *et al.* (2003): Three-dimensional maximum probability atlas of the human brain, with particular reference to the temporal lobe. *Hum Brain Mapp* 19: 224–247.
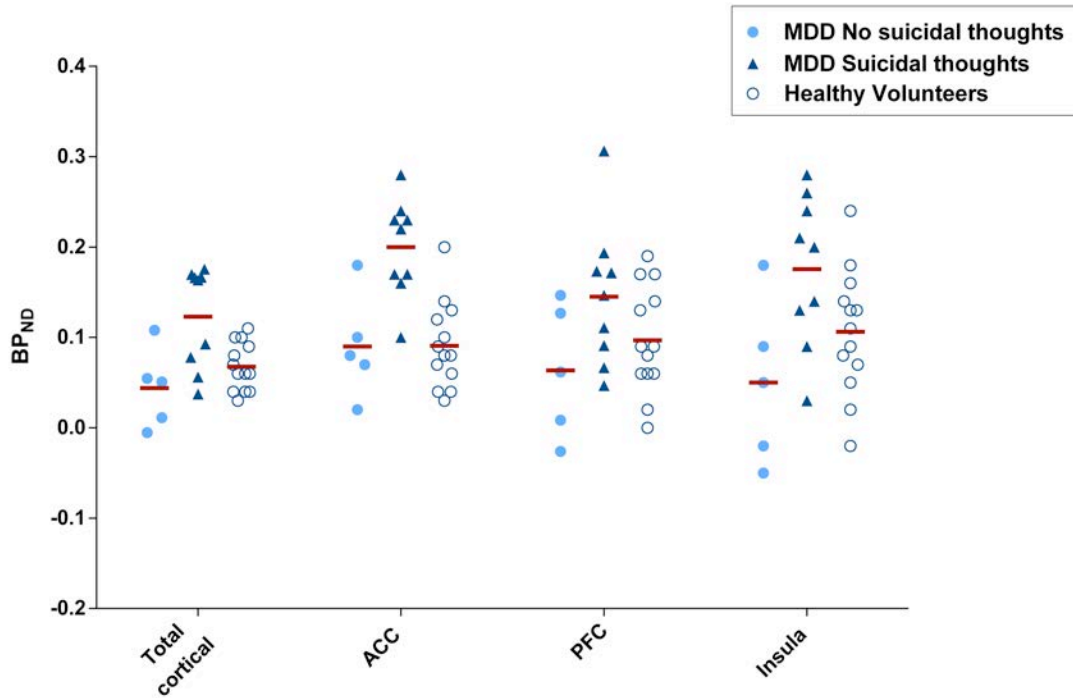
Relationships between corticostriatal functional connectivity and striatal [11C]raclopride availability in social drinkers and nontreatment-seeking alcoholics

M Halcomb[1], E Chumin[1,2], J Contreras[1,2], J Goni[1,3,4], M Dzemidzic[1,5], KK Yoder[1,2,6]

[1]Center for Neuroimaging, Department of Radiology and Imaging Sciences, Indiana University School of Medicine, Indianapolis, IN USA; [2]Stark Neurosciences Research Institute, Indiana University School of Medicine, Indianapolis, IN   USA; [3]Weldon School of Biomedical Engineering, Purdue University, West Lafayette, IN USA; [4]School of Industrial Engineering, Purdue University, West Lafayette, IN, USA ; [5]Department of Neurology, Indiana University School of Medicine, Indianapolis, IN USA ; [6]Department Psychology, Indiana University Purdue University at Indianapolis, Indianapolis, IN USA

Introduction: The striatal dopamine system is regulated, in part, by inputs from the prefrontal cortex.   Given the major role that the dopamine system plays in cognitive processes related to addiction, it is of great importance to understand how cortical activity may influence dopaminergic function *in vivo* in humans.   Broadly stated, resting-state functional magnetic resonance imaging (rs-fMRI) permits assessment of interregional correlations of brain activity (functional connectivity, FC).   Combining FC methodology with dopaminergic positron emission tomography (PET) has the potential to provide unique information about how corticostriatal activity may relate to dopamine function in healthy and diseased states.   A handful of studies   have implemented this approach in healthy subjects (Cole 2012), Parkinson's Disease (Baik 2014) and methamphetamine addiction (Kohno 2016).   However, no such data are available in alcohol use disorders.   Here, we examined whether FC between known corticostriatal projections was related to striatal [11C]raclopride (RAC) binding potential (BP).   We hypothesized that significant relationships would be detected, and that the nature of relationships between BP and FC would differ between social drinkers (SD) and nontreatment-seeking alcoholics (NTS).

Methods: Sixteen SD (39.3±2.9 y.o.; 9M/7F) and 13 NTS (39.8±2.9 y.o.; 10M/3F) received a baseline RAC PET scan (Siemens mCT), an rsFC scan, and an anatomical MRI (Siemens 3T Skyra: 8 SD, 9 NTS; 3T Prisma: 8 SD, 4 NTS). NTS subjects met DSM-IV criteria for alcohol dependence. For each subject, gray matter was parcellated into 278 functionally-defined regions of interest (ROIs) per Shen 2013.   After extensive data processing and QC (data between MR scanners were deemed compatible), FC was quantified using Pearson's *r* for each pair of ROIs.   ROI pairs that most closely corresponded to known or likely corticostriatal projections (e.g., Haber 2006) were analyzed.   Cortical regions included anterior cingulate, medial prefrontal, orbitofrontal, ventromedial prefrontal, dorsolateral prefrontal, and other prefrontal cortical areas. Striatal parcellations included the accumbens, putamen, and caudate body and tail, which were also used to extract time-activity curves from the RAC PET data.   BP was estimated with MRTM, with cerebellar gray matter as the reference region.   For each group, correlations were assessed for all respective PET and FC pairs (e.g., left accumbens BP with left accumbens-left orbitofrontal FC).   For significant correlations, Fisher's *r*-to-*z* transformation was used to determine group differences.

Results: Results for SD and NTS are presented in the attached table.   There were multiple trend-level and significant group differences in BP:FC correlations.   The majority of correlations were inverse.

Conclusions: The spatial pattern of BP:FC relationships was different between SD and NTS, which could indicate differential regulation of striatal dopamine in alcoholism.   The data suggest that increased regional connectivity may lead to higher dopamine tone; alternatively, increased connectivity may be a function of increased D_2/D_3 signaling. Additional data and new studies are required to guide interpretation of this important multi-modality approach. These pilot results may provide an important platform for understanding the neurobiological substrates of alcohol dependence and other addictive disorders.

References:

1. Cole DM, Beckmann CF, Searle GE, Plisson C, Tziortzi AC, Nichols TE, Gunn RN, Matthews PM, Rabiner EA, Beaver JD. Orbitofrontal connectivity with resting-state networks is associated with midbrain dopamine D3 receptor availability.   Cereb Cortex. 2012 Dec;22(12):2784-93. doi: 10.1093/cercor/bhr354. Epub 2011 Dec 19. PMID: 22186675

2. Kohno M, Okita K, Morales AM, Robertson CL, Dean AC, Ghahremani DG, Sabb FW, Rawson RA, Mandelkern MA, Bilder RM, London ED.   Midbrain functional connectivity and ventral striatal dopamine D2-type receptors: link to impulsivity in methamphetamine users.   Mol Psychiatry. 2016 Feb 2. doi: 10.1038/mp.2015.223. [Epub ahead of print] PMID: 26830141
3. Baik K, Cha J, Ham JH, Baek GM, Sunwoo MK, Hong JY, Shin NY, Kim JS, Lee JM, Lee SK, Sohn YH, Lee PH.   Dopaminergic modulation of resting-state functional connectivity in de novo patients with Parkinson's disease.   Hum Brain Mapp. 2014 Nov;35(11):5431-41. doi: 10.1002/hbm.22561. Epub 2014 Jun 17. PMID: 24938993
4. Shen X, Tokoglu F, Papademetris X, Constable RT.   Groupwise whole-brain parcellation from resting-state fMRI data for network node identification.   Neuroimage. 2013 Nov 15;82:403-15. doi: 10.1016/j.neuroimage.2013.05.081. Epub 2013 Jun 4. PMID: 23747961

Group	BP:FC pair	r	p	Group	r	p	Group Difference in r
Social Drinkers n = 16	L acccum151: L accum151- L ACC161	-0.8	<0.0001	NTS n = 13	-0.3	0.28	Z = -1.67 p = .095
	L caud body263: L caud body263-L mPFC182	-0.6	0.022		0.1	0.68	Z = -1.85 p = 0.064
	L caud body263: L caud body263-L ACC161	-0.6	0.008		-0.1	0.66	Z = -1.47 p = 0.142
	L caud tail273: L caud tail273- L ACC161	-0.5	0.04		0.2	0.59	Z = -1.77 p = 0.077
	L caud tail273: L caud tail273- L OFC179	0.52	0.041		-0.6	0.03	Z = 3.06 p = 0.002
Nontreatment- seeking alcoholics n = 13	L accum151: L accum151- L ACC176	-0.6	0.028	SD n = 16	-0.1	0.64	Z = -1.37 p = 0.171
	L accum151: L accum151- L PFC209	-0.6	0.038		0.5	0.07	Z = -2.97 p = 0.005
	L caud tail273: L caud tail273- L OFC179	-0.6	0.027		0.5	0.04	Z = -3.06 p = 0.002
	L put149: L put149- L dlPFC164	0.57	0.044		-0.3	0.28	Z = 2.25 p = 0.024
	R accum114: R accum114- R PFC037	-0.6	0.03		-0.2	0.55	Z = -1.26 p = 0.208
	R put128: R put128- R dPFC002	-0.6	0.046		0.3	0.28	Z = -2.21 p = 0.027

SD: social drinkers; NTS: nontreatment-seeking alcoholics; L: left; R: right; accum: accumbens; caud: caudate; put: putamen; ACC: anterior cingulate cortex; m: medial; d: dorsal; dl: dorsolateral; PFC: prefrontal cortex; OFC: orbitofrontal cortex. Region numbers indicate Shen (2013) parcellation label designations.

Biodistribution and dosimetry of [^{18}F]fluortriopride, a dopamine D3 receptor selective PET radiotracer, in healthy humans

Robert Doot, Jacob Dubroff, Joshua Scheuermann, Jenny Cai, Chia-Ju Hsieh, Hsiaoju Lee, Erin Schubert, Catherine Hou, Regan Sheffer, Kuiying Xu, Shihong Li, and Robert Mach

Division of Nuclear Medicine and Molecular Imaging, Department of Radiology, Perelman School of Medicine, University of Pennsylvania, Philadelphia, Pennsylvania, USA

Introduction: Dopamine D3 receptors are thought to represent principal neural substrates in the dopaminergic mesolimbic circuit, the primary reward pathway in the mammalian brain. D3 receptor dysfunction has been implicated in many diseases including drug addiction, Parkinson's disease, and schizophrenia. In anesthetized non-human primates, [^{18}F]fluortriopride (FTP) binding was sensitive to levels of endogenous dopamine [1] but reflected the distribution of D3 receptors as determined by autoradiography [2]. The purpose of this study was to assess the biodistribution and radiation dose resulting from administration of the dopamine D3 receptor selective radiotracer [^{18}F]FTP in healthy humans.

Methods: Five healthy adult volunteers (2 females and 3 males, ages 23-53, mean 36) underwent 7 PET whole body and up to 4 low dose CT attenuation scans using a Philips Ingenuity PET/CT scanner over 4 hours following the intravenous administration of [F-18]FTP (mean 244 MBq, 159-270 MBq (6.6 mCi, 4.3-7.3 mCi)). The patients provided signed informed consent for the PET/CT studies according to the guidelines of the University of Pennsylvania Institutional Review Board. Activity concentrations in participant blood and urine samples were assessed using a gamma counter. The total activity residing in relevant organs for each time point was determined from volumes of interest (VOIs) measurements of the PET images using Pmod v3.7 image analysis software package. Individual VOIs completely encompassed each patient's brain, gall bladder, heart wall, heart contents, intestines, kidneys, liver, lungs, spleen, and urinary bladder to measure total activity by organ using the software's VOI analysis tools. We also measured the total activity and total volume in 5 manually drawn lumbar vertebrae marrow spaces to combine with a red marrow density of 1.03 g/cc [3], and an assumption that the red marrow weight is 1.6% of total body weight [4] to estimate the total activity in red bone marrow. The resulting total activity by organ data was converted into % injected activity residing in each organ at each time point and entered into the exponential modeling module of the OLINDA | EXM v.1.1 software package. The cumulated activity for each organ was used as the input for the dosimetry estimates in OLINDA | EXM. All dose estimates were calculated using the Standard Adult Male phantom in OLINDA.

Results: The [^{18}F]FTP average absorbed dose estimates for healthy volunteers are in Table 1. The highest individual organ dose is in the gall bladder. The average effective dose was 0.0227 ± 0.0028 mSv/MBq. An anticipated standard 240.5 MBq (6.5 mCi) injected dose of [^{18}F]FTP results in an effective dose of 5.46 mSv.

Conclusion: [^{18}F]Fluortriopride PET/CT dosimetry results confirm expectations that the biodistribution and levels of absorbed doses are adequately low to continue researching [^{18}F]FTP radiotracer uptake in humans.

References:
1. Mach RH, Tu Z, Xu J, et al. Endogenous dopamine (DA) competes with the binding of a radiolabeled D(3) receptor partial agonist in vivo: a positron emission tomography study. *Synapse.* 2011;65(8):724-732.
2. Sun J, Xu J, Cairns NJ, Perlmutter JS, Mach RH. Dopamine D1, D2, D3 receptors, vesicular monoamine transporter type-2 (VMAT2) and dopamine transporter (DAT) densities in aged human brain. *PloS one.* 2012;7(11):e49483.
3. ICRU, Tissue substitutes in radiation dosimetry and measurement, ICRU Report 44. International Commission on Radiation Units and Measurements, Bethesda, MD, 1989: Table 4.2, page 21.
4. Vieira JW, Lima FRA, and Kramer R. Calculation of red bone marrow equivalent dose to the MAX (Male Adult voXel) model for external exposures to photons. VI National Meeting on Nuclear Applications – ENAN, Rio de Janeiro, Brazil, 11-16 August 2002, p 2.

Table 1:
Mean [^{18}F]fluortriopride absorbed dose estimates in mSv/MBq for 5 subjects.

Target organ	Mean	Standard deviation
Adrenals	1.50E-02	1.12E-03
Brain	4.75E-03	4.13E-04
Breast	6.56E-03	8.81E-04
Gallbladder wall	3.44E-01	1.57E-01
Lower large intestine (LLI) wall	3.27E-02	1.26E-02
Small intestine	8.19E-02	3.54E-02
Stomach wall	1.32E-02	5.50E-04
Upper large intestine (ULI) wall	9.42E-02	4.03E-02
Heart wall	1.58E-02	3.70E-03
Kidneys	2.77E-02	2.83E-03
Liver	6.44E-02	7.32E-03
Lungs	3.04E-02	1.57E-02
Muscle	8.73E-03	1.40E-04
Ovaries	1.97E-02	5.49E-03
Pancreas	1.73E-02	1.41E-03
Red marrow	1.55E-02	1.10E-03
Osteogenic cells	1.36E-02	8.53E-04
Skin	5.53E-03	2.94E-04
Spleen	3.01E-02	1.08E-02
Testes	5.98E-03	3.07E-04
Thymus	7.46E-03	1.12E-03
Thyroid	5.95E-03	6.93E-04
Urinary bladder wall	2.11E-02	4.91E-03
Uterus	1.67E-02	3.91E-03
Total body	1.18E-02	2.68E-04
Effective dose equivalent	4.95E-02	8.85E-03
Effective dose	2.27E-02	2.79E-03

PET neuroimaging and kinetic evaluation in non-human primates of the glycogen synthase kinase-3 radiotracer [11C]PF367

Nicolas J. Guehl[1], Dustin W. Wooten[1], Elijahu Livni[1], Thomas L. Collier[1], Kira Grogg[1], Steven H. Liang[1], Georges El Fakhri[1], Neil Vasdev[1], Marc D. Normandin[1]

[1]*Gordon Center of Medical Imaging, Division of Nuclear Medicine and Molecular Imaging, Massachusetts General Hospital & Department of Radiology, Harvard Medical School, Boston, MA, USA.*

Objectives: [11C]PF367 was developed as a radiotracer for positron emission tomography (PET) imaging of the glycogen synthase kinase-3 (GSK-3). The target enzyme represents an essential locus of convergence and crosstalk between several important signal transduction pathways. Dysregulation of GSK-3 has been implicated in the etiology of pathological conditions including Alzheimer's disease, schizophrenia, bipolar disorder and major depression. Here we describe initial evaluation of [11C]PF367 for brain imaging in non-human primates.

Methods: Two rhesus macaques underwent nine scans. Paired baseline-blocking studies at two doses of unlabeled PF367 (0.135 and 1 mg/kg) were performed in each animal. Blocking scans entailed co-administration of cold PF367 with the radiotracer and were preceded 4 hours earlier by baseline imaging. One chase study was conducted with 1 mg/kg PF367 administered 45 min after radiotracer. Arterial samples were drawn and radioactivity concentration measured in whole blood and plasma. Selected plasma samples were analyzed by column-switching radio-HPLC to generate metabolite-corrected input functions. Regional time activity curves were analyzed by compartmental models in one- (1T) and two- (2T) tissue configurations, with or without blood volume correction, and the 2T model was assessed in irreversible (K_1-k_3 estimated, k_4=0) and reversible (K_1-k_4 estimated) implementations. The Patlak and Logan graphical analysis techniques were also applied to region-based curves and for parametric mapping.

Results: The ratio of plasma to whole blood concentration was stable at 1.3±0.1 after 1 minute post-injection. Plasma parent fraction was best fitted with biexponential function ($T_{1/2s}$ = 5.9±1.8 min, 109±58 min). Metabolism was relatively fast with ~40% of plasma activity from unmetabolized [11C]PF367 at 15 min after tracer administration. [11C]PF367 peaked quickly in brain with SUV of 1.0±0.2 at ~4 min post-injection. The 1T model gave poor fits regardless of inclusion of blood volume and was not further considered. The 2T reversible binding model with vascular correction (2T4k1v) produced best fits by Akaike information criterion and visual inspection but the total volume of distribution calculated from the micro-parameters (V_T=[K_1/k_2]/[1+k_3/k_4]]) was unstable and failed to correlate with V_T estimated by Logan graphical analysis. The 2T irreversible binding model with vascular correction, (2T3k1v) gave satisfactory fits and the net influx rate calculated from the micro-parameters (K_i=[$K_1 k_3$]/[k_2+k_3]) was found to be robust. K_i obtained from the Patlak slope correlated strongly with the 2T3k1v outcomes (K_i^{Patlak}=1.07 x K_i^{2T3k1v}-0.05, R^2= 0.98; mean difference: -4.3±7.5%). K_i decreased 30±7% compared to baseline with similar results at the 0.135 and 1 mg/kg doses. In the chase study, time activity curves revealed displacement shortly after administration of cold PF367.

Conclusions: [11C]PF367 is brain penetrant and metabolizes rapidly. Blocking and chase studies demonstrated specific and displaceable binding in vivo, characteristics not exhibited by previously reported GSK-3 radiotracers, although quantification of [11C]PF367 based on irreversible uptake methods proved more robust than an unconstrained reversible binding model. Additional studies at lower mass doses will elucidate a more detailed dose-response profile to confirm optimal analytic methods and outcome parameters for [11C]PF367, which warrants further evaluation while serving as a lead compound toward discovery of GSK-3 radiotracers with even more favorable imaging properties.
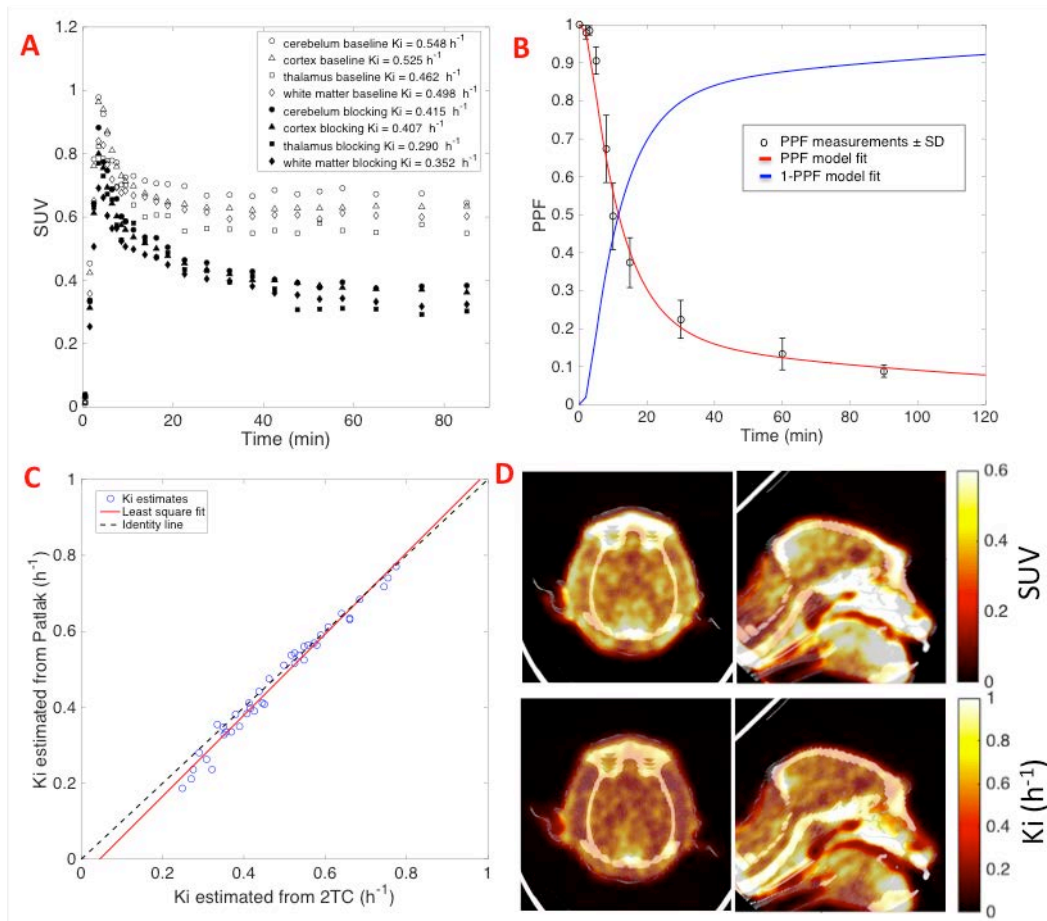
Figure 1S: **A:** PET time activity curves for different brain regions from baseline and blocking studies. **B.** Mean PPF measurements across all studies and associated standard deviation. Model fit obtained with a sum of two-exponentials is also shown. **C.** Correlation plot between Ki obtained from Patlak analysis and Ki calculated from the 2T3k1v model estimates. **D:** [11C]PF367 SUV images (Top) for a baseline scan (45-90 min after tracer injection) and Ki parametric map (bottom) obtained with Patlak graphical method for the same scan overlaid on CT images.

Quantifying variation in compartmental model estimates of binding potential using Sequential Monte Carlo

Adam Hall[1,2], John Aston[2], Franklin Aigbirhio[1], John O'Brien[3]

[1]*Molecular Imaging Chemistry Laboratory, Wolfson Brain Imaging Centre, University of Cambridge, UK;*
[2]*Statistics Laboratory, University of Cambridge, UK;* [3]*Department of Psychiatry, University of Cambridge, UK*

Introduction and objectives: Due to the large volumes of data in PET images, robust analyses of fit and quantification of corresponding error have not previously been easy to conduct. A statistical method known as Sequential Monte Carlo (SMC) [1] can be readily applied to PET data [2], which can provide robust and easily interpreted estimates of uncertainty of model fit. These estimates are broadly useful, but especially so in scenarios involving dementias, where this information has the potential to assist with or reaffirm diagnoses with more confidence than where the PET imaging-derived information is limited to binding potential (BP) maps alone.

Quantification of error in PET models traditionally proceeds using asymptotics under the assumption that the estimated parameters provide a good model fit [3], though this is not entirely robust.

Instead of a single set of `best fit' parameter values, it is proposed that a collection of parameter values called particles is maintained. These particles describe a probability distribution for a `plausible fit', from which the variance and correlation in the parameters can be readily extracted.

Methods: SMC is a mature and robust technique for computing such a particle distribution, and though any thorough analysis of PET data can be computationally challenging, SMC is computationally scalable in modern computing environments via parallelisation (and could also make effective use of GPUs).

[11C]PK11195 is used here to demonstrate the approach. This tracer has been widely used as a PET ligand for studying neuroinflammation in dementia brain disorders through binding to TSPO receptor expression. Here, plasma input is unavailable so the standard simplified reference tissue model (SRTM) is used with cluster-derived input [4], which consists of one compartment to describe the reference region and another compartment for a region/tissue of interest, with different tissues treated independently.

This is easily implemented (as indeed are other PET compartmental models) using the vSMC framework [5]. For speed reasons, a spectral basis of exponential decay coefficients are pre-calculated from a physically informed range. The SMC sampler then only has to calculate linear combinations of these basis functions while evaluating likelihoods.

Results: The method was first validated on synthetic data before being applied to the PK11195 data. For PK11195, the estimates of the SRTM micro parameters had large variances for a number of regions, but the corresponding binding potential variances and fitted curves were generally much more stable with lower variances. For time-activity curves (TACs) that did not fit the SRTM dynamics, the corresponding variances were much larger. Results as shown in the indicative figure below were obtained by the SMC sampler in under 2 hours on the local compute server.

The upper left part of the figure shows the expected value of the BP over one slice of the brain for PK11195 for a particular subject, using AAL-derived regions of interest to improve signal compared to a voxel-wise approach. The lower left part shows the corresponding standard deviations of the BP values. The upper right part shows the highlighted TAC and corresponding band of fits with high posterior density. The lower right component shows the posterior marginal distribution of binding potentials for this voxel.

Key references
[1] Arnaud Doucet and Adam M. Johansen. In *Handbook of Nonlinear Filtering* (2009): 656-704.
[2] Yan Zhou. PhD thesis, University of Warwick. (2014).
[3] John Aston, et al. Neuroimage 12.3 (2000): 245-256.
[4] Federico E. Turkheimer, et al. J Nucl Med. (January 2007). 48:158-167

[5] Yan Zhou. arXiv preprint:1306.5583. (2013).
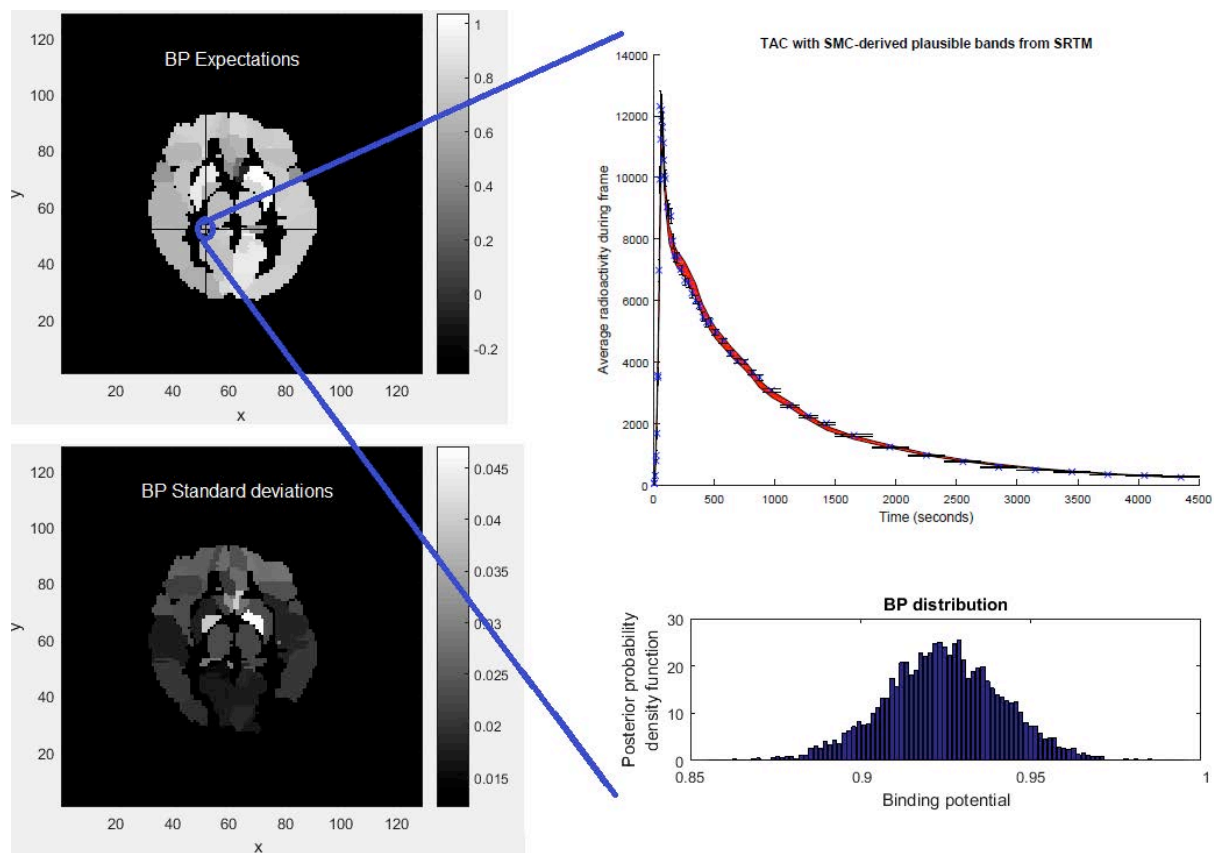
Test-retest reproducibility of the NMDA receptor ligand [18F]PK-209 in humans

Jasper van der Aart[1,4], Sandeep SV Golla[1], Marieke van der Pluijm[1], Patricia A. McCarthy[1], Lothar A. Schwarte[2], Patrick Schober[2], Robert C. Schuit[1], Pieter J Klein[1], Adriaan A. Lammertsma[1], Albert D. Windhorst, Ronald Boellaard[1,3], Bart N.M. van Berckel[1]

[1]Department of Radiology and Nuclear Medicine, VU University Medical Centre, Amsterdam, Netherlands; [2]Department of Anesthesiology, VU University Medical Center, Amsterdam, The Netherlands; [3]Department of Nuclear Medicine and Molecular Imaging, University Medical Center Groningen, Groningen, Netherlands; [4]Centre for Human Drug Research, Leiden, Netherlands

Objectives: Aberrant NMDA receptor neurotransmission and glutamate mediated neurotoxicity are implicated in the pathogenesis of neurodegenerative CNS disorders. Positron emission tomography provides a sensitive instrument to assess the NMDA receptor system *in vivo*, provided that a selective tracer for this receptor is available. [18F]PK-209 is a methylguanidine derivative that binds to the PCP site of the NMDA ion channel with high affinity and selectivity. In addition, it was shown its uptake could be modulated by MK-801 administration in rhesus monkeys [1]. The purpose of the present study was to investigate the kinetics of [18F]PK-209 in man and to evaluate plasma input kinetic models for quantification of NMDA receptor binding.

Methods: 5 healthy volunteers completed two PET scans each. The time between the two scans ranged from 31 to 61 days. Dynamic data were acquired for 120 minutes following intravenous injection of 182±6 MBq (mean±SD) [18F]PK-209. For each scan a metabolite corrected arterial input function was obtained using on-line sampling together with manual samples at 8 set times to determine metabolite fractions. Co-registered T1 MRI scans were used to segment PET images into grey matter, white matter, and extra-cerebral fluid. Time activity curves (TACs) were extracted using PVE-lab. Whole brain grey-matter TACs were fitted to single- and two-tissue (reversible and irreversible) compartment models, both with and without an additional (fit) parameter for fractional blood volume. Additional plasma input functions (IF) were generated to investigate their effect on model parameter test-retest (TRT) variability: an IF with the mean parent fractions and mean plasma-to-blood (PB) ratios of the 2 scans within each subject, and an IF that includes the population averaged parent fractions (i.e. at each time point the mean of 10 measurements) and PB ratios.

Results: [18F]PK-209 was synthesized with >97% radiochemical purity. Mean (±SD) specific activity at time of injection was similar between the first (64±22 GBq/μM) and the second (80±28 GBq/μmole) PET scans (P=0.21, paired T-test). Mean parent fractions were 35±5% at 20 minutes, 20±2% at 60 minutes and 15±3% at 120 minutes post injection. Best model fits were obtained using an irreversible two-tissue model with blood volume parameter (2T3k_Vb) in 8 out of 10 scans according to the Akaike information criterion. Table 1 shows the net influx rate constant (K_i) values obtained using the three different plasma input functions, and TRT variability for all subjects.

Conclusions: TACs were well described by a 2T3k model with blood volume parameter. Input functions with individual metabolite data resulted in high [18F]PK-209 TRT variation of K_i. Natural fluctuation of glutamate levels, or a different degree of [18F]PK-209 trapping within the NMDA receptor channel might explain variability in irreversible binding. However, the substantial reduction in K_i TRT variability when using the within-subject mean parent fractions may indicate that K_i is affected by rapid radiotracer metabolism and the associated uncertainties in metabolite analysis at later time points.

Reference
Golla SSV, Klein PJ, Bakker J, Schuit RC, Christiaans JAM, van Geest L, Kooijman EJM, Oropeza-Seguias GM, Langermans JAM, Leysen JE, Boellaard R, Windhorst AD, van Berckel BNM. Metaxas A. Preclinical evaluation of [18F]PK-209, a new PET ligand for imaging the ion-channel site of NMDA receptors. Nucl Med Biol; 2014.

IF		Subject1		Subject2		Subject3		Subject4		Subject5		TRT Mean ± SD
		PET1	PET2	PET1	PET2	PET1	PET2	PET1	PET2	PET1	PET2	
Single scan	K_i	0.0148	0.0108	0.0157	0.0125	0.0166	0.0152	0.0235	0.0148	0.0208	0.0182	
	TRT	31.5 %		22.7 %		8.7 %		45.1 %		13.5 %		24.3 ± 14.5%
Within-subject	K_i	0.0118	0.0126	0.0131	0.0127	0.0154	0.0162	0.0202	0.0170	0.0200	0.0191	
	TRT	-6.4 %		3.1 %		-5.3 %		17.0 %		4.6 %		7.3 ± 5.6%
Population average	K_i	0.0136	0.0142	0.0113	0.0136	0.0193	0.0201	0.0147	0.0115	0.0170	0.0156	
	TRT	-4.3 %		-18.1 %		-4.2 %		24.1 %		8.8 %		11.9 ± 8.9%

Blunted endogenous opioid release in abstinent alcohol dependent patients examined using [11C]carfentanil PET and dexamphetamine

Turton S[1], Myers J[1], Mick I[1], Stokes PRA[1], Rabiner EA[2,3], Gunn RN[2,4], Nutt DJ[1], Lingford-Hughes A[1]

[1]Centre for Neuropsychopharmacology, Division of Brain Sciences, Imperial College London, UK; [2]Imanova Ltd, London, UK; [3]Centre for Neuroimaging Sciences, King's College, London, UK; [4]Centre for Restorative Neuroscience, Division of Brain Sciences, Imperial College London, UK

Introduction: 24% of adults in England consume alcohol in a harmful manner, with 4% meeting the criteria for alcohol dependence. Pharmacotherapy for alcohol dependence includes opioid receptor antagonists naltrexone and nalmefene. These medications target the endogenous opioid system, modulating the mesolimbic dopaminergic pathway to reduce the rewarding effects of alcohol. There is increased binding of selective and non-selective opioid receptor PET radioligands in newly abstinent alcohol dependent individuals, implicating dysregulation of the endogenous opioid system in alcohol dependence (Williams 2009).
[11C]carfentanil is a selective mu-opioid receptor (MOR) agonist radioligand that can be used to measure endogenous β-endorphin release following a pharmacological challenge with dexamphetamine (Colasanti 2012, Mick 2014). Pathological gamblers have blunted β-endorphin release compared with healthy volunteers in several brain regions, but normal baseline MOR availability (Mick 2015). This study will test the hypothesis that alcohol dependence is associated with blunted β-endorphin release and higher baseline MOR availability.

Methods: Ten alcohol dependent (ADP) males, abstinent for a minimum of 4 weeks (mean 282 days, range 59-720 days), were recruited along with 10 healthy controls (HV) (<21 UK units/168g of alcohol per week). Participants underwent two [11C]carfentanil PET scans, before and 3 hours following a 0.5 mg/kg oral dose of dexamphetamine. Dynamic PET imaging was carried out on a Siemens PET Biograph. MOR binding potential (BP_{ND}) values were determined by applying the simplified reference tissue model, using the occipital cortex as the reference tissue, to region-of-interest (ROI) time-activity data. ΔBP_{ND} was calculated as (BP_{ND}Baseline–BP_{ND}PostAmphetamine)/BP_{ND}Baseline. All image processing and kinetic analysis was performed using MIAKAT™ (www.miakat.org). ROI were chosen a priori based on data from previous studies showing increased [11C]carfentanil BP_{ND} in alcohol dependence (See figure 1).

Results: ADP have a significantly ($p<0.05$) reduced ΔBP_{ND} in all ROIs compared with HV (see table 1). For example in the caudate ADP have a mean ΔBP_{ND} of -0.020 (-0.051 to 0.010 95% CI) compared with -0.090 (-0.133 to -0.046 95% CI) in the HV. There were no significant differences in baseline [11C]carfentanil BP_{ND} between HV and ADP.

Conclusions: These results show that abstinent alcohol dependent individuals have reduced β-endorphin release in all nine ROI investigated. This replicates our findings in pathological gamblers and supports the hypothesis that the opioid system is dysregulated in alcohol dependence. We found no support for our hypothesis that baseline MOR availability is elevated in ADP. This may be due to the longer duration of abstinence in our ADP sample compared with other cohorts.

References:
T.M. Williams et al. Brain opioid receptor binding in early abstinence from alcohol dependence and relationship to craving: an [11C]diprenorphine PET study. Eur Neuropsychopharmacol. **2009;19(10):740-8**
A. Colasanti et al. Endogenous Opioid Release in the Human Brain Reward System Induced by Acute Amphetamine Administration. Biol Psychiatry. 2012;72(5):371-7
I. Mick et al. Amphetamine induced endogenous opioid release in the human brain detected with [11C]carfentanil PET: replication in an independent cohort. Int J Neuropsychopharmacol. 2014;17(12):2069-74
I. Mick et al. Blunted Endogenous Opioid Release Following an Oral Amphetamine Challenge in Pathological Gamblers. Neuropsychopharmacology. 2015 [Epub ahead of print]

Figure 1 – Mean [^{11}C]carfentanil ΔBP_{ND} by ROI following amphetamine challenge comparing ADP and HV (95% confidence intervals)
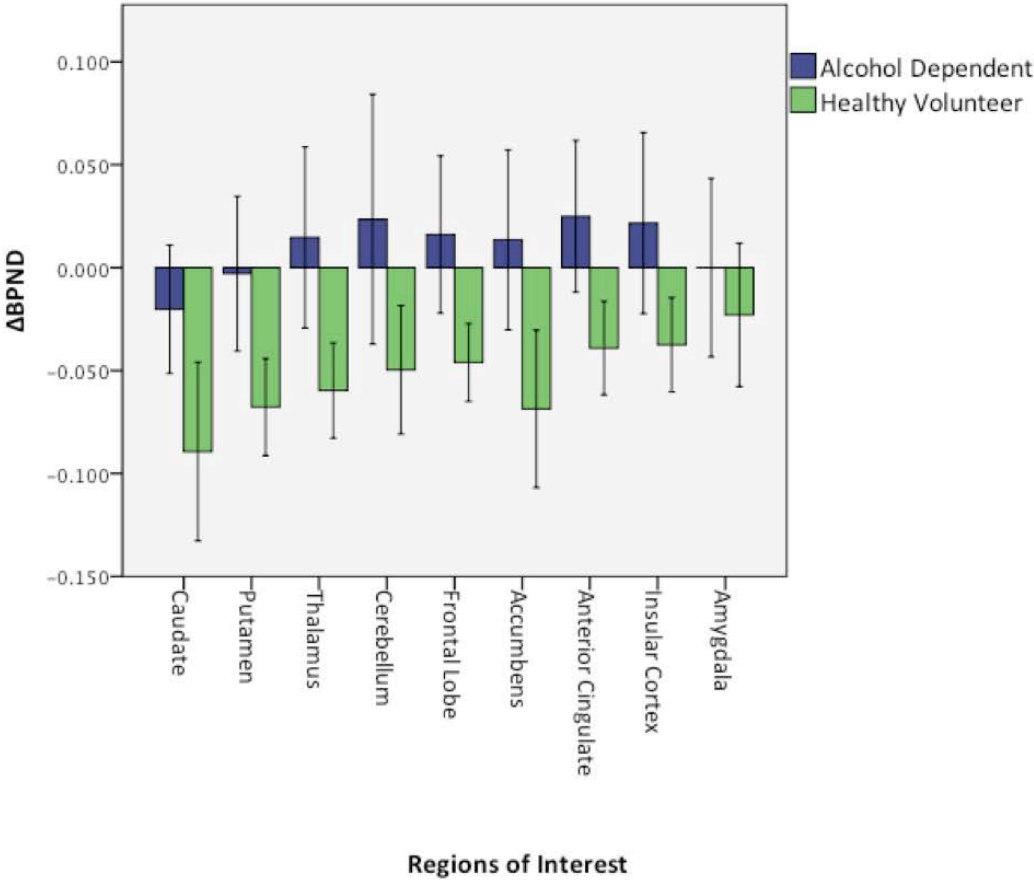
Gender specific changes in metabotropic glutamate receptor type 5 during chronic abstinence in a mouse model of chronic cocaine

Ayon Nandi[1], Hiroto Kuwabara[1], Heather Valentine[1], Mary E. McCaul[2], Dean Wong[1,2,3]

[1]The Johns Hopkins University School of Medicine, Russell H. Morgan Department of Radiology, Nuclear Medicine – PET Center, Baltimore, MD; [2]The Johns Hopkins University School of Medicine, Department of Psychiatry and Behavioral Sciences, Baltimore, MD; [3]The Johns Hopkins University School of Medicine, Solomon H. Snyder Department of Neuroscience, Baltimore, MD.

Introduction: According to the National Survey on Drug Use and Health, over 913,000 people over the age of 12 met the criteria for cocaine use disorder in 2014 [1]. It is also known that females are less affected but may suffer more severe consequences once affected. Since the glutamate system has been implicated in cocaine use and recovery, we attempted to study changes in metabotropic glutamate receptor, type 5 (mGluR5), during two weeks' abstinence in a mouse model of chronic cocaine use, using microPET and a selective mGluR5 ligand, 18F-FPEB.

Methods: A total of ten (10) male and nine (9) female, age-matched C57-BL/6 mice were studied. After a baseline PET scan under isoflurane (2%) anesthesia, daily intraperitoneal injections of cocaine were administered for 7 consecutive days, a regimen which has previously been shown to elicit molecular changes in the glutamate system (Ben-Shahar, 2013). Mice had two additional scans at days 14 and 21 days post cocaine abstinence. In all scans, 60 min of dynamic frames were obtained using the SuperArgus microPET/CT (Sedecal) scanner, starting immediately following an intravenous bolus injection of ~200 uCi of 18F-FPEB. Using locally developed data analysis packages for mouse brain PET studies (Nandi et al., 2013), values of non-displaceable binding potential (BPND) were obtained in template-based regions by cerebellum-reference multivariable reference tissue method (MRTM2; Ichise et al 2003).

Results: At baseline, mGluR5 binding was highest in the entorhinal cortex, followed by striatum, and hippocampus, and lowest in thalamus and hypothalamus. **Male vs. Female:** At baseline, the female mice had significantly higher BPND than the male mice, across all regions ($p < 0.05$). **Baseline vs. post-abstinence scan:** Female mice showed significantly decreased binding at 14 and 21 days across all regions compared to baseline. In contrast, male mice showed significantly decreased binding at 14 days, but not 21 days. (See figure 1)

Conclusions: In contrast to previous studies (Akkus, et al 2013), the results of this study show a sex difference in terms of 18-FPEB binding. The sex differences in the time courses of mGluR5 changes during abstinence in this mouse model of chronic cocaine use, supports the hypothesis that females suffer prolonged elevation of BPND during cocaine abstinence, and agree with several clinical reports of sex differences in the effects of cocaine (Collins, et al, 2007; Evans and Foltin, 2010). Our current data supports the hypothesis that mGluR5 differentially affected males and females with chronic cocaine use and abstinence. Further studies will be required to test if this male/female differences also occur during initial exposure to cocaine vs. abstinence.
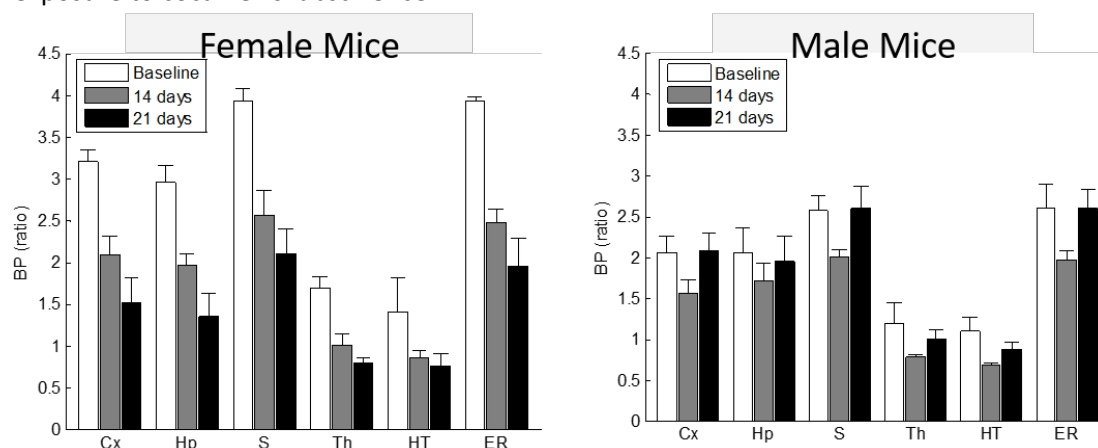
Characterization of ^{18}F-LY2459989 as the First ^{18}F-Labeled Antagonist Radiotracer for PET Imaging of Kappa Opioid Receptor in Non-Human Primates

Songye Li, Zhengxin Cai, Daniel Holden, Jim Ropchan, David Labaree, Shu-fei Lin, Michael Kapinos, Teresa Lara-Jaime and Yiyun Huang

PET Center, Department of Radiology and Biomedical Imaging, Yale University School of Medicine, New Haven, CT, USA

Objectives: The kappa opioid receptor (KOR) is an important target for the investigation of stress-related disorders and for drug development in depression and alcoholism. Availability of KOR specific PET radiotracers will facilitate the investigation of this target *in vivo*. We have previously reported ^{11}C-LY2459989 as an KOR antagonist radiotracer suitable for PET imaging (1). The objective of this study was to synthesize ^{18}F-LY2459989 and characterize its performance as the first ^{18}F-labeled antagonist radiotracer for PET imaging of KOR in non-human primates.

Methods: ^{18}F-LY2459989 was synthesized by ^{18}F-displacement of an aromatic iodonium ylide. PET imaging with ^{18}F-LY2459989 under baseline and blocking conditions were conducted in rhesus monkeys on a Focus-220 scanner to assess the ligand's pharmacokinetics and the strength, specificity and selectivity of its binding *in vivo*. Measurement of arterial blood activity and metabolite analysis were performed for each scan to generate metabolite-corrected arterial plasma activity curve as input function. Regional time-activity curves were analyzed with compartmental models and the multilinear analysis-1 (MA1) method to estimate regional volume of distribution (V_T).

Results: LY2459989 displayed high *in vitro* affinity (K_i = 0.18 nM) and good selectivity for KOR. ^{18}F-LY2459989 was prepared from a recently developed aromatic iodonium ylide precursor (Figure 1) with high radiochemical yield, high radiochemical purity (> 99 %), and excellent specific activity (50.2 ± 29.5 Ci/µmol at end of synthesis, n = 4). In evaluation in rhesus monkeys ^{18}F-LY2459989 was found to have moderate metabolism rate, with ~26% of parent tracer in plasma at 30 min post-injection. Fast and reversible kinetics was observed in the monkey brain, with radioactivity uptake peaking at <20 min after tracer injection in all regions. Pre-treatment of the animal with the selective KOR antagonist LY2456302 (0.1 mg/kg, iv)) reduced uptake levels in high binding regions to that in the cerebellum, thus demonstrating the binding specificity and selectivity of ^{18}F-LY2459989 for KOR *in vivo*. Regional time activity curves were well fitted by the MA1 model with a fitting start time (t^*) of 30 min to obtain reliable estimates of regional distribution volume (V_T). Regional binding potential (BP_{ND}) was calculated using cerebellum as the reference region, with values of 1.56 ± 0.17, 1.14 ± 0.19, 1.08 ± 0.10, 0.96 ± 0.05, 0.71 ± 0.02, 0.53 ± 0.07 and 0.47 ± 0.17 (n = 3), respectively, for the cingulate cortex, insula, caudate, putamen, frontal cortex, temporal cortex and thalamus. These regional BP_{ND} values were similar to those of ^{11}C-LY2459989 (1).

Conclusions: ^{18}F-LY2459989 is synthesized in good radiochemical yield, high radiochemical purity and high specific activity. In rhesus monkeys it demonstrated many attractive characteristics as a PET imaging tracer: fast tissue kinetics, KOR binding specificity and selectivity, amenability to kinetic analysis with reliable measures of kinetic parameters, and high levels of specific binding signals. Taken together, ^{18}F-LY2459989 is an excellent radiotracer for PET imaging and quantification of KOR *in vivo*. Advancement of this radiotracer to evaluation in humans is warranted.

References:
1. Zheng MQ, Kim SJ, Holden D et al. *J Nucl Med.* 2014; 55:1185-1191.
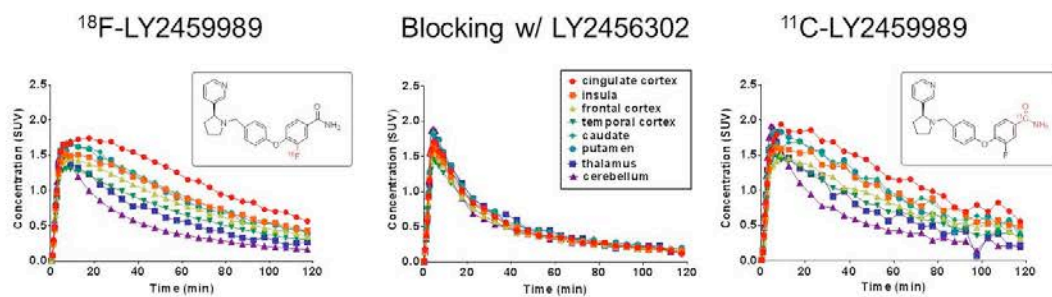
Figure 1. Time-activity curves from a ^{18}F-LY2459989 baseline scan (left), a blocking scan (middle) with pretreatment of the monkey with 0.1 mg/kg of LY2456302, and from a corresponding baseline scan of ^{11}C-LY2459989 (right). Structures and radiolabeling positions of ^{18}F-LY2459989 and ^{11}C-LY2459989 are also shown.

P-116

Test-retest of [11C]SCH23390 binding in the brain of healthy volunteers using PET. Comparing manual and automated definition of anatomical Regions of Interests.

Per Stenkrona M.D., Granville J. Matheson, MSc, Simon Cervenka, MD, PhD, Pontus Plavén Sigray, MSc, Christer Halldin, PhD, Lars Farde, MD, PhD

Department of Clinical Neuroscience, Center for Psychiatric Research, Karolinska Institutet, S-171 76 Stockholm, Sweden

BACKGROUND: The methods of analyzing Positron Emission Tomography (PET) data have developed considerably in recent years. In particular, the delineation of regions of interest (ROIs) has evolved from manual methods using crude templates to automated methods using anatomical information. The different ROI definition methods have trade-offs with regard to validity and reliability of the outcome measures such as the non-displaceable binding potential (BP_{ND}). Particularly in populations with structural brain changes and in repeated studies, the chosen methodology may impact effect sizes and statistical power. Previous cross-validation of manual and automated ROI methods have been found to be in good agreement [1], however, to our knowledge different methods of ROI definitions have not been compared with regard to test-retest reliability.

In this study we compared the test-retest reliability of BP_{ND} derived from manual and automated ROI definitions. Fifteen healthy volunteers were examined twice with the D_1 dopamine radioligand [11C]SCH23390. This radioligand has been widely used since the 1980s on patient populations, in experimental studies and for drug development [2-4]. The test-retest reliability of [11C]SCH23390 has previously been evaluated in a limited sample [5]. Here we reexamined the reproducibility of [11C]SCH23390 binding in a larger sample and using both manual and automated methodology for ROI definition.

Methods: Each of 15 healthy male subjects was examined twice, in the morning and afternoon respectively. After injection of [11C]SCH23390 (300 MBq, <1 µg) the PET-system ECAT EXACT HR was used for data acquisition in sequential time frames during 51 minutes and reconstruction to a 4-D data set. The time frames were corrected for head motion using a post-reconstruction frame-to-frame realignment algorithm. Each subject had their T1-weighted MR image re-oriented to AC-PC orientation using SPM5 software and coregistered to the PET image. Two sets of ROIs was generate: manually using the human brain atlas software [6], and automatically by FreeSurfer (www.surfer.nmr.mgh.harvard.edu, version 5.0) [7].   For both methods, ROIs were applied to each image frame (using the SPM coregistration matrix) to generate regional TACs. The BP_{ND} for each ROI was derived using the simplified reference tissue model [8]. For each regional BP_{ND} the absolute percentage variability and Intraclass correlation coefficient (ICC) were calculated.

Results: Reproducibility, as measured by absolute percentage differences of BP_{ND}, did not differ significantly between the manual and the FreeSurfer derived ROIs. The regional ICC values were also similar for most regions. The BP_{ND} did not differ significantly between the morning and afternoon in any of the regions. The absolute values of BP_{ND} were significantly higher for the manually generated ROIs compared to FreeSurfer generated ROIs in all regions (p<0.005).

Conclusions: The reproducibility of BP_{ND} values was similar for both the manual and automated methods of ROI delineation.   The results are in agreement with previous results on [11C]SCH23390 binding generated by less advanced image analysis procedures [5]. The observation that higher BP_{ND} values were obtained using the manually generated ROIs suggests that the choice of method for ROI definition in PET studies may be based on issues of validity rather than reliability.

References:

1.   Schain, M., et al., Evaluation of two automated methods for PET region of interest analysis. Neuroinformatics, 2014. **12**(4): p. 551-62.

2.   Farde, L., et al., PET analysis of human dopamine receptor subtypes using 11C-SCH 23390 and 11C-raclopride. Psychopharmacology, 1987. **92**(3): p. 278-84.

3.   Suhara, T., et al., Age-related changes in human D1 dopamine receptors measured by positron emission tomography. Psychopharmacology, 1991. **103**(1): p. 41-5.

4.   Karlsson, P., et al., PET study of D(1) dopamine receptor binding in neuroleptic-naive patients with schizophrenia. Am J Psychiatry, 2002. **159**(5): p. 761-7.

5.   Hirvonen, J., et al., Measurement of cortical dopamine d1 receptor binding with 11C[SCH23390]: a test-retest analysis. J Cereb Blood Flow Metab, 2001. **21**(10): p. 1146-50.

6.   Roland, P.E., et al., Human Brain Atlas: For High-Resolution Functionel and Anatomical Mapping. Human Brain Mapping, 1994. **1**: p. 173-184.

7.   Fischl, B., et al., Whole brain segmentation: automated labeling of neuroanatomical structures in the human brain. Neuron, 2002. **33**(3): p. 341-55.

8.   Lammertsma, A.A. and S.P. Hume, Simplified reference tissue model for PET receptor studies. NeuroImage, 1996. **4**(3): p. 153-158.

Region	Method	BP_{ND} mean AM-PM Mean ± SD	Absolute diff AM-PM (%) Mean ± SD	ICC
Caudate	Manual	1.62 ±0.21	7.74 ±4.24	0,88
	FreeSurfer	1.35 ±0.24	8.23 ±4.56	0,88
Putamen	Manual	1.78 ±0.11	4.19 ±3.00	0,74
	FreeSurfer	1.58 ±0.14	4.23 ±2.81	0,84
Accumbens	Manual	1.39 ±0.14	5.98 ±4.34	0,76
	FreeSurfer	1.30 ±0.13	9.65 ±9.14	0,52
Dorsolateral prefrontal cortex	Manual	0.28 ±0.04	14.43 ±9.16	0,55
	FreeSurfer	0.26 ±0.05	13.71 ±10.00	0,70
Insula	Manual	0.53 ±0.04	9.11 ±8.05	0,28
	FreeSurfer	0.51 ±0.04	9.65 ±8.13	0,33

Glial activation assessed with [11C]PBR28 co-localizes with brain structural abnormalities in amyotrophic lateral sclerosis

*Mohamad J. Alshikho[a,b] , *Nicole R. Zürcher[a] , Marco L. Loggia[a] ,   Paul Cernasov [b] , Daniel B. Chonde[a] , David Izquierdo-Garcia[a] , Julia E. Yasek[b] , Oluwaseun Akeju[c] , Ciprian Catana[a] , Bruce R. Rosen[a] , Merit E. Cudkowicz[b] , Jacob M. Hooker[a] , Nazem Atassi[b]

[a] A. A. Martinos Center for Biomedical Imaging, Department of Radiology, Massachusetts General Hospital, Harvard Medical School, Charlestown, MA, USA; [b] Neurological Clinical Research Institute (NCRI), Department of Neurology, Massachusetts General Hospital, Harvard Medical School, Boston, MA, USA; [c] Department of Anesthesiology, Massachusetts General Hospital, Harvard Medical School, Boston, MA, USA
*Contributed equally

Introduction: Amyotrophic lateral sclerosis (ALS) is a severe neurodegenerative disease in which upper and lower motor neurons degenerate, resulting in progressive muscle weakness, respiratory failure and death often within 2–5 years [1]. The pathophysiology of ALS is poorly understood, but the immune system has increasingly been implicated. We have recently provided *in vivo* evidence for glial activation in the motor cortices and the corticospinal tract in individuals with ALS using [11C]-PBR28 PET [2]. Here, we aim to investigate the relationship between brain glial activation and brain structural abnormalities in the same ALS patients.

Methods: Ten ALS patients (7 males) and 10 healthy controls (CTRL) (6 males) matched for age (ALS: 53.2 years ± 10.75 (mean ± SD), CTRL: (51.1 years ± 11.01)) and binding affinity (4 mixed, 6 high affinity binders) underwent simultaneous magnetic resonance (MR) and positron emission tomography (PET) imaging on a 3 Tesla Siemens Tim Trio with an integrated PET camera. [11C]-PBR28 was injected as a slow intravenous bolus, with a mean administered dose of 430 MBq ± 34 for ALS and 424 MBq ± 42 for CTRL. T1 weighted multi-echo magnetization prepared rapid acquisition gradient echo (MEMPRAGE) and diffusion tensor imaging scans were acquired simultaneously with [11C]-PBR28 PET. Standardized uptake values (SUV) were calculated from 60-90 minutes post radiotracer injection and normalized to whole brain mean (SUVR). Fractional anisotropy (FA) was assessed using tract-based spatial statistics (TBSS) and a region of interest (ROI) approach. Surface-based cortical thickness was determined using FreeSurfer. Spearman correlation was carried out to study the relationship between [11C]-PBR28 SUVR, FA, cortical thickness and upper motor neuron burden scores.

Results: [11C]-PBR28 binding was increased in the motor cortex and corticospinal tract in ALS compared to CTRL, with a greater increase in the left hemisphere. TBSS and ROI analyses revealed significantly decreased FA in the corticospinal tract ($P_{FWE} < 0.05$) and in the left primary motor cortex in ALS ($P < 0.05$). Surface based morphometric analysis revealed cortical thinning, particularly in the left primary motor cortex ($P_{corr} < 0.05$) in ALS. Overall, in ALS patients the regions that showed increased [11C]-PBR28 SUVR compared to CTRL also exhibited decreased FA (see Figure) and cortical thinning compared to CTRL. Specifically, [11C]-PBR28 binding in the left motor cortex was negatively correlated with FA (r=-0.68, P<0.05) and cortical thickness (r=-0.75, P<0.05).   Disease severity assessed using the upper motor neuron burden scale correlated positively with [11C]-PBR28 SUVR (r=+0.75, P<0.05) and negatively with both FA (r=-0.77, P<0.05) and cortical thickness (r=-0.75, P<0.05) in the primary motor cortex, reflecting that with increased disease severity [11C]-PBR28 binding increases while FA values and cortical thickness decrease.

Conclusion: Our findings show that glial activation (neuroinflammation) co-localizes with white matter changes in the corticospinal tract and cortical thinning in the motor cortex in the same patients. These findings provide a unique *in vivo* link between mechanisms involved in ALS, namely inflammation, cortical thinning and alterations in tissue integrity in the same set of individuals.

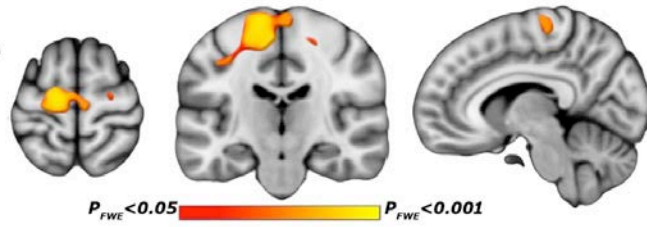**References:**
[1] Ferraiuolo et al. Nature Reviews Neurology 2011.   [2] Zurcher et al. NeuroImage Clinical 2015

[^{11}C]PBR28 SUVR$_{60\text{-}90min}$ in ALS

0.2   1.7

L
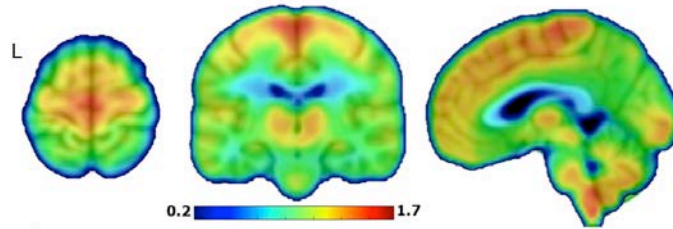
Increased [^{11}C]PBR28 SUVR$_{60\text{-}90min}$ in ALS vs. CTRL

$P_{FWE} < 0.05$ $P_{FWE} < 0.001$

Decreased fractional anisotropy in ALS vs. CTRL

$P_{FWE} < 0.05$ $P_{FWE} < 0.001$
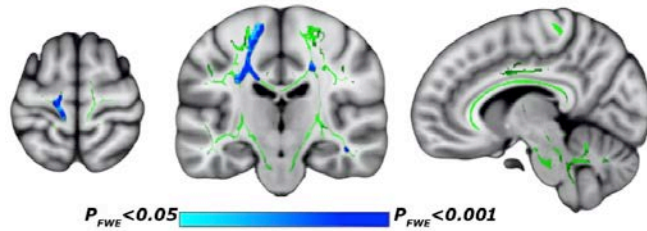
Brain glial activation in fibromyalgia: a [11C]PBR28 pilot study

Daniel S. Albrecht[1], Ekaterina Protsenko[1], Yvonne Lee[2], Robert R. Edwards[3,4], Ciprian Catana[1], Oluwaseun Akeju[5], George Cohen[6,7], Jacob M. Hooker[1], Vitaly Napadow[1,3,8], Marco L. Loggia[1,3]

[1] MGH/MIT/HMS Athinoula A. Martinos Center for Biomedical Imaging, MGH, Harvard Medical School, Charlestown, MA 02129, USA; [2] Division of Rheumatology, Immunology and Allergy, Brigham and Women's Hospital, Boston, MA; [3] Department of Anesthesiology, Perioperative and Pain Medicine, BWH, Harvard Medical School,Boston, MA 02155, USA; [4] Department of Psychiatry, BWH, HMS, Boston, MA 02155, USA; [5] Department of Anesthesia, Critical Care and Pain Medicine, MGH/HMS, Boston, MA 02114, USA; [6] Department of Rheumatology, Allergy, and Immunology, MGH, Boston, MA; [7] Department of Medicine, MGH, Boston, MA; [8] Department of Biomedical Engineering, Kyung Hee University, Seoul 130-872, Republic of Korea

Introduction: Fibromyalgia (FM) is a debilitating disorder, characterized by chronic pain, fatigue and other symptoms. While FM pathophysiology is poorly understood, the central nervous system (CNS) has been strongly implicated, with putative evidence of pathological neuroinflammation. FM patients exhibit increased CSF concentrations of pro-inflammatory cytokines produced in the brain by microglia and astrocytes[1-3]. Furthermore, FM benefits from treatments thought to inhibit glial activation – e.g., low-dose naltrexone[4,5]. Additionally, novel evidence from our laboratory suggests that CNS glial activation might play an important role in the pathophysiology of human chronic pain disorders[6], as predicted by the animal literature[7,8]. To investigate the hypothesis that FM is associated with brain glial activation, we conducted a study using integrated Positron Emission Tomography / Magnetic Resonance (PET/MR) imaging and the recently developed radioligand [11C]PBR28. This ligand binds to the 18 kDa translocator protein (TSPO), which is a marker of glial activation.

Methods: Nine FM patients (8F; 51.0 ± 10 y/o) and 9 healthy controls (4F; 51.4 ± 12 y/o) received 90 minute [11C]PBR28 scans. 60-90 minute standardized uptake value (SUV) images were reconstructed for each subject, and normalized by whole-brain signal to create SUV ratio (SUVR) maps. SUVR maps were compared across groups, and their associations with FM symptoms (e.g. pain, depression) performed using voxelwise t-tests and linear regressions, respectively. The resulting statistical maps were cluster corrected for multiple comparisons using a cluster-forming voxel-wise threshold of $z > 2.3$, and a (corrected) cluster significance threshold of $p < 0.05$. In addition, within regions exhibiting significant group differences, exploratory regression analyses were performed at the more liberal threshold of $z = 3.1$, uncorrected. Finally, in order to investigate whether FM patients demonstrate elevated thalamic [11C]PBR28 binding (as we had observed in chronic low back pain patients[6]), an ROI analysis was performed to compare thalamic SUVRs between FM and controls.

Results: In FM patients, SUVR was higher than controls in bilateral cerebellar cortex and medulla ($p < 0.05$, corrected). There were no regions where SUVR was higher in controls than in FM patients. Within FM patients, pain (measured by the revised Fibromyalgia Impact Questionnaire [FIQR]) was positively correlated with SUVR in the right posterolateral cerebellum. ROI analyses revealed that FM patients did not have elevated thalamic SUVR compared to controls ($p = 0.26$).

Conclusions: The current data are in line with previous evidence of elevated glial activation in chronic pain patients. As opposed to chronic low back pain, however, in FM we observed elevation of the glial marker TSPO in the medulla and cerebellum, raising the possibility that different glial signatures might be identified for different pain disorders. The cerebellum has been associated with FM pain catastrophizing[9], and altered cerebellar gray and white matter morphometry in FM patients has been associated with FM symptoms[10]. If confirmed on a larger sample size, our data support the involvement of glial activation in the pathophysiology of FM.

References: 1. Ehrlich, L. C. *et al.Journal of immunology* **160**, 1944-1948, (1998); 2. Lu, Y. *et al.PLoS One* **9**, e108318, (2014); 3. Wallace, D. J. *et al.Rheumatology (Oxford)* **40**, 743-749, (2001); 4. Mattioli, T. A. *et al.Mol Pain* **6**, 22, (2010); 5. Younger, J. *et al.Pain medicine* **10**, 663-672, (2009); 6. Loggia, M. L. *et al.Brain*, (2015); 7. Okada-Ogawa, A. *et al.J Neurosci* **29**, 11161-11171, (2009); 8. Zhao, P. *et al.J Neurosci* **27**, 8893-8902, (2007); 9. Morris, L. D. *et al.Journal of physical therapy science* **27**, 3461-3467, (2015); 10. Kim, H. *et al.NeuroImage. Clinical* **7**, 667-677, (2015).

Quantification of reward associated dopamine release through late adolescence from simultaneous PET-MR imaging

Calabro FJ[1], Minhas D[2], Larson BL[1], Murty VP[1], Becker C[2], Laymon CM[2], Price JC[2], Luna B[1]

Departments of [1]Psychiatry, [2]Radiology, University of Pittsburgh, Pittsburgh, PA, USA

Objectives: Adolescence is characterized by increased risk taking and reward-driven behaviors, which has been hypothesized to reflect increases in striatal dopamine transmission. However, direct *in vivo* evidence for this in humans has been elusive. To address this, we collected simultaneous [11C]raclopride PET and fMRI data from a cohort of subjects from late adolescence through early adulthood while they performed a reward learning task.

Methods: Task-related changes in [11C]raclopride (RAC) binding and striatal BOLD activation were assessed in 19 subjects (4 female:15 male, 24.5±3.0 years, range 18-30). Subjects performed a reward learning task in which they explored a map containing locations of varying reward probabilities. On each trial, subjects selected a new map location and received a high reward, low reward, or no reward. Subjects were instructed to determine map locations corresponding to high and low probabilities of reward in order to maximize their earnings. The RAC was administered using a bolus+infusion (B+I) paradigm [1]. MRI and PET data were collected over 90 min on a Siemens Biograph mMR PET/MRI scanner. The PET attenuation correction was performed using a combined segmentation- and atlas-based approach [2], and the RAC data were reconstructed using filtered back projection (30x3-min time frames). The fMRI task paradigm was conducted for 30 min and began 41.5±3.1 min after initiation of the B+I RAC injection. Regional RAC tissue ratios were computed over pre-task (~25-40 min) and task (~40-80 min) time intervals. Late-time (~60-80 min) cerebellum was used as reference for both pre-task and task tissue ratios.

Results: fMRI data showed significant reward-related activation across the striatum, including nucleus accumbens (NAcc), caudate, and putamen, as well as in the ventral tegmental area and substantia nigra. Task-related changes in [11C]raclopride tissue concentration were identified in NAcc (3.25±0.34 pre-task; 2.98±0.29 task), caudate (3.85±0.32 pre-task; 3.55±0.31 task), and putamen (4.43±0.36 pre-task; 4.18±0.31 task). Greater percent change of [11C]raclopride was significantly predictive of better reward learning (Pearson correlation between %RAC decrease and performance) in NAcc ($r=-0.64$, $p=0.005$), caudate ($r=-0.48$, $p=0.04$) and putamen ($r=-0.46$, $p=0.05$) (Figure 1). Overall, this produced a significant relationship between striatal %RAC decrease and performance (GLM, $F(1,48)=18.9$, $p<0.001$), but no interaction between %RAC decrease and region ($F(2,48)=0.02$, $p>0.9$), suggesting the effect was similar across striatal regions. Further, task-related RAC changes computed across the striatum showed a significant relationship with age (Pearson correlation between %RAC decrease and inverse age, $r=-0.61$, $p=0.006$), although we found no significant relationship between pre-task tissue ratios and age within our sample.

Conclusions: Our data suggest that task-induced dopamine transmission across the striatum facilitates reward learning, complementing rodent and primate literature which shows a causal role for striatal dopamine in reward learning [3,4]. This initial finding and that of age-related differences in the RAC reward response require further validation with regard to the quantification of baseline and task RAC specific binding within a single scan, particularly in small regions such as the NAcc that are vulnerable to PET partial volume effects. Overall, this study further highlights the promise of simultaneous PET/MR imaging for multi-modal functional assessments.

References:
[1] Martinez, D. et al. Imaging human mesolimbic dopamine transmission with positron emission tomography. Part II: amphetamine-induced dopamine release in the functional subdivisions of the striatum. J. Cereb. Blood Flow Metab. Off. J. Int. Soc. Cereb. Blood Flow Metab. 23, 285–300 (2003).
[2] Izquierdo-Garcia D, Hansen AE, Förster S, Benoit D, Schachoff S, Fürst S, Chen KT, Chonde DB, Catana C. An SPM8-based approach for attenuation correction combining segmentation and nonrigid template formation: application to simultaneous PET/MR brain imaging. J Nucl Med. 2014 Nov;55(11):1825-30. doi: 10.2967/jnumed.113.136341. Epub 2014 Oct 2.
[3] Schultz W. 2016. "Dopamine Reward Prediction-Error Signalling: A Two-Component Response." Nature Reviews. Neuroscience, February. doi:10.1038/nrn.2015.26.

[4] Schultz W, Carelli RM, and Wightman RM. 2015. "Phasic Dopamine Signals: From Subjective Reward Value to Formal Economic Utility." Current Opinion in Behavioral Sciences 5: 147–54.
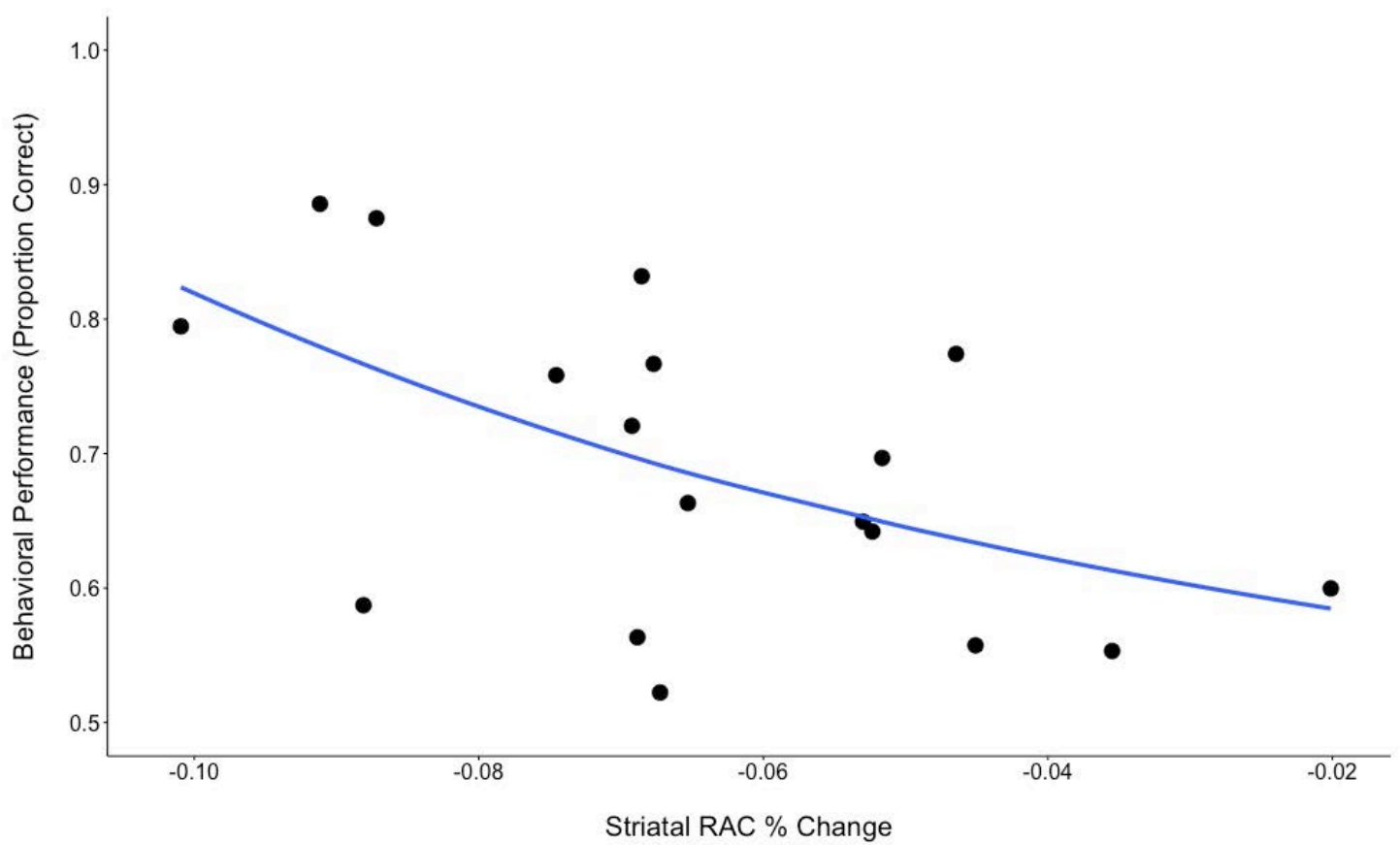
Translational Evaluation of the Corpus Callosum as a Reference Region for [18F]Flubatine

Shivani Bhatt[1,2], Ansel T. Hillmer[2,3], Jean-Dominique Gallezot[2], Osama Sabri[4], Irina Esterlis[2,3,5], Richard E. Carson[2,3], Nabeel Nabulsi[2], Yiyun Huang[2], Kelly P. Cosgrove[1,2,3,5]

[1]Department of Neuroscience, Interdepartmental Neuroscience Program, Yale University School of Medicine, New Haven, CT; [2]Yale PET Center, Yale University School of Medicine, New Haven, CT; [3]Department of Radiology and Biomedical Imaging, Yale University School of Medicine, New Haven; [4]Department of Nuclear Medicine, University of Leipzig, Leipzig, Germany; [5]Department of Psychiatry, Yale University School of Medicine, New Haven, CT

Introduction: In vivo imaging of α4β2-containing nicotinic acetylcholine receptors (α4β2-nAChRs) with PET has important clinical applications for studying addiction and other neuropsychiatric disorders. (-)-[18F]Flubatine is an effective PET tracer for *in vivo* imaging of α4β2-nAChRs in non-human primates[1] and was shown to have fast kinetics in humans[2]. To date however, most brain PET studies of α4β2-nAChRs have required arterial sampling as there are no known gray matter reference regions. The goal of this study was to evaluate whether the corpus callosum, a white matter region previously found to have low distribution volume (V_T) for (-)-[18F]Flubatine and likely low α4β2-nAChR density, may be suitable as a reference region for analysis of PET data.

Methods: Two rhesus monkeys and one 27-year-old female tobacco smoker were imaged with (-)-[18F]Flubatine PET. PET data were acquired with a Focus 220 camera for animals and with a High-Resolution Research Tomograph for the tobacco smoker. In a previous study, each animal underwent two baseline scans and one nicotine-blocking scan in which nicotine was administered (5 min of 0.08 mg/kg plus 2 hours of 0.18 mg/kg nicotine) starting 5 minutes before the bolus injection of 36.7 ± 0.9 MBq (-)-[18F]Flubatine[1]. The tobacco smoker abstained from smoking for 5 days and was imaged with 244 MBq (-)-[18F]Flubatine administered as bolus plus constant infusion with a K_{bol} = 360 minutes. The tobacco smoker smoked a cigarette after 125 minutes into the scan, taking 1 puff every 30 seconds for 5 minutes. The ROI for the corpus callosum was drawn on consecutive sagittal slices of rhesus monkey and human MRI templates (Figure 1A). In animals, distribution volumes (V_T) and free-fraction corrected distribution volume (V_T/f_p) were estimated from MA1 modeling analysis (t*= 45 min). Drug occupancy (O_{Drug}) and non-displaceable binding (V_{ND}) were estimated from occupancy plots[3]. In the tobacco smoker, V_T and V_T/f_p were estimated by (C_{PET}/C_{Plasma})/f_P at equilibrium (90-120 min) and after the cigarette (150-210 min). Displacement was measured by comparing both V_T and V_T/f_p before and after cigarette smoking.

Results: Our preliminary results in animals showed a baseline V_T of 9.56 mL/cm³ and V_T/f_P of 10.89 mL/cm³ in corpus callosum. In the previous study, a V_{ND} of 6.15 mL/cm³ and V_{ND}/f_P of 6.91 mL/cm³ were estimated from drug occupancy plots (r^2=0.992)[1], which were approximately 35.7% and 36.5% lower, respectively, than the V_T findings in corpus callosum. In the tobacco smoker, smoking a cigarette reduced baseline V_T and V_T/f_P values in corpus callosum by 28.6% from 7.95 mL/cm³ and 9.13 mL/cm³ to 5.68 mL/cm³ and 6.52 mL/cm³, respectively, while V_T was reduced by 46.3% in cerebellum, 53.7% in thalamus, and 24.3% in frontal cortex (Figure 1B).

Conclusion: These preliminary findings suggest there is displaceable binding of (-)-[18F]Flubatine in the corpus callosum of rhesus monkeys and human smokers and that the corpus callosum may not be a valid reference region for (-)-[18F]Flubatine PET for smokers. Further studies are ongoing.

References:

Bois, F., Gallezot, J. D., Zheng, M. Q., Lin, S. F., Esterlis, I., Cosgrove, K. P., Carson R. E. Huang, Y. (2015). Evaluation of [18F]-(-)-norchlorofluorohomoepibatidine ([18F]-(-)-NCFHEB) as a PET radioligand to image the nicotinic acetylcholine receptors in non-human primates. *Nucl Med Biol, 42*(6), 570-577.

Sabri, O., Becker, G. A., Meyer, P. M., Hesse, S., Wilke, S., Graef, S., Patt M., Luthardt J., Wagenknecht G., Hoepping A., Smits R., Franke A., Sattler B., Habermann B., Neuhaus P., Fischer S., Tiepolt S., Deuther-Conrad W., Barthel H., Schönknecht P., Brust, P.

(2015). First-in-human PET quantification study of cerebral alpha4beta2* nicotinic acetylcholine receptors using the novel specific radioligand (-)-[^{18}F]Flubatine. *Neuroimage, 118*, 199-208.

Cunningham, V. J., Rabiner, E. A., Slifstein, M., Laruelle, M., & Gunn, R. N. (2010). Measuring drug occupancy in the absence of a reference region: the Lassen plot re-visited. *J Cereb Blood Flow Metab, 30*(1), 46-50.

Figure 1
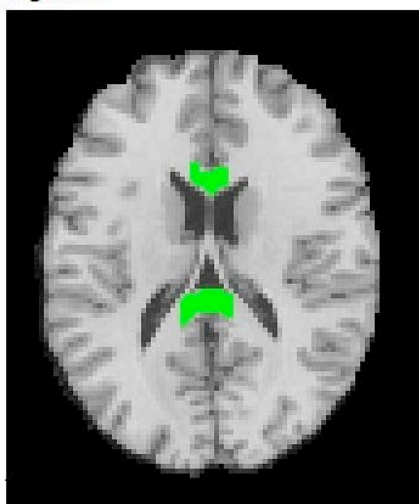
A. ROI of Corpus Callosum

Corpus callosum indicated in green shown overlaid in transverse orientation on human MRI template.
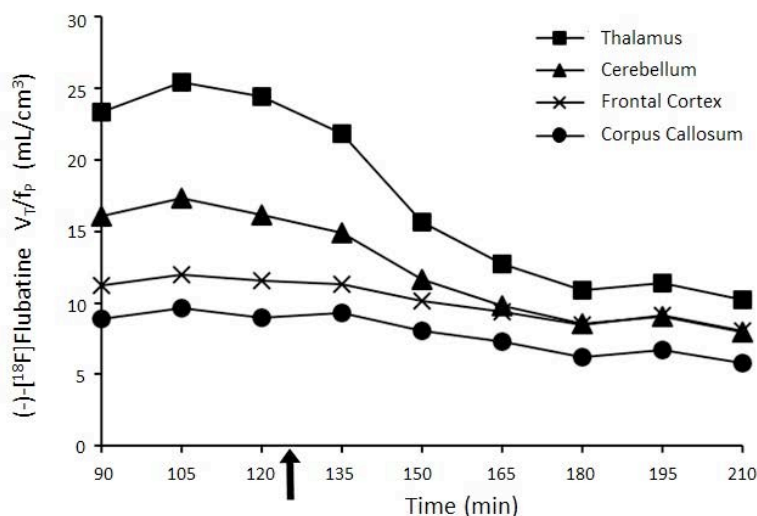
B. Distribution Volumes of (-)-[^{18}F]Flubatine across ROIs

V_T/f_P for thalamus, cerebellum, frontal cortex, and corpus callosum as obtained from equilibrium analysis of time activity curves in each region of interest. Arrow indicates start of cigarette smoking at 125 min.

Differences in Kappa Opioid Receptor Drug Occupancy Measured with PET, a Comparison of [11C]GR103545 and [11C]LY2459989

Michael S. Placzek[†‡], Jacob M. Hooker[‡]

[†]*Department of Psychiatry McLean Imaging Center, McLean Hospital, Harvard Medical School, Belmont, MA, US;*
[‡]*Department of Radiology, Athinoula A. Martinos Center for Biomedical Imaging, Massachusetts General Hospital, Harvard Medical School, Charlestown, MA, US.*

Introduction: Differences in side effect profiles of opioid receptor targeting drugs has been linked to activation of specific intracellular signaling pathways following agonist binding [1-2]. In addition, *in silico* studies have revealed opioid receptors (OR) undergo unique conformation changes upon ligand binding, with different opioids inducing different conformation states of the receptor [3-4]. In an effort to study this phenomenon *in vivo*, we investigated OR binding changes with PET in rodents. We conducted pharmacological PET experiments of kappa opioid receptors (KOR) in the rat brain to determine differences, if any, of radioligand sensitivity towards drug challenge with structurally and pharmacologically unrelated KOR drugs. We chose to study the kappa opioid receptor due to the availability of two pharmacologically different classes of KOR radiotracers, the KOR agonist [11C]GR103545 and the KOR antagonist [11C]LY2459989. Comparing binding changes of these two radiotracers following drug challenge will aid in the understanding of opioid receptor-ligand dynamics *in vivo*, which may benefit future opioid occupancy PET experiments, and help understand opioid neuropharmacology.

Methods: Male Sprague-Dawley rats were anesthetized with isoflurane and treated with the KOR agonist salvinorin A (0.01 – 10 mg/kg, i.v.) or KOR antagonists (10 mg/kg nor-BNI or 2mg/kg naltrexone). Following drug administration, either the kappa opioid agonist radiotracer [11C]GR103545 or antagonist radiotracer [11C]LY2459989 was administered as a bolus (i.v.) and animals underwent a 60 minute dynamic PET brain scan. Images were co-registered to a rat brain atlas and regional binding potential values (BP_{ND}) were calculated using the Logan reference analysis method with the cerebellum as a reference region.

Results: Comparing baseline PET scans of agonist [11C]GR103545 to the antagonist [11C]LY2459989 revealed a similar regional uptake in the rodent brain, consistent with previously reported KOR distribution in the rat brain. Blocking experiments with KOR antagonist drugs (10 mg/kg nor-BNI or 2 mg/kg naltrexone) indicated both radiotracers were sensitive to this pharmacological challenge, resulting in comparable drug occupancy at KORs (nor-BNI, 50 % & 44 %; naltrexone, 86 % & 95 % occupancy). Pharmacological PET studies with the KOR agonist salvinorin A resulted in conflicting occupancy determinations when measured with either agonist radiotracer [11C]GR103545 or antagonist radiotracer [11C]LY2459989. While we observed a dose response relationship between increasing doses of salvinorin A with decreases in [11C]GR103545 BP_{ND}, a dose response relationship was not observed with salvinorin A and [11C]LY2459989 BP_{ND}. Salvinorin A failed to decrease [11C]LY2459989 BP_{ND}, at 0.6 mg/kg (~50% occupancy at KOR when measured with [11C]GR103545) and 10 mg/kg (10x the dose required for ~ 90% occupancy with [11C]GR103545).

Conclusions: We have observed differences in KOR drug occupancy from the KOR agonist salvinorin A when measured with the agonist KOR radiotracer [11C]GR103545 or the antagonist KOR radiotracer [11C]LY2459989. We have expanded our pharmacological PET experiments to include a number of KOR agonists and antagonists to further characterize the sensitivity of these two radiotracers. In addition, we are conducting *in vitro* competition experiments to clarify the differences observed in the pharmacological PET experiments.

References:
[1] Zhou, L. and Bohn, L.M., 2014. Functional selectivity of GPCR signaling in animals. Current opinion in cell biology, 27, pp.102-108.
[2] White, K.L., et al., 2015. The G Protein–Biased κ-Opioid Receptor Agonist RB-64 Is Analgesic with a Unique Spectrum of Activities In Vivo. Journal of Pharmacology and Experimental Therapeutics, 352(1), pp.98-109. [3] O'Connor, C., et al., 2015. NMR structure and dynamics of the agonist dynorphin peptide bound to the human kappa opioid receptor. Proceedings of the National Academy of Sciences, 112(38), pp.11852-11857. [4] Yuan, S., et al., 2015. The Mechanism of Ligand-Induced Activation or Inhibition of μ-and κ-Opioid Receptors. Angewandte Chemie International Edition, 54(26), pp.7560-7563.

First human PET/MRI study with sigma-1 receptor highly selective radioligand [18F]FTC-146

Bin Shen[1]; Trine Hjørnevik[1,2]; Jun Hyung Park[1]; Deepak Behera[1]; Peter Cipriano[1]; Dawn Holly[1]; Harsh Gandhi[1]; Daehyun Yoon[1]; Praveen K Gulaka[1]; Christopher R. McCurdy[3]; Sandip Biswal[1]; Frederick T. Chin[1]

[1] Department of Radiology, Stanford University, Stanford, CA 94305, USA; [2] The Intervention Centre, Oslo University Hospital & Norwegian Medical Cyclotron Centre, Oslo, Norway; [3] Department of BioMolecular Sciences, School of Pharmacy, The University of Mississippi, University, MS, 38677, USA

Objective: Sigma-1 receptors (S1Rs) have been implicated to play an important role in many known neurological disorders. Simultaneous PET/MR imaging with S1R radioligands may provide valuable information towards diagnosis and treatment guidance of these diseases. Our previously reported S1R radioligand ([18F]FTC-146) [1-3] demonstrated high affinity for S1R (K_i = 0.0025 nM) and excellent selectivity for S1R over S2R (K_i = 364 nM) across several species (from mouse to non-human primate). Herein, we are reporting the first experience with human subject PET/MR imaging with this radioligand.

Methods: Quality control criteria for [18F]FTC-146 were set and the tests were performed according to USP 823. Two healthy volunteers underwent a serial whole body examination involving time-of-flight (TOF) based PET/MR scans (Signa PET/MR, GE Healthcare, WI) acquired at 0, 30, 60, and 120 minutes after the tracer injection. We acquired at least six bed positions, covering from head to middle of thigh, with 2 min PET acquisition per bed and simultaneous anatomical MRI scans (T1 and T2-weighted images). The PET data was reconstructed using a fully 3D TOF iterative ordered subsets expectation maximization (OSEM) algorithm (28 subsets, 2 iterations, temporal resolution = 400 ps) and analyzed with PMOD 3.7. 1 mL blood samples were obtained specifically at 1, 3, 5, 10, 30, 60, 90 and 120 minutes post-tracer administration. At each time point, 0.5 mL blood sample was counted for radioactivity using a gamma counter; the remaining 0.5 mL blood sample was extracted with acetonitrile and analyzed by radio-HPLC.

Results: Figure panels **a-e** show the distribution of [18F]FTC-146 at 30 min after intravenous tracer administration in human brain and whole body. [18F]FTC-146 rapidly crosses the blood brain barrier and accumulates in S1R-rich areas such as thalamus; hippocampus; cingulate cortex; striatum; brainstem and cerebellum (Fig. **f**). Additionally, [18F]FTC-146 accumulates in other organs containing S1Rs, including the lungs, spleen, pancreas, thyroid, heart, kidneys and liver (Fig. **g**). Nearly no tracer uptake (< 0.7 SUV) was observed in bone (spine, skull, femur) and muscle (thigh) at 120 min. Peak values of radioactivity in blood appear at 3 min post administration. 39% (30 min), 29% (60 min), 24% (90 min) and 21% (120 min) of radioactivity remained in the circulation relative to the radioactivity at 3 min (Fig. **h**). Radio-HPLC results show 50% intact [18F]FTC-146 in the acetonitrile extraction of blood at 5 min post-tracer injection.

Conclusions: In these pilot studies, there were no adverse events or clinically important changes in vital signs or electrocardiographic findings. We will continue to perform additional scans on healthy volunteer subjects to determine radiation dosimetry and biodistribution of [18F]FTC-146 over time and across subjects (n=10).

References:
[1] James ML, et al (2012) J Med Chem, 55, 8272-82. [2] James ML, et al (2014) J Nucl Med, 55, 147-53. [3] Shen B, et al (2015) EJNMMI Res, 5: 49
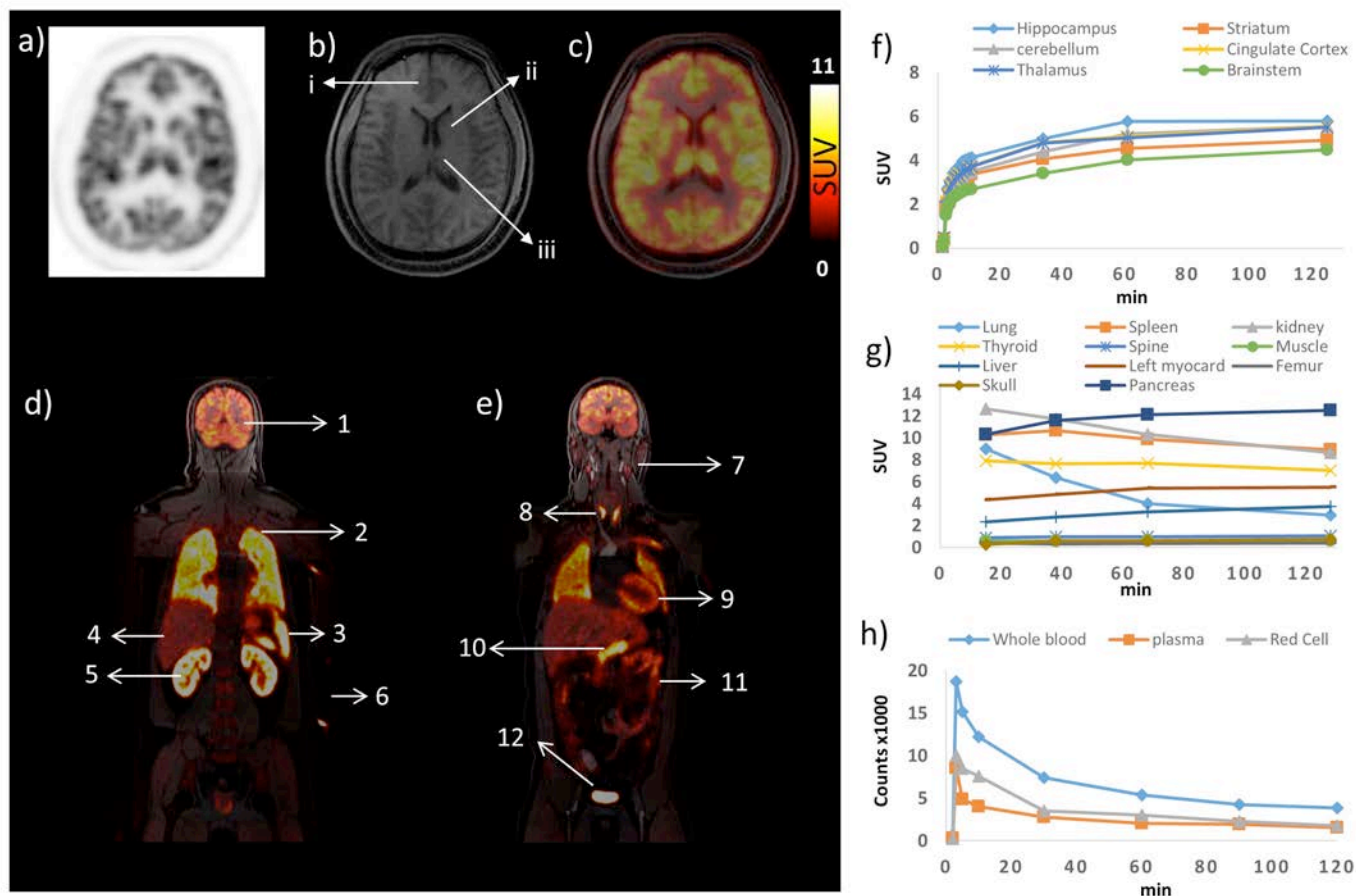
Figure. Selected transverse brain PET at 30 min post injection **(a)**, MR **(b)**, and fused **(c)** PET/MR images: cingulate cortex (i), striatum (ii) thalamus (iii); **(d)** Whole body coronal PET/MR images at 30 min post injection: brain (1), lungs (2), spleen (3), liver (4), kidneys (5), injected vein (6); **(e)** Whole body coronal PET/MR images at 30 min post injection: salivary glands(7), thyroid gland (8), heart (9), pancreas (10), bowel (11) and urinary bladder (12); **(f)** TAC of brain regions; **(g)** TAC of peripheral organs; **(h)** [^{18}F]FTC-146 clearance in blood.

The effect of TSPO expression on brain structures in Transgenic model of amyloidosis

Min Su Kang[1, 2], Sulantha S. Mathotaarachchi[1, 2], Maxime J. Parent[1, 2], Monica Shin[1, 2], Antonio Aliaga[4], Sonia Do Carmo[5], Jean-Paul Soucy[4], Serge Gauthier[2], A. Claudio Cuello[5], Pedro Rosa-Neto[1, 2, 3, 4, 5]

Translational Neuroimaging laboratory[1], McGill Centre for Studying in Aging[2], Brain Imaging Centre – Douglas Research Centre[3], McConnell Brain Imaging Centre – McGill University[4], Department of Pharmacology – McGill University[5]

Background: A growing body of literature suggests that neuroinflammation is an integral part of Alzheimer's disease (AD) pathophysiology imposing neuronal vulnerability or neuroprotection depending the phase of the disease. However, it remains to be demonstrated whether microglial activation might modulate structural changes observed in AD. Here, we test the hypothesis that amyloid-induced translocator protein (TSPO) expression modulates brain structural changes in a transgenic rat model of overexpressing human APP with Swedish and Indiana mutation. TSPO is an 18kDa protein mainly found on the outer mitochondrial membrane of activated microglia.

Methods: We conducted longitudinal imaging studies in the McGill-R-Thy1-APP rat model. This transgenic rat displays brain amyloidosis without neurofibrillary tangles. A total 12 rats (3 WT and 9 Tg) had [18F]PBR06 and structural MRI acquisitions conducted at 11.5 months (baseline) and 16.8 months (follow-up). MRI acquisitions were acquired in a Brooker 7T system during 60 minutes under anesthesia with isoflurane 2% delivered via nose cone. Deformation images were also generated following a 60-minute structural MRI scans with volumetric coil. Individual deformation maps were generating using structural images co-registered linearly and nonlinearly to the average standard map. Dynamic PET [18F]PBR06 were acquired in a CTI R4 concorde PET scanner during 60 min. Trnasmission images were acquires using a [57Co] point source. PET acquisitions were conducted using isoflurane as previously described. List mode acquisitions were reconstructed using maximum a posteriori (MAP) estimation. BP_{ND} images were generated using Simplified Reference Tissue Method (SRTM) following a 60-minute dynamic scans using reference region. Individual differences between baseline and follow up [18F]PBR06 BP_{ND} were estimated. The synergistic effect of neuroinflammation and group on deformation was tested using a general linear model. The statistical analysis was performed using VoxelStats, a statistical voxel based analytical framework. General linear model is depicted in the figure 1.

Results: Results are summarized in figure 1. The interaction effect between Δ[18F]PBR06 BP_{ND} and group revealed that the cumulative neuroinflammation was associated with structural stability in Tg compared as compared WT in dorsal hippocampus, basal lateral amygdaloid region, hypothalamus, and corpus callosum.

Conclusion: TSPO expression modulates mechanism underlying structural changes present in the animal model of AD.

Follow-up Deformation ~ Group*△[18F]PBR06
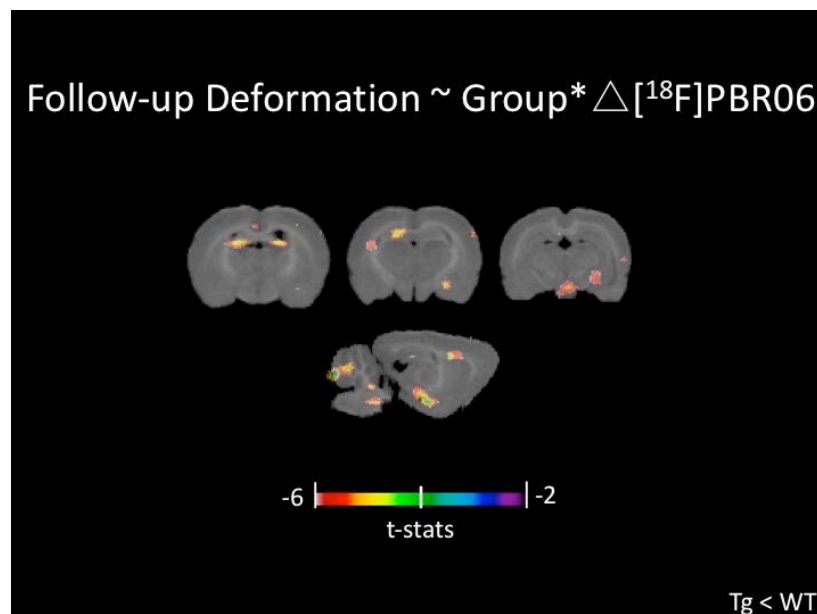
Insights into neuroepigenetics through human histone deacetylase imaging

H-Y Wey[1†], T.M. Gilbert[1†], N.R. Zürcher[1], A. Bhanot[1], F.A. Schroeder[1], C. Wang[1*], J.M. Hooker[1*]

[1]*Athinoula A. Martinos Center for Biomedical Imaging, Massachusetts General Hospital, Harvard Medical School, Charlestown, MA, US;* [†], [*] *Equal contribution*

Introduction: Histone deacetylases (HDACs) are epigenetic enzymes that repress gene transcription to alter downstream cellular functions. Although there is growing evidence for HDAC dysfunction in neurological disease, a fundamental knowledge gap exists regarding the expression and distribution of HDACs in healthy individuals for comparison to disease states. Moreover, the pathological consequences of *in vivo* HDAC dysregulation are not understood in humans. The goal of this study is to quantitate *in vivo* regional HDAC expression in the healthy human brain using a novel HDAC-selective radiotracer, [11C]Martinostat, and to confirm the binding targets of   [11C]Martinostat in brain tissue through *ex vivo* biochemical profiling.

Methods: [11C]Martinostat PET images were acquired from eight healthy volunteers (4M/4F, 28.6±7.6 years) on a 3T Siemens BrainPET. Dynamic 90 min PET image acquisition was initiated with the start of IV bolus injection of [11C]Martinostat (4.8 ± 0.4 mCi). PET data were stored in list mode format and binned into 28 frames of progressively longer duration. Data were processed using FSL, FreeSurfer, and PMOD. A two-tissue compartmental model was applied to the regional time-activity curves extracted from 28 VOIs (AAL atlas), using the metabolite-corrected arterial plasma as an input function to derive volume of distribution (V_T). An averaged SUV image ($SUV_{60-90min}$) was calculated from 60 to 90 min post-radiotracer injection. To assess regional differences in [11C]Martinostat binding, we biochemically profiled postmortem human brain tissue across gray matter (superior frontal gyrus, dorsal lateral prefrontal cortex, hippocampus, anterior cingulate). Cellular thermal shift assays (CETSA) were performed with brain homogenates and increasing concentrations of Martinostat, such that inhibitor-binding results in thermal stabilization.

Results and Discussion: The uptake and retention of [11C]Martinostat in the human brain was high, with regional heterogeneity observable at the individual subject level (Fig 1). A two-tissue compartmental model fits the PET data sufficiently and the V_T values can be determined robustly (Fig 1c). Regional $SUV_{60-90min}$ correlated positively with V_T values (r^2=0.96; p<0.0001) (Fig. 1b), suggesting that $SUV_{60-90min}$ is an appropriate surrogate outcome measurement for V_T. Regional $SUV_{60-90min}$ showed that HDAC expression is strikingly reproducible between individuals, thus establishing the first *in vivo* baseline of normal HDAC expression throughout the brain. Specifically, we found that HDAC expression is higher in cortical gray matter ($SUV_{60-90min}$ 3.2 ± 0.4) than white matter (1.7 ± 0.3). Among gray matter regions, HDAC expression is highest in the cerebellum (3.6 ± 0.5) and lowest in the hippocampus (2.4 ± 0.3) and amygdala (2.4 ± 0.3). Since HDACs inhibit gene transcription, lower levels of [11C]Martinostat uptake may serve as a marker for transcriptionally active brain regions undergoing neuronal plasticity. Using CETSA, we confirmed that across gray matter, [11C]Martinostat binds HDAC1/2/3, the subtypes most associated with cognitive function.

Conclusions: The first-in-human epigenetic imaging study with [11C]Martinostat establishes that HDACs are highly expressed throughout the healthy brain with region-specific distribution. We believe [11C]Martinostat PET holds great potential for detecting aberrant HDAC expression and assessing novel HDAC therapeutics in neurodegenerative and psychiatric disorders.
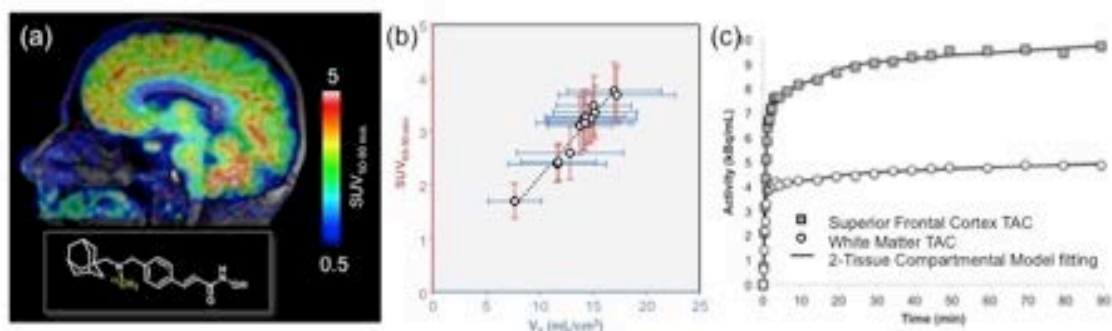
Figure 1. (a) [^{11}C]Martinostat SUV$_{60\text{-}90min}$ images of an individual subject overlaid on the subject's anatomical MR images. Bottom panel shows the structure of [^{11}C]Martinostat. (b) Correlation of regional distribution volume (V_T) values and SUV$_{60\text{-}90min}$ values (r^2=0.96; correlation analysis, $p<0.0001$, n=6). (c) Time activity curves (TACs) and a two-tissue compartmental model fitting results for superior frontal cortex and white matter.

Development of a PET tracer for tracer for imaging of reactive oxygen species in the brain

Thomas J. A. Graham, Catherine Hou and Robert H. Mach

Department of Radiology, University of Pennsylvania, Philadelphia, PA 19104

Objective: Unregulated production of reactive oxygen species (ROS) have been implicated in pathogenesis of neurodegenerative diseases such as Parkinson's disease (PD), Alzheimer's disease (AD) and amyotrophic lateral sclerosis (ALS). Imaging tools capable of studying ROS *in vivo* remains an unmet challenge. We recently reported the development a superoxide sensitive PET imaging probe based upon the fluorescent probe dihydroethidium. While this tracer was capable of imaging ROS levels *in vivo* it lacked brain uptake. As a result, we focused on the development of a second generation tracer with increased brain uptake.

Methods: Using *in vivo* dynamic optical imaging in mice, candidate (fluordihydromethidine, FDM) was identified as being likely to possess increased brain uptake relative to our previously described candidate. FDM and its tosylate precursor were then synthesized and radiolabeled with [18F]F⁻/Kryptofix. *Ex vivo* biodistribution studies were carried out in healthy untreated mice (BALB/c; n=3). Dynamic PET imaging studies were carried out in healthy, untreated mice (BALB/c, n=x) and mice treated with LPS (systemic, 5 mg/kg).

Results: FDM and tosylate precursor were prepared from commercially available materials in 11 and 12 steps, respectively. Labeling of FDM was achieved with [18F]F⁻/Kryptofix (100 °C, DMSO, 5 min) followed by deprotection (100 °C, 1 N HCl, 5 min). After HPLC purification [18F]FDM was isolated with a non-decay corrected yield of 3.3% (>99% radiochemical purity). Stability studies with [18F]FDM formulated with ascorbic acid (1 mg/mL) in saline/EtOH showed no decomposition for at least 5 hours. Biodistribution studies with [18F]FDM showed total brain uptake of 4.38±0.66 at 2 min, 1.42±0.30 at 30 min and 1.32±0.13 %ID/g.MicroPET imaging studies in control and LPS-treated mice demonstrated selective retention in the brain in the treated versus control animals.

Conclusion: [18F]FDM was prepared and radiolabeled for evaluation in an LPS model of neuroinflammation. Biodistribution studies with [18F]FDM showed good brain uptake and washout in mice suggesting that it would be a viable candidate for brain imaging studies. Imaging studies in LPS-treated mice indicate that this radiotracer is a potential probe for imaging ROS levels in the CNS under conditions of neuroinflammation.
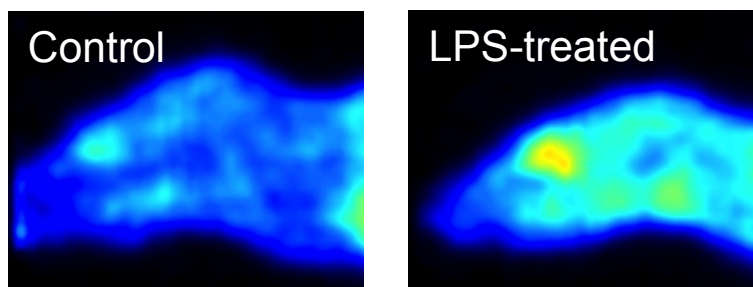
Figure. PET imaging studies in a control (left) and LPS-treated mouse.

PET/MR and Mathematical Modeling of Drug Delivery in Brain Tumors

Ahmed Boujelben[1], Michael Watson[1], Steven McDougall[1], Mark Chaplain[2], Elizabeth Gerstner[3], Ciprian Catana[3], David Boas[3], Tracy Batchelor[3], Jacob Hooker[3], Jayashree Kalpathy-Cramer[3], Bruce Rosen[3]

[1] Heriot-Watt University, Edinburgh, Scotland; [2] St. Andrews University, Scotland; [3] Massachusetts General Hospital, Boston, MA

Introduction: Patients diagnosed with glioblastoma, a kind of primary brain tumor, have a grim prognosis with a median overall survival of less than 15 months. Vasculature within these tumors is typically abnormal, with increased tortuosity, dilation and disorganization and these tumors typically exhibit a disrupted blood brain barrier (1). Although it has been hypothesized that the "normalization" of the vasculature resulting from anti-angiogenic therapies (2) could improve drug delivery through improved blood flow, there is also evidence that suggests that the restoration of blood brain barrier integrity might limit the delivery of therapeutic agents and hence their effectiveness (3, 4). In this work, we apply mathematical models of blood flow, permeability and diffusion through the tumor microenvironment to investigate the effect of these competing factors on drug delivery (5). PET/MR studies using radiolabeled drugs may provide insights into the delivery of therapeutic agents during concomitant therapy with anti-angiogenic agents.

Methods: We had previously developed a hybrid discrete-continuum mathematical model of flow through vascular networks allowing for dynamic adaptivity of the vessels, with applications to tumor induced angiogenesis and drug delivery, wound healing and retinal development (6, 7). Recent extensions to the model incorporated permeability of the vasculature and diffusion of the extravasated agent through heterogeneous media in 3D. Advances in optical imaging technology have enabled us to develop Vascular Anatomical Network (VAN) models based on two-photon microscopy in rodents (8). These "virtual voxels", representing realistic vascular networks, were used as input to the mathematical models to calculate the flow and distribution of agents within the "virtual voxel". We present preliminary results based on exploring the effects of modeling parameters on drug delivery.

In human studies, we present PET/MR imaging data from an ongoing clinical trial of patients with glioblastoma treated with bevacizumab. We performed MR-PET scans in patients receiving bevacizumab and radiolabeled [11C] temozolomide. Patients were scanned pre and post bevacizumab therapy. In addition to standard anatomical MRI, we also performed perfusion/permeability imaging. Parametric maps were generated for cerebral blood flow, volume and permeability as well as SUV for uptake of the radiolabeled temozolomide and quantified within regions of interest identified by the clinician.

Results: Preliminary results from the modeling indicate that delivery of the agent to the tumor bed is affected by flow, permeability and diffusion in the interstitial space. Reductions in the permeability of the vasculature, as would be expected from restoration of the blood brain barrier in response to anti-angiogenic therapy, could potentially reduce the delivery of the drug to the tumor while increased flow could increase drug delivery.

Preliminary PET/MR data on the patients similarly demonstrated a range of vascular responses. In one patient we observed increases in enhancing tumor volume, median permeability and median SUV, perhaps suggesting increased drug delivered to the tumor while another patients exhibited a marked reduction in tumor volume, permeability and uptake after treatment with bevacizumab.

Conclusions: Mathematical modeling combined with empirical data from animal models can provide insights into the role that the vascular architecture, permeability and microenvironment heterogeneity can play in the drug distribution in the tumor bed in response to anti-angiogenic therapies. PET/MR with radiolabeled drugs such as temozolomide in humans can be used to non-invasively validate these models and provide patient specific guidance for therapy.

References:

1. Folkman J. Role of angiogenesis in tumor growth and metastasis. Semin Oncol. 2002;29(6 Suppl 16):15-8. doi: 10.1053/sonc.2002.37263. PubMed PMID: 12516034.

2. Jain R. Normalization of Tumor Vasculature: An Emerging Concept in Antiangiogenic Therapy2005. PubMed PMID: 13174295468459881802related:SvWWm-1_1LYJ.

3. Van der Veldt AA, Lubberink M, Bahce I, Walraven M, de Boer MP, Greuter HN, Hendrikse NH, Eriksson J, Windhorst AD, Postmus PE, Verheul HM, Serne EH, Lammertsma AA, Smit EF. Rapid decrease in delivery of chemotherapy to tumors after anti-VEGF

therapy: implications for scheduling of anti-angiogenic drugs. Cancer cell. 2012;21(1):82-91. doi: 10.1016/j.ccr.2011.11.023. PubMed PMID: 22264790.

4.   Arjaans M, Oude Munnink TH, Oosting SF, Terwisscha van Scheltinga AG, Gietema JA, Garbacik ET, Timmer-Bosscha H, Lub-de Hooge MN, Schroder CP, de Vries EG. Bevacizumab-induced normalization of blood vessels in tumors hampers antibody uptake. Cancer Res. 2013;73(11):3347-55. doi: 10.1158/0008-5472.CAN-12-3518. PubMed PMID: 23580572.

5.   McDougall SR, Anderson AR, Chaplain MA. Mathematical modelling of dynamic adaptive tumour-induced angiogenesis: clinical implications and therapeutic targeting strategies. J Theor Biol. 2006;241(3):564-89. doi: 10.1016/j.jtbi.2005.12.022. PubMed PMID: 16487543.

6.   Macklin P, McDougall S, Anderson AR, Chaplain MA, Cristini V, Lowengrub J. Multiscale modelling and nonlinear simulation of vascular tumour growth. J Math Biol. 2009;58(4-5):765-98. doi: 10.1007/s00285-008-0216-9. PubMed PMID: 18781303; PubMed Central PMCID: PMC3037282.

7.   Machado MJ, Watson MG, Devlin AH, Chaplain MA, McDougall SR, Mitchell CA. Dynamics of angiogenesis during wound healing: a coupled in vivo and in silico study. Microcirculation. 2011;18(3):183-97. doi: 10.1111/j.1549-8719.2010.00076.x. PubMed PMID: 21166934.

8.   Gagnon L, Sakadzic S, Lesage F, Musacchia JJ, Lefebvre J, Fang Q, Yucel MA, Evans KC, Mandeville ET, Cohen-Adad J, Polimeni JR, Yaseen MA, Lo EH, Greve DN, Buxton RB, Dale AM, Devor A, Boas DA. Quantifying the Microvascular Origin of BOLD-fMRI from First Principles with Two-Photon Microscopy and an Oxygen-Sensitive Nanoprobe. J Neurosci. 2015;35(8):3663-75. doi: 10.1523/JNEUROSCI.3555-14.2015. PubMed PMID: 25716864.

There is more to "Lassen" plots than Lassen's plot

Araj Khodaei J[1], Araj Khodaei M[2], Vafaee M[3,4], Gjedde A[3,4]

[1]Mechanical Engineering Department, Amirkabir University of Technology, Tehran, Iran; [2] Iranian Traditional Medicine Clinical trial Research Center, Shahed University, Tehran, Iran; [3]Department of Neuroscience and Pharmacology, University of Copenhagen, Copenhagen, Denmark; [4]Neuroscience Research Center, Tabriz University of Medical Sciences, Tabriz, Iran

Introduction: Neuroreceptor studies by PET often compare radioligand binding potentials in baseline and inhibition states in cases where an apparent reference region of no binding is unknown. The quantitative comparison often uses the basic equation of receptor availability in molecular imaging to obtain separate estimates of receptor saturation and non-displaceable radioligand volume of distribution, according to the equation,

$$1 - s = \frac{V_{T(i)} - V_{ND}}{V_{T(b)} - V_{ND}}$$ (1)

where s is the fraction of receptors occupied, V_{Ti} is the total volume of distribution of specifically bound and non-specifically dissolved radioligand in the occupied state of the receptor, V_{ND} is the volume of distribution of the radioligand in the absence of specific binding, also known as the partition volume or coefficient, and V_{Tb} is the total volume of distribution in the unoccupied state of the receptor. The equation was linearized by Turton et al (1995) 1, Gjedde & Wong 2, and Cunningham et al (2010) 3, respectively, as the Saturation, Inhibition, and Occupancy plots, listed here in that order,

$$V_{T(b)} = \frac{1}{s} \Delta V_T + V_{ND}$$ (2)

$$V_{T(i)} = (1-s)V_{T(b)} + s V_{ND}$$ (3)

$$\Delta V_T = s V_{T(b)} - s V_{ND}$$ (4)

Objectives: Two of the three linearizations, the Occupancy and Saturation plots, use commingled variables in the form of the difference between the volume parameters. The aim of this work was to determine which linearization has a better convergence with measured data, and how regression methods affect the resulting estimates of the fraction of receptors occupied (s) and the volume of distribution of non-displaceable radioligand (V_{ND}).
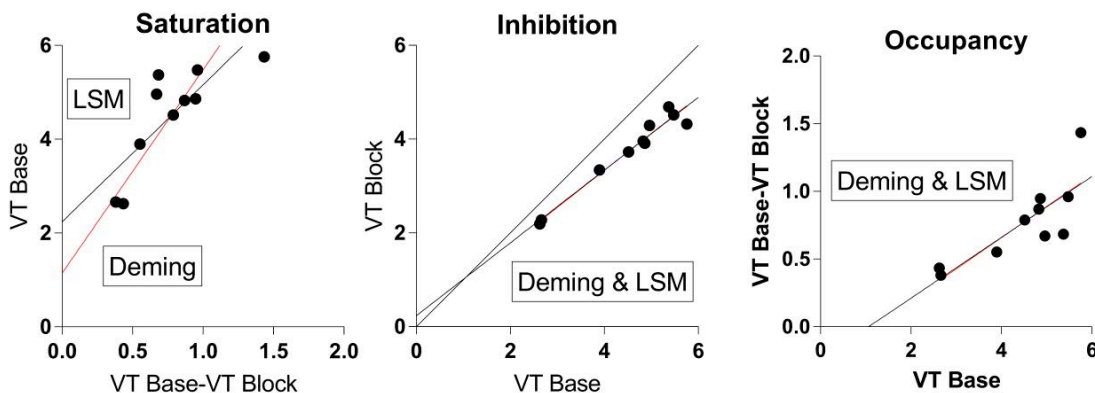

Figure 1. Example of LSM and Deming II Regressions of Data Extracted from Kågedal et al. [12]

Methods: To accomplish this goal, we subjected 24 published reports of 98 sets of data to reanalysis. In six cases, the authors submitted data [4-9], and for the remaining 18 reports, we extracted the data from the graphs with Getdata software. We used two linear regression methods, the *Least Squares* (LSM) and *Deming* methods to obtain parameter estimates, as implemented in *Matlab*. Using the slope and intercept estimates, we calculated s (fraction of receptors occupied) and V_{ND} and evaluated the accuracy. In LSM, the R^2 value is the linearization accuracy. When the R^2 value is closer to one, the results are considered more accurate 1. In the Deming II method, Sigma X^2 is the standard error of

regression. When the Sigma X^2 value is closer to zero, the results are considered more accurate 11. The results of the three linearizations for raw and extracted data were compared and the comparison showed that the mean error was less than 0.85%, confirming that extractions were accurate. As an example, values of $V_{T(E)}$ and ΔV_T were extracted from the report of Kågedal et al. 11, and $V_{T(i)}$ values were calculated from the digitization. Using Inhibition plot, Saturation plot, and Occupancy plot linearizations, and *LSM* and *Deming* method regressions, we obtained parameter values from the linear regressions to the data, as presented in Figure 1. The resulting regressions and *s* and V_{ND} estimates are listed in Table 1.

Table 1. Equations and s and V_{ND} Estimates from Figure 1 Regressions

Regression	Plot	Equation	s	V_{ND}	R^2 or SigmaX^2
Least Squares	Inhibition	Y=(0.558059×X) + 0.61993	0.441941	1.402742	0.960357
	Occupancy	Y=(0.441941×X) - 0.61993	0.441941	1.402742	0.938244
	Saturation	Y=(2.123006×X) + 1.59359	0.47103	1.593594	0.938244
Deming II	Inhibition	Y=(0.56357×X) + 0.59516	0.43643	1.363713	0.006893
	Occupancy	Y=(0.446737×X) - 0.64148	0.446737	1.435920	0.007567
	Saturation	Y=(2.238451×X) + 1.43592	0.446737	1.435920	0.007567

Results: Using the linearization accuracy parameters R^2 for LMS and Sigma X^2 for Deming, the comparison yielded the following results: As seen in Table 2, the mean value of R^2 (for 86 samples) in LSM for the Inhibition plot was closest to unity, as the most accurate of the linearizations. In addition, the mean value of Sigma X^2 in the Deming Method for the Inhibition plot was closest to zero, also as the most accurate of the three plots. The Saturation plot uses ΔV_T as the **X** component, and $V_{T(E)}$ as the **Y** component, while the Occupancy plot uses ΔV_T as the **Y** component, and $V_{T(E)}$ as the **X** component, yielding similar trend and regression accuracy parameter values.

Table 2. Accuracy vs Precision

Regression	Method	Mean Accuracy Parameter
Least Squares	Inhibition	0.7459
	Occupancy	0.7257
	Saturation	
Deming II	Inhibition	0.1089
	Occupancy	0.1457
	Saturation	

Conclusions: Three linearizations have been derived from the equation of receptor availability in molecular imaging. In this comparison of 98 cases culled from the literature, the accuracy for each equation of the linear regressions was evaluated with the Least Squares and Deming methods of regression. Due to the absent commingling of dependent and independent variable, the Inhibition plot emerged as the most accurate of the regressions.

References:
1. Turton, D. R., et al. Benzodiazepine receptor quantification in vivo in humans using [11C]flumazenil and PET: application of the steady-state principle. J Cereb Blood Flow Metab 15.1 (1995).
2. Gjedde, A., and D. F. Wong. Receptor occupancy in absence of reference region. Neuroimage 11.6 (2000): S48.
3. Cunningham, Vincent J., et al. Measuring drug occupancy in the absence of a reference region: The Lassen plot re-visited. Journal of Cerebral Blood Flow & Metabolism 30.1 (2010): 46-50
4. Ettrup, Anders, et al. 11C-NS14492 as a Novel PET Radioligand for Imaging Cerebral α7 Nicotinic Acetylcholine Receptors: In Vivo Evaluation and Drug Occupancy Measurements. Journal of Nuclear Medicine 52.9 (2011): 1449-1456.

5. Ramakrishnan, Nisha K., et al. Cutamesine Overcomes REM Sleep Deprivation-Induced Memory Loss: Relationship to Sigma-1 Receptor Occupancy. Molecular Imaging and Biology 17.3 (2015): 364-372.

6. Paul, Soumen, et al. Use of ^{11}C-MPDX and PET to study adenosine A1 receptor occupancy by nonradioactive agonists and antagonists. Journal of Nuclear Medicine 55.2 (2014): 315-320.

7. Phan, Jenny-Ann, et al. Quantification of [11C]yohimbine binding to α2 adrenoceptors in rat brain in vivo. Journal of Cerebral Blood Flow & Metabolism (2015).

8. Horti, Andrew G., et al. ^{18}F-ASEM, a Radiolabeled Antagonist for Imaging the α7-Nicotinic Acetylcholine Receptor with PET. Journal of Nuclear Medicine 55.4 (2014): 672-677.

9. Narendran, Rajesh, et al. Evaluation of dopamine D2/3specific binding in the cerebellum for the positron emission tomography radiotracer [11C] FLB 457: Implications for measuring cortical dopamine release. Synapse 65.10 (2011): 991-997.

10. Miller, Steven J. The method of least squares. Mathematics Department Brown University (2006): 1-7.

11. Pollock, M. A., et al. Method comparison—a different approach. Annals of Clinical Biochemistry: An international journal of biochemistry in medicine29.5 (1992): 556-560.

12. Kågedal, Matts, et al. A positron emission tomography study in healthy volunteers to estimate mGluR5 receptor occupancy of AZD2066—estimating occupancy in the absence of a reference region. NeuroImage 82 (2013): 160-169.

GLP-1 Analog Raises Glucose Transport Capacity of Blood-Brain Barrier in Alzheimer's disease

Albert Gjedde[1], Michael Gejl[2, 3,4], Jørgen Rungby[5], Lærke Egefjord[2], Birgitte Brock[2, 4]

[1]Department of Neuroscience and Pharmacology, University of Copenhagen, Copenhagen, Denmark; [2]Institute of Biomedicine, Aarhus University, Aarhus, Denmark; [3]Department of Nuclear Medicine and PET Center, Aarhus University Hospital, Aarhus, Denmark; [4]Department of Clinical Biochemistry, Aarhus University Hospital, Aarhus, Denmark; [5]Center for Diabetes Research and Department of Clinical Pharmacology, Copenhagen University Hospital, Gentofte and Rigshospitalet, Copenhagen, Denmark.

Introduction: Glucose enters the brain tissue from plasma by facilitated diffusion across the two membranes of the endothelium of the blood–brain barrier (BBB), mediated by the glucose transporter 1 (GLUT1). There is evidence in Alzheimer's disease (AD) of reduction of glucose transport across the blood-brain barrier, due to diminished GLUT1 translocation and expression at the BBB. Reduced BBB GLUT1 expression is known to aggravate AD pathology and further impair cognitive function, implying that GLUT1 may be a potential target of therapy directed towards AD neurovascular dysfunction and degeneration. The incretin hormone GLP-1 prevents the decline of the cerebral metabolic rate of glucose that signifies cognitive impairment, synaptic dysfunction, and disease evolution in AD, and GLP-1 may directly activate GLUT1 transport in brain capillary endothelium. For this reason, we here claim that the GLP-1 analog liraglutide may prevent the decline of blood-brain glucose transfer in AD.

Methods: In this 26-week test of the hypothesis, we randomized 38 patients with AD to treatment with the GLP-1 analog liraglutide (n=18) or placebo (n=20). We determined blood-brain glucose transport capacity (T_{max}) with [^{18}F]FDG (FDG) (ClinicalTrials.gov NCT01469351).

Results: Unlike the placebo treatment, the GLP-1 analog treatment significantly (P<0.0001) raised T_{max} in cerebral cortex as a whole from 0.72 to 1.1 mmol/hg/min, a 50% increase (2-way ANOVA of qui-squared).

Conclusion: The results are consistent with the claim that GLP-1 analog treatment raises GLUT1 activity in the BBB and hence may represent a therapeutic target for neurovascular dysfunction and degeneration in AD.

Tmax before and after 6 months' treatment
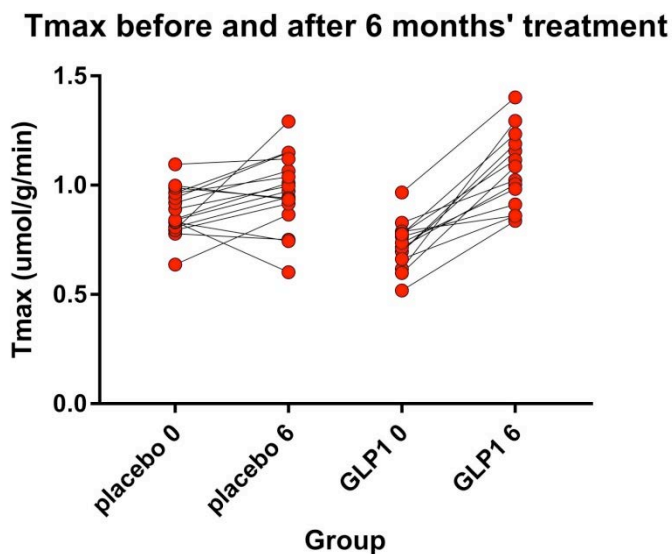
Baseline binding potential of [^{11}C]raclopride at true transient equilibrium predicts magnitude of amphetamine-stimulated dopamine release

Yoshitaka Kumakura,[1,2] Dean F. Wong,[1,3] Albert Gjedde[1,3]

[1]Department of Neuroscience and Pharmacology, University of Copenhagen, Denmark; [2]Department of Nuclear Medicine & PET Centre, Aarhus University, Denmark; [3]Department of Radiology and Radiological Sciences, Division of Nuclear Medicine PET Center, Departments of Psychiatry and Neurology and Neuroscience, Johns Hopkins Medical Institutions, Baltimore, MD, U.S.A.

Objectives: Quantitation of the binding of [^{11}C]raclopride in human brain is challenged by the extreme temporal changes of synaptic concentration of endogenous dopamine after intravenous administration of amphetamine. We used the exact approach of True Equilibrium Bolus Estimation (TREMBLE, Soelling et al., 1997; Wong et al, 1998) to quantify the specific binding of tracer raclopride at true transient equilibrium by means of simple rearrangement of differential kinetic equations. We reasoned that baseline dopamine occupancy would indicate the capacity for additional dopamine release and hence the increase of dopamine's receptor occupancy expected by the action of amphetamine. Therefore, we tested the hypothesis that the baseline binding potential (BP_{ND}) of raclopride predicts the receptor occupancy by stimulated dopamine release in relation to baseline dopamine in young healthy volunteers.

Methods: We selected PET data of 23 males and 14 females aged 19-29 years (mean 22.4; SD 3.1) from a cohort of 84 subjects (Kuwabara et al., 2012). The exclusion criteria of the PET data included the following: (1) irregularity of arterial plasma blood sampling for entire scan duration; (2) outliers of kinetic estimates obtained by one-tissue two-compartment model analysis for cerebellum. Subjects underwent two consecutive 90-min PET sessions with [^{11}C]raclopride. A high specific activity intravenous bolus injection of approximately 18 mCi was administered at the beginning of each scan. The first scan was preceded at 5min by an i.v. injection of saline; the second scan was preceded at 5 min by 0.3 mg/kg AMPH. Arterial blood was sampled at rapid intervals (< 5s) initially, with increasing intervals. Selected samples were analyzed by HPLC for radioactive plasma metabolites. The imaging protocol included as many as 30 acquisitions, frame durations increasing from 15 sec to 6 min, with the GE Advance PET device. First, the raw time-activity-curves (TACs) of striatum and reference tissues were interpolated and resampled every 0.1 min. Then, we employed the Savitzky–Golay polynomial filter (Savitzky and Golay, 1964) to calculate first-order differential terms by numerical differentiation. We analyzed the filtered noise-attenuated TACs with TREMBLE to obtain BP_{ND} at the time of the transient true equilibrium (T_{EQ}). Linear regression analysis was performed between baseline BP_{ND} ($BP_{ND\{b\}}$) and receptor occupancy (%) estimated as [1-($BP_{ND\{amph\}}$)/$BP_{ND\{b\}}$]x100. The few outliers that exceeded 2 SDs were excluded from final analysis after proof that there inclusion did not significantly affect the results and conclusions.

Results: The mean and SD estimates of baseline BP_{ND} for caudate and putamen were 3.36 ± 0.38 and 4.09 ± 0.46, respectively. Likewise, the mean estimates of amphetamine BP_{ND} were 3.25 ± 0.39 and 3.50 ± 0.31. The mean estimates of RO(%) were 2.33 ± 14.88 and 13.23 ± 13.02, meaning significantly smaller "displacement" in caudate. The slopes of linear regression analysis were significantly non-zero, at the significance level of P<0.0002 for caudate, and P<0.0001 for putamen. Likewise, the 95% confidence intervals of X-intercept were 3.019 to 3.442, and 3.232 to 3.672, where BP_{ND} changes were minimal by amphetamine challenge. As shown in Figure, we observed negative RO estimates in some subjects with the lowest baseline BP_{ND}.

Conclusions: We conclude that the principles of competitive binding failed to explain these results, suggesting that both the apparent maximum binding and affinity may vary, depending on individual differences. Given that reduction in affinity of D2 receptors may be due to internalization and/or affinity state interaction from D2high towards D2low receptors in subjects with high baseline binding, the sensitivity of D2 receptors appears to be associated inversely with the degree of receptor occupancy in the baseline, as predicted by the baseline binding potential obtained with this novel kinetic approach.

References

1. Kuwabara H, McCaul ME, Wand GS, Earley CJ, Allen RP, Weerts EM, Dannals RF, Wong DF (2012). Dissociative changes in the Bmax and KD of dopamine D2/D3 receptors with aging observed in functional subdivisions of the striatum: a revisit with an

improved data analysis method. J Nucl Med. 2012 May;53(5):805-12. doi: 10.2967/jnumed.111.098186. Epub 2012 Apr 9. PubMed PMID: 22492734; PubMed Central PMCID: PMC4533866.

2. Savitzky, A.; Golay, M.J.E. (1964). Smoothing and Differentiation of Data by Simplified Least Squares Procedures. Analytical Chemistry 36 (8): 1627–39. doi:10.1021/ac60214a047.

3. Sølling, T., Brust, P., Cunningham, V., Wong, D. F., and Gjedde, A. (1997). True Equilibrium Bolus Estimation (TREMBLE) confirms rapid transient equilibrium. NeuroImage 5: A29.

4. Wong DF, Sølling T, Yokoi F, Gjedde A (1998). Chapter 69 - Quantification of Extracellular Dopamine Release in Schizophrenia and Cocaine Use by Means of TREMBLE, Quantitative Functional Brain Imaging with Positron Emission Tomography Edited by:Richard E. Carson, Margaret E. Daube-Witherspoon and Peter Herscovitch, pp. 463-468, ISBN: 978-0-12-161340-2

Figure
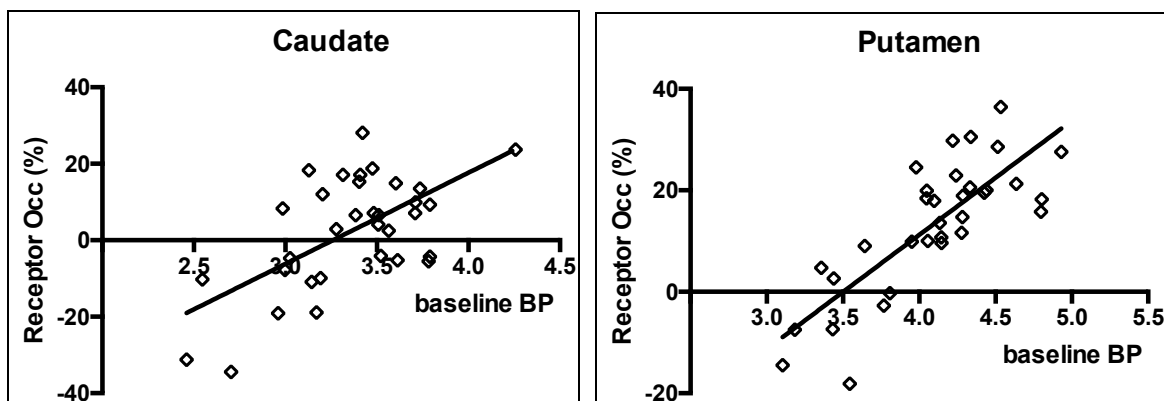
Effect of noradrenergic denervation on alpha2-adrenoceptor binding in rat brain in vivo

Jenny-Ann Phan[1,2], Steen Jakobsen[2], Albert Gjedde[2,3]

[1]*Department of Biomedicine, Aarhus University, Denmark,* [2]*Department of Nuclear Medicine & PET centre, Aarhus University Hospital, Denmark.* [3]*Department of Neuroscience and Pharmacology, University of Copenhagen, Denmark*

Introduction: Disrupted noradrenergic neurotransmission is implicated in Parkinson's and Alzheimer's diseases. However, the relative effects on noradrenaline levels and receptor density *in vivo* are uncertain.   Tracer [11C]yohimbine is a radioligand of alpha2 adrenoceptors with sensitivity to noradrenaline release in pigs and rats. Here, we use measures of [11C]yohimbine binding to alpha2 adrenoceptor sites and noradrenaline release in rat brain *in vivo* to test the hypothesis that noradrenaline levels decline more than the available receptors in selected brain regions after noradrenergic denervation.

Methods: Noradrenergic denervation was induced by IP treatment (50 mg/kg) of the selective neurotoxin (N-(2-chloroethyl)-N-ethyl-2-bromobenzylamine (DSP-4)) 7 days prior to positron emission tomography (PET). We determined [11C]yohimbine binding potentials at two levels of receptor occupancy, at baseline followed by amphetamine challenge (2 mg/kg) in DSP-4 pretreated and naïve animals. We calculated [11C]yohimbine binding potentials as bound vs. free ratios, using the yohimbine partition coefficient (V_{ND}), obtained from the Inhibition plot, a linearization of the Michaelis Menten equations applied to baseline and inhibition.

Results: The binding potentials in naïve animals were greatest in striatum, followed in descending order by thalamus, frontal cortex, pons and cerebellum. Amphetamine challenge significantly reduced the binding potentials with a uniform magnitude of 38% in all regions of interest (Figure 1), indicating uniform noradrenaline increase. DSP-4 denervation exhibited significantly lower binding potentials than naïve animals, suggesting acute decline of alpha2 adrenoceptor density. The effect of amphetamine challenge after DSP-4 treatment was greater than in naïve animals but with regional heterogeneity. With amphetamine, the binding potentials declined 51-67%, indicating variable and regionally differential release from surviving projections.

Conclusion: The greater decline of receptors than of noradrenaline levels is at variance with the original hypothesis stated above.

[11C]Yohimbine Binding of Noradrenergic Denervation